The Importance of Micro-Scale Processes on the Release of Macro-Nutrients from Estuarine Suspended Sediments

by

Emma Louise Pidduck

A thesis submitted to the University of Plymouth in partial fulfilment for the degree of

Doctor of Philosophy

School of Marine Science & Engineering

Faculty of Science & Engineering

2016

Copyright Statement

Signed .....

Emma Louise Pidduck

Date .....

Declaration

At no time during the registration for the degree of Doctor of Philosophy has the author been registered for any other University award without prior agreement of the Graduate Committee.

This study was financed by the Natural Environment Research Council (NERC) and the National Oceanography Center (NOC) Liverpool. Funding from Ifremer and a grant provided by the British Sedimentological Research Group (BSRG) was received with thanks, to enable fieldwork to be conducted in the Seine estuary, France.

Word count of main body of thesis: 49,045

Abstract

The Importance of Micro-Scale Processes on the Release of Macro-Nutrients from Estuarine Suspended Sediments

Emma L. Pidduck

The quality of water within an estuary is inseparable from the component parts; suspended particulate matter (SPM) and the balance of macro-nutrients. Long-term temporal variations and the horizontal advection of both SPM and macro-nutrient concentrations are well-constrained, but the vertical fluxes associated with micro-scale processes, such as turbulence and flocculation, are poorly constrained. The importance of three micro-scale processes on the interactions between SPM and inorganic macro-nutrients, nitrate (NO_3^-), ammonium (NH_4^+) and phosphate (PO_4^{3-}), are examined in four field campaigns and five laboratory experiments.

Field campaigns were conducted in two turbid estuaries. One field campaign was conducted in the Seine estuary, France, and three campaigns in the Tamar estuary, U.K., in order to consider the effects of seasonal variations (spring, summer and autumn). Physical conditions measured included current velocity, turbidity, turbulence and particle size, were recorded using a suite of oceanographic instrumentation. Five different laboratory studies were conducted using the same mini annular flume, with different background conditions. Inorganic macro-nutrients were measured spectrophotometrically on a continuous flow analyser (for NO_3^- and PO_4^{3-}) and fluorimetry

(NH_4^+).

Three hypotheses are presented as potential mechanisms controlling the release and uptake of macro-nutrients from sediments. Mechanism One (M1) described an exchange process between inorganic macro-nutrients and flocculation/disaggregating particles. It was hypothesised that flocculating particles would decrease water column macro-nutrient concentrations, and vice versa. In this study, flocculation was observed in both field sites, but there was no significant relationship between flocculation and macro-nutrient concentration. Similarly, the five laboratory studies demonstrated no statistically significant relationships between flocculation and macro-nutrient concentrations.

Mechanism Two (M2) hypothesised that turbulence would enhance the release portion of the exchange processes described in M1. Furthermore, it was proposed that increased turbulence would break bonds between macro-nutrients and the surface of particle faces. Turbulence was observed to limit the floc size in all experiments (both field and laboratory), but this study determined that it did not promote a significant release mechanism for inorganic macro-nutrients. However, this study observed that turbulence played a key role in the vertical distribution of PO_4^{3-} and NH_4^+. In both the Seine and Tamar estuaries, surface and near-bed concentrations were observed to be statistically significantly different ($p = <0.05$).

Finally, Mechanism Three (M3) hypothesised that increased salinity provides additional salt water cations that would enhance flocculation

and M1. This study measured an increase in floc size with increasing salinity in but did not enhance the proposed M1. Instead, as with turbulence, differences in water density as a result of the salinity affected the vertical distribution of NO_3^-.

This research concluded that micro-scale processes have no significant impact on the water-column concentration of inorganic macro-nutrients. Instead, it was observed that two of the three micro-scale processes, turbulence and salinity, play a key role in the vertical distribution of inorganic macro-nutrients in the Tamar and Seine estuaries.

Acknowledgements

This thesis has taken longer than I had originally planned and hoped, but, thankfully, is not without a final, positive outcome and invaluable lessons. This would not have been possible without support and advice from a wide range of people. I would like to thank my PhD supervisors, Dr Andrew Manning, Dr Mark Fitzsimons, Dr Alex Nimmo Smith, Professor Paul Worsfold and Dr Alejandro Souza for their support throughout this study. They have provided invaluable advice and assistance throughout the PhD process and have taught me a lot more than I ever could have wished for.

I would also like to thank the technical staff for all of their assistance during the project, including the hours of work in the laboratory. Especially to Dr Claire Williams for her patience and persistence with the Skalar; to Dr Alan Tappin for his ever-lasting patience and humour with the Shimadzu and finally, to the geology staff, Ian King and Christie Teece, for providing laboratory space, coffee and company when I needed it most.

And last, but not least, this work would not have been possible without the continued support of my wonderful family and friends. They have been a constant guiding light through an extraordinarily, long, dark tunnel! Thanks to my brother, Jamie, and Edward and Alexander, for their help and humour with the Tamar fieldworks, and to my many office and laboratory mates over the years for the distractions and bizarre conversations. I wish I could have stayed longer for those!

Thanks also go to Jonas, my housemate and buddy, for providing invaluable advice and laughs for the last 8 years. To Marcus, my best friend and hero, for supporting me, calming me, encouraging me and reading every last word of this thesis without a single complaint - I wouldn't have done this without you! And finally, to my ever-young and fantastic parents, who have had to endure countless phone calls, tears, frustrations and my company at home, but who have provided laughs, love and unwavering support all the way through.

Contents

List of Figures

List of Tables

Acronyms

ADCP	Acoustic Doppler Current Profiler
ADV	Acoustic Doppler Velocimeter
BB	Borate Buffer
CFA	Continuous Flow Analyser
CTD	Conductivity, Temperature & Depth instrument
DIP	Dissolved Inorganic Phosphorus
DOP	Dissolved Organic Phosphorus
EPS	Extra-Polycellular Substances
ESD	Equivalent Spherical Diameter
ETM	Estuarine Turbidity Maximum
HDPE	High Density PolyEthelene
IN	Inorganic Nitrogen
INSSEV	IN Situ SEttling Velocity (instrument)
LabSFLOC	Laboratory Spectral Flocculation Characteristics
LISST	Laser In-Situ Scattering Transmissometry system
LNS	Low Nutrient Seawater
MRP	Molybdate Reactive Phosphorus
N	Nitrogen
NTU	Nephelometric Turbidity Units
OBS	Optical BackScatter
P	Phosphorus
PAT	Potassium Antimony Tartrate
PSD	Particle Size Distribution
RSD	Relative Standard Deviation
RMS	Root Mean Square
SPM	Suspended Particulate Matter
TDN	Total Dissolved Nitrogen
TKE	Turbulent Kinetic Energy
TON	Total Oxidised Nitrogen
TP	Total Phosphorus
UHP	Ultra High Purity water
WR	Working Reagent
WWTP	Waste Water Treatment Plant

Chapter 1

Introduction

'What do we tell people you're doing?'

Sarah Pidduck

1. INTRODUCTION

An estuary is *'a semi-enclosed coastal body of water which has a free connection to the open sea, extending into the river as far as the limit of tidal intrusion, and within which sea water is measurably diluted with freshwater derived from land drainage'* (Dyer, 1997; Cochran, 2014). They have long been identified as one of the most important ecosystems on Earth. The typically opposing flows of the predominately riverine fresh water input and saline water associated tides provide high concentrations of suspended sediment and macro-nutrients in the water column, making them one of the most productive natural habitats in the world (Dyer, 1997; Wolanski, 2007; Cochran, 2014). Although estuaries are a particularly young and ephemeral feature, in terms of morphology and dynamics, they retain their importance throughout time as vital economic and industrial pathways and have been extremely important in the development of most countries (Dyer, 1997; Lotze et al., 2006).

The quality of water within an estuarine environment is inseparable from both suspended particulate matter (SPM) (Fisher et al., 1988; Droppo and Ongley, 1994; Turner, 1996; Turner and Millward, 2002; Maggi, 2009), and the balance of the macro-nutrients, nitrogen (N) and phosphorus (P) (Statham, 2012). Macro-nutrients are defined as nutrients required by organisms to survive; including plants, animals and humans. An excess of SPM may limit light penetration through the water and, therefore, the primary productivity. On the other hand, an excess input of macro-nutrients, also termed 'eutrophication', can lead to an excess of primary productivity. Eutrophication describes the result of increased nutrient concentrations that can lead to the increase in growth of 'choking' phytoplankton, such as algae (e.g. *Gyrodinium aureolum* and *Alexandrium*). Subsequently, light limitation and a depletion of oxygen in the water mean that many marine organisms (fish and shellfish) cannot survive (Painting et al., 2007; Dupas et al., 2015; Lemley et al., 2015). These algal events and toxins contaminate sea food for human consumption (as well as birds and marine mammals), giving

rise to a number of different poisoning syndromes (e.g. neurotoxic shellfish poisoning).

Historically, the highly variable conditions within and between estuarine systems have made it difficult to clearly discern the relationships between sedimentary processes, nutrient concentrations and the consequent biological impact (Elliott et al., 1999). The high degree of temporal and spatial variability in both SPM and macro-nutrient concentrations can be attributed to the changes in factors such as river discharge, tides, weather and climate that further result in changes to current speeds, turbidity, temperature and salinity (Dyer, 1997).

The delicate and complex nature of an estuary requires continuous monitoring and management due to the anthropic stresses imposed on them. As such, it is important to constrain each component, be it physical, chemical or biological, and understand the corresponding interactions. Long-term temporal variations in both SPM and macro-nutrient concentrations are, individually, well-documented (Kaul and Froelich Jr, 1984; Sin et al., 1999; Kormas et al., 2002; Huang et al., 2003; Pérez-Ruzafa et al., 2005; Li et al., 2007) and in estuarine environments with high riverine input and high SPM concentrations, it has generally been assumed that the dominant source of macro-nutrient concentrations is due to horizontal advection (Jay et al., 1997), i.e. river input. However, 'micro-scale' (see Figure 2.1) temporal variations and vertical fluxes of macro-nutrients are poorly constrained (Statham, 2012; Couceiro et al., 2013).

1.1 Aims

The overarching aim of this research was to investigate the significance of 'micro-scale' physical processes, such as flocculation and turbulence, as sources of inorganic macro-nutrients from suspended sediments and their mobility in the

water column. Secondary aims include:

- To investigate the effects of 'macro-scale' seasonal changes on the 'micro-scale' processes occurring in turbid estuaries.
- The identify controlling 'mechanisms' (see section 1.2 for each inorganic macro-nutrient tested in this study.

1.2 Hypotheses

The primary aim of the study was to establish the importance of sediments and small-scale physical processes as sources of inorganic N and P to the water column. With this in mind, it was proposed that several small-scale physical processes could affect the release and uptake of N and P ions, depending on the meso-scale conditions in the estuary. The hypothesised mechanisms were tested in both field work and laboratory experiments, as described in the following chapters.

Figure 1.1 (page 7) shows the proposed mechanisms that were tested in this study. Figure 1.1A illustrates the small-scale physical processes occurring in the water column (Maggi, 2009), all of which will be described in this chapter.

Starting Particle - Figure 1.1B represents a typical floc found in estuarine conditions in terms of shape and structure. The coloured particles attached to and surrounding the floc are ions of N and P species (colour and concentration irrelevant). In this case, there are nutrients bound to the floc, held in the interstitial water and in the surrounding water column.

Mechanism One (M1) - Figure 1.1C - This theory describes an exchange process associated with sorption and desorption of macro-nutrients and particles. Firstly, it is hypothesised that an increase in SPM concentration will

increase the opportunities for flocculation to occur and thus potentially create new 'pockets' of interstitial water through the formation of larger macroflocs (Eisma, 1986; Manning, 2001), as advocated by Krone (1963)'s order of aggregation. It is hypothesised that when two or more flocs aggregate, water containing macro-nutrients would become trapped and encourage the sorption of macro-nutrients onto the particle faces. This would reduce the concentration of macro-nutrients in the water column, and increase the potential of transport and dispersion of both nutrients elsewhere in the estuary. It is not, however, proposed to be a more efficient method than dispersion in the dissolved phase (Tian et al., 1992; Cruzado et al., 2002), but an additional unquantified component of macro-nutrient distribution in a turbid estuary. On the other side of the exchange, the increase in SPM concentration provides an additional source of already-bound macro-nutrients that, when exposed to other micro-scale processes, undergo desorption from the faces and lead to an increase in water-column macro-nutrient concentrations. When the micro-scale processes are in equilibrium (i.e. flocculation is limited by turbulence), it is anticipated that no flux will be observed, but that where one process is dominant, an uptake or release of macro-nutrients will occur.

Mechanism Two (M2) - Figure 1.1D - Increased levels of turbulence both aid and hinder the process of flocculation (Eisma and Li, 1993; Markussen and Andersen, 2014). Turbulence forms flocs through constructive collisions, but higher levels of shear will fracture weaker floc joints creating disaggregation (Manning, 2004). When the process of flocculation is increased by turbulence, flocs will aggregate and as described in Mechanism One, new pockets of interstitial water will be created. However, the primary hypothesis of Mechanism Two is that the turbulence physically breaks the bonds between sediments and attached nutrients, instead of a chemical process or exchange. It is further hypothesised that increased turbulence may also affect the charge of the particle faces and there-

fore change the strength of the attraction between the particle faces and PO_4^{3-} / NH_4^+ ions in the water.

Mechanism Three (M3) - Figure 1.1E - During the flood tide, sea water flushes the estuarine system increasing the salinity, thereby increasing the concentration of salt water cations and anions in the water column (Figure 1.1E). Gardner et al. (1991) has shown that increased salt water cations in the water leads to ion exchange between cations (e.g. Mg^{2+}, Ca^{2+}) and NH_4^+, on the particle face. Similarly, PO_4^{3-} is also subject to ion exchange processes as described by Pomeroy et al. (1965); Jones (1989). As another potential exchange process, Mechanism Three may encourage uptake and release of macro-nutrients.

1.3 Objectives

To address the aim of this study, the main objectives of this thesis are as follows:

- In order to determine the impacts of micro-scale physical processes on sediment-nutrient behaviour, hydrodynamic conditions, including salinity, turbidity, current velocity, etc. and inorganic macro-nutrient concentrations will be recorded at a high temporal resolution in both field and laboratory experiments.
- To determine the effects of 'macro-scale' processes on sediment-nutrient behaviour, identical field campaigns will be repeated in different seasons.
- A laboratory experiment, consisting of multiple runs, will seek to constrain each of the hypotheses discussed previously and compare results with field studies.

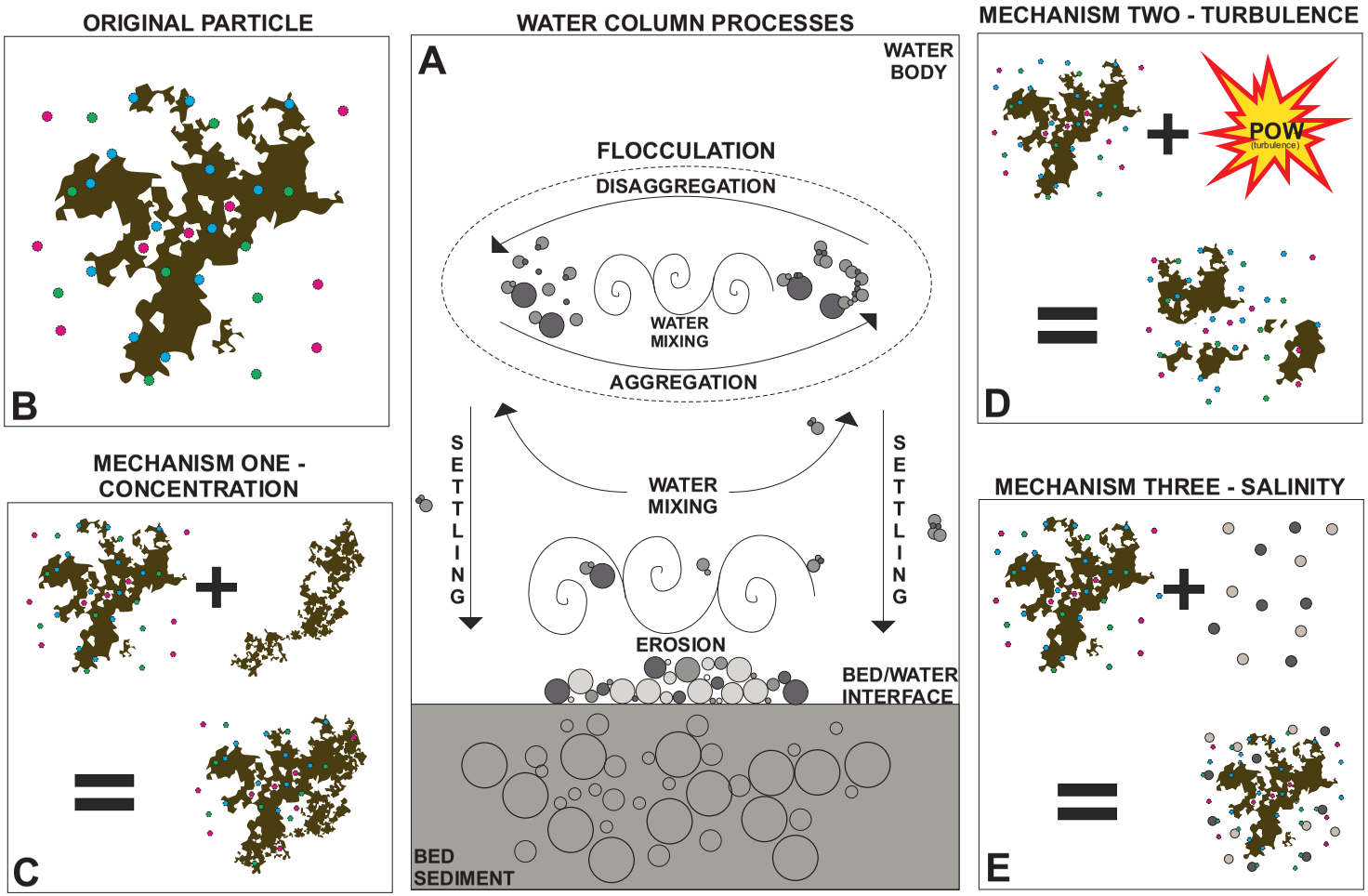

Figure 1.1: *Figure 1.1A illustrates the typical SPM physical processes occurring in an estuarine environment (adapted from Maggi, 2009) Figures 1.1B-E illustrate proposed mechanisms between suspended sediments, physical processes and nutrient concentrations. Blue, pink and green particles in Figures 1.1B - E represent inorganic macro-nutrients. Grey and green particles shown in Figure 1.1E represent saltwater cations.*

1.4 Thesis Structure

Background literature is presented in chapter 2 where existing understanding of both sediment and nutrient behaviour in estuaries is explored. Chapter 3 describes the instrumentation and methods employed in the fieldwork. Chapters 4 and 5 provide examples of two contrasting macro-tidal turbid estuaries, whereby the objectives in section 1.1 were met. Any variations from the methods described in chapter 3 are highlighted in the respective chapters. Finally, in chapter 6, preliminary work is presented on determining relationships between sediments and nutrients by way of a laboratory experiment. Chapter 7 presents a discussion of the results obtained in this study, including conclusions and future work.

Chapter 2

Physical and chemical properties of estuaries

'Why did you choose this subject in particular?'

Terry Cox

2. PHYSICAL AND CHEMICAL PROPERTIES OF ESTUARIES

This Chapter introduces the individual components of this interdisciplinary research before discussing the relationship between each component. The section refers to the aforementioned Mechanisms with a view to identifying supporting literature, as well as gaps in research. Each topic is broadly reviewed but analysis and evaluation was only conducted on areas that relate to the main aims and objectives of this research, as presented in section 1.1.

Estuaries are a constantly evolving, dynamic environment that provide the transformation zones from fresh water to salt water, between land, coastal seas and the global ocean (Pritchard, 1967; van Rijn, 1993; Dyer, 1997; Flemming and Hansom, 2011). They originated from the Flandrian transgression during the last ice age, approximately 10,000 years ago, making them relatively 'young' on a geological timescale (Emmett et al., 2000; Dyer, 1997; Simenstad and Yanagi, 2011). Their form is continually altered by the erosion and deposition of sediment, while sea level rise due to climate change can cause drastic effects (van Rijn, 1993; Dyer, 1997; Lotze et al., 2006). Estuaries are susceptible to large inputs of nutrients from the land, from both anthropogenic and natural sources, making them ecologically highly productive. Natural sources include riverine input and precipitation, while anthropogenic sources include agricultural fertilisers and storm sewer outfalls. However, the number of different nutrient species within an estuary is limited by the broad variations in conditions, such as temperature and salinity (Dyer, 1997; Simenstad and Yanagi, 2011; Wolanski and Elliot, 2016). Furthermore, each estuary responds differently to these varying conditions, with differing magnitudes and time scales for each physical process, as well as varying aquatic conditions.

Figure 2.1 shows the typical temporal and spatial range of physical processes in an estuarine environment. These scales were designed to categorise the different processes occurring within an estuary. Each scale was created using existing

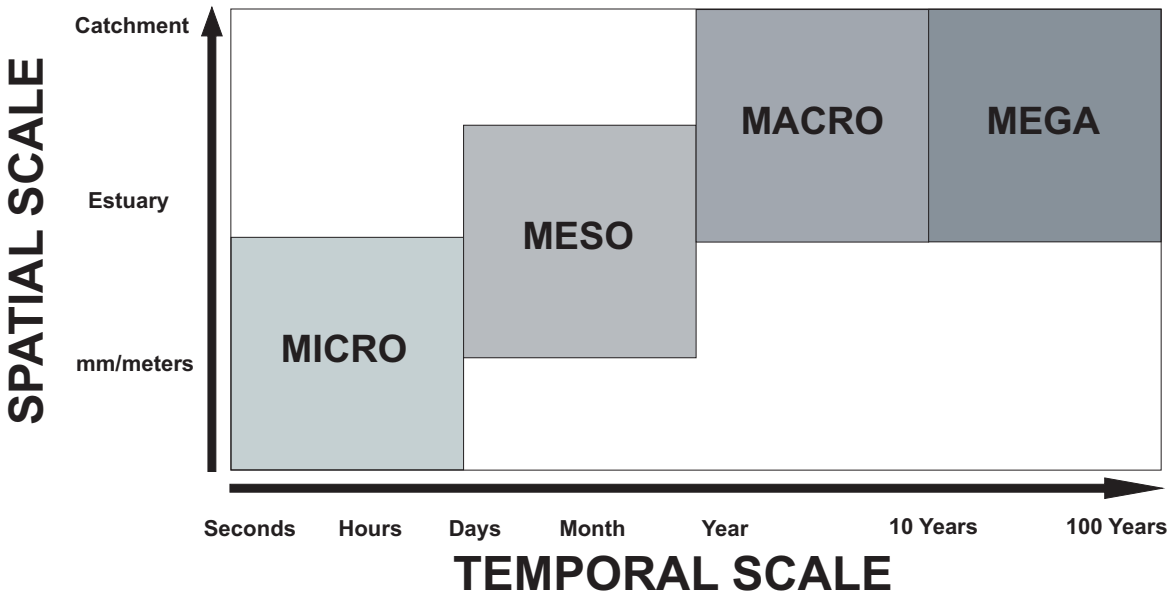

Figure 2.1: *Diagrammatic representation of the temporal and spatial scales affecting estuaries. Micro-scale processes include turbulence and flocculation. Meso-scale processes include semi-diurnal and spring-neap tides. Macro-scale processes include seasonal variations. Mega-scale processes include major morphological changes as a result of climate change.*

literature and an analysis of the typical timescales reported, and the physical size of the process, where quantifiable. 'Mega-scale' processes, such as sea level rise due to climate change, take place over decades and centuries and can affect the entire estuary (Dyer, 1997; Struyf et al., 2004; Pachauri et al., 2014). This study ignores 'mega-scale' processes.

'Macro-scale' physical processes include seasonal and annual variations (Bale et al., 1985; Childers et al., 1993). Seasonal variations can affect the physical conditions; wetter-than-normal conditions experienced in winter may provide additional river run-off and thus increase the amount of sediment or macro-nutrients transported into the estuary (Bale et al., 1985), as well as diluting saline water. In drier, warmer periods, the surface water temperature may increase as a result of increased solar radiation, thus changing the density and stratification of the water column (Simpson et al., 1990). Longer term effects, particularly across the equator, can include the El Niño–Southern Oscillation

(ENSO) (Dyer, 1997) and monsoon events (Khodse and Bhosle, 2012). 'Macro-scale' chemical processes are typically related to anthropogenic events such as industrial revolutions and land development. The effects of such industrial revolutions have been documented for many estuaries, worldwide (Cun and Vilagines, 1997; Billen et al., 1999; Ruiz-Fernandéz et al., 2002; Sritrairat et al., 2012). Macro-scale processes for SPM and macro-nutrients have both been well-documented, both individually and as related components of an estuary (Correll et al., 1992; Smith et al., 1999; Dauer et al., 2000; Weller et al., 2003; Soataert and Middelburg, 2006; Howarth, 2008). However, these studies have predominately considered the horizontal advection associated with increased riverine flow, or the impact of seasonality on biology within the estuary (Jickells et al., 2015; Wengrove et al., 2015). This study included a short-term seasonal investigation of the Tamar Estuary (spring, summer and autumn) in order to consider the impact of seasons on micro-scale physical process, such as increased turbulence in adverse weather conditions.

'Meso-scale' processes are typically between a day and a month in duration, and include physical processes such as spring-neap cycles, semi-diurnal tides and short-term weather events (Boersma and Terwindt, 1981; Griffin and LeBlond, 1990; Allen and Duffy, 1998a,b). Weather events typically last for between 2 and 5 days and generate a number of different effects (Pugh, 2004); for example, in a low pressure system, wind can affect the estuarine circulation, while the creation of surface waves can generate additional mixing and turbulence (Dyer, 1997; Allen and Duffy, 1998a). Cyclic changes in sea level are caused by semi-diurnal and spring-neap tides (Kvale, 2006). The currents produced in these tidal movements generate turbulence and internal waves, create mixing and invoke further erosion, deposition and transport of sediments (Dyer, 1997). Chemically, the nutrient concentration of an estuary is affected predominately by the meso-scale weather events. Varying weather conditions may lead to changes in

the amount of river run-off, as well as the dilution of estuaries and rivers and thus may invoke M3 (Salinity).

Finally, 'micro-scale' physical processes are typically short-term and localised (Trevethan et al., 2007; Orton and Visbeck, 2009; Stacey et al., 2011), but can have significant effects on water column structure, suspended sediment transport and pollutant dispersion (Roberts and Webster, 2002; Thorpe, 2007). Micro-scale processes have a temporal scale of between seconds and hours with most processes contributing to meso- and macro-scale measurements. For example, turbulence on a micro-scale as a result of a meso-scale process such as tides can enhance the process of resuspension of SPM from the bed and increase the SPM concentration within the estuary. Turbulence and SPM behaviour, including particle size, have been previously studied (Shinnar and Church, 1960; Gore and Crowe, 1989; Rashidi et al., 1990), however, the consequence of turbulence on the relationship between SPM and macro-nutrients has not been constrained. Examples of micro-scale physical processes include turbulence and flocculation. While each of these has been well-documented (Thorpe, 2007; Manning et al., 2006; Manning and Bass, 2006; Manning et al., 2010b), the processes have not been related to nutrient biogeochemistry in estuaries. Fitzsimons et al. (2006) investigated the kinetics of methylamines and ammonium with respect to cumulative concentration within samples, as well as temporal release. This study reported the sources of NH_4^+ (and methylamines) during a tidal cycle, highlighting the injection of pore-waters to the water column during sediment inundation events. These results and studies closely mimic the hypothesised Mechanism One, without consideration of the effects of flocculation.

The scales described in Figure 2.1 highlight the complexity of the estuarine environment, of which it is further enhanced by the interactions between each scale. With the aims and objectives in mind (section 1.1), the primary focus of this

literature review will be to examine the current understanding of the physico-chemical processes occurring at the micro-scale level in relation to sediments and macro-nutrients. Some inferences will be drawn from the meso-scale level to provide context.

2.1 Sediments in the Estuarine Environment

Input principally by the river watershed and controlled and manipulated by tidal flow and waves, sediments play a role in macro-, meso- and micro-scale processes (Grabowski et al., 2011). On a macro-scale, sediments form the bulk of the topography of an estuary and as bed sediment they form the banks and bottom morphology. These features are typically not static, with evolution occurring from weeks to years, and so can contribute to meso- and micro-scale sedimentary processes. On a meso- and micro-scale, suspended sediments are known for their capacity to transport nutrients, pollutants and contaminants during erosion and deposition cycles (Colin, 1995; Walling et al., 1997; Statham, 2012). Additional sources of estuarine sediments include continental shelf input, erosion and resuspension of bed sediment, biological activity and aeolian transport[†] (Grabowski et al., 2011).

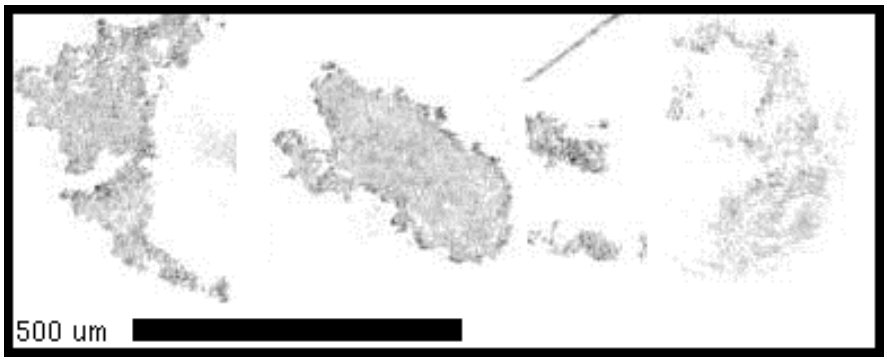

Figure 2.2: *Six images of flocs taken from a LISST-HOLO instrument deployed in the Menai Strait in 2012- courtesy of Emlyn J. Davies (2012).*

The composition of sediments in rivers, estuaries and coastal zones varies greatly, both spatially and seasonally. Changes in the composition of sediments can af-

[†]*Relating to, or caused by, or carried by the wind*

fect the resuspension and transport, while changes in the structure of the sediments may limit or enhance the ability to retain nutrient-laden interstitial water. Spatially, it has been seen that 'patches' of different types of bed-sediment (i.e. sand, gravel and mud), or 'segregation' are found on the bed alongside each other (Van Ledden, 2003), while suspended sediment has seen the incorporation of large sand particles into the compositional matrix together with smaller clay and silt minerals, depending on the location in the estuary and the physical conditions (Manning et al., 2011). On a macro-scale, the composition of suspended sediment changes with the availability of organic matter, i.e. seasonally. The variability of sediment composition will significantly affect the types and concentrations of macro-nutrients that can be adsorbed onto the particle face (Pavanelli and Selli, 2013).

2.1.1 Flocculation of Estuarine Sediments

Flocculation is the micro-scale process of aggregation of existing primary particles and suspended particles to form 'flocs'. It occurs in rivers, lakes and estuaries and the process is controlled by a number of different physical, chemical and biological factors, such as salinity, turbulence, particle concentration and particle biology. Flocculation is not limited to cohesive sediments, as it has been shown that with sufficient energy, sand can be incorporated into the floc structure when adequate biology based adhesion is present within the sedimentary matrix (Manning et al., 2006, 2013).

2.1.1.1 Cohesive Sediments and Initial Bonding Mechanisms

Cohesive sediments (mud) are a mixture of organic and non-organic compounds including, silt, sand, water and gas (Van Ledden, 2003; Maggi, 2005; Grabowski et al., 2011). The smallest component of cohesive sediments are clay particles of between 1 and 5 μm that are shaped like discs. Clay particles have negatively charged faces that allow for the initial bonding to create 'primary particles' and

subsequent flocculation (McAnally, 1999). Primary particles are typically between 5 and 20 μm in size with a 'face-to-face' bonding mechanism that forms highly resilient structures. As the primary particles flocculate, they can form 'macroflocs' that can exceed 1000 μm in size. Macroflocs are typically filamentous and random in structure (Maggi, 2005) (Figure 2.2).

Initial bonding of the clay particles is a complex interaction between turbulent shear stresses, repulsive electrostatical and attractive van-der-Waals force (Edzwald and O'Melia, 1975; Zhou et al., 1994; Hallez, 2012). Repulsive forces are a result of the diffusive double layer (van Leussen, 1994). The negatively charged faces of the particles, also expressed as the ζ potential (Mietta et al., 2009), may be surrounded by a solution of cations, whereby the concentration is high immediately adjacent to the particle face (called the 'Stern layer'). Next to the Stern layer is the 'Gouy layer' where the concentration of cations is less. The type of mineral and the ion concentration has a great effect on the thickness of the double layer and, thus, the strength of the repulsion experienced by two particles in close proximity (Maggi, 2005). Overcoming the repulsive forces relies on hydrodynamic conditions and, once particles are within a certain distance, particles may be kept together by attractive forces (Hallez, 2012). Research has shown that the presence of biology, such as extracellular polymeric substances (EPS), significantly enhances the cohesive strength of floc particle bonds (Kiorboe et al., 1990; Paterson and Black, 1999; Maggi, 2009; Tolhurst et al., 2009; Manning et al., 2010b).

The rate of aggregation and the strength of created flocs depends upon the aforementioned ζ potential; uniformly charged particles with lower ζ potential are more likely to aggregate than particles with a higher ζ potential. This, however, is affected by the solution that particles are held in and is usually affected by salinity and acidity of the water (Mietta et al., 2009).

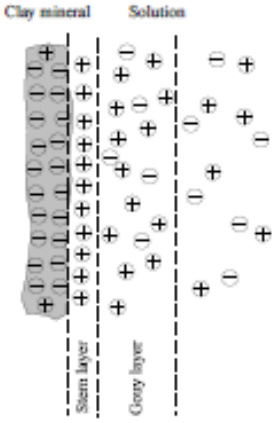

Figure 2.3: *Illustration of the 'double layer' (Gouy Layer and Stern Layer) from Valioulis (1983).*

2.1.1.2 Effect of Salinity on Particle Cohesion

Of particular interest in the initial bonding of clay particles is the effect of salinity on cohesion, as well as the effect of salinity on macro-nutrient bonding with particles. The naturally-occurring anions and cations present in salt water cause a decrease in the repulsive strength of the double layer and, ultimately, elimination of the barrier with mid to high concentrations of salt water. The decrease in the strength of the repulsive double layer encourages the cohesion of clay particles and further aggregation (Valioulis, 1983; Maggi, 2005). This suggests an inability of particles to undergo cohesion in fresh water situations based on electro-chemical bonding alone. Drake (1976) reported that an average salinity of 2 PSU will enhance the cohesion of clay particles, while Krone (1962) reported that a salinity of approximately 6 did not produce any significant increases in particle electrostatic cohesion. van Leussen (1994) and McAnally (1999) suggest that the salinity required to increase cohesion is related to the mineral type. For example, kaolinite has a much weaker bond than smectite.

The aforementioned effects of salinity on particle interactions highlights a contrast between salinity-sediment interactions and salinity-nutrient interactions. An increase in salt water cations has been shown to enhance flocculation of par-

ticles and thereby, as per M1 (SPM concentration increase) (Einstein and Krone, 1962; Kranck, 1981; Hunter and Liss, 1982), it would indicate that the creation of interstitial water during aggregation could reduce the water concentration of macro-nutrients. However, it has also been demonstrated by Gardner et al. (1991) that the increase in cations (and anions) associated with an increase in salinity can break the bonds between NH_4^+ and the particle faces. This is particularly relevant to Mechanism 3, which describes the potential for an increase in the water column macro-nutrient concentration due to the increase in cations and anions associated with increased salinity.

The information described in this section implies that there may be a balance between increased flocculation due to salinity, and increased desorption of macro-nutrients from particle faces as a result of increased salinity. It is expected that, with no salinity, flocculation will be negligible. As per the objectives in section 1.1, to establish controlling factors in sediment-nutrient interaction, observations were made in estuarine conditions whereby both salt and freshwater conditions were seen (Chapters 5 and 4). Furthermore, the laboratory experiments (Chapter 6) were designed to establish differences in sediment-nutrient behaviour in both fresh and salt water.

2.1.2 Aggregation and Break-up Mechanisms

The most important physical mechanism in the flocculation process are the collisions between particles in suspension; this means that particles in suspension need to be brought into contact. Turbulent shear is regarded as the most efficient way of achieving this (Manning, 2001, 2004; Winterwerp et al., 2006). Conversely, it can also break fragile flocs at high shear stress levels. Collision mechanisms between two particles are described below (Saffman and Turner, 1956; Broadway, 1978; Hunt, 1980; McCave et al., 1984; Tsai and Hwang, 1995).

Brownian motion is the random moving of particles in a fluid as a result of collisions with fast-moving atoms of molecules in the fluid. However, Brownian motion has been shown to have negligible effects in estuarine waters (Krone, 1962; O'Melia, 1980; McCave et al., 1984; van Leussen, 1994; Maggi, 2005).

Concentration – increased concentration of particles increases the chance of particle collisions, and thus flocculation. However, as flocs grow in size, they may become more fragile and so are broken up by further collisions, limiting their size and demonstrating an equilibrium mechanism as described in M1.

Differential settling is the process whereby particles with a larger settling velocity will overtake those with a lower settling velocity. Differential settling is still a subject of debate with studies by Burban et al. (1990) and Lick et al. (1993) reporting that it has a significant impact on flocculation. Stolzenbach and Elimelich (1994), however, reports that differential settling is inefficient for flocculation and may only occur in the incidences of very small particles and very large particles. Stolzenbach and Elimelich (1994) reported that 'when the ratios of settling velocity and the excess density of two particles exceed critical values determined by the theory, the trajectory of the small particle is closed in a region of finite size surrounding the large particle.' This finite surround deflects approaching/overtaking particles and alters the trajectory preventing particle collision.

Turbulent and laminar shear enable particles carried by eddies to collide and form flocs, while turbulent shear may disrupt flocs causing floc breakup. Turbulent and laminar shear and differential settling mechanisms are the most important for inter-particle collision and these are further aided by biological processes. Turbulence (described in section 2.1.4) is a micro-scale process that has, so far, not been related to the concentration of nutrients in the water col-

umn. Further details are presented and discussed in section 2.1.4.

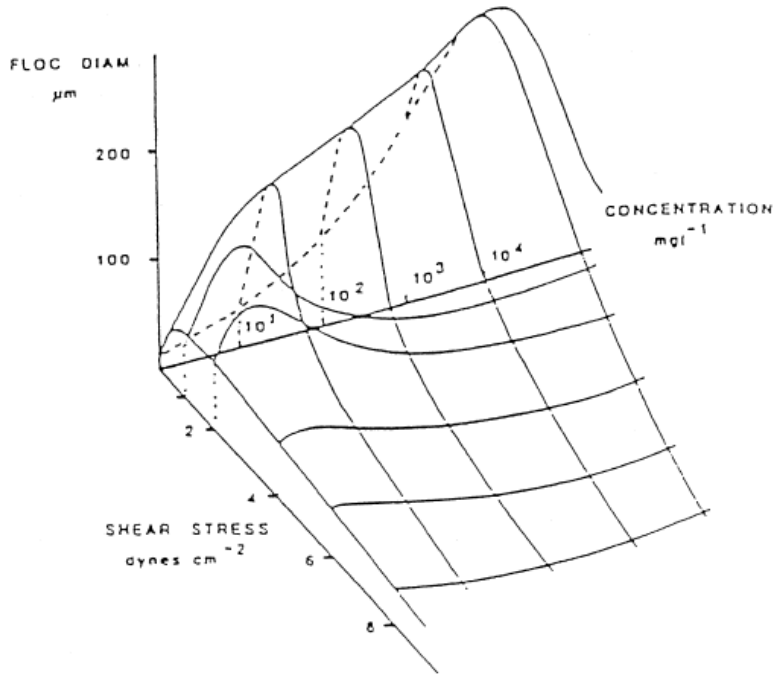

Figure 2.4: *The conceptual relationship between sediment concentration, shear stress and floc size (from Dyer (1989)).*

In relation to the scales of spatial and temporal variability in an estuary, SPM concentration can form both a micro- and a meso-scale process. Mean SPM concentration ranges vary widely in estuaries globally. Short-term events, such as an estuarine turbidity maximum (ETM), are micro-scale temporal events that significantly increase the SPM concentration of the water column for a short period of time. For example, in the Scheldt estuary, an ETM has been observed with SPM concentrations of between 50 - 500 mg l^{-1} with approximate time scales of 1 - 2 h (Manning et al., 2007c). The effects of SPM concentration on water column nutrient concentrations have previously been investigated in studies by the likes of Mortimer et al. (1999); Fitzsimons et al. (2006); Shepherd et al. (2007); Garnier et al. (2008, 2010); Bartley et al. (2012). However, there are few studies considering the particle characteristics within these SPM concentration increases. Of the few studies investigating nutrient concentrations in relation

to particle characteristics and SPM concentrations, Pavanelli and Selli (2013) reported that during flood events in the Reno River, Italy, nutrient concentrations were shown to have a linear relationship with silt particle size. Pavanelli and Selli (2013) concluded that silts appear to be the preferential vehicle for nutrient transfer. This research was conducted in a purely riverine environment, but has relevance as silts are a common component of flocs in both the Tamar (Bale et al., 1985; Tattersall et al., 2003; Bass et al., 2007) and Seine estuaries (Avoine, 1982; Brenon and Le Hir, 1999; Garnier et al., 2010). Furthermore, silts are commonly transported from the riverine environment into the estuarine environment (Grabowski et al., 2011), whereby they may be affected by different physical processes that affect the nutrient bonds with the sediment.

The aforementioned physical mechanisms are not sufficient alone to cause aggregation of suspended particles. The physico-chemical properties, including repulsive and van der Waals forces, and organic compounds (such as polysaccharides) on and within the particles have to be considered in flocculation. Van Leussen (1994) and Winterwerp et al. (2002) utilised an efficiency parameter α_c to relate the likelihood for two aggregates to adhere and bond together following collision, to physico-chemical properties of the sediment and surrounding water, and to floc shape and structure (Edzwald and O'Melia, 1975; Maggi, 2005).

2.1.3 Composition of Flocs

Floc formation in the natural environment encourages a wide variety of flocs in shape, size and composition. This is due to differing salinities, changing levels of turbulence, and changing biology. Flocs range from being large and round, to thin and stringy (Figure 2.2) with the structure forming as a result of the flocculation process, deformation due to turbulence and collision with other aggregates, consolidation and torquing (to twist or rotate). Floc structure also dictates the response to different physical forcings and interactions with other

particles (Maggi, 2005). Furthermore, flocs may be composed of up to 10^6 individual particles (Lick and Lick, 1988; Milligan and Hill, 1998; Manning and Dyer, 1999).

2.1.3.1 Size, Porosity & Effective Density

Particle size is a difficult parameter to measure due to the complexities of the shape and structure, and the vast number of methods and instruments available to measure floc size. At present, there is no accepted standard definition of floc size (Maggi, 2005). Two of the most common methods used to determine the size of the floc include a geometric average of the sizes measured in different directions, and the diameter of a circumscribed sphere; equivalent spherical diameter (ESD) (Maggi, 2005). Alternatively, the principles of laser diffraction and light angle scattering can be used. Regardless of which method is used, they both have the same disadvantage; invariably one or more dimensions of a particle may be over- or underestimated, or missed altogether. This means that assumptions must be made in the calculation of further values, such as effective density and porosity. While a significant disadvantage, few methods exist for the accurate measurements of particles with more than one dimension.

The varying methods of formation affect the subsequent size and shape of a floc. For example, low shear conditions, such as in deep oceans, will predominately produce long, chain-like flocs (Wells and Goldberg, 1993), while higher shear rates found in estuaries will produce smaller, spherical flocs (van Leussen, 1994).

Particle size, while important to the composition of flocs, is not easily or accurately measured. This is due to the inherently small size, often poor visibility in the water column and the number of planes/faces/dimensions of a floc. Furthermore, there is no universal agreement as to what defines a ‘floc size’ or

'diameter'. In terms of the relationship between particle size and nutrient concentration, it could be theorised that the larger the particle and availability of surface space, the more ions may bond with the particle, thus reducing water column concentrations and increasing the possibility of uptake by flocculation. As a one-dimensional value representing a typically three-dimensional particle of irregular shape forms a practical but inaccurate measurement, the relative changes in particle size distribution between samples is considered as a measure of flocculation or disaggregation in this thesis.

Porosity and effective density of particles are closely related. The porosity of a floc is related to the space-filling ability of the floc structure; where the porosity is high, the amount of interstitial, or pore water, is greater in the floc. Typically, larger, filamentous flocs would be quite porous. As a result of the high amount of interstitial water, a porous floc is likely to have a lower effective density ($\approx$ 16 kg m^{-3} (Fennessy et al., 1997)).

The interstitial water found in a floc is usually the water trapped by two or more components of a floc, when formed. It is in this way, as well as particle surface-bonding, that contaminants are transported in an estuary. They are trapped in the interstitial water - disaggregation could release any unbound contaminant back into the water column. This is particularly relevant to the aim of this study whereby the significance of sediments as a source of nutrients to the water column is to be established. In areas of high SPM ($\approx$ 2 g L^{-1}) and nutrient concentration, large porous flocs may be a source of nutrients when later broken up.

Effective density is calculated using a derivation of Stokes' law, including the particle size and settling velocity:

$$\rho_c = (\rho_f - \rho_w) = \frac{W_s 18\mu}{D_y D_x g} \tag{2.1}$$

where ρ_f is the density of the floc bulk, ρ_w is the density of the water, W_s is the settling velocity, g is the acceleration due to gravity, μ is the dynamic viscosity, D_y is the axis normal to the settling velocity, D_x.

The value is based on particle geometric self-similarity an assumes a constant primary particle size. As such, it requires additional information (such as fractal dimension) in order to highlight any anomalous results. It is, however, a particularly useful descriptor of the type of measured particle. The density affects the rate at which particles can settle and so it is proposed that it will affect the time in which nutrients could bond to particle surfaces; i.e. fast settling particles have less chance to adsorb nutrients. Those that do settle quickly, if they have nutrients attached, the nutrients will be taken down to the bed whereby they may be consolidated. In this thesis, only the LabSFLOC I instrumentation was capable of measuring settling velocity in conjunction with particle size. The advantages and disadvantages of this methodology are discussed in Chapter 3.

2.1.4 Turbulence

Turbulence is a naturally occurring physical process in the marine environment that is responsible for the transfer of heat and momentum and dispersion of solutes, organic and inorganic particles. Characterised by chaotic and stochastic behaviour, turbulence has been identified as 'the most important unsolved problem of classical physics' (Falkovich and Sreenivasan, 2006; Thorpe, 2007). Thorpe (2007) defined turbulence as *'an energetic, rotational and eddying state of motion that results in the dispersion of material and the transfer of momentum, heat and solutes at rates far higher than those of molecular processes'*. This description includes the dispersion of flocs and the dilution of chemical species in the water, such as N and P. Turbulence is characterised by a number of different features; irregularity, diffusivity, rotationality, dissipation, energy cascade, integral length scales, Kolmogorov microscales and Taylor microscales (Kolmogorov,

1941b,a; Tennekes, 1975).

Turbulence is produced by friction at the bed, and the shear stress[††] linearly diminishes with height above the bed. Generally, there are two regions; inner and outer. The inner region or the 'wall region' is the region close to the bed. This is where, typically, the first 20 - 30% of the water depth consists of a logarithmic layer of velocity increase from the bed (Dyer et al., 2004). The area close to the bed can include a viscous sub-layer and this is dependent on the presence of any bedforms (e.g. sandwaves, etc.). The velocity profile associated with turbulence is affected by changes in the hydrodynamic conditions of the water column, and in particular, the density stratification. Meanwhile, suspended sediment has been shown to absorb turbulent energy, appearing as an increase in effective viscosity (Krestenitis et al., 2007).

Turbulent Kinetic Energy (TKE) is the *mean kinetic energy per unit mass* associated with eddies in turbulent flow. As eddies have been shown to affect the properties of flocculation sediment (Krestenitis et al., 2007), it is a useful way to characterise the conditions (Pope, 2000). TKE is typically characterised using root mean square (RMS) velocity fluctuations. In Reynolds-averaged Navier Stokes equations, the TKE can be calculated based on the 'closure method' in that TKE can be quantified by the mean of the turbulence-normal stresses (Pope, 2000):

$$k = \frac{1}{2}\left(\overline{(u_1')^2} + \overline{(v_1')^2} + \overline{(w_1')^2}\right) \tag{2.2}$$

TKE can be produced by fluid shear, friction or buoyancy, or through external forcing at low-frequency eddy scales. TKE is then transferred down the 'energy cascade', and is dissipated by the viscous forces at the Kolmogorov scale (see section 2.1.4.2). The full descriptive equation is written as follows:

[††]Denoted τ, is defined as the component of stress coplanar with a material cross section.

$$\frac{\delta k}{\delta t} + \overline{u_j}\frac{\delta k}{\delta x_j} = -\frac{1}{\rho_0}\frac{\delta \overline{u_i' p'}}{\delta x_i} - \frac{1}{2}\frac{\delta \overline{u_j' u_j' u_i'}}{\delta x_i} + v\frac{\delta^2 k}{\delta x_j^2} - \overline{u_i' u_j'}\frac{\delta \overline{u_i}}{\delta x_j} - v\frac{\overline{\delta u_i' \delta u_i'}}{\delta x_j \delta x_j} - \frac{g}{\rho_0}\overline{\rho' u_i'}\delta_i \quad (2.3)$$

Within Equation 2.3, the following components can be separated into the following components (not limited to): TKE dissipation rate (ϵ), TKE production (P), transport of TKE ($\bigtriangledown \cdot T'$):

$$\epsilon = v\frac{\overline{\delta u_i' \delta u_i'}}{\delta x_j \delta x_j} \quad (2.4)$$

$$P = -\overline{u_i' u_j'}\frac{\delta \overline{u_i}}{\delta x_j} \quad (2.5)$$

$$\bigtriangledown \cdot T' = -\frac{1}{2}\frac{\delta \overline{u_j' u_j' u_i'}}{\delta x_i} \quad (2.6)$$

By examining each of the phenomena listed above, the TKE budget can be determined for a particular flow. The aforementioned TKE and equations will be considered in Chapter 3 (section 3.3.2.1) where the methods for calculating TKE and Kolmogorov microscales are presented.

2.1.4.1 Diffusivity and Dispersion

Dispersion is the spreading of solid particles and particles of fluid by turbulent motion (Thorpe, 2007). Turbulent diffusion, in contrast to dispersion, is the transport of fluid properties, such as salinity, at a molecular scale. Diffusion by turbulence occurs more rapidly than molecular diffusion and is, therefore, very important in dynamic, fast-moving environments, such as an estuary (Roberts and Webster, 2002), and forms a micro-scale process. Diffusion is particularly relevant when considering the transport and movement of ions, such as N and P species, in the water column. In turbulent environments, such as the ETM, the rate of diffusion may be relevant to the bonding of ions to particles, or trapping

within the interstitial water of flocculated particles. Dispersion, meanwhile, is a relevant micro-scale to the particulates held in suspension. Together, dispersion and diffusion may play a role in the relationship between sediments and nutrients in the water column. These parameters, however, are difficult to measure.

2.1.4.2 Energy Scales & Measuring Turbulence: The Kolmogorov Microscale

One of the major challenges in modern physics is the accurate measurement of turbulence (Falkovich and Sreenivasan, 2006). There are many methods to measure aspects of turbulence. Of particular relevance to this study are Kolmogorov Microscales. Kolmogorov described how energy is transferred from larger to smaller eddies; how much energy is contained by eddies of a given size; and how much energy is dissipated by eddies of each size. There are three main turbulent length scales, as shown in Figure 2.5: the integral scale, the Taylor scale and the Kolmogorov scale, of which each can be expressed using Reynolds numbers (Pope, 2000; Thorpe, 2007) and described the 'energy cascade'. The energy cascade describes the process in which 'energy is transferred to successively smaller and smaller eddies' and continues until the Reynolds number is sufficiently small that the eddy motion is stable (Bakker, 2006).

The first scale, the integral scale, describes larger eddies and their characteristic velocity, $u_0 \equiv u(l_0)$, is on the order of the root mean square (r.m.s.) turbulence intensity: $u' \equiv (2k/3)^{(1/2)}$. The integral scale assumes that the energy of an eddy with a velocity scale u_0 is dissipated in time τ_0 (Pope, 2000; Bakker, 2006).

The second scale of turbulence is the Taylor Microscale and it describes the turbulent structures within the inertial subrange (the scales between the smallest and largest turbulent structures). It is calculated as follows: $\lambda \approx (10vk/\epsilon)^{1/2}$.

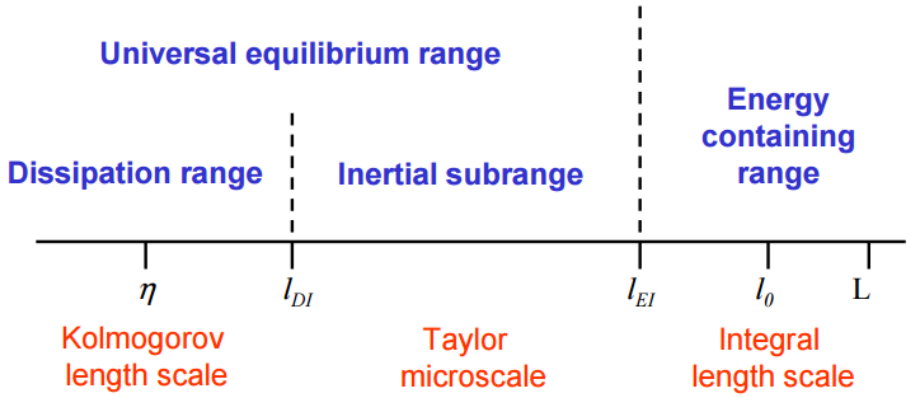

Figure 2.5: *Turbulent scales as described by Pope (2000). From Bakker (2006). The suffixes EI and DI indicate that l_{EI} is the demarcation line between Energy (E) and inertial (I) ranges, as l_{DI} is that between the dissipation (D) and inertial (I) ranges.*

Finally, and the most relevant to this project, are the Kolmogorov microscales (Kolmogorov, 1941b). Kolmogorov microscales, or Kolmorogov length scales, are the smallest scales of turbulent flow and can be measured in lengths, time-scales or velocities:

$$\text{length scale: } \eta = (v^3/\epsilon)^{1/4} \tag{2.7}$$

$$\text{velocity scale: } u_\eta = (\epsilon v)^{1/4} \tag{2.8}$$

$$\text{time scale: } \tau_\eta = (v/\epsilon)^{1/2} \tag{2.9}$$

The microscales are based upon Kolmogorov's first similarity hypothesis: *'that in every turbulent flow at sufficiently high Reynolds number, the statistics of small-scale motions ($l < l_{EI}$ have a universal form that is uniquely determined by ϵ and v.* Generally, smaller Kolmogorov microscale values indicate higher levels of turbulence (smaller structures) (Mîkes, 2011).

The microscales are particularly relevant to this project as the length of tur-

bulent structures in the water column (measured in μm) is directly comparable to measured particle sizes. Using this parameter, it has been found that particle size is limited by the Kolmogorov microscales (Berhane et al., 1997; Van Leussen, 1997; Fettweis et al., 2006; Braithwaite et al., 2010). The Kolmogorov Length Microscale will be used throughout this thesis as an indication of the level of turbulence in the water.

2.1.4.3 Turbulence and Suspended Sediment

As highlighted previously, turbulence (and shear) can both cause and disrupt the process of flocculation. Primary particles bonded electrochemically are typically resistant to turbulent action, plus small flocs are bonded in a stronger way due to their low porosity and EPS on particles. Meanwhile, low-to-mid values of shear rate can enhance flocculation.

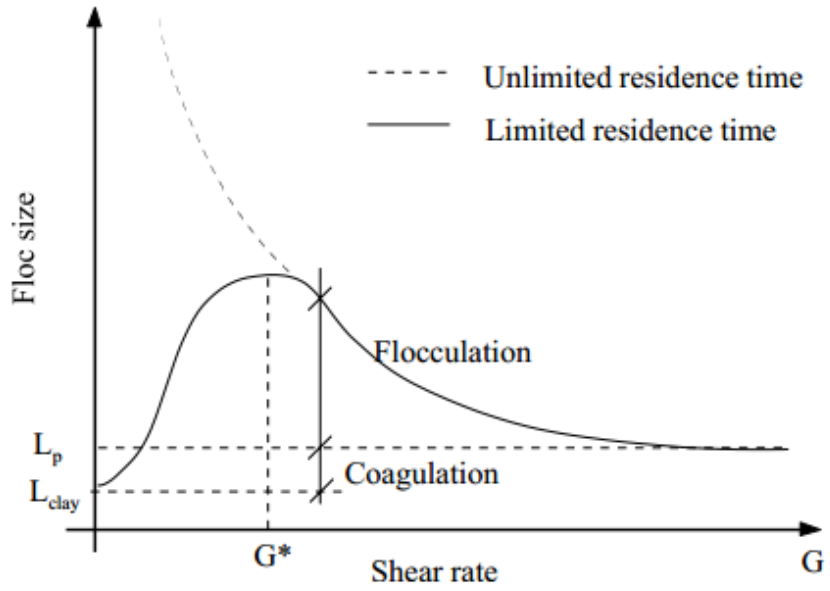

Figure 2.6: *Qualitative representation of the modal floc size against the rate of turbulent shear (G) for limited and unlimited residence time (Winterwerp, 1993).*

Figure 2.6 demonstrates the delicate balance between the generation of flocs due to turbulence and the disruption. It should be noted that flocculation and coagu-

lation are two different processes. Coagulation is the process by which colloidal particles and very fine solid suspensions are combined into larger agglomerates which can be separated via sedimentation, flocculation, filtration, and other separation methods. G is a measure of the rate of turbulent shear and is expressed as follows:

$$\mathrm{G} = \sqrt{\frac{\epsilon}{\mathrm{v}}} \tag{2.10}$$

Where ϵ is the energy dissipation rate per unit mass and v is the kinematic viscosity. Kinematic viscosity is the ratio between the dynamic viscosity and the density of the water and has units of $\mathrm{m}^2\ \mathrm{s}^{-1}$. The rate of turbulent shear can also be expressed as the inverse of Kolmogorov length microscales: $\mathrm{G} = \mathrm{l}_\mathrm{k}^{-1}$ (Winterwerp, 1993).

2.2 Nutrients in the Estuarine Environment

As key elements in primary productivity, in both terrestrial and marine environments, nitrogen (N) and phosphorus (P) are often classed as 'limiting' nutrients (Hecky and Kilham, 1988; Vitousek et al., 1997; Tyrrell, 1999; Worsfold et al., 2008; Statham, 2012; Jickells et al., 2015). Nutrients are elements that are actively taken up by organisms and are essential in processes of living organisms, such as reproduction and growth. Of the 30 bioelements (chemical elements vital for life) that have been identified, the macro-nutrients N and P are required in greater quantities. N forms a component of amino acids and is found in all cell proteins. N is also of great importance to the rate of primary productivity, and the production of arable crops, forests and marine phytoplankton relies heavily upon the availability of inorganic N (such as nitrate or ammonia) (White, 1993; Hessen, 1999; Tyrrell, 1999; Jickells et al., 2015). P, on the other hand, is vital for all living organisms as it forms a principle constituent (nucleic acid) of bones, nerves, brain tissue and teeth (Hessen, 1999; Williams, 2001). Other macro-

nutrients include, calcium (Ca^{2+}), chloride (Cl^{-}), magnesium (Mg^{2+}), potassium (K^{+}), sodium (Na^{+}) and sulphate ($SO_4{}^{2-}$). Macro-nutrients, despite being crucial, can be detrimental if an excess occurs.

Despite strict legislation to maintain the balance of natural waters, water quality has remained a key global issue. Eutrophication and harmful algal blooms, such as blue-green algal blooms, in estuarine and coastal waters have also been attributed to increased fluxes of N and P (Howarth, 2008). On a 'mega-scale' (see Figure 2.1), nutrient concentrations in U.K. rivers have been significantly increased by human activity, spanning centuries and decades before control measures were implemented (Seitzinger et al., 2005; Statham, 2012; Moore et al., 2013; Jickells et al., 2015). In 2003, the cost of annual freshwater eutrophication control in the U.K., was estimated by Pretty et al. (2003) to be between £75 - 114.3 million in 2003. Since then, the Environment Agency have, in line with the European Union Urban Waste Water Treatment Directive (UWWTD), spent approximately £1.3 bn capital in attempts to reduce the point sources of P (Environment Agency, 2012). Despite this expenditure, the EA report that, still, 36% of rivers will fail to meet the P threshold set by the UWWTD (Environment Agency, 2012). Smith et al. (1999) wrote that *'human activity has profoundly altered the global biogeochemical cycle of N'* and stated that *'humans have approximately doubled the rate of N input into the terrestrial ecosystem'*. Indeed, Smith et al. (1999) explained that current levels of anthropogenic input of N are at least equal to that of all natural sources combined. Similarly, Burt et al. (2011a) reported that ground-water dominated rivers demonstrate increasing levels of nitrate and propose that it could be decades before surface-water concentrations decrease to values consistent with water quality legislation (Burt et al., 2011b; Tappin et al., 2012). In the Seine estuary, France, before 2000, most effluents from Paris were treated with a 'standard' activated sludge treatment of carbon, thus releasing high concentrations of ammonium to the water. This increase in

ammonium to water column caused a significant growth in nitrifying bacteria and a subsequent dissolved oxygen deficit (Aissa-Grouz et al., 2015). Subsequent efforts to reduce the issues associated with untreated waste have yielded the elimination of ammonium from effluent and 30% of the nitrate formed was denitrified, considerably improving water quality in the Seine estuary (Aissa-Grouz et al., 2015).

Point sources and non-point sources of nutrients, including anthropogenic inputs, to the marine environment are summarised in Table 2.1. Notably, sediments as a source of nutrients to the water column were not identified by Smith et al. (1999).

Table 2.1: *Sources of point and non-point chemical inputs from Smith et al. (1999).*

Point Sources
Waste water effluent (municipal and industrial)
Runoff and leachate from waste disposal sites
Runoff and infiltration from animal feedlots
Runoff from mines, oil fields and unsewered industrial sites
Storm sewer outfalls from cities with populations $>$ 100,000
Runoff from construction sites with an area $>$ 2ha
Non-point sources
Runoff from agriculture (including return flows from irrigated agriculture)
Runoff from pastures and rangelands
Urban runoff from unsewered areas and sewered areas with populations $<$ 100,000
Septic tank leachage and runoff from failed septic systems
Runoff from construction sites with area $<$ 2 ha
Runoff from abandoned mines
Atmospheric deposition over a water surface
Activities on land that generate contaminants, such as logging, wetland conversion, construction and development of land and waterways

2.2.1 Nitrogen in the Marine Environment

N is a non-metal that, in the form dinitrogen (N_2), is the most abundant, but least reactive, form of N in the global environment. As a colourless, odourless, inert gas, it contributes to approximately 78%, by volume, of the Earth's atmosphere (Capone et al., 2008). N_2 also exists as the following inorganic species; nitrate (NO_3^-), nitrite (NO_2^-) and ammonium (NH_4^+). It can be converted into organic N compounds such as amines, amides and amino acids. Both forms of N are found in the particulate and dissolved phase (Capone et al., 2008).

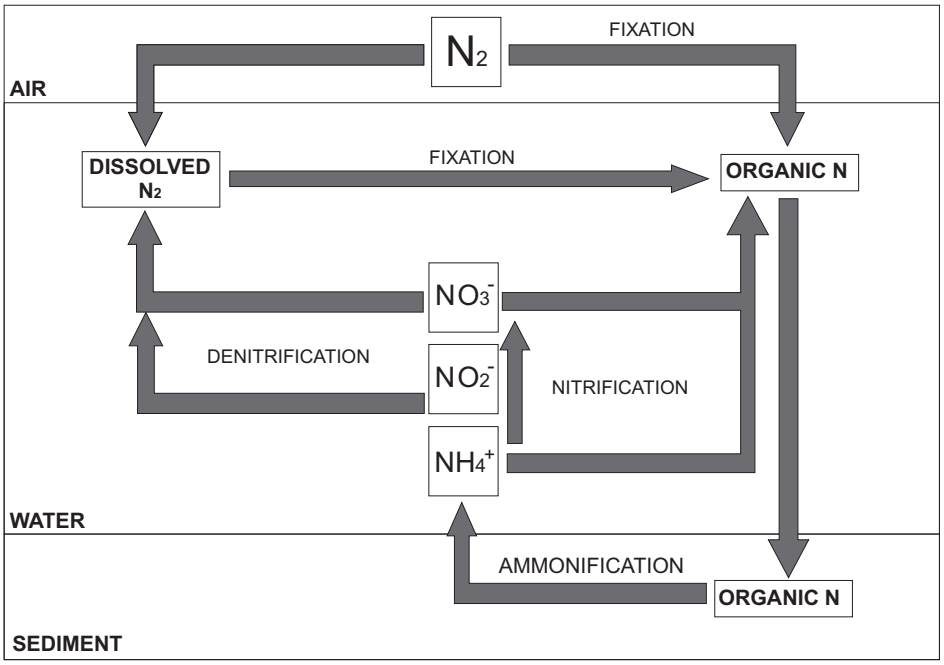

Figure 2.7: *A schematic of the marine N cycle – adapted from Hanrahan et al. (2002).*

Nitrogen is converted into bio-available forms by one of three processes (listed below), while the process of denitrification converts fixed N back into gaseous species.

- *Fixation* – N_2 gas is converted, either by micro-organisms or root nodule symbiosis, to NH_4^+. A natural example of N fixation is lightning.
- *Nitrification* – the process of oxidisation of NH_4^+ into NO_2^- through am-

monium oxidising bacteria (AOB) or ammonia oxidising archaea (AOA). Nitrification then continues to oxidise NO_2^- into NO_3^- by way of bacteria such as *nitrobacter*.

- *Ammonification* – when plants or animals die, organic N is converted back into NH_4^+ by forms of bacteria and/or fungi.

There are three routes for N to enter an estuarine environment; atmosphere, groundwaters and, primarily, rivers. In estuarine waters, N occurs at small concentrations in its inorganic and organic forms. The most prominent of the inorganic forms are NH_4^+, NO_2^- and NO_3^- ions, which play a crucial role in the nitrogen cycle. The species abundance depends on the location within an estuary: for example, an unperturbed system may have a concentration of 0.01 - 0.1 mg L^{-1} NO_3^- in estuarine waters compared to between 0 - 30+ mg L^{-1} NO_3^- in riverine waters. The Tamar estuary has a typical NO_3^- concentration of 12.4 mg L^{-1} (Tappin et al., 2012). Figure 2.8 highlights the operational definitions of N in the marine environment (Galloway, 2003). Total oxidised N (TON) (not in Figure 2.8) is defined as NO_3^- + NO_2^- and will be used throughout this thesis (referred to as NO_3^-), assuming that NO_2^- represents only a minor component of the total nitrate plus nitrite under oxic conditions (Tappin et al., 2012).

N in the marine environment occurs both naturally and anthropogenically. Natural sources include the fixation of gases by cyanobacteria and algae, and the breakdown of nitrogeneous matter in sediments, water and excrement from biota (Capone et al., 2008). Riverine input of N is estimated to be between 35 - 64 Mt yr^{-1} (Tappin, 2002). However, the natural concentrations of approximately 0.1 mg L^{-1} may be enhanced by anthropogenic sources.

One of the greater anthropogenic sources of N to the marine environment is N-fertiliser used in agriculture. Smith et al. (1999) estimated that between 37

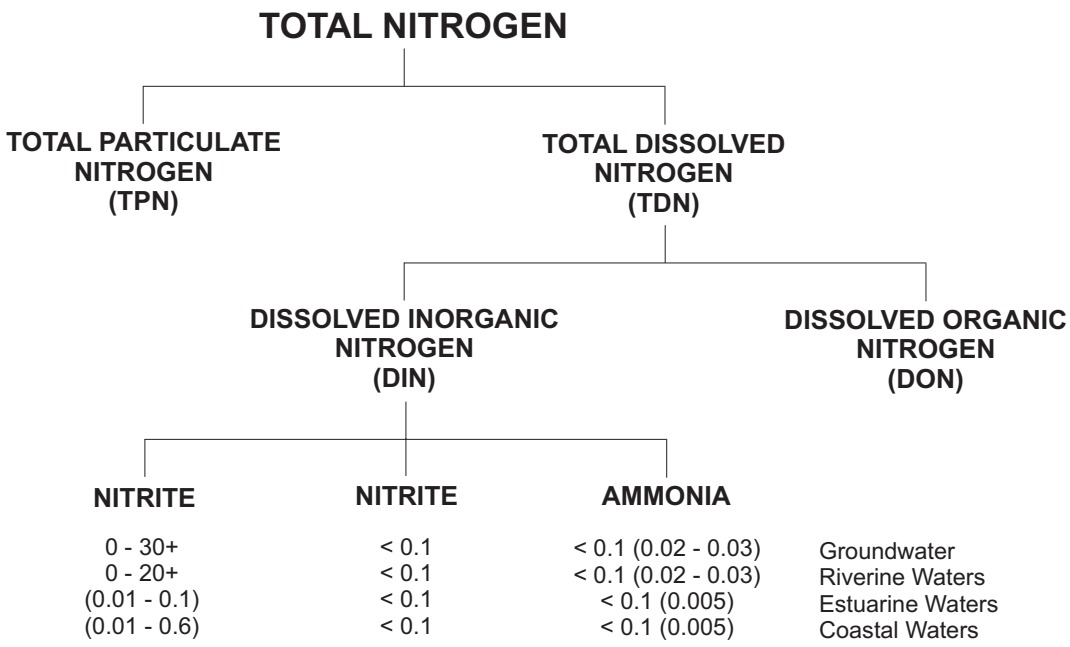

Figure 2.8: *The operational definition of N and typical concentrations in marine water (mg L^{-1} N) (adapted from Robards et al. (1994)).*

- 82% of all emissions to surface water in Europe are the result of N-fertiliser and Vitousek et al. (1997) noted that the production of agricultural fertilisers increased from $<$ 10 million metric tonnes in 1950 to approximately 80 million metric tonnes in 1990, with a predicted increase to 135 million metric tonnes by the year 2030. The N-fertiliser produced is applied to cropland in the form of animal manure, for which the regulatory standards are much less stringent than those applied to human sewerage (Vitousek et al., 1997). Smith et al. (1999) explained that a small fraction of applied fertiliser is not required by the plants for growth. As well as diffusion through land to the surface layer of water bodies, a surplus of N may accumulate in soils, migrate into groundwaters or enter the atmosphere as nitrous oxide (Smith et al., 1999).

Further input of N to the water column arrives through the burning of fossil fuels such as coal, gas and oil. Vitousek et al. (1997) disclosed that the burning of fossil fuels transfers fixed N from geological reservoirs to the atmosphere and in

the high-temperature combustion of fossil fuels, a small amount of atmospheric N_2 is fixed. Vitousek et al. (1997) further estimated that greater than 20 Tg y^{-1} of fixed N is emitted to the atmosphere during fossil-fuel combustion.

A third mechanism involves the fixing of N through leguminous crops such as soybeans, peas and alfalfa. The crops support symbiotic N-fixing micro-organisms who derive much of the required N directly through the atmosphere (Vitousek et al., 1997). Fixation of N in excess of natural background rates in communities that legume crops have replaced represents a new source of anthropogenic N to coasts and estuaries. It is estimated by Galloway et al. (1995) that N fixation by leguminous crops is between 32 and 53 Tg y^{-1}, while Smith et al. (1999) estimate that approximately 40 Tg y^{-1} is fixed - the variations occur as a result of difficulty in measuring the fixation, in comparison to industrial measurements (Vitousek et al., 1997).

A fourth, and final input to the N cycle, arises not from anthropogenic N fixation, but from the release of natural N from long-term biological reservoirs. Activities such as biomass burning, deforestation, land clearing and conversion, drainage of wetlands and the consequent oxidation of organic soils can be termed 'mobilisation' and can account for a proportion of the anthropogenic contribution to the N cycle (Vitousek et al., 1997). It is estimated that, combined, these activities could account for approximately 50 Tg y^{-1}. Furthermore, the drainage of wetland removes a significant 'sink' (an accumulation of a mineral in soils, effectively taken out of the cycle for a period of time) for fixed nitrogen and thus increases the mobility of N through soils into streams and rivers (Vitousek et al., 1997).

2.2.1.1 Partitioning of N onto Particles in the Marine Environment

Tappin (2002) reported that over 50% of the annual global riverine N flux is in

the form of particulate N, most of which is entirely organic. However, it is unclear how species of N transfer from the dissolved phase to the particulate phase (Hedges and Keil, 1999). Fitzsimons et al. (2011) highlighted that the partitioning[§] of N to SPM may be different for each molecule. For example, NO_3^- and NO_2^- are negatively charged, the same as the surfaces and edges of the particles (Loder and Liss, 1985), and so bonding between the particle surface and NO_3^- and NO_2^- does not typically occur. Instead, NO_3^- is typically assimilated into the pore-waters of sediments (Koike and Sorensen, 1988). NH_4^+, on the other hand, is positively charged and so can form ionic bonds with the negatively-charged sites on the particle surface. Despite the lack of bonding between NO_3^- and particle surface, it was still measured in this thesis as a method of determining the possible magnitude of uptake by interstitial water during creation of flocs (Kalnejais et al., 2010). Ammonium was also recorded as a means of testing all proposed Mechanisms.

The partitioning of N to the surfaces of the particle is dependant on the species of N. NO_3^- and NO_2^- are not likely to be sorbed to sediments and so observable fluxes of NO_3^- and NO_2^- are likely to be a result of advected river water into the sampling site. NH_4^+, on the other hand, has been shown to bond with particles and so is likely to be affected by the theories discussed in Chapter 1.

2.2.2 Phosphorus in the Marine Environment

Phosphorus is a highly reactive, non-metallic element that, like N, is essential to living organisms. Unlike N, however, it is highly reactive and classed as an 'allotrophic' element, which means that the element can exist in many different physical forms while retaining identical chemical composition (Williams, 2001). In the environment, P mainly occurs as P minerals that are commonly found in P rocks, suspended solids in rivers and oceans, and less commonly found in

[§]Distribution of a solute between two immiscible solvents.

dust in the air (Ryther and Dunstan, 1971; Knauer et al., 1979; Eberlein and Kattner, 1987; Williams, 2001).

P is often classed as a limiting nutrient as it is an essential element in living organisms (Karl, 2000) and forms a major constituent of bones, nerves, brain tissue and teeth (Hessen, 1999; Williams, 2001) as well as being a component of adenosine triphosphate (ATP), the fundamental energy source for all life forms (Thurman, 1985). In the terrestrial environment, P predominately occurs as P minerals of the apatite family, or as inorganic phosphates of aluminium, calcium and iron (Williams, 2001). In the aquatic environment, dissolved PO_4^{3-} often dominates. Phosphates are naturally occurring throughout terrestrial and marine ecosystems (Williams, 2001). P plays an important role in estuarine biogeochemistry with inorganic P (mono- or di-protonated orthophosphate) forming the most bioavailable form of P in the environment (Worsfold et al., 2008).

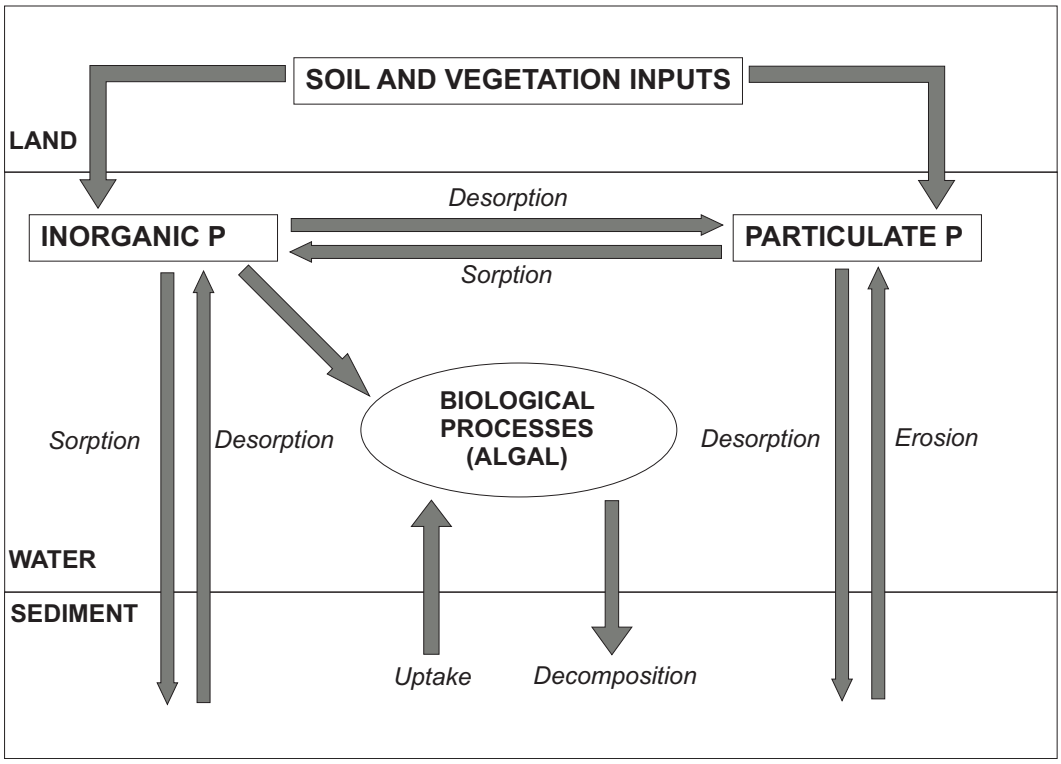

Figure 2.9: *The aquatic phosphorus cycle as defined by Worsfold et al. (2005).*

In contrast to N, marine P differs in two ways (Statham, 2012): 1) oxidation-reduction processes do not play a significant part in the distribution of P; 2) P does not exist in a gaseous form. Bacterial processes are responsible for the conversion of dissolved organic phosphorous (DOP) into dissolved inorganic phosphorous (DIP).

Catchment run-off, including weathered rock (e.g. hydroxyapatite, fluorapatite and berlinite) and agricultural run-off and sewage effluent, is the main source of P in estuaries and deposition/settling of SPM is the major pathway for P transfer from water to sediment. The settling of sediment allows for the trapping of P within an estuary in undisturbed sediments as insoluble calcium components (Emsley, 1980; Mitchell and Baldwin, 2005; Worsfold et al., 2008). Froelich et al. (1982) and Howarth et al. (1995) estimated natural riverine fluxes of P to be between 2.6 and 3.3 $\times$ 10^{11} mol P yr^{-1}. When considering the anthropogenic input through use of fertilisers and deforestation, the value rises to between 7.4 and 15.6 $\times$ 10^{11} mol P yr^{-1} (Froelich et al., 1982; Howarth et al., 1995; Statham, 2012).

Additional sources (point sources) of P include waste water from waste water treatment plants (WWTPs) and industrial processes, leakage from animal waste storage facilities and sewered urban runoff. WWTPs inputs are more significant during periods of low flow. Non-point sources include agricultural runoff, fertilisers used for agriculture (Cole et al., 1990), erosion and sedimentation due to human activities (such as digging or dredging), atmospheric deposition and direct input by livestock.

P species can be characterised by a number of operationally defined fractions, as defined by Worsfold et al. (2005) and illustrated in Figure 2.10. Of particular importance is the Molybdate Reactive Phosphorus (MRP) which is often

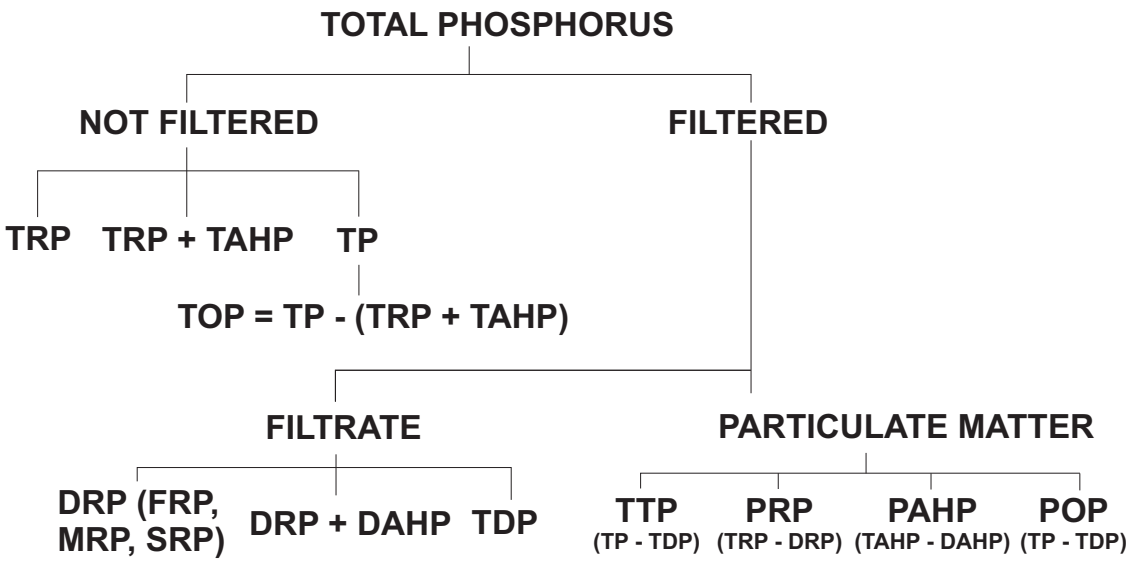

DAHP	Dissolved acid hydrolysable phosphorus	**POP**	Particulate organic phosphorus	**TP**	Total phosphorus
DOP	Dissolved organic phosphorus	**PRP**	Particulate reactive phosphorus	**TPP**	Total particulate phosphorus
DRP	Dissolved reactive phosphorus	**SRP**	Soluble reactive phosphorus	**TRP**	Total reactive phosphorus
FRP	Filterable reactive phosphorus	**TAHP**	Total acid hydrolysable phosphorus		
MRP	Molybdate reactive phosphorus	**TDP**	Total dissolved phosphorus		
PAHP	Particulate acid hydrolysable phosphorus	**TOP**	Total organic phosphorus		

Figure 2.10: *Operationally defined aquatic P fractions from Worsfold et al., (2005).*

assumed to be the inorganic P fraction, but may also contain acid-labile colloidal and organic phosphorus. For the purposes of this thesis, inorganic P will refer to MRP and will be the only form of P measured to determine possible micro-scale processes occurring between sediments and macro-nutrients.

2.2.2.1 Partitioning of P onto Particles in the Marine Environment

Numerous studies have concluded that fluvial SPM is an abundant source of estuarine P, providing between 27.6 and 60% of the total P (TP) (Deborde et al., 2007; Fang, 2000; Nemery and Garnier, 2007; Shen et al., 2008). The exchange between P, SPM and the water column is a complex relationship, involving several physico-chemical and biological processes (Louchouarn et al., 1997). Processes include molecular diffusion, increased temperature, water turbulence, gas ebullition and bioturbation. Micro-scale physical processes such as turbulence allow for the resuspension of sediments from the bed, as well as the accumu-

lation of SPM in an ETM. The increase in SPM causes an increase in surface area to water volume ratio and therefore facilitates the release of P from the surface of particles, back into the water column (Kleeburg and Gruneberg, 2005; Kalnejais et al., 2010). Undisturbed sediments contribute dissolved species via pore-water diffusion across the sediment-water interface (Kalnejais et al., 2010).

The uptake and release of P to particles occurs as a two-step process: 1) rapid surface adsorption onto (or desorption from) the particle surface; 2) a slow penetration by solid-state diffusion of this phosphate into (or out of) sub-surface horizons within the interior of the particles (Froelich, 1988). Step one has fast kinetics of between minutes and hours in duration (micro-scale), while step two has slow kinetics (meso-scale) (Fitzsimons et al., 2011).

The release rate of dissolved P to the water column has been said to be a result of four primary environmental variables; temperature, dissolved oxygen concentration, pH and redox potential (Kim et al., 2003; Hou et al., 2013). Hou et al. (2013) also highlighted that research into the dynamic release of P has been limited to date. Of the limited research, Kalnejais et al. (2010) conducted erosion chamber experiments to determine the solute release associated with known shear stresses. The results of the study indicated the increased shear stress lead to increase concentrations of PO_4^{3-}, as well as copper, manganese, iron, and silver. In this study, using Boston Harbour sediments, the release of solutes from disturbed sediments contributed more to the water column, than could be accounted for by conservative behaviour (Kalnejais et al., 2010). This study seeks to investigate whether suspended particulate matter could contribute a significant concentration of PO_4^{3-} in the same way that resuspension events were shown to contribute to the water column macro-nutrient concentration by Kalnejais et al. (2010).

2.2.3 Interactions of N and P with SPM in an Estuary

As transporters of chemical species and pollutants, understanding the interactions between estuarine SPM and macro-nutrients is both an important and complex task. It has generally been assumed that in estuaries with high riverine input and SPM concentrations, the lateral advection component is dominant (Jay et al., 1997). However, the vertical flux of nutrients, and micro-scale flux of nutrients from sediments to the water are also thought to be able to significantly affect the macro-nutrient concentration (Jay et al., 1997; Kornman and de Dekere, 1998). The release of macro-nutrients from sediments depends on both the sediment geochemistry and local hydrodynamics (Lorke et al., 2003). Of the studies conducted previously, many have examined direct fluxes under quiescent conditions, usually based on molecular diffusion (Fitzsimons et al., 2006; Warnken et al., 2000; Berelson et al., 2003), with little evidence of consideration of fluxes within the field. At a micro-scale, interactions between estuarine SPM and macro-nutrients consist of several different chemical processes, such as remineralisation, adsorption, desorption and ion exchange (Froelich, 1988; Lucotte and d'Anglejan, 1988; Loring et al., 1983; Fitzsimons et al., 2011). However, the aforementioned processes are highly affected by the physical conditions in which they take place (Fitzsimons et al., 2011). A brief description of each process can be found below.

- **Remineralisation** – the transformation of organic to inorganic forms mediated by biological activity.
- **Desorption** – the phenomenon whereby a substance is released from or through a surface (Nic et al., 1997; Thompson and Goyne, 2012). It occurs in a system being in a state of sorption equilibrium between bulk phase and an adsorbing surface.
- **Adsorption** – the adhesion of atoms, ions or molecules from a gas, liquid

or dissolved solid to a surface (Nic et al., 1997). *Note that this process is different from absorption whereby a fluid permeates or is dissolved by a liquid or solid.*

- **Ion exchange** – the exchange of ions between two electrolytes or between an electrolyte solution and a complex (Harland, 1994).

Adsorption processes are of particular interest in relation to Mechanism One of the physical theories outlined in chapter 1. It was hypothesised that an increase in SPM concentration attributed to hydrodynamic processes, may enhance the uptake of nutrients through sorption of sediment to the particle faces. With increased availability of SPM comes increased surface area with enhanced opportunities for the bonding of macro-nutrients with particle surfaces. This uptake could then be further enhanced by the formation of flocs and the trapping of interstitial water into the floc matrix, decreasing water column concentrations. Adsorption has been shown to be particularly important in the control of concentrations of P in soils, lakes and estuaries (Pomeroy et al., 1965; Khalid et al., 1977; Stirling and Wormald, 1977) and so Mechanism One may be relevant to estuarine PO_4^{3-} concentrations.

Similarly, it could also be hypothesised that an increase in SPM concentration enhances the possibility of **desorption** of previously bound nutrients. The desorption reactions of these nutrients typically have two phases: an initial rapid-release associated with loosely bound ions on the surface of the particle (Froelich, 1988; Fitzsimons et al., 2006, 2011), followed by a slower release of ions held within the sediment matrix (Froelich, 1988; Luthy et al., 1997; Turner and Millward, 2002). Temporally, the slower release phase of desorption relates to the meso-scale processes identified in Figure 2.1, as constituents originally bound to the surface migrate into the matrix of the solid over a period of weeks to months (Millward and Liu, 2003). To complicate things further, the aforemen-

tioned desorption, are dependent on the residence time of water, nutrients and SPM in the estuary (Morris, 1990) - all of which are controlled by meso-/macro-scale physical processes.

Mechanism 2 of the detailed aims outlined in chapter 1 proposed that the influence of turbulence on particles in the water column might increase the concentration of macro-nutrients. Turbulence has been shown to both enhance and limit the generation of flocs in the water column, as it is synonymous with the increased energy required to increase SPM concentrations (Braithwaite et al., 2010). With relation to macro-nutrient concentrations, it is thought that increased turbulence could break down particles, releasing nutrient-laden interstitial water from the floc matrix. Further to this, it is proposed that increased turbulence will break down any weak bonds between PO_4^{3-} and the particle surface.

The process of ion exchange is relevant to Mechanism 3 (described in chapter 1), particularly with regard to NH_4^+. It was proposed that with increasing salinity, and therefore cation availability, the concentration of macro-nutrients in the water column may increase due to ion exchange between surface-bound NH_4^+ ions and salt water cations such as Mg^+ and Ca^{2+}.

Chapter 3

Methods & Instrumentation

'She's going to look at the Estuarine Turbidity Maximum... did I get that right?'

Andy Pidduck

3.1 Introduction

This chapter describes the methods and instrumentation used in the fieldwork and laboratory experiments reported in chapters 4 and 5. Any variations from the methods described in this chapter are stated in the respective chapters. The mini annular flume methods for the laboratory experiments can be found in chapter 6. The aims of this chapter are as follows:

- To select and evaluate suitable instrumentation and processing methodologies for the measurement of hydrodynamic conditions.
  - Instrumentation needs to achieve a high temporal resolution (at least 1Hz) in order to capture the micro-scale processes occurring in the water column.
  - Instrumentation must be easy to deploy.
- To optimise methods for the measurement of N and P species (NO_3^-, PO_{43}^- and NH_4^+) within the typical ranges found in the Tamar and Seine estuary.
- To establish a sampling regime that captures meso- to micro-scale processes occurring in the water column, while remaining practical in terms of processing and sampling.

Section 3.2 provides an overview of the sampling strategy and setup, while sections 3.3 and 3.4 present details of the instrumentation and methodologies used to acquire physical and chemical data, respectively. As highlighted in chapter 1, for the purposes of this study, nitrate + nitrite is referred to as 'nitrate'.

3.2 Field Methodology

Fieldwork was conducted in two estuaries; the Tamar estuary (UK) and the Seine estuary (France). Fieldwork locations were selected based on the typical range of SPM concentrations, with both locations falling within the tidal

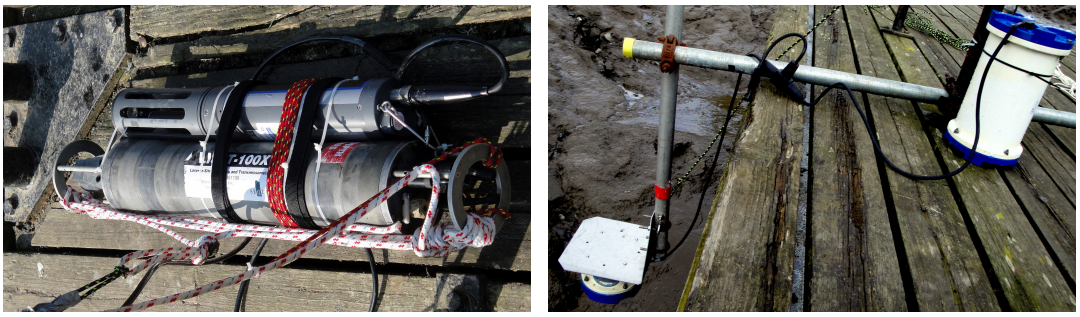

(a) *CTD and LISST apparatus.* ***(b)*** *ADCP Mount location and set-up.*

Figure 3.1: *a) The CTD and LISST strapped together for profiling in a horizontal orientation. The LISST provided sufficient weight to enable a vertical profile of the water column. b) The ADCP mounted on bracket with battery pack at the Tamar estuary sampling site, Calstock (picture taken at low tide).*

trajectory of an ETM although this was a desirable parameter, not a required parameter. The Tamar estuary had mid to high SPM concentrations (0.1 – 2 g L^{-1}) with a meso/macro-tidal regime providing a broad range of turbulent conditions (Davies, 1964). The Seine estuary provided a more 'extreme' case, with a larger tidal range and SPM concentration range (0.1 – 4 g L^{-1}). Further details of each location are provided in chapters 4 and 5, respectively.

Estuarine variables, including temperature, salinity and turbidity, were recorded using a conductivity, temperature and depth (CTD) profiler. A surface mounted 1200 KHz RDI Teledyne Acoustic Doppler Current Profiler (ADCP) (Figure 3.1b) recorded the current velocity, shear and turbulent dissipation of the water column (section 3.3.2). A LISST-100X (Laser In-Situ Scattering and Transmissometry system) (section 3.3.3) was used to determine the particle size distribution. The LISST-100X was attached to the CTD and profiled at the same time (Figure 3.1a).

Instruments were profiled every 30 min. throughout the sampling period (where water was available), while water samples for nutrient analysis were collected every hour by way of a 2.2 L horizontal Van Dorn water sampler. Instrument profiles took approximately 2 - 3 minutes per profile. Instrument profiles were

conducted every 30 minutes as this was deemed achievable with the requirement to filter water samples immediately after collection. To reduce the possibility of contamination of water samples, sample bottles and the Van Dorn water sampler should be conditioned prior to collecting a sample (Mart, 1979). Both were rinsed with surface water from the sampling site prior to filling. The hourly collection of water samples was considered the most effective to capture meso/micro-scale processes, in line with the number of samples to be collected and processed (n = 9). For each Van Dorn water sample collected, this sample volume was further divided into four bottles. Three of these bottles were used to obtain samples for determination of macro-nutrient concentrations, and the fourth was used to complete gravimetric determination of the SPM concentration.

Water samples were filtered on-site using a vacuum pump connected to three independent glass filtration systems (Figure 3.2). As a preliminary treatment, sample were filtered to remove SPM. Water samples for the determination of nitrate and phosphate were filtered through Nuclepore polycarbonate 47 mm diameter, 0.4 $\mu\mathrm{m}$ pore-size filters, while samples for ammonium determination were filtered through Fisherbrand MF300 (GF/F equivalent) 47 mm diameter, 0.7 $\mu\mathrm{m}$ pore-size filters. The instrumentation for the determination of nitrate and phosphate required that a smaller pore size be used to remove as much of the SPM as possible - this prevents contamination in future measurements, particularly with phosphate. The nominal pore size for the removal of SPM from water samples is 0.45 $\mu\mathrm{m}$ (Wilde et al., 2004 - 2011). Sample volumes for nitrate, phosphate and ammonium determinations were transferred into 20 mL HDPE scintillation vials, labelled and transferred into sealable plastic bags (Dore et al., 1996; Gardolinski et al., 2001). Sample vials of this material are considered appropriate, when acid washed, for storage as minimal adsorption of nutrients or bacteria onto the storage container surface occurs (Dore et al., 1996).

Figure 3.2: *Three independent glass filtration rigs attached to vacuum pump to filter water samples before analysis - photo taken during the Tamar estuary spring sampling campaign.*

Samples were stored in a cool box packed with ice at approximately 5^{o}C in the field, before transport to the laboratory and subsequent storage at -20^{o}C. It should be noted that all storage methods for nutrient analysis will involve some alteration of the nutrient to eventually be measured (Intergovernmental Oceanographic Commission, 1993). However, freezing of samples is a widely-accepted method of slowing down biological processes that may cause the depletion of nutrients in the sample (Dore et al., 1996; Gardolinski et al., 2001). Water samples collected for PO_4^{3-} were refrigerated without further acidification as it was shown by Morse et al. (1982) that acid made no significant difference to the quality of sample collected. The results demonstrated that quality of the sample was safe for up to 60 days - consequently, samples were processed within 60 days. This was the same for NO_3^{-}. For NH_4^{+}, samples were frozen as soon as

possible as a study by Vesely (1978) indicated that refrigerated samples degrade within 1 - 2. The MF300 filter papers were retained for gravimetric determination of SPM concentration. Filter papers were dried in an oven at 80°C for 4 h before being weighed. Prior to sampling, 50 filter papers were weighed to obtain average filter weight. The weight of the filter papers prior to sampling was subtracted from the new filter weight to give the amount of SPM in the recorded volume of water filtered. This was then normalised to give the concentration of SPM in g L^{-1}.

3.3 Physical Measurements

3.3.1 CTD - Conductivity, Temperature & Depth Profiler

CTD instruments carry many advantages that make them suitable for use in the Tamar and Seine estuaries (Williams, 2009). Foremost, they allow the acquisition of high resolution data, both spatially and temporally. The instrument is light-weight and practical for use in both shallow and deep water. However, they must be attached to other instruments or a frame when profiling to ensure a vertical profile in strong current velocities. CTD instruments are limited in that measurements can only be made at one point in space and time and so several instruments are required to obtain measurements over a broader area, or when making measurements to assess the impact of advection.

Table 3.1: *A comparison of specifications for the YSI 6600 V2 Sonde and the Seabird SBE 19plus V2 SeaCAT.*

		YSI 6600 V2	
Parameter	**Range**	**Resolution**	**Accuracy**
Conductivity	0 - 10 S / m	0.001 - 0.1 mS / cm	± 0.5% of reading
Temperature	-5 to +50°C	0.01 °C	±0.15°C
Depth	Up to 200 m	0.001 m	up to 0.3 m*
Turbidity	Up to 1,000 NTU	0.1 NTU	± 2% or 0.5 NTU

		Seabird CTD	
Parameter	**Range**	**Resolution**	**Accuracy**
Conductivity	0 - 9 S / m	0.0005 S / m	± 0.00005 S / m
Temperature	- 5 to 35°C	0.0002°C	0.001°C
Depth	Up to 100 m	0.001 m	± 0.1% of scale
Turbidity	Up to 1,000 NTU	0.1 NTU	± 2% or 0.5 NTU

A CTD can carry a variety of sensors with the 'primary' three sensors measuring conductivity, temperature and depth, from which the salinity is calculated internally. Additional sensors can be attached including an optical backscatter sensor (OBS) for the measurement of turbidity, as well as pH, dissolved oxygen and chlorophyll. During the Tamar and Seine estuary experiments, variables were recorded to the instrument memory at a rate of 2 Hz by the YSI CTD, while the Seabird CTD sampled at 4 Hz in the Seine estuary. Salinity, temperature and turbidity probes were calibrated prior to sampling days with a 3 point calibration, as described in the user manual. Specifications, including accuracy, of the YSI 6600 V2 Sonde and the Seabird SBE 19plus V2 SeaCAT (with Campbell Scientific OBS3+ turbidity sensor) used in field campaigns are shown in Table 3.1. The Seabird CTD was more accurate and had a higher resolution than the Seabird CTD, except for the turbidity probe which had the same accuracy and resolution.

The instrument required a short period (30 s) of adjustment upon entering the water, especially in conditions where the air temperature was above or below the water temperature. This initial data was removed during processing. Once

adjusted, the instrument was profiled from surface to bottom recording data on both descent and ascent. On data interpretation, the data were averaged into depth bins (10 cm) to create a smooth profile of each variable.

3.3.1.1 Turbidity Measurements

Data collected by the turbidity probe were measured in Nephelometric Turbidity Units (NTU). A beam of light was shone through the water and a light detector recorded the amount of light visible through the water column. The turbidity of the water was a function of the light reflected into the detector. This data was used in conjunction with filtered water samples (section 3.2) to calculate the SPM concentration in g L^{-1} using linear least-squares regression analysis.

Turbidity measurements recorded by the CTD require conversion to the SI units of turbidity (g L^{-1}). This is done by performing a linear least-squares regression analysis of the gravimetric filter weights against the concentration measured by the CTD at the same time for each sample. The equation of the line can then be used to convert the NTU to g L^{-1}. Site-specific sediment data (i.e. gravimetrically filtered samples) are required because the calibration of the turbidity probe to SPM concentration can vary significantly with the mineral type and colour, as well as particle size Connor and De Visser (1992); Sutherland et al. (2000); Guillén et al. (2000).

Figure 3.3 shows the linear regression analysis performed for each of the field campaigns completed. Table 3.2 shows the details of the regression analysis, including equations of lines of best fit and r^2 values. The equations were used to turn NTU values from each CTD into grams per litre using the following equation:

$$\text{SPM Conc}(g.L^{-1}) = m \times \text{NTU/OBS} + C_0 \tag{3.1}$$

where: m is the gradient of the line and C_0 is the y-intercept of the regression analysis.

Linear regression analysis results presented in Table 3.2 showed that, for most cases, there was a general increase in recorded NTU values and gravimetrically filtered SPM samples. R^2 values for the summer season Tamar estuary campaign demonstrated minimal gradient indicating a weak correlation. In the absence of another calibration, this was used. Reasons for changes in the gradient, m, are a result of changes in the grain size of sediments in suspension (Guillén et al., 2000).

Table 3.2: *Calibration equations for the determination of SPM concentration for each field campaign from gravimetric filtration and OBS measurements.*

Location & Season	Calibration Equation	R-squared
Seine Estuary	y = 0.0023 x + 0.1585	0.702
Tamar Estuary - Spring	y = 0.0021 x + 0.9208	0.704
Tamar Estuary - Summer	y = 0.0073 x - 0.0208	0.486
Tamar Estuary - Autumn	y = 0.0063 x - 0.672	0.796

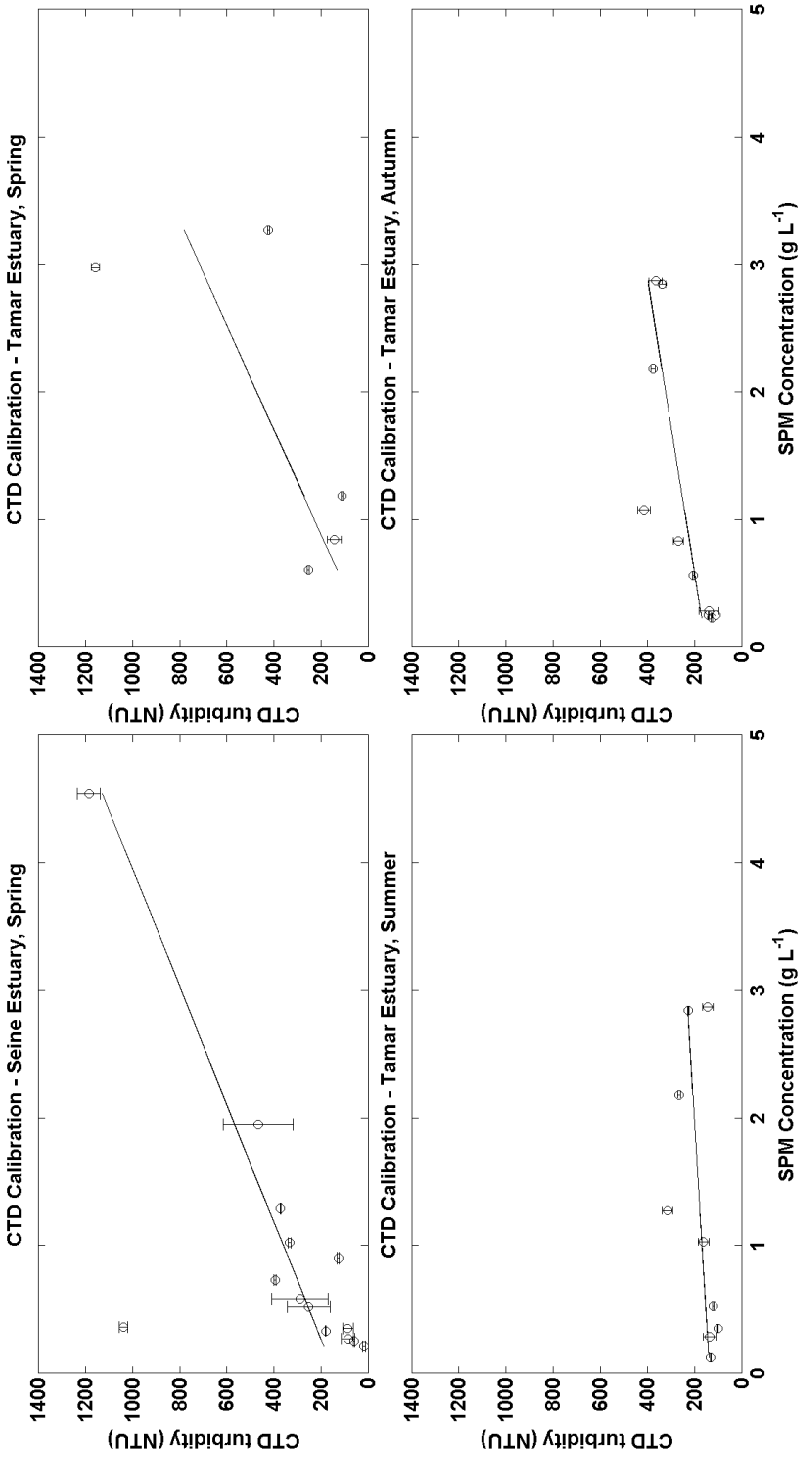

Figure 3.3: *Linear regression analysis of gravimetric filter weights against the concentration recorded by the CTD for each field campaign conducted. Equations of line and further details are presented in Table 3.2.*

3.3.2 ADCP - Acoustic Doppler Current Profiler

ADCP instruments are widely used to measure vertical profiles of currents in estuarine, river and oceanic conditions, using Doppler Effect principles (Figure 3.4) (Emery, 2001). The Doppler Effect is a shift in wavelength (or other periodic event) to an observer (or, in this case, a sensor) as a result of motion. They hold many advantages over alternative instruments. They provide high definition, accurate current velocity data of the entire water column. Instruments such as the Valeport current meter use impellors and only take point measurements and profiles. An added benefit is that the instrument has no external moving parts and is therefore less susceptible to biofouling (e.g. transducer head fouling, plus issues during phytoplankton blooms). Deployment logistics are also simplified by the use of battery packs and autonomous data recording to the internal disk drive.

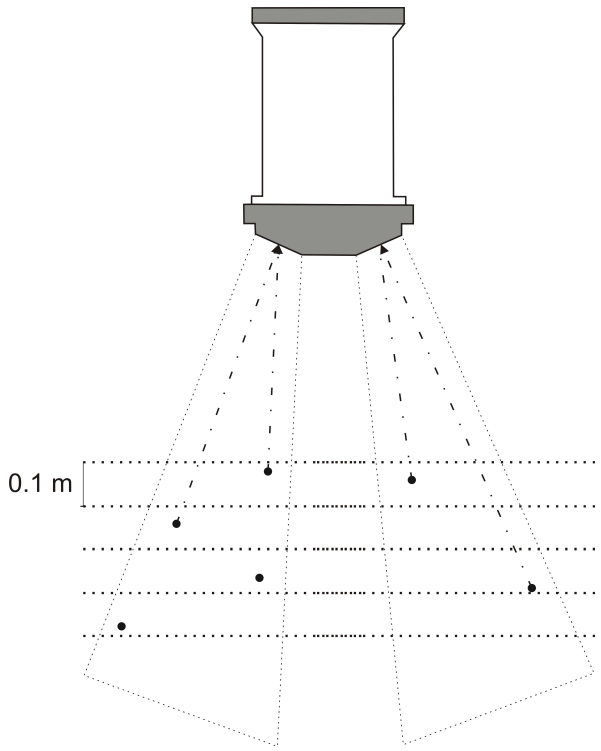

Figure 3.4: *An ADCP uses doppler shift theory to determine current velocity and direction.*

The ADCP transmits a series of acoustic pulses at a fixed frequency, while 'listening' for the resulting backscatter from 'sound scatterers'. Sound scatterers are small particles or plankton that reflect the acoustic pulse back to the ADCP. Reflected sounds are Doppler shifted to a different frequency (depending on the direction of the scatterer in relation to the ADCP) and the Doppler shift is proportional to the relative velocity between the scattering object and the ADCP. It is assumed that scatterers will move in the same direction and at the same velocity as the current (Nystrom et al., 2002; Muste et al., 2004). Higher frequencies (e.g. 1200 KHz) permit higher resolution data, but are limited in the depth of water that they can profile as lower frequencies travel further (Nystrom et al., 2002; Muste et al., 2004). In the Seine and Tamar estuaries, a 1200 KHz ADCP was used, as the depth was no greater than 8 and 4 m, respectively. These depths are well within the remit of a 1200 KHz ADCP. An ADCP instrument also has a compass, a pitch/roll sensor, temperature sensor and a clock.

3.3.2.1 Calculating Kolmogorov Microscales using an ADCP

As well as current velocity and direction, the ADCP can be used to determine Reynold's stress, friction velocity (u_*) and Kolmogorov's microscales (length). Reynold's stress components were calculated using ADCP data. Three components of velocity data, $\widehat{\mathrm{u}}$, $\widehat{\mathrm{v}}$ and $\widehat{\mathrm{w}}$ (in a co-ordinate system fixed relative to Earth), and an error, $\widehat{\mathrm{e}}$, were recorded at 0.2 m depth intervals at a rate of 2 Hz. The error component is described as being 'proportional to the difference between the vertical velocity components estimated along the two planes of the instrument' (van Haren et al., 1994; Nidzieko et al., 2006). Data were averaged into 30 minute bins allowing 15 mins either side of a water profile. Velocity measurements, u, v and w, were used to obtain Reynolds stress estimates using the following format: $u' = u - \overline{u}$. Where u' is the turbulent fluctuation, $\overline{\mathrm{u}}$ is the average velocity and u is the instantaneous velocity. Stress components are then related to Reynolds shear stress using equation 3.2:

$$\tau_{\mathrm{RE}} = -\rho(\overline{\mathrm{u'w'}} + \overline{\mathrm{v'w'}}) \tag{3.2}$$

where ρ is averaged water density.

The aforementioned Reynolds Stress is obtained from the averaging operation over the Navier-Stokes equations to account for turbulent fluctuations in fluid momentum. The method assumes a homogeneous and incompressible flow, where flow velocities are split into a mean part and a fluctuating part. This method, whereby the flows are assumed as homogeneous, avoids the issue of TKE production.

Estimates of the Kolmogorov length microscale ($\mathrm{l_K}$; Kolmogorov, 1941b) were obtained using Equation 3.3:

$$\mathrm{l_K} = \left(\frac{\eta^3}{\varepsilon}\right)^{\frac{1}{4}} \tag{3.3}$$

where η is the averaged kinematic viscosity and ε is the TKE dissipation rate. Kinematic viscosity was calculating using CTD data obtained for each sampling campaign and the following equation:

$$\upsilon = \mu/\rho \tag{3.4}$$

where μ is the dynamic viscosity and ρ was the water density. Kinematic viscosity was calculated using the Gibbs-Seawater Oceanographic MATLAB toolbox (McDougall and Barker, 2011).

For TKE dissipation rate (shown in Equation 3.3), on the basis that the Reynolds stresses were calculated assuming a homogeneous flow where production and dissipation are equal, the results of Equation 3.5 , described below, was used as a measure of the TKE dissipation rate.

$$\varepsilon = \frac{1}{2}\left(\mathrm{u}'^2 + \mathrm{v}'^2 + \mathrm{w}'^2\right) \tag{3.5}$$

3.3.3 LISST 100X - Laser In-Situ Scattering and Transmissometry System

A LISST-100X (Sequoia Scientific) uses the theory of small-angle forward scattering of light (laser diffraction) from particles, also known as Mie theory, to determine the *in situ* particle size distribution and volume concentration (Agrawal and Pottsmith, 2000; Mikkelsen et al., 2005). The 'X' in the name, refers to the type of LISST (A, B, C or ST, etc.). Mie theory states 'that at small forward scattering angles, laser diffraction by spherical particles is essentially identical to diffraction by an aperture of equal size (Fraunhofer approximation)' (Agrawal and Pottsmith, 1994; Gartner et al., 2001). The primary benefit of a LISST-100X, henceforth referred to as a LISST unless otherwise specified, is the ability to measure particle size distributions *in situ*. Alternative methods include wet and dry sieving, while optical backscatter methods only give a concentration of SPM. The instrument is self-contained with internal memory and battery, or the ability to run connected to the mains and computer.

The LISST transmits a red 670 nm laser from a collimated laser diode through the water which is detected by a bespoke ring-detector with 32 logarithmically sized bins (Figure 3.5). The angles determined from the ring detector are computationally inverted to give the particle size distribution of the sample volume (for LISST-100B: 1.25 - 250 $\mu\mathrm{m}$, for LISST-100C: 2.5 to 500 $\mu\mathrm{m}$). This means small particles in the water will scatter light at large angles, while larger particles will scatter light at smaller angles.

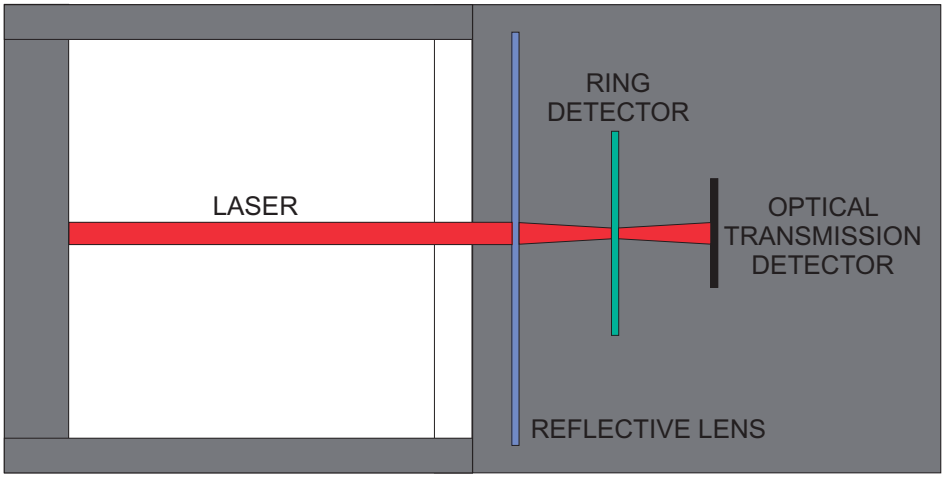

Figure 3.5: *A birds-eye view schematic of the LISST-100X instrument.*

3.3.4 Sampling and Processing

For each sampling day, a background scattering file (or zscat) was created using pure water. This measurement records the scattering of light due to micro-roughness of the optics system and is subtracted from further measurements (Agrawal and Pottsmith, 2000). The corrected scattering from a sample was then calculated using Equation 3.6:

$$s = \left[\overline{d}/\tau\right] - zscat \tag{3.6}$$

where $\overline{\mathrm{d}}$ is the 32-element scattering distribution and τ is the attenuation factor as calculated by Beer's law. The quantities $\overline{\mathrm{d}}$, τ and *zscat* are measured in digital counts. s is further corrected for the 'non-ideal detector responsivity' correction factor, $\overline{\mathrm{D}}$ (see Agrawal and Pottsmith (2000) for details) using Equation 3.7.

$$S(i) = s(i)\overline{D}(i) \tag{3.7}$$

The final step includes dividing the inverse of the scattering by the *volume conversion constant*, $\mathrm{C_v}$, which yields the volume concentration (Equation 3.8):

$$C_n = INV(S)/C_v \tag{3.8}$$

Further processing was applied to PSD data to obtain particle mean, median (D_{50}), standard deviation, surface area (cm^2/L), silt density and silt volume.

Due to the high concentrations of SPM experienced in the Tamar and Seine estuaries, it was necessary to add a path reduction module (PRM) to the LISST configuration. This reduces the optical path length in the water that the laser has to travel through and thus ensures that the laser signal reaches the sensor for measurements. As such, the path reduction must be taken into account when calculating the beam attenuation (Equation 3.9), where r is the path length in meters:

$$(-1/r) \times ln(\tau) \tag{3.9}$$

There are a number of disadvantages of using a LISST. Foremost is the inability to determine what is being viewed. It may be that 'particles' measured in the size distribution are, in fact, biological material or small copepod-like animals. Secondly, for work in coastal and estuarine environments, the measurable size range of the LISST (up to 500 μm) is limited in range. Further to this, Davies et al. (2012) reported that particles larger than the size range of the instrument produces volume distributions that peak at varying sizes between 250 and 400 μm. This is a result of the principal peaks in scattering moving off the inside of the ring detectors, leading to the remaining peaks being interpreted as principal peaks (Mikkelsen et al., 2005; Davies et al., 2012).

Finally, the LISST is susceptible to the refractive properties of density interfaces, known as 'schlieren' (Styles, 2006; Mikkelsen et al., 2008; Boss et al., 2009; Hill et al., 2011; Slade et al., 2011). Schlieren in the water column can be observed in the water column between two different bodies of water with different densities. Mikkelsen et al. (2008) wrote that schlieren can cause increases in

beam attenuation due to an increase in the volume scattering function at smaller angles (1.5 - 2^{o}), resulting in a false accumulation of particles. Mikkelsen et al. (2008) recommended that care be taken when interpreting data that has been obtained in conditions where the buoyancy frequency exceeds 0.025 s^{-1}.

3.3.4.1 Buoyancy Frequency

Buoyancy frequency in the ocean, or the Brunt-Väisälä frequency, is calculated as:

$$N = \sqrt{-\frac{g}{\rho}\frac{d\rho}{dz}} \tag{3.10}$$

where ρ is the potential density, z is the geometric height and g is the local acceleration of gravity. Buoyancy frequency for CTD data was calculated using the MATLAB toolbox by McDougall and Barker (2011). This was only applied in the Tamar estuary where the LISST-100X was the primary instrument to determine particle characteristics.

3.3.5 LabSFLOC - Laboratory Spectral Flocculation Characteristics

While the LISST-100X utilised lasers and light scattering to determine particle size, an alternative method included camera systems, such as LabSFLOC (Manning, 2006; Manning et al., 2007b) (Figure 3.6). The primary advantage of using a camera system was the ability to see exactly what was being measured, unlike the LISST. However, the camera system could only see particles in 2-D, preventing measurement of a third dimension, and therefore requiring several assumptions.

LabSFLOC (version 1.0) utilised a monochrome Puffin Pasecon UTC 341 high resolution video camera (Manning and Dyer, 2002) to observe flocs as they settled in a bespoke settling column. The column was illuminated with a low-heat

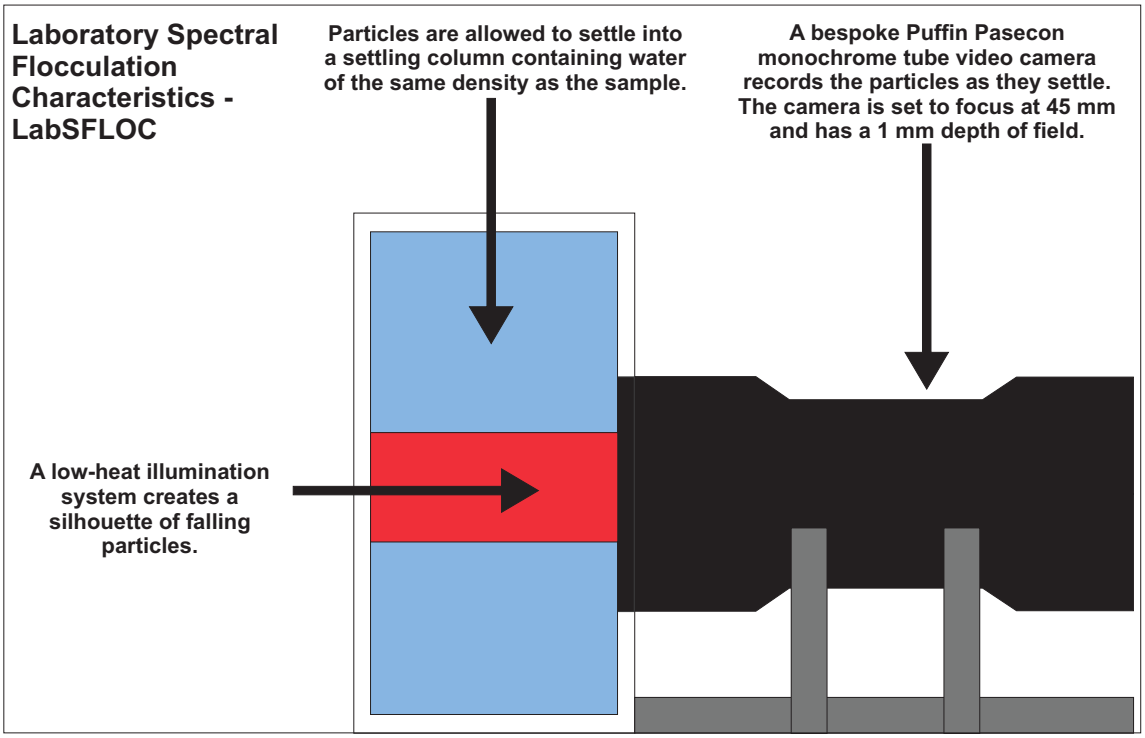

Figure 3.6: *LabSFLOC I Camera System.*

red LED to capture falling particles as silhouettes. As particles settled, the camera captured images of particles that fell within a 1 mm depth of field, 45 mm from the lens and 75 mm above the base of the column (Manning et al., 2007*b*).

Particles were extracted from the sample volume, either from the flume or a water sampler, by modified glass pipette (4 mm internal diameter). The subsample was transferred to the settling column as quickly as possible to minimise the disruption to the floc structures. The aperture of the pipette was brought into contact with the water of the settling column, allowing the flocs to undergo gravitational settling (Gratiot and Manning, 2007). The settling column was filled with water of the same density (temperature and salinity) as the sample volume being extracted.

3.3.5.1 Sampling and Processing

A number of floc properties were obtained from the images of the particles. Equivalent spherical diameter (ESD) of the floc (D), floc shape (height to width ratio) and settling velocity (Ws) were calculated from images alone. Ws was determined by tracking the distance a particle settled between consecutive video frames. Effective density (ρ_{e}) was calculated using a Stokes' Law relationship (Manning et al., 2007*b*):

$$\rho_e = (\rho_f - \rho_w) = \frac{Ws18\mu}{D^2 g} \tag{3.11}$$

where μ is the dynamic molecular viscosity, g is gravitational acceleration, ρ_{f} is the floc bulk density and ρ_{w} is the water density. Calculations of ρ_e using Equation 3.11 were only applicable where the particles settling had low particle Reynolds numbers (i.e. $\mathrm{WsD}/\eta < 0.5$, where η is kinematic viscosity). For particles with higher particle Reynolds numbers, the Oseen modification was applied (Oseen, 1927) to account for the inertial drag on the settling particles (Brun-Cottan, 1986; ten Brinke, 1994).

Floc porosity, as described in section 2.1.3, indicates how compact the floc or aggregate is. It therefore required that the volume of the floc and the volume of the interstitial water associated with the floc were calculated:

$$P_f = \frac{V_{iw}}{V_f} \times 100 \tag{3.12}$$

where V_{iw} is the interstitial water between the particles in a floc, and V_f is the volume of the floc:

$$V_f = \frac{4\pi D_y D_x}{3} \tag{3.13}$$

$$V_{iw} = 1 - \frac{\rho_c}{\rho_{cnp}} \times V_f \tag{3.14}$$

where ρ_{e} is the effective density and ρ_{cnp} is the mean effective density for solid non-porous aggregates.

3.3.5.2 Assumptions

LabSFLOC uses one fundamental assumption in all of the calculations done in post-processing; that all particles are spherical. The camera system can only take 2-D images and so additional dimensions and axes of the particles may be missed. By omitting other faces or axes of a particle, it may result in errors in calculation of effective density, porosity and the volume of interstitial water. Furthermore, particles that appear small and round, may actually be an image of a long, stringy floc, of which the largest axis is missed.

3.4 Chemical Measurements

3.4.1 Labware Cleaning Protocol

Prior to use, all plasticware and glassware used for sampling, analysis, standards and reagents were scrubbed and cleaned with ultra high purity (UHP) water ($\leq$ 18 MΩ·cm). Following a rinse, the items were left to soak in 2% Decon Neutracon[†] (low nutrient) for a minimum of 24 h. Once removed, items were rinsed three times with UHP water and transferred to a 10% v/v hydrochloric acid (HCl) bath for a further 24 h. A final rinse with UHP water was conducted five times before the items were either dried under a laminar flow hood, or ashed in a muffle furnace at 450 ^{o}C for 6 h. Once dried, all plasticware and glassware were stored in two sealable plastic bags.

[†]A specialised surface active cleaning agent/decontaminant

All reagents were supplied by Fisher Scientific or Sigma-Aldrich and were of analytical grade. Solutions were prepared with UHP water, unless otherwise stated. Further details of reagents used can be found in each methodology listed in this chapter.

3.4.2 Continuous Flow Analysis (CFA)

Nitrate and phosphate concentrations were determined on an automated, air-segmented, continuous flow analyser (CFA) (Skalar SANplus). The instrument incorporated an autosampler, capable of holding 300 samples, a Skalar SA 4000 chemistry unit equipped with two 16 channel peristaltic pumps, a 4-channel module holder for up to four different chemical methodologies, and four flow-through, dual-channel, single-beam photometer heads. It also included a Skalar SA 6250 dual-channel, single-beam photometer unit linked to a Microsoft Windows operating system through a Skalar 8502 interface, designed to modulate the analogue voltage signal to digital data. Under optimum conditions, the absorbance measured is directly proportional to the concentration of the nutrient and is measured in arbitrary peak height values. Peak height values were recorded by the Skalar Flow Access (2.0.11) software. Calculations to account for the drift of the baseline could be conducted by the software, or independently.

The Skalar Flow Access software calculated nitrate and phosphate concentrations based on 'corrected peak heights'. The peak heights measured during experiments were adjusted for changes in sensitivity in the baseline and drift measurements. Once the corrections had been completed, the software used a first order regression (linear calibration curve) to calculate the slope, intercept and correlation coefficient. However, in the case of a large drift or an unstable baseline, results and calculations were found to be exaggerated. Zhao (2009) reported that, for the determination of phosphate, changes in temperature of the reagents would change the sensitivity of the baseline measurement, thus chang-

ing the 'corrected peak height'. As such, reagents were equilibrated to room temperature prior to use and manual calculations of nutrient concentrations were performed.

3.4.3 Nitrate Determination

Nitrate determination was based upon the reduction of nitrate in copperised cadmium to nitrite, followed by diazotisation of nitrite with sulphanilamide and coupling with N-(1-napthyl) ethylenediamine dihydrochloride to form an azo dye (Figure 3.7) with a maximum molar absorptivity (ϵ) at 540 nm (Armstrong et al., 1967). The Skalar nitrate manifold (Figure 3.8) required 2 reagents; a buffer solution and a colour reagent.

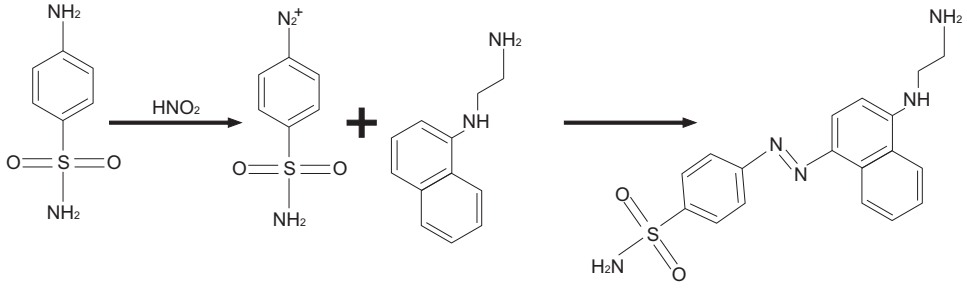

Figure 3.7: *A schematic example of the diazonium coupling reaction in the presence of nitrite to form an azo dye.*

The buffer solution was composed of 50 g ammonium chloride, 1 mL ammonium hydroxide and 2 mL low-nutrient surfactant (Brij 24, Skalar analytical), made up to 1 L with water. The colour reagent comprised 150 mL o-phosphoric acid (85%), 10 g sulphanilamide, 0.5 g N-(1-napthyl) ethylenediamine dihydrochloride and made up to 1 L with water. Stock solutions were prepared using 0.6067 mg pre-dried sodium nitrate, accurately weighed and dissolved in 1 L water. Working standards were produced on the day of analysis by serial dilution of the stock solution with helium degassed water. An example of the typical concentration range used for calibration, including dilution volumes, are shown in Table 3.3.

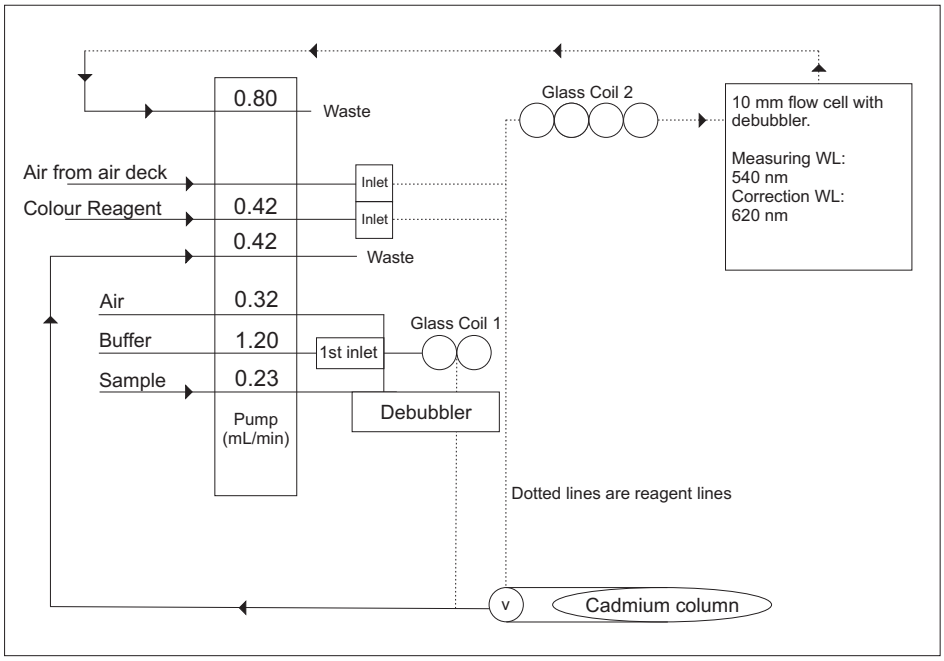

Figure 3.8: *The CFA manifold for the determination of NO_3^-. Modified from Tuckwell (2007a).*

Table 3.3: N Standard Set *- A typical calibration set for the determination of NO_3^-.*

Standard	**NO_3^- N mg L^{-1}**	**Vol. 10 mg L^{-1} stock required (in 100 mL) mL**	μM
S0	0	0	0
S1	2	20	142
S2	4	40	285
S3	6	60	428
S4	8	80	571
S5	10	100	714

3.4.3.1 Nitrate Calibration

Table 3.4 shows the regression analysis calibration equations for the nitrate determination for samples collected in the Tamar and Seine estuary. Results were linear for samples in the range 2 - 6 μg L^{-1}. Above 6 μg L^{-1}, results began to deviate. For the Tamar estuary, the analytical variability for the 4 μg L^{-1} standard ranged between 0.2 and 3.4 % Relative Standard Deviation (RSD) (n = 3), with R-squared values of between 0.93 and 0.98. An R-squared value of 1

represents that the regression line fits perfectly. For the Seine estuary experimental runs, the RSD values were 0.62 and 2.8%, and R-squared values were 0.987. The R-squared values for calibrations in this study were acceptable, with all values above 0.9. The variability in gradients is thought to be a result of changes in ambient temperature during the course of the experimental runs. Intercept variations are thought to be a result of changes in UHP water quality and changes in quality and concentration of the reagents over the period of analysis.

Table 3.4: *Calibration equations for the determination of nitrate for the range 2 - 10 $\mu g\ L^{-1}$. RSD is the relative standard deviation of the 4 $\mu g\ L^{-1}$ standard for each experiment.*

Sample Set	Calibration Equation	R-squared	RSD % (n = 3)
Seine ETM 1	y = 534.15 x + 174.9	0.987	2.8
Seine ETM 2	y = 418.71 x - 284.48	0.987	0.62
Tamar March 2011	y = 355.29 + 377.07	0.925	2.3
Tamar June 2011	y = 474.89 x + 243.65	0.9825	0.2
Tamar Sept 2011	y = 305.52 x - 248.65	0.9734	3.4

The limit of detection (LOD) was calculated as the intercept of the regression plus three times the standard deviation of the peak height of five blanks, resulting in an LOD of 1.42 μM for this method. This value is approximately 1% of the lowest standard used for the calibration and so is acceptable for this method.

3.4.4 Phosphate Determination

Detection of phosphate was based on the method by Murphy and Riley (1962), and optimised by Drummond and Maher (1995). It involves the reaction of phosphorus with molybdate under acidic conditions (pH 2) to produce phosphomolybdic acid. The heteropoly acid (a class of acid made up of a particular combination of hydrogen and oxygen with certain metals) produced is subsequently reduced by ascorbic acid to form a blue complex that can be detected spectrophotometrically at 880 nm. The linear detection range for phosphate determination is 20 - 500 $\mu g\ L^{-1}$ (0.016 - 16.14 μM).

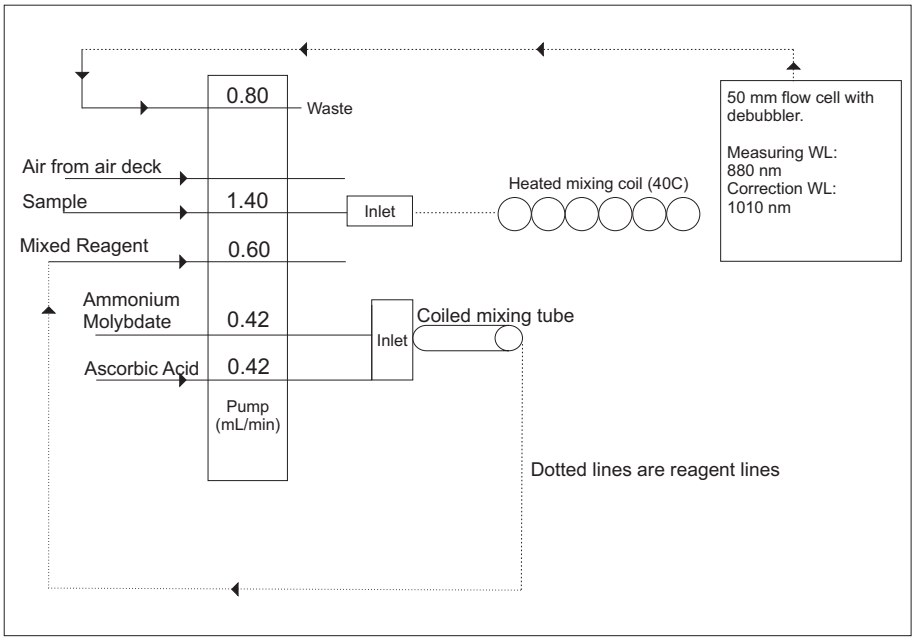

Figure 3.9: *The CFA manifold for the determination of PO_4^{3-}. Modified from Tuckwell (2007a).*

The Skalar manifold required two reagents (Figure 3.9); an ammonium molybdate solution, and an ascorbic acid solution. Ammonium molybdate was prepared using 0.230 g of potassium antimony tartrate (PAT), 69.4 mL of sulphuric acid, 6 g ammonium molybdate, 2 mL of FFD6 surfactant and made up to 1 L with water. Ascorbic acid solution was composed of 11 g ascorbic acid, 60 mL acetone, 2 mL FFD6 surfactant and made up to 1 L with water.

Table 3.5: P Standard Set *- A typical calibration set for the determination of phosphate.*

Standard	**PO_4-P μg L^{-1}**	**Vol. PO_4-P 10 mg L^{-1} stock required (in 100 mL) mL**	μM
S0	0	0	0
S1	20	200	0.65
S2	40	400	1.29
S3	60	600	1.94
S4	80	800	2.58
S5	100	1000	3.22

A 100 mg L^{-1} PO_4-P solution was produced using 0.4393 g pre-dried potassium dihydrogen phosphate (POP) dissolved in 1 L water. From this, a 10 mg L^{-1} intermediate stock solution was prepared using a dilution of the original 100 mg

L^{-1} stock solution. As with nitrate determination, 6 standards (including blank) were created using serial dilutions with helium degassed water. An example of the concentration range used, including dilution volumes, can be found in Table 3.5.

3.4.4.1 Phosphate Calibration

Table 3.6 shows the typical regression analysis calibration equations for the phosphate determinations conducted during this research. The phosphorus calibration graphs were linear over the range 20 - 100 $\mu g\ L^{-1}$ (with R-squared values ranging between 0.978 and 0.992). For the Tamar estuary, the analytical variability for the 40 $\mu g\ L^{-1}$ standard was consistently below 2 % RSD (n = 3). For the experiment runs for the samples collected in the Seine estuary, the RSD was 20 % (n = 3). The variability in gradients is thought to be associated with changes in temperature during course of the experimental runs. Intercept variations are thought to be a result of changes in UHP water quality and changes in the quality and concentrations of reagents over the period of analysis. The limit of detection (LOD) was calculated as the intercept of the regression plus three times the standard deviation of the peak height of five blanks, resulting in an LOD of 0.024 μM for this method.

Table 3.6: *Calibration equations for the determination of phosphate for the range 20 - 100 $\mu g\ L^{-1}$. RSD is the relative standard deviation of the 40 $\mu g\ L^{-1}$ standard for each experiment.*

Sample Set	Calibration Equation	R-squared	RSD % (n = 3)
Seine ETM 1	y = 28.446 x - 13.365	0.979	16.76
Seine ETM 2	y = 21.856 x + 0.2	0.971	15.69
Tamar March 2011	y = 9.9308 x + 96.054	0.968	1.6
Tamar June 2011	y = 11.411 x - 32.34	0.992	1.5
Tamar Sept 2011	y = 14.442 x - 68.085	0.978	1.5

3.4.5 Ammonium Determination

A number of methods exist for the determination of ammonium (Garside et al., 1978; Goyal et al., 1988; Genfa and Dasgupta, 1989; Gibbs et al., 1995; Kerouel and Aminot, 1997), with the indophenol blue method most widely used (Holmes et al., 1999). However, increasing publication and widespread variance of methods demonstrate the complexity and issues associated with the accurate measurement of ammonium, particularly at sub-micromolar concentrations (Holmes et al., 1999).

Holmes et al. (1999) described two fluorimetric methods for the determination of ammonium. Protocol A was reported to be suitable for sub-micromolar concentrations while Protocol B was reported to be suitable for higher concentrations. The motivation to use Protocol B of the method outlined by Holmes et al. (1999) was the suitability of the applicable concentration range to both the Tamar and the Seine estuary, and the disadvantages of using the indophenol blue method. Disadvantages of the indophenol blue method included high and variable blanks, difficulties with high limits of detection and the use of toxic reagents. Comparatively, the adapted continuous-flow fluorimetric technique used instead was simple and accurate, there were no toxic reagents, and the method could be used for samples from a range of aquatic environments, both fresh and saline.

3.4.5.1 Instrumentation

The determination of ammonium required an Hitachi F-4500 fluorescence spectrophotometer to measure fluorescence. The excitation and emissions slits were set to 5 nm, the PMT voltage was 700 V and the response was set to ‘auto’. Maximum fluorescence was achieved at an excitation wavelength of 362 nm and an emission wavelength of 422 nm. Fluorescence measurements were 3 second integrations of the peak height.

3.4.5.2 Reagents

The method used a stable working reagent (WR) of which the active ingredient was orthophthaldialdehyde (OPA). The OPA reacted with ammonium to form a highly fluorescent product. Further components included a borate buffer (BB) and sodium sulfite. In the presence of sodium sulfite, OPA loses its sensitivity to amino acids and becomes specific for ammonium (Kerouel and Aminot, 1997; Holmes et al., 1999).

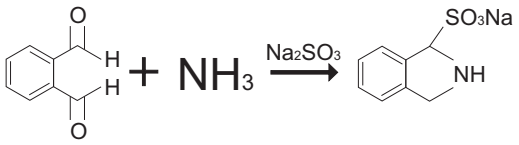

Figure 3.10: *A schematic example of the fluorimetric determination of ammonium.*

The sodium sulfite solution was composed of 1 g sodium sulfite dissolved in 125 mL water. The solution was stable for approximately 1 month. BB was composed of 80 g sodium tetraborate is dissolved in 2 L water. The BB requires agitating/stirring/shaking until the sodium tetraborate is totally dissolved. The OPA solution was composed of 4 g of OPA added to 100 mL ethanol (high-grade). The solution was light sensitive and was stored in the dark.

The WR, stored in a 2 L Winchester bottle, was composed of 1 L borate buffer solution, 5 mL sodium sulfite solution and 50 mL OPA solution. The WR was left for at least 24 hours, as the blank fluorescence measurement decreased over time. The WR was stable for 3 months when stored in the dark at room temperature.

3.4.5.3 Standards , Analytical Procedure and Calibration

A stock solution, created on the day of processing, was created using 53.49 mg ammonium chloride dissolved in 100 mL water, giving a concentration of 10

mM NH_4^+. A 100 μM solution was achieved by a 1:10 dilution. From this, 6 standards were made. Concentrations and dilutions used for the determination of ammonium in this research are listed in Table 3.7.

Table 3.7: NH_4^+ Standard Set *- A typical calibration set for the determination of NH_4^+.*

Standard	NH_4^+ Concentration (μM)	Vol. required in 25 mL
S0	0	0.00
S1	10	0.25
S2	20	0.50
S3	30	0.75
S4	40	1.00
S5	50	1.25

The analytical procedure of the methodology required the determination of background fluorescence, matrix effect fluorescence and sample fluorescence. Background fluorescence was determined by the addition of 2.5 mL BB to 10 mL water in scintillation vials.

For each sample, 2.5 mL was pipetted into 2 scintillation vials. 1.25 mL was also pipetted into a third vial to account for the matrix effect. The first vial containing 2.5 mL sample and 10 mL WR gave the fluorescence of the sample itself ($F_{sample(obs)}$). The second vial containing 2.5 mL sampling and 10 mL BB, gave the background fluorescence for the sample ($F_{sample_{(BF)}}$). The final vial, containing 1.25 mL sample, 1.25 ml standard (spike) and 10 mL WR takes into account the matrix effect ($F_{sample(spike)}$).

To calculate the corrected ammonium concentration ($F_{sample(corrected)}$), the following formulae were applied:

$$F_{sample_{(NH_4)}} = F_{sample_{(obs)}} + F_{sample_{(BF)}} \tag{3.15}$$

$$ME = \left\{ \frac{\left[\left(F_{standard_{spike}} - F_{standard_{zero}} \right) - \left(F_{sample_{spike}} - F_{sample_{obs}} \right) \right]}{\left(F_{standard_{spike}} - F_{standard_{zero}} \right)} \right\} \times 100\% \quad (3.16)$$

$$F_{sample_{(corrected)}} = F_{sample_{(NH_4)}} + \left[F_{sample_{(NH_4)}} \times \left(\frac{ME}{100} \right) \right] \quad (3.17)$$

3.4.5.4 Ammonium Calibrations

Ammonium concentrations were subsequently calculated using basic regression analysis. Fluorescence values of known concentration were plotted against the known concentration range and an equation produced. Fluorescence was shown to be linear over the required range (0 - 50 μM). The equation of the line was $\mathrm{y} = 125.84\mathrm{x} + 109.73$ and the regression coefficient was 0.997. The limit of detection (LOD) was calculated as the the intercept of the regression curve plus three times the standard deviation of the fluorescence of 5 blanks, resulting in an LoD for this method of 0.075 μM.

3.5 Conclusions

Instrumentation to measure the hydrodynamic conditions was selected on the ability to record at a high frequency, and ease of sampling. The CTD, ADCP and LISST-100X all sampled at a rate of 2 Hz, meeting the requirements for high temporal resolution sampling. As a self-contained stationery profiling unit, the ADCP was set to record at the start of the day and stopped when the last sample was collected - data was stored internally and downloaded post deployment. The CTD and LISST-100X were strapped together for simultaneous sampling and ease of profiling. It also provided the weight required to record a straight profile in strong current velocities.

Determination of NO_3^- and PO_4^{3-} was conducted by spectrophotometric CFA on

a Skalar system. Methods were optimised for the range of concentrations previously reported in the Tamar and Seine estuaries, as well as for experiments in the flume studies. Initial testing and results revealed a good linear range of 142 - 285 μM for NO_3^-, and 0.65 - 3.22 for PO_4^{3-}, with a limit of detection of 1.42 and 0.024 μM, respectively. For NO_3^-, results were not linear above 428 μM but values below this were within the expected range and so met the aims outlined at the start of the chapter. Precision and accuracy of the methods showed values of between 0.2 - 2.8 % RSD for NO_3^-, and 1.5 - 16.76 % RSD for PO_4^{3-}.

Concentrations of NH_4^+ were determined using a fluorimetry method reported by Holmes et al. (1999). Method B was reported to be suitable for concentrations over 1 μM and results obtained in this study showed a linear range between 10 and 50 μM, meeting the aims of this chapter. The LOD for this method was 0.075 μM.

Chapter 4

Sediment-Nutrient Interactions in the Seine Estuary, France

'Going in-Seine... get it?'

Mark Fitzsimons

4.1 Introduction

This chapter presents the results and discussion of the field campaign conducted in the Seine estuary, France. A single field campaign of 10 h was conducted in April 2010, at the approximate location of the ETM. The aim of this chapter was to determine whether micro-scale processes affecting macro-nutrient concentrations could be observed in a turbid estuarine environment. The objectives of this chapter are outlined below:

- to make *in situ* hydrodynamic, particle and chemical measurements in a turbid estuary;
- to determine nutrient concentrations in collected water samples;
- to analyse particle and nutrient data to determine micro-scale relationships between sediments and nutrients.

4.2 Location

The Seine estuary (Figure 4.1) is a controlled (the estuary has been significantly altered from its natural state), tide-dominated, macro/hyper-tidal estuary located within the regions of *Ile-de-France* and *Haute-Normandie* (Darymple et al., 1992; Lesourd et al., 2003). Characterised by both freshwater and saline tidal sections, the estuary is approximately 160 km in length from the mouth to a man-made lock at Poses. The estuarine section is approximately 20% of the 776 km total length of the Seine River and has a hyper-tidal range of 8.5 m during spring tides (Davies, 1964) and a meso-tidal range of 3 m during neap tides at the mouth, and a small tidal range of 30 cm at Poses lock (Deloffre et al., 2005; Garnier et al., 2008). At Poses lock, the Seine river has a 15-year annual mean flow of 500 m^3 s^{-1} (Garnier et al., 2008), and extreme values of around 2,000 m^3 s^{-1} (winter) have also been observed (Lesourd et al., 2001).

Historically, the Seine estuary has been heavily manipulated to allow access for large ocean-going vessels. Between Le Havre and Rouen, the estuary has been dyked to a single channel and dredged up to 9 m (Deloffre et al., 2005). These changes have reduced the water volume within the estuary and subsequently increased the current flows to between 1 - 2 m s^{-1} (Avoine, 1982). As a result of the fast current flows and altered shape of the estuary, deposition of fine-grained sediments is limited to areas of low erosion, such as the inner of a large meander, and in the docks of ports (Deloffre et al., 2005).

An ETM is formed as a result of tides, waves and river flows in the brackish mixing zone, and the longitudinal oscillation of the ETM is approx. 20 km. During periods of high river flow it can move out to the Seine Bight (Avoine, 1987; Deloffre et al., 2005; Garnier et al., 2008). Every semi-diurnal tidal cycle, large quantities of sediment are suspended during peak current periods (up to 2 m s^{-1}) and concentrations of SPM can reach 4,000 mg L^{-1} (Lesourd et al., 2003; Garnier et al., 2008). Tidal asymmetry in the Seine estuary induces stronger flood current compared with ebb current velocities, with a longer high water slack period (approx. 3 h) giving rise to increased settling of particles (Brenon and Le Hir, 1999).

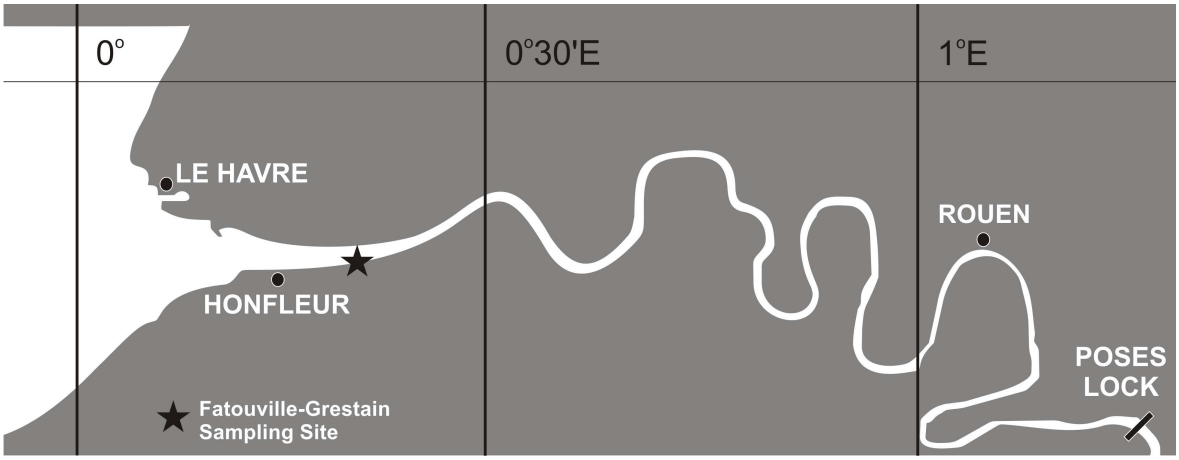

Figure 4.1: *The Seine estuary from mouth to Poses Lock – sampling location: 49°N 26' 13.32", 0°W 21' 17.21".*

(a) *The sampling jetty at Fatouville-Grestain*

(b) *A view of the river looking East towards Rouen.*

Figure 4.2: *a) The jetty used for sampling and deployment at Fatouville Grestain. b) Looking east along the River Seine from the sampling jetty.*

The Seine River supplies a large quantity of suspended silt and clay to the estuary. It is reported that the dry weight mean annual flux of sediment at Poses is 5 $\times$ 10^5 t per year (Lesourd et al., 2003). During wet periods, this value can increase to around 1 $\times$ 10^6 t per year, and can drop to as little as 2 $\times$ 10^5 t year^{-1} in drier periods (Avoine, 1987; Lesourd et al., 2003). Examination of the sediments carried in suspension in the Seine estuary revealed three distinct fractions: fine-grained (3 - 5 μm), medium-grained (8 - 20 μm) and coarse-grained (over 100 μm) (Avoine et al., 1984; Avoine, 1987).

Whilst the riverine input of sediment is predominately fine clay and silt, the composition of the bed sediment is more varied. In the Bay of Seine, sediment sizes are seen to decrease from the English Channel (gravelly) to the estuary mouth (coarse sand). In the mouth of the estuary, patches of different sediments can be observed; the main estuary channel is largely composed of clean fine sand of marine origin (Germaneau, 1968, 1971; Avoine, 1987). Along the northern side of the estuary, fine, thinly-bedded silts and clays form the tidal flats and

marshes (Avoine, 1987).

The SPM concentrations of the Seine estuary made it a suitable candidate for the examination of physical and chemical processes, in line with the aim highlighted in section 4.1. Other physical conditions highlighted in this section indicate conditions whereby it was expected that Mechanisms and processes would be amplified and easier to observe.

4.3 Methodology

The methods used for the Seine sampling were as described in chapter 3, with a few adaptations (listed below).

- LISST data were not used due to 'saturation' of the instrument as a result of high SPM concentrations. Unlike the Tamar estuary, a path reduction module was not used. Instead, the LabSFLOC I camera system was used to determine floc characteristics.

- Water samples were collected hourly and filtered on-site with a vacuum pump. Water samples for the determination of nitrate and phosphate were filtered through Nuclepore polycarbonate 47 mm diameter, 0.4 $\mu\mathrm{m}$ pore-size filters, while samples for ammonium determination were filtered through Fisherbrand MF300 (GF/F equivalent) 47 mm diameter, 0.7 $\mu\mathrm{m}$ pore-size filters. Subsequently, filter papers and samples were stored in an ice box until they could be frozen. Samples were frozen within 24 h of collection.

- The 1200 KHz ADCP was set to record at a higher resolution (0.1 m bin size). The increased frequency of sampling provided higher resolution data, however this resulted in more memory being used and the instrument did not have enough memory for the entire day of sampling. Consequently, data is only available for the flood tide.

The adaptations to the method above were deemed suitable for the 'extreme' conditions highlighted in section 4.1. LabSFLOC I is suitable for SPM concentrations of up to 8 g L^{-1} making it more suitable for the conditions than the LISST.

4.4 Results & Discussion: The Effect of Micro-Scale Processes on Macro-Nutrient Concentrations in the Seine Estuary

Sampling in the Seine estuary was conducted from a short jetty at Fatouville-Grestain (Figure 4.1) in April 2010. Figure 4.3 presents the air temperature and precipitation data for the week preceding and day of sampling. Conditions were warm and there was very little precipitation during the day or the week preceding sampling (17/4/2010 – 23/04/2010). The average precipitation for the month of April 2010 is depicted by the black line in Figure 4.3b. The maximum air temperature during sampling reached 14.9 °C, while the average was 8.9 °C. These conditions were close to the average temperatures typically recorded for April in the Seine estuary. Low levels of precipitation throughout the month prior to sampling would impact the river run off levels for that month. This, in turn, will affect the meso-scale processes occurring in the estuary including, the limit of tidal intrusion, the formation and strength of an ETM, and the concentrations of nutrient species within the estuary.

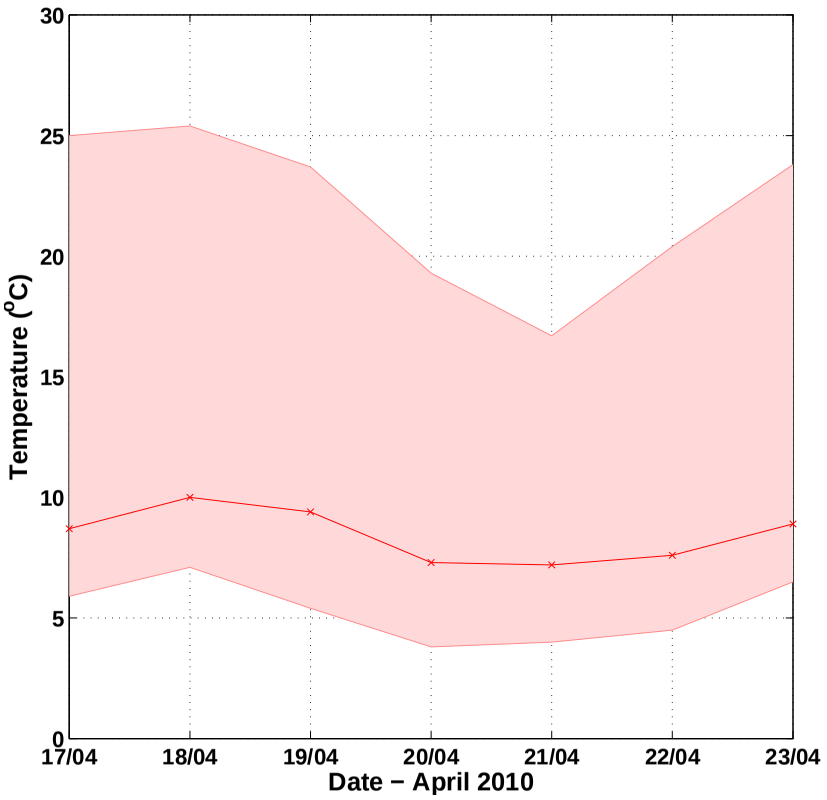

(a) Temperature data

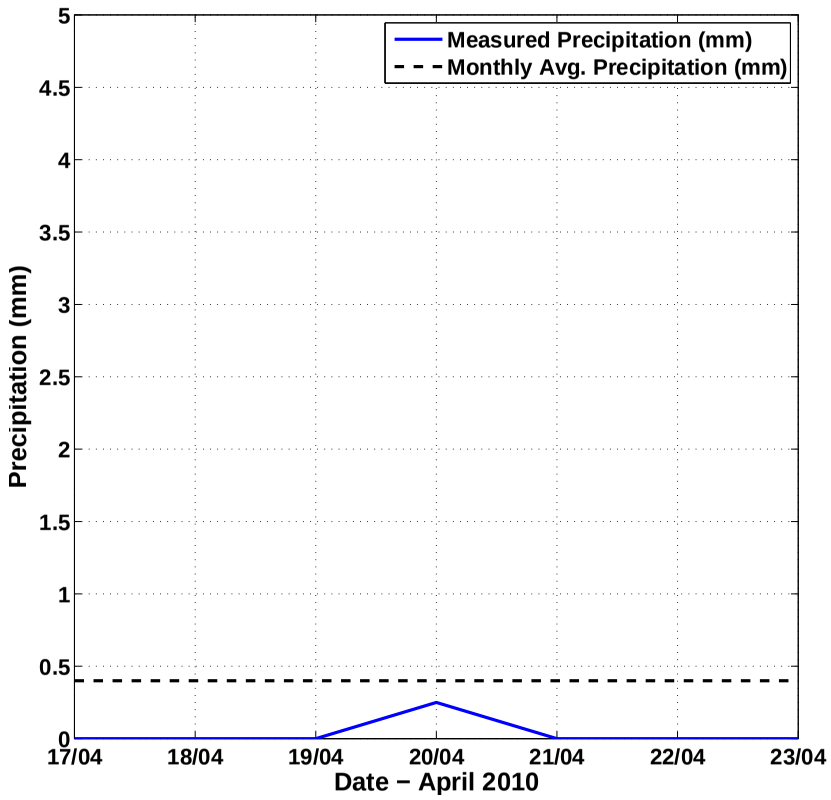

(b) Precipitation data

Figure 4.3: *a) Temperature data for the week preceding sampling (17/4/2011 – 23/04/2011). Average temperatures are marked by the solid red line, while the pink bounding box marks the maximum and minimum temperature for each day. b) Actual and average precipitation data for the week preceding sampling.*

4.4.1 An overview of the hydrodynamic conditions in the ETM

Time series plots of temperature, salinity and turbidity from CTD profiles are presented in Figure 4.4 (Page 87). High water (HW+0) was at 1446 (Coordinated Universal Time (UTC +2)). Increased depth, temperature and salinity gradients were observed at the start of the flood tide at HW-3, with the influx of salt water. The start of the ebb tide was observed at HW+1, with strong stratification caused by the intrusion of warmer, fresher water at the surface and the retreat of salt water close to the bed (Day et al., 1945; Simpson et al., 1990). Salinity ranged from 0 (HW-5 to HW-2) to 24 (HW+0 to HW+3), while temperature ranged from 10.5 - 12.5 ^{o}C. Physical conditions were in agreement with previous studies conducted in the Seine estuary, despite lower than average levels of precipitation (Garnier et al., 2008, 2010).

The maximum SPM concentration, calculated gravimetrically, was 4.5 g L^{-1} at HW-2 (near-bed SPM concentration), while the minimum value was 0.2 g L^{-1} at HW+3 (surface SPM concentration). Gravimetric SPM concentrations were used to calibrate the OBS instrument measurements and, consequently, OBS SPM concentrations from the CTD profiles were in the range 0 - 2.5 g L^{-1} (Figure 4.4c). Measured OBS concentrations were lower due to 'resolution bias' in water sampling (see section 3.3.1 for calibration information). At approximately HW-2, as indicated by increased turbidity in Figure 4.4c, an ETM was observed for approximately 90 min. Concentrations of SPM observed using OBS measurements in the ETM were similar in magnitude to those reported in previous studies (Lesourd et al., 2003; Deloffre et al., 2005; Garnier et al., 2008, 2010). Results in Figure 4.4c show that, at its peak, the ETM height reached a height of approximately 6.5 m above the bed.

Current velocity (u) and Kolmogorov microscale length ($\mathrm{l_K}$) data are presented

in Figures 4.5a & b (Page 88). Both variables have been temporally averaged (15 minutes). The time-step for temporal averaging was chosen as it was the approximate time interval between CTD profiles collected. As mentioned in section 2.1.4.2, Kolmogorov microscale lengths are a useful measure of turbulence as they are directly comparable to particle sizes (Braithwaite et al., 2010). Lower values of l_K are indicative of higher levels of turbulence (McCabe, 1991; Hill et al., 1992; Fugate and Friedrichs, 2003; Mîkes, 2011) and values in estuaries typically range from 100 - 1000 μm, depending on the depth and flow conditions (Winterwerp et al., 2002). The values recorded here reflect atypical, highly turbulent conditions; thought to be a result of current velocities up to 2.2 $\mathrm{m\ s^{-1}}$. Values previously reported for the Seine estuary were between 100 - 1000 μm (Mikes et al., 2004; Verney et al., 2009). It is also possible that localised turbulence from the jetty used for sampling could have influenced ADCP values (Geyer et al., 2008; Trowbridge, 2008; Roman et al., 2010). Highest current velocities were observed at approximately HW-2 (2.2 m $\mathrm{s^{-1}}$) and were coincident with temperature and salinity gradients marking the incoming flood tide (Figure 4.4). Current velocities presented in Figure 4.3a are temporally averaged and therefore do not show the actual maximum as recorded in the raw data.

The implication of high levels of turbulence in addition to high SPM concentrations was that M1 and M2 would potentially be in direct competition. Despite an increase in SPM, increased levels of turbulence may hinder the process of flocculation, and thus uptake of macro-nutrient species to the interstitial water. Furthermore, increased turbulence may provide additional energy to break stronger bonds between macro-nutrient species and the particle surfaces and thus increase the dissolved nutrient concentration.

Near-bed l_K values (averaged over each hour that LabSFLOC and water samples were taken) at HW-2 indicate that turbulence increased (from 83 - 67 μm) with

increasing current velocity, both of which were coincident with the ETM. Maximum near-bed l_K values (84 μm) were found at HW-4, where current velocity values were lowest. Despite the atypical range of l_K values observed, this would indicate calmer conditions.

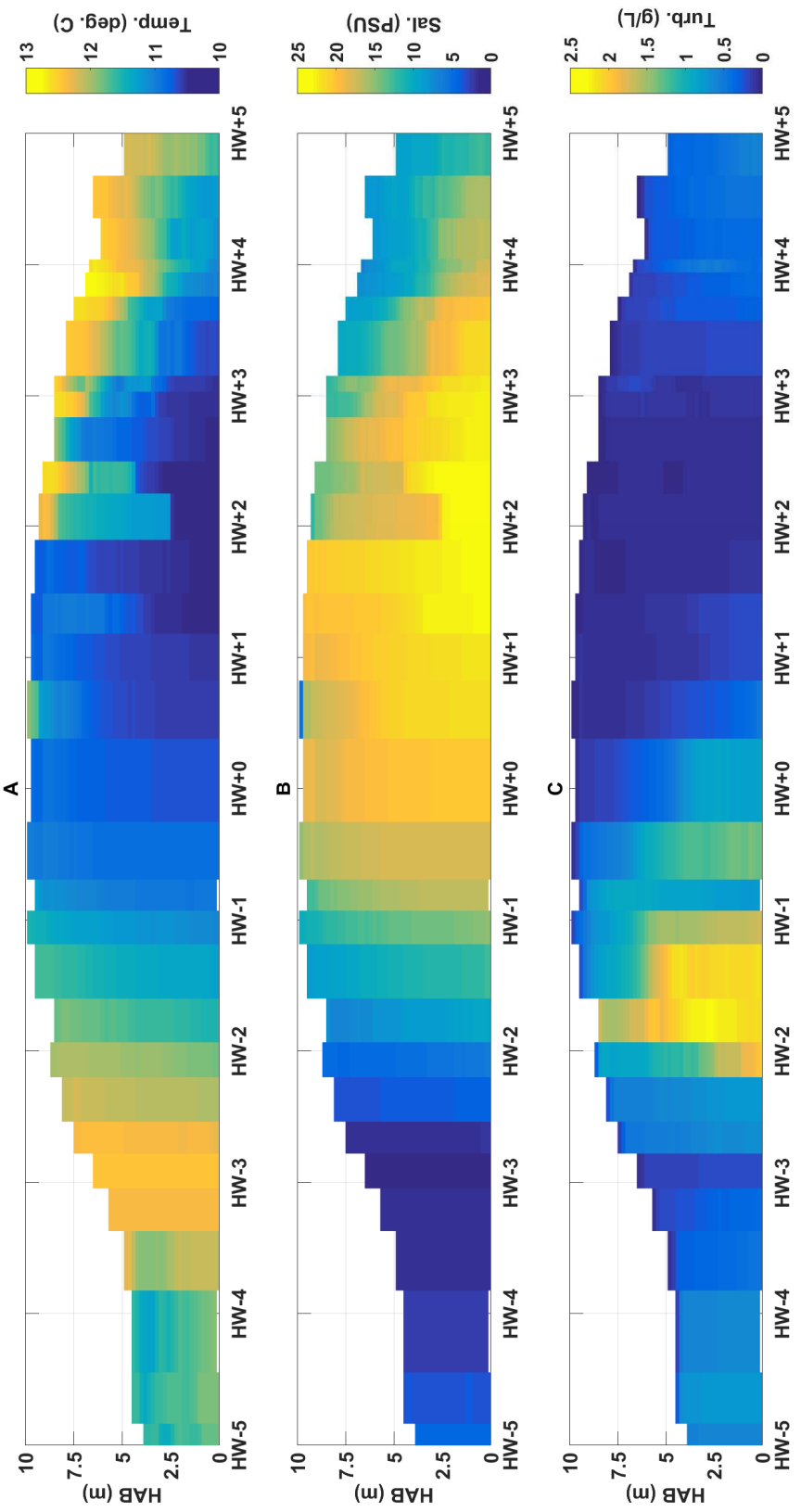

Figure 4.4: *Time series data from the CTD showing temperature (a) salinity (b) and turbidity (c). At HW-3 and HW+2, temperature and salinity gradients were observed at the onset of the flood and ebb tide.*

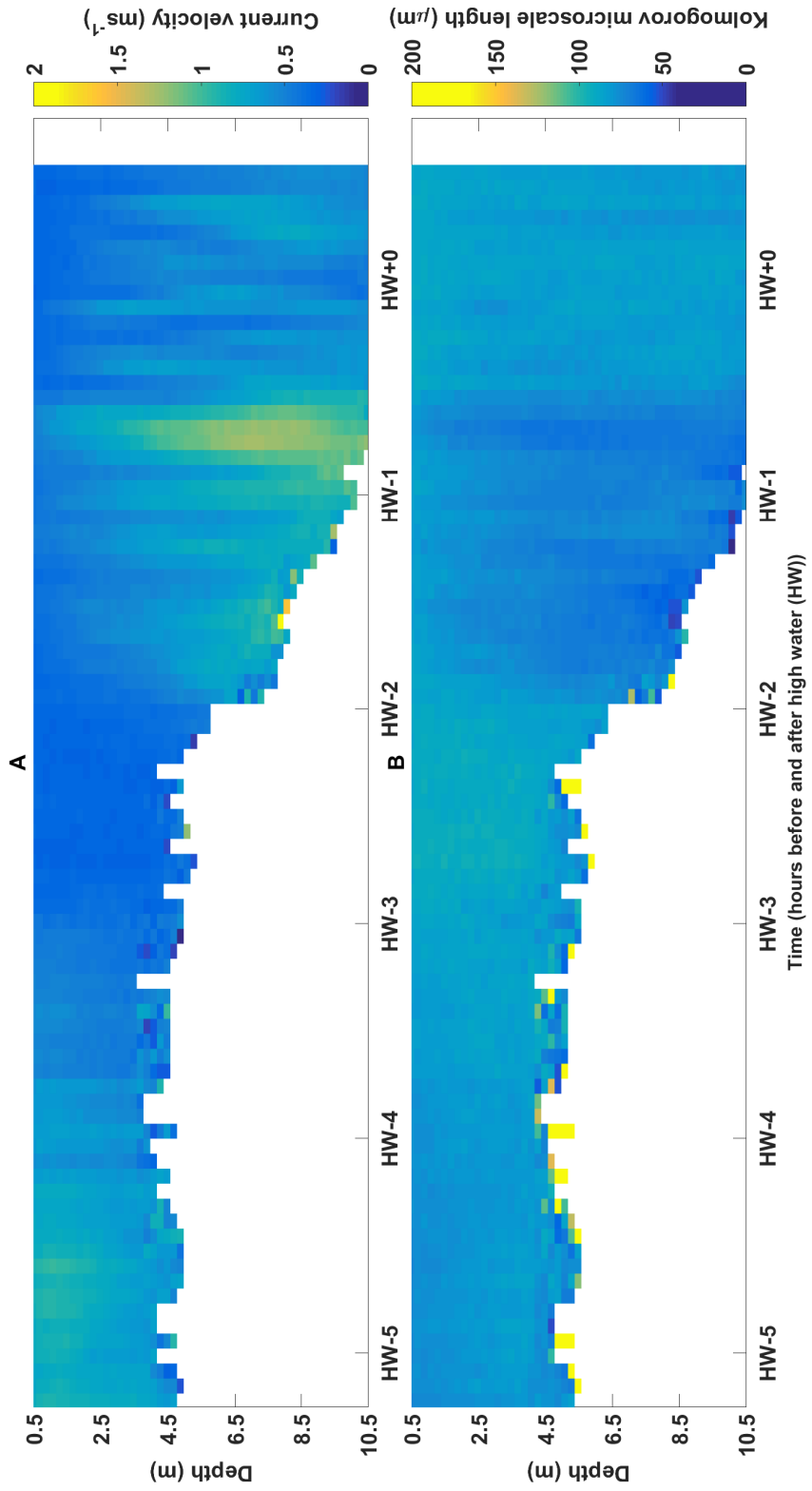

Figure 4.5: *Current velocity (u) and Kolmogorov microscale length (μM) data from ADCP measurements.*

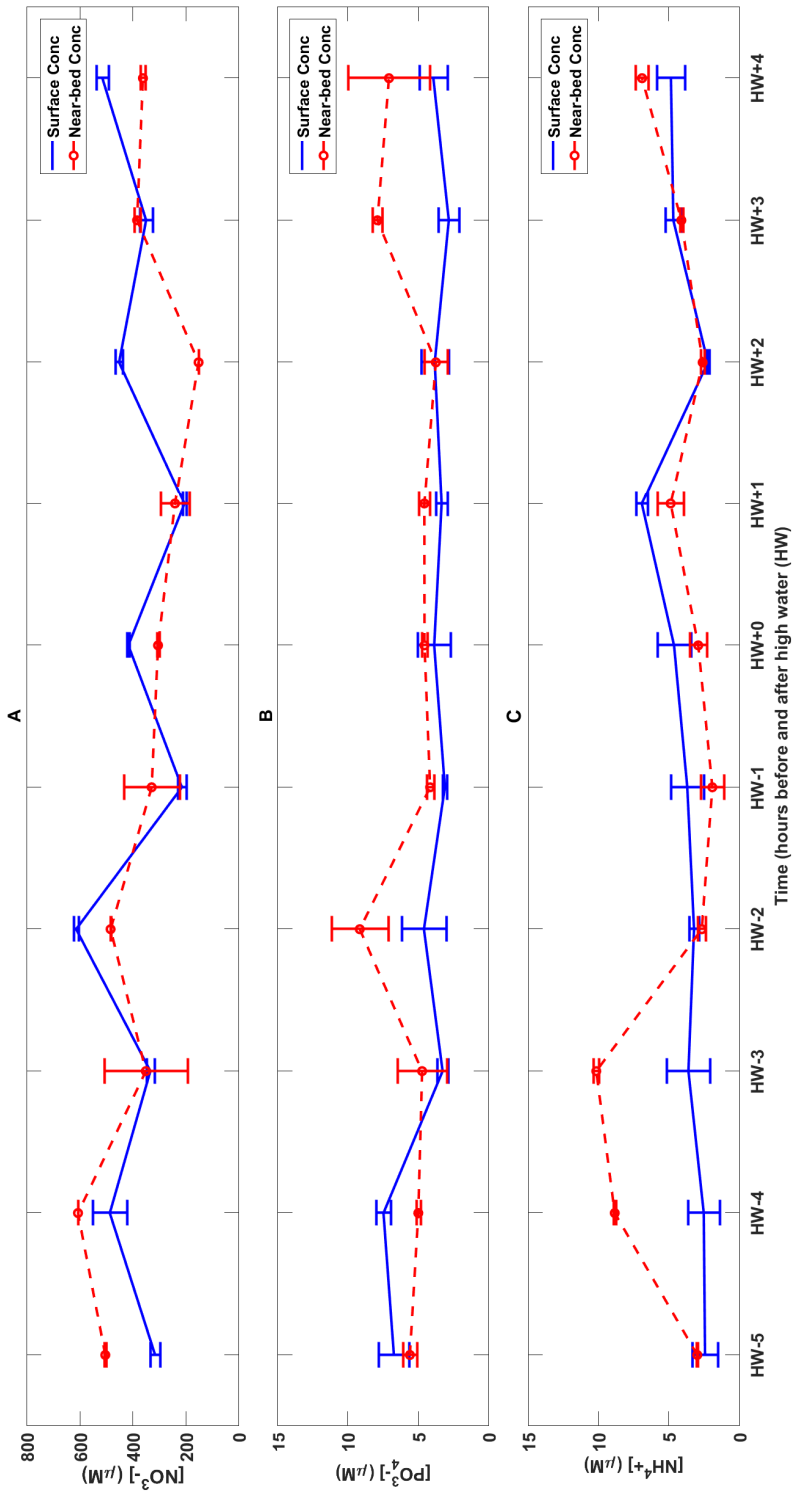

Figure 4.6: *Inorganic macro-nutrient concentrations measured during the Seine estuary sampling campaign. Surface concentrations are marked by the blue solid line, while near-bed concentrations are marked by the dashed red line.*

4.4.2 Nutrient concentrations in the water column

The measured concentrations of NH_4^+, NO_3^- and PO_4^{3-} (mean $\pm$ 1 s.d.) are shown in Table 4.1 for surface and near-bed water samples from HW-5 to HW+4. These concentrations were broadly in agreement with the values reported for the Seine ETM by Garnier et al. (2010). Nitrate was detected in all surface and near-bed water samples (Table 4.1), with maximum concentrations of 613 μM (surface) and 606 μM (near-bed), both at HW-2. Minimum concentrations were 204 μM (surface) at HW+3 and 151 μM (near-bed) at HW+2.

Table 4.1: *Surface and near-bed concentrations of NO_3^-, PO_4^{3-} and NH_4^+.*

	Surface					
	NO_3^+ (μM)	+/-	PO_4^{3-} (μM)	+/-	NH_4^+ (μM)	+/-
HW-5	315	19	6.71	1.09	2.42	0.91
HW-4	486	65	7.45	0.52	2.51	1.11
HW-3	333	15	3.24	0.38	3.60	1.53
HW-2	613	10	4.57	1.57	3.13	0.33
HW-1	214	16	3.08	0.15	3.68	1.16
HW+0	416	5.8	3.84	1.17	4.62	1.20
HW+1	204	6.3	3.31	0.42	6.91	0.40
HW+2	451	15	3.80	0.98	2.22	0.09
HW+3	349	34	2.80	0.74	4.67	0.57
HW+4	514	23	3.90	0.99	4.84	1.00
	Near-bed					
	NO_3^+ (μM)	+/-	PO_4^{3-} (μM)	+/-	NH_4^+ (μM)	+/-
HW-5	506	4.85	5.57	0.49	2.97	0.05
HW-4	606	0.93	4.97	0.15	8.84	0.08
HW-3	350	157	4.70	1.77	10.1	0.21
HW-2	483	0.98	9.14	2.02	2.66	0.28
HW-1	328	105	4.13	0.26	1.90	0.82
HW+0	304	5.13	4.53	0.21	2.90	0.59
HW+1	240	53.4	4.54	0.40	4.87	0.93
HW+2	151	0.17	3.72	0.84	2.59	0.12
HW+3	383	11.6	7.88	0.35	4.11	0.11
HW+4	361	8.83	7.06	2.92	6.89	0.45

The general behaviour of NO_3^- was not consistent with the conservative mixing of NO_3^- with salinity (Loder and Reichard, 1981), as shown in Figure 4.7, indicating addition or removal processes. Linear regression analysis results cal-

culated a near-bed r-squared value of 0.54 ($y = -11.01x + 532.2$), and a surface r-squared value of 0.05 ($y = -4.95x + 436.8$). Conservative mixing and mixing diagrams such as shown in Figure 4.7, are an indication of the processes affecting a nutrient. That is, if the distribution of a nutrient is subject to physical mixing processes alone, there should be a linear relationship between salinity and the nutrient (Chester, 2000; Jickells et al., 2015). Where the relationship deviates from a linear line, this can indicate addition or removal processes (Jickells et al., 2015). In this case, results demonstrated both addition and removal processes occurring. Linear regression analysis for PO_4^{3-} and NH_4^+ with salinity were also performed with no indication of conservative behaviour for either macronutrient.

Results of analysis of variance (ANOVA) are presented in Table 4.2. ANOVA showed that there was a significant temporal difference (p = $<$0.05) in NO_3^- concentration for both the near-bed and surface water samples at HW-2 (highest), compared with HW-1. Concentrations of NO_3^- at HW-2 coincided with the highest current velocity and SPM concentrations (4.5 and 2.0 g L^{-1} for near-bed and surface waters, respectively), as well as the lowest Kolmogorov microscale length values, whilst at HW-1, significantly lower NO_3^- concentrations coincided with the maximum particle settling velocity. The significant decrease in surface and near-bed NO_3^- concentrations were coincident with a significant increase in salinity indicating the dominant influx of typically low-nutrient saline water. This significant decrease could also be associated with the uptake of interstitial water during flocculation at HW-2 and the subsequent settling of particles before HW-1, as per Mechanism 1 described in chapter 1.

Concentrations of NH_4^+ varied through the sampling period (Table 4.1). Near-bed concentrations increased from 2.98 μM in the first sample to a maximum of 10.14 μM at HW-3. This maximum occurred one hour prior to the maximum

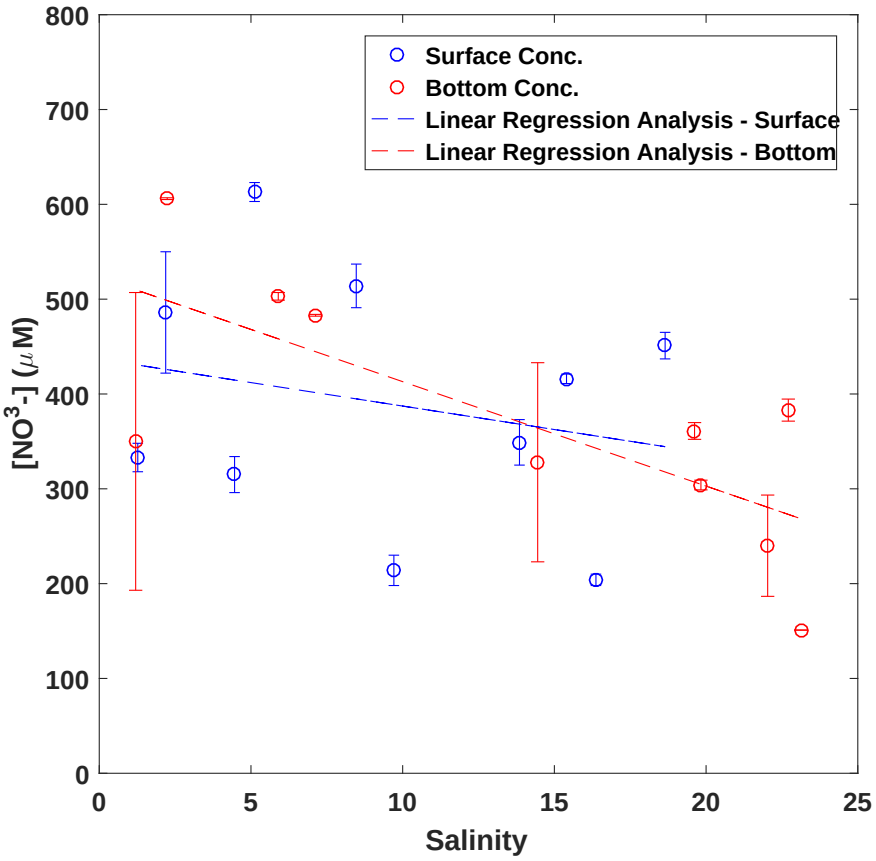

Figure 4.7: *Observed salinity and nitrate concentrations for sampling conducted in the ETM. Conservative mixing is identified by a linear relationship between salinity and nitrate.*

SPM concentration and the onset of the salt water intrusion. It was also coincident with a change in current direction of approximately 100 degrees at HW-3. The near-bed NH_4^+ maximum was out of phase with the SPM maximum and formation of the ETM. This behaviour was not observed in previously reported field studies, where dissolved NH_4^+ correlated with SPM (Morin and Morse, 1999; Fitzsimons et al., 2006); however, these studies were not depth-resolved. It is proposed that a benthic NH_4^+ flux occurred prior to formation of the ETM as a result of the stresses imposed by the change in current direction, while a more strongly-bound PO_4^{3-} fraction was desorbed from particles ejected into the water column once the ETM had formed (Froelich, 1988), as indicated by the near-bed concentration maximum (9.14 μM) at HW-2. This is consistent

with a study completed in the Gironde Estuary, France, by Robert et al. (2004), who examined the mobilisation of metals and macro-nutrients at the continuum of the estuarine turbidity maximum. The study found that an intense period of metal mobilisation at the near-bed as a result of a fluid mud layer (defined as an SPM concentration of between 50 - 500 g L^{-1}). The report also describes the 'soft mud' layer, which is generally re-worked at the spring-neap time scale. The soft mud layer is typically nitrate-free and ammonium-rich, providing a significant source (Robert et al., 2004). Additionally, Lillebø et al. (2004) reported the release of PO_4^{3-} at slack water associated with increased contact between water particles and the mud. Subsequent peaks in the NH_4^+ concentration may have indicated a flux from a slow-release particulate fraction, where repartitioning of occluded NH_4^+ occurred to replace earlier NH_4^+ loss from the exchangeable fraction (Morin and Morse, 1999).

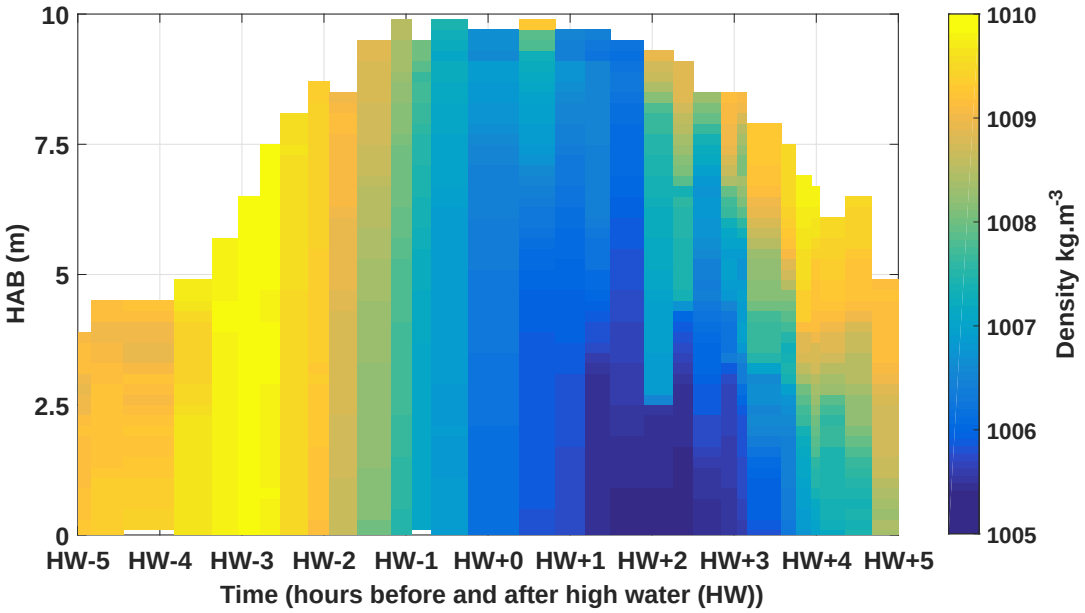

Figure 4.8: *Calculated water density for the Seine Estuary during the spring sampling campaign. Densities indicate the riverine water observed at HW-3 and again at HW+3.*

Additionally, consideration of the density of the water column allowed a comparison between water samples collected at HW-3 and HW+3, which demonstrated similar temperature and salinity values, albeit where HW-3 was well-mixed, and

Surface Sample	PO_4^{3-} Mean	Grouping	NO_3^-. Mean	Grouping	NH_4^+ Mean	Grouping
HW-5	5.57	B C D	314	E	2.41	B
HW-4	4.96	C D	486	B C	2.51	B
HW-3	4.69	C D	333	E	3.59	A B
HW-2	9.14	A	613	A	3.13	B
HW-1	4.13	D	214	F	3.69	A B
HW+0	4.54	C D	416	D	4.62	A B
HW+1	4.45	C D	204	F	6.91	A
HW+2	3.72	D	450	C D	2.22	B
HW+3	7.88	A B	348	E	4.67	A B
HW+4	7.05	A B C	514	B	4.85	A B
HW-5	6.705	A	537	A B	2.98	D E
HW-4	7.448	A	587	A	8.84	A
HW-3	3.245	B	442	B C	10.14	A
HW-2	4.573	B	601	A	2.65	D E
HW-1	3.073	B	190	E F	1.86	E
HW+0	3.838	B	301	D E	2.9	D E
HW+1	3.303	B	240	E F	4.87	C
HW+2	3.797	B	162	F	2.6	D E
HW+3	2.805	B	382	C D	4.11	C D
HW+4	3.473	B	452	B C	6.9	B

Table 4.2: *Tukey's test results for an analysis of the significance of each sample collected for near-bed and surface water samples.*

HW+3 was stratified (see Figure 4.8). The similarity in density of the less saline water is consistent with riverine input; however, the contrast in NH_4^+ concentrations, both between HW-3 & HW+3 and near-bed and surface concentrations, indicates addition or removal processes, such as the benthic input discussed previously.

A second near-bed NH_4^+ peak occurred during the period of maximum measured salinity, which may represent desorption of a more strongly-bound, slow-release NH_4^+ fraction (Morin and Morse, 1999). This is in line with M3 outlined in chapter 1.

Mechanisms 1 (concentration) and 3 (salinity), were identified as potential mech-

anisms for the release of NH_4^+ to the water column. The dominant mechanism was proposed to be SPM concentration due to a peak in NH_4^+ shortly after the SPM concentration maximum.

Phosphate (PO_4^{3-}) concentrations were in the range 3.7 - 9.1 μM for surface water samples and 2.8 - 7.5 μM for near-bed water samples (Table 4.1). The maximum PO_4^{3-} concentration was reached at HW-2 in the near-bed water, coincident with the maximum SPM concentration. Analysis by ANOVA revealed that there was a significant temporal difference (p = $<$0.05) in PO_4^{3-} concentrations prior to HW-3 for near-bed samples. These results are broadly in agreement with the reported rapid release of PO_4^{3-} due to ion exchange from suspended sediment particles, at the onset of the observed ETM and salinity gradients on the flood tide (Froelich, 1988; Gardolinski et al., 2004). ANOVA analysis also revealed a significant spatial difference between the near-bed (2.66 μM) and surface (5.13 μM) concentrations of PO_4^{3-} at HW-4 (surface: 7.45 μM, near-bed: 4.96 μM) and HW-2 (surface: 4.573 μM, near-bed: 9.14 μM) . This statistically significant result was co-incident with stratified water as a result of the ebb tide and subsequent dominance of riverine flow over tidal flow (see Figure 4.4), indicating the affect of stratification on the vertical transport of nutrients. SPM concentrations during this time were homogeneous and therefore suggest that changes in macro-nutrient concentrations are a result of hydrodynamic processes, rather than micro-scale physical processes.

4.4.3 An overview of near-bed particle characteristics in the ETM

Maximum particle size measurements decreased by approximately 40% 1 h before the maximum occurred (HW-3) (from 724 μm to 386 μm), coincident with the peak in NH_4^+. The decrease in floc size and count at HW-3 coincided with a decrease in current velocity and slack water, indicating unsuitable conditions for particle aggregation and/or suspension, as well as the settling of larger macroflocs

prior to high water.

Minimum floc sizes were consistent throughout the sampling period, at approximately 30 μm. The absolute minimum occurred at the same time as the minimum SPM concentration and settling velocity, shortly after high water (HW+2). During this time, conditions were quiescent, with flocs in suspension settling slowly. Shortly after high water, the maximum floc size for each sample decreased to approximately 20% of the floc size samples recorded for HW-2 and HW-1 (from 920 μm at HW-2, to $\approx$ 132 μm at HW+1). Average floc size also remained consistent throughout all samples. The prolonged period of slack water (relative to the ebb) is synonymous with the tidal asymmetry of the Seine estuary and would only allow for fine, light materials to be held in suspension, either by salinity and/or temperature gradients (Figure 4.4), or low velocity currents as the ebb tide current velocity starts to increase (Brenon and Le Hir, 1999).

The floc count measured for each profile (from the 400 mm^3 LabSFLOC sample chamber) was broadly consistent with recorded SPM concentrations; floc count increased with SPM concentration, as would be expected (Dyer, 1997; Manning and Dyer, 1999; Manning et al., 2006). The maximum floc count (147) and broadest range (892 μm) of floc sizes occurred at HW-2, where the SPM concentration was highest, and coincided with the maximum near-bed PO_4^{3-} concentration. This condition is in contradiction to the proposed Mechanism 1 in which it was hypothesised that the increase in flocculation would remove interstitial water from the water column concentrations. Instead, this suggests that the increase in SPM concentration serves as a source of PO_4^{3-}, and that flocculation has no significant effect on macro-nutrient concentration. Figure 4.9d shows that the floc size reached a maximum of 920 μm, with an average floc size of 132 μm. The flocs recorded had an average settling velocity of 2.8 mm s^{-1} and an average

effective density of 642 kg m^{-3}. The porosity of flocs ranged between 0 and 99%, with an average porosity of 47%. A floc of 99% porosity will typically be solid with little interstitial water and have a fast settling velocity. Conversely, a floc of low porosity will settle slowly and contain large amounts of interstitial water. The average value of 47% implies roughly half of the flocs contained interstitial water, and half did not. This implies that a number of the large particles were not capable of retaining interstitial water and acting in accordance with Mechanism 1. This would further reduce the magnitude of any of the proposed Mechanisms.

The distribution of flocs in Figure 4.9d shows that the larger flocs had a lower effective density that is typically indicative of large, stringy flocs created with the increased SPM concentration. Meanwhile, the smaller flocs, usually with faster settling velocities, have much higher effective densities and could indicate grains of entrained sand, or tightly bound flocs. Flocculation theory usually indicates that for pure-mud suspensions, large, low-density flocs tend to settle quicker than microflocs, even when the latter have a relatively high effective density (Manning et al., 2006). When the ratio of mud:sand falls in favour of sand, the microflocs consistently settle quicker than the larger macroflocs (Winterwerp and van Kesteren, 2004).

Statistics for this sample of flocs (HW-2) show that microflocs accounted for 81% of the total population, with an average settling velocity of 2.72 mm s^{-1} and an average effective density of 843 kg m^{-3}. Macroflocs accounted for 19% of the population, with an average settling velocity of 3.58 mm s^{-1} and an average effective density of 100 kg m^{-3}. In this case, the higher average settling velocity of the macroflocs indicates that the flocs conform to the theory that larger macrofloc settle quicker. The maximum settling velocity of the microflocs (9.10 mm s^{-1}) could still indicate the presence of sand grains within the flocs.

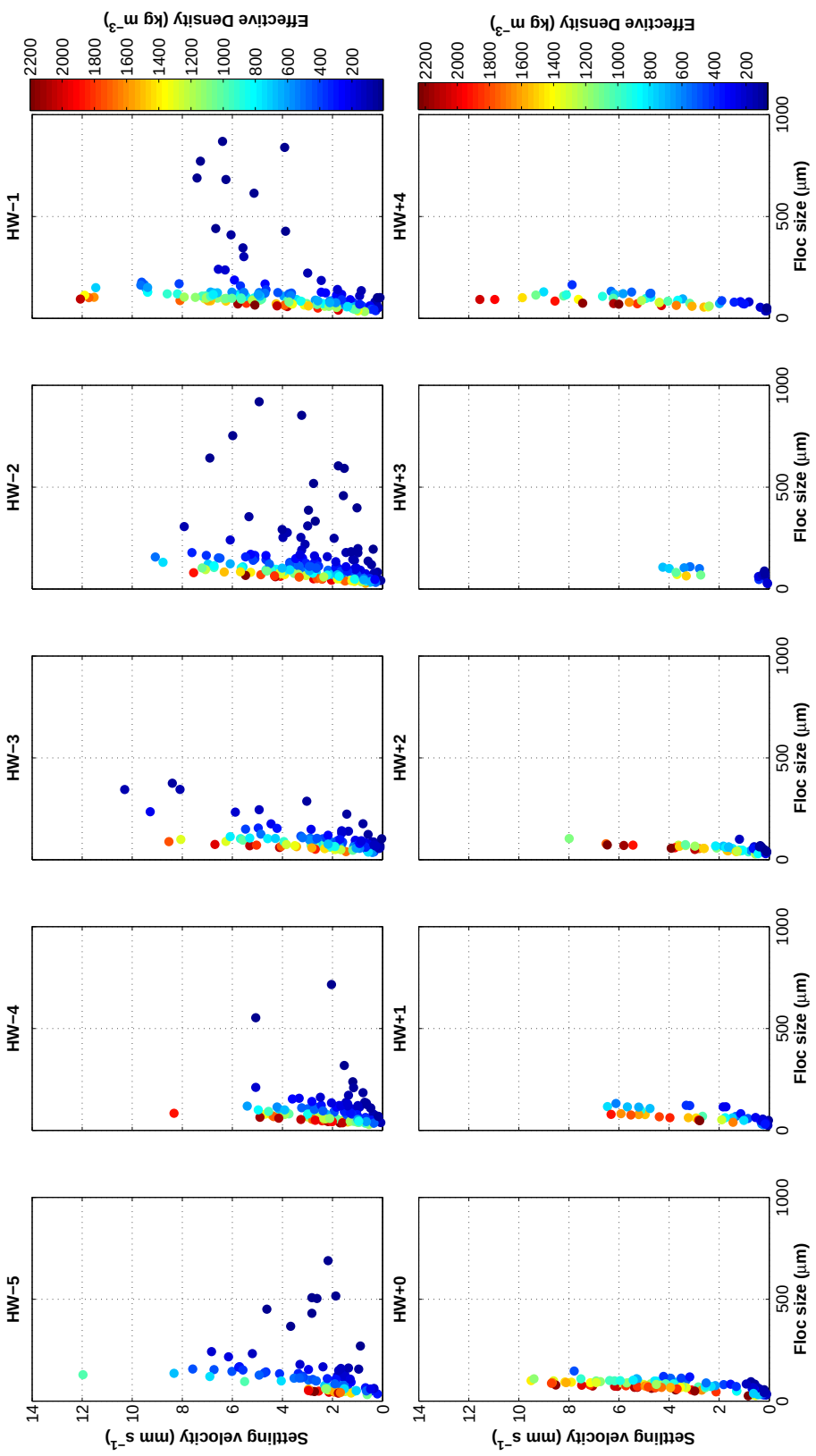

Figure 4.9: *Scatter plots showing particle size verses settling velocity. The colour scale represents the effective density of each particle.*

4.5 Conclusions

The primary aim of this chapter was to determine whether the hypothesised mechanisms described in chapter 1 could be observed in field data.

A 10 h sampling campaign was conducted measuring the required variables to determine hydrodynamic, chemical and particle characteristics. Measurements were taken at a sufficient temporal scale so as to capture the micro-scale processes and changes occurring throughout the tidal cycle. The results obtained in this sampling campaign were taken at one location and therefore do not consider the effects of horizontal advection. Instead, this chapter highlights instances where sediment-nutrient behaviour may be explained by one, or several, of the mechanisms outlined in section 1.2 (chapter 1).

Surface and near-bed concentrations of NO_3^- were seen to peak at HW-2, however, as mentioned in section 4.4.2, this is likely a result of advection, as any benthic fluxes of NO_3^- are typically swamped by natural water concentrations, as reported by Knox et al. (1986). Concentrations of NO_3^- were lower during the ebb tide which was consistent with a period of saline water diluting the fresher, nitrate-loaded river water. As the salt water began to retreat, NO_3^- concentrations increased again, confirming that NO_3^- is controlled by the physical mixing processes, rather than micro-scale sediment.

Ammonium concentrations saw a peak of 10.14 μM (near-bed) at HW-3 and a statistically significant decrease in near-bed NH_4^+ at HW-2 ($p = 0.05$) supporting the evidence reported by Robert et al. (2004); Fitzsimons et al. (2006) that benthic fluxes are a significant source of NH_4^+ to the water column. This condition was, however, contradictory to all proposed mechanisms as the flux was not a result of flocculation processes, increased salinity, or increased turbulence.

Concentrations of NH_4^+ were different at the surface, with two peaks in surface NH_4^+ recorded at HW-1 and HW+1, before decreasing significantly. The surface peak recorded at HW-1 was coincident with the formation of the ETM and an increase in SPM concentration from the bed, possibly indicating a vertical transport of NH_4^+ as a result of and during the ETM, signifying the importance of hydrodynamic processes such as turbulence on the distribution on macro-nutrients in the water column. The maximum concentration occurred one hour after the SPM concentration maximum and reflected the desorption of an exchangeable NH_4^+ fraction via exchange with seawater cations in alignment with M3. This scenario is consistent with previous resuspension studies (Morin and Morse, 1999; Fitzsimons et al., 2006).

Surface concentrations of PO_4^{3-} peaked at HW-3, with the near-bed peak occurring at HW-2 and coincident with the maximum SPM concentration indicating that the hypothesised M1 (flocculation and disaggregation) did not have a role in PO_4^{3-} concentrations, but that the increase in SPM concentration provides a significant portion of total P to the water column via desorption processes (Fang, 2000; Deborde et al., 2007; Nemery and Garnier, 2007; Shen et al., 2008). The broad range of floc sizes (820 μm) suggest that increased SPM concentration, in conjunction with turbulent conditions in the ETM, outweigh the opportunities for a decrease in PO_4^{3-} due to trapping of macro-nutrients in interstitial waters.

Stratification was identified to be a key factor in the distribution of macro-nutrients in the water column. At HW+3, stratified waters yielded a statistically significant ($p = 0.05$) difference in near-bed and surface concentrations of PO_4^{3-}, NO_3^- and NH_4^+. SPM concentrations at this time were homogeneous within the water column and highlight that variation in the water column of macro-nutrient concentrations was a result of hydrodynamic processes. Turbulence, as a micro-scale process was likely not occurring during this time and was

not recorded using the ADCP due to insufficient memory to record such high resolutions. Stratification in the water column and the statistically significant differences in near-bed and surface macro-nutrient concentrations confirms the role of turbulence in the distribution of macro-nutrients in line with results presented by numerous reports (Ward and Twilley (1986); Geyer (1993); Falco et al. (2010); Maar et al. (2010); Wild-Allen et al. (2013).

This study of the relationship between micro-scale physical processes, such as flocculation and turbulence, and nutrient distributions in the Seine estuary has demonstrated the variance in effect of each Mechanism on different nutrient species.

For example, M1, an exchange mechanism describing the uptake of macro-nutrients into interstitial waters as a result of flocculation, was not observed in the Seine estuary. Instead, increased SPM concentrations were coincident with increased levels of PO_4^{3-}, with a proposed mud-water interface benthic flux of NH_4^+, as per Robert et al. (2004). Nitrate was not subject to micro-scale sedimentary processes but was affected by micro- to meso-scale hydrodynamic processes such as tides, mixing and stratification. PO_4^{3-} and NH_4^+ were also affected by micro- to meso-scale sedimentary processes in a period of stratification at HW+3.

NH_4^+ was dominated by M2; the ion exchange between cations and anions associated with salt water. Here, an increase in SPM concentration played a secondary role in that increased SPM concentration provided greater opportunity for ion exchange in the presence of salt water. PO_4^{3-} on the other hand was entirely dominated by M1, with turbulence potentially playing a secondary role.

Micro-scale physical processes, such as current velocity and turbulence, were controlling factors in the generation of large, stringy flocs at HW-2, primarily by

an increase in SPM concentration (up to 2.2 g L^{-1}). High levels of turbulence (l_k $\approx$ 70 μm) constrained the maximum floc size and generated larger numbers of smaller particles.

Finally, concentrations of NO_3^- did not demonstrate a pattern or relationship with floc or SPM characteristics, and hence, any of the mechanisms outlined in chapter 1. It is proposed that any benthic fluxes of NO_3^- would be negligible due to the magnitude of naturally occurring concentrations in the water column (Bale et al., 1985). NO_3^- showed conservative behaviour during the sampling day; concentrations of NO_3^- decreased with increasing salinity likely as a result of dilution by salt water, and increase during periods of fresher water (Knox et al., 1986) whereby nutrient-laden river water would be advected downstream.

Chapter 5

Sediment-Nutrient Interactions in the Tamar Estuary, U.K.

'Why are we sticking these things in the water so early in the morning?'

Jamie Pidduck

5.1 Introduction

This chapter presents and discusses the results of field campaigns conducted in the Tamar estuary, U.K. Three field campaigns to determine the hydrodynamic conditions and nutrient concentrations were conducted for approximately half a tidal cycle (one ebb and one flood tide) in spring (March), summer (June) and autumn (September) 2011. The aim of this work was to examine sediment-nutrient relationships in the field on both a seasonal and a high-resolution temporal scale. The objectives of this campaign were as follows:

- to make *in situ* hydrodynamic, particle/floc and chemical measurements in a moderately turbid estuary;
- to collect comparative seasonal nutrient and sediment characteristics;
- to analyse particle and nutrient data for relationships relating to theories presented in the hypotheses.

The objectives of this chapter are similar to those in chapter 4 with the added addition of a seasonal component to consider the implications of increased and decreased riverine run-off, as well as different sediment types. The Tamar estuary has lower average SPM concentrations and current velocities, but is similar to the Seine estuary in that an ETM has also been observed and measured.

5.2 Site Description

The Tamar estuary (Figure 5.1) is a flood-dominant, meso/macrotidal (Davies, 1964) drowned river valley located in the south-west of England (Dyer, 1997). It is the product of sea level rise during the Flandrian Transgression of the late Holocene (12,000 years ago - present). It forms the boundary between the counties Devon and Cornwall, both of which are known for their fishing, mining and farming industries (Langston, 1980; Readman et al., 1987; Clason et al., 2004;

Mighanetara et al., 2009). The Tamar estuary is also host to one of three of the U.K.'s Royal Naval bases (Devonport), as well as several commercial shipping and passenger transport companies, highlighting the importance of the estuary as a commercial port. Commercial fisheries are also based in the lower estuary with numerous marinas and a strong sailing community uses the length of the River Tamar.

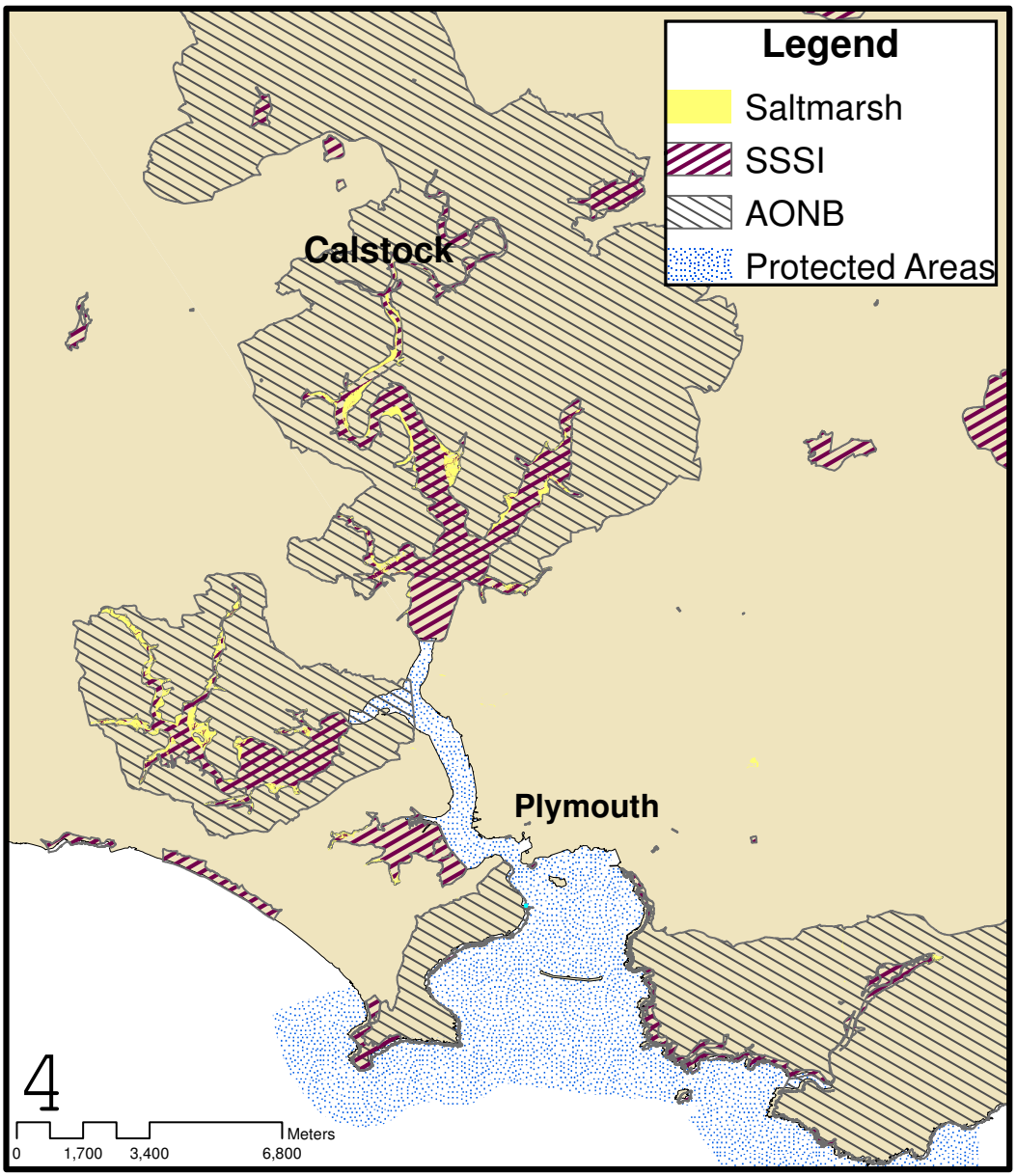

Figure 5.1: *An overview map of the Tamar Estuary, U.K., including protected areas and notable features.*

Much of the water, including a large portion of the lower brackish estuary is a

protected area, with large portions of the north estuary marked as Areas of Outstanding Natural Beauty (AONB) and a Site of Special Scientific Interest (SSSI). The Tamar-Tavy SSSI comprises the upper reaches from the Tamar Bridge to the limit of tidal influence of the Rivers Tamar and Tavy, and has been invoked to protect a series of protected birds, as well as a rare plant.

Historically, the land surrounding the Tamar estuary and its tributaries has been used for mining and agriculture (Mighanetara et al., 2009). Mining was conducted for several centuries with the extraction of tin, copper, lead, silver, arsenic and granite as the primary products from the river source, Dartmoor (Kavanagh et al., 1997; Hamilton, 2000). Products were transported via barge along the Tamar estuary to larger commercial ships, further signifying its long-standing importance as a port in the U.K. At the start of the 20^{th} century, mining activity reduced and animal grazing and agriculture became the major influences on terrestrial inputs to the estuary, with approximately 75% of the Tamar catchment area land cover designated as agriculture (National Rivers Authority, 1996; Tappin et al., 2012). Both agriculture and mining still have an effect on the nutrient biogeochemistry of the Tamar estuary (National Rivers Authority, 1996; Tappin et al., 2012).

Of the 915 km^2 estuarine catchment area (Environment Agency, 1999), the river Tamar forms the largest portion and has a total length of 75 km, with 9 additional sub-catchments (Tappin et al., 2012). The limit of tidal intrusion to the river Tamar is approximately 31 km, and reaches Weir Quay near Gunnislake (Manning et al., 2006). Tidal height in the estuary ranges between 2.2 m - 4.7 m during neap and spring tides, respectively, and the entire estuary has an average river discharge of 22 $\text{m}^3\ \text{s}^{-1}$ (Dyer, 1997). Winter values of river discharge have been reported to reach 70 $\text{m}^3\ \text{s}^{-1}$, with values falling to around 3 $\text{m}^3\ \text{s}^{-1}$ in the summer months (Bale et al., 1985).

Bathymetrically, the upper portion of the estuary is narrow (40 - 200 m) and the mean depth reduces to between 1 - 2 m at low water. In the lower portion of the estuary, the channel widens to 900 m with depths of between 18 - 25 m in the navigation channels. The shape of the estuary and the friction effects produce asymmetry in the tidal curve and a flood current dominance at the head of the estuary (George, 1975). Sampling was conducted close to the limit of the tidal intrusion, at Calstock (Figure 5.2). At this location, current velocities on the ebb tide peak at approximately 1 m s^{-1}, with flood current velocities reaching a maximum of 0.8 m s^{-1} (Uncles et al., 2010). Calstock also falls within the tidal trajectory of the ETM (Manning and Bass, 2006). Within the ETM, SPM concentrations range between 0.1 - 8.6 g L^{-1}, with greatest concentrations occurring during spring tide conditions (McCabe, 1991; Manning and Dyer, 2007). The SPM concentrations and hydrodynamic conditions experienced at Calstock make it a suitable sampling site.

Suspended, bed and intertidal sediment in the Tamar estuary consists largely of silt and clay particles with an increasing fraction of silt and clay from the mouth of the estuary, to the head of the river Tamar (60% to 99% of dry weight) (Uncles and Stephens, 1993). Previous studies of flocculation properties have been conducted in the Tamar estuary, with many being conducted in Calstock (Dyer et al., 2002; Fennessy et al., 1994; Manning et al., 2006; Uncles et al., 2010). Floc sizes of between 15 $\mu\mathrm{m}$ -1 mm have been recorded in the Tamar estuary, with settling velocities of up to 9 mm s^{-1} (Dyer et al., 2002; Uncles et al., 2002; Manning and Dyer, 2007; Uncles et al., 2010). Manning and Dyer (2007) divided the floc population into two groups: microflocs (up to 160 $\mu\mathrm{m}$) and macroflocs (greater than 160 $\mu\mathrm{m}$). Microflocs are considered to be the building blocs of larger macroflocs (Eisma, 1986) and consist of mineral particles and organic matter. Macroflocs, meanwhile, are a fragile composition of several mi-

croflocs and are formed in water under conditions of viscous flow (Eisma, 1986).

Figure 5.2: *The sampling site at Calstock is marked by the yellow pin. Image from Google Earth.*

Of the data collected in the Tamar, and in particular, around Calstock, the general composition of the SPM is composed of macroflocs, indicating conditions suitable for flocculation. Manning et al. (2006) proposed that the greater proportion of organic matter in the sediment is responsible for the greater proportion of macroflocs in this region. Furthermore, Manning and Dyer (2002) reported that SPM in the ETM has around 5 - 7 times the concentration of carbohydrate than regions outside the ETM, which may also affect flocculation processes in the estuary.

5.2.1 Nutrient Concentrations in the Tamar Estuary

Reported annual mean concentrations of NO_3^- in the Tamar Estuary are between 147 - 255 μM (Knox et al., 1986; Tappin et al., 2012), with values varying

(a) *The Van Dorn water sampler.* ***(b)*** *CTD/LISST sampling.*

Figure 5.3: *Images of sampling instrumentation deployed in turbid water during sampling conducted at Calstock in autumn 2011.*

according to location within the estuary. The upper estuary is subject to larger variation, with typically higher concentrations, due to short-term changes in parameters such as river run off (Morris et al., 1981; Knox et al., 1986), short flushing times of estuarine waters and restricted levels of primary productivity (Morris et al., 1985). The lower estuary, meanwhile, demonstrates lower concentrations with less variability. Concentrations are also subject to seasonal variation.

Tappin et al. (2012) highlighted that NO_3^- concentrations were highest during winter, reflecting increased river run off. Previous studies have indicated that NO_3^- in the Tamar estuary behave conservatively (Morris et al., 1981, 1985; Knox et al., 1986). Any variation from the conservative behaviour occurred in lower salinity waters and was attributed to short-term variability in the composition of fresh water entering the system (Morris et al., 1981). Furthermore, at the lower end of the estuary (close to the mouth), concentrations were consistently lower than for the upper estuary (near Gunnislake), across all seasons.

Despite the implementation of directives to control the input and concentration of NO_3^- in coastal waters, NO_3^- has not shown a significant decrease in the past 30 years, indicating the difficulty in controlling diffuse inputs of N to the system (Littlewood and Marsh, 2005; Maier et al., 2009; Tappin et al., 2012). Prior to the introduction of legislation to improve water quality across the U.K., algal blooms were observed in the Upper Tamar Lake of the River Tamar catchment area (Environment Agency, 1999; Tappin et al., 2012). Analysis of NH_4^+ data by Tappin et al. (2012) highlighted annual mean concentrations of between 1.94 - 7.58 μM, with a maximum value of 15.2 μM. Similar values were reported by Knox et al. (1986), with maximum values occurring in the summer months. The minimum and maximum measurements of NH_4^+ demonstrate a large range and are typical of U.K. estuaries (Maier et al., 2009; Tappin et al., 2012).

Tappin et al. (2012) evaluated concentrations of PO_4^{3-} in the Tamar estuary across a 30 year period. Mean concentrations of PO_4^{3-} were between 1.38 - 3.44 μM. There were also intermittent peaks of approx. 9 μM between 1975 - 1991. Fewer peaks were experienced in the later decades, either as a result of the introduction of directives to prevent nutrient pollution, or a coarser temporal sampling regime (Bowes et al., 2009; Neal et al., 2010; Tappin et al., 2012). Tappin et al. (2012) also highlighted that PO_4^{3-} concentrations have decreased over the past few decades; also likely a result of the implementation of EU directives such as the Water Framework Directive (WTD), including the Nitrate Directive, and the Urban Waste Water Treatment Directive (UWWTD). Morris et al. (1981) also measured concentrations of PO_4^{3-} between 0.3 - 1.76 μM, with higher concentrations occurring during spring and summer months. The concentrations recorded by Morris et al. (1981) were lower than those evaluated by Tappin et al. (2012); this is likely a result of measurements being taken at a different location. The nature of the Tamar estuary means that phosphate concentrations are lower than those found in more populous areas, such as the

Thames (Neal et al., 2010; Tappin et al., 2012).

5.3 Methodology

The methods used in the Tamar estuary were as described in chapter 3 with a few variations (listed below). The same instruments were used throughout. Water samples collected for the analysis of nutrients were labelled with T for surface concentrations and B for near-bed concentrations. The number of the sample corresponded to the hour on which the sample was collected (T01 = 0900 surface sample; B01 = 0900 near-bed sample).

- During the sampling conducted in March 2011, samples were filtered using a hand-pump, rather than the vacuum pump. It was decided during this campaign that the hand-pump was inefficient and sampling could not be conducted at regular intervals, as planned. Subsequently, filtration in June and September was done by vacuum pump, thus reducing the time to filter water samples between collections.

- The times and number of samples collected changed with conditions on the day; fewer hours of daylight in March prevented sampling late into the evening, while power issues (invertor failure) during June lead to a reduced number of samples being collected in the morning.

- LabSFLOC instrumentation was not used during any of the Calstock sampling campaigns due to the lack of electrical power in the field.

5.4 Results and Discussion

This section details the results obtained during the three field campaigns conducted in the Tamar estuary in 2011. Results are presented and discussed on a month-by-month basis, followed by a comparison of the three months.

5.4.1 Weather and river flow data

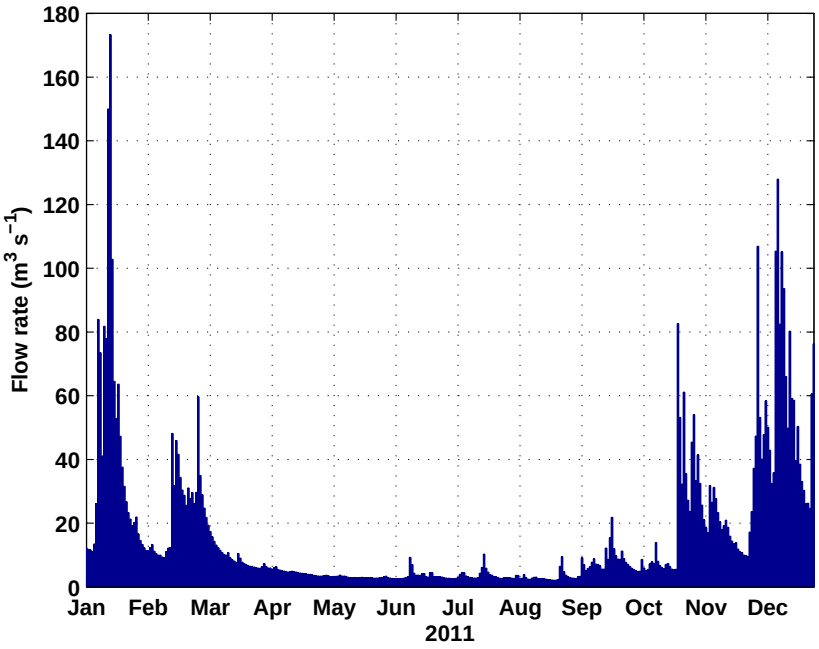

Figure 5.4: *Flow data for the Gunnislake tidal station (#47001) as collected by the CEH (Wallingford, Oxford). Gunnislake is located upstream of Calstock and was the closest flow gauge available.*

Discharge of the River Tamar was measured by the Environment Agency (EA) at the gauging station located at Gunnislake (#47001) and reported to the National River Flow Archive (NRFA), maintained by the Center for Ecology and Hydrology (CEH) in Wallingford (downloaded from the CEH website: http://www.ceh.ac.uk/data/nrfa). Data were provided as average daily flow in $\mathrm{m}^3\ \mathrm{s}^{-1}$. Weather data, including temperature, rainfall and wind speed, were obtained from Plymouth University weather archive (http://www.plymouth.ac.uk/metnet). Measurements were taken at Plymouth University campus and were used as an overall picture of the weather experienced on the day, and the week prior to sampling.

River flow data for 2011 is presented in Figure 5.4. Data presented is the mean value for each day of flow measurement. A typically wet winter lead to high flows during January and February, with maximum values of 173.3 and 59.68

$m^3\ s^{-1}$, respectively. The summer period showed lower flow with peaks of around 12.7 $m^3\ s^{-1}$ in June and July, before rising again in the winter months (November and December).

Along with tidal range, river flow data is a useful indicator of the likely residence times of SPM and nutrients (Uncles et al., 2002), as well as the relative importance of internal processes. Uncles et al. (2002) reported that in large, slowly-flushed estuaries, the internal processes of SPM resuspension, settling and accumulation were more important than in faster-flushing estuaries. This theory would suggest that during the summer months, when the river flow rate was low, the availability of SPM for resuspension, settling and accumulation would be lower than seen in the winter or spring months, where river flow rates are higher. Furthermore, the advection of nutrients with river flow would be less during the summer months.

5.4.2 Hydrodynamic, particle/floc and nutrient data obtained in spring

Sampling was conducted on the 23rd March 2011, two days after the peak spring tide (Figure 5.5a). Sampling began shortly after the first high water at 0835 GMT and continued for the duration of the ebb tide until water was no longer available to sample (approx. 1230 GMT). Flood tide sampling began as soon as water was available (1740 GMT) and continued until there was insufficient light to continue sampling (approx. 1930 GMT). Tidal range and rainfall data are presented in Figures 5.5a and b. Conditions on the day were consistently dry with an average temperature of 12^{o}C; slightly above the average U.K. temperature (in March) of 9.6^{o}C (calculated using historic data obtained from Plymouth University Metnet).

In the week preceding sampling, a total of 9.2 mm of rain fell (Figure 5.5b). Flow gauge data showed an average flow of 7.82 $m^3\ s^{-1}$ in the week preceding

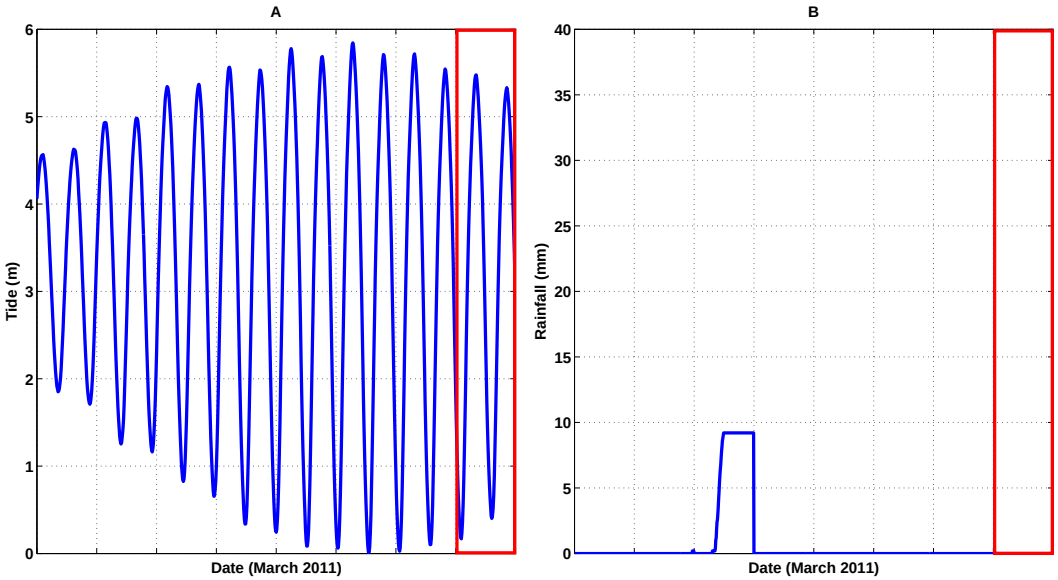

Figure 5.5: *Tide (a) and rainfall (b) data for the week preceding the sampling date (marked in red), in spring 2011. Sampling was conducted shortly after the spring tide and there was no precipitation during the sampling period. Rainfall data were obtained from Plymouth University Metnet. Red boxes indicate the sampling period.*

sampling, with a daily average flow rate of 6.65 $\mathrm{m}^3\ \mathrm{s}^{-1}$ on the sampling day. Flow rates for the week preceding and day of sampling were significantly lower than the average values for the time of year (calculated from historic flow gauge data obtained from the CEH website). The calculated average flow rate for the same week in March (10 year average) was 16.1 $\mathrm{m}^3\ \mathrm{s}^{-1}$.

5.4.2.1 Physical Data - ADCP, CTD and LISST

Figures 5.6a, b & c (Page 118) show the water temperature, salinity and turbidity data collected during the spring sampling campaign. Ebb and flood tide were separated by a long period where there was insufficient water for sampling approximately 2 hours either side of low water (LW). Water temperature in the morning ranged between 7.1 - 10.2 $^{\circ}$C, with the lowest temperatures measured at the start of the sampling period. Figure 5.5a shows that there was no precipitation during the ebb tide and so the patch of lower temperature surface water is likely to be a result of nocturnal cooling. Minimum current velocities (Figure

5.7a) of approximately 0.1 m s^{-1} were coincident with cooler surface water, indicating little mixing within the water column.

Salinity ranged between 0 - 8.4 PSU, with maximum values found at the near-bed of the water column during the first hour of sampling (HW+0), after which fresh water dominated the water column (Figure 5.6a). Turbidity ranged between 0.8 - 2.2 g L^{-1}. The hydrodynamic conditions observed were consistent with previous studies conducted in the Tamar estuary (see Dyer et al. (2002); Tattersall et al. (2003); Bale et al. (2006)), and more specifically Calstock (Manning et al., 2007a). As mentioned previously (section 5.2), SPM concentrations in the Tamar estuary can reach 8.2 g L^{-1}, particularly at the bed (Manning et al., 2006). The lower SPM concentrations recorded were consistent with the absence of mobile sediment in the upper reaches of the estuary due to low run-off conditions, as reported by Bale et al. (1985). Furthermore, reduced flow rates would decrease the availability of riverine SPM; consequently, SPM concentrations would be more heavily influenced by internal processes such as turbulence and shear stresses (Bale et al., 1985; Uncles and Stephens, 1993; Uncles et al., 2002). The lower SPM concentration may also have been a result of measurements being taken at the edge of the river, rather than in the centre of the channel where peak flow and concentrations would typically be observed (Manning et al., 2006).

Compared to the ebb tide, both temperature and salinity during the flood tide remained consistent (range of 0.5 ^{o}C and 2 PSU, respectively), with a maximum salinity of 3 PSU. Turbidity, on the other hand, demonstrated a broader range with a maximum concentration of 3.5 g L^{-1} at the start of the flood tide (LW+3 - LW+4).

The maximum SPM concentration was coincident with the maximum current

velocity (Figure 5.7a), highlighting the requirement of greater energy to resuspended more sediment, and the importance of internal physical processes (Bale et al., 1985; Uncles et al., 2002). Increased SPM concentration during this time would also increase opportunity for flocculation to occur, in line with M1.

Figures 5.7a & b (Page 119) show ADCP data collected during the ebb and flood tide in spring. Data presented is between 1.2 m and the bed due to the set-up of the ADCP on the day resulting in a large blanking distance between the water surface and the first 'true' measurement. On the ebb tide, current velocity (u) (Figure 5.7a) ranged between 0.1 - 0.4 m s^{-1} with peak flows at approximately 0930 GMT. Kolmogorov microscale (length) ($\mathrm{l_K}$), shown in Figure 5.7b, ranged between 180 - 510 $\mu\mathrm{m}$. Lowest $\mathrm{l_K}$ values were coincident with maximum u measurements indicating turbulent conditions with small eddies and structures. This phenomenon was consistent with other studies (Van der Lee, 2000; Bowers et al., 2007).

Due to limited daylight hours in the spring, only 2 hours of ADCP data were recorded during the flood tide sampling. Current velocities were greater than the in the morning ranging between 0 - 0.6 m s^{-1}. These values are consistent with the results reported by George (1975) whereby the shape of the estuary results in a stronger flood tide current velocity in the head of the estuary in contrast to the typically ebb tide dominant system of the Tamar estuary (Uncles and Stephens, 1993). Peak flow occurred between LW+3 - LW+4. As with the ebb tide, smaller $\mathrm{l_K}$ measurements were coincident with greater current velocities, indicating higher levels of turbulence.

Data recorded by the LISST on the ebb and flood tide are shown in Figures 5.8a & b. Particle concentrations recorded by the LISST instrument are shown in Figure 5.8 b, and correlate closely with those recorded using the CTD. Concen-

tration output from the LISST is recorded in $\mu\mathrm{L/L}$ and concentrations on both the ebb and flood tide ranged between 850 - 4900 $\mu\mathrm{L/L}$ with maximum concentrations occurring in shallower waters, as expected. The median ($\mathrm{d_{50}}$) floc size is presented in Figure 5.8a, and values during the day ranged from 11 - 228 $\mu\mathrm{m}$. While comparable with the median floc size reported by Dyer et al. (2002) and Uncles et al. (2002), measured values were lower than those reported in previous studies (Bass et al., 2007; Manning et al., 2006; Braithwaite et al., 2010). Manning et al. (2006) reported typical floc sizes at Calstock, as determined by LabSFLOC I and INSSEV, to be between 20 - 320 $\mu\mathrm{m}$, with larger floc sizes of up to 607 $\mu\mathrm{m}$ occurring during periods of high SPM concentrations (around 4.2 g $\mathrm{L^{-1}}$). Reported values are more closely aligned with the $\mathrm{l_K}$ values experienced in this study (Figure 5.7a), indicating that the floc size was limited by turbulent structures in the water column (Braithwaite et al., 2010). The limitation of floc size by turbulence in the water column was indicative of M1 and M2 acting in competition on SPM.

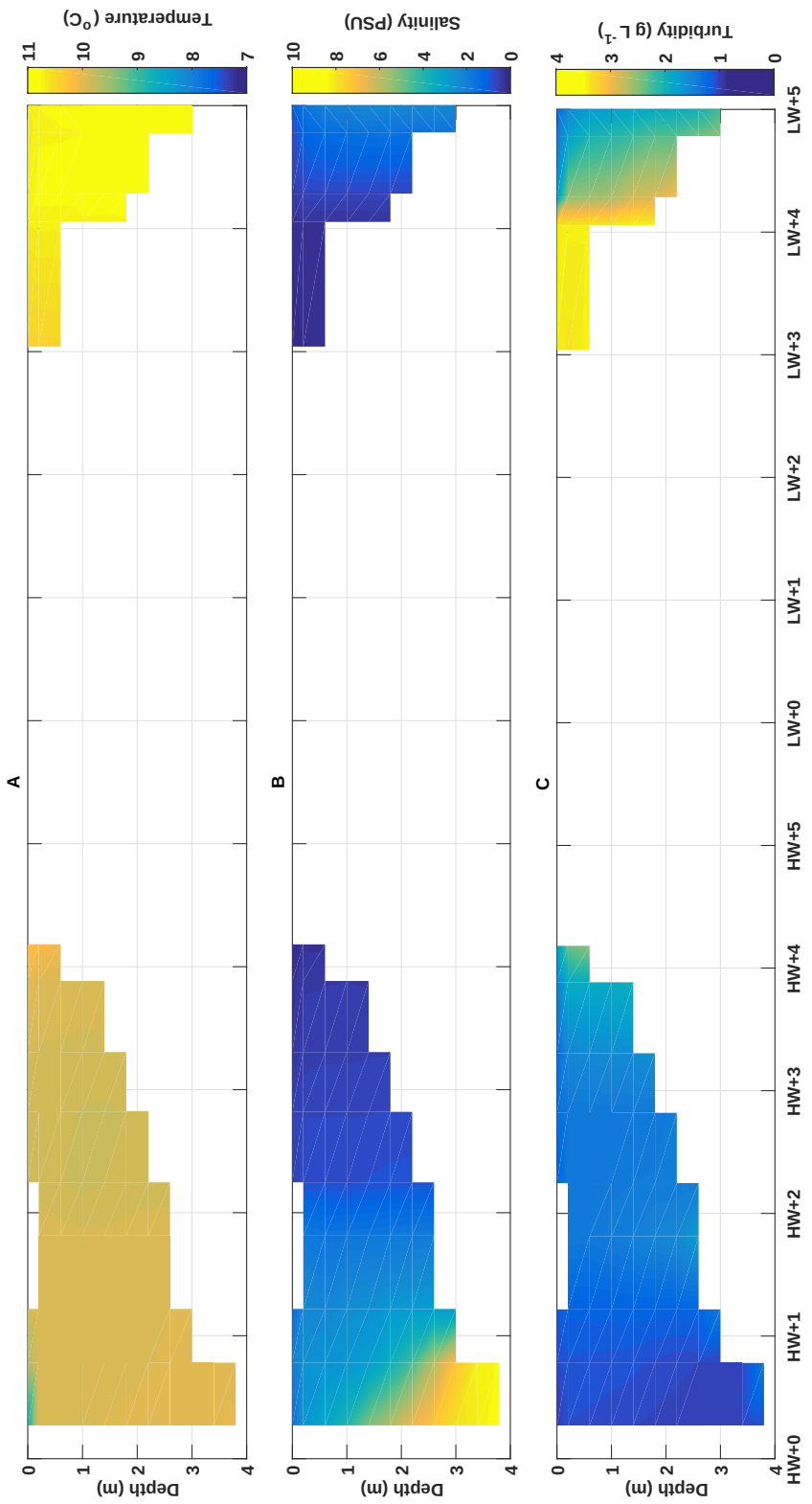

Figure 5.6: *Temperature, salinity and turbidity data collected in spring 2011. Missing data at the surface between 0900 - 1030 hours is a result of profiling the instrument too quickly. Frequency of sampling in the afternoon was less than in morning, resulting in reduced temporal resolution.*

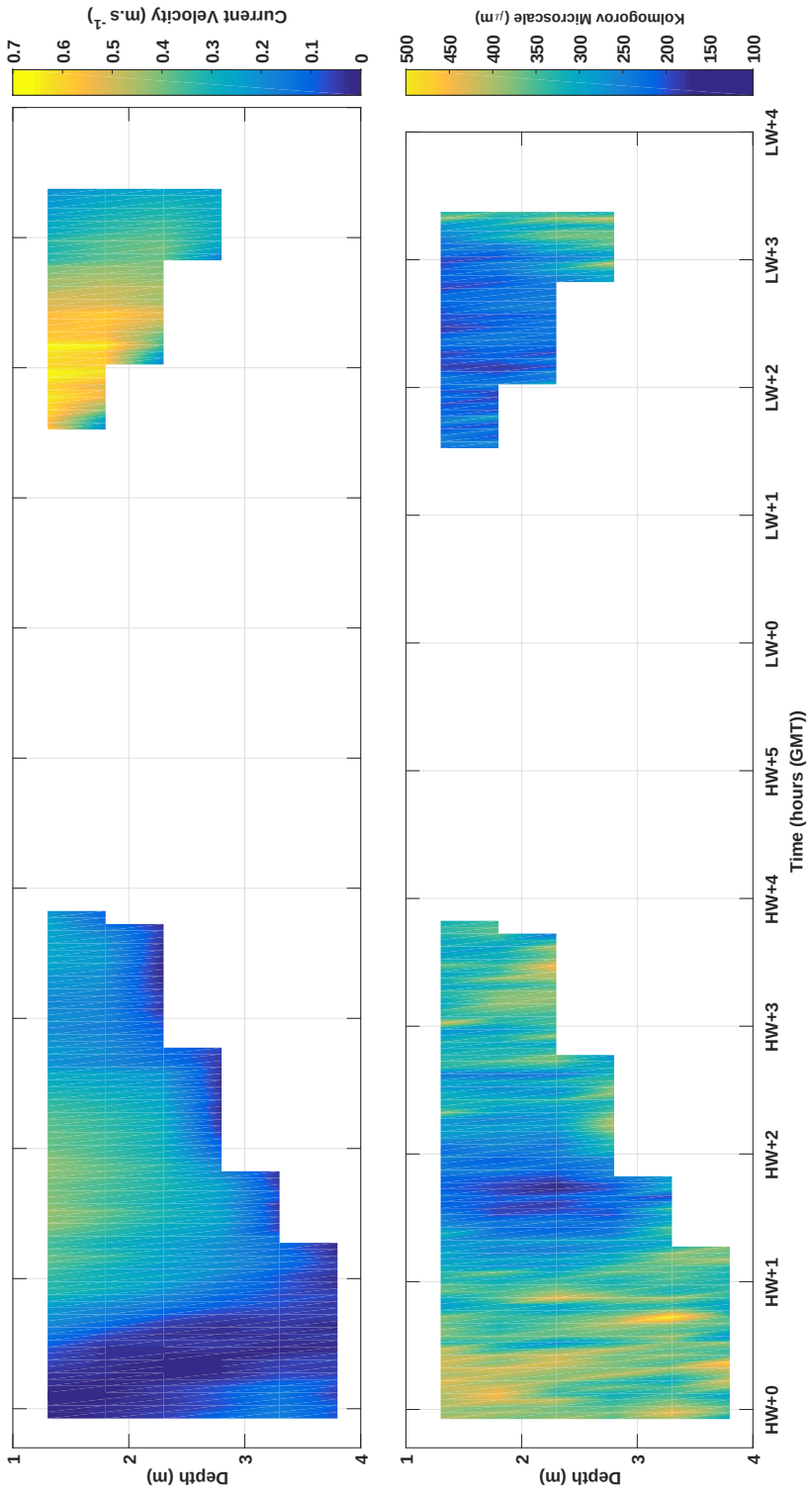

Figure 5.7: *ADCP data collected during spring 2011. Current velocity (Figures 4.5a) and Kolmogorov microscale (length) (Figures 4.5b) are presented for both the ebb and flood tide. Timings are different to the CTD data due to an earlier sampling start time (0800 GMT) and an earlier finish due to limitations of measurements of ADCP data below 0.5 m of water.*

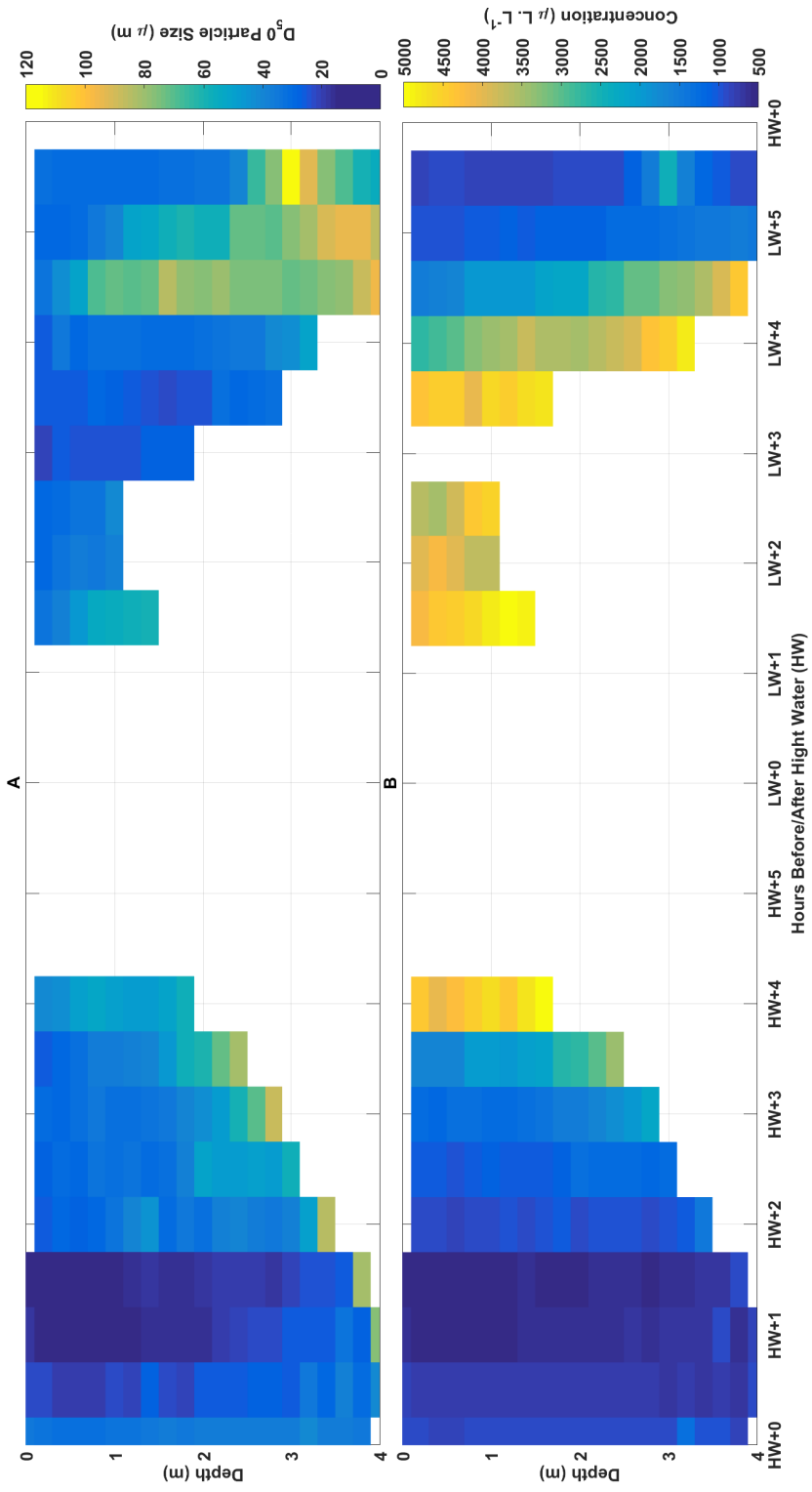

Figure 5.8: *Median (d_{50}) floc size collected during a) the ebb tide sampling and b) the flood tide sampling in spring 2011. Corrupted data, due to 'saturation' of the LISST, has been removed and therefore limited flood tide data is available.*

Maximum particle sizes occurred during periods of lower current velocity (Figure 5.7) where turbulence and disruptive processes were lower allowing for the aggregation of flocs. This was following the increase in SPM concentration observed at LW+1 to LW+3. During this time, l_K values were between 250 - 450 μm. As expected, the size of the floc was limited by the size of the eddies and structures in the water as indicated by the minimum l_K measurement of 250 μm and a maximum particle size of 228 μm. Concentrations of SPM during the flood tide were too high for the LISST to measure particle sizes, despite the PRM (see section 3.3.4), and so the 'saturated' data was removed (two out of the five profiles were removed). Figure 5.8b shows the particle size values between LW+4 - LW+5. During this time, the range of particle sizes was lower than that of the ebb tide (range = 60 μm) and values did not rise above 100 μm. During this time, l_K measurements were between 300 - 450 μm, which would suggest hydrodynamic conditions were conducive for the creation of larger flocs. However, SPM concentrations and current velocity at this time were low and so little flocculation occurred due to a lack of sediment to aggregate and energy to force them together.

5.4.2.2 Nutrient Data - spring 2011

Surface and near-bed concentrations of NO_3^-, NH_4^+ and PO_4^{3-} data for sampling conducted in spring 2011 are presented in Table 5.1. Surface concentrations were recorded every hour on the ebb tide and the sample interval was reduced to 30 min. during the flood tide due to insufficient light. Near-bed water concentrations were only collected on the ebb tide. Concentrations of NO_3^-, NH_4^+ and PO_4^{3-} obtained were in agreement with previous values reported for the Tamar estuary (Worsfold et al., 2008; Tappin et al., 2012).

NO_3^- was detected in all but two samples collected during spring; near-bed con-

Table 5.1: *Surface and near-bed concentrations of NO_3^-, NH_4^+ and PO_4^{3-} for samples collected in spring 2011. PO_4^{3-} concentrations for samples T07 - T09 were below the limit of detection (<LOD). Near-bed concentrations were only collected during the morning sampling.*

Time	NO_3^- (μM)	+/- (n=9)	PO_4^{3-} (μM)	+/- (n=9)	NH_4^+ (μM)	+/- (n=3)
T01	82	19	0.61	0.19	10.0	0.5
T02	137	22	1.07	0.14	7.95	0.3
T03	133	36	0.99	0.19	8.40	1.1
T04	128	58	0.72	0.22	6.40	0.4
T05	175	26	0.06	0.07	8.50	0.4
T06	194	7	0.10	0.06	5.60	0.2
T07	162	45	<LOD	<LOD	6.50	0.2
T08	184	20	<LOD	<LOD	6.90	0.2
T09	150	43	<LOD	<LOD	8.10	0.2
B01	<LOD	<LOD	1.65	0.75	11.6	1.4
B02	133	22	0.89	0.44	7.20	0.1
B03	139	49	0.72	0.19	8.50	1.8
B04	165	31	0.76	0.21	6.70	0.7

centrations at T01 and T05 were below the LOD. The maximum surface concentration of NO_3^- occurred at T06. This sample was collected at the start of the flood tide, before the influx of saline water and was coincident with the maximum SPM concentration. However, Morris et al. (1981) stated that any fluxes of NO_3^-, by processes other than advection, are typically swamped by the magnitude of NO_3^- entering the system through alternative sources, such as riverine water (Morris et al., 1981; Knox et al., 1986).

Surface concentrations of NO_3^- on the ebb tide (T01 - T05) showed a statistically significant increase (from 82 - 175 μM), as calculated by ANOVA and Tukey's test (p = 0.05). This result is consistent with a NO_3^- laden freshwater input, also shown by the salinity gradient in Figure 5.6b. Although the data is limited, ebb tide near-bed concentrations of NO_3^- also increased (from 133 - 165 μM), however ANOVA and Tukey's test did not reveal any significant differences. The minimum concentration of NO_3^- occurred at T01 at the start of the ebb tide. This lower value is consistent with the dilution of higher NO_3^- concen-

tration freshwater by lower NO_3^- concentration salt water (Knox et al., 1986). During the flood tide, results demonstrated a minor decrease in NO_3^- concentration, as would be expected with the increase in salinity associated with the incoming tide (Knox et al., 1986).

The behaviour of nutrient species in relation to hydrodynamic conditions in estuaries, particularly salinity, was determined by linear regression analysis. Conservative behaviour is marked by a linear relationship with salinity in estuaries. For the results obtained in spring 2011, regression analysis was conducted for sub-sets of the data, as shown in Table 5.2. Where results are shown as 'N/A', insufficient samples were available to conduct linear regression analysis. This is due to near-bed samples not being collected during the ebb tide.

Table 5.2: *Linear regression analysis of NO_3^-, NH_4^+ and PO_4^{3-} including r^2 values. Where values are listed as 'N/A', insufficient data was available for performing linear regression analysis.*

	Nitrate		Ammonium		Phosphate	
Analysis	Lin. Reg.	r^2	Lin. Reg.	r^2	Lin. Reg.	r^2
Surface Ebb	y = -0.024x + 4.43	0.71	y = 0.49x - 2.81	0.57	y = 1.176x + 0.47	0.42
Near-bed Ebb	y = -0.015x + 3.16	0.74	y = 1.46x - 9.31	0.88	N/A	N/A
Surface Flood	y = -0.05x + 9.42	0.71	y = 0.4x - 2.24	0.96	y = 8.25x - 5.125	0.98
Near-bed Flood	N/A	N/A	N/A	N/A	N/A	N/A

The relationship between NO_3^- and salinity demonstrated a negative correlation in all sub-sets of data. The r^2 values, while high, do not indicate a linear relationship and thus non-conservative behaviour. Liss (1976) highlighted that deviation above or below the theoretical linear relationship can indicate addition or removal processes. In this case, most values were below the linear fit suggesting removal processes, such as the recycling of NO_3^- by denitrifying bacteria, were occurring in the water column (Liss, 1976; Burgin and Hamilton, 2007).

Ammonium was present in all samples collected during both the flood and ebb

tide sampling. There was no general pattern of increase or decrease with time; but there was a relationship with salinity. NH_4^+ demonstrated an increase in concentration with an increase in salinity, as demonstrated by the positive correlations shown in Table 5.2. Of the three sub-sets of data on which linear regression analysis was performed, the ebb tide samples showed non-conservative behaviour, with most of the data points falling above the theoretical linear line indicating addition processes (Liss, 1976). The surface flood-tide samples, on the other hand, demonstrated conservative behaviour, with an r^2 value of 0.96.

Concentrations of NH_4^+ ranged between 5.6 - 11.6 μM with the maximum concentration occurring at the start of sampling (B01 and T01). The maximum concentration was shown to be statistically significantly different from all other samples collected by way of ANOVA and Tukey's test analysis (P = 0.05) and was coincident with the salinity gradient experienced at the start of sampling indicating the function of M2 (Salinity). Near-bed waters had salinities of up to 8 PSU, while surface waters were closer to 1 PSU. The stratification experienced at this time was associated with the onset of the ebb tide and was not reflected in the near-bed and surface concentrations of NH_4^+, suggesting that the high NH_4^+ concentration was not a result of salinity alone. The maximum particle size occurred at this time and indicates the process of flocculation and therefore the potential uptake of NH_4^+ as described in M1. The subsequent decrease in NH_4^+ would support this. On the other hand, it is possible that the high concentration of NH_4^+ was a result of processes occurring during the flood tide. Concentrations may have been higher prior to this sample, or there may have been a lag associated with the release of more strongly bound NH_4^+. For example, increased current velocity and turbulence associated with the flood tide may have increased SPM concentration, while the tidal intrusion would have increased the concentration of salt water cations. These conditions would be conducive to a benthic release of NH_4^+ by the exchange of NH_4^+ ions with other

cations present in the salt water (Fitzsimons et al., 2006). This theory would be aligned with all Mechanisms outlined in chapter 1 with M2 (Salinity) playing a more dominant role.

PO_4^{3-} was present in all samples collected during the ebb tide. However, three of the four samples collected during the flood tide were below the LOD, despite the high SPM concentrations. Additionally, two samples collected from very shallow waters at T05 (end of ebb tide) and then T06 (start of the flood tide), contained up to 0.1 μ M of PO_4^{3-}, with 1 standard deviation calculations as high as the recorded values.These results are consistent with results presented by Lillebø et al. (2004) and Mitchell and Baldwin (1998), who described the effects of P release from air-exposed sediments. These samples collected were shortly before the inter-tidal mud flats were exposed, and shortly after the inter-tidal mud flats had been exposed. Mitchell and Baldwin (1998) reported that air-exposed sediments have significantly higher P sorption capacity than submerged sediments, suggesting that any water column PO_4^{3-} coming into contact with the sediment, would be quickly removed.

Table 5.2 illustrates the linear regression analysis results for the relationship between PO_4^{3-} and salinity. Due to a number of samples falling below the LOD, it was not possible to perform the analysis for the near-bed ebb tide samples. However, as with NH_4^+, the ebb tide surface samples showed non-conservative behaviour with measurements lying above the linear line. This suggests addition of PO_4^{3-} from alternative sources, such as a benthic or riverine input. On the flood tide, surface samples showed conservative behaviour with an r^2 value of 0.98.

ANOVA and Tukey's test revealed a number of statistically significant temporal differences; surface PO_4^{3-} concentration peaked at T02, one hour after high

water and was highlighted as being statistically significant from T01, while T05 and T06 were significantly different from samples T01 - T04. The significant difference between T01 - T02 is not marked by significant changes in temperature, or turbidity, but there a gradient in salinity was experienced at T01, and an overall decrease in salinity occurred at T02. Current velocity and l_K demonstrated an increase in current velocity at T02 and T03, with lower l_K values at the same time. Floc size was also greater at T01, than T02. These conditions are indicative of a benthic input of PO_4^{3-} at T01, but with a time lag in the measurement associated with a consistent SPM concentration throughout the ebb tide. The low l_K values would suggest high levels of turbulence and mixing within the water, causing the breakdown of the salinity gradient at T01.

5.4.3 Hydrodynamic, particle/floc and nutrient data obtained in summer

Sampling was conducted on 16th June 2011 at the peak of the spring-neap tidal system. Longer hours of daylight allowed for extended hours of sampling and so sampling began at approx. 0630 BST (British Summer Time = GMT+1). Unlike sampling conducted in spring 2011, the conditions on the day were variable with both wet and dry spells. The average temperature was 12.8^{o}C, and approx. 9 mm of rain fell over the 24 h period. Despite cooler than usual conditions for June, as well as prolonged periods of rain prior to sampling, the daily average flow rate was lower than the average flow rate for June over the past decade (3.6 $m^3\ s^{-1}$ in June 2011, compared to 7.9 $m^3\ s^{-1}$). However, as a result of 35 mm of rain falling in one 24 h period, the maximum flow rate in the week preceding sampling was 9.3 $m^3\ s^{-1}$, which was greater than the average in the same period during the past decade (6.2 $m^3\ s^{-1}$).

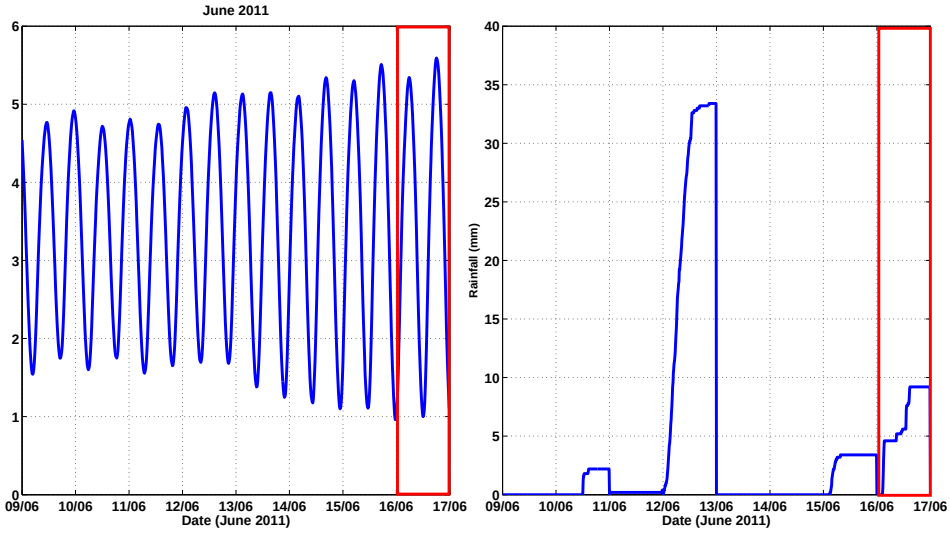

Figure 5.9: *a) Tide height (m) and b) rainfall (mm) data for the week preceding the sampling date (marked in red), in June 2011. Red boxes indicate the sampling period.*

5.4.3.1 Physical data - ADCP, CTD and LISST

Figures 5.10a, b & c (Page 129) show the temperature, salinity and turbidity data collected during the summer 2011 sampling campaign. Temperature during the ebb tide ranged between 17.2 - 17.6°C. During the flood tide, precipitation throughout the sampling period gave surface water temperatures of 15.5°C. Salinity ranged between 0 - 7 PSU, with higher salinities occurring at the start of the ebb tide (between HW+0 - HW+1). Turbidity ranged between 0.8 - 2.5 g L^{-1}. Maximum concentrations were found close to the bed in shallower water, with one 'patch' of higher SPM concentration at approx. HW+2, coinciding with a peak in current velocity.

Similar to the ebb tide, and aside from minor surface variations, the temperature during the flood tide showed little variation with an average temperature of 17.4°C. Salinity, on the other hand, showed a broader range (between 0 - 10.2 PSU) with the tidal intrusion shown clearly between LW+3 - LW+4. The second ebb tide of the day was seen to commence at HW+0, after LW+5. Turbidity,

like the first ebb tide, was consistently above 1 g L^{-1}, with patches of SPM concentrations up to 3.2 g L^{-1}. The maximum concentration was found in shallow water at the onset of sampling. This was likely a result of water covering the bed and the rate at which it did so, caused the resuspension of previously settled sediment. Higher SPM concentrations recorded in summer 2011 were consistent with the mobilisation of sediment in the mid-estuarine region and the subsequent accumulation of the mobile sediment in the upper estuary during the summer months, as reported by Bale et al. (1985).

Figures 5.11a & b (Page 130) show the ADCP data collected during the ebb and flood tide sampling in summer 2011. Similar to the data collected in spring 2011, the set-up of the ADCP resulted in a blanking distance of 1 m. On the ebb tide, current velocities peaked at 0.37 m s^{-1} at approx. HW+2. A secondary peak of 0.34 m s^{-1} occurred at HW+3. Kolmogorov microscales (length; l_K) during the ebb tide ranged between 160 - 224 μm.

During the flood tide sampling, current velocities peaked at 0.61 m s^{-1} between LW+4 and LW+5. This peak in current velocity on the flood tide is coincident with higher SPM concentrations. In contrast to the ebb tide, l_K values on the flood tide demonstrated a broader range (60 - 245 μm) with a very distinct 'band' of higher values between LW+5 and HW+2. This period of higher l_K values coincides with the decrease in current velocity, starting at the surface and progressing to the near-bed of the water column over the 2 h period.

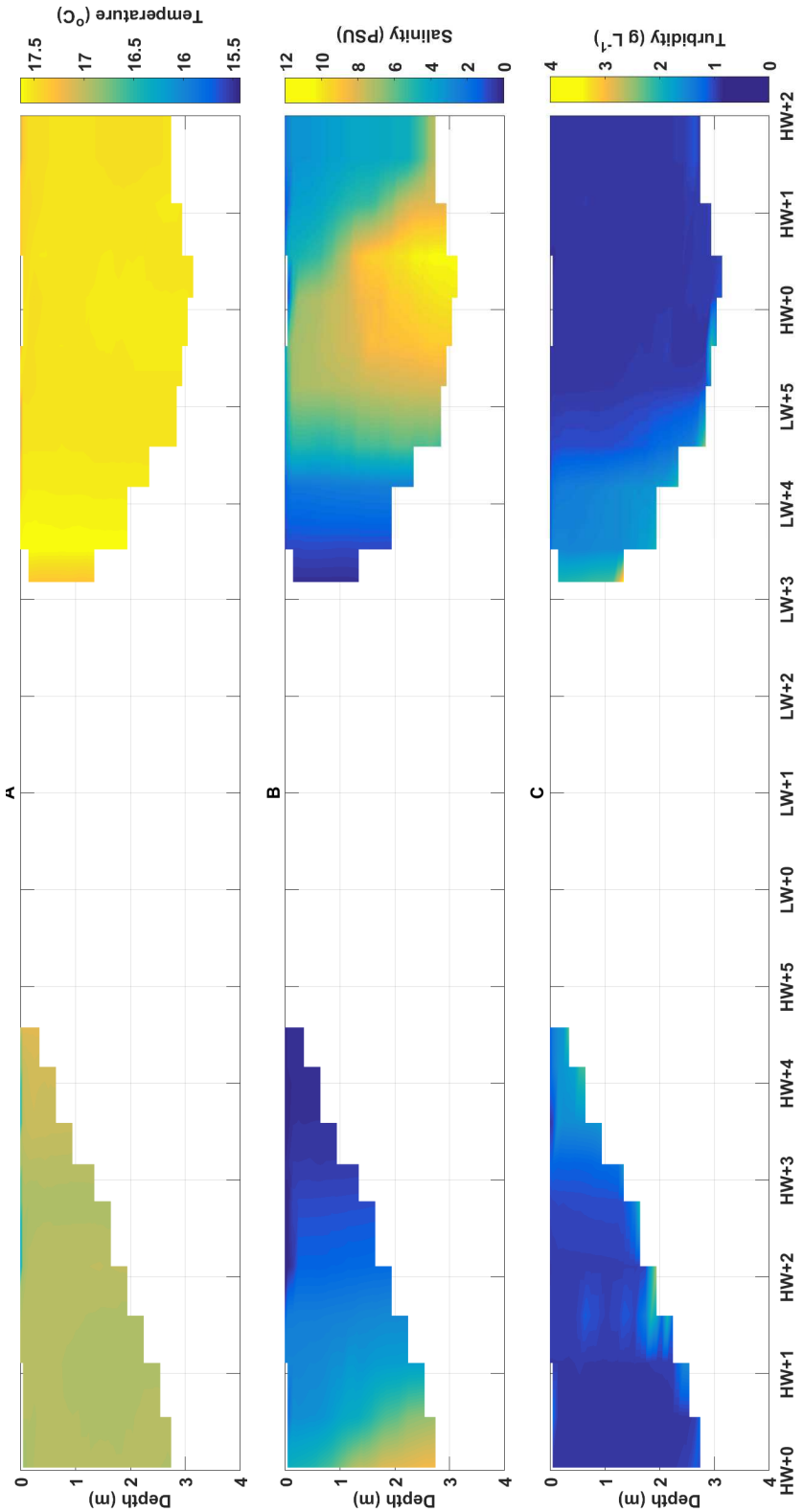

Figure 5.10: *Temperature (A), salinity (B) and turbidity (C) data collected in summer 2011.*

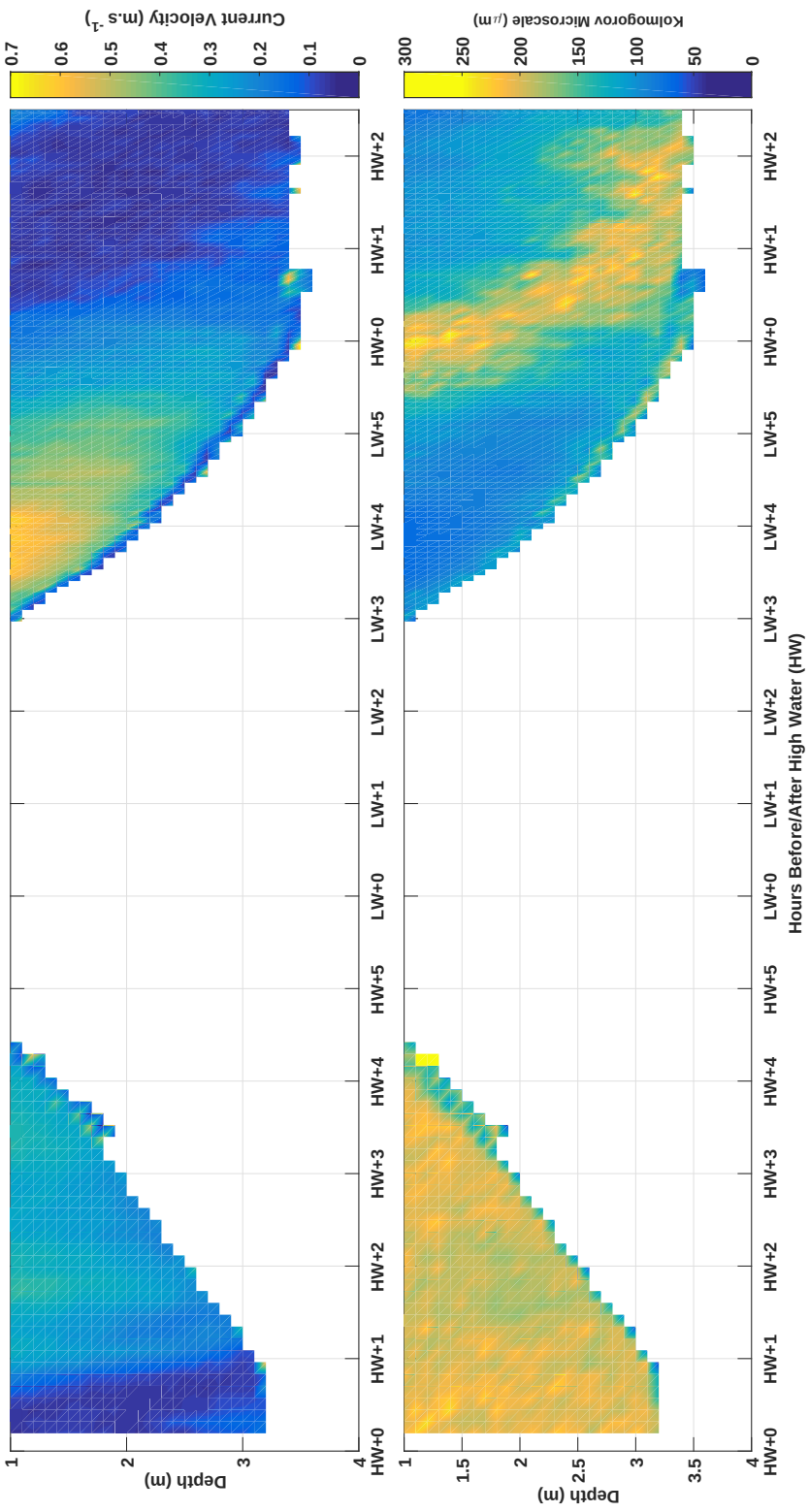

Figure 5.11: *ADCP data collected during summer 2011. Current velocity (Figures 4.5a) and Kolmogorov microscale (length) (Figures 4.5b) are presented for both the ebb and flood tide.*

Figure 5.12a shows the median (d_{50}) particle size data collected during summer 2011 using the LISST. Particle size range was similar to that recorded in March 2011 and ranged between 20 - 155 μm. Again, these values are a fraction of those reported in previous studies (see Bass et al. (2007); Manning et al. (2006); Braithwaite et al. (2010)). The atypical range of sizes exhibited in summer 2011 is likely a result of increased rainfall and river flows transporting fine silts downstream. Maximum particle size occurred at the start of sampling, shortly after high water and close to the bed where salinities were higher (Figure 5.10b). At this time, current velocities were close to 0 m s^{-1} and l_K values were approaching the maximum seen during the summer 2011 sampling campaign. The SPM concentration, combined with slow current velocity and low intensity turbulence (Figure 5.11 b) provided conditions conducive for flocculation.

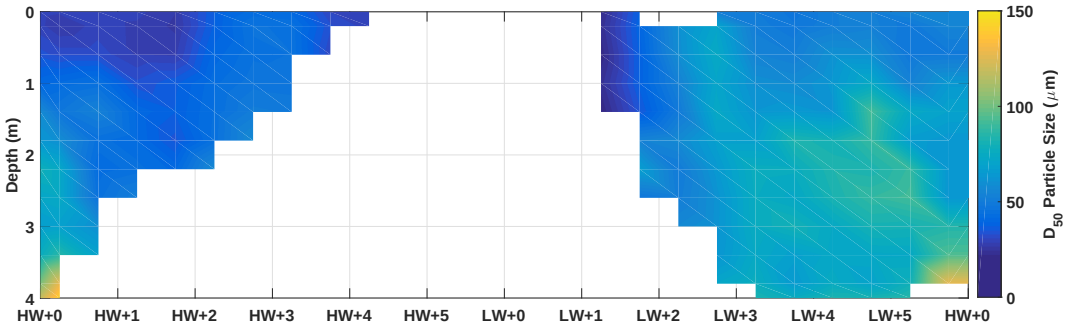

Figure 5.12: *Median floc size data collected using the LISST for the a) ebb tide and b) the flood tide in summer 2011.*

As with current velocity and l_k data presented in Figures 5.11a & b, the median particle size (d_{50}) presented in Figure 5.12 shows the same 'band' between LW+5 and HW+2. In this band, where l_k values are high and current velocity is low, an increase in particle size can be seen. Above this band, particles are approximately 40 μm smaller than those in it. l_k values at this point were approximately twice those outside of the band. As this band approaches the bed at approx. HW+2, another peak in median particle size was seen.

Contrary to expectation, periods of high SPM concentration seen at low water

sampling periods did not lead to a peak in particle size. This is a result of high current velocities causing higher intensity turbulence that limited floc growth. When conditions are quiescent and turbulent intensity is lower, particle sizes increase as a result of flocculation.

5.4.3.2 Nutrient data - summer 2011

NO_3^- and PO_4^{3-} were present in all samples collected during summer 2011 and are presented in Table 5.3. Due to sampling issues†, only 8 samples were collected during the day. Surface and near-bed samples were collected hourly, with the exception of near-bed samples when the water depth went below 0.5 m. This was because the Van Dorn water sampler could not sample twice in that depth of water. Measured concentrations were consistent with samples collected in March 2011, as well as previous studies conducted in the Tamar estuary (Worsfold et al., 2005; Tappin et al., 2012).

Table 5.3: *Surface and near-bed concentrations of NO_3^-, PO_4^{3-} and NH_4^+ for samples collected in summer 2011.*

Time	NO_3^- (μM)	+/- (n=9)	PO_4^{3-} (μM)	+/- (n=9)	NH_4^+ (μM)	+/- (n = 3)
T01	63	13	7.88	1.15	5.00	1.14
T02	57	8	2.27	0.50	3.00	2.23
T03	61	6	1.68	0.90	5.00	0.85
T04	72	7	2.61	0.24	4.90	2.27
T05	89	10	1.64	0.08	<LOD	<LOD
T06	79	9	1.49	0.30	2.50	1.49
T07	50	19	1.54	0.16	3.30	2.18
T08	54	22	1.05	0.38	2.30	0.86
B01	64	7	3.35	0.02	1.50	0.46
B02	70	10	2.16	0.15	2.21	0.87
B03	83	3	2.44	0.13	2.56	1.10
B06	35	2	1.42	0.20	N/A	N/A
B07	26	2	1.6	0.25	N/A	N/A
B08	59	4	1.97	0.37	N/A	N/A

†invertor failure prevented filtration by vacuum pump

Concentrations of NO_3^- ranged between 26 and 89 μM with the maximum concentration occurring at T05, one hour after the low water. The maximum concentration occurred at the surface and was coincident with the maximum SPM concentration and current velocity. At this point, l_k values were small and indicative of an area of high turbulence (Figure 5.11d). Typically, NO_3^- is not bound to sediments and, combined with low salinity (river) water and low current velocity at this time, the NO_3^- concentration at this time was likely a result of the advection of nutrient-laden freshwater shortly before the flood tide commenced. The minimum concentration of NO_3^- was measured in a near-bed sample collected at B07. This sample was collected with approx. 1 m of water available and where the salinity gradient of the incoming tide was just visible (Figure 5.10).

Linear regression analysis of 4 sub-sets of data was performed to establish the relationship between the salinity and the concentration of each nutrient species. Results are presented in Table 5.4. Unlike March, linear regression analysis performed for NO_3^- samples collected in summer 2011 revealed that there was no conservative behaviour during the flood or the ebb tide, with r^2 values of between 0.18 and 0.69. These low r^2 values indicate a poor relationship between salinity and NO_3^- and thus, non-conservative behaviour. Non-conservative behaviour of inorganic nutrients is typically a result of biological processes and chemical removal during the mixing of riverine and estuarine waters (Billen, 1975; Cloern and Oremland, 1983; Morris et al., 1985; Knox et al., 1986). The poor fit of the data for both ebb and flood tide data illustrates both removal and addition processes (Liss, 1976).

NH_4^+ concentrations were measured for surface samples during the ebb and flood tide but, due to sampling constraints, were not collected for near-bed water samples during the flood tide. NH_4^+ was present in all but one sample collected during the day; the first sample of the flood tide (T05) was below the LOD. Con-

Table 5.4: *Linear regression analysis of NO_3^-, NH_4^+ and PO_4^{3-} including r^2 values. Where values are listed as 'N/A', there was insufficient data to perform linear regression analysis.*

	Nitrate		Ammonium		Phosphate	
Analysis	Lin. Reg.	r^2	Lin. Reg.	r^2	Lin. Reg.	r^2
Surface Ebb	y = -0.78x + 64.57	0.28	y = 0.04x + 4.4	0.08	y = 1.39x + 1.38	0.95
Near-bed Ebb	y = -2.13x + 80.12	0.18	y = -0.12x + 1.64	0.99	y = 0.13x + 2.12	0.87
Surface Flood	y = -5.39x + 84.33	0.69	y = 0.26x + 1.64	0.99	y = 0.06x + 1.42	0.04
Near-bed Flood	y = 2.31x +27.48	0.69	N/A	N/A	y = 0.05x + 1.37	0.97

centrations ranged between 2.3 and 5.0 μM, with the maximum concentrations occurring on the ebb tide at T01 and T03. ANOVA and Tukey's test revealed that NH_4^+ at T01 and T03 were statistically significantly different from results collected at T02 and T04.

Linear regression analysis (Table 5.4) revealed that samples collected on the ebb tide at the near-bed, and surface samples collected during the flood tide, showed conservative behaviour with r^2 values of 0.99. On the flood tide, this would indicate that with increasing salinity, ammonium increases. The ebb tide conservative behaviour was only seen in near-bed samples. It is thought that aeolian inputs of NH_4^+ are marked addition processes in the non-conservative behaviour experienced at the surface.

PO_4^{3-} concentrations ranged between 1.05 - 7.88 μM. These values, while consistent with previous research, demonstrated a relatively extreme maximum concentration typically occurring only once or twice a year (Tappin et al., 2012). The maximum concentration occurred in a surface sample at the start of sampling and was coincident with a salinity gradient as seen in Figure 5.10c. The salinity gradient here showed fresher water at the surface and higher salinities closer to the bed. This situation is typical of the ebb tide and the peak in PO_4^{3-} was likely a result of the flow of nutrient-laden river water. The minimum concentration of PO_4^{3-} occurred at T08. This surface sample was collected at high water where current velocities were close to 0 m s^{-1}. SPM concentrations were low and the fresh water associated with the beginning of the ebb tide had just

started to appear at the surface (Figure 5.10d).

Analysis of conservative behaviour of PO_4^{3-} illustrated that ebb tide surface samples showed conservative behaviour with an r^2 value of 0.95; as the salinity decreased, so did the concentration of PO_4^{3-}. Near-bed samples were close to being conservative with an r^2 value of 0.87. The slight deviation from being conservative appeared to be a results of removal processes occurring (Liss, 1976).

5.4.4 Hydrodynamic, particle/floc and nutrient data obtained in autumn

Sampling was conducted on the 16th September 2011 one day after the peak in the spring-neap cycle. As with summer, longer hours of daylight allowed for a longer sampling day. Figure 5.13 shows the tidal range and precipitation data for the day of sampling and the week preceding. Temperatures ranged between 13 and 19.5°C, with an average temperature of 16.5°C; slightly warmer than the ten-year average for September (14.4°C). Conditions in September were consistently damp, with up to 5 mm of precipitation per day prior to, and including, the sampling day. The average river flow rate on the day of sampling was 7.1 m^3 s^{-1} and the average flow rate for the week preceding sampling was 6.9 m^3 s^{-1}. These flow rates are approximately half of the 10 year average river flow rate for the same week (13.8 m^3 s^{-1}).

5.4.4.1 Physical data - ADCP, CTD and LISST

Figures 5.15a – f show the CTD data collected during the ebb and flood tide sampling campaign in autumn 2011. Water temperatures ranged between 14 and 17°C with only a subtle difference visible in the ebb tide sampling that is consistent with cooler fresh water dominating the water column. A striking and contrasting difference to samples collected in March and June is the salinity of the water column throughout the sampling day. Salinities ranged from 0 - 2.5

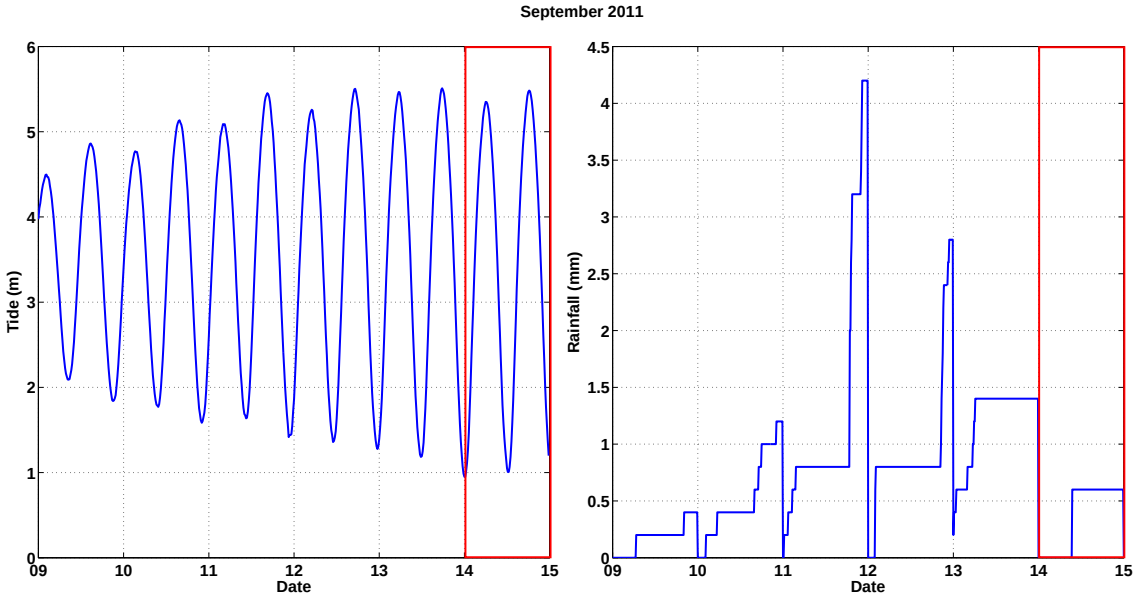

Figure 5.13: *Tide (a) and rainfall (b) data for the week preceding the sampling date (marked in red), in autumn 2011. Red boxes indicate the sampling period.*

PSU with maximum salinities occurring at the start of the ebb tide, and the onset of the flood tide. Fresh water conditions such as this are usually the result of increased river flows inhibiting the limit of the tidal intrusion. River flow velocities, however, were lower than those experienced in March and the same conditions were not seen. An alternative possibility is the dilution of saline water by constant and persistent precipitation and a weaker spring tide than experienced in March or June.

Turbidity during the sampling day ranged from 0 - 5 g L^{-1} with maximum concentrations occurring at low water periods, coincident or just after periods of high current velocity. In line with the study by Bale et al. (1985), SPM concentrations in the upper estuary in early autumn are a result of the same processes seen in summer: the erosion of mid-estuary sediment leads to the accumulation of mobile sediment in the upper estuary, resulting in higher SPM concentrations. The SPM concentration in autumn 2011 was higher than those experienced in spring indicating the addition of sediment by prolonged periods

of rainfall. The recorded SPM concentrations at this time were also closer to concentrations experienced in concentrated benthic suspensions, as reported by Manning and Dyer (2007).

Figures 5.16a – d show the ADCP data collected during the ebb and flood tide sampling campaign. As per the data collected in March and June, the ADCP had a blanking distance of 1 m. Current velocity ranged between 0.05 and 0.55 m s^{-1}, with maximum velocities found on the flood tide. This is consistent with results obtained during the March and June sampling campaigns. The speeds are also consistent with the results reported by George (1975) whereby the shape of the estuary results in a stronger flood tide current in the head of the estuary in contrast to the typically ebb tide dominant system in the Tamar (Uncles and Stephens, 1993).

During the ebb tide, current velocities reached a maximum of 0.33 m s^{-1} at approx. 0830 BST and were lowest between 0700 to 0800 BST. This period of slack water was coincident with the maximum salinity experienced on the ebb tide. Maximum current velocities occurred during the retreat of the saline water where the presence of riverine water increased, as shown in Figure 5.15c. Kolmogorov microscale length values during the ebb tide were between 95 and 184 μm. Unlike June, there were no distinct periods of turbulence or quiescence, indicating a well mixed water column.

Flood tide velocities reached a maximum of 0.55 m s^{-1}, with the maximum velocity occurring at the very start of the flood tide (1630 BST). This is typical of flood tide conditions, however the salinities shown in Figure 5.15 are atypical of flood tide conditions. Minimum current velocities during the flood tide occur as the depth approaches 3 m at approx 1830 BST. In contrast to the data obtained during the ebb tide, the flood tide demonstrates a clear change in current ve-

locity and a clearer change in l_k values. l_k measurements ranged between 115 and 200 μm. The maximum current velocity was coincident with the minimum l_k measurements and the maximum SPM concentrations. As per the results in March and June, it is proposed that the intense energy in such a shallow volume of water causes the high SPM concentration. It is also possible that a concentrated benthic suspension (CBS) formed. The formation of a CBS is a result of near-bed turbulence causing the entrainment and resuspension of loose bed sediments into existing high SPM concentration waters. A CBS can also be formed as a result of a significant deposition event, such as the collapse of an ETM. Figures 5.14a and b show the d_{50} particle size during the ebb and flood tide, collected with the LISST in autumn 2011. Measurements in September were lower than those recorded in both March and June, with values between 11 and 115 μm. These values are lower than median floc sizes reported by Dyer et al. (2002) and Uncles et al. (2002), but fit the theory that particle size is limited by turbulence (l_k values between 95 and 200 μm). Maximum particle sizes occurred on flood tide during increasing salinity and as a result of increased velocity, but during a period of decreasing SPM concentration.

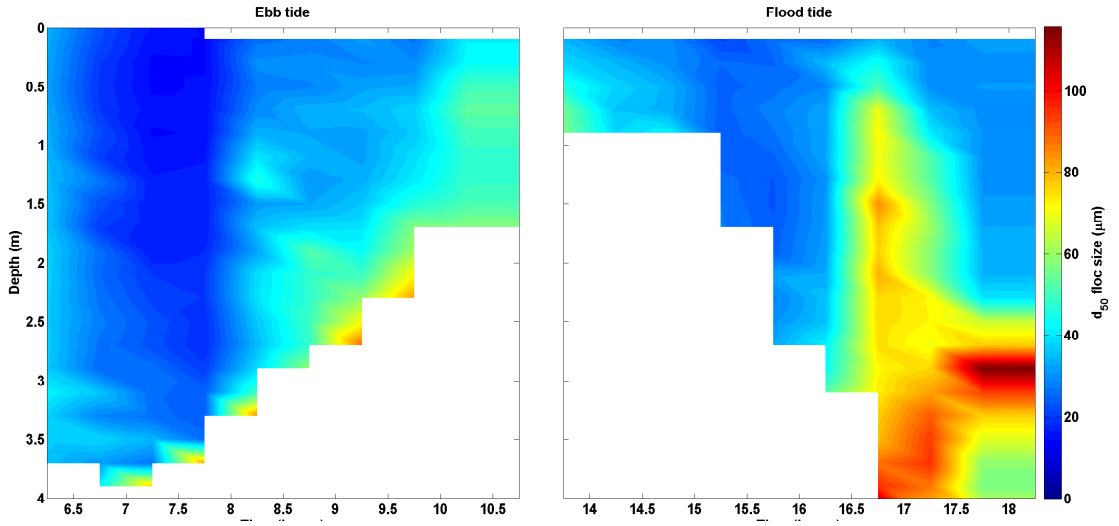

Figure 5.14: *a) LISST data collected during the ebb tide sampling and b) the flood tide in autumn 2011.*

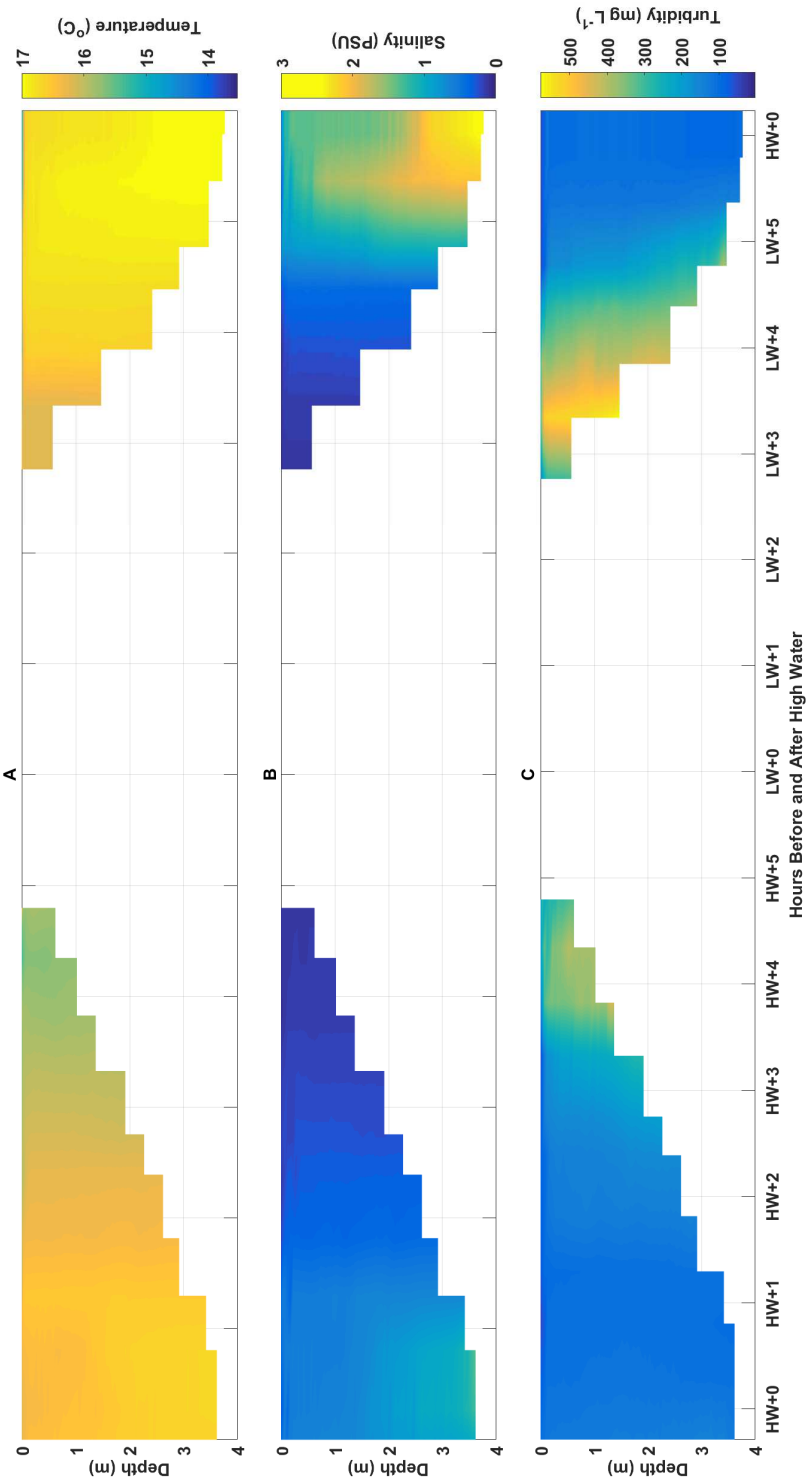

Figure 5.15: *Temperature, salinity and turbidity data collected in autumn 2011.*

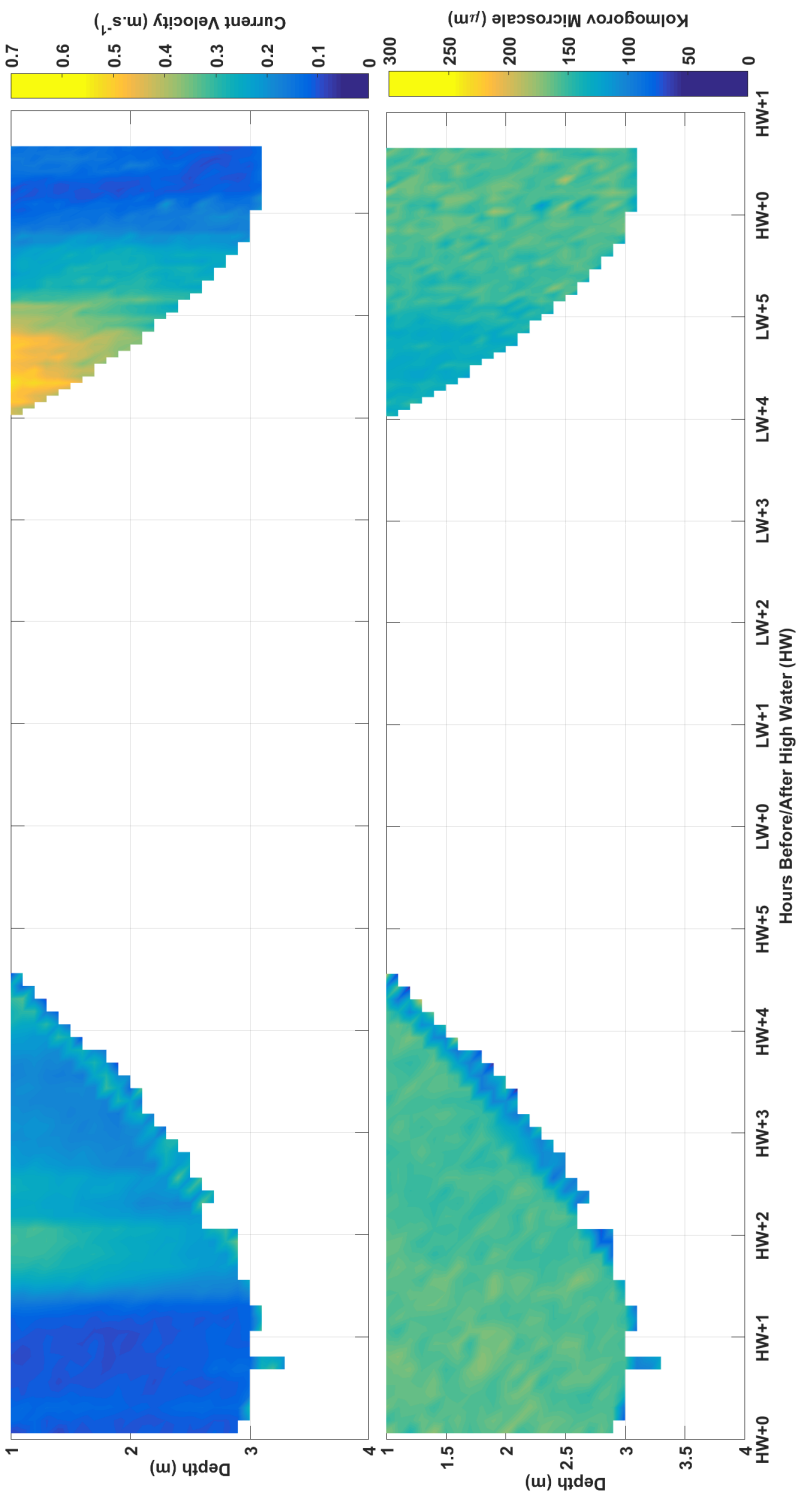

Figure 5.16: *ADCP data collected during autumn 2011. Current velocity (Figures 5.16a & 5.16c) and Kolmogorov microscale (length) (Figures 5.16b & 5.16d) are presented for both the ebb and flood tide.*

5.4.4.2 Nutrient data - autumn 2011

Surface and near-bed concentrations of NO_3^-, PO_4^{3-} and NH_4^+ data for sampling conducted in autumn 2011 are presented in Table 5.5. Surface and near-bed concentrations were recorded every hour during the flood and ebb tides. Due to failing light, the number of samples collected during the ebb tide was reduced to three. Measured concentrations of NO_3^- and PO_4^{3-} were in agreement with previous values recorded in the Tamar estuary (Worsfold et al., 2008; Tappin et al., 2012), and comparable to concentrations in March and June. Samples collected for the determination of NH_4^+ were all below the LOD. The calibration curve during this time did not identify any issues with the NH_4^+ processing and so there is no methodological reason that the results should be below the limit of detection, particularly as prolonged periods of rainfall would typically cause an increase in NH_4^+ (and NO_3^-) (Ryther and Dunstan, 1971; Paerl, 1985; Duce, 1986; Paerl et al., 1990).

Table 5.5: *Surface concentrations of NO_3^-, PO_4^{3-} and NH_4^+ for samples collected in autumn 2011. Note that for all samples collected during the sampling campaign, NH_4^+ was not present.*

Time	NO_3^- (μM)	+/- (n=9)	PO_4^{3-} (μM)	+/- (n=9)	NH_4^+ (μM)	+/- (n = 9)
T01	102	1	7.11	3.57	<LOD	<LOD
T02	85	13	4.50	0.61	<LOD	<LOD
T03	80	8	2.68	0.70	<LOD	<LOD
T04	86	7	2.77	0.42	<LOD	<LOD
T05	75	9	2.07	1.46	<LOD	<LOD
T06	80	17	2.08	0.61	<LOD	<LOD
T07	86	13	3.45	0.15	<LOD	<LOD
T08	99	16	3.59	0.28	<LOD	<LOD
B01	70	15	1.89	0.5	<LOD	<LOD
B02	87	12	0.90	0.02	<LOD	<LOD
B03	110	6	0.74	0.04	<LOD	<LOD
B04	95	10	0.59	0.18	<LOD	<LOD
B05	105	6	0.58	0.03	<LOD	<LOD
B06	102	9	1.49	0.3	<LOD	<LOD
B07	100	6	1.54	0.16	<LOD	<LOD
B08	88	7	<LOD	<LOD	<LOD	<LOD

NO_3^- was detected in all samples collected in autumn 2011. The maximum concentration was 110 μM and the minimum concentration was 70 μM. Recorded concentrations were similar to those recorded in June, despite the prolonged rain. The maximum concentration occurred in a near-bed water sample during the ebb tide and was coincident with the retreat of saline water at approx. 0830. This increase was marked as statistically significant and is consistent with conservative behaviour as outlined by Loder and Reichard (1981). Similarly, when the salinity increased during the flood tide, NO_3^- was seen to decrease in near-bed samples, but not in surface samples. Surface samples, on the other hand, show a statistically significant increase in concentration that is consistent with an input by precipitation.

PO_4^{3-} was present in all but one water sample collected during the flood and ebb tide. The final near-bed sample collected on the ebb tide was below the limit of detection. The maximum concentration of PO_4^{3-} occurred in the surface water sample collected at the start of sampling. This maximum was coincident with the retreating salinity associated with the ebb tide. At this point, there were no significant particle and SPM concentration behaviours.

5.5 Seasonal Comparisons

Clear seasonal differences were seen in hydrodynamic conditions of the water column and macro-nutrient concentrations. Turbidity values reached a maximum of 5 g L^{-1} in autumn with the lowest maximum of 2.2 g L^{-1} occurring in spring. SPM concentrations in spring, summer and autumn were consistent with previous studies conducted in the Tamar estuary and specifically, the study by Bale et al. (1985). Upper estuary SPM concentrations in spring were lower than summer as a result of an absence of mobile sediment, while summer demonstrated consistently higher SPM concentrations associated with the mo-

bilisation and transport of mid-estuarine sediments to the upper estuary.

Current velocity was consistent across all field campaigns with maximum values of up to 0.6 m s^{-1} occurring on the flood tide. This was in contrast to the reported ebb-dominant system and was a reflection of the shape of the estuary (George, 1975; Bale et al., 1985). Minimum current velocities were indicative of periods of slack water associated with high and low tide. Kolmogorov microscale (length; l_k) was used as an indicator of the level of turbulence experienced in the water column and measurements were found to be directly related to the current velocity, as expected. However, the levels of turbulence recorded in the Tamar estuary were lower than those reported in previous studies. Studies by McCabe (1991); Hill et al. (1992); Fugate and Friedrichs (2003); Mîkes (2011) reported that typical Kolmogorov microscale length values are between 100 - 1000 μm and values in summer and autumn did not exceed 200 μm, indicating high levels of turbulence. Kolmogorov microscale length measurements were greater in spring and reached 510 μm, identifying less turbulent conditions. Higher current velocities resulted in greater energy and thus, turbulence. Induced turbulence was found to be a controlling factor in the size of flocs; in all seasons, median particle size did not exceed Kolmogorov microscales consistent with the aforementioned studies.

SPM concentration measurements in spring, summer and autumn, combined with current velocity and turbulence data, highlighted the importance of controlling factors such as current speed and river flow in the availability and mobility of sediments at Calstock. The impact of variations in SPM concentrations could affect both the uptake and release of nutrient species from sediments as outlined in M1 (chapter 1). Further to this, the effect of higher levels of turbulence would limit the equilibrium floc size and partly control the size of the largest macroflocs. Limited floc size would impact the amount of interstitial wa-

ter that could be trapped when flocs are generated and, thus, reduce the uptake of macro-nutrients. On the other hand, the high levels of turbulence could potentially break up larger flocs and release previously trapped interstitial water, or provide sufficient energy to break bonds between nutrient species and particle faces. This would be in line with M3.

Measurements of salinity in spring and summer were comparable, with a maximum PSU of 8 and 10, respectively. Autumn, on the other hand, showed much lower salinities with a maximum of 2 PSU. It is proposed that this was a result of the prolonged rainfall experienced during autumn leading to increased river flow and a reduction in the limit of the tidal intrusion.

The impact of the lower salinity experienced in autumn on the concentration of macro-nutrients was different for each species. For NO_3^-, theory would suggest that increased rainfall and river run off would lead to an increase in nitrate concentration - it was observed, however, that concentrations were lower than those seen in spring or summer. This is proposed to have been a result of increased denitrification during the summer and autumn months (Whitehead et al., 2008). The effect of lower salinity in autumn on concentrations of NH_4^+ could not be determined as all results were below the limit of detection. However, it is theorised that, in relation to M3, concentrations of NH_4^+ would not show any significant increases with increasing salinity, as they did in spring. This is because a lower salinity would result in fewer salt water cations and thus less chance of ion exchange processes.

Ammonium concentrations recorded in spring were in line with studies by Watson et al. (1985); Law et al. (1991) and Fitzsimons et al. (2006) and demonstrated processes closely aligned with M1 and M3, as described in chapter 1. M1 described the increase of NH_4^+ with the increase in sediments; this was indicated

by the increase in SPM concentration at T02 consistent with a benthic input, followed by an increase in NH_4^+ at T03, associated with the slow-release from particulate fraction (Morin and Morse, 1999). An additional peak in NH_4^+ at T05 was coincident with an increase in salinity and was indicative of M3. In contrast to spring, the maximum concentration of NH_4^+ was not coincident with any significant changes in turbidity or salinity. Unexpected results of NH_4^+ concentrations that below the limit of detection collected in autumn prevented any comparison to the Mechanisms described in chapter 1.

Maximum NO_3^- concentrations were recorded in spring (up to 194 μM) and were almost double those recorded in summer and autumn. This is in line with previous studies that demonstrate an increase in NO_3^- during the winter months due to increased rainfall and run-off and decreased biological activity in the water. As reported earlier, NO_3^- is not typically bound to sediments and thus not directly related to Mechanisms 1 - 3. A previous study indicated that NO_3^- can behave conservatively in estuaries (Morris et al., 1981), however in spring, summer and autumn, results indicated non-conservative behaviour of NO_3^-.

The maximum concentration of PO_4^{3-} occurred in summer and was closer to the highest concentrations recorded between 1975 and 1991 (Tappin et al., 2012), than the typical annual mean value. Similarly, concentrations recorded in autumn were also elevated. These high measurements were proposed to be a result of increased SPM concentration associated with the seasonal movement of sediments in the upper estuary. It could also have been a result of increased levels of river run-off. In contrast, concentrations recorded in spring were significantly lower and within the range of those typically experienced.

5.6 Conclusions

The aim of this study was to examine sediment-nutrient relationships in the field on a seasonal and high resolution temporal scale. To investigate the aim, a field campaign was conducted in spring, summer and autumn of 2011 using a suite of oceanographic instruments and collecting water samples to measure macro-nutrient concentrations on the best possible temporal scale. Water samples were collected hourly, while CTD and LISST profiles were collected every 30 min.

Hydrodynamic data and macro-nutrient concentrations were recorded in spring, summer and autumn 2011. Concentrations and values of both physical and chemical parameters were within the range of measurements previously recorded in the Tamar estuary and there were marked differences in hydrodynamic conditions and nutrient concentrations across the seasons. In particular, gravimetrically recorded SPM concentrations were greater in autumn in line with reports by Bale et al. (1985) and reached a maximum of 5 g L^{-1}.

SPM and current velocity data obtained in the field campaigns highlighted the importance of meso-scale internal physical processes, such as changes in flow conditions associated with spring-neap tides and seasons, on the mobility and availability of sediments in the upper estuary. In turn, the availability of sediments in the upper estuary was seen to be related to concentrations of PO_4^{3-}, particularly in summer and autumn. When SPM concentrations were elevated, so were concentrations of PO_4^{3-}; an indication of a benthic release of PO_4^{3-}. Despite the aforementioned coincidence, it was not possible to observe if the hypothesised exchange mechanism of macro-nutrients associated with flocculation. It was concluded that an SPM concentration increase supplies a source of macro-nutrients on which other mechanisms act.

The relationship between SPM concentration and current velocity was also shown to influence the particle size. Particle sizes were observed to be limited by the size of Kolmogorov microscales, indicating the restrictive nature of turbulence in the formation of larger flocs. M1 described the uptake of nutrients into the interstitial water when flocs were formed, however, it was feasible that flocs were both created and broken in turbulent conditions and therefore uptake or release mechanisms were insignificant in these field studies.

Concentrations of NH_4^+ were observed to be related to both M1 and M3. During spring, concentrations demonstrated a benthic release associated with peaks in SPM concentration, followed by a second slow-release from the particulate fraction in line with studies conducted by Morin and Morse (1999). Contrastingly, results in summer did not show any relationship with SPM concentration, but aligned more closely with the salinity and the exchange of NH_4^+ with salt water cations present in the water column, consistent with a report by Gardner et al. (1991).

5. SEDIMENT-NUTRIENT INTERACTIONS IN THE TAMAR ESTUARY, U.K.

Chapter 6

A Laboratory Examination of Micro-Scale Physical Processes Affecting Sediment Characteristics and Nutrient Concentration

'You keep rowing the distance... I will bail the water out!'

Marcus Zanacchi

6.1 Introduction

Following the field campaigns conducted in the Seine and Tamar estuaries, this chapter presents the results and discussion of the laboratory experiments. A series of experiments were conducted to identify the controlling factors in the relationships between micro-scale physical processes, SPM characteristics and nutrient concentrations.

The primary aim of this chapter was to establish which of the Mechanisms outlined in chapter 1, if any, result in a change in concentration of macro-nutrients (NH_4^+, NO_3^- & PO_4^{3-}) to the water column. Additionally, as a result of observations in chapters 4 and 5, to determine whether an equilibrium state occurred between the effects of flocculation and turbulence in the control of uptake and release of macro-nutrients in the water column. The objectives of this chapter are as follows:

- to configure the mini-annular flume to create similar physical conditions to those measured in the Tamar estuary;
- to quantitatively measure the changes in sediment characteristics in controlled conditions;
- to identify the dominance of each Mechanism outlined in chapter 1

6.2 Instrumentation & Methodology

The laboratory set-up consisted of a number of instruments including, ADV, LISST-100C and a mini-annular flume. In addition to this, three glass filtration kits were assembled to filter water samples for the determination of NO_3^-, PO_4^{3-} and NH_4^+ as per section 3.4 (chapter 3).

6.2.1 Acoustic Doppler Velocimeter (ADV)

Acoustic Doppler Velocimeters (ADV), like ADCPs (section 3.3.2), measure instantaneous flow velocity components by way of the Doppler shift effect described in section 3.2 of chapter 3. Unlike ADCPs, however, ADVs sample a smaller, fixed volume and do not have diverging beams. It is implemented as a bistatic (focal point) acoustic Doppler system and consists of a transmitter and three 10 MHz receivers. The transmitters are positioned in 120° increments around a 10 MHz transmitter and slanted at 30° from the axis of the transmit transducer. This focuses on a common sample volume located 10.8 cm from the probe (Voulgaris and Trowbridge, 1997). The system operates by transmitting short acoustic pulses along the transmit beam. In the same way as the ADCP, as the pulses pass through the water a part of the pulse is reflected by small particles suspended in the water. The phase data subsequently converted into velocity estimates using the method identified by Miller and Rochwarger (1972).

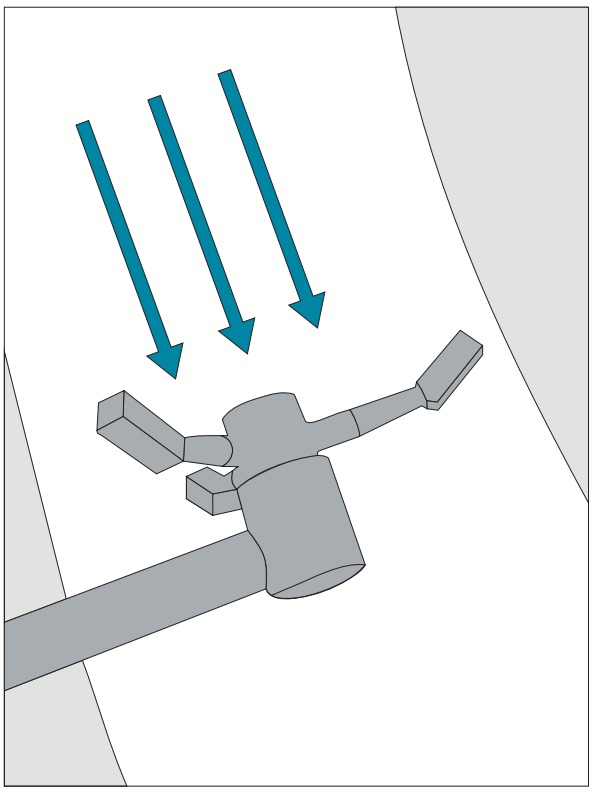

Figure 6.1: *A diagram of the ADV in place in the flume channel.*

6.2.1.1 Data Quality and Filtering

ADV measurements, while capable of capturing 3-D velocity profiles, are subject to 'spike noise' as a result of Doppler signal aliasing, air bubble effects, etc. (Voulgaris and Trowbridge, 1997). The biggest issue with spikes is that they can look similar to turbulent components in the velocity data (Goring and Nikora, 2002). Several algorithms for the de-spiking of ADV data have been proposed. The method proposed by Mori et al. (2007) consists of a 3-D phase space method. All data presented in this section were 'de-spiked' according to the methods of Goring and Nikora (2002), using the MATLAB toolbox developed by Nobuhito Mori (Mori et al., 2007).

In addition to noise filtering, the 'checksum' and 'velocity correlation' factors were also used as a means of removing bad data. Checksum values equal to 1 were removed as they indicate low quality data, and velocity correlation values of less than 70% were also removed.

6.2.1.2 ADV Usage

The ADV was only used during the set-up of the flume to establish the current velocities in the flume and to calibrate the motor; the ADV probe was removed during the experiment sets as it had a continuous leak and it was thought that repeated applications of sealant may interfere with the nutrient concentrations within the flume. Within the calibration phase, turbulence conditions were established and it was assumed that these conditions would remain the same when the probe was removed.

6.2.2 Mini-Annular Flume

Sediment dynamics have commonly been interpreted through the use of an annular flume, in which the flow is induced by a rotating annular ring (Figure

6.2) (Lau and Droppo, 2000; Bale et al., 2002). Advantages include the development of a fully formed boundary layer as a result of the infinite flow length. In contrast to straight re-circulating flumes, annular flumes are more appropriate for investigations of cohesive sediment dynamics as aggregates are not affected by pumps and filters required for re-circulation of water (Manning et al., 2007*b*).

Numerous annular flume studies have been conducted in the past, as indicated by the selection of examples listed in Table 6.1. An annular flume has been used for a variety of experiments, spanning several disciplines, with the majority of experiments examining the interactions between hydrodynamics and sediment characteristics. Prior to the development of *Sedflume* (a commercial tool for the characterisation of sediment transport), the annular flume was the leading method of erodability and critical shear stress measurement for sediment transport studies (Thibodeaux and Mackay, 2010).

In later years, annular flume experiments evolved to examine other disciplines, in relation to sediments (Table 6.1). Of particular relevance to this study, Zhao (2009) used an annular flume to examine the effects of turbulent resuspension events in relation to the release and transformation of both DIP and DOP from sediments. Zhao (2009) observed that DIP had a strong linear relationship with shear stress in pure water and artificial seawater, but that there was no significant relationship between DOP and shear stress. Following the establishment of physical controls, Zhao (2009) went on to examine the chemical transformations that occurred as a result of a release from suspended sediment. In contrast to the experiment conducted by Zhao (2009), the experiment conducted in this study focused solely on the micro- and meso-scale controls on the release of inorganic macro-nutrients.

The advantages of annular flumes over conventional recirculating straight flumes

Table 6.1: *Examples of the types of experiments conducted in annular flumes.*

Authors	Brief Description
Bale et al., 2006	Critical erosion threshold of sediments
Barlow et al., 2004	Phosphorus interactions with bed sediments
Couceiro et al., 2009	Reactivity of nickel in estuarine sediments
Lansard et al., 2006	Plutonium mobilisation from marine sediment resuspension
Manning et al., 1999	Floc characteristics with regard to turbulent shearing
Manning et al., 2007	Flocculation properties recorded by LabSFLOC
Orvain et al., 2006	Influence of cohesiveness on bioturbation effects
Partheniades et al., 1966	Erosion and deposition effects
Pope et al., 2006	Estimation of bed stress by TKE
Prochnow et al., 2002	Biogenic sediment stabilisation simulation
Wang et al., 2011	Suspended sediment concentration vs. shear stress

were described by Partheniades et al. (1966), who used an annular flume to measure the erosion and deposition of cohesive sediments (Rodi and Fueyo, 2002). Advantages included the lack of pumps that have been reported to break down suspended sediment; the loss of effects created by inflow and outflow of water in a recirculating system (Partheniades et al., 1966; Booij, 1994), as well as the uniformity of flow in the longitudinal direction (Rodi and Fueyo, 2002). Annular flumes also have the advantage of being a closed system; this means that potential entrance effects can be avoided (Thibodeaux and Mackay, 2010). Entrance effects represent a pressure change that cause abrupt changes in the velocity profile, commonly related to capillary flow (Jastzebski, 1967).

A disadvantage of an annular flume is that the curvature of the system invokes secondary flow velocities, yielding a more complex 3-D flow field instead of a 2-D flow field (Booij, 1994). To date there is only one way to counteract the 3-D flow field; by rotating the flume lid and the flume walls in opposite directions (Partheniades et al., 1966). For the purposes of this study, the flume will remain stationary due to the inherent difficulties in rotating the base of the flume and the ring in opposite directions.

The experiments in this chapter used equipment and adapted methods defined by Manning and Dyer (1999). The experiment conducted by Manning and Dyer (1999) aimed to examine floc characteristics of sediments collected from the Tamar Estuary, in relation to turbulent shearing, which has been established as the more dominant mechanism in the process of flocculation (Mehta and Partheniades, 1975; Manning and Dyer, 1999). By looking at the inter-relationships between floc characteristics over increasing turbidity and turbulent shear environments, the authors were able to calculate the effective density and porosity of the flocs. This was achieved using measurements (settling velocity and floc size) recorded with the flume and camera system, LabSFLOC I (used in chapter 4) devised by Dr Andrew Manning (Manning and Dyer, 1999; Manning et al., 2010a). In contrast to the method used by Manning and Dyer (1999), the LabSFLOC I camera system was not used in this experiment due to lack of availability. Instead, a LISST (in laboratory configuration) was used to determine particle

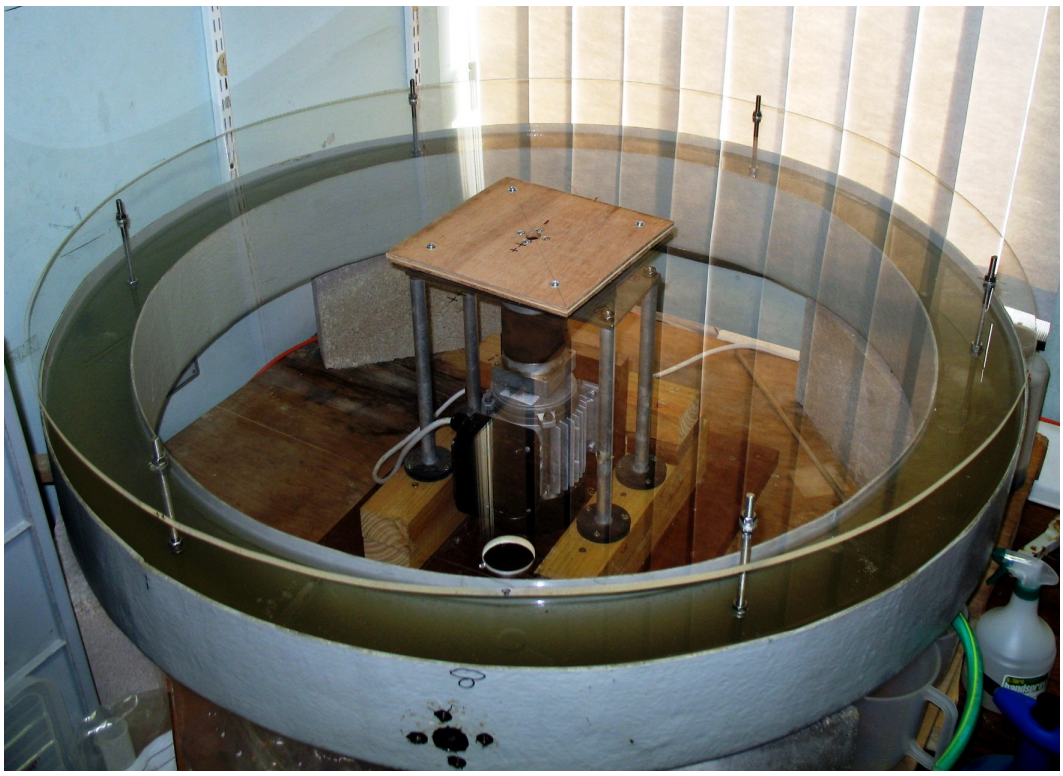

Figure 6.2: *The mini-annular flume set up at Plymouth University.*

concentration and changes in particle size (see section 6.2.3).

In the experiment conducted by Manning and Dyer (1999), four different SPM concentration levels, 80, 120, 160 and 200 mg L^{-1}, were examined in the flume at increasing shear stress rates. The water in the flume was kept at the same temperature (20°C) and the salinity of the water was maintained at 10 PSU (Manning and Dyer, 1999). The initial sediments in the flume were sheared for 30 minutes at a shear stress of 0.6 N m^{-2} before the motor was stopped and the camera started recording. The motor was started again but at a different speed to generate a different shear stress; decreasing increments of 0.1 N m^{-2} down to 0.1 N m^{-2} (Manning and Dyer, 1999). This reduction in shear stress was to emulate the turbulent shear stresses found in a natural marine environment (Manning and Dyer, 1999). This method was adapted in order to emulate the conditions experienced in the Tamar estuary (chapter 5):

- Three shear stress increments were used for 15 min. (determined using calibration/set-up procedures).
- A number of experiments were conducted with 0 PSU salinity with a view to establishing baseline conditions. Later, a salinity of 5 PSU was selected.
- The motor was not stopped to take particle size measurements.

The annular flume was identified as a suitable instrument to achieve the objectives for this chapter. The instrument has been used in a variety of experiments as outlined in Table 6.1 but the method described by Manning and Dyer (1999) was chosen as the base method for the laboratory experiments in this chapter.

For this study, a mini annular flume of width 1.2 m, with an internal channel width and depth of 0.1 m and 0.15 m, respectively was used (Figure 6.2). The original design has a detachable roof holding a ring, fitted to the dimensions of

the flume with six 15 mm (depth) paddles placed equi-distant around the ring. The ring is driven by an AC motor that was controlled by a variable frequency AC motor control unit (Manning and Whitehouse, 2009).

A number of preliminary flume experiments were conducted with a view to ensuring that the conditions were suitable for the experimental runs to be conducted in line with the aims and objectives outlined at the start of the chapter. The primary objective in the method development was to achieve a current velocity of similar magnitude to the conditions experienced in the Tamar estuary. The maximum velocity, seen in chapter 5, was 0.6 m s^{-1}, with an average velocity of 0.21 m s^{-1} (flume flow conditions are reported in section 6.2.6). The results of the performance assessment can be see in Appendix 1.

6.2.2.1 Calculating Turbulence in the Flume

Using the same method as Manning and Dyer (1999), frictional (shear) velocity (U_*), average shear stress (τ), turbulent velocity fluctuations (G) and the microscale of turbulence (η) were calculated.

The equation for frictional (shear) velocity is (Delo, 1988):

$$U_* = ung^{-1}/h^{1/6} \tag{6.1}$$

where n is Manning's bed roughness coefficient, g is acceleration due to gravity, and h is the depth of the flow. The flume had a very smooth channel surface and a Manning bed roughness coefficient of 0.011 was estimated (Manning and Dyer, 1999). The average shear stress (τ) was then calculated as:

$$\tau = \rho_w U_*^2 \tag{6.2}$$

where ρ_w is the density of the water. Turbulent velocity fluctuations were cal-

culated in order to further calculate the Kolmogorov microscales of turbulence (length):

$$G = U_*(u/v.H)^{0.5} \tag{6.3}$$

where H is the water column depth, v is the kinematic viscosity (molecular viscosity divided by the density of water), U_* and u are the frictional and mean current velocities, respectively. Kolmogorov microscale of turbulences (length) were calculated using Equation 6.4.

$$\eta = (v/G)^{0.5} \tag{6.4}$$

Results of the above calculations are presented in Table 6.3.

6.2.3 LISST-100C - Laboratory Set-up

A LISST-100C (2.5 - 250 μm) was used to determine the particle size distribution and volume concentration. Basic details of operation can be found in section 3.3.3 of chapter 3 and this following section outlines the adjustments made to suit the laboratory set up. The LISST-100C in laboratory mode used 'burst' mode sampling. The LISST-100C used in this particular laboratory study could be used as a LISST-ST whereby a settling chamber is attached to the LISST and a propeller used to suspend particles for measurement of the settling velocity. This particular method was deemed unsuitable as no measurements of particle size are available with settling velocity data.

6.2.4 Cleaning Protocol

The cleaning protocol for all plastic- and glassware was the same as that outlined in chapter 3. The material of the flume, however, required an alternative application method and strength of cleaning agents. Prior to all experiments, the mini annular flume was first rinsed of dirt and dust with UHP water. A

weak (5% v/v HCl) acid solution was applied throroughly using a spray bottle before being rinsed thoroughly with UHP water three times. The fitted tap that was used to drain the flume and to take water and LISST samples, was removed from the flume and rinsed before being sprayed with a weak acid solution. The o-ring was removed and rinsed separately to prevent damage to the rubber. Once sprayed with acid, the tap was rinsed clean with UHP water before being re-attached to the flume. Each time the tap was removed, it required a new PTFE seal when re-attaching it to the flume. This cleaning protocol, while not as rigorous as for the plastic- and glassware, was the most appropriate method to ensure clean apparatus while preventing damage to the equipment. When the flume was not in use, the equipment was covered with a large plastic sheet to limit contamination. Filtration equipment was stored in air-tight bags and an acid-washed, clean air-tight box.

6.2.5 Experiment Design

Prior to each run, the flume was cleaned as per the protocol outlined above. Once clean, the flume was filled with 37 L UHP water. The volume of water in the flume was slightly reduced during the adaptations - this was a result of the ring without paddles being lower than with the paddles. To input the correct volume of suspended sediment, a sediment slurry was pre-mixed in an acid-washed glass beaker. The same sediment slurry was used throughout the procedure and sub-samples of the slurry were frozen in between experimental runs.

The sampling experiments were designed to emulate the Tamar estuarine environment (as far as possible), with particular focus on the changing current speeds over a tidal cycle and the introduction of saline water, as per the Mechanisms outlined in chapter 1. Five experiments (A - E) were devised in line with the aims and objectives of this chapter and are presented in Table 6.2.

The first, **Experiment A**, was devised to determine whether the concentration of suspended sediment in the flume was sufficient to adequately observe changes in particle concentration and size. This experiment would also confirm that background concentrations of macro-nutrients were low and that there was no observable contamination of equipment. The second, **Experiment B**, was to establish the 'baseline' conditions; the concentration of nutrients released by 1 g L^{-1} of sediment; and to examine the physical characteristics of sediments, such as particle size and SPM concentration. **Experiment C** saw the introduction of low nutrient seawater (LNS) to determine the effect of a salinity increase on particle size and macro-nutrient behaviour, in line with M2 (chapter 1). For **Experiment D**, the concentration was increased to 4 g L^{-1} to investigate M1 further (chapter 1). As a development of Experiment C, **Experiment E** served to examine the effect of an SPM concentration increase on saline waters; it was chosen to continue using LNS as theory suggests that without the cations, flocculation could not occur.

6.2.5.1 Sediment Input & Slurry

A bed sediment sample was collected following the autumn (September) sampling campaign. Sediment was collected from the first 2 cm of the inter-tidal sediment, which was presumed to be the oxic layer, at low tide and frozen shortly after in acid-washed HDPE 150 mL sample pots. The collection of the sediment from the intertidal seabed, while not ideal as it is not representative of sediments in the water column, was a more practicable method of obtaining samples to use in the flume and was an adaptation of the methods deployed by Manning and Dyer (1999); Zhao (2009) and Fitzsimons et al. (2006).

A total of four (4) sample pots were collected supplying approx. 600 g of sediment. The sample remained frozen until use where one (1) pot was withdrawn and a sediment slurry made using UHP water. A slurry was the most appro-

Table 6.2: *Flume experiments to be conducted, including sediment concentrations, water type and aims of the experiment. LNS is Low Nutrient Seawater.*

Set	Sediment Concentration	Water type	Aim
A	0.5 g L^{-1}	UHP Water	To determine whether the concentration of suspended sediment was sufficient to observe changes in particle size.
B	1.0 g L^{-1}	UHP Water	To establish background concentrations of nutrients and their response to changing physical conditions.
C	1.0 g L^{-1}	LNS	Introduction of salt water (low nutrient) to establish the response of nutrient concentrations to changing shear stresses and particle sizes in saline/estuarine conditions.
D	4.0 g L^{-1}	UHP water	To determine whether higher concentrations of SPM result in more pronounced changes in macro-nutrient concentrations.
E	4.0 g L^{-1}	LNS	To determine whether SPM concentration and salinity combined change macro-nutrient concentrations.

priate method of adding sediment to the rotating flume as it would be a homogeneous mixture and would most easily be dispersed into the flow. A sediment slurry of 2,213 g L^{-1} was created using the bed sediment sample and 300 mL UHP water. The slurry created was sufficient to be used for all laboratory experiments. Between experiments, the slurry was refrigerated for up to 24 h and frozen where flume runs were to be conducted more than 24 h apart. This was an attempt to minimise the biological degradation of thawed samples.

6.2.5.2 Sampling regime and collection

Once the experiment sets had been determined, the sampling regime was designed. Sampling was conducted as per Figure 6.3, with samples being collected at each point labelled 'S'. Samples were collected from the installed tap/spigot.

The alternative method was to collect using a glass pipette from the sampling point. This method was discounted because it would require stopping the flume for every sample and the water would lose momentum, requiring longer equilibrium time.

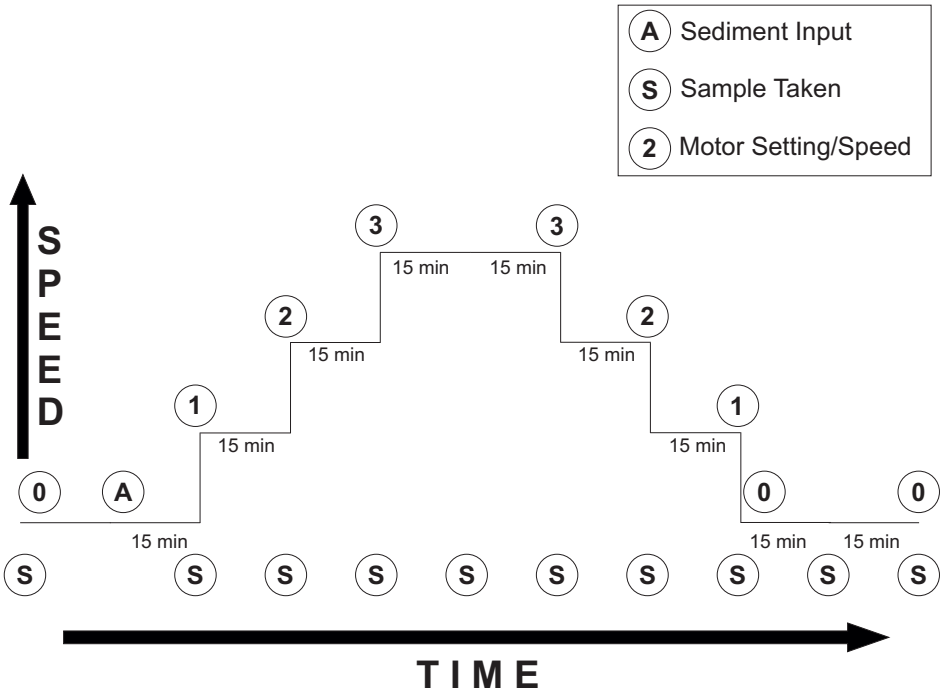

Figure 6.3: *Sampling regime for experiment sets A - E. A marks the point where the sediment slurry was inserted. S marks the point where each water sample was taken. Numbers 0 - 3 show the motor setting, where 0 is stationary and 3 is the maximum speed.*

When the water had been added to the flume, a 'baseline' sample was taken to establish the background concentration of the water. The sediment slurry was then poured into the flume and the next sample was taken. From this point forward, samples were collected at the start of each change in motor speed. The increase and decrease in shear stress that changes in motor speed invoked was designed to emulate the current velocities experienced during the flood and ebb tide experiments seen in chapter 5 (Figure 5.7). At the end of each experiment, the water was left to still in the flume and a final sample was collected when all the sediment had settled.

As per the samples collected in the Tamar and Seine estuary, water samples were collected in triplicate and further divided into 3 for analysis on the relevant instrument. 125 mL of water was taken from the flume and filtered in the same way as for the Tamar estuary and filter papers were saved to determine the suspended sediment concentration in the flume.

Particle size and concentration measurements were taken at the same time as water samples for macro-nutrient analysis using the the LISST-100C instrument. The sample volume of the chamber was 75 mL and so 75 mL of the flume water was taken from the tap and transferred by glass beaker to the settling chamber. Between each sample, the chamber was emptied back into the flume and rinsed thoroughly with UHP water to ensure it had no residual sediment in it.

6.2.6 Flume Flow Conditions

A performance assessment of the mini annular flume was conducted prior to the experiments. This aimed to determine the suitability of the instrument in its standard configuration and to make modifications, where required. The results of the assessment are presented in Appendix A and a summary is supplied below.

The first flume performance assessments were calculated with the same set up as described by Manning and Dyer (1999), including six paddles of 15 mm depth (10% of the total water depth). Current velocities ranged between 0.1 - 0.2 m s^{-1}; significantly lower than those reported by Manning and Dyer (1999). Manning and Dyer (1999) reported velocities of up to 1 m s^{-1} using exactly the same parameters. It is possible that some of the original instrumentation may have changed in the years preceding this study, including the strength/type of the motor; in the time frame of this study, it was not possible to find an alternative

and re-configure the flume. Shear stress (τ) ranged between 0.12 - 0.47 Pa, with Kolmogorov microscale (length) (η) ranging between 13 - 22 μm. An assessment of the individual flow current velocities revealed a number of inconsistent turbulent bursts in the flow and so the paddles were removed in an attempt to make a more consistent flow. The same assessment was completed without the paddles and the comparative results of physical parameters are presented in Table 6.3. Modification of the flume yielded a more consistent flow (see section A.1) but at the cost of minorly reduced current speeds and shear stresses. Calculated current velocities for both set-ups were approximately consistent with the average flow conditions experience in the Tamar estuary (0.12 m s^{-1}), but the maximum current velocity obtained in the Tamar estuary (0.6 m s^{-1}) could not be obtained using the flume. This was due to insufficient motor power to generate higher current velocities.

Table 6.3: *A summary of physical parameters calculated during the flume performance assessment. Where u = current velocity (m s^{-1}), τ = shear stress (Pa) and η is the Kolmogorov microscale length (μm).*

Parameter	**Without Paddles**			**With Paddles***		
u (m s^{-1})	0.07	0.10	0.15	0.10	0.15	0.20
N m^{-2}	0.94	1.36	2.00	1.36	2.00	2.67
τ (Pa)	0.05	0.12	0.26	0.12	0.26	0.47
η (μm)	29	22	16	22	16	13

6.3 Results

This section presents and discusses the results obtained from each experiment set. Results are presented and discussed for each individual run, with a further discussion as to the differences between each experiment type and the relevance of each proposed Mechanism in chapter 1.

Of note, before each experiment is discussed in detail; concentrations of NO_3^-

*As per Manning and Dyer (1999)

and NH_4^+ were below the limit of detection for all experiments. This will be discussed in detail in the discussion section (section 6.4).

6.3.1 Experiment A - UHP water with 0.5 g L^{-1} sediment

The primary aim of **Experiment A** was to determine whether the proposed cleaning protocol was sufficient to prevent background concentrations of macronutrients contaminating future samples. The secondary aim was determine whether changes in particle size and concentration were apparent and detected by the LISST instrument.

A volume of the pre-made sediment slurry (8.4 mL) was added to the 37 L of water in the flume to make a maximum SPM concentration of 0.5 g L^{-1}. It was anticipated that some of the sediment may not be in suspension at any one time due to insufficient current velocities to entrain and carry larger, heavier particles. Filter papers from water samples were kept and SPM concentrations obtained to determine actual SPM concentrations from each sample (Table 6.4). The maximum concentration obtained by gravimetric filtering was 0.31 g L^{-1} shortly after the slurry was added to the water, while the lowest concentration was 0 g L^{-1} and found prior to the addition of the slurry, and again at the end when the flume had been stationary for 15 min. where all sediment had settled to the bottom of the flume.

Figure 6.4a demonstrates the total volume concentration (calculated by summing the volume concentration of each size bin for each sample taken), while Figure 6.4b presents the volume concentration of each size bin. Background concentrations at the start of the flume run indicate low concentrations (approx 1 μL L^{-1}) of particles between 20 - 500 μm in size. The maximum total volume concentration was 57 μL L^{-1} (approx. equivalent to mg L^{-1}), obtained during the 6th sample when the current velocity was fastest. The increase in concentration

Table 6.4: *Gravimetric filter SPM concentrations - Experiment A.*

Sample Number	**SPM conc. (mg L^{-1})**
1	00
2	310
3	130
4	150
5	160
6	160
7	140
8	110
9	00

was a result of the increased current speed entraining more sediments that had previously settled to the base of the flume. The largest particle size range was seen at sample number 5 where the current velocity had been 0.15 m s^{-1} for 15 min. At this point, the increase in current speed generated conditions conducive for flocculation. It was observed that during the course of the experiment, when current speed increased, so did the particle range and concentration. While the current velocity decreased, the particle size range decreased, but the concentration of particles between 20 - 60 μm remained consistent until the motor had ceased. These conditions indicated an equilibrium in the particle size.

Water samples collected before sediment was added to the flume demonstrated that concentrations of $NO_3{}^-$, $NH_4{}^+$ and $PO_4{}^{3-}$ were all below the level of detection (LOD) by each instrument and the cleaning protocol was, therefore, validated. It was observed, however, that there were no observable peaks or changes in any of the macro-nutrients following addition of the slurry indicating the requirement for a higher SPM concentration to observe changes. The results highlighted, however, that changes in sediment sizes and concentrations were being recorded and that the flume speeds were sufficient to observe changes.

Figure 6.4: *a) SPM concentration (g L^{-1}) and PO_4^{3-} concentration (if applicable). b) Particle size distribution data for the samples collected in Experiment A with 0.5 g L^{-1}. The y-axis shows the median particle size while the colour bar shows the volume concentration in μL/L. Current velocity is on the x-axis.*

6.3.2 Experiment B: UHP water with 1 g L^{-1} sediment

Allowing for a UHP water volume of 37 L in the flume, 16.8 mL of the 2,213 g L^{-1} pre-made sediment slurry was transferred to the flume to make a maximum theoretical SPM concentration of 1 g L^{-1}. The sediment slurry was transferred to the still water in the flume and another sample taken. Once the motor was started, samples were taken every 15 min. after the motor speed was changed, as per the sampling regime (Figure 6.3). In contrast to the sampling regime shown in Figure 6.3, a sample was taken immediately after sediment addition instead of waiting for 15 min. and no sample was taken 30 min. after the flume had stopped, giving only 9 samples per flume run for **Experiment B**.

Results of **Experiment B** are shown in Figure 6.6. Figure 6.6a shows the PO_4^{3-} concentration for each sample and total volume concentration for each sample, while Figure 6.6b shows the volume concentration in each particle size band.

Table 6.5: *Gravimetric filter SPM concentrations and PO_4^{3-} concentrations, including error (+/-) -* ***Experiment B****.*

Sample Number	SPM Conc. (mg L^{-1})	[PO_4^{3-}] (μM)	+/-
1	112	0.97	0.13
2	1008	0.72	0.09
3	608	0.71	0.28
4	576	0.55	0.07
5	704	0.65	0.21
6	496	0.57	0.17
7	360	0.47	0.08
8	384	0.52	0.03
9	400	0.02	0.00

Gravimetric filter SPM concentrations and PO_4^{3-} concentrations are presented in Table 6.5. The maximum gravimetric SPM concentration (1,008 mg L^{-1}) was recorded shortly after the sediment slurry had been added to the flume. The second peak (704 mg L^{-1}) in SPM concentration according to the gravimetric sample results was recorded at sample 5.

Particle size distribution results in Figure 6.6b demonstrate volume concentrations of up to 14 μL L^{-1}, with particle sizes reaching the limit of the LISST instrument (500 μm). The maximum volume concentration measured by the LISST was at sample 6 in the upper size band (460 - 500 μm) and was coincident with the maximum current velocity. The increase in the number of larger particles found in sample 6 indicated flocculation of smaller particles, or the entrainment of larger particles as a result of the increase in SPM concentration that occurred at sample 5. When the current velocity decreased to 0.07 m s^{-1}, the number of larger particles decreased with the volume of smaller particle remaining the same. If the particles had broken up due to turbulence effects, the number of smaller particles would have increased. This suggests that the newly created flocs, or entrained larger particles, had settled when the current velocity decreased.

Macro-nutrient data presented in Figure 6.6b shows the concentration of PO_4^{3-}. Concentrations of NO_3^- and NH_4^+ were below the LOD for all samples. It was not expected to see NO_3^- concentration in the water samples as it is not typically bound to sediments (Fitzsimons et al., 2011) and there was no other source. It was proposed that the concentrations of NH_4^+, if any, were below the LOD due to the low concentration of SPM. It is also possible that the lack of salt water cations present may have prevented ion exchange as described in M2 (Salinity). This indicated that a greater amount of energy and SPM are required to make a significant contribution of NH_4^+ from micro-scale suspended sediment processes.

The PO_4^{3-} concentration ranged between 0.41 - 0.98 μM and demonstrated a linear relationship (see Figure 6.5). The highest concentration was found in the first sample taken and analysis of the data by ANOVA identified this sample as significantly different to all other samples. This was supposed to be when

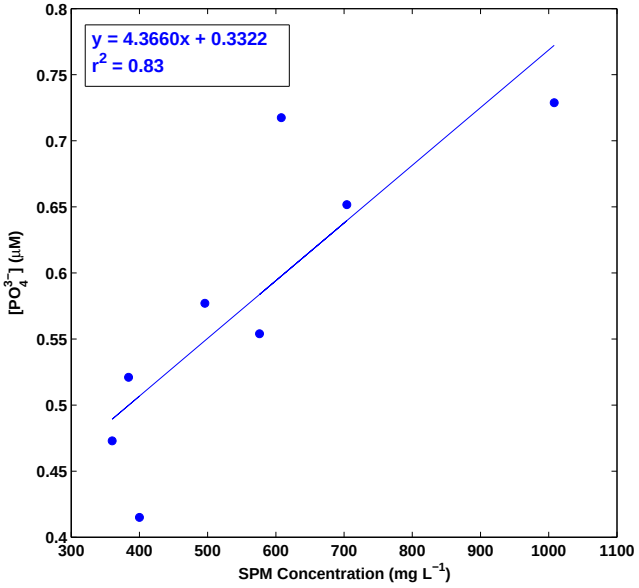

Figure 6.5: *SPM concentration data versus PO_4^{3-} concentration for* ***Experiment B****. This figure does not include the presumed-anomalous results obtained prior to addition of the slurry.* r^2 *is 0.83.*

the water was 'clean' and prior to the addition of the sediment slurry. This was likely due to a contaminated sample; either at the filtering and bottling stage, or during the processing on the instrument. If this data point is omitted and assumed anomalous, the concentration ranges between 0.41 - 0.74 μM with the highest concentration occurring just as the slurry is added to the water (sample 2). Ignoring the anomalous point at the start of sampling gives a linear relationship between SPM concentration and PO_4^{3-} (see Figure 6.5), with an r^2 value of 0.83 indicating a good relationship. After this, the PO_4^{3-} concentration is seen to decrease until sample number 5. At sample number 5, with the increase in concentration of SPM, a slight increase in PO_4^{3-} occurs (from 0.55 to 0.65 μM). However, this sample was not marked as statistically significantly different from samples 4 or 6; likely a result of the error on this sample (0.21 μM). During the identified period of flocculation, PO_4^{3-} decreases again (samples 5 and 6). The implication of the decrease in PO_4^{3-} is that either the increase in concentration of SPM increases the available surface areas for particles to bond with, or that the formation of larger flocs traps a portion of PO_4^{3-} within the interstitial wa-

ter, thus lowering the overall concentration of PO_4^{3-} in the water, in line with M1.

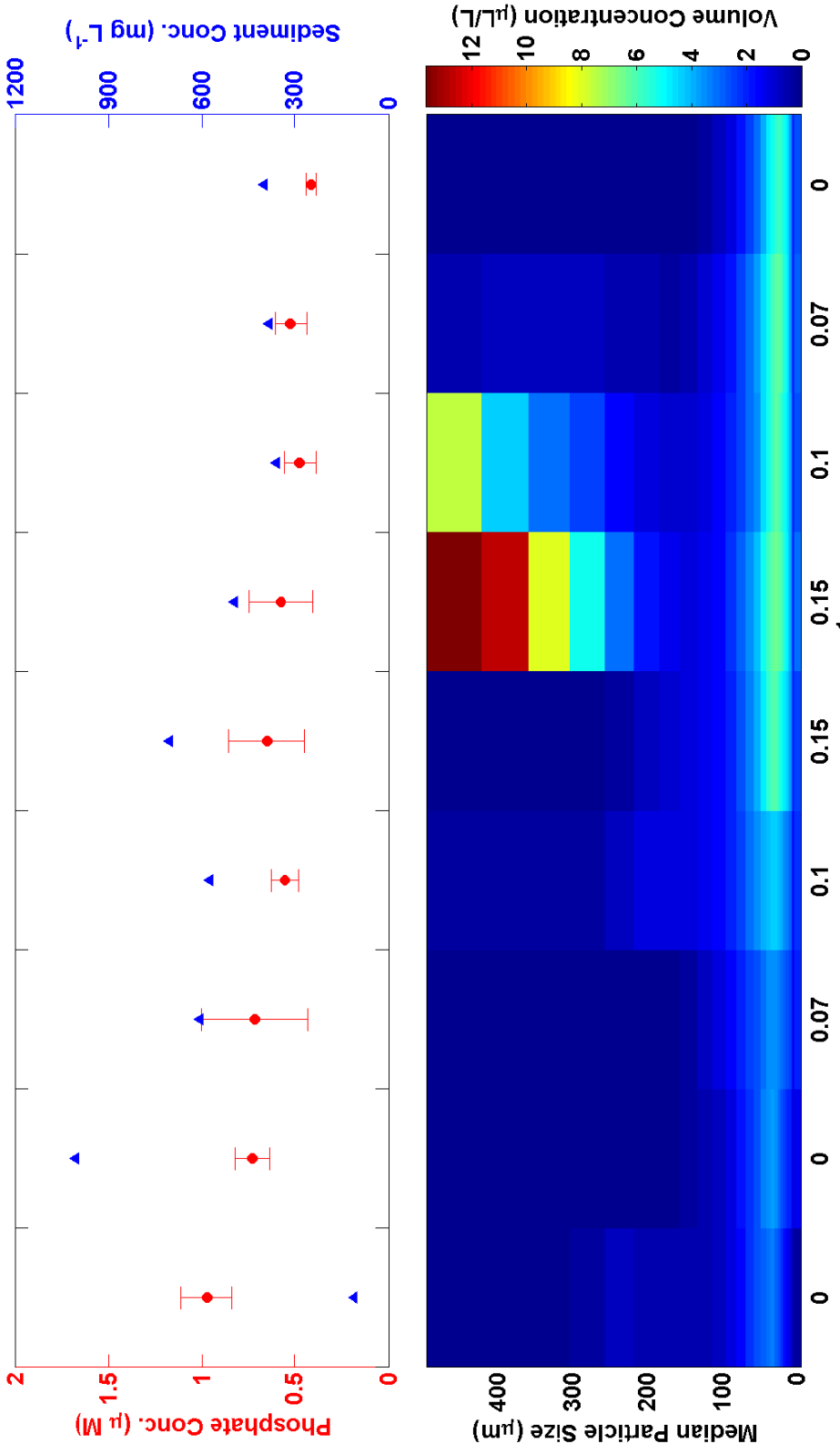

Figure 6.6: *a) PO_4^{3-} concentration and SPM concentration for each sample. b) Particle size distribution data for the samples collected in Experiment Set B. The y-axis shows the size bands of the LISST instrument and the colour bar the volume concentration in* μL/L. *Current speed of the water is on the x-axis.*

6.3.3 Experiment C: Low Nutrient Seawater with 1 g L^{-1} sediment

Prior to increasing the SPM concentration, **Experiment C (ExpC)** was devised to determine whether salinity played a role in the sediment-nutrient processes occurring in the flume. Low nutrient seawater (LNS) was added to UHP water to create a salinity of 5 PSU. Prior to the experiments, a set of LNS standards were prepared and compared to standards made using UHP water. Results of the performance assessment of LNS are presented in Appendix A. An adjustment was made to the sampling regime for **ExpC**; a sample was collected shortly after the slurry was added, and then again 15 min. later, before the flume was started. This sample was added to establish whether the concentration remained constant prior to the flume starting after the sediment was added.

Allowing for a UHP water volume of 37 L in the flume, 16.8 mL of the 2,213 g L^{-1} pre-made slurry was transferred to the flume to make a maximum theoretical SPM concentration of 1 g L^{-1}. The sediment slurry was transferred to the still water in the flume and another sample taken. Once the motor was started, samples were taken every 15 min. after the motor speed was changed, as per the sampling regime (Figure 6.3).

Figure 6.9 shows the results of **Experiment C**. SPM and PO_4^{3-} concentration data is shown in Figure 6.9a, while particle size distribution data is presented in Figure 6.9b. SPM concentration and PO_4^{3-} concentrations are also shown in Table 6.6. The maximum SPM concentration recorded gravimetrically was 568 mg L^{-1}, where the sediment was added to the flume (sample 2). Later, at sample 8, the SPM concentration peaked for a second time with a concentration of 520 mg L^{-1}, shortly after the maximum current velocity had been maintained for 30 min. Despite the same input concentration of sediment (1 g L^{-1}), the concentration of sediment that occurred during sampling was approximately 42%

lower than those experienced in **ExpB**. It was anticipated that the SPM concentration would remain the same with the addition of sediment and that volume of larger particles would significantly increase due to increased salinity aiding flocculation processes (Pomeroy et al., 1965; Jones, 1989; Gardner et al., 1991).

Table 6.6: *Gravimetric filter SPM concentrations and PO_4^{3-} concentrations - **Experiment C**.*

Sample Number	Current Velocity (m s^{-1})	SPM Conc. (mg L^{-1})	[PO_4^{3-}] (μM)	+/-
1	0.00	160	0.00	0.00
2	0.00	568	0.36	0.04
3	0.00	464	0.32	0.15
4	0.07	408	0.32	0.22
5	0.10	392	0.37	0.21
6	0.15	384	0.12	0.02
7	0.15	424	0.13	0.08
8	0.10	520	0.23	0.04
9	0.07	448	0.65	0.15
10	0.00	432	0.29	0.09
11	0.00	392	0.21	0.05

As with **ExpB**, SPM concentration and PO_4^{3-} demonstrated a linear relationship (see Figure 6.7). While a strong relationship occurred (r^2), the relationship was considerably weaker than **ExpB**. This was proposed to be a result of greater variability in particle size associated with larger floc formation due to the presence of saltwater cations.

Figure 6.8a demonstrates two example particle size distributions recorded during **ExpC**. Sample 2 was taken shortly after sediment was added to the flume and the increase in volume concentration across all particle sizes increased.

Sample 6 was taken after 30 min. of 0.15 m s^{-1} and, although small, an increase in larger particle sizes can be seen. Figure 6.8b shows the same two profiles collected during **ExpB**. In contrast to Figure 6.8a, the volume concentration recorded by the LISST instrument demonstrated a lower volume concentration

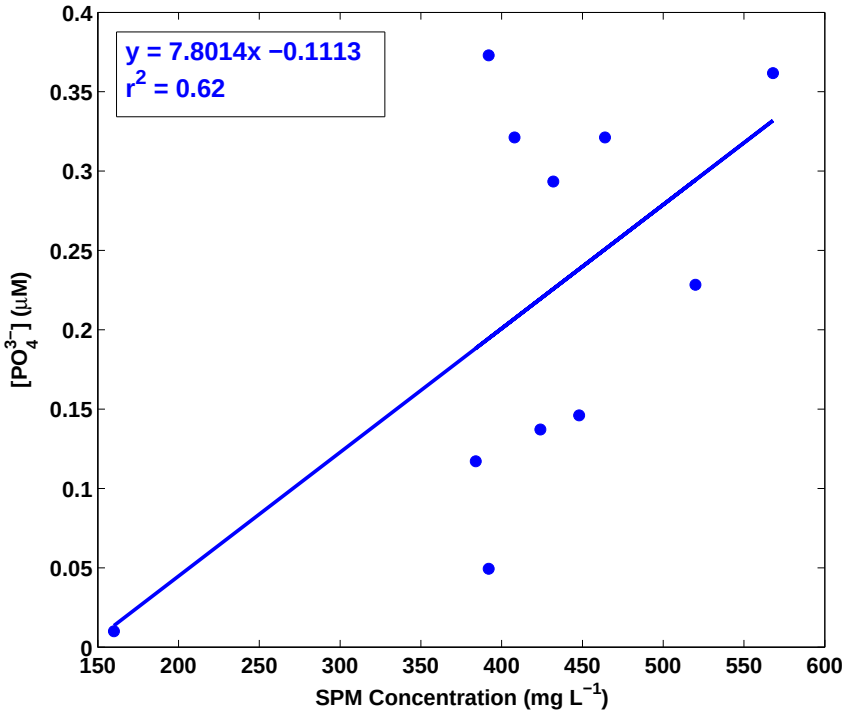

Figure 6.7: *Linear regression analysis of SPM concentration and PO_4^{3-} for* ***Experiment C****.*

for both profiles, and there was no significant difference between the two. Most significantly, during Sample 6 where the flume had generated a current velocity of 0.15 m s^{-1}, there were very few larger flocs in comparison to **ExpC**. This confirms that the addition of LNS to the water increased the ability to flocculate, despite the lower SPM concentration (Gardner et al., 1991).

The SPM concentration decreased to 392 mg L^{-1} when the current speed decreased. Despite the decrease in current velocity for the final two samples, the SPM concentration did not decrease significantly. This suggested that the effective density of the particles in suspension was lower than those experienced in **ExpB**, possibly a result of the salt water cations present due to the LNS water.

The maximum concentration of PO_4^{3-} was 0.65 μM and occurred during sample 9 when the flume had stopped spinning and before settling could occur. At

this point, total volume concentration measured by the LISST had peaked for the second (169 μm). Analysis of the data by ANOVA and a Tukey's test identified sample 9 as significantly different from all other samples (p = 0.05). The concentration of PO_4^{3-} increased from 0 to 0.36 μM shortly after the sediment slurry was added to the flume and both sample 1 and sample 2 were marked as statistically significant in the ANOVA analysis (p = 0.05). The concentration remained stable until the current velocity had remained at 0.15 m s^{-1} for 15 min. whereby the concentration dropped from 0.37 (sample 5) to 0.12 μM (sample 6); samples 5 and 6 were marked statistically significantly different from each other in ANOVA analysis (p = 0.05). The decrease in PO_4^{3-} and increase in particle size during a period of higher velocity could indicate that M1 is occurring; flocculation in the water column removed PO_4^{3-} by trapping it in interstitial water, or the increase in concentration, number of particles and flocculation increased the available surface area for PO_4^{3-} to bond to. The decrease in PO_4^{3-} was greater than that experienced during **ExpB** suggesting that salinity may increase the chances of bonding with particle faces in line with work completed by Gardner et al. (1991).

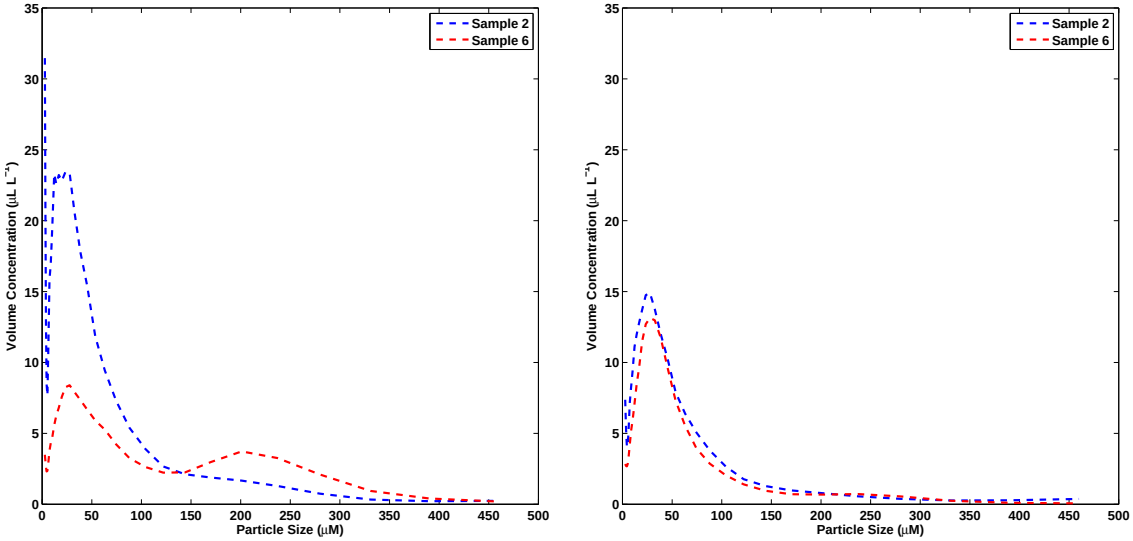

(a) *Experiment C.* ***(b)*** *Experiment B.*

Figure 6.8: *PSD for both Experiment C and Experiment B. The blue lines indicate the PSD shortly after the sediment slurry was added, and the red a sample taken during the experiments.*

Despite the addition of LNS water to increase the salinity, NO_3^- and NH_4^+ were still below the limit of detection.

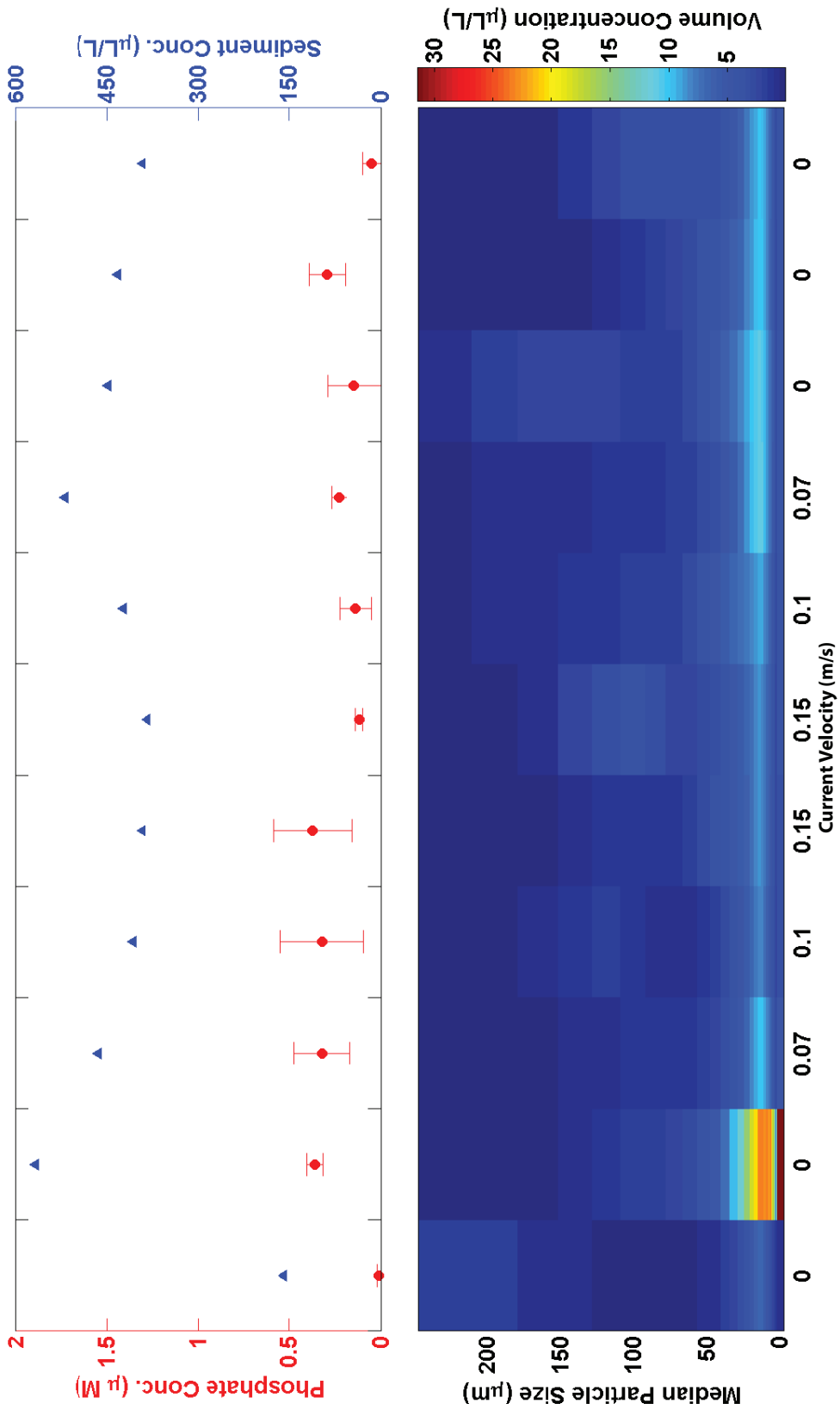

Figure 6.9: *a) PO_4^{3-} concentration and total volume concentration for each sample. b) Particle size distribution data for the samples collected in Experiment C. The y-axis shows the size bands of the LISST instrument and the colour bar the volume concentration in* μL/L*. Current speed of the water is on the x-axis.*

6.3.4 Experiment D - UHP Water with 4 g L^{-1} Sediment

The aim of **Experiment D (ExpD)** was to further investigate the effect of SPM concentration on macro-nutrient concentrations in the water. The SPM concentration was made up to 4 g L^{-1} using the same sediment slurry. UHP water was used in order to compare with results obtained in **Experiment B**. There were no changes to the sampling regime described in Figure 6.3.

Results of **ExpD** are shown in Figure 6.11. Figure 6.11a shows the SPM concentration measuring using gravimetric filter weights, while Figure 6.11b shows the concentration of PO_4^{3-}. SPM concentrations and PO_4^{3-} concentrations are also shown in Table 6.7. Despite the input of 4 g L^{-1}, SPM concentrations in suspension were approximately one quarter of the total input with a maximum gravimetric SPM concentration of 1.61 g L^{-1}, occurring shortly after the sediment slurry had been added to the flume. The second peak in SPM concentration was 1.40 g L^{-1} and was coincident with increasing, but not maximum, current velocity (u = 0.1 m s^{-1}).

Table 6.7: *Gravimetric filter SPM concentrations and PO_4^{3-} concentrations - Experiment D. Note that SPM concentrations are now in g L^{-1}. PO_4^{3-} concentrations are also shown.*

Sample Number	SPM Conc. (g L^{-1})	$[PO_4^{3-}]$ (μM)	+/-
1	0.37	1.06	0.17
2	1.61	12.30	0.55
3	1.30	11.79	0.48
4	1.30	13.85	0.65
5	1.40	11.35	0.24
6	1.23	11.46	0.64
7	1.35	11.78	0.69
8	1.12	11.73	0.53
9	1.40	11.25	0.35
10	0.92	12.04	1.05

LISST results recorded particle sizes up to 500 μm (the limit of the instrument).

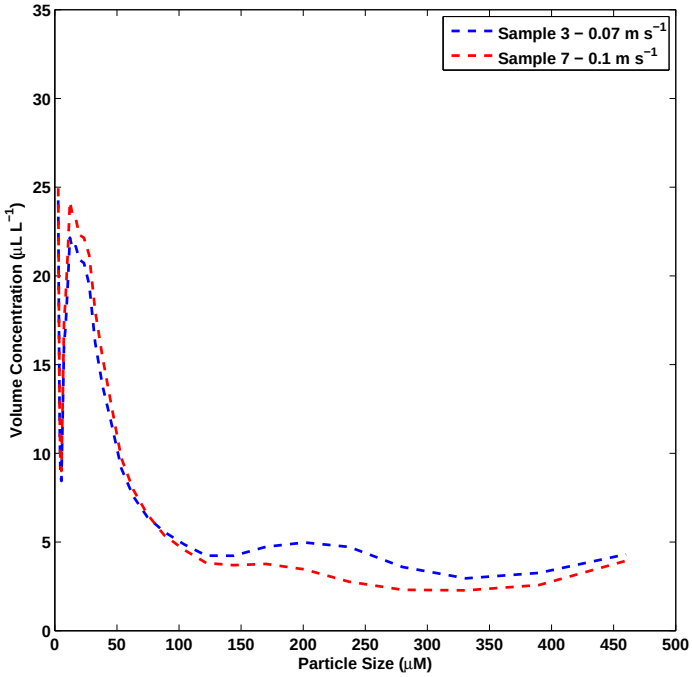

Figure 6.10: *Particle Size Distributions for Experiment D. The blue lines indicate the PSD shortly after the sediment slurry was added, and the red a sample taken during the experiments.*

However, unlike **ExpC** and similar to **ExpB**, particle size distributions indicated that minimal flocculation processes occurred during the period of maximum current velocity (see Figure 6.10).

Once again, concentrations of NO_3^- and NH_4^+ were below the limit of detection, despite the significant increase in SPM concentration. PO_4^{3-} concentrations were between 11.06 and 13.85 μM, with the maximum concentration occurring during sample 4 where the flume had just started to spin at 0.1 m s^{-1}. Concentrations in general were an order of magnitude higher than those measured in **Experiments A, B and C**. Sample 4 was identified as statistically significantly different to all other samples by ANOVA and Tukey's analysis. This maximum PO_4^{3-} concentration did not coincide with the maximum SPM concentration. This, combined with the absence of salt water cations, suggests a kinetic process such as turbulence was occurring at this point. Following the maximum

concentration at sample 4, sample 5 was also identified as statistically significantly different from sample 4 with a concentration of 11.37 μM. This drop in concentration was coincident with a minor increase in volume concentration of larger particles suggesting that flocculation may have occurred and trapped PO_4^{3-} within the interstitial waters, corresponding with M1.

The concentration of PO_4^{3-} at sample 2 was also marked as statistically significant from all other samples ($p = 0.05$). This is where the slurry had been added to the water and gave a concentration of 12.30 μM. The increase in concentration that occurred here was a result of the input of sediment to the flume suggesting that loosely bound PO_4^{3-} was broken away from the sediment in the process. This could indicate the turbulence (M3) contributed to increasing the concentration of PO_4^{3-} in the water column.

Unlike **ExpB** and **ExpC**, there was no linear relationship or correlation between SPM concentration and PO_4^{3-} concentration. This may be a result of the higher concentrations of PO_4^{3-} hiding changes that previously would have been significant.

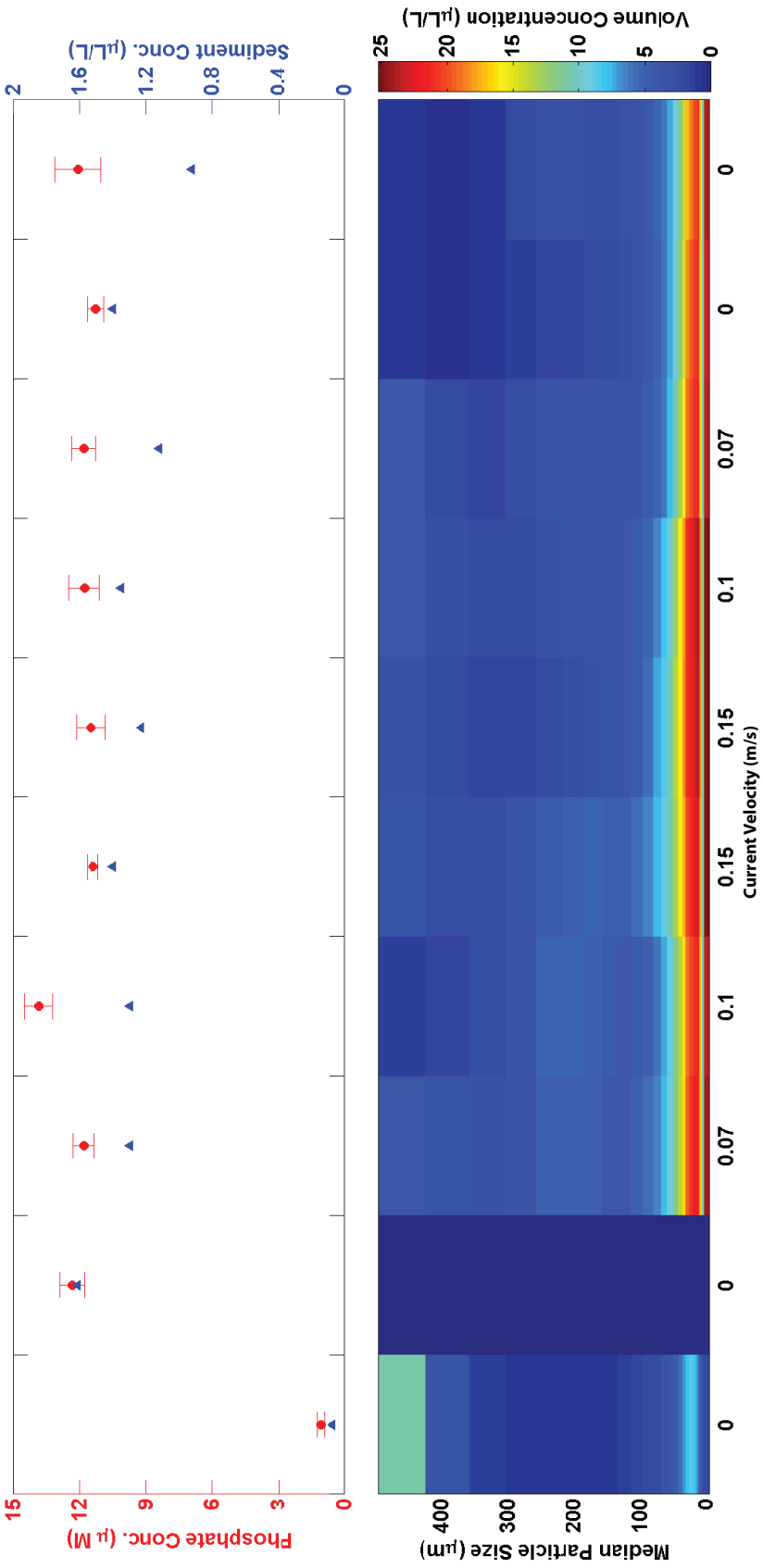

Figure 6.11: *a) PO_4^{3-} concentration and total volume concentration for each sample. b) Particle size distribution data for the samples collected in Experiment Set D - Run 1. The y-axis shows the size bands of the LISST instrument and the colour bar the volume concentration in μL/L. Current speed of the water is on the x-axis.*

6.3.5 Experiment E - Low Nutrient Seawater with 4 g L^{-1}

The aim of **Experiment E (Exp E)** was to determine whether an increase in SPM concentration combined with LNS water would yield more variations in all macro-nutrient concentrations. For **ExpE**, LNS was used to create a salinity of 5 PSU, as per **ExpC**. However, 67.2 mL of the 2,213 g L^{-1} pre-made slurry was transferred to the 37 L flume to make a maximum theoretical SPM concentration of 4 g L^{-1}. There only adjustment to the sampling regime was a corrupt LISST sample at the end of sampling.

Results of **ExpE** are presented in Figure 6.13. SPM concentrations and PO_4^{3-} are presented in Figure 6.13a while volume concentrations in particle size bins measured by the LISST are in Figure 6.13b. SPM concentrations and PO_4^{3-} concentrations are also presented in Table 6.8.

Table 6.8: *Gravimetric filter SPM concentrations and PO_4^{3-} concentrations - Experiment E. Note that SPM concentrations are now in g L^{-1}. PO_4^{3-} concentrations are also shown.*

Sample Number	SPM Conc. (g L^{-1})	[PO_4^{3-}] (μM)	+/-
1	0.39	0.47	0.13
2	1.14	11.07	0.55
3	1.12	10.98	0.32
4	1.87	10.69	0.40
5	1.55	11.11	0.43
6	1.46	11.04	0.46
7	1.42	12.18	1.89
8	1.36	11.09	0.60
9	1.29	10.77	0.45
10	1.12	10.75	0.34

SPM concentrations measured by gravimetric filtration ranged between 0.39 - 1.87 g L^{-1}, with the maximum SPM concentration occurring shortly after addition of sediment to the flume, as per previous experiments. Despite a predetermined concentration of 4 g L^{-1}, the maximum suspended concentration

only reached 1.87 g L^{-1}. As with previous runs, a large portion of sediment settled to the bottom of the flume and there was insufficient current velocity to entrain all the sediment. The final SPM sample measured did not have a corresponding LISST profile as the file was found to be corrupt; however, despite 30 min. of u = 0 m s^{-1}, 1.12 g L^{-1} remained in suspension. This was a result of less dense particles taking longer to settle.

Volume concentrations recorded by the LISST were an order of magnitude higher than recorded in Experiments A - D; in the range 0 - 160 μL L^{-1}. Unlike **Experiment D**, the addition of the sediment slurry at sample 2 did not saturate the LISST and so it was possible to examine the particle size distribution at this point (Figure 6.12a). This is where the volume concentration of smaller particles (between 0 - 25 μm) increased to 160 μL L^{-1}.

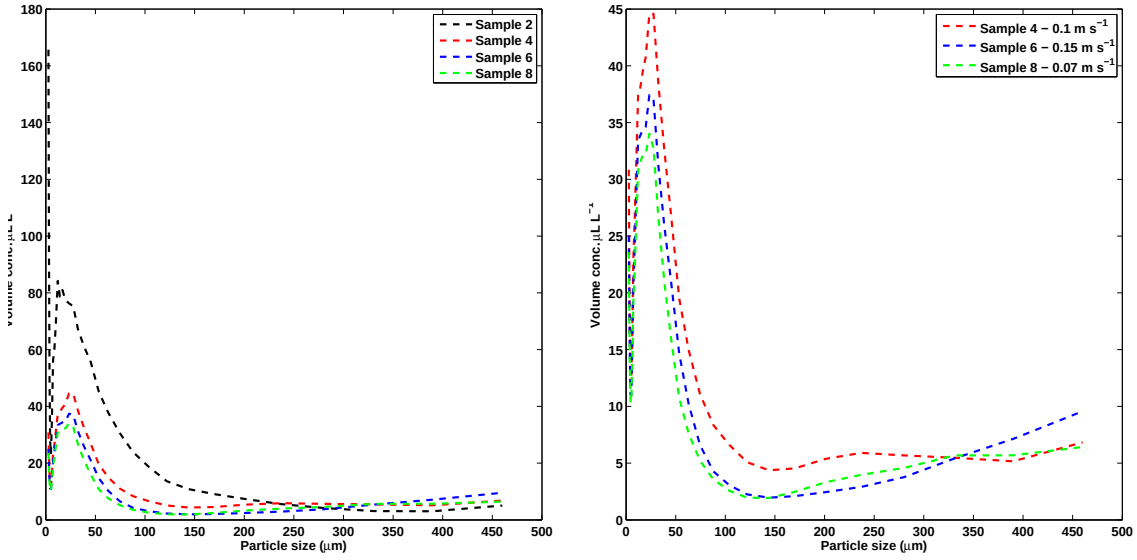

(a) *PSD including Sample 2.* ***(b)*** *PSD excluding Sample 2.*

Figure 6.12: *Particle Size Distributions allowing detailed examination of micro-scale processes affecting particle size.*

Figure 6.12a demonstrates that the volume of particles input at sample 2 dilutes the observable particle changes in subsequent samples. As such, Figure 6.12b shows three separate samples (samples 4, 6 and 8) of particle size distribution.

Here, one can observe that sample 6 collected during maximum current velocity (u = 0.15 m s^{-1}) shows an increase in the volume of larger particles. This was a result of flocculation of smaller particles apparent in sample 4. It could also have been a result of entrainment of larger, denser particles with increased current velocity. Later, during sample 8 (u = 0.07 m s^{-1}), the volume of larger particles decreases again.

Concentrations of PO_4^{3-} ranged between 0.47 - 12.18 μM, consistent with **Experiment D**. The maximum PO_4^{3-} concentration occurred at sample 7, shortly after the period of maximum SPM concentration and a period of flocculation (as shown in Figure 6.12b). This maximum was likely contrasts the theory that increasing floc sizes will trap more interstitial water and, thus, PO_4^{3-}. It should be noted, however, that the error of this sample (1.89 μM) prevented the sample from being statistically significantly different and some caution was used in interpretation.

The PO_4^{3-} concentration measured at sample 5 was identified as being statistically significant from samples 4 and 6. This apparent peak in PO_4^{3-} at sample 5 follows an increase in SPM concentration at sample 4, and preceeded a decrease in SPM concentration at sample 6 where PO_4^{3-} was also observed to decrease. This is consistent with benthic desorption of PO_4^{3-} upon resuspension (reference).

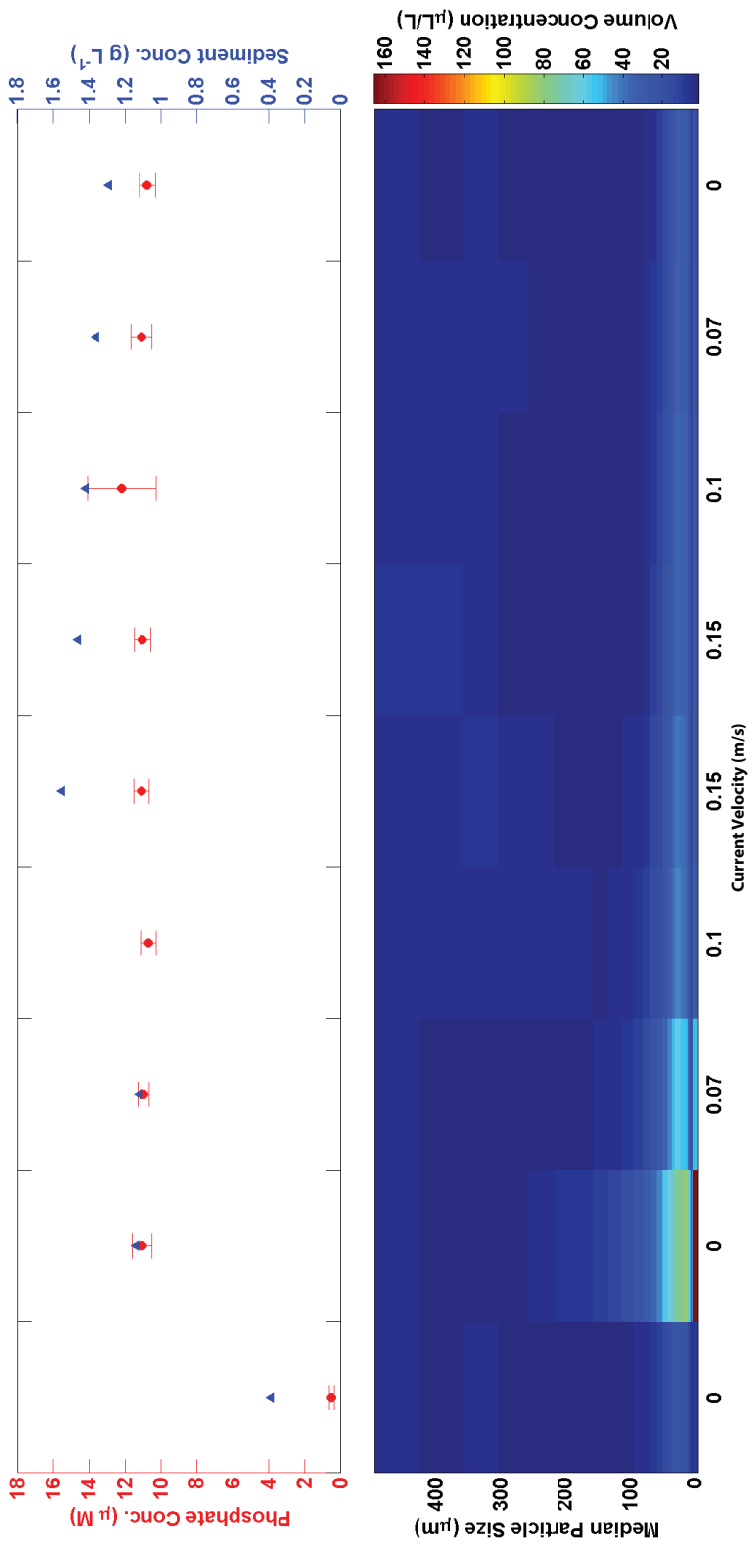

Figure 6.13: *a) PO_4^{3-} concentration and total volume concentration for each sample. b) Particle size distribution data for the samples collected in Experiment E. The y-axis shows the size bands of the LISST instrument and the colour bar the volume concentration in μL/L. Current speed of the water is on the x-axis.*

6.4 Discussion & Conclusions

This section discusses the results of **Experiments A - E** with respect to the objectives outlined in section 6.1, and the Mechanisms outlined in Chapter 1.

Experiments A - E were designed to examine the micro-scale processes affecting macro-nutrient concentrations in the water and, if possible, determine the dominance of each mechanism outlined in chapter 1. The flume experiments served to constrain particular variables, such as temperature and salinity, and eliminate other factors, such as advection and riverine run-off. SPM concentrations and particle characteristics were observed using gravimetric filtration and LISST measurements, while macro-nutrient concentrations were determined using spectrophotometry and fluorimetry, as per the method outlined in chapter 3. Prior to conducting each experiment, the flume physical conditions, such as shear stress and TKE were calculated independently (see Appendix A).

As mentioned in the results section, of particular note was the lack of NO_3^- and NH_4^+ concentrations in all experiments. It was not expected to measure NO_3^- as it is not typically bound to sediments; although nitrification of NH_4^+ to NO_2^- and NO_3^- is widely reported to occur in marine sediments under the correct conditions (Risgaard-Petersen et al., 2004). In this case, it was possible that the freezing of the sample prevented nitrification and thus concentrations of NO_3^- were below the LOD. This did not, however, explain the lack of NH_4^+. As it was not detected in any sample in any experiment, it was unlikely a result of methodical error, but a result of the sediment collection method and conditions. Sediment was collected in September from the top 2 cm of the inter-tidal seabed at Calstock, which was presumed to be the oxic layer, and frozen within 6 h of collection. This method was derived from that reported by Fitzsimons et al. (2006) who successfully measured release kinetics of NH_4^+ and methylamines

from sediments collected from four sites in the Thames estuary.

Sediment collected was from the, presumed, oxic layer of inter-tidal sediment, of which the sediment-nutrient behaviours in oxic and anoxic layers are reportedly different (Falcao and Vale, 1998). Falcao and Vale (1998), reported that a number of factors can affect the concentration of NH_4^+ in sediments, including: ammonium production as organic matter decomposes (Nowicki and Nixon, 1985); nitrification (Lohse et al., 1993); excretion by benthic organisms (Lomstein et al., 1989) and consumption by primary predators. As consumption by primary predators was unlikely, it could be assumed that nitrification by bacteria in the sediment occurred between collection and freezing. Additionally, the inter-tidal sediment was not collected until after sampling had finished, approx. 2 h after exposure giving greater opportunity for chemical processes to remove NH_4^+. Mackin and Aller (1984) reported that reversible ion exchange and the subsequent equilibrium of NH_4^+ in sediments could be modified 'in minutes'. It was plausible that, in transport until freezing, nitrifying bacteria present in the sediment could have converted NH_4^+ into prior to collection.

The objectives of **Experiment A** were to determine whether the cleaning protocol was sufficient and that particle size changes could be observed using the LISST instrumentation. Both objectives were met but it was established that 0.5 g L^{-1} was not sufficient to measure any macro-nutrient species.

The LISST instrument adequately recorded changing particle size distributions and it was possible to see flocculation of smaller particles. It was observed, however, that the upper size limit of the particle size meant that particles above 500 μm were not recorded. The LabSFLOC I camera system was not available during the flume experiments.

The concentration was subsequently increased in **Experiment B** to 1 g L^{-1}, and once again in **Experiment D** to 4 g L^{-1}. The increase in concentration in **Experiment B** yielded clearer observations of changes in particle size, and concentrations of PO_4^{3-} in the range 0.02 - 0.97. However, the maximum concentration of PO_4^{3-} was identified to be an anomalous result - likely a result of contamination. Excluding this first measurement, concentrations of PO_4^{3-} ranged from 0.02 - 0.72 with the new maximum occurring shortly after the sediment slurry was added and consistent with the fast kinetics of desorption and adsorption reported by Froelich (1988). A second peak occurred with an increase current velocity and SPM concentration, indicating desorption processes associated with increased SPM concentration and a possible influence of increasing turbulence in the amount of PO_4^{3-} released.

A subsequent increase in SPM concentration to 4 g L^{-1} in **Experiment D** did not make any clearer the micro-scale processes occurring. Phosphate concentrations increased by an order of magnitude with the 4-fold increase in SPM concentration and the relative change in PO_4^{3-} between samples was less noticeable.

As was clear from the increase in PO_4^{3-} with increase in SPM concentration, M1 plays a dominant role in the release and uptake of PO_4^{3-}, although it was not clear what role flocculation had on the concentrations of PO_4^{3-}, if any. The secondary processes affecting PO_4^{3-} were turbulence, in line with kinetic desorption processes.

The level of turbulence in the flume was controlled by the current velocity in the flume and three values of turbulence were established during the performance assessment of the flume (see Table 6.3 and Appendix A). It was not possible to create a wide range of turbulent conditions in the flume, as per those recorded in the field, and so fewer conclusions can be drawn at this stage. Furthermore, as

it was not possible to separate current velocity and turbulence, it was also not possible to constrain turbulence and particle size. Increasing current velocity gave decreased Kolmogorov microscale (lengths) indicating increased turbulence and smaller irregular features, but increased current velocity also increased the SPM concentration in the water column.

The increase in particle size and number associated with increased SPM concentration, combined with the maximum particle size of 500 μm implied that an equilibrium state between turbulence and particle size had not yet been reached during these experiments. Particle sizes far exceeded the calculated Kolmogorov microscale lengths of 16 - 29 μm. During periods of equilibrium, it would be expected that conditions (i.e. particle size range), including PO_4^{3-} would remain constant.

Experiments C and E were designed to examine the influence of salinity on micro-scale processes affecting macro-nutrient concentrations. The absence of NH_4^+ in these experiments was not expected as it was anticipated that the dominant controlling mechanism in the behaviour of NH_4^+ would be salinity, as indicated in chapters 4 and 5. In terms of particle bonding and flocculation, there were a wide variety of reports of salinities that both enable, enhance and support the processes, ranging from 2 PSU (Drake, 1976) to 12 PSU (McAnally, 1999). This study used an arbitrary 5 PSU based on the volumes of LNS water required for each experiment, and it falling within the range previously reported.

Salinity was observed to affect the flocculation processes occurring in the flume, but there was no observable effect on PO_4^{3-} at either SPM concentration. Changes in PO_4^{3-} between each sample were of a similar order of magnitude to those in **Experiments B** and **D**. This result served to indicate that the proposed uptake of PO_4^{3-} due to flocculation, described in M1, does not exist or does not sig-

nificantly affect the concentration of PO_4^{3-} and, consequently, that sediments are predominately a source and sink of phosphate through means of desorption/adsorption. It was subsequently proposed that the rate/amount available for desorption (or adsorption) is a function of mineral type and surface area available, combined with kinetics.

Chapter 7

A Discussion & Synthesis of the Results Obtained in Field Campaigns and Laboratory Experiments

'What are you going to do next, Em?'

Nora Cox (December 1934 – September 2014)

7.1 Introduction

The aim of this thesis was to investigate the importance of micro-scale physical processes, such as flocculation, on the release of inorganic macro-nutrients nitrate, ammonium and phosphate to the water column. Attempts to address this aim comprised four field campaigns at two sites, and a laboratory study.

The field campaigns were designed to measure *in situ* micro-scale physical processes and inorganic macro-nutrients at a high temporal resolution for at least one ebb and flood tide. The laboratory study was then designed around the observed conditions of one of the field campaigns (Tamar Estuary, autumn campaign) with a view to constraining each variable individually, thereby examining each Mechanism in detail, if present.

This section considers the results obtained in relation to the primary aim, and draws comparisons between field campaigns, seasonal implications and the laboratory studies. The suitability of the method will be discussed, followed by an analysis of each proposed Mechanism outlined in chapter 1.

7.2 Methodology Discussion and Critique

To achieve the aims and objectives outlined in chapter 1, the objectives of the methods included:

- determine suitable methodologies for the measurement of high resolution (temporally and spatially) chemical and physical parameters;
- quantitatively measure the hydrodynamic and chemical conditions of two turbid estuaries;
- design and administer a series of mini-annular flume experiments to quantify the release of macro-nutrients as a result of micro-scale processes.

7.2.1 Field Instrumentation & Methods

Instrumentation was chosen and evaluated according to the requirements for the measurements collected in the Tamar and Seine estuaries (chapters 4 and 5). One requirement for instrumentation used in the field was the portability and ease-of-use in the marine environment. Instrumentation was to be handled manually from a jetty and so needed to be of reasonable weight for one person to profile ($<$ 20 kg), while maintaining the ability to obtain simultaneous measurements of each physical parameter. Power at both sites was limited, and so instruments were required to be battery powered.

For both estuaries, a battery-powered CTD profiler was selected to measure salinity, temperature and turbidity. In the Tamar estuary, a YSI 6600V2 CTD profiler was used at the highest frequency of 2 Hz and sampled every 30 minutes. The availability of instrumentation in the Seine estuary was greater than that of the Tamar and so both a YSI 6600V2 and a Seabird CTD were used. The data presented in chapter 3 (Seine Estuary) were from the Seabird CTD as the instrument was sampled more frequently (every 15 min.), and the resolution and accuracy was greater (see Table 3.1 in chapter 3). However, the Seabird CTD was in a large metal frame that added additional weight (approx. 4 kg) and so the CTD was sampled separately to the LISST. The YSI CTD, being lighter, was sampled at the same time and rate of lowering as the LISST instrument. The minor difference in sample time (estimated to be a maximum of 5 min. apart), combined with the fast current speeds seen in the Seine estuary (up to 4 m s^{-1}) further highlights the issue of advection in this study; measurements were not exactly simultaneous and so introduce error in the results presented. However, the instrumentation adequately met the objectives of the method.

Particle size measurements were conducted using a LISST in both the Seine and

Tamar estuaries. It was observed during the Seine estuary sampling that the high suspended sediment concentrations of up to 4.5 g L^{-1} prohibited the accurate and continuous measurement of particle size by the LISST alone, and so a Path Reduction Module (PRM) was fitted during the Tamar estuary campaigns. The PRM served to reduce the optical path of the LISST instrument by 50%. The LabSFLOC I camera system was available during the Seine sampling campaign and so alternative detailed particle characteristics could be obtained in lieu of the LISST. One disadvantage of the LabSFLOC I camera was that, due to the size of the data of each sample and the time taken to collect the data, it was not possible to sample more than once per hour, drastically reducing the temporal resolution that would have been obtained from the LISST. In the Tamar estuary, the LISST was fitted with a PRM and so samples were obtained at a better temporal resolution during each campaign. The disadvantage of the LISST instrument was the lack additional sediment characteristics such as settling velocity and effective density, which are usually used to indicate flocculation characteristics (Manning and Dyer, 1999; Manning et al., 2007b).

An additional disadvantage observed during this campaign was the post-processing of LabSFLOC I data; despite attempts to automate the process, it was necessary to manually measure particle sizes and settling velocities for each sample collected by LabSFLOC I. This introduces an element of subjectivity into the measurements, particularly as the particle boundaries were not always clearly defined. The definition of the particle boundaries was a result of sampling being conducted in broad daylight, reducing the contrast of image. An attempt to increase the contrast in post-processing resulted in a loss of several smaller particles. Further to this, the depth of field of the instrument (1 mm) meant that if particles dispersed outside of the focal point during settling, they could not be accurately measured as there is no third axis (z) to determine how far away the particles are from the lens. This disadvantage was removed in using the LISST.

The latest LabSFLOC II camera system uses a different light source to enhance the contrast and therefore the definition of the particles.

The LISST was not without its own disadvantages; a known issue of data collected using a LISST is the impact of schlieren (Mikkelsen et al., 2008) on size measurements. Schlieren is the blurring of or altering of a materials refractive properties due to the interaction between two materials of different density (i.e. fresh and salt water). It was shown by Styles (2006), that the occurrence of schlieren in the water can falsely manipulate the sizes seen by the sensor of a LISST; in particular, an increase in the number of large particles were present in samples affected by schlieren. To date, there are no common filtering techniques for post-processing data that are subject to schlieren. Instead, careful monitoring of density interfaces (buoyancy frequency) was conducted in line with post-processing of LISST data. Mikkelsen et al. (2008) observed that data recorded where buoyancy frequencies as low as 0.025 s^{-1} should be interpreted with caution as they may be subject to schlieren. Mikkelsen et al. (2008) also identified that schlieren may be visible in camera imagery at 0.12 s^{-1}. LISST volume scattering function profiles were examined and compared where buoyancy frequency exceeded both 0.025 and 0.12 s^{-1}. Schlieren was only relevant in the Tamar estuary where the LISST instrument was profiled in waters where the temperature or salinity may vary throughout the water column (i.e. not in the laboratory flume studies). Of the 30 profiles taken between spring - autumn, the majority of the profiles had buoyancy frequencies between 0.025 - 0.12 s^{-1}. Examination of the VSF profiles for data that exceeded 0.12 s^{-1} in buoyancy frequency, indicated that only the measurements recorded at the surface of the water column were subject to schileren and, when compared with salinity/temperature profiles, were consistent with a layer of different temperature and salinity. At depth, buoyancy frequencies greater than 0.12 s^{-1} did not appear to affect the VSF profiles. This meant that approx. 93% of the LISST data obtained in the

Tamar estuary were valid for use in this study.

Figure 7.1a demonstrates an example profile (Profile 1 Spring Sampling Campaign - Tamar Estuary) where the buoyancy frequency varied greatly and exceeded 0.12 s^{-1}. Figure 7.1b shows the corresponding particle size and concentration data obtained by the LISST. In this example, the retreating tide and stratified waters potentially caused higher levels of schlieren, particularly at the surface, that may have affected measurements of particle size. If schlieren were apparent, it could be identified by a skewed profile of the Volume Scattering Function (VSF) towards the larger rings causing an apparent increase in the volume of smaller particles (Mikkelsen et al., 2008). Figure 7.1c illustrates 3 VSF profiles taken at different water depths with different apparent levels of schlieren; two with buoyancy frequency values above the 0.025 s^{-1} threshold, and one below. For the sample collected at the surface (red line), there is a pronounced increase in volume concentration in the larger rings when compared to the VSF profiles of deeper samples. The VSF profile for the mid-depth sample indicated a buoyancy frequency above 0.025 s^{-1} but did not demonstrate a significant increase in the larger rings as would have been expected were schlieren apparent.

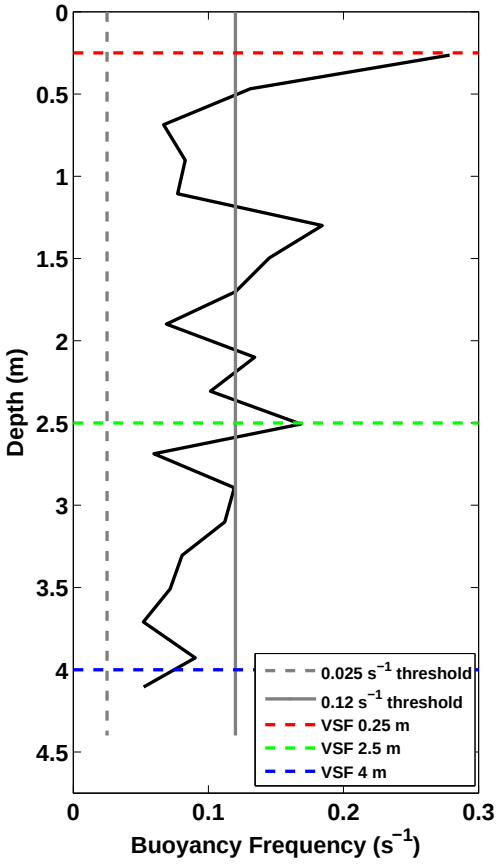

(a) *Profile 1: Buoyancy Frequency*

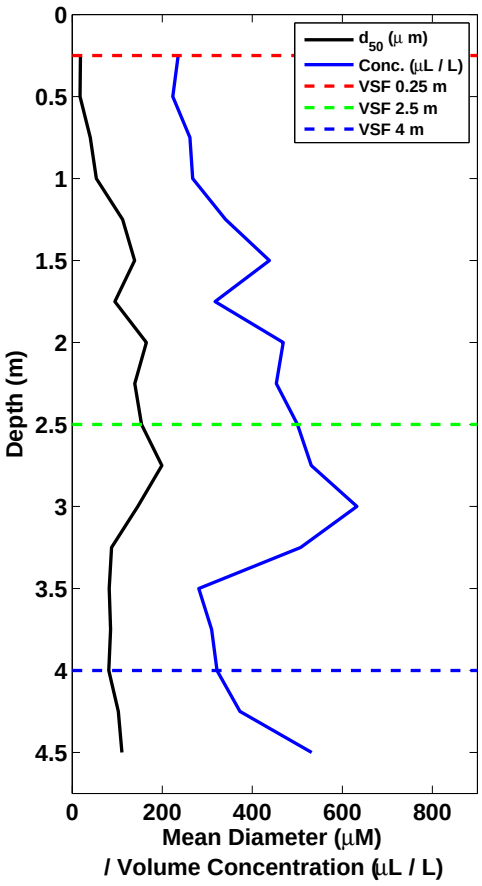

(b) *Profile 1: d_{50} Particle Size*

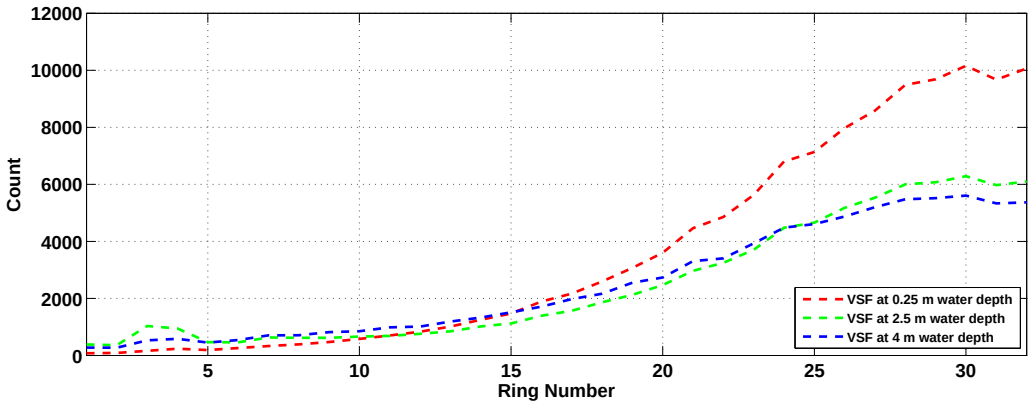

(c) *Profile 1: Volume Scattering Function*

Figure 7.1: *a) An example buoyancy frequency profile from the ebb tide. The solid purple line indicates the threshold 0.025* s^{-1} *as identified by Mikkelsen et al. (2008).*

Current velocity and turbulent kinetic energy (TKE) data were collected using a high-frequency ADCP (1200 KHz). A high-frequency ADCP was chosen as it has been demonstrated by ADCP manufacturers that higher resolutions are able to capture smaller spatial resolution (10 cm bin size) and are more suitable for shallower depths (Rowe Technologies, 2013). The benefit of high-resolution temporal measurements is the ability to see smaller-scale processes and more detail. However, as observed in the Seine estuary, it also creates larger data files. During the Seine sampling campaign, the instrument stopped recording halfway through the day and, due to a lack of user interface (such as a hand-held monitor), it was undiscovered until the instrument was recovered at the end of the day. In the Tamar estuary, it was possible to ensure data was collected throughout the day and sufficient data storage was made available prior to deployment. The same settings were applied in the Seine and Tamar estuary to allow direct comparison.

Turbulent kinetic energy can be calculated using several methods (Wiles et al., 2006). The 'three-beam solution' as described by van Haren et al. (1994) was used in this study as the ADCP was set up in the basic method to measure parameters u, v, w and e, where u, v and w are directional current velocity components and e is the error estimate. Alternative methods, such as the structure function method proposed by (Wiles et al., 2006), require raw measurements from each beam and were based on a setting that was not present on this particular ADCP.

7.2.2 Chemical Methodologies

The methodology for each nutrient (i.e. PO_4^{3-}, NO_3^-, NH_4^+) were required to be determined by individual methodologies as, to date, there was no such instrument that could be used to determine concentrations *in situ*. The inability to measure each nutrient simultaneously introduced an element of error in that

several sub-samples of each sample were required, thus increasing the possibility of contamination during transferral to the vials. In attempt to reduce this, all sample containers were acid washed, dried and stored in the same way. Samples were stored in sealed bags in freezers until analysis and, where required, samples were acidified to preserve them.

Additional errors were potentially introduced by the methodologies themselves. For example, the determination of ammonium from samples requires a very strict incubation time. Furthermore, the efficacy of working reagents required to process each sample increased with age up to a point where they became ineffective. Holmes et al. (1999) recommended that the working reagent be left for at least 24 hours before use. In attempt to reduce errors associated with this, the storage protocol described by Holmes et al. (1999) was followed; working reagents were left for at least 48 h prior to processing, with no set of working reagents ageing beyond 14 days. Additionally, a calibration set was conducted at the start of each 'batch.

As with the ammonium methodology, the storage protocols of reagents required to measure the concentrations of phosphate and nitrate were also observed and calibration sets were performed prior to each batch. It was advised (Williams, pers comm., 2012) that reagents for the determination of phosphate and nitrate were more effective at room temperature and so reagents, buffers and samples were left to reach room temperature prior to processing on the SKALAR CFA instrument.

The number of methodologies required, and the resulting number of sub-samples, introduced a significant element of error. In cases where nitrate and phosphate were observed, ammonium results were contaminated, and vice versa. Despite sampling being collected in triplicate and processed in triplicate (n = 9), it was

not always possible to eliminate the error. For all sample processing, calibration curves were created using a standard set for each nutrient to ensure the quality of results was sufficient for the studies.

7.2.3 Field Campaigns

Sampling was conducted in two estuaries with established records of high turbidity, which was deemed to be important for the observation of flocculation and suspended sediment processes. Additionally, a high-energy environment was required in order to assess the effects of turbulence on sediment-nutrient behaviour. Finally, a range of salinities were required in order to assess the effects of salt water cations on inorganic macro-nutrient concentrations. For this reason, a sampling site in the brackish area of the estuary was chosen.

Both the Seine and Tamar estuary fulfilled the aforementioned requirements, with varying but similar SPM concentration, salinity and turbulent conditions. Wherever possible, the field sampling method, as described in chapter 3, was used. However, there were a few differences resulting from refinement of the method as each field campaign was completed, or due to unforeseen circumstances. Differences in the sampling methodologies are outlined below:

- The primary difference between the Seine and the Tamar estuary was the inclusion of a seasonal assessment for the Tamar estuary. It was not possible to complete a seasonal campaign of the Seine estuary due to cost and time constraints.
- The Tamar estuary was sampled from a jetty over an intertidal mud flat. This meant that water was not always present for sampling. In contrast, the jetty used in the Seine estuary had access to water at all states of the tide, with a 4 m minimum water depth.
- LabSFLOC I instrumentation was used in the Seine estuary but was not

available for any of the Tamar estuary field campaigns. Conversely, comprehensive LISST data was obtained for the Tamar estuary, but SPM concentrations were too high in the Seine estuary and no data was recorded here.

7.3 Discussion of the Proposed Mechanisms

7.3.1 Mechanism One – SPM Concentration Increase

Mechanism 1 (shown in Figure 7.2) described an exchange mechanism as a result of the increase in SPM concentration in the water column. The SPM concentration increase would typically be a result of increased current velocity acting to re-suspend particles from the bed, or the development of an estuarine turbidity maximum. As described in chapter 1, it was hypothesised that an increase in SPM concentration would increase the opportunity for flocculation, as reported by Verney et al. (2009), Soulsby et al. (2013), and Manning and Schoellhamer (2013) (among others). During flocculation, pockets of interstitial water can be created, forming a delicate and porous floc. It was proposed that these pockets could trap inorganic macro-nutrients, increasing the contact time between particle faces and nutrient-laden water, thereby reducing the water column macro-nutrient concentration. Similarly, SPM concentration increase (and other factors such as turbulence) can also cause the disruption of fragile flocs that contain the aforementioned trapped interstitial water, thereby releasing the trapped macro-nutrients to the water column and increasing the water column macro-nutrient water column. It was proposed that, when flocculation and disaggregation processes reach an equilibrium, there would be a constant macro-nutrient concentration.

An SPM concentration increase was observed in both the Tamar and Seine estuary, giving an increase in particle size associated with flocculation; how-

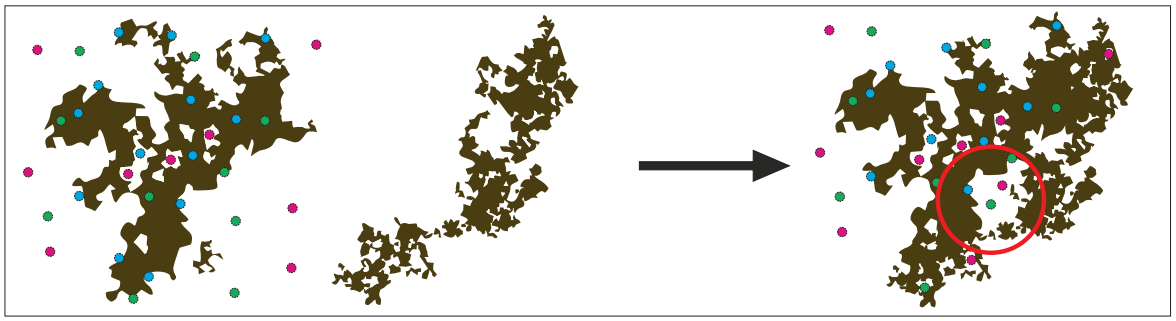

Figure 7.2: *One part of the proposed exchange mechanism associated with SPM concentration increase - for more detail, see chapter 1.*

ever, the timing of the flocculation processes differed in each estuary. In the Seine estuary, an ETM was observed in which increased SPM concentration was coincident with increased current velocity (max 2.2 m s^{-1}), and both were coincident with the increase in floc size observed at HW-2. Effective density values calculated using LabSFLOC I for the Seine estuary demonstrated large, porous flocs with low effective density (values of approx 1200 kg m^{-1}), as well as several smaller particles with higher effective density (around 300 kg m^{-3}), which could be sand particles. When the SPM concentration decreased, so did the number of larger, porous flocs (see Figure 4.9, Page 98). It was not possible to separate disaggregation and flocculation processes occurring as the hydrodynamics associated with tides meant that conditions changed too quickly to observe an equilibrium. Increased sampling frequency, or continuous LISST measurements would have allowed for a higher frequency observation of changing particle size.

In the Tamar estuary, flocculation was not as easily observed and minimal variability was observed with changing seasons. It was anticipated that increased biology in summer months would yield larger particle sizes (McAnally and Mehta, 2001) and therefore possibly enhance Mechanism 1. Each campaign (spring, summer and autumn) showed a range of particle sizes, including increased particle size over time; but in the Tamar, the size of the flocs was controlled by the current velocity, not the increase in SPM concentration. That is, there was

a phase lag in the generation of larger particles. In all field campaigns, flocs formed following the increase in SPM concentration, but only as the current velocity decreased and the corresponding Kolmogorov microscales increased. It was not possible to calculate effective density or settling velocity for the Tamar estuary and so the types of sediments in suspension could not be verified. However, typically, the relatively low current velocities would typically be insufficient to entrain heavier sand particles and so it is proposed that the effective densities associated with the larger particles after the SPM increase would be low and contain interstitial water. Observed particle sizes were consistently considerably smaller than those reported in other studies conducted in the Tamar estuary. This may be due to the location of sampling; samples were collected from a jetty that, as a physical object in the channel flow, may have generated more turbulence than would be experienced at centre of the channel. This increased turbulence may have limited the size of floc generation and therefore uptake of interstitial water.

In comparing the macro-nutrient concentrations associated with this mechanism for each estuary, it was observed that neither estuary demonstrated a quantifiable exchange mechanism such as described in chapter 1. In particular, in the Seine estuary, ammonium concentrations were observed to peak one hour prior to the SPM maximum where flocculation and disaggregation were not observed. This was similar to studies completed by Mitchell and Baldwin (1998) and Lillebø et al. (2004), who observed a slack water benthic input of near-bed nutrients to the water column. Here it is proposed that the shear stresses associated with the current changing direction at slack water may have started to re-suspend bed sediments, contributing source of phosphate to the water column by way of efflux. The lack of current velocity at this time increased the contact time of the sediment-water interface, thereby allowing measurement before advection took over. This was in contrast to studies reported by Fitzsimons et al.

(2006) who observed a peak in ammonium at the same time as the SPM maximum in studies in the Thames estuary.

As per historic studies (e.g. Pomeroy et al. (1965), Stirling and Wormald (1977), Froelich (1988), Jones (1989)), SPM concentration provided a significant source of phosphate to the water as demonstrated by correlated increase in phosphate concentration with SPM increase in the Seine estuary. However, there was no measurable contribution from observed flocculation or disaggregation.

In the Tamar estuary, the seasonal variability of the macro-nutrient behaviour, including the absence of any phosphate following intertidal sediment air exposure in autumn, meant that the effect of Mechanism 1 could not be measured or observed. Instead, it was observed that salinity played a key role in the behaviour of inorganic macro-nutrients, as will be discussed in section 7.3.3.

Following the field campaigns, the flume study used intertidal sediment collected at low water in an attempt to establish the controlling parameters and whether Mechanism 1 could be significant source of inorganic macro-nutrients. The result of this study concluded that Mechanism 1 does not perform as described in chapter 1. Instead, it confirmed that SPM concentration increase provides a source of phosphate to the water column on which salinity was observed to affect phosphate concentrations. Notably, neither ammonium nor nitrate were measured in the flume study. Ammonium and nitrate were likely not quantifiable as a result of nitrifying bacteria in the inter-tidal sediment.

7.3.2 Mechanism Two – Turbulence

Mechanism Two, as described in chapter 1, proposed that turbulence in the marine environment would serve to enhance M1. It is well-documented that flocculation and turbulence are closely related, with turbulence acting as a limiter

to the growth of flocs and, eventually, reaching an equilibrium state (McAnally and Mehta, 2001; Jago et al., 2006; Winterwerp et al., 2006). This was further confirmed in all four field campaigns.

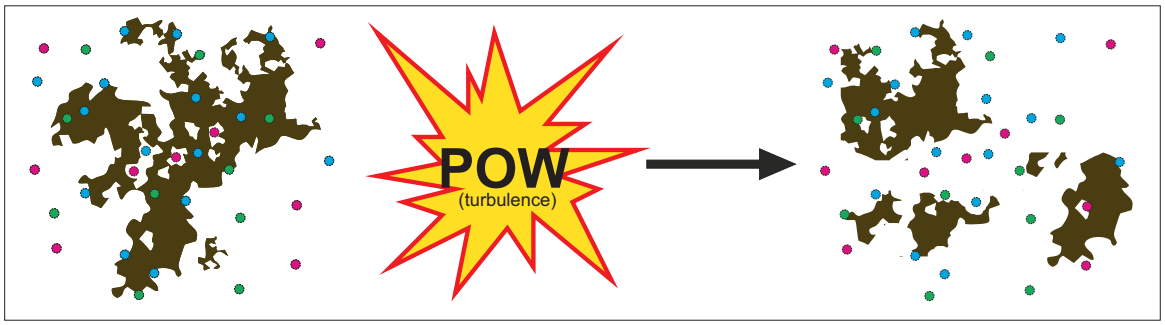

Figure 7.3: *Illustration of the proposed impact of turbulence on SPM, as described in chapter 1. Turbulence was proposed to encourage disaggregation of flocs and the subsequent release of macro-nutrients from interstitial water.*

However, as it was determined that flocculation does not significantly contribute to the relationship between sediments and nutrients in the water column, it stands that the effect of turbulence described in M2 does not have the hypothesised release of inorganic macro-nutrients. It was established, however, that on a micro/meso-scale, turbulent mixing within the water column played an important role in the vertical transport of macro-nutrients released from sediments. In the Tamar estuary, it was recorded that near-bed PO_4^{3-} concentrations had a linear relationship with SPM concentration increase, but that the surface did not. The significant feature at this point was the clear stratification in the water column (see Figure 7.4) as a result of the opposing flow of tidal and riverine water. Stratification effects will be discussed further in section 7.3.3.

This study attempted to consider the effects of turbulence in the flume studies performed following field campaigns. However, the conditions in the flume were naturally turbulent, as shown by the low Kolmogorov microscale numbers, as the flume shape/design did not allow laminar flow. Therefore, increased turbulence was as a result of increased current velocity, which was shown to increase

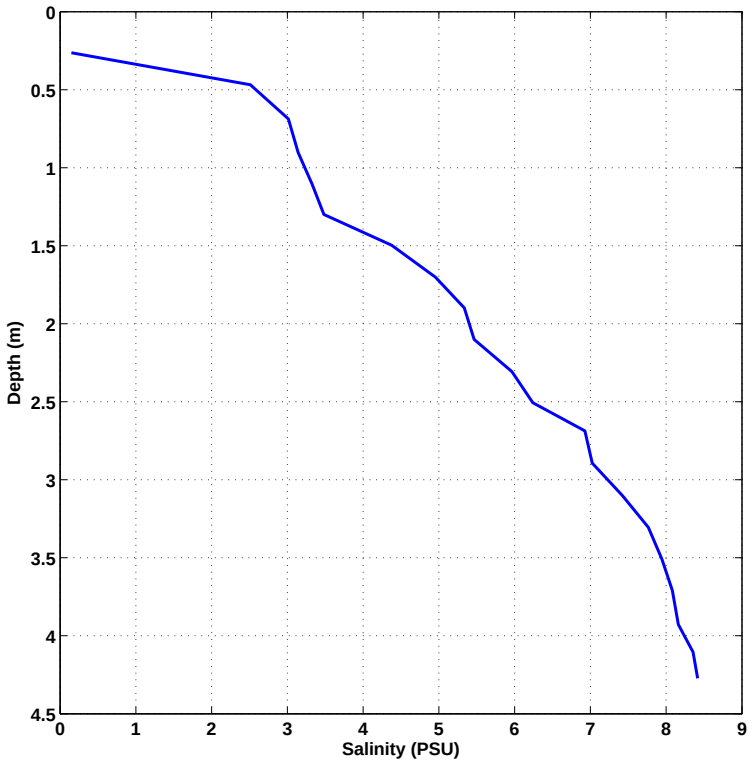

Figure 7.4: *An example of a stratified water column from Spring sampling campaign.*

the SPM concentration.

7.3.3 Mechanism Three – Salinity

Salinity is already an established parameter that affects the inorganic macro-nutrient concentrations in estuaries. Conservative behaviour of nutrients is widely reported (Officer, 1979; Treguer and Queguiner, 1989; Dyer and Orth, 1994), and Gardner et al. (1991) and Weston et al. (2010) reported the effects of ion exchange with ammonium in estuaries. In this study, it was proposed that salinity would play a key role in the generation of larger flocs, thereby enhancing the described Mechanism 1.

A wide range of salinities were observed across all field campaigns, with each campaign demonstrating a subtly different range of salinities. The Seine estuary

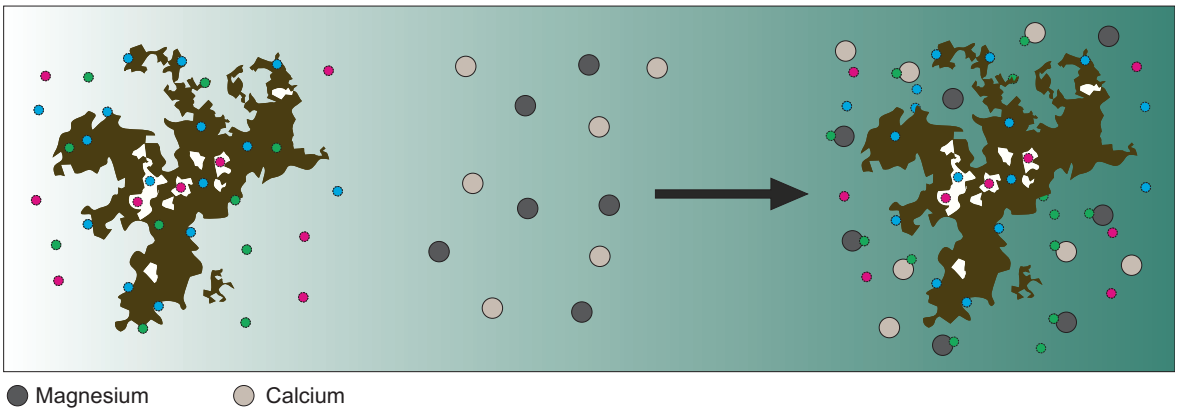

Figure 7.5: *An increase in salinity has been reported to aid flocculation processes which may enhance Mechanism One. Alternatively, cations present in the water column may compete for space on particle faces, thus breaking bonds between sediment and nutrients.*

ranged from 0 to 25 PSU, and increased salinity was observed to coincide with increased particle size, and vice versa. In the Tamar estuary, the salinity varied across each season. Notably, increased riverine run-off during the autumn campaign saw a maximum salinity of 3 PSU, while spring and summer reached 10 and 12 PSU, respectively, both of which were considerably lower than the maximum observed in the Seine estuary. Despite the salinity variation across each campaign in the Tamar estuary, there was minimal variation in particle size indicating that turbulence was dominant in controlling the floc size, even if salinity were to increase flocculation.

On the basis that Mechanism 1 was not observed or quantifiable in either estuarine field campaign, the flume study provided the final attempt to measure the effect of salinity on sediment-nutrient behaviour. As discussed in section 7.3.1, nitrate and ammonium were below the limit of detection and so cannot be considered when discussing the flume experiments. Phosphate concentrations, however, were observed in all flume experiments and increased with increasing SPM concentration. The introduction of low nutrient seawater in Experiment B (1 g L^{-1}) saw a change in the behaviour of phosphate; the peak in phosphate was observed shortly after the peak in SPM and current velocity, rather than coinci-

dent. This experiment was subsequently conducted using a higher SPM concentration (4 g L-1). Here, it was observed that the variability in phosphate was harder to discern as the phosphate was approximately 10 times higher with a four-fold increase in SPM concentration. Still, it could be observed that the peak in phosphate of 12.08 μM occurred shortly after the peak in SPM concentration and following 15 minutes of decreased current velocity. This was in contrast to Experiment D where a four-fold increase in SPM concentration yielded 10x the phosphate concentration, but the peak occurred at the onset of increase current velocity.

These results were related to particle size using a particle size distribution PSD from the LISST measurements. In Experiment E, where low nutrient seawater was used with a high SPM concentration, it was observed that at the maximum current velocity, particle size increased. It is proposed that salt water cations supported the development of larger flocs, since the current velocity did not change and therefore, in theory, resuspended particles would be the same in both experiments. In contrast, Experiment D was completed using UHP water at a high concentration, and there was no observed increase in particle size at maximum current velocity and SPM concentration. This is consistent with studies completed by Winterwerp and van Kesteren (2004) who described the increased flocculation with increased salinity, even at low salinities.

It is proposed that salinity may play a role in the generation of flocs, but that it requires slower and less turbulent conditions for an ion exchange event to occur, as contact time between ions would increased.

As stated in section 7.3.2, turbulence and salinity were observed to play a role in the vertical transport of inorganic macro-nutrients within the water column. There were several occasions in both the Seine and Tamar estuary where near-

bed and surface concentrations of inorganic nutrients were statistically significantly different. In each case, this was a result of two distinct water bodies, such as seen in Seine estuary between HW+2 and HW+5 (Figure 4.4, Page 87). In the Tamar estuary, near-bed and surface concentrations of nitrate were calculated to be statistically significantly different as a result of stratification. Where conditions were observed to be well-mixed, near-bed and surface concentrations were not statistically significant.

7.4 Summary & Conclusions

The intricacies of sediment-nutrient behaviour in turbid estuaries, such as the effect of micro-scale physical processes, are relatively unconstrained and may represent a significant source of macro-nutrients to the water column. This study aimed to investigate the importance, if any, of flocculation, turbulence and salinity on the behaviour of nitrate, phosphate and ammonium. Three Mechanisms were proposed and investigated in four field campaigns and five laboratory experiments: 1. flocculation as an exchange mechanism; 2. turbulence as a release mechanism; 3. salinity as an exchange mechanism and supporting function to Mechanism 1.

A summary of the findings of this study in relation to each hypothesised Mechanism are presented below:

- Mechanism 1: Both the field campaigns and flume experiment results showed that M1 did not demonstrate any observable effect of macro-nutrient uptake in any of the field or laboratory experiments. Instead, and in agreement with previous studies, it was established that an increase in SPM concentration serves as a significant source of PO_4^{3-} and NH_4^{+}, as demonstrated by the 10-fold increase in PO_4^{3-} with a 4-fold increase in SPM concentration in **Experiment D** of the flume experiments (chapter 6).

- Mechanism 2: As Mechanism 2 was partly related to Mechanism 1, it is logical that the disaggregation of flocs due to turbulence does not serve as a significant source of inorganic macro-nutrients to the water column. Instead, turbulence was demonstrated to affect the vertical distribution of macro-nutrients. Indeed, where turbulence was low and stratification occurred, there were statistically significant ($p = 0.05$) differences between near-bed and surface concentrations of inorganic macro-nutrients.

- Mechanism 3: This Mechanism was partly related to Mechanism 1 in that it was proposed to enhance flocculation processes and therefore the proposed exchange mechanism described above. It was observed that salinity increases the rate of flocculation but it was not proven to affect the release and uptake of inorganic macro-nutrients. NH_4^+ and sediment demonstrated an ion exchange process as a result of competition for space on particle faces between NH_4^+ and salt water cations, consistent with previous studies and somewhat in line with Mechanism 3. This relationship was established in both field studies but was not demonstrated in the flume studies as there was no NH_4^+ present in the sediment collected. Flume studies demonstrated that salinity plays a role in the development of larger flocs, and inhibited the release of PO_4^{3-} when SPM concentration increased with current velocity.

7.4.1 Key Issues

A number of key issues were identified during this study and are discussed throughout this chapter. To summarise:

- **Advection** - described as a lateral or horizontal transfer of mass, heat or other property. The tides in an estuary, and the flows of a river are a lateral transfer of fluid, or advection, and so what is occurring at one sample point may not be occurring at a different sample point. The aim of this thesis was

not to measure the impact of advection on nutrient concentrations, but to examine the impact of small-scale physical processes on sediments and the subsequent change in nutrient concentrations. However, it should be noted that measurements taken downstream of the dominant flow direction in the field may be subject to processes that have already occurred upstream. The flume experiments isolated this parameter by recirculating the water.

- **Contamination** - the nutrients measured in this study were subject to contamination and efforts were made to prevent this, where possible. Despite the efforts, there were contaminated samples in this study. These were discussed in each chapter, but are further discussed in this chapter as to the impact on the results as a whole.

- **Representation** - only the inorganic species of N and P were considered in this study. It is known that the organic species of nutrient also interact with sediments. For example, Tappin et al. (2010) investigated the adsorption of amino acids as surrogates for DON and found them the adsorption onto natural SPM was greater than abiotic particles. This was thought to be a result of the bacteria associated with the particles (Statham, 2012). However, only inorganic species were measured due to time constraints associated with sampling and processing of samples for all species of nutrients. It would be prudent to fully examine all species of N and P, as well as additional parameters such as bacteria and carbon to determine the impact of small-scale physical processes on the sedimentary behaviour of nutrients.

- **Sediment Collection** - Later, when considered under laboratory conditions, it was observed that both NH_4^+ and NO_3^- were below the limit of detection for all experiments. This was to be expected for NO_3^-, but studies by Morin and Morse (1999) and Fitzsimons et al. (2006) reported significant increases in NH_4^+ from benthic sources. It was concluded that the

sediment sample taken from the top 2 cm of mud did not contain sufficient NH_4^+ to be observed at either SPM concentration in the flume, nor with increased salinity. This was concluded to be a result of nitrification processes occurring in the sediment, either prior to collection or during transport before storage.

7.5 Future Work

7.5.1 Field Studies

One of the primary constraints of the field work conducted in this thesis was *advection*. To consider the impact of moving volumes of water, it would be prudent to collect samples from multiple sampling locations at the same time. Ideally, 5 sampling stations could be established along the estuary with samples collected at the same time to accurately assess the changing conditions within the estuary. The downside of the sampling campaign are the required resources to collect so many samples at so many different locations.

Another constraint identified in this project was the temporal resolution of sampling, in terms of both seasonality and micro-scale changes. Three sampling campaigns were undertaken and a fourth season was omitted due to time constraints. Increasing the temporal resolution to sampling monthly would increase the understanding of biological factors within sediments that may impact the efficacy of the proposed mechanisms on the release and uptake of macro-nutrients. Add to this that the effects of natural macro-nutrient input through precipitation events could be observed.

In relation to the micro-scale processes, future work could consider taking more samples in a shorter time-scale. Samples were collected hourly in this project due to the constraints of processing and storing all samples, as well as filter-

ing them on site. Samples collected on a shorter time-scale would give more information about the rapid exchange processes that may be a occurring during rapidly changing suspended sediment conditions.

7.5.2 Laboratory Studies

The laboratory work conducted in this thesis highlighted a number of problems that would be better addressed in additional studies. Primarily, the size of the experiment, when considering all variables and the addition of organic nutrients to the repertoire of macro-nutrients studied, would warrant a PhD thesis in itself. Each experiment took approximately 150 minutes with all runs required to be, at least, duplicated. To increase the validity of the results, it would be beneficial to conduct the runs 3 times. This has implications for the number of samples to taken for each run. Each sample required three vials for each type of nutrient. This means that 90 samples were collected for each. Each experiment would therefore require 270 samples to be processed.

References

Y. C. Agrawal and H. C. Pottsmith. Laser diffraction particle sizing in STRESS. *Continental Shelf Research*, 14(10/11):1101 – 1121, 1994.

Y. C. Agrawal and H. C. Pottsmith. Instruments for particle size and settling velocity observations in sediment transport. *Marine Geology*, 168:89 – 114, 2000.

N. Aissa-Grouz, J. Garnier, G. Billen, B. Mercier, and A. Martinez. The response of river nitrification to changes in wastewater treatment (The case of the lower Seine River downstream from Paris). *Ann. Limnol. - Int. J. Lim.*, 51:351 – 364, 2015. doi: 10.1051/limn/2015031.

J. R. L. Allen and M. J. Duffy. Medium-term sedimentation on high intertidal mudflats and salt marshes in the Severn Estuary, SW Britain: the role of wind and tide. *Marine Geology*, 150(1-4):1–27, 1998a. ISSN 0025-3227. doi: DOI:10.1016/S0025-3227(98)00051-6.

J. R. L. Allen and M. J. Duffy. Temporal and spatial deposition patters in the Severn Estuary, southwestern Britain: iintertidal studies at spring-neap and seasonal scales, 1991 - 1993. *Marine Geology*, 146:147 – 171, 1998b.

F. A. J. Armstrong, C. R. Stearns, and J. D. H. Strickland. The measurement of upwelling and subsequent biological processes by means of the Technicon Autoanalyser and associated equipment. *Deep-Sea Research*, 14:381 – 389, 1967.

J. Avoine. Mécanismes contrôlant la dynamique des sédiments en suspension dan l'estuaire de la Seine. *Mémoires de la Société Géologique de France*, 144: 17 – 25, 1982.

J. Avoine. Sediment exchanges between the seine estuary and its adjacent shelf. *Journal of the Geological Society of London*, 144:135 – 148, 1987.

J. Avoine, A. Caillot, R. Hoslin, C. Larsonneur, J. Massias, and M. Quesney. Mise en évidence des mouvements sédimentaires en Baie de Seine à l'aide de traceurs radioactifs. *Société Hydrotechnique de France, XVIIIémes Journées de l'Hydraulique*, XVIII:1.2.1 – 1.2.8, 1984.

A. Bakker. Appied computational fluid dynamics - lecture 9 - kolmogorov's theory. Website, 2006. URL http://www.bakker.org/dartmouth06/engs150/09-kolm.pdf.

A. J. Bale, A. W. Morris, and R. J. M. Howland. Seasonal sediment movement in the Tamar Estuary. *Oceanologica Acta*, 8:1 – 16, 1985.

A. J. Bale, R. J. Uncles, J. Widdows, M. D. Brinsley, and C. D. Barrett. Direct observation of the formation and break-up of aggregates in an annular flume using laser reflectance particle sizing. In J. C. Winterwerp and C. Kranenberg, editors, *Fine Sediment Dynamics in the Marine Environment*, volume 5 of *Proceedings in Marine Science*, pages 189 – 201. Elsevier, 2002.

A. J. Bale, J. Widdows, C. B. Harris, and J. A. Stephens. Measurements of the critical erosion threshold of surface sediments along the Tamar Estuary using a mini-annular flume. *Continental Shelf Research*, 26:1206 – 1216, 2006.

R. Bartley, W. J. Speirs, T. W. Ellis, and D. K. Water. A review of sediment and nutrient concentration data from Australia for use in catchment water quality models. *Marine Pollution Bulletin*, 65:101 – 116, 2012.

S. J. Bass, A. J. Manning, and K. R. Dyer. Preliminary findings of a study of the upper reaches of the Tamar Estuary, UK, throughout a complete tidal cycle: Part I: likning hydrodynamics and sediment cycles. In *Estuarine and Coastal Fine Sediment Dynamics*. Elsevier, 2007.

W. Berelson, J. McManus, K. Coale, K. Johnson, D. Burdige, T. Kilgore, D. Colodner, F. Chavez, R. Kudela, and J. Boucher. A time series of benthic flux measurements from Monterey Bay, CA. *Continental Shelf Research*, 23:457 – 481, 2003.

I. Berhane, R. W. Sternberg, G. C. Kineke, T. Milligan, and K. Kranck. The variability of suspended aggregates on the amazon continental shelf. *Continental Shelf Research*, 17(3):267–285, 1997.

G. Billen. Nitrification in the Scheldt estuary. *Estuarine Coastal Mar. Sci.*, 3:79 – 89, 1975.

G. Billen, J. Garnier, C. Deligne, and C. Billen. Estimates of early-industrial inputs of nutrients to river systems: implication for coastal eutrophication. *Science of the Total Environment*, 243 - 244:43 – 52, 1999.

J. R. Boersma and J. H. J. Terwindt. Neap-spring tide sequences of intertidal shoal deposits in a mesotidal estuary. *Sedimentology*, 28:151 – 170, 1981.

R. Booij. *Measurements of the flow field in a rotating annular flume*. PhD thesis, Civil Engineering and Geosciences, TU Delft, 1994.

E. Boss, W. H. Slade, M. Behrenfeld, and G. Dall'Olmo. Acceptance angle effects on the beam attenuation in the ocean. *Optics Express*, 17(3):1535–1550, 2009.

D. G. Bowers, C. E. Binding, and K. M. Ellis. Satellite remote sensing of the geographical distribution of suspended particle size in an energetic shelf sea. *Estuarine, Coastal and Shelf Science*, 73:457 – 466, 2007.

M. J. Bowes, J. T. Smith, H. P. Jarvie, C. Neal, and R. Barden. Changes in point and diffuse source phosphorus inputs to the River Frome (Dorset, UK). *Science of the Total Environment*, 407:1954 – 1966, 2009.

K. M. Braithwaite, D. G. Bowers, W. A. M. Nimmo Smith, G. W. Graham, Y. C. Agrawal, and O. A. Mikkelsen. Observations of particle density and scattering in the Tamar Estuary. *Marine Geology*, 277:1 – 10, 2010.

I. Brenon and P. Le Hir. Modelling the turbidity maximum in the Seine estuary (France): identification of formation processes. *Estuarine, Coastal and Shelf Science*, 49:525 – 544, 1999.

J. D. Broadway. Dynamics of growth and breakage of alum floc in the presence of fluid shear. *Journal of the Environmental Engineering Division*, EE5:901 – 915, 1978.

J. C. Brun-Cottan. *Vertical transport of particles in the ocean*, pages 83 – 111. D. Reidel Publishing Company, 1986.

P.-Y. Burban, Y.-J. Xu, J. McNeil, and W. Lick. Settling speeds of flocs in fresh water and seawater. *Journal of Geophysical Research*, 95:18213 – 18220, 1990.

A. J. Burgin and S. K. Hamilton. Have we overemphasized the role of denitrification in aquatic ecosystes? A review of nitrate removal pathways. *Frontiers in Ecology and the Environment*, 5:89 – 96, 2007.

T. P. Burt, N. J. K. Howden, F. Worrall, and J. J. McDonnell. On the value of the long-term, low-frequency water quality sampling: avoiding throwing the baby out with the bathwater. *Hydrological Processes*, 25:828–830, 2011a.

T. P. Burt, N. J. K. Howden, F. Worrall, and M. J. Whelan. Nitrate in United Kingdom rivers: policy and its outcomes since 1970. *Environmental Science and Technology*, 45:175 – 181, 2011b.

D. G. Capone, D. A. Bronk, M. R. Mulholland, and E. J. Carpenter. The marine nitrogen cycle: overview and challenges. In *Nitrogen in the Marine Environment*, chapter 1, pages 1 – 50. Elsevier, 2nd edition, 2008.

R. Chester. *Marine Geochemistry*. Blackwell Science Ltd., 2nd edition, 2000. ISBN 0-632-05432-8.

D. L. Childers, F. H. Sklar, B. Drake, and T. Jordan. Seasonal measurements of sediment elevation in three mid-Atlantic estuaries. *Journal of Coastal Research*, 9(4):986 – 1003, Autumn 1993.

B. Clason, W. J. Langston, and G.-P. Zauke. Bioaccumulation of trace metals in the amphipod Chaetogammarus marinus (Leach, 1815), from the Avon and Tamar estuaries (UK): comparison of two-compartment and hyperbolic toxicokinetic models. *Marine Environmental Research*, 57:171 – 195, 2004.

J. E. Cloern and R. S. Oremland. Chemistry and microbiology of a sewage spill in south San Francisco Bay. *Estuaries*, 6:399 – 406, 1983.

J. K. Cochran. Estuaries. In *Reference Module in Earth Systems and Environmental Sciences*, pages –. Elsevier, 2014. ISBN 978-0-12-409548-9. doi: http://dx.doi.org/10.1016/B978-0-12-409548-9.09151-X. URL http://www.sciencedirect.com/science/article/pii/B978012409548909151X.

J. J. Cole, N. F. Caraco, and G. E. Likens. Short-range atmospheric transport: a significant source of phosphorus to an oligotrophic lake. *Limnology and Oceanography*, 35:1230 – 1237, 1990.

T. A. Colin. Recent advances in statistical methods for the estimation of sediment and nutrient transport in rivers. *Review of Geophysics*, 33:1117 – 1123, 1995.

C. S. Connor and A. M. De Visser. A laboratory investigation of particle size effects on optical backscatterrance sensor. *Marine Geology*, 108:151 – 159, 1992.

D. L. Correll, T. E. Jordan, and D. E. Weller. Nutrient flux in a landscape: effects of coastal land use and terrestrial community mosaic on nutrient transport to coastal waters. *Estuaries*, 15(4):431 – 442, December 1992.

F. Couceiro, G. Fones, G. L. Thomson, P. Statham, D. Sivyer, R. Parker, B. Kelly-Gerreyn, and C. L. Amos. Impact of resuspension of cohesive sediments at the Oyster Grounds (North Sea) on nutrient exchange accross the sediment-water interface. *Biogeochemistry*, 113:37 – 52, 2013.

A. Cruzado, Z. Velásquez, and M. del Carmen Pérez. Nutrient fluxes from the Ebro River and subsequent across-shelf dispersion. *Continental Shelf Research*, 22(2):349 – 360, 2002.

C. Cun and R. Vilagines. Time series analysis on chlorides, nitrates, ammonium and dissolved oxygen concentrations in the Seine river, near Paris. *Science of the Total Environment*, 208:56 – 69, 1997.

D. M. Dauer, J. A. Ranasinghe, and S. B. Weisberg. Relationships between benthic community condition, water quality, sediment quality, nutrient loads, and land use patterns in Chesapeake Bay. *Estuaries*, 15(4):431 – 442, December 2000.

E. J. Davies, W. A. M. Nimmo Smith, Y. C. Agrawal, and A. J. Souza. LISST-100 response to large particles. *Marine Geology*, 307 - 310:117 – 122, 2012.

J. H. Davies. A morphogenetic approach to world shorelines. *Z. Geomorphol.*, 8: 127–142, 1964.

J. W. Day, B. C. Crump, W. M. Kemp, and A. Yáñez-Arancibia. *Estuarine Ecology*. Wiley, 1945.

J. Deborde, P. Anschutz, G. Chaillou, H. Etcheber, M.-V. Commarieu, P. Lecroat, and G. Abril. The dynamics of phosphorus in turbid estuary systems: example of the Gironde estuary (France). *Limnology and Oceanography*, 52:862 –872, 2007.

E. A. Delo. The behaviour of estuarine muds during tidal cycles. Technical Report SR138, HR Wallingford, February 1988.

J. Deloffre, R. Lafite, P. Lesueur, S. Lesourd, R. Verney, and L. Guezennec. Sedimentary processes on an intertidal mudlfat in the upper macrotidal Seine estuary, France. *Estuarine, Coastal and Shelf Science*, 64:710 – 720, 2005.

J. E. Dore, T. Houlihan, D. V. Hebel, G. Tien, L. Tupas, and D. M. Karl. Freezing as a method of sample preservation for the analysis of dissolved inorganic nutrients in seawater. *Marine Chemistry*, 53:173 – 185, 1996.

D. E. Drake. Suspended sediment transport and mud depostion on continental shelves. In *Marine Sediment Transport and Environment Management*, pages 127 – 158. Wiley & Sons, New York, 1976.

I. Droppo and E. D. Ongley. Flocculation of suspended sediment in rivers of southeasouth Canada. *Water Research*, 28(8):1799 – 1809, 1994.

L. Drummond and W. Maher. Determination of phosphorus in aqueous-solution via formation of the phosphoantimonylmolybdenum blue complex - re-examination of optimum conditions for the analysis of phosphate. *Analytica Chimica Acta*, 302:69 – 74, 1995.

R. A. Duce. *The role of air-sea exchange in geochemical cycling*, chapter The impact of atmospheric nitrogen, phosphorus and iron species on marine biological productivity, pages 497 – 529. D. Reidel Publishing Company, 1986.

R. Dupas, M. Delmas, J. Dorioz, J. Garnier, F. Moatar, and C. Gascuel-Odoux. Assessing the impact of agricultural pressures on N and P loads and eutrophication risk. *Ecological Indicators*, 48:396 – 407, 2015.

K. R. Dyer. Sediment processes in estuaries: future research requirements. *Journal of Geophysical Research: Oceans*, 94:14327 – 14339, 1989.

K. R. Dyer. *Estuaries: A Physical Introduction*. John Wiley & Sons, 2nd edition, 1997. ISBN 0-471-97471-4.

K. R. Dyer and R. J. Orth. *Changes in Fluxes in Estuaries: Implications from Science to Management*. 1994.

K. R. Dyer, A. J. Bale, M. C. Christie, N. Feates, S. Jones, and A. J. Manning. The turbidity maximum in a mesotidal estuary, the Tamar Estuary, UK: II The Floc Properties. In J. Winterwerp and C. Kranenberg, editors, *Fine sediment dynamics in the marine environment*, pages 203 – 218. Elsevier Science, 2002.

K. R. Dyer, M. C. Christie, and A. J. Manning. The effects of suspended sediment on turbulence within an estuarine turbidity maximum zone. *Estuarine, Coastal and Shelf Science*, 59:237 – 248, 2004.

K. Eberlein and G. Kattner. Automatic method for the determination of orthophosphate and total dissolved phosphorus in the marine environment. *Fresenius' Zeitschrift für Analytische Chemie*, 326(4):354–357, 1987.

J. K. Edzwald and C. R. O'Melia. Clay distributions in recent estuarine sediments. *Clays and Clay Minerals*, 23:39 – 44, 1975.

H. A. Einstein and R. B. Krone. Experiments to determine modes of cohesive sediment transport in salt water. *Journal of Geophysical Research*, 67(4):1451–1461, 1962.

D. Eisma. Flocculation and deflocculation of suspended matter in estuaries. *Netherlands Journal of Sea Research*, 20:183 – 199, 1986.

D. Eisma and A. Li. Changes in suspended-matter floc size during the tidal cycle in the dollard estuary. *Netherlands Journal of Sea Research*, 31(2):107 – 117, 1993. ISSN 0077-7579. doi: http://dx.doi.org/10.1016/0077-7579(93)90001-9. URL http://www.sciencedirect.com/science/article/pii/0077757993900019.

M. Elliott, V. N. de Jonge, S. J. Malcolm, and M. Wilkinson. Impact of nutrients in estuaries. Technical Report P269, Environment Agency, 1999.

W. J. Emery. Data Aquisition and Recording. In W. J. Emery and R. E. Thomson, editors, *Data Analysis Methods in Physical Oceanography*, chapter 1, pages 1 – 158. Elsevier, 2001.

R. Emmett, R. Llansó, J. Newton, R. Thom, and M. Hornberger. Geographic signatures of North American west coast estuaries. *Estuaries*, 23(6):765 – 792, 2000.

J. Emsley. The phosphorus cycle. In *The natural environment and the biogeochemical cycles*. Springer-Verlag, Berlin, 1980.

Environment Agency. Freshwater Tamar and its Tributaries. Technical report, Environment Agency, 1999.

Environment Agency. Freshwater eutrophication: a nationally significant water management issue. Briefing note for workshop, Environment Agency, 2012.

M. Falcao and C. Vale. Sediment-water exchanges of ammonium and phosphate in intertidal and subtidal areas of a mesotidal coastal lagoon (Ria Formosa). *Hydrobiologica*, 373:193 – 201, 1998.

S. Falco, L. F. Niencheski, M. Rodilla, I. Romero, J. Gonzalez del Rio, J. P. Sierra, and C. Mosso. Nutrient flux and budget in the Ebro estuary. *Estuarine, Coastal and Shelf Science*, 87:92 – 102, 2010.

G. Falkovich and K. R. Sreenivasan. Lessons from hydrodynamic turbulence. *Physics Today*, 59:43, 2006.

T. H. Fang. Partitioning and behaviour of different forms of phosphorus in the Tanshui estuary and one of its tributaries, northern Taiwan. *Estuarine, Coastal and Shelf Science*, 50:689 – 701, 2000.

M. J. Fennessy, K. R. Dyer, and D. A. Huntley. INSSEV: An instrument to measure the size and settling velocity of flocs in situ. *Marine Geology*, 117:107–117, 1994.

M. J. Fennessy, K. R. Dyer, and D. A. Huntley. Estimation of settling flux spectra in estuaries using inssev. In N. Burt, R. Parker, and J. Watts, editors, *Cohesive Sediments*, pages 87–104. John Wiley & Sons, 1997.

M. Fettweis, F. Francken, V. Pison, and D. Van den Eynde. Suspended particulate matter dynamics and aggregate sizes in a high turbidity area. *Marine Geology*, 235(1):63–74, 2006.

T. Fisher, L. Harding, D. Stanley, and L. Ward. Phytoplankton, nutrients, and turbidity in the Chesapeake, Delaware, and Hudson estuaries. *Estuarine Coastal and Shelf Science*, 27:61–93, July 1988. doi: 10.1016/0272-7714(88)90032-7.

M. F. Fitzsimons, G. E. Millward, D. M. Revitt, and M. D. Dawit. Desorption kinetics of ammonium and methylamines from estuarine sediments: consequences for the cycling of nitrogen. *Marine Chemistry*, 101:12 – 26, 2006.

M. F. Fitzsimons, M. C. Lohan, A. D. Tappin, and G. E. Milward. The role of suspended particles in estuarine and coastal biogechemistry. In G. Shimmield, editor, *Treatise on Estuarine and Coastal Science*, volume 4, chapter Geochemistry of Estuaries and Coasts, pages 71 – 144. Elsevier, 2011.

B. Flemming and J. Hansom. 3.01 - estuarine and coastal geology and geomorphology a synthesis. In E. Wolanski and D. McLusky, editors, *Treatise on Estuarine and Coastal Science*, pages 1 – 5. Academic Press, Waltham, 2011. ISBN 978-0-08-087885-0. doi: http://dx.doi.org/10.1016/B978-0-12-374711-2.00301-6. URL http://www.sciencedirect.com/science/article/pii/B9780123747112003016.

P. N. Froelich. Kinetic control of dissolved phosphate in natural rivers and estuaries: a primer on the phosphate buffer mechanism. *Limnology and Oceanography*, 33(4):649 – 668, 1988.

P. N. Froelich, M. L. Bender, N. A. Luedtke, G. R. Heath, and T. Devries. The marine phosphorus cycle. *Am. J. Sci.*, 282:474 – 511, 1982.

D. C. Fugate and C. T. Friedrichs. Controls on suspended aggregate size in partially mixed estuaries. *Estuarine, Coastal and Shelf Science*, 58(2):389–404, 2003. ISSN 0272-7714. doi: DOI:10.1016/S0272-7714(03)00107-0.

J. Galloway, W. Schlesinger, H. Levy, A. Michaels, and J. Schnoor. Nitrogen fixation: anthropogenic enhancement - environmental response. *Global Biogeochem. Cycles*, 9:235 – 252, 1995.

J. N. Galloway. The global nitrogen cycle. In J. H. Schlesinger, editor, *Treatise on geochemistry*, volume 8, pages 557 – 583. Elsevier, 2003.

W. G. Gardner, S. P. Seitzinger, and J. M. Malczyk. The effects of sea salts on the forms of nitrogen released from estuarine and freshwater sediments: does ion pairing affect ammonium flux? *Estuaries and Coasts*, 14:157 – 166, 1991.

P. C. F. C. Gardolinski, G. Hanrahan, E. P. Achterber, M. Gledhill, A. D. Tappin, W. A. House, and P. J. Worsfold. Comparison of sample storage protocols for the determination of nutrients in natural waters. *Water Research*, 35:3670 – 3678, 2001.

P. C. F. C. Gardolinski, P. J. Worsfold, and I. D. McKelvie. Seawater induced release and transformation of organic and inorganic phosphorus from river sediments. *Water Research*, 38:688 – 692, 2004.

J. Garnier, G. Billen, S. Even, H. Etcheber, and P. Servais. Organic matter dynamics and budgets in the turbidity maximum zone of the seine estuary (france). *Estuarine, Coastal and Shelf Science*, 77:150 – 162, 2008.

J. Garnier, G. Billen, J. Nemery, and M. Sebilo. Transformations of nutrients (n, p and si) in the turbidity maximum zone of the seine estuary and export to the sea. *Estuarine, Coastal and Shelf Science*, 90:129 – 141, 2010.

C. Garside, G. Hull, and S. Murray. Determination of sub-micromolar concentrations of ammonia in natural waters by a standard addition method using a gas sensing electrode. *Limnology and Oceanography*, 23:1073 – 1076, 1978.

J. W. Gartner, R. T. Cheng, W. P-F., and K. Richter. Laboratory and field evaluations of the lisst-100 instrument for suspended particle size determinations. *Marine Geology*, 175(14):199 – 219, 2001. ISSN 0025-3227. doi: http://dx.doi.org/10.1016/S0025-3227(01)00137-2. URL http://www.sciencedirect.com/science/article/pii/S0025322701001372.

Z. Genfa and P. K. Dasgupta. Fluorometric measurement of aqueous ammonium ion in flow-injection system. *Analytical Chemistry*, 61:408 – 412, 1989.

K. J. George. *The tides and tidal streams of the Tamar Estuary*. PhD thesis, University of London, 1975.

J. Germaneau. Etude de la sédimentation dan l'estuaire de la Seine. Origine, déplacement et dépôt des suspensions. *Travaux du Centre du Recherches et d'Etudes Océanographiques*, VIII:1 – 63, 1968.

J. Germaneau. Sédiments actuels et sédiments fossiles dans la Seine maritime et dans la Seine fluvial. *Travaux du Centre du Recherches et d'Etudes Océanographiques*, XI:55 – 110, 1971.

R. Geyer. The importance of suppression of turbulence by stratification on the Estuarine Turbidity Maximum. *Estuaries*, 16:113 – 125, 1993.

R. Geyer, M. E. Scully, and D. K. Ralston. Quantifying vertical mixing in estuaries. *Environmental Fluid Mechanics*, 8(5-6):495 – 509, 2008.

S. W. Gibbs, R. F. C. Mantoura, and P. S. Liss. Analysis of ammonia and methylamines in natural waters by flow-injection gas diffusion coupled to ion chromatography. *Analytica Chimica Acta*, 316:291 – 304, 1995.

R. A. Gore and C. T. Crowe. Effect of particle size on modulating turbulent intensity. *International Journal of Multiphase Flow*, 15(2):279 – 285, 1989.

D. G. Goring and V. I. Nikora. Despiking Acoustic Doppler Velocimeter Data. *Journal of Hydraulic Engineering*, 128:117 – 126, 2002.

S. S. Goyal, D. W. Rains, and R. C. Huffanaker. Determination of ammonia ion by fluorometry or spectrophotometry after on-line derivation with o-phthaldehyde. *Analytical Chemistry*, 60:179, 1988.

R. C. Grabowski, I. G. Droppo, and G. Wharton. Erodibility of cohesive sediment: the importance of sediment properties. *Earth Science Reviews*, 105(3 - 4):101 – 120, 2011.

N. Gratiot and A. J. Manning. A laboratory study of dilute suspension mud floc characteristics in an oscillatory diffusive turbulent flow. *Journal of Coastal Research*, SI 50:1142–1146, 2007.

D. A. Griffin and P. H. LeBlond. Estuary/ocean exchange concontrol by spring-neap tidal mixing. *Estuarine, Coastal and Shelf Science*, 30:275 – 297, 1990.

J. Guillén, A. Palanques, P. Puig, X. Durrieu de Madron, and F. Nyffeler. Field calibration of optical sensors for measuring suspended sediment concentration in the western Mediterranean. *Scientia Marina*, 64:427 – 435, 2000.

Y. Hallez. Analytical and numerical computations of the van der Waals force in complex geometrics: Application to the filtration of colloidal particles. *Colloids and Surfaces, A: Physicochemical and Engineering Aspects*, 414:466 – 476, 2012.

E. I. Hamilton. Environmental variabiles in a holistic evaluation of land contaminated by historic mine wastes: a study of multi-element mine wastes in West Devon, England using arsenic as an element of potential concern to human health. *Science of the Total Environment*, 249:171 – 221, 2000.

C. E. Harland. *Ion Exchange*. Royal Society of Chemistry, Cambridge, 1994.

R. E. Hecky and P. Kilham. Nutrient limitation of phytoplankton in freshwater and marine environments: a review of recent evidences of the effects of enrichment. *Limnology and Oceanography*, 49:796–822, 1988.

J. I. Hedges and R. G. Keil. Organic geochemical perspectives on estuarine processes: sorption reactions and consequences. *Marine Chemistry*, 65:55 – 65, 1999.

D. O. Hessen. Catchment properties and the transport of major elements to estuaries. In D. B. Nedwell and D. G. Raffaelli, editors, *Advances in Ecological Research: Estuaries*, pages 1–34. Academic Press Inc., 1999.

P. Hill, E. Boss, J. Newgard, B. Law, and T. Milligan. Observations of the sensitivity of beam attenuation to particle size in a coastal bottom boundary layer. *Journal of Geophysical Research: Oceans (1978–2012)*, 116(C2), 2011.

P. S. Hill, R. M. Nowell, and P. A. Jumars. Encounter rate by turbulent shear of particles similar in diameter to the Kolmogorov scale. *Journal of Marine Research*, 50(4):643 – 668, 1992.

R. M. Holmes, A. Aminot, R. Kerouel, B. A. Hooker, and B. J. Peterson. A simple and precise method for measuring ammonium in marine and freshwater ecosystems. *Can. J. Fish. Aquat. Sci.*, 56:1801–1808, 1999.

D. Hou, J. He, C. Lu, F. Zhang, and K. Otgonbayar. Effects of environmental factors on nutrients release at sediment-water interface and assessment of trophic status for a typical shallow lake, Northwest China. *The Scientific World Journal*, 716342, 2013. doi: doi:10.1155/2013/716342.

R. W. Howarth. Coastal nitrogen pollution: A review of sources and trends globally and regionally. *Harmful Algae*, 8(1):14–20, 2008. ISSN 1568-9883. doi: DOI:10.1016/j.hal.2008.08.015. HABs and Eutrophication.

R. W. Howarth, H. S. Jensen, R. Marino, and H. Postma. Transport to and processing of p in nearshore and oceanic waters. In *Phosphorus in the Global Environment*. Wiley, New York, 1995.

X. P. Huang, L. M. Huang, and W. Z. Yue. The characteristics of nutrients and eutrophication in the Pearl River estuary, South China. *Marine Pollution Bulletin*, 47(1):30 – 36, 2003.

J. R. Hunt. Prediction of oceanic particle size distribution from coagulation and sedimentation mechanisms. In *Advances in Chemistry*, volume 189, chapter Particle in Water, pages 243 – 257. American Chemical Society, 1980.

K. A. Hunter and P. S. Liss. Organic matter and the surface charge of suspended particles in estuarine waters1. *Limnology and Oceanography*, 27(2):322–335, 1982. ISSN 1939-5590. doi: 10.4319/lo.1982.27.2.0322. URL http://dx.doi.org/10.4319/lo.1982.27.2.0322.

Intergovernmental Oceanographic Commission. *Nutrient analysis in tropical marine waters - practical guidance and safety notes for the performance of dissolved micronutrient analysis in sea water with particular reference to tropical waters*. UNESCO, 28 edition, 1993.

C. Jago, S. Jones, P. Sykes, and T. Rippeth. Temporal variation of suspended particulate matter and turbulence in a high energy, tide-stirred, coastal sea: Relative contributions of resuspension and disaggregation. *Continental Shelf Research*, 26:2019 – 2028, 2006. ISSN 0278-4343. doi: DOI:10.1016/j.csr.2006.07.009. Special Issue in Honor of Richard W. Sternberg's Contributions to Marine Sedimentology.

Z. D. Jastzebski. Entrance effects and wall effects in an extrusion rheometer during the flow of concentrated suspensions. *Ind. Eng. Chem. Fundamen.*, 6: 445 – 453, 1967.

D. A. Jay, R. J. Uncles, J. Largier, R. W. Geyer, and J. Boynton. A review of recent developments in estuarine scalar flux estimation. *Estuaries*, 20(2):262 – 280, 1997.

T. D. Jickells, J. E. Andrews, D. J. Parkes, S. Suratman, A. A. Aziz, and Y. Y. Hee. Nutrient transport through estuaries: the importance of estuarine geography. *Estuarine, Coastal and Shelf Science*, 150:215 – 229, 2015. doi: 10.1016/j.ecss.2014.03.014.

M. A. Jones. Sediment preservation: the effects on phosphate exchange between sediment and water. *Oceanologica Acta*, 12(1):87 – 90, 1989.

L. H. Kalnejais, W. R. Martin, and M. H. Bothner. The release of dissolved nutrients and metals from coastal sediments due to resuspension. *Marine Chemistry*, 121(14):224 – 235, 2010. ISSN 0304-4203. doi: http://dx.doi.org/10.1016/j.marchem.2010.05.002. URL http://www.sciencedirect.com/science/article/pii/S0304420310000678.

D. M. Karl. Aquatic Ecology: Phosphorous, the staff of life. *Nature*, 406(6971): 31 – 33, 2000.

L. W. Kaul and P. N. Froelich Jr. Modelling estuarine nutrient geochemistry in a simple system. *Geochimica Cosmochimica Acta*, 48(7):1417 – 1433, 1984.

P. J. Kavanagh, M. E. Farago, I. Thornton, and R. S. Braman. Bioavailability of arsenic in soil and mine wastes of the Tamar Valley, SW England. *Chemical Speciation and Bioavailability*, 9:77 – 81, 1997.

R. Kerouel and A. Aminot. Fluorometric determination of ammonia in sea and estuarine waters by direct segmented flow analysis. *Marine Chemistry*, 57: 265 – 275, 1997.

E. R. Khalid, W. H. Patrick, and R. D. Delaune. Phosphorous sorption characteristics of flooded soils. *Aust. J. Mar. Freshwater Res.*, 41:305 – 310, 1977.

V. B. Khodse and N. B. Bhosle. Nature and sources of suspended particulate organic matter in a tropical estuary during the monsoon and pre-monsoon: Insights from stable isotopes ($\delta^{13}\ C_{POC}$, $\delta^{15}\ N_{TPN}$) and carbohydrate signature compounds. *Marine Chemistry*, 145 - 147:16 – 28, 2012.

L. H. Kim, E. Choi, and M. K. Stenstrom. Sediment characteristics, phosphorus types and phosphorus release rates between river and lake sediments. *Chemosphere*, 50(1):53 – 61, 2003.

T. Kiorboe, K. P. Andersen, and H. G. Dam. Coagulation efficiency and aggregate formation in marine-phytoplankton. *Marine Biology*, 107:235 – 245, 1990.

A. Kleeburg and B. Gruneberg. Phosphorus mobility in sediments of acid mining lakes, Lusatia, Germany. *Ecological Engineering*, 24:89 – 100, 2005.

G. A. Knauer, J. H. Martin, and K. W. Bruland. Fluxes of particulate carbon, nitrogen, and phosphorus in the upper water column of the northeast pacific. *Deep Sea Research Part A. Oceanographic Research Papers*, 26(1):97–108, 1979.

S. Knox, M. Whitfield, D. R. Turner, and M. I. Liddicoat. Statistical analysis of estuarine profiles: Part III Application to nitrate, nitrite and ammonium in Tamar Estuary. *Estuarine, Coastal and Shelf Science*, 22:619 – 636, 1986.

I. Koike and J. Sorensen. *Nitrogen Cycling in Coastal Marine Environments*, chapter Chapter 11 - Nitrate reduction and denitrification in marine sediments, pages 251 – 273. SCOPE. John Wiley & Sons, 1988.

A. Kolmogorov. Dissipation of energy in locally isotropic turbulence. *C.R. Acad Sci URSS*, 32(16), 1941a.

A. N. Kolmogorov. The local structure of turbulence in incompressible viscous fluid for very large Reynolds numbers. *C. R. Acad. Sci. URSS*, 30:301, 1941b.

K. A. Kormas, A. Nicolaidou, and S. Reizopoulou. Temporal variations of nutrients, chlorophyll α and particulate matter in three coastal lagoons of Amvrakikos Gulf, (Ionian Sea, Greece). *Marine Ecology*, 22(3):201 – 213, 2002.

B. A. Kornman and E. M. G. T. de Dekere. Temporal variation in sediment erodibility and suspended sediment dynamics in the Dollard estuary. In K. S. Black, D. M. Patterson, and A. Cramp, editors, *Sedimentary processes in the intertidal zone*, pages 231 – 241. Geological Society, 1998.

K. Kranck. Particulate matter grain-size characteristics and flocculation in a partially mixed estuary. *Sedimentology*, 28(1):107–114, 1981.

Y. N. Krestenitis, K. D. Kombiadou, and Y. G. Savvidis. Modelling the cohesive sediment transport in the marine environment: the case of Thermaikos Gulf. *Ocean Science*, 3:91 – 104, 2007.

R. B. Krone. Flume studies of the transport of sediment in estuarial shoaling processes, final report. Technical report, Hydraulic Engineering and Sanitary Engineering Research Laboratory, University of California, Berkeley (CA), 1962.

R. B. Krone. A study of rheological properties of estuarine sediments. Technical Report Hydraulic Engineering Laboratory and Sanitary Engineering Research Laboratory, University of California, Berkley, Tech. Bull 7, Committee of Tidal Hydraulics, 1963.

E. P. Kvale. The origin of neap-spring tidal cycles. *Marine Geology*, 235:5 – 18, 2006.

W. J. Langston. Arsenic in u.k. estuarine sediments and its availability to benthic organisms. *Journal of the Marine Biology Association of the United Kingdom*, 60:869 – 881, 1980.

Y. L. Lau and I. G. Droppo. Influence of antecedent conditions on critical shear stress of bed sediments. *Water Research*, 34:663 – 667, 2000.

C. S. Law, A. P. Rees, and N. J. P. Owens. Temporal variability of denitrification in estuarine sediments. *Estuarine, Coastal and Shelf Science*, 33:37 – 56, 1991.

D. A. Lemley, J. B. Adams, S. Taljaard, and N. A. Strydom. Towards the classification of eutrophic condition in estuaries. *Estuarine, Coastal and Shelf Science*, 2015.

S. Lesourd, P. Lesueur, J. C. Brun-Cottan, J. P. Auffret, N. Poupinet, and B. Laignal. Morphosedimentary evolution of a macrotidal estuary subjected to human impact: the example of the seine estuary (france). *Estuaries*, 6B:940 – 949, 2001.

S. Lesourd, P. Lesueur, J. C. Brun-Cottan, S. Garnaud, and N. Poupinet. Seasonal variations in the characteristics of superficial sediments in a macrotidal estuary (the seine inlet, france). *Estuarine, Coastal and Shelf Science*, 58(1): 3–16, 2003. ISSN 0272-7714. doi: DOI:10.1016/S0272-7714(02)00340-2.

M. Li, K. Xu, M. Watanabe, and Z. Chen. Long-term variations in dissolved silicate, nitrogen and phosphorus flux from the Yangtze River into the East China Sea and impacts on estuarine ecosystem. *Estuarine, Coastal and Shelf Science*, 71:3 –12, 2007.

W. Lick and J. Lick. Aggregation and disaggregation of fine-grained lake sediment. *Journal of Great Lakes Research*, 14(4):514 – 523, 1988.

W. Lick, H. Huang, and R. Jepsen. Flocculation of fine-grained sediments due to differential settling. *Journal of Geophysical Research*, 98(C6):10279–10288, 1993.

A. I. Lillebø, J. M. Neto, M. R. Flindt, J. C. Marques, and M. A. Pardal. Phosphorous dynamics in a temperate intertidal estuary. *Estuarine, Coastal and Shelf Science*, 61(1):101–109, 2004. ISSN 0272-7714. doi: DOI:10.1016/j.ecss.2004.04.007.

P. S. Liss. Conservative and non-conservative behaviour of dissolved constituents during estuarine mixing. In *Estuarine Chemistry*. Academic Press, 1976.

I. G. Littlewood and T. J. Marsh. Annual freshwater river mass loads from Great Britain 1975 - 1994: estimation algorithm, database and monitoring network issues. *Journal of Hydrology*, 304:221 – 237, 2005.

T. C. Loder and P. S. Liss. Control by organic coating of the surface charge of estuarine suspended sediments. *Limnology and Oceanography*, 30(2):418 – 421, 1985. doi: 10.4319/lo.1985.30.2.0418.

T. C. Loder and R. P. Reichard. The dynamics of conservative mixing in estuaries. *Estuaries*, 4:64 – 69, 1981.

L. Lohse, J. F. P. Malschaert, C. P. Slomp, W. Helder, and W. Van Raaphorst. Nitrogen cycling in North Sea sediments: interaction of denitrification and nitrification in offshore and coastal waters. *Mar. Ecol. Prog. Ser.*, 101:283 – 296, 1993.

B. A. Lomstein, T. H. Blackburn, and K. Kenriksen. Aspects of ntirogen and carbon cycling in the northern Bering Shelf sediments. I. The significance of urea turnover in mineralisation of ammonium. *Mar. Ecol. Prog. Ser.*, 57:237 – 247, 1989.

D. Loring, R. Rantala, A. Morris, A. Bale, and R. Howland. Chemical composition of suspended particles in an estuarine turbidity maximum zone. *Canadian Journal of Fisheries and Aquatic Sciences*, 40(S1):s201–s206, 1983.

A. Lorke, B. Muller, M. Maerki, and A. Wuest. Breathing sediments: the control of diffusive transport across the sediment-water interface by periodic boundary-layer turbulence. *Limnology and Oceanography*, 2003.

H. K. Lotze, H. S. Lenihan, B. J. Bourque, and R. H. Bradbury. Depletion, degradation, and recovery potential of estuaries and coastal seas. *Science*, 2006.

P. Louchouarn, M. Lucotte, R. Canuel, J. P. Gagne, and L. F. Richard. Sources and early diagenesis of lignin and bulk organic matter in the sediments of the lower St Lawrence Estuary and the Saguenay Fjord. *Marine Chemistry*, 58:3 – 26, 1997.

M. Lucotte and B. d'Anglejan. Seasonal changes in the phosphorus-iron geochemistry of the st. lawrence estuary. *Journal of coastal research*, pages 339–349, 1988.

R. G. Luthy, G. R. Aiken, M. L. Brusseau, S. D. Cunningham, P. M. Gschwend, J. J. Pignatello, M. Reinhard, S. J. Traina, W. J. J. Weber, and J. C. Westall. Sequestration of hydrophobic organic contaminants by geosorbens. *Environmental Science and Technology*, 31:3341 – 3347, 1997.

M. Maar, K. Timmermann, J. K. Petersen, K. E. Gustafsson, and L. M. Storm. A model study of the regulation of blue mussels by nutrient loadings and water column stability in a shallow estuary, the Limfjorden. *Journal of Sea Research*, 64:322 – 333, 2010.

J. E. Mackin and R. C. Aller. Ammonium adsorption in marine sediments. *Limnology and Oceanography*, 29:250 – 257, 1984.

F. Maggi. *Flocculation dynamics of cohesive sediment*. PhD thesis, Delft, 2005.

F. Maggi. Biological flocculation of suspended particles in nutrient-rich aqueous ecosystems. *Journal of Hydrology*, 376:116 – 125, 2009.

G. Maier, R. J. N. Smith, G. A. Glegg, A. D. Tappin, and P. J. Worsfold. Estuarine eutrophication in the UK: current incidences and future trends. *Aquatic Conservation: Marine and Freshwater Ecosystems*, 19:43 – 56, 2009.

A. Manning and K. Dyer. A Comparison of Floc Properties Observed During Neap and Spring Tidal Conditions. In J. Winterwerp and C. Kranenburg, editors, *Fine Sediment Dynamics in the Marine Environment*, volume 5, pages 233–250. Elsevier, Amsterdam, 2002.

A. Manning, J. Baugh, J. Spearman, and R. Whitehouse. Flocculation settling characteristics of mud:sand mixtures. *Ocean Dynamics*, 2010a.

A. J. Manning. *Study of the effect of turbulence on the properties of flocculated mud*. PhD thesis, University of Plymouth, 2001.

A. J. Manning. The observed effects of turbulence on estuarine flocculation. In *Sediment transport in European Estuaries*, volume SI41, pages 90 – 104. Journal of Coastal Research, 2004.

A. J. Manning. LabSFLOC – a laboratory system to determine the spectral characteristics of flocculating cohesive sediments. Technical Report TR 156, HR Wallingford, 2006.

A. J. Manning and S. Bass. Variability in cohesive sediment settling fluxes: Observations under different estuarine tidal conditions. *Marine Geology*, 235: 177 – 192, 2006.

A. J. Manning and K. R. Dyer. A laboratory examination of floc characteristics with regard to turbulent shearing. *Marine Geology*, 160:147–170, 1999.

A. J. Manning and K. R. Dyer. Mass settling flux of fine sediments in Northern European estuaries: measurements and predictions. *Marine Geology*, 245:107 – 122, 2007. doi: doi:10.1016/j.margeo.2007.07.005.

A. J. Manning and D. H. Schoellhamer. Factors controlling floc settling velocity along a longitudinal estuarine transect. *Marine Geology*, 345:266 – 280, 2013.

A. J. Manning and R. J. S. Whitehouse. Uop mini-annular flume operation and hydrodynamic calibration. Technical report, HR Wallingford, 2009.

A. J. Manning, S. J. Bass, and K. R. Dyer. Floc properties in a turbidity maximum of a mesotidal estuary during neap and spring tide conditions. *Marine Geology*, 235:193 – 211, 2006.

A. J. Manning, S. J. Bass, and K. J. Dyer. Preliminary findings of a study of the upper reaches of the tamar estuary, uk, throughout a complete tidal cycle: Part ii: In-situ floc spectra observations. In J.-Y. Maa, L. P. Sanford, and D. H. Schoellhamer, editors, *Estuarine and Coastal Fine Sediments Dynamics Intercoh 2003*, volume 8 of *Proceedings in Marine Science*, pages 15 – 33. Elsevier, 2007a.

A. J. Manning, P. L. Friend, N. Prowse, and C. L. Amos. Estuarine mud flocculation properties determined using an annular mini-flume and the labsfloc system. *Continental Shelf Research*, 27:1080 – 1095, 2007b.

A. J. Manning, C. Martens, T. de Mulder, J. Vanlede, H. Winterwerp, P. Ganderton, and G. W. Graham. Mud floc observations in the turbidity maximum zone of the Scheldt estuary during neap tides. *Journal of Coastal Research*, SI50: 832 – 836, 2007c.

A. J. Manning, W. J. Langston, and P. J. C. Jonas. A review of sediment dynamics in the Severn Estuary: Influence of flocculation. *Marine Pollution Bulletin*, 61: 37 – 51, 2010b.

A. J. Manning, J. V. Baugh, J. R. Spearman, E. L. Pidduck, and R. J. S. Whitehouse. The settling dynamics of flocculating mud-sand mixtures: Part 1 - empirical algorithm development. *Ocean Dynamics*, 61:311 – 350, 2011.

A. J. Manning, J. R. Spearman, R. J. S. Whitehouse, E. L. Pidduck, J. V. Baugh, and K. L. Spencer. Flocculation dynamics of mud:sand mixed suspensions. In A. J. Manning, editor, *Sediment transport processes and their modelling applications*, chapter 6, pages 119 – 165. INTECH, 2013.

T. N. Markussen and T. J. Andersen. Flocculation and floc break-up related to tidally induced turbulent shear in a low-turbidity, microtidal estuary. *Journal of Sea Research*, 89:1 – 11, 2014. ISSN 1385-1101. doi: http://dx.doi.org/10.1016/j.seares.2014.02.001. URL http://www.sciencedirect.com/science/article/pii/S1385110114000252.

L. Mart. Prevention of contamination and other accuracy risks in voltammetric trace metal analysis of natural waters. *Fresenius' Zeitschrift fur analytische Chemie*, 296(5):350–357, 1979. ISSN 0016-1152. doi: 10.1007/BF00479972.

W. McAnally. *Aggregation and deposition of estuarial fine sediment*. PhD thesis, University of Florida, FL., 1999.

W. H. McAnally and A. J. Mehta. *Coastal and estuarine fine sediment processes*. Elsevier, 2001.

J. C. McCabe. *Observations of estuarine turbulence and floc size variations*. PhD thesis, Polytechnic South West, Plymouth, 1991.

I. N. McCave, R. J. Bryant, H. F. Cook, and C. A. Coughanowr. Evaluation of a laser-diffraction-size analyzer for use with natural sediments. *Journal of Sedimentary Petrology*, 56:561–564, 1984.

T. J. McDougall and P. M. Barker. *Getting started with TEOS-10 and the Gibbs Seawater (GSW) Oceanographic Toolbox*. SCOR/IAPSO, 2011.

A. J. Mehta and E. Patheniades. An investigation of the depositional properties of flocculated. *Journal of Hydrology Research*, 92:361–381, 1975.

F. Mietta, C. Chassagne, A. J. Manning, and J. C. Winterwerp. Influence of shear rate, organic matter content, pH and salinity on mud flocculation. *Ocean Dynamics*, 59:751 – 763, 2009.

K. Mighanetara, C. B. Braungardt, J. S. Rieuwerts, and F. Azizi. Contaminant fluxes form point and diffuse sources from abandoned mines in the River Tamar catchment, UK. *Journal of Geochemical Exploration*, 100:116 – 124, 2009.

D. Mîkes. A simple floc-growth function for natural flocs in estuaries. *Mathematical Geosciences*, 43:593 – 606, 2011.

D. Mikes, R. Verney, R. Lafite, and R. Belorgey. Controlling factors in estuarine flocculation processes: experimental results with material from the Seine estuary, Northwestern France. In P. Ciavola and M. Collins, editors, *Sediment transport in European estuarine environments*, volume 41, pages 82 – 89, 2004.

O. A. Mikkelsen, P. S. Hill, T. G. Milligan, and R. J. Chant. In situ particle size distributions and volume concentrations from a lisst-100 laser particle sizer and a digital floc camera. *Continental Shelf Research*, 25:1959 – 1978, 2005.

O. A. Mikkelsen, T. G. Milligan, P. S. Hill, R. J. Chant, C. Jago, S. E. Jones, V. Krivtsov, and G. Mitchelson-Jones. The influence of schlieren on in situ optical measurements used for particle characterisation. *Limnology and Oceanography: Methods*, 6:133 – 143, 2008.

K. S. Miller and M. M. Rochwarger. A covariance approach to spectral moment estimation. *IEEE Trans. Inform. Theory.*, IT-18:588 – 596, 1972.

T. G. Milligan and P. S. Hill. A laboratory assessment of the relative importance of turbulence, particle composition, and concentration in limiting mmaxima floc size and settling behaviour. *Journal of Sea Research*, 39(3):227 – 241, 1998.

G. E. Millward and Y. Liu. Modelling metal desorption kinetics in estuaries. *Science of the Total Environment*, 314 - 316:613 – 623, 2003.

A. M. Mitchell and D. S. Baldwin. Effects of desiccation/oxidation on the potential for bacterial mediated P release from sediments. *Limnology and Oceanography*, 4:481 – 487, 1998.

A. M. Mitchell and D. S. Baldwin. Organic phosphorus in the environment. In *Organic phosphorous in the aquatic environment: speciation, transformations interactions with nutrient cycles*, page 309. CABI, London, 2005.

C. M. Moore, M. M. Mills, K. R. Arrigo, I. Berman-Frank, L. Bopp, P. W. Boyd, E. D. Galbraith, R. J. Geider, C. Guieu, S. L. Jaccard, T. D. JickeJickells, J. La Roche, T. M. Lenton, N. M. Mahowald, E. Maranon, I. Marinov, J. K. Moore, T. Nakatsuka, A. Oschlies, M. A. Saito, T. F. Thingstad, A. Tsuda, and O. Ulloa. Processes and patterns of oceanic nutrient limitation. *Nat. Geoscience.*, 6:701 – 710, 2013.

N. Mori, T. Suzuki, and S. Kakuno. Noise of acoustic doppler velocimeter data in bubbly flows. *Journal of engineering mechanics*, 133:122 – 125, 2007.

J. Morin and J. W. Morse. Ammonium release from suspended sediments in the Laguna Madre estuary. *Marine Chemistry*, 65:97 – 110, 1999.

A. W. Morris. Kinetic and equilibrium approaches to estuarine chemistry. *Science of the Total Environment*, 97/98:253 – 266, 1990.

A. W. Morris, A. J. Bale, and R. J. M. Howland. Nutrient distributions in an estuary: evidence of chemical precipitation of dissolved silicate and phosphate. *Estuarine, Coastal and Shelf Science*, 12:205 – 216, 1981.

A. W. Morris, R. J. M. Howland, E. M. S. Woodward, A. J. Bale, and R. F. C. Mantoura. Nitrite and ammonia in the Tamar estuary. *Netherlands Journal of Sea Research*, 19(34):217 – 222, 1985. ISSN 0077-7579. doi: 10.1016/0077-7579(85)90026-2. URL http://www.sciencedirect.com/science/article/pii/0077757985900262.

J. W. Morse, M. Hunt, J. Zulling, A. Mucci, and T. Mendez. A comparison of techniques for preserving dissolved nutrients in open ocean seawater samples. *Ocean Science & Engineering*, 7:75 – 106, 1982.

R. J. G. Mortimer, M. D. Krom, P. G. Watson, P. E. Frickers, J. T. Davey, and R. J. Clifton. Sediment-water exchange of nutrients in the intertidal zone of the Humber Estuary, UK. *Marine Pollution Bulletin*, 37:261 – 279, 1999.

J. Murphy and J. P. Riley. A modified single solution method for the determination of phosphate in natural waters. *Analytica Chimica Acta*, 27:31 – 36, 1962.

M. Muste, K. Yu, and M. Spasojevic. Practical aspects of ADCP data use for quantification of mean river flow characteristics; part i: moving-vessel measurements. *Flow Measurement and Instrumentation*, 15(1):1 – 16, 2004. ISSN 0955-5986. doi: http://dx.doi.org/10.1016/j.flowmeasinst.2003.09.001. URL http://www.sciencedirect.com/science/article/pii/S0955598603000670.

National Rivers Authority. Freshwater Tamar and tributaries catchment management plan consultation report. Technical report, NRA South West Region, 1996.

C. Neal, H. P. Jarvie, P. J. A. Withers, B. A. Whitton, and M. Neal. The strategic significance of wastewater sources to pollutant phosphorus levels in English rivers and to environmental management for rural, agricultural and urban catchments. *Science of the Total Environment*, 408:1485 – 1500, 2010.

J. Nemery and J. Garnier. Typical features of particulate phosphorus in the Seine Estuary, France. *Hydrobiologica*, 588:271 – 290, 2007.

M. Nic, J. Jirat, and B. Kosata. *Compendium of Chemical Terminology*. Blackwell Scientific Publications, 2nd edition, 1997.

N. J. Nidzieko, D. A. Fong, and J. L. Hench. Comparison of reynolds stress estimates derived from standard and fast-ping adcps. *Journal of Atmospheric and Oceanic Technology*, 23(6):854–861, 2006.

B. L. Nowicki and S. W. Nixon. Benthic community metabolism in a coastal lagoon system. *Mar. Ecol. Prog. Ser.*, 22:21–30, 1985.

E. Nystrom, K. Oberg, and R. C. Measurement of turbulence with acoustic doppler current profilers - sources of error and laboratory results. In *Hydraulic Measurements and Experimental Methods*, volume 55, pages 1 – 10, 2002.

C. B. Officer. Discussion on the behaviour of nonconservative dissolved constituents in estuaries. *Estuarine and Coastal Marine Science*, 9:91 – 94, 1979.

C. R. O'Melia. Aquasols: the behaviour of small particles in aquatic systems. *Environmental Science and Technology*, 14(9):1052–1060, 1980.

P. M. Orton and M. Visbeck. Variability of internally generated turbulence in an estuary, from 100 days of continuous observations. *Continental Shelf Research*, 29:61 – 77, 2009.

C. W. Oseen. *Neuere Methoden un d Ergebnisse in der Hydrodynamik*. Akad. Verl.-Ges, 1927.

R. K. Pachauri, M. R. Allen, V. R. Barros, J. Broome, W. Cramer, R. Christ, J. A. Church, L. Clarke, Q. Dahe, P. Dasgupta, N. K. Dubash, O. Edenhofer, I. Elgizouli, C. B. Field, P. Forster, P. Friedlingstein, J. Fuglestvedt, L. Gomez-Echeverri, S. Hallegatte, G. Hegerl, M. Howden, K. Jiang, B. Jimenez Cisneroz, V. Kattsov, H. Lee, K. J. Mach, J. Marotzke, M. D. Mastrandrea, L. Meyer, J. Minx, Y. Mulugetta, K. O'Brien, M. Oppenheimer, J. J. Pereira, R. Pichs-Madruga, G. K. Plattner, H. O. Portner, S. B. Power, B. Preston, N. H. Ravindranath, A. Reisinger, K. Riahi, M. Rusticucci, R. Scholes, K. Seyboth, Y. Sokona, R. Stavins, T. F. Stocker, P. Tschakert, D. van Vuuren, and J. P. van Ypserle. Climate Change 2014: Synthesis Report. Contribution of Working Groups I, II and III to the Fifth Assessment Report of the Intergovernmental Panel on Climate Change . Technical report, IPCC, 2014.

H. W. Paerl. Enchancement of marine primary production by nitrogen-enriched acid rain. *Nature*, 316:747 – 749, 1985.

H. W. Paerl, J. Rudek, and M. A. Malin. Stimulation of phytoplankton production in coastal waters by natural rainfall inputs: nutritional and trophic implications. *Marine Biology*, 107(2):247 – 254, 1990.

S. J. Painting, M. J. Devlin, S. J. Malcolm, E. R. Parker, D. K. Mills, C. Mills, P. Tett, A. Wither, J. Burt, R. Jones, and K. Winpenny. Assessing the impact of nutrient enrichment in estuaries: susceptibility to eutrophication. *Marine Pollution Bulletin*, 55:74 – 90, 2007.

E. Partheniades, J. F. Kennedy, R. J. Etter, and R. P. Hayer. *Investigations of the depositional behaviour of fine cohesive sediments in an annular rotating channel*. Department of Civil Engineering, Massachusetts Institute of Technology, 1966.

D. M. Paterson and K. S. Black. Water flow, sediment dynamics and benthic biology. In D. B. Nedwell and D. G. Raffaelli, editors, *Advances in Ecological Research: Estuaries*, pages 155–182. Academic Press Inc., 1999.

D. Pavanelli and L. Selli. Effective size characteristics of suspended sediment and nutrient concentrations during flood events in the Reno River Tributaries (Northern Italy). *Procedia Environmental Studies*, 19:723 – 732, 2013.

A. Pérez-Ruzafa, A. I. Fernández, C. Marcos, J. Gilabert, J. I. Quispe, and J. A. Garcia-Charton. Spatial and temporal variation of hydrological conditions, nutrients and chlorophyll α in a Mediterranean coastal lagoon (Mar Menor, Spain). *Hydrobiologica*, 550:11 – 27, 2005.

L. R. Pomeroy, E. E. Smith, and C. M. Grant. The exchange of phosphate between estuarine water and sediments. *Limnology and Oceanography*, 10:167 – 172, 1965.

S. B. Pope. *Turbulent Flows*. Cambridge University Press, August 2000.

J. N. Pretty, C. F. Mason, D. B. Nedwell, R. E. Hine, S. Lead, and R. Dils. Environmental costs of freshwater eutrophication in England and Wales. *Environmental Science and Technology*, 37:201 – 208, 2003.

D. W. Pritchard. What is an estuary: physical viewpoint. In G. H. Lauf, editor, *Estuaries*, pages 3 – 5. A.A.A.S Publ. No 83, 1967.

D. Pugh. *Changing sea levels: effects of tides, weather and climate*. Cambridge University Press, 2004.

M. Rashidi, G. Hetsroni, and S. Banerjee. Particle-turbulence interaction in a boundary layer. *International Journal of Multiphase Flow*, 16:935 – 949, 1990.

J. W. Readman, R. F. C. Mantoura, and M. M. Rhead. A record of polycyclic aromatic hydrocarbon (PAH) pollution obtained from accreting sediments of the Tamar Estuary, U.K.: Evidence for non-equilibrium behaviour of PAH. *Science of the Total Environment*, 66:73 – 94, 1987.

N. Risgaard-Petersen, R. L. Meyer, M. C. Schmid, M. S. M. Jetten, A. Enrich-Prast, S. Rysgaard, and N. P. Revsbech. Anaerobic ammonium oxidation in an estuarine sediment. *Aquatic Microbial Ecology*, 36(3):293 – 304, 2004.

K. Robards, I. D. McKelvie, R. L. Benson, P. J. Worsfold, N. J. Blundell, and H. Casey. Determination of carbon, nitrogen, phosphorus and silicon species in waters. *Analytica Chimica Acta*, 287:147 – 190, 1994.

S. Robert, G. Blanc, J. Schafer, G. Lavaux, and G. Abril. Metal mobilization in the Gironde Estuary (France): the role of the soft mud layer in the maximum turbidity zone. *Marine Chemistry*, 87:1–13, 2004.

P. J. W. Roberts and D. R. Webster. Turbulent Diffusion. In *Environmental fluid mechanics: theories and applications*. New York: American Society of Civil Engineers, 2002.

W. Rodi and N. Fueyo. *Engineering Turbulence Modelling and Experiments 5*. Elsevier, 2002.

F. Roman, V. Armenio, R. Inghilesi, and S. Corsini. Large eddy simulation of turbulent mixing in an estuary region. In B. Geurts, editor, *Direct and Large-Eddy Simulation VII*, volume 13 of *ERCOFTAC Series*, pages 451–456. Springer Netherlands, 2010. ISBN 978-90-481-3651-3.

Rowe Technologies. ADCP application technologies. Technical report, Rowe Technologies, 2013.

A. C. Ruiz-Fernandéz, C. Hillaire-Marcel, B. Ghaleb, M. Soto-Jiménez, and F. Páez-Osuna. Recent sedimentary history of anthropogenic impacts on the Culiacan River Estuary, northwestern Mexico: geochemical evidence from organic matter and nutrients. *Environmental Pollution*, 118:365 – 377, 2002.

J. H. Ryther and W. M. Dunstan. Nitrogen, phosphorus, and eutrophication in the coastal marine environment. *Science*, 171(3975):1008–1013, 1971.

P. G. Saffman and J. S. Turner. On the collision of drops in turbulent clouds. *Journal of Fluid Mechanics*, 1:16 – 30, 1956.

S. P. Seitzinger, J. A. Harrison, E. Dumont, A. H. W. Beusen, and A. F. Bouwman. Sources and delivery of carbon, nitrogen and phosphorus to the coastal zone: an overview of Global Nutrient Export from Watersheds NEWS models and their application. *Global Biogeochem. Cycles*, 19(GB4S01), 2005.

Z. L. Shen, S. Q. Zhou, and S. F. Pei. Transfer and transport of phosphorus and silica in the turbidity maximum zone of the Chiangjiang estuary. *Estuarine, Coastal and Shelf Science*, 78:481 – 492, 2008.

D. Shepherd, D. Burgess, T. D. Jickells, J. Andrews, R. Cave, R. K. Turner, J. Aldridge, E. R. Parker, and E. Young. Modelling the effects and eeconomic of managed realignment on the cycling and storage of nutrients, carbon and sediments in the Blackwater estuary, UK. *Estuarine, Coastal and Shelf Science*, 73:355 – 367, 2007.

R. Shinnar and J. M. Church. Statistical theories of turbulence in predicting particle size in agitated dispersions. *Industrial & Engineering Chemistry Research*, 1960.

C. Simenstad and T. Yanagi. 1.01 - introduction to classification of estuarine and nearshore coastal ecosystems. In E. Wolanski and D. McLusky, editors, *Treatise on Estuarine and Coastal Science*, pages 1 – 6. Academic Press, Waltham, 2011. ISBN 978-0-08-087885-0. doi: http://dx.doi.org/10.1016/B978-0-12-374711-2.00101-7. URL http://www.sciencedirect.com/science/article/pii/B9780123747112001017.

J. H. Simpson, J. Brown, J. Matthews, and G. Allen. Tidal straining, density currents, and stirring in the control of estuarine stratification. *Estuaries and Coasts*, 13(2):125 – 132, 1990.

Y. Sin, R. L. Wetzel, and I. C. Anderson. Spatial and temporal characteristics of nutrient and phytoplankton dynamics in the York River Estuary, Virginia: analysis of long-term data. *Estuaries*, 22:260 – 275, 1999.

W. H. Slade, E. Boss, and C. Russo. Effects of particle aggregation and disaggregation on their inherent optical properties. *Optics express*, 19(9):7945–7959, 2011.

V. H. Smith, G. D. Tilman, and J. C. Nekola. Eutrophication: impacts of excess nutrient inputs on freshwater, marine, and terrestrial ecosystems. *Environmental Pollution*, 100:179 – 196, 1999.

K. Soataert and J. J. Middelburg. Long-term change in dissolved inorganic nutrients in the heterotrophic Scheldt estuary (Belgium, the Netherlands). *Limnology and Oceanography*, 51(1):409 – 423, January 2006.

R. Soulsby, A. J. Manning, J. Spearman, and R. J. S. Whitehouse. Settling velocity and mass settling flux of flocculated estuarine sediments. *Marine Geology*, 339:1 – 12, 2013.

S. Sritrairat, D. Peteet, T. C. Kenna, R. Sambrotto, D. Kurdyla, and T. Guilderson. A history of vegetation, sediment and nutrient dynamics at Tivoli North Bay, Hudson Estuary, New York. *Estuarine, Coastal and Shelf Science*, 102 - 103:24 – 35, 2012.

M. T. Stacey, T. Rippeth, and J. D. Nash. 2.02 Turbulence and Stratification in Estuaries and Coastal Seas. In Editors-in-Chief: Eric Wolanski and Donald McLusky, editor, *Treatise on Estuarine and Coastal Science*, pages 9 – 35. Academic Press, Waltham, 2011. doi: 10.1016/B978-0-12-374711-2.00204-7.

P. Statham. Nutrients in estuaries - an overview and the potential impacts of climate change. *Science of the Total Environment*, 434:213 – 227, 2012.

H. P. Stirling and A. P. Wormald. Phosphate/sediment interaction in Tolo and Long Harbours, Hong Kong, and its role in estuarine phosphorus availability. *Estuarine Coastal Mar. Sci.*, 5:631 – 642, 1977.

K. D. Stolzenbach and M. Elimelich. The effect of density on collisions between sinking particles: implications for particle aggregation in the ocean. *Journal of Deep Sea Research I*, 41(3):469–483, 1994.

E. Struyf, S. Van Damme, and P. Meire. Possible effects of climate change on estuarine nutrient fluxes: a case study in the highly nutrified Schelde estuary (Belgium, the Netherlands. *Estuarine, Coastal and Shelf Science*, 60:649 – 661, 2004.

R. Styles. Laboratory evaluation of the LISST in a stratified fluid. *Marine Geology*, 225:151 – 162, 2006.

T. F. Sutherland, P. M. Lane, C. L. Amos, and J. Downing. The calibration of optical backscatter sensors for suspended sediment of varying darkness levels. *Marine Geology*, 162:587 – 597, 2000.

A. D. Tappin. An examination of the fluxes of nitrogen and phosphorus in temperate and tropical estuaries: current estimates and uncertainties. *Estuarine, Coastal and Shelf Science*, 55:885 – 901, 2002.

A. D. Tappin, G. E. Millward, and M. F. Fitzsimons. Particle-water iinteraction of organic nitrogen in turbid estuaries. *Marine Chemistry*, 122:28 – 38, 2010.

A. D. Tappin, U. Mankasingh, I. D. McKelvie, and P. J. Worsfold. Temporal variability in nutrient concentrations and loads in the River Tamar and its catchment (SW England) between 1974 and 2004. *Environmental Monitoring and Assessment*, 185(6):791 – 818, June 2012. doi: 10.1007/s10661-012-2905.

G. R. Tattersall, A. J. Elliott, and N. M. Lynn. Suspended sediment concentrations in the Tamar estuary. *Estuarine, Coastal and Shelf Science*, 57:679 – 688, 2003.

W. B. M. ten Brinke. Settling velocities of mud aggregates in the Oosterschelde Tidal Basin (The Netherlands), determined by a submersible video system. *Estuarine, Coastal and Shelf Science*, 39:549 – 564, 1994.

H. Tennekes. Eulerian and lagrangian time microscales in isotropic turbulence. *Journal of Fluid Mechanics*, 67(03):561–567, 1975.

L. J. Thibodeaux and D. Mackay. *Handbook of Chemical Mass Transport in the Environment*. CPC Press, 2010.

A. Thompson and K. W. Goyne. Introduction to the sorption of chemical constituents in soils. *Nature Education Knowledge*, 4:7, 2012.

S. A. Thorpe. *An Introduction to Ocean Turbulence*. Cambridge University Press, 2007. ISBN 978-0-521-67680-9.

E. M. Thurman. *Organic geochemistry of natural waters*. Nijhoff & Junk, Boston, 1985.

R. C. Tian, F. X. Hu, and A. Saliot. Biogeochemical processes controlling nutrients at the turbidity maximum and the plume water fronts in the Changjiang Estuary. *Biogeochemistry*, 19:83 – 102, 1992.

T. J. Tolhurst, K. S. Black, and D. M. Paterson. Muddy sediment erosion: insights from field studies. *Journal of Hydraulic Engineering*, 135(2):73 – 85, 2009.

P. Treguer and B. Queguiner. Seasonal variations in conservative and nonconservative mixing of nitrogen compounds in a West European macrotidal estuary. *Oceanologica Acta*, 12(4):371 – 380, 1989.

M. Trevethan, H. Chanson, and M. Takeuchi. Continuous high-frequency turbulence and suspended sediment concentration measurements in an upper estuary. *Estuarine, Coastal and Shelf Science*, 73:341 – 350, 2007.

J. H. Trowbridge. Quantifying turbulence in the coastal environment. Technical report, Woods Hole Oceanographic Institution, 2008.

C.-H. Tsai and S.-C. Hwang. Flocculation of sediment from the Tanshui River Estuary. *Mar. Freshwater Research*, 46:383 – 392, 1995.

A. Turner. Trace metal partitioning in estuaries: importance of salinity and particle concentration. *Marine Chemistry*, 1996.

A. Turner and G. E. Millward. Suspended particles: their role in estuarine biogeochemical cycles. *Estuarine, Coastal and Shelf Science*, 55:857 – 883, 2002.

T. Tyrrell. The relative influences of nitrogen and phosphorus on oceanic primary production. *Nature*, 400:525–531, 1999.

R. J. Uncles and J. A. Stephens. Nature of the turbidity maximum zone in the Tamar Estuary, UK. *Estuarine, Coastal and Shelf Science*, 36:413 – 431, 1993.

R. J. Uncles, J. A. Stephens, and R. E. Smith. The dependence of estuarine turbidity on tidal intrusion length, tidal range and residence time. *Continental Shelf Research*, 22:1835 – 1856, 2002.

R. J. Uncles, A. J. Bale, J. A. Stephens, P. E. Frickers, and C. Harris. Observations of floc sizes in a muddy estuary. *Estuarine, Coastal and Shelf Science*, 87:186 – 196, 2010.

I. A. Valioulis. Particle collisions and coalescence in fluids. Technical Report KH-R-44, W. M. Keck Laboratory of Hydraulics and Water Resources - Division of Engineering and Applied Science - California Institute of Technology, Pasadena, California, 1983.

W. T. B. Van der Lee. Temporal variation of floc size and settling velocity in the dollard estuary. *Continental Shelf Research*, 20:1495 – 1511, 2000.

H. van Haren, N. Oakey, and C. Garrett. Measurements of internal wave band eddy fluxes above a sloping bottom. *Journal of Marine Research*, 52:909 – 946, 1994.

M. Van Ledden. *Sand-mud segregation in estuaries and tidal basins*. PhD thesis, Delft University of Technology, The Netherlands, 2003. Report No 03-2, ISSN 0169-6548.

W. van Leussen. *Estuarine macroflocs and their role in fine-grained sediment transport*. PhD thesis, University of Utrecht, The Netherlands, 1994.

W. Van Leussen. The Kolmogorov Microscale as a limiting value for the floc sizes of suspended fine-grained sediments in estuaries. *Cohesive sediments*, pages 45–62, 1997.

L. C. van Rijn. *Principles of sediment transport in rivers, estuaries and coastal seas*. Aqua Publications, 1993.

R. Verney, R. Lafite, and J.-C. Brun-Cottan. Flocculation potential of estuarine particles: the importance of environmental factors and of the spatial and seasonal variability of suspended particulate matter. *Estuaries and Coasts*, 32(4): 678 – 693, 2009.

J. Vesely. Stability of pH and the contents of ammonium and nitrate in precipitation samples. *Atmospheric Environment*, 24A:3085 – 3089, 1978.

P. M. Vitousek, J. Aber, R. W. Howarth, G. E. Likens, P. A. Matson, D. W. Schindler, W. H. Schlesinger, and G. D. Tilman. Human alterations of the global nitrogen cycle: sources and consequences. *Ecol. Appl.*, 7:737–750, 1997.

G. Voulgaris and J. H. Trowbridge. Evaluation of the Acoustic Doppler Velocimeter (ADV) for turbulence measurements. *Journal of Atmospheric and Oceanic Technology*, 15:272 – 289, 1997.

D. E. Walling, B. W. Webb, and M. A. Russell. Sediment-associated nutrient transport in UK rivers. Technical report, IAHS Publications, 1997.

L. G. Ward and R. R. Twilley. Seasonal distributions of suspended particulate material and dissolved nutrients in a coastal plain estuary. *Estuaries*, 9(3): 156–168, 1986.

K. W. Warnken, G. A. Gill, P. H. Santschi, and L. L. Griffen. Benthic exchange of nutrients in Galveston Bay, Texas. *Estuaries*, 23(5):647 – 661, 2000.

P. G. Watson, P. E. Frickers, and C. M. Goodchild. Spatial and seasonal variations in the chemistry of sediment interstitial waters in the Tamar Estuary. *Estuarine, Coastal and Shelf Science*, 21:105 – 119, 1985.

D. E. Weller, T. E. Jordan, D. L. Correll, and Z. Liu. Effect of land-use change on nutrient discharges from the Patuxent river watershed. *Estuaries*, 26(2A):244 – 266, April 2003.

M. L. Wells and E. D. Goldberg. Colloid aggregation in seawater. *Marine Chemistry*, 41(4), 1993.

M. E. Wengrove, D. L. Foster, L. H. Kalnejais, V. Percuoco, and T. C. Lippman. Field and laboratory observations of bed stress and associated nutrient release in a tidal estuary. *Estuarine, coastal and shelf science*, 161:11 – 24, April 2015. doi: 10.1016/j.ecss.2015.04.005.

N. B. Weston, A. E. Giblin, G. T. Banta, C. S. Hopkinson, and J. Tucker. The effects of varying salinity on ammonium exchange in estuarine sediments of the Parker River, Massachussetts. *Estuaries and Coasts*, 33:985 – 1003, 2010.

T. C. White. *The inadequate environment: Nitrogen and the abundance of animals*. Springer, Berlin, 1993.

P. Whitehead, D. Butterfield, and A. Wade. Potential impacts of climate change on river water quality. Technical Report SC070043, Environment Agency, 2008.

K. Wild-Allen, J. Skerratt, J. Whitehead, F. Rizwi, and J. Parslow. Mechanisms driving estuarine water quality: 3-D biogeochemical model for informed management. *Estuarine, Coastal and Shelf Science*, 135:33 – 45, 2013.

F. D. Wilde, D. B. Radtke, Gibs, Jacob, and R. T. Iwatsubo. Processing of water samples (ver 2.2). In *U.S. Geological Survey Techniques of Water-Resources Investigations*. U.S.G.S., 2004 - 2011.

P. J. Wiles, T. P. Rippeth, J. H. Simpson, and P. J. Hendricks. A novel technique for measuring the rate of turbulent dissipation in the marine environment. *Geophysical Research Letters*, 33, 2006.

A. J. Williams. CTD (Conductivity, Temperature, Depth) Profiler. In E. in Chief: John H. Steele, K. K. Turekian, , and S. A. Thorpe, editors, *Encyclopedia of Ocean Sciences (Second Edition)*, pages 708 – 717. Academic Press, Oxford, 2nd edition, 2009. ISBN 978-0-12-374473-9. doi: 10.1016/B978-012374473-9.00724-4.

I. Williams. *Environmental Chemistry*. Wiley, 2001.

H. Winterwerp. *On the dynamics of high-concentrated mud suspensions*. PhD thesis, Delft University of Technology, 1993.

J. Winterwerp, A. Manning, C. Martens, T. de Mulder, and J. Vanlede. A heuristic formula for turbulence-induced flocculation of cohesive sediment. *Estuarine, Coastal and Shelf Science*, 68(1-2):195–207, 2006. ISSN 0272-7714. doi: DOI:10.1016/j.ecss.2006.02.003.

J. C. Winterwerp and W. G. M. van Kesteren. Flocculation processes. In T. van Loon, editor, *Introduction to the physics of cohesive sediment in the marine environment*, Developments in Sedimentology. Elsevier, 1st edition, 2004.

J. C. Winterwerp, A. J. Bale, M. C. Christie, K. J. Dyer, S. Jones, D. G. Lintern, A. J. Manning, and W. Roberts. Flocculation and settling velocity of fine sediments. *Proceedings in Marine Science*, 5:25 – 40, 2002.

E. Wolanski. *Estuarine Ecohydrology*. Elsevier, 2007. ISBN 978-0-444-53066-0.

E. Wolanski and M. Elliot. Introduction. In *Estuarine Ecohydrology*, pages 1 – 33. Elsevier, Boston, second edition edition, 2016. ISBN 978-0-444-63398-9. doi: http://dx.doi.org/10.1016/B978-0-444-63398-9.00001-5. URL http://www.sciencedirect.com/science/article/pii/B9780444633989000015.

P. J. Worsfold, L. J. Gimbert, U. Mankasingh, O. N. Omaka, G. Hanrahan, P. C. F. C. Gardolinski, P. M. Haygarth, B. L. Turner, M. J. Keith-Roach, and I. D. McKelvie. Sampling, sample treatment and quality assurances for the determination of phoshorus species in natural water and soils. *Talanta*, 66:273 – 293, 2005.

P. J. Worsfold, P. Monbet, A. D. Tappin, M. F. Fitzsimons, D. A. Stiles, and I. D. McKelvie. Characterisation and quantification of organic phosphorus and organic nitrogen components in aquatic systems: A review. *Analytica Chimica Acta*, 624(1):37–58, 2008. ISSN 0003-2670. doi: DOI:10.1016/j.aca.2008.06.016.

J. Zhao. *Transformation of organic and inorganic phosphorus in estuarine particle-water systems*. PhD thesis, University of Plymouth, 2009.

J. L. Zhou, S. Rowland, R. Fauzi, C. Mantoura, and J. Braven. The formation of humic coatings on mineral particles under simulated estuarine conditions - a mechanistic study. *Water Research*, 28(3):571 – 579, March 1994.

Appendices

Appendix A

Calibration & Performance Assessment

A.1 Flume Performance Assessment

Three runs with the existing set-up were conducted to identify any changes that needed to be made. Figure A.1a demonstrate the results of the first assessment run that was conducted for approx. 6000 seconds with 4 velocity steps. The maximum current velocity achieved was 0.20 m s^{-1}. This value is considerably different to the value obtained by Manning and Dyer (1999); it was not understood why this value was so low, but changes to the set up failed to the 1 m s^{-1}. The primary component of velocity, stream-wise velocity (z), ranged between 0.14 and 0.20 m s^{-1} and demonstrated an increase in current velocity with an increase in motor speed, as expected (Figure A.1a). The cross stream velocity component (y) and the vertical velocity component (x) showed negative values of velocity (Figure A.1c) indicating that the flow was shearing towards the inner wall of the flume. All three assessment runs demonstrated similar results as shown in Table A.1.

Run No.	Max. vel. (m s^{-1})	% Data good
1	0.24	91
2	0.24	94
3	0.24	95

Table A.1: *Results of initial flume calibrations*

Initial examination of results revealed conditions suitable for use. However, upon closer examination at a shorter timescale (5 seconds - see Figures A.1b, c & d), all velocity components demonstrated fluctuations of the range 0.06 m s^{-1}. Of particular relevance, is the fluctuation of between 0.075 and 0.095 m s^{-1} in the stream-wise velocity component (z) during a 5 s period. Fluctuations in velocity components are indicative of turbulence and it was presumed to be the result of the paddles attached to the rotating ring.

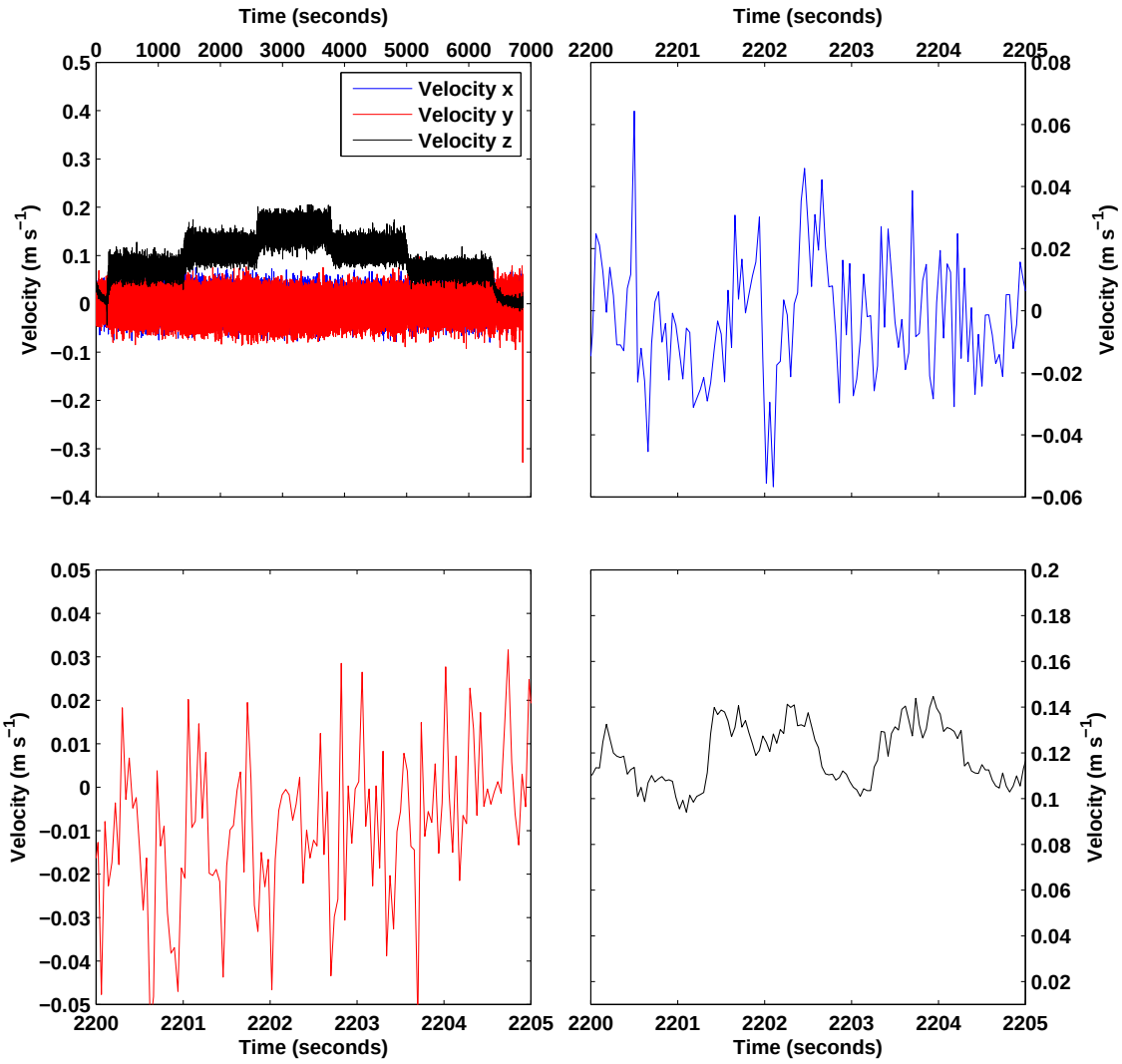

Figure A.1: *a) ADV results of the initial flume experiment with paddles attached to the rotating ring. b-d) A 5-second excerpt of the fluctuating x, y and z velocity data.*

Turbulent flow, while similar to conditions in the Seine and Tamar estuaries, was highlighted as a minor issue as the turbulent flow would not be a controllable variable and may prevent the formation of flocs. It was proposed that a more laminar flow might be achieved by removing the paddles and thus increase the opportunities for flocculations. However, the smooth surface of the perspex ring would not provide sufficient drag friction to create a flow. A layer of 'window frosting' was applied with adhesive to the ring with a light patterned texture to induce drag friction.

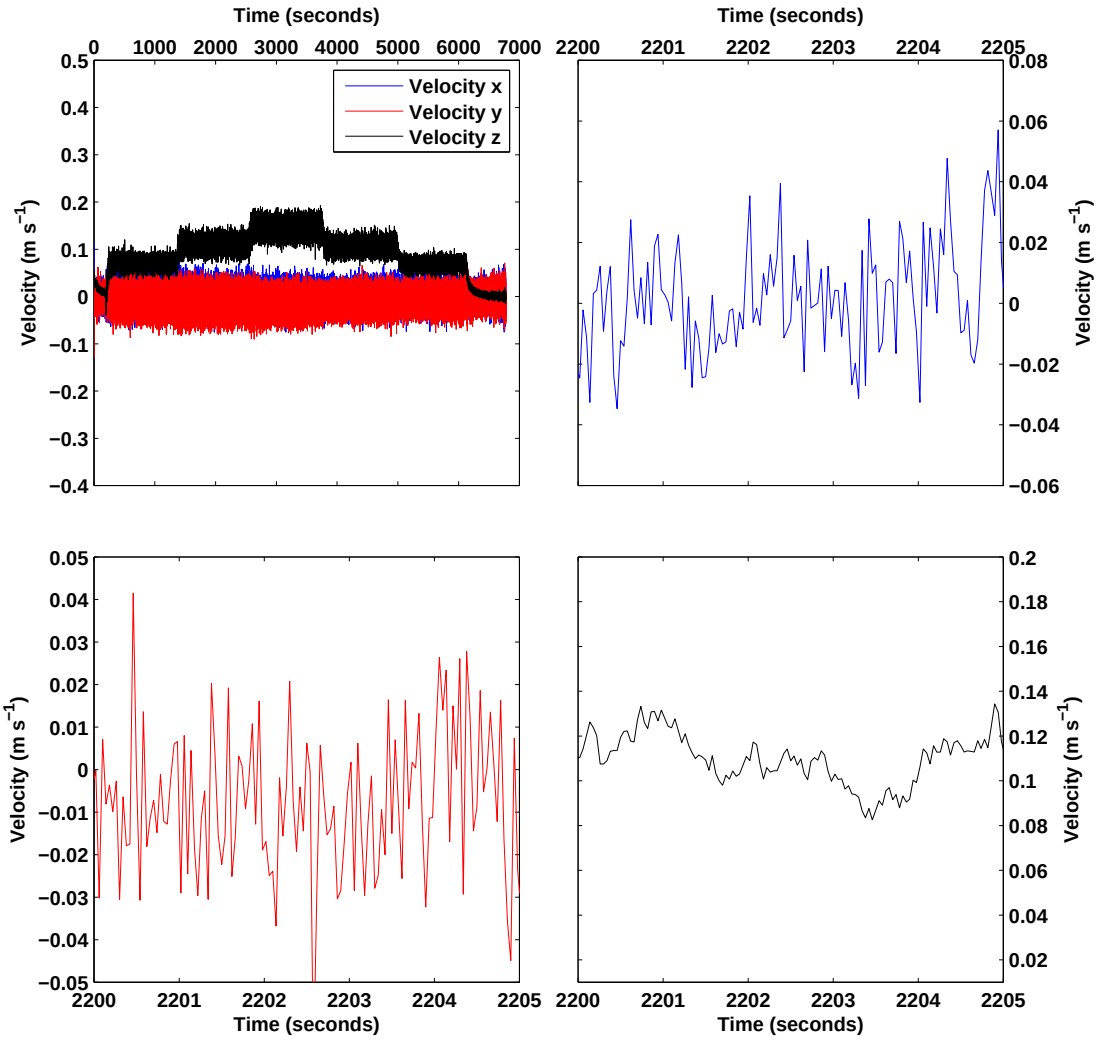

Figure A.2: *ADV results of the initial flume experiment without paddles attached to the rotating ring. A 5-second excerpt of the reduced fluctuations x, y and z velocity data is shown in Figures b, c, & d.*

The results of the flume adaptations are presented in Figures A.2a - d. Figure A.2a shows the stepped increments of the motor throughout the run for all velocity components, while Figures A.2b - d show each individual component of velocity during a 5 s window, as per A.1b - d. In comparison to the initial run with paddles, the fluctuations of each velocity component were very subtly reduced (by approx. 0.03 m s^{-1}); however, while reducing the fluctuations, the overall velocity of each component also decreased resulting in a maximum current velocity of 0.19 m s^{-1} (from 0.2 m s^{-1}). The flume adaptations were insufficient to remove turbulence from the flow; but it was decided to continue using the 'frosted' flume adaptation as it was thought to have less impact on any flocs in the water column.

A.2 Low Nutrient Seawater Performance Assessment

This was to ensure that the LNS was not contaminated or likely to artificially change macro-nutrient concentrations measured in samples. The results of both calibration sets are presented in Figure A.3. Results demonstrated that LNS standards and blanks were of the same order and linear relationship as the UHP standards and was suitable to use in the flume.

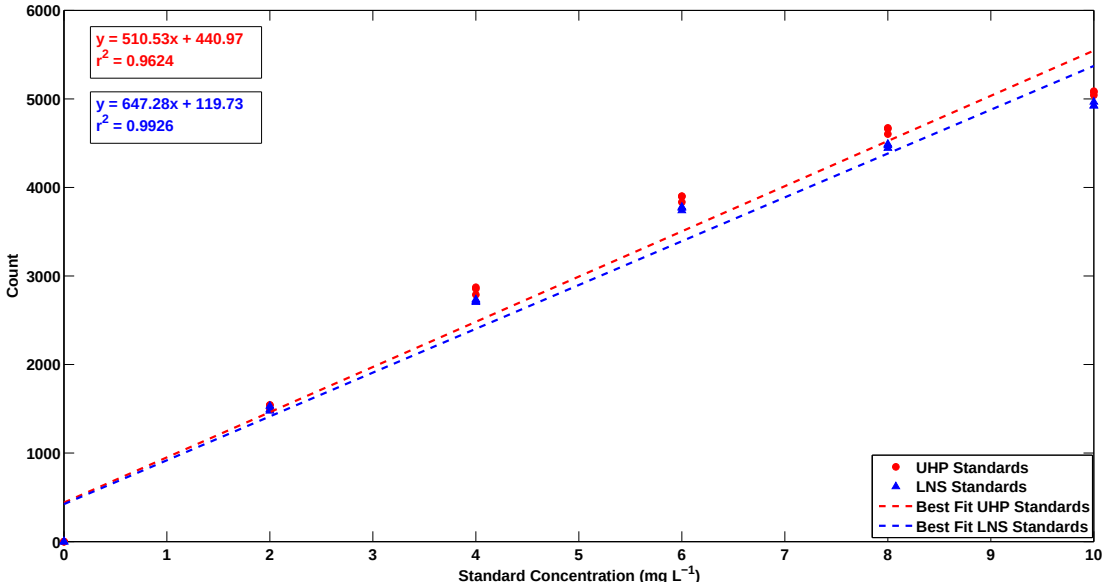

Figure A.3: *UHP Standards comparison with LNS Standards*

Appendix B

Achievements

B.1 PEER REVIEWED PUBLICATIONS

- Manning, A. J., Van Kessel, T., Melotte, J., Sas, M., Winterwerp, H. and Pidduck, E. L. (2011), 'On the consequence of a new tidal dock on the sedimentation regime in the Antwerpen area of the Lower Sea Scheldt', *Continental Shelf Research* **31**, 150 - 164.
- Manning, A. J., Baugh, J. V., Spearman, J. R., Pidduck, E. L. and Whitehouse, R. J. S. (2011), 'The settling dynamics of flocculation mud-sand mixtures: Part 1 - Empirical algorithm development', *Ocean Dynamics* **61**, 311 - 350.
- Manning, A. J., Baugh, J. V., Spearman, J. R., Pidduck, E. L. and Whitehouse, R. J. S. (2010), 'Flocculation settling characteristics of mud:sand mixtures', *Ocean Dynamics - Special Issue: PECS 2008*, **60**, 237 - 253.

B.2 POSTERS

- Pidduck, E. L., Manning, A. J., Verney, R., Fitzsimons, M. F., Nimmo Smith, W. A. M., Worsfold, P. J. & Souza, A. J., 'Sediment-nutrient dynamics in the Seine estuary', AGU Ocean Science Conference, Salt Lake City - February 2012.

B.3 ORAL PRESENTATIONS

- Pidduck, E. L. and Manning, A. J., 'A laboratory examination of flocculation properties exhibited by sediments from Portsmouth Harbour', Biogeochemistry Research Centre Conference, December 2009 - University of Plymouth.
- Pidduck, E. L., Manning, A. J., Verney, R., Fitzsimons, M. F., Worsfold, P. J. and Souza, A. J., 'Marine nutrient dynamics in turbid estuaries - A case study of the Seine estuary, France', Challenger Society Biennial Conference 2010 - National Oceanography Centre, Southampton.

- Pidduck, E. L., Manning, A. J., Verney, R., Fitzsimons, M. F., Worsfold, P. J. and Souza, A. J., 'Marine nutrient dynamics in turbid estuaries - A case study of the Seine estuary, France', British Sedimentological Research Group Annual General Meeting and Conference, December 2010 - National Oceanography Centre, Southampton.
- Pidduck, E. L., Manning, A. J., Verney, R., Fitzsimons, M. F., Worsfold, P. J. and Souza, A. J., 'Marine nutrient dynamics in turbid estuaries - A case study of the Seine estuary, France', Biogeochemistry Research Centre Conference, December 2010 - University of Plymouth.
- Pidduck, E. L., Manning, A. J., Verney, R., Fitzsimons, M. F., Worsfold, P. J. and Souza, A. J., 'Marine nutrient dynamics in turbid estuaries - A case study of the Seine estuary, France', Marine Institute Research Conference, March 2011 - University of Plymouth.

Appendix C

Paper: The Settling Dynamics of Flocculating Mud-Sand Mixtures: Part I - Empirical Algorithm Development

Ocean Dynamics (2011) 61:311–350
DOI 10.1007/s10236-011-0394-7

The settling dynamics of flocculating mud-sand mixtures: Part 1—Empirical algorithm development

Andrew James Manning · John V. Baugh · Jeremy R. Spearman · Emma L. Pidduck · Richard J. S. Whitehouse

Received: 17 January 2010 / Accepted: 14 February 2011 / Published online: 30 March 2011

Abstract European estuaries tend to be regarded as being either predominantly muddy or sandy. In some estuaries, the cohesive and non-cohesive fractions can become segregated. However, recent laboratory tests have revealed that mud and sand from many coastal locations can exhibit some degree of flocculation. A clear understanding of the dynamic behaviour of sediments in the nearshore region is of particular importance for estuarine management groups who want to be able to accurately predict the transportation routes and fate of the suspended sediments. To achieve this goal, numerical computer simulations are usually the chosen tools. In order to use these models with any degree of confidence, the user must be able to provide the model with a reasonable mathematical description of spatial and temporal mass settling fluxes. However, the majority of flocculation models represent purely muddy suspensions. This paper assesses the settling characteristics of flocculating mixed-sediment suspensions through the synthesis of data, which was presented as a series of algorithms. Collectively, the algorithms were referred to as the mixed-sediment settling velocity (MSSV) empirical model and could estimate the mass settling flux of mixed suspensions. The MSSV was based entirely on the settling and mass distribution patterns demonstrated by experimental observations, as opposed to pure physical theory. The selection of the algorithm structure was based on the concept of macroflocs—the larger aggregate structures—and smaller microflocs, representing constituent particles of the macroflocs. The floc data was generated using annular flume simulations and the floc properties measured using the video-based LabSFLOC instrumentation. The derived algorithms are valid for suspended sediment concentrations and turbulent shear stress values ranging between 0.2–5 g l^{-1} and 0.06–0.9 Pa, respectively. However, the MSSV algorithms were principally derived using manufactured mixtures of Tamar Estuary mud and a fine silica sand, which means that the algorithms presented are site-specific in nature, and not fully universal in application. In terms of mass settling flux (MSF) accuracy: at the lower flux range (195–777 mg m^{-2} s^{-1}) most MSSV predictions were within a few percent of the observations, whilst for the largest observed MSFs (1.3–21 g m^{-2} s^{-1}), the MSSV demonstrated a close fit with the data. Even for the highest observed MSF of 33 g m^{-2} s^{-1} (produced by a 75M:25S mixed suspension), the MSSV only under-estimated the flux by 18%. The MSSV algorithms indicated a trend whereby a rise in sand content, and a subsequent decrease in mud, favours the microflocs as the dominant flux contributor. Parameter comparison testing indicated that by applying a single-sediment assumption to a mixed-sediment environment, pure mud algorithms under-predicted at each concentration by as much as 25% and did not handle sandy mud sediments particularly well. Slow constant settling velocity (0.5 and 1 mm s^{-1}) parameters severely under-predicted MSF (at times down to only 13% of the observed flux), whilst the fastest constant fall rate (5 mm s^{-1}) parameter over-predicted by as much as 246%. Fixed settling velocity parameters produced quite large mean errors in MSF estimation. A concentration

Responsible Editor: Susana B. Vinzon

A. J. Manning · J. V. Baugh · J. R. Spearman · R. J. S. Whitehouse
HR Wallingford,
Howbery Park,
Wallingford, Oxfordshire OX10 8BA, UK

A. J. Manning (✉) · E. L. Pidduck
Marine Physics Research Group, School of Marine Science & Engineering, University of Plymouth,
Portland Square Building (A410),
Plymouth, Devon PL4 8AA, UK
e-mail: andymanning@yahoo.com

Power Law and van Leussen (1994) approaches generally under-predicted by 25–37%, with extremely high mean errors and standard deviations. By assuming every suspension scenario was pure sand, over-estimated the mass settling flux by over 400% at dilute suspensions, reducing to about 100% at a concentration of 5 g l^{-1}. One would assume that if we knew what percentage of mud and sand were in suspension at any one point in time and space, we should be able to predict the MSF with greater accuracy. However, the modification of one of a purely cohesive parameterisation with the addition of a pure sand fall velocity to account for the sand fraction, tended to create even greater MSF predictive errors, and in most cases produced excessive over-estimations in MSF. The reason for these predictive errors was that this hybrid approach still treated mud and sand separately. This is potentially reasonable if the sediments are segregated and non-interactive, but appears to be unacceptable when the mud and sand are flocculating via an interactive matrix. The MSSV empirical model may be regarded as a 'first stage' approximation for scientists and engineers either wishing to investigate mixed-sediment flocculation and its depositional characteristics in a quantifiable framework, or simulate mixed-sediment settling in a numerical sediment transport model where flocculation is occurring. The preliminary assessment concluded that in general when all the SPM and shear stress range data were combined, the net result indicated that the new mixed-sediment settling velocity empirical model was only in error by −3 to −6.7% across the experimental mud:sand mixture ratios. Tuning of the algorithm coefficients is required for the accurate prediction of depositional rates in a specific estuary, as was demonstrated by the algorithm calibration using data from Portsmouth Harbour. The development of a more physics-based model, which captures the essential features of the empirical MSSV model, would be more universally applicable.

Keywords Mixed sediments · Mass settling flux · Flocculation · Turbulent shear stress · Macrofloc · Settling velocity · Suspended particulate matter · Cohesive sediment · LabSFLOC instrument · Parameterisation · Numerical sediment transport models

1 Introduction

Sediments present in many European estuaries tend to be regarded as being either predominantly muddy or sandy. However, in many estuarine systems and tidal inlets mud can become mixed with sandy sediments. The proportion of mud and sand in the subtidal and intertidal sediments can vary in both space and in time (e.g. Jacobs 2006; Uncles et al. 1998). In some locations, the cohesive and non-cohesive fractions can become segregated and appear to behave independently, in terms of aggregation (Van Ledden 2003). For example, van Wijngaarden et al. (2002a,b) observed the effects of the segregation of the mud:sand content distributions in Haringvliet–Hollands Diep (The Netherlands). Williamson (1991) has reviewed the characteristics of mud:sand mixtures in the natural environment.

There are however many estuarial environments where mud and sand co-exist as a single mixture (Mitchener et al. 1996) and this creates the potential for these two fractions to combine and exhibit some degree of interactive flocculation (Manning et al. 2007, 2009). Whitehouse et al. (2000) describe a process whereby cohesive sediments mix into a predominately cohesionless sandy region can create a 'cage-like' structure which can fully encompass the sand grains, thus trapping the sand within a clay floc envelope. Biological activity, more commonly associated with cohesive sediments, has been highlighted to play an important role in the cohesion of sediments (e.g. Paterson and Hagerthey 2001) and previous research has shown that a clay content of between 5% and 10% can cause natural sediment mixtures to behave in a cohesive manner (Dyer 1986; Raudkivi 1998). Thus different ratios of mud and sand, can vary the level of cohesion, which will influence the resultant level of flocculation occurring. However, one may appreciate that due to the wide-ranging variability in the mixed-sediment compositional properties, it is extremely difficult to quantitatively describe such a complex sedimentary matrix in a fundamental manner, primarily as a result of a lack of verification data.

A clear understanding of the dynamic behaviour of sediments in the nearshore region is of particular importance for estuarine management groups who want to be able to accurately predict the transportation routes and fate of the suspended sediments. To achieve this goal, numerical computer simulations are usually the chosen tools. However, in order to use these models with any degree of confidence, the user must be able to provide the model with a reasonable mathematical description of spatial and temporal mass settling fluxes.

Pure cohesive sediments can flocculate into larger aggregates called 'flocs' (e.g. Lick et al. 1993; Manning 2001; Winterwerp and van Kesteren 2004). These flocs tend to become less dense and more porous as they grow in size (Koglin 1977; Tambo and Watanabe 1979; Klimpel and Hogg 1986), but display faster settling velocities (Ws) due to a Stokes Law relationship between Ws and the floc diameter (e.g. Dyer and Manning 1999). To complicate matters further, mud flocculation is a dynamically active process which readily reacts to changes in turbulent hydrodynamic conditions (e.g. Krone 1962; Argaman and Kaufman 1970; Parker et al. 1972; McCave 1984; van Leussen 1994; Winterwerp 1998; McAnally 1999; Manning 2004a; Cuthbertson et al. 2008).

The specification of the flocculation term within numerical models depends upon the sophistication of the model. The most simplistic parameterisation is a settling velocity value that remains constant in both time and space. These fixed settling values are typically selected on an arbitrary basis and can be adjusted by model calibration, but they hold no link to the naturally turbulent environment. A conceptual model of the effect of shear and concentration on the median floc settling velocity was proposed by Dyer (1989). Since the 1990s, numerous mud flocculation models have been developed, which include: heuristic approaches (e.g. van Leussen 1994; Malcherek 1995); predominantly theoretical (Boadway 1978; Casamitjana and Schladow 1991, 1993; Krishnappan 1990, 1991); those based on in situ and/or laboratory-derived data (e.g. Ayesa et al. 1991; Lick et al. 1993; Lee et al. 1994; Manning 2008); fractal-based (Kranenburg 1994; Hill 1996; Chen and Eisma 1995; Winterwerp 1998; Sanford et al. 2005; Winterwerp et al. 2006 amongst others) and population balance approaches (e.g. Maggi 2005; Mietta et al. 2008).

Many of these flocculation approaches listed have been applied to real estuarine locations. For example: the Manning (2008) empirical algorithms have been applied to the Tamar Estuary, UK (Manning and Dyer 2007) and were also used in numerical simulations of the Thames Estuary in the UK (Baugh and Manning 2007). The heuristic approach by Malcherek (1995) has been applied to the Wesser Estuary in Germany (Malcherek et al. 1996); and the Winterwerp et al. (2006) fractal model has been implemented in a Delft 3-D model of the Scheldt Estuary (Belgium) in the Antwerpen region. However, the majority of flocculation models represent purely muddy suspensions. This paper presents a new empirical model which quantitatively describes the mass settling behaviour of flocculating mud:sand mixtures.

The aim of the research presented in this paper was to identify potential trends in terms of the settling characteristics of flocculating mixed-sediment suspensions. It is not the intention of this paper to present a new theory on flocculation. Instead it attempts to assess the settling characteristics of mixed-sediment suspensions through the synthesis of a unique empirical data set. In order to provide some degree of quantification for the comparison of their behavioural dynamics, it was decided that the floc data set would be used to create a series of empirical algorithms, from which one could inter-relate the settling velocity and mass distributional characteristics demonstrated by different ratios of mud and sand. The algorithms would be derived in terms of the ambient total sediment particulate matter (SPM) concentration and turbulent shear stress (τ) within the water column. The work extends the Manning (2004b, 2008) analysis which developed similar algorithms for muddy suspensions.

The empirical 'Mixed Sediment Settling Velocity (MSSV) model' was based entirely on laboratory experimental observations made using low intrusive data acquisition techniques, from simulations over a wide range of water column conditions (Manning et al. 2007). The MSSV algorithms were principally derived using manufactured mixtures of Tamar Estuary mud and a fine silica sand, as both are well-documented sediments. This means that the algorithms will be site-specific in nature, and not fully universal in application. Testing of the MSSV against benchmark data are presented, followed by an alternative model calibration with naturally occurring mixed sediments from Portsmouth Harbour. The implementation of the MSSV within a 1DV numerical model will be presented in the companion paper by Spearman et al. (2011).

2 Data acquisition and sources

2.1 Overview of primary experiments

The new mud:sand settling velocity algorithms were based on laboratory-derived data. Laboratory simulations have been previously used to examine many aspects of mud:sand behaviour (e.g. Ockenden and Delo 1988; Williamson and Ockenden 1993; Torfs 1994; Torfs et al. 1996; Dankers et al. 2007). The laboratory flume study (Manning et al. 2007) examined the flocculation/aggregation dynamics for three different mud:sand (M:S) mixtures of the following ratios: 75:25 (Run A), 50:50 (Run B), and 25:75 (Run C). For each mixed-sediment run, three different SPM concentrations were used: 200, 1,000 and 5,000 mg l^{-1}; i.e. a progressive increase by a factor of five in ambient SPM concentration. Sediment mixtures were sheared for 30 min at each shear stress (τ) increment (τ ranging from 0.06 to 0.9 Pa) to allow each suspension to attain floc equilibrium. This time duration was predetermined in accordance with theoretical flocculation time (TF), as the time required to decrease the number of individual unflocculated particles in a suspension to 10% of the initial number as a result of flocculation (van Leussen 1994). A fourth run comprised a set of settling tests conducted on suspensions of 100% sand, with the same three total SPM concentrations employed in the mixed-sediment runs. No shear stress was induced on the 100% sand test as it was not expected to flocculate. Although the main tests only produced a dataset with a total of 36 mixed floc/aggregate spectral samples, the wide range in τ, SPM and M:S, means that significantly different conditions exist between neighbouring data points. A complete matrix of the experimental runs and samples collected is illustrated in Table 1.

Table 1 Overview of Tamar Estuary mixed-sediment experimental runs and samples

Run	Sample	Mud (%)	Sand (%)	τ (Pa)	SPM (mg/l)
A	1	75	25	0.9	200
A	2	75	25	0.6	200
A	3	75	25	0.35	200
A	4	75	25	0.06	200
A	5	75	25	0.9	1,000
A	6	75	25	0.6	1,000
A	7	75	25	0.35	1,000
A	8	75	25	0.06	1,000
A	9	75	25	0.9	5,000
A	10	75	25	0.6	5,000
A	11	75	25	0.35	5,000
A	12	75	25	0.06	5,000
B	1	50	50	0.9	200
B	2	50	50	0.6	200
B	3	50	50	0.35	200
B	4	50	50	0.06	200
B	5	50	50	0.9	1,000
B	6	50	50	0.6	1,000
B	7	50	50	0.35	1,000
B	8	50	50	0.06	1,000
B	9	50	50	0.9	5,000
B	10	50	50	0.6	5,000
B	11	50	50	0.35	5,000
B	12	50	50	0.06	5,000
C	1	25	75	0.9	200
C	2	25	75	0.6	200
C	3	25	75	0.35	200
C	4	25	75	0.06	200
C	5	25	75	0.9	1,000
C	6	25	75	0.6	1,000
C	7	25	75	0.35	1,000
C	8	25	75	0.06	1,000
C	9	25	75	0.9	5,000
C	10	25	75	0.6	5,000
C	11	25	75	0.35	5,000
C	12	25	75	0.06	5,000

2.2 Mini-annular flume

Data for this study was acquired from a series of mini-annular flume experiments conducted at the University of Plymouth (Manning et al. 2007; see Fig. 1a). This created a consistent and repetitively turbulent environment, within which sediment suspensions could be sheared in controlled conditions. The annular flume has an outer diameter of 1.2 m, a channel width of 0.1 m and a maximum depth of 0.15 m, along with a detachable roof of 10 mm thickness. The flume channel is constructed of fibreglass with a rotating roof section. An adjustable annular ring, which has six 15-mm deep paddles on the underside, was rigidly suspended from the roof. The annular ring fits into the channel, and is set to the height of the fluid—0.13 m above the channel base. This produced a nominal fluid volume of 45 l present in the flume channel during each experimental run. A detailed description of the mini-annular flume operation is reported by Manning and Whitehouse (2009). The flume hydrodynamics, in terms of velocity and turbulent kinetic energy (TKE), were measured by a Nortek mini-acoustic Doppler velocimeter at a distance of 22 mm above the flume channel base, which was also the floc extraction height.

2.3 Floc/aggregate properties

The low intrusive video-based LabSFLOC—Laboratory Spectral Flocculation Characteristics—instrument (Manning 2006) was used to measure floc/aggregate properties from each population (see Fig. 1b). Sampling comprised careful extraction of a suspension from a distance of 22 mm above the flume channel base. The sample was then quickly transferred to a Perspex column containing clear water with the same salinity as used in the flume runs (salinity of 20 ±0.2), and then each floc/aggregate was observed using a high-resolution miniature underwater video camera as they were settling in the column. All settling aggregates for each extracted population were measured for both size (D) and settling velocity, which permits their effective density (ρ_e) to be calculated via Stokes Law. Computational techniques originally derived by Fennessy et al. (1997), and adapted by Manning (2004c), were then applied to calculate individual floc dry mass, porosity and the MSF distributions for each LabSFLOC population.

2.4 Sediment sources

The laboratory experiments primarily utilised predetermined mixed sediments, which were a combination of natural Tamar Estuary (UK) mud mixed with sand, in order to produce the desired mud:sand ratio. The Tamar Estuary is a ria, which is tidally classified as mesotidal at neap tides, and macrotidal during spring conditions, with respective average tidal ranges of 2.2 and 4.7 m. A natural mud sample, from the surface down to a depth of about 5 cm, was collected from the intertidal area adjacent to the slipway at Calstock, located in the upper reaches approximately 30 km from the mouth within the tidal trajectory of the mobile turbidity maximum. This mud was used as its characteristics are widely reported from previous international experiments, such as COSINUS (see Manning and Dyer 2002). The sand used in these experiments was

Ocean Dynamics (2011) 61:311–350

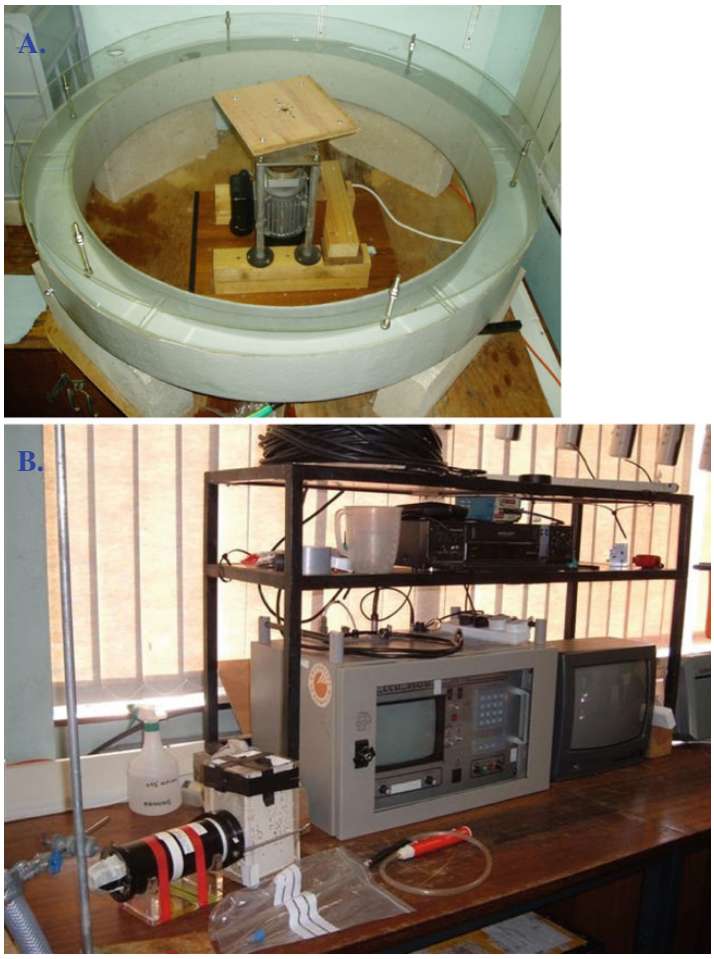

Fig. 1 The mini-annular flume (**a**) and· the LabSFLOC instrument set-up (**b**)

Redhill 110, which is a closely graded silica sand with a d_{10} of about 0.070 mm, d_{50} of about 0.110 mm and a d_{90} of about 0.170 mm.

A second floc/aggregate data set was produced from a series of mini-annular flume experiments conducted on naturally occurring mixed-sediment samples collected from within Portsmouth Harbour (Pidduck and Manning 2009). An overview of the Portsmouth Harbour experimental runs and samples is shown in Table 2. This data was used to provide an independent set of mixed-sediment settling algorithms. Portsmouth Harbour is a tidal inlet on the south coast of the UK. Regular dredging activities for military vessel access to the Royal Naval Base, combined with an ebb-dominant macrotidal regime, mean that the fine mud and coarser sands that reside in the Harbour can become mixed. It was estimated that the average d_{50} of sand fraction from the Portsmouth samples was estimated to be 0.127 mm (±0.003 mm). Sediment transport in Portsmouth Harbour has been reviewed by Hydraulics Research (1959), Lonsdale (1969) and Harlow (1980).

2.5 Example data sets

To illustrate typical ranges and patterns depicted by the non-parameterised floc/aggregate data measured by Lab-SFLOC instrumentation during the flume simulations, some examples of data from each sediment type will be presented.

2.5.1 Tamar estuary manufactured mixed-sediment floc/aggregates

Figure 2 shows the aggregate characteristics for Sample A3, which was obtained from a 75M:25S sediment run. The

Table 2 Overview of Portsmouth Harbour natural mixed-sediment experimental runs and samples

Run	Sample	Mud (%)	Sand (%)	τ (Pa)	SPM (mg/l)
4_A	1	38	62	0.6	200
4_A	2	38	62	0.35	200
4_A	3	38	62	0.1	200
4_A	4	38	62	0.6	600
4_A	5	38	62	0.35	600
4_A	6	38	62	0.1	600
4_A	7	38	62	0.6	2,000
4_A	8	38	62	0.35	2,000
4_A	9	38	62	0.1	2,000
6_B	1	70	30	0.6	200
6_B	2	70	30	0.35	200
6_B	3	70	30	0.1	200
6_B	4	70	30	0.6	600
6_B	5	70	30	0.35	600
6_B	6	70	30	0.1	600
6_B	7	70	30	0.6	2,000
6_B	8	70	30	0.35	2,000
6_B	9	70	30	0.1	2,000
8_C	1	90	10	0.6	200
8_C	2	90	10	0.35	200
8_C	3	90	10	0.1	200
8_C	4	90	10	0.6	600
8_C	5	90	10	0.35	600
8_C	6	90	10	0.1	600
8_C	7	90	10	0.6	2,000
8_C	8	90	10	0.35	2,000
8_C	9	90	10	0.1	2,000

SPM concentration was 200 mg l^{-1} at a τ of 0.35 Pa. The scatterplot illustrates spherical-equivalent floc sizes (D) plotted against settling velocity (Ws) for the sample. The diagonal lines represent contours of constant floc effective density ρ_e (units=kg m^{-3}). The 204 individual flocs which comprised Sample A3, ranged from 42 to 182 μm in diameter. Their settling velocities spanned from just below 0.3–3.4 mm s^{-1}. When comparing the settling velocities, the macrofloc fraction (Ws_{macro}; D>160 μm) settled at an average fall rate of 1.7 mm s^{-1}, compared to the smaller sized aggregates/flocs (i.e. the microflocs; D<160 μm) which were settling at a velocity (Ws_{micro}) of 0.9 mm s^{-1}; this was 0.6 mm s^{-1} slower.

The microflocs' effective densities (ρ_{e_micro}) ranged from 200 to 1,580 kg m^{-3} and generally exceeded those of the macroflocs (ρ_{e_macro}) which were more closely grouped between 30 and 100 kg m^{-3}. The denser microflocs were 30–58% porous—the porosity reducing and the mineral content rising, with successively decreasing floc size; this demonstrates the encapsulation of fine sand grain into the microfloc structure during the flocculation process.

Sample C6, was acquired from a 1 g l^{-1} suspension with a greater sand proportion (25M:75S), which was sheared at a stress of 0.6 Pa. The scatterplot of D vs. Ws (Fig. 3) indicates the total population comprises four main aggregate clusters, together with four lesser clusters that were more fragmented. The slurry mixture produced a resultant dominance by the microflocs throughout the 25M:75S suspension. For example, one of the microfloc-based clusters comprised aggregates 42–66 μm in diameter, which exhibited settling velocities of 1–4.5 mm s^{-1}, were less than 30% porous and had effective densities of 1,200–1,700 kg m^{-3}. Since some individual flocs have effective densities greater than 1,200 kg m^{-3}, but are also less dense

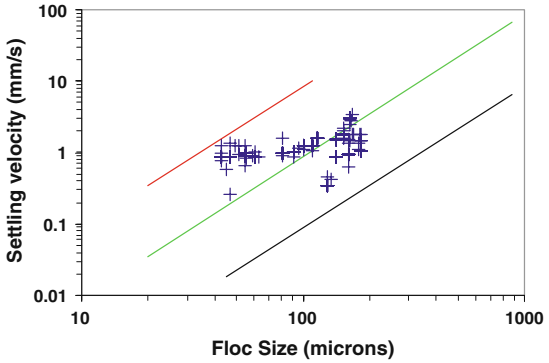

Fig. 2 Distribution floc/aggregate size and settling velocity characteristics for Sample A3. The nominal 200 mg l^{-1} suspension comprised 75% mud and 25% sand had been sheared at τ=0.35 Pa. Diagonal lines represent contours of constant Stokes equivalent effective density: *red* 1,600 kg m^{-3}, *green* 160 kg m^{-3}, and *black* 16 kg m^{-3}

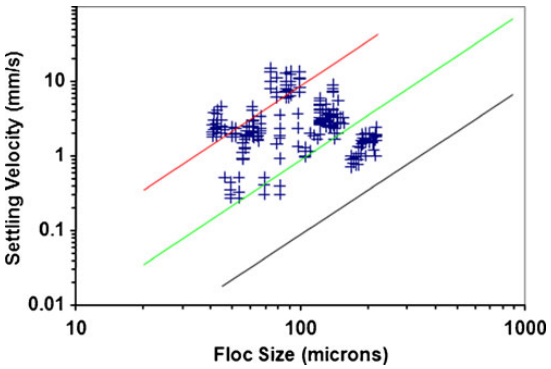

Fig. 3 Distribution floc/aggregate size and settling velocity characteristics for Sample C6. The nominal 1 gl^{-1} suspension comprised 25% mud and 75% sand had been sheared at τ=0.6 Pa. Diagonal lines represent contours of constant Stokes equivalent effective density: *red* 1,600 kg m^{-3}, *green* 160 kg m^{-3}, and *black* 16 kg m^{-3}

than a quartz particle, implies sand particles constitute a portion of the floc structure. Another microfloc cluster with sizes between 76 and 99 μm, demonstrated even faster settling velocities ranging between 6 and 15 mm s^{-1}.

Contrastingly, the macrofloc cluster only spans a 55 μm range: 160–215 μm. This was a 40% reduction in size when compared to the corresponding 75% mud suspension flocs. The average D_{macro} was just 191 μm. These small, low-density ($\rho_e \sim 70$ kg m^{-3}) macroflocs were approximately 94% porous and fell at a combined average Ws_{macro} of 1.35 mm s^{-1}. When the slower settling dynamics of the macrofloc fraction are compared to the microflocs, the microflocs were seen to settle at an average velocity of 3.6 mm s^{-1}; 160% faster than Ws_{macro}. Further examples of the sediment floc/aggregate population dynamics are reported by Manning et al. (2007).

2.5.2 Portsmouth harbour naturally mixed-sediment floc/aggregates

Two Portsmouth Harbour samples at a constant SPM concentration of 2 g l^{-1} and sheared at 0.35 Pa are described. The first example, 6_B-8 (Fig. 4), was cohesive containing 70% mud (70M:30S) within its matrix. The *D* vs. Ws distribution depicts a population more characteristic of a purely muddy suspension, as would be expected (e.g. Fennessy et al. 1994; Eisma et al. 1997; Gratiot and Manning 2004, 2008). The smaller size flocs were distinctly slower in settling speed than the larger flocs/aggregates—a common dynamical pattern observed with pure mud flocs. In terms of settling velocities, the microfloc sized fractions fell at rates between 2 and 8 mm s^{-1}, whilst the macroflocs predominantly spanned 4–11 mm s^{-1}. The macroflocs also constituted 60% of the individual 6_B-8 population (i.e. 1,756 of the 2,909 flocs), which represented approximately 80% of the ambient SPM.

The second example, 4_A-8 (Fig. 5) was less cohesive comprising 38% mud and 62% sand (including coarse silts). Although the 4_A-8 flocs/aggregates ranged in size from 29 to 313 μm, the sandier matrix resulted in a population that was microfloc-focused. The microfloc fraction represented 3,835 (i.e. three quarters) of the total 5,023 aggregates/flocs. This translated into the microfloc fraction comprising 58% of the SPM concentration and the majority of the smaller size fraction exhibiting effective densities greater than 800 kg m^{-3}. Contrastingly, the macroflocs demonstrated $\rho_e < 233$ kg m^{-3}. The 4_A-8 settling velocities span three orders of magnitude from 0.36 to 34 mm s^{-1}, with an abundance of fast settling flocs in the 80–160 μm size range.

3 Algorithm development

Ideally, a model which describes a particular oceanographic process would be in the form of a physics-based model, as this allows a universal application. By comparison a heuristic model can be problematic as there are calibration issues which can stem from a low level of representation of a complex natural marine process. Therefore, an empirical approach can provide a good compromise. Empirical models can identify key physical components which contribute to a process, in terms of how the independent variables relate to the dependent variables; plus they can

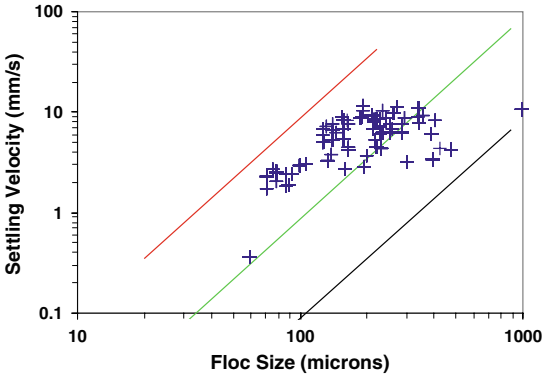

Fig. 4 Distribution floc/aggregate size and settling velocity characteristics for Portsmouth Harbour Sample 6_B-8. The nominal 2,000 mg l^{-1} suspension comprised 70% mud and 30% sand had been sheared at τ= 0.35 Pa. *Diagonal lines* represent contours of constant Stokes equivalent effective density: *red* 1,600 kg m^{-3}, *green* 160 kg m^{-3}, and *black* 16 kg m^{-3}

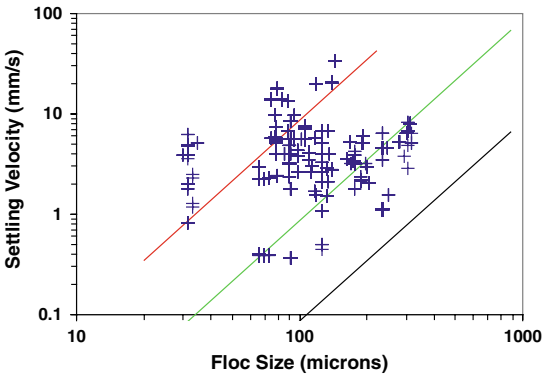

Fig. 5 Distribution floc/aggregate size and settling velocity characteristics for Portsmouth Harbour Sample 4_A-8. The nominal 2,000 mg l^{-1} suspension comprised 38% mud and 62% sand had been sheared at τ= 0.35 Pa. *Diagonal lines* represent contours of constant Stokes equivalent effective density: *red* 1,600 kg m^{-3}, *green* 160 kg m^{-3}, and *black* 16 kg m^{-3}

provide an output (e.g. a settling velocity) which is correctly scaled to the natural process. The drawback is that empirical models quite often tend to be restricted in terms of their 'universal' applicability due to the site-specific nature of the phenomena under consideration; this is the case with both cohesive and mixed-sediment environments.

In the present study, statistical relationships were generated from the mixed-sediment experimental dataset, and compared with existing purely cohesive models and non-cohesive settling values. In a similar way to the Manning floc settling velocity (MFSV; see Manning 2008) empirical model for purely cohesive sediment, this empirical approach would also allow the development of depositional algorithms for incorporating into existing numerical simulation models. The algorithms describe the settling and mass distribution trends of different sediment mixtures within turbulent flow, at varying levels of total SPM concentrations. An example of the type of settling distributions the algorithms needed to describe is illustrated in (Fig. 6; Whitehouse and Manning 2007). The statistical package *Minitab for Windows—version 14.13* was used for the parametric multiple regression analysis, with a default statistical confidence level of 95%.

Most floc/aggregation parameterisations are reliant on a single or mean fall rate, in both time and space. However, a conclusion drawn from an intercomparison experiment of various floc measuring devices conducted in the Elbe estuary (Dyer et al. 1996), was that a single mean or median settling velocity *did not* adequately represent an entire floc spectrum, especially in considerations of flux to the bed. Dyer et al. (1996) recommended that the best approach for accurately representing the settling characteristics of a floc population, was to split a floc/aggregate distribution into two or more components, each with their own mean settling velocity. Both Eisma (1986) and Manning (2001) suggest a more realistic and accurate generalisation of floc populations can be derived from the macrofloc and microflocs. To keep the parameterisations consistent with the MFSV model, this study employed a floc/aggregate diameter of 160 μm as the size limit between the macro- and microfloc fractions (Manning 2001). Analysis of mud:sand flocculating mixtures by Manning et al. (2009), demonstrated that the 160 μm demarcation zone could be used to parameterise mixed-sediment flocs. In a similar way to the MFSV model (Manning 2008), these mixed-sediment algorithms represent the particulate mass and dual settling velocities, both of which vary in response to shear stress and SPM concentration changes.

The following floc/aggregate characteristics were considered the most important and relevant (abbreviations used in brackets):

- Macrofloc settling velocity (Ws_{macro})
- Microfloc settling velocity (Ws_{micro})
- Total SPM concentration (SPM)
- Percentage of SPM constituting the macrofloc portion of a floc population ($SPM\%_{macro}$)
- Percentage of SPM constituting the microfloc portion of a floc population ($SPM\%_{micro}$)
- Turbulence parameters (τ or TKE)

The division of particulate matter within a floc population, and the relative rates at which they settle, are the key variables that govern the deposition of the matter in suspension; i.e. the mass settling flux, and these are represented by the first five terms. Also, the physical descriptors of SPM concentration and a turbulence parameter represent the basic factors which govern the collision rate and

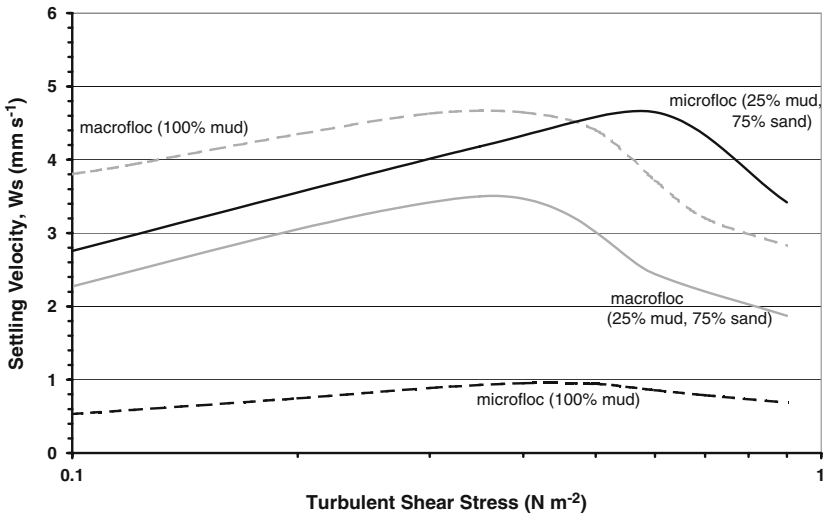

Fig. 6 Conceptual illustration of Ws_{macro} and Ws_{micro} trends for a mixed-sediment suspension comprising 25% mud and 75% sand (*solid lines*), and a pure mud (*dotted lines*) suspension, both at a total suspended concentration of 5 gl^{-1} and are plotted against shear stress (from Whitehouse and Manning 2007)

subsequent degree of flocculation of particles in estuarine waters.

For consistency, the following units were used for each parameter included in the multiple regression and comparison analysis: τ = Pa or N m^{-2}, SPM=mg l^{-1}, Ws=mm s^{-1}, D=μm, and $SPM\%_{macro}$ and $SPM\%_{micro}$ were both expressed as a percentage. In order to differentiate between observations and predictions in this report, the sub-script EM will identify values computed by the empirical model algorithms.

4 Results

4.1 Overview of the mixed-sediment model

The MSSV model (version 1.0) was derived from an empirical data base. The MSSV was based entirely on the settling and mass distribution patterns demonstrated by experimental observations, as opposed to pure physical theory. The selection of the algorithm structure was based on the concept of macroflocs—the larger aggregate structures—and smaller microflocs, representing constituent particles of the macroflocs. The complete data matrix from which the MSSV is derived is listed in Appendix 1. This applies a similar approach used to derive the MFSV algorithms for purely muddy sediments (Manning 2004b). Therefore, the MSSV empirical model is also composed of three principle component algorithms: Ws_{macro_EM}, Ws_{micro_EM} and SPM_{ratio_EM}. However, a fourth component, $M:S_{\_mi:MA\ \_EM}$, is also required when implementing the complete MSSV. This fourth algorithm provides the sediment transport model with quantities/information of how much mud and sand is contained within both the macrofloc and microfloc sub-fractions of a specific population.

The derived algorithms are valid for SPM concentration and τ values ranging between 200–5,000 mg l^{-1} and 0.06–0.9 Pa, respectively. The upper shear stress limit was dictated by the annular flume motor. If a modeller thinks that they may use values outside of the algorithm coverage zone (e.g. higher shear stress, etc.), then they have the option of either taking the equation limit value as a constant thereafter, or alternatively employing a form of exponential decay; both would prevent the Ws = zero scenario occurring.

4.2 Tamar mixtures—macrofloc settling velocity (Ws_{macro_EM})

The macrofloc size fraction (D>160 μm) is recognised as the most important sub-group of flocs, as their fast settling velocities tend to have the most influence on the mass settling flux. The Ws_{macro_EM} equations representing each ratio of mud and sand, for each shear stress range, are as follows:

75% Mud:25% Sand

- For τ ranging between 0.06 and 0.6 Pa:

$$Ws_{macro\_EM} = -0.956 + 17.1 \times \tau - 23.5 \times \tau^2 + 0.000798 \times SPM \qquad R^2 = 0.921 \tag{4.1a}$$

- For τ ranging between 0.6 and 0.9 Pa:

$$Ws_{macro\_EM} = 3.6 - 4.73 \times \tau + 1.45 \times \tau^2 + 0.000586 \times SPM \qquad R^2 = 0.969 \tag{4.1b}$$

50% Mud:50% Sand

- For τ ranging between 0.06 and 0.6 Pa:

$$Ws_{macro\_EM} = -0.24 + 11.7 \times \tau - 15.4 \times \tau^2 + 0.000528 \times SPM \qquad R^2 = 0.868 \tag{4.2a}$$

- For τ ranging between 0.6 and 0.9 Pa:

$$Ws_{macro\_EM} = 3.59 - 4.41 \times \tau + 1.33 \times \tau^2 + 0.00044 \times SPM \qquad R^2 = 0.978 \tag{4.2b}$$

25% Mud:75% Sand

- For τ ranging between 0.06 and 0.6 Pa:

$$Ws_{macro\_EM} = 0.259 + 5.76 \times \tau - 7.61 \times \tau^2 + 0.000317 \times SPM \qquad R^2 = 0.835 \tag{4.3a}$$

- For τ ranging between 0.6 and 0.9 Pa:

$$Ws_{macro\_EM} = 2.02 - 1.6 \times \tau + 0.324 \times \tau^2 + 0.000219 \times SPM \qquad R^2 = 0.978 \tag{4.3b}$$

Equations 4.1–4.3 are valid for the entire experimental total SPM concentration (i.e. 200 mg l^{-1}–5 g l^{-1}). The

multiple regression analysis revealed that Ws_{macro_EM} showed a dependency on both τ and SPM concentration variations at each ratio of mud and sand. Each formulation is valid for suspended mixed-sediment concentrations as low as 200 mg l^{-1} and up to 5 g l^{-1}. Due to the variability of the inter-relationships over the parameter ranges, it was not possible for a single equation to encompass the entire experimental range of turbulent shear stress. Therefore, the data was split into two shear stress zones: 0.06–0.6 and 0.6–0.9 Pa (the MFSV purely cohesive sediment algorithms utilised three τ zones, as they were based on in situ data which had a higher stress range). For suspensions where the %mud and %sand do not directly match the individual MSSV algorithms, a modeller can employ the two bordering equations and interpolate between them. For example: if one needs to calculate a Ws_{macro_EM} for a 63M:37S mixture, they would need to calculate Ws_{macro_EM} using both the 75M:25S and 50M:50S algorithms and then interpolate accordingly to obtain a resultant Ws_{macro_EM} a 63M:37S representative mixture.

The complete regression curves for 75M:25S are displayed graphically in Fig. 7. The solid lines on Fig. 7a represent equations 4.1a–4.1b, whilst the individual points are the data upon which the regression analysis is based. The regression fit is very good, with R^2 values of 0.92 and 0.97 for each sub-algorithm. First impressions show that Ws_{macro_EM} curves display a similar shape to that of both the pure mud empirical algorithms of Manning (2004b), and the conceptual relationship for pure mud flocculation proposed by Dyer (1989). There is an increase in settling velocity at low shear stresses due to flocculation enhanced by shear, and a decrease in settling velocity due to floc disruption at higher stresses for the same concentration.

For example, at a concentration of 200 mg l^{-1} (75M:25S) the low turbulent environment of 0.06 Pa produced a Ws_{macro_EM} of 0.15 mm s^{-1}. As the shear stress increased, so the flocculation dynamics responded and the settling velocity increased to a maximum of 2.1 mm s^{-1} at 0.35 Pa. Thereafter, the macrofloc settling velocity progressively decreased with rising turbulence, resulting in a Ws_{macro_EM} of 0.6 mm s^{-1} at 0.9 Pa which mirrors the more quiescent end of the scale. In fact, the macrofloc 75M:25S mixed fraction attained maximum settling velocities throughout the concentration ranges at a shear stress of 0.35 Pa, as demonstrated by a peak Ws_{macro_EM} of 6.2 mm s^{-1} at a SPM concentration of 5 g l^{-1}. This peak macrofloc fall rate was 1.4 mm s^{-1}, or 31%, faster than the equivalent prediction for pure mud flocs (Manning 2004a). The shear stress of 0.35 Pa is similar to stress which provides maximum flocculation stimulation for natural estuarine mud flocs (e.g. Manning 2004a; Manning and Dyer 2002), and also corresponds very closely to the value observed during a series of pure mud laboratory mini-annular flume experiments by Manning and Dyer (1999).

The macrofloc algorithms representative of an equal mixture of mud and sand suspensions (Eqs. 4.2a–4.2b) indicate a decrease in Ws_{macro_EM} across each base SPM concentration range (see Fig. 7b). However, the general shape of the regression curves are similar to those of 75% Mud:25% Sand mixtures and pure mud suspensions. For 200 mg l^{-1} sheared at 0.35 Pa, the equally mixed sediment produced a Ws_{macro_EM} of 2.1 mm s^{-1}, which was a reduction of 0.2 mm s^{-1} from the 75% mud suspension, and was 14% or 0.3 mm s^{-1} slower at settling than the equivalent pure mud benchmark of the MFSV estimate. Interestingly, if we examine the macrofloc settling characteristics at the highest concentration (5 g l^{-1}) and a τ of 0.35 Pa, the 50M:50S algorithms infer a fall velocity of 4.6 mm s^{-1}; this is identical to the value predicted by the MFSV for pure mud, but 25% or 1.5 mm s^{-1} slower than the equivalent 75% Mud suspension.

This large Ws_{macro} difference between the 75M:25S and 50M:50S mixtures, decreased as the turbulent shear stress was reduced to a lower level. Whereas at a τ of 0.06 Pa, the predicted Ws_{macro_EM} for 50M:50S was 3.1 mm s^{-1} which was just 1 mm s^{-1} slower than the 75% mud mixture predicted Ws_{macro_EM} at the same shear stress. However, both mixed suspension macroflocs at the low shear stress were still slower than the pure mud macrofloc settling predictions of the MFSV, which settled considerably faster at about 3.8 mm s^{-1}.

The sandy mud suspension conditions (25M:75S) represented by Eqs. 5.3a–5.3b, demonstrate significantly less macrofloc flocculation; a result of less cohesion. The shear stress threshold for peak Ws_{macro_EM} is higher with decreasing mud content, moving closer to 0.4 Pa with a 75% sand suspension (see Fig. 7c). The maximum Ws_{macro_EM} across the entire shear stress and SPM ranges was 3 mm s^{-1}, and this only just exceeded the equivalent settling velocity of a d_{10} sand grain. In contrast, a 5 g l^{-1} mixed suspension comprising double the mud content (i.e. 50M:50S), produced macroflocs which exceeded the fall velocity of d_{10} sand from shear stresses ranging from 0.06 Pa through to 0.9 Pa (see Fig. 7b).

4.3 Tamar mixtures—microfloc settling velocity (Ws_{micro_EM})

The smaller microflocs ($D<160$ μm) are generally considered to be the building blocks from which the macroflocs are composed; this is the basis of the order of aggregation theory by Krone (1963). The microfloc class of aggregate tend to display a much wider range in effective densities and settling velocities than the macrofloc fraction. It is plausible that for mixed sediments, this size fraction will

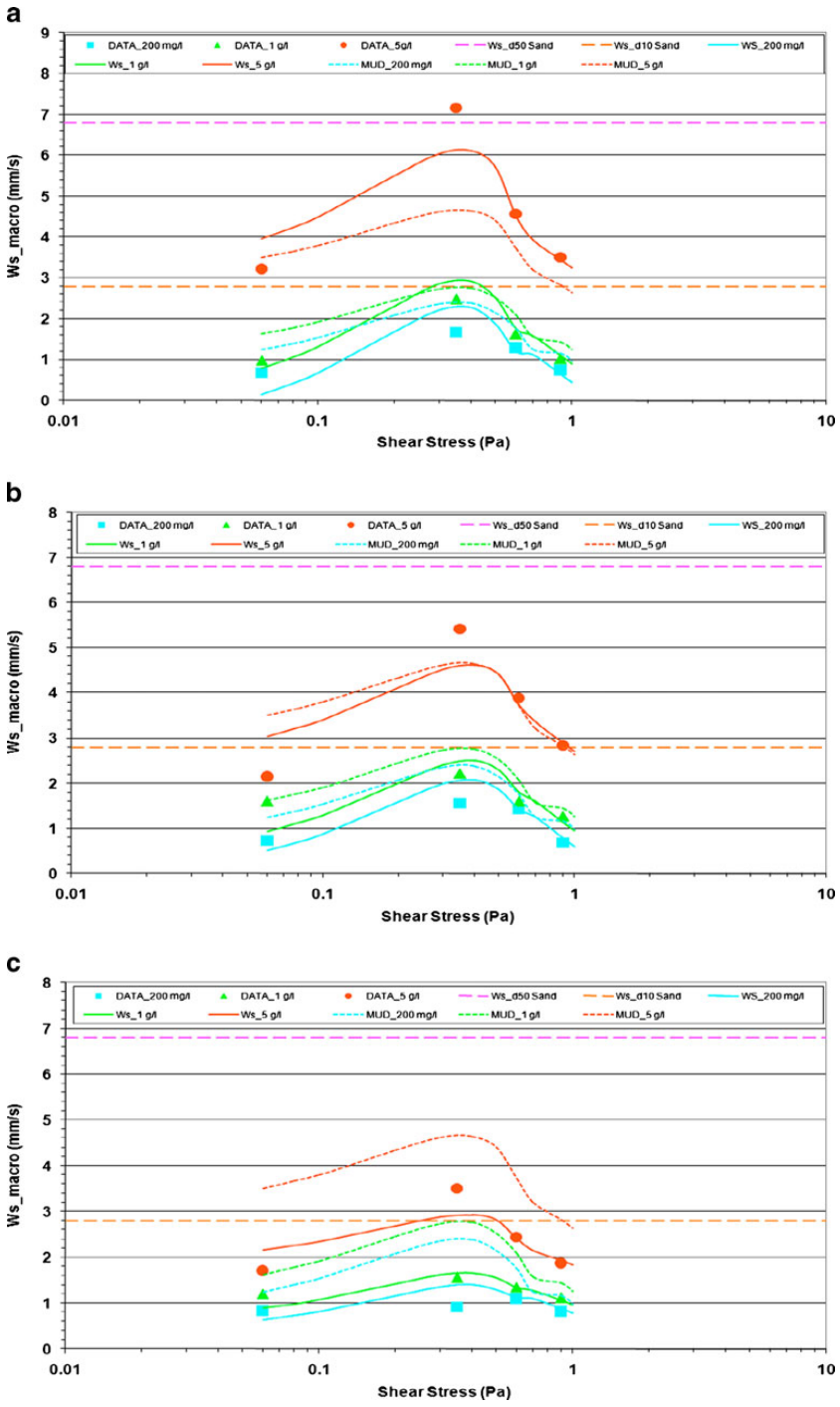

Fig. 7 Ws_{MACRO_EM} regression curves (*solid lines*) and data points for Tamar Estuary manufactured sediment mixtures at the following ratios: **a** 75% Mud:25% Sand; **b** 50% Mud:50% Sand; and **c** 25% Mud:75% Sand. *Line* representative of constant sand grain and pure Tamar mud settling velocities are also shown

comprise a large proportion of unflocculated sand grains under certain conditions. The density aspect will be examined later. The Ws_{micro_EM} equations representing each total ratio of mud and sand (valid for total SPM concentration of 200 mg l^{-1}–5 g l^{-1}), for each shear stress range, are as follows:

75% Mud:25% Sand

- For τ ranging between 0.06 and 0.6 Pa:

$$Ws_{micro\_EM} = 0.224 + 2.63 \times \tau - 1.08 \times \tau^2 + 0.000237 \times SPM \quad R^2 = 0.880 \tag{4.4a}$$

- For τ ranging between 0.6 and 0.9 Pa:

$$Ws_{micro\_EM} = 1.76 - 0.64 \times \tau + 0.057K \times \tau^2 + 0.000246 \times SPM \quad R^2 = 0.911 \tag{4.4b}$$

50% Mud:50% Sand

- For τ ranging between 0.06 and 0.6 Pa:

$$Ws_{micro\_EM} = 0.561 + 5.66 \times \tau - 4.84 \times \tau^2 + 0.000185 \times SPM \quad R^2 = 0.803 \tag{4.5a}$$

- For τ ranging between 0.6 and 0.9 Pa:

$$Ws_{micro\_EM} = 3.13 - 1.64 \times \tau + 0.354 \times \tau^2 + 0.000161 \times SPM \quad R^2 = 0.888 \tag{4.5b}$$

25% Mud:75% Sand

- For τ ranging between 0.06 and 0.6 Pa:

$$Ws_{micro\_EM} = 1.59 + 5.66 \times \tau - 3.99 \times \tau^2 + 0.000185 \times SPM \quad R^2 = 0.695 \tag{4.6a}$$

- For τ ranging between 0.6 and 0.9 Pa:

$$Ws_{micro\_EM} = 5.91 - 4.64 \times \tau + 1.39 \times \tau^2 + 0.000148 \times SPM \quad R^2 = 0.913 \tag{4.6b}$$

As with the mixed-sediment macrofloc settling relationships, the microfloc algorithms also show good all-round statistical fits with the laboratory data, with all but one of the sub-algorithms demonstrating R^2 values exceeding 0.8. Algorithm 4.6a produced the lowest R^2 fit of 0.7, but this is still valid for natural flocculated sediment data suggesting that the scatter is relatively small. In fact, Manning (2004b, 2008) also demonstrated slightly lower statistical regression fits for the MFSV pure mud microfloc algorithms, when compared to those representative of the pure mud macroflocs. This can be generally interpreted as being partly a result of the greater variability in the individual settling velocities and effective densities exhibited by the microfloc fractions, from which each of the average microfloc settling velocities was calculated; this distribution would be potentially wider for different ratios of mixed-sediment suspensions. The most noticeable difference to be revealed when comparing the $Ws_{micro\ EM}$ algorithms for the mixed sediments and the pure cohesive suspensions of the MFSV (Manning 2004a,b), was the significant influence of SPM concentration variations on the former, but statistically negligible in the latter pure mud scenario. This results in the production of different regression curves in response to rising or falling total SPM concentration levels for the mixed-sediment $Ws_{micro\ EM}$; as opposed to the generation of a single regression curve for pure mud $Ws_{micro\ EM}$, regardless of SPM concentration.

The shape of the regression curve for Eqs. 4.4a–4.4b (75M:25S), is illustrated graphically in Fig. 8a, where it is plotted together with the corresponding data points. A transition zone between Eqs. 4.4a and 4.4b occurs at a τ of 0.6 Pa. A single $Ws_{micro\ EM}$ value is obtained by linear interpolation between the two values calculated by both equations in this transitional shear zone. A similar "linking" computation is employed for the other microfloc settling velocity algorithms (i.e. Eqs. 4.5 and 4.6). As with the pure mud MFSV microfloc settling velocity algorithms, the settling trends of the MSSV microflocs are represented by two sub-algorithms. However, the mixed-sediment Ws_{micro_EM} equations required both SPM and shear stress components in order to attain a realistic quantifiable representation of the data. This was in contrast to the MFSV pure mud microfloc representation, which were only statistically dependent on the shear stress component; this is an indication of the greater complexity in mixed-sediment flocculation, and a higher level of interdependency of the various component parameters in the mixed-sediment algorithms. Thus, it is apparent that the mixed-sediment Ws_{micro_EM} appears to be more sensitive to changes in SPM concentration, compared to pure mud microflocs whose dynamics only seem to vary with turbulent shear stress.

At 75M:25S, the predicted mixed-sediment microfloc fractions all settled faster than the pure mud MFSV estimates, at each stress increment. Where the macrofloc mixed fraction showed settling peaks at 0.35 Pa, similar to natural muds, the

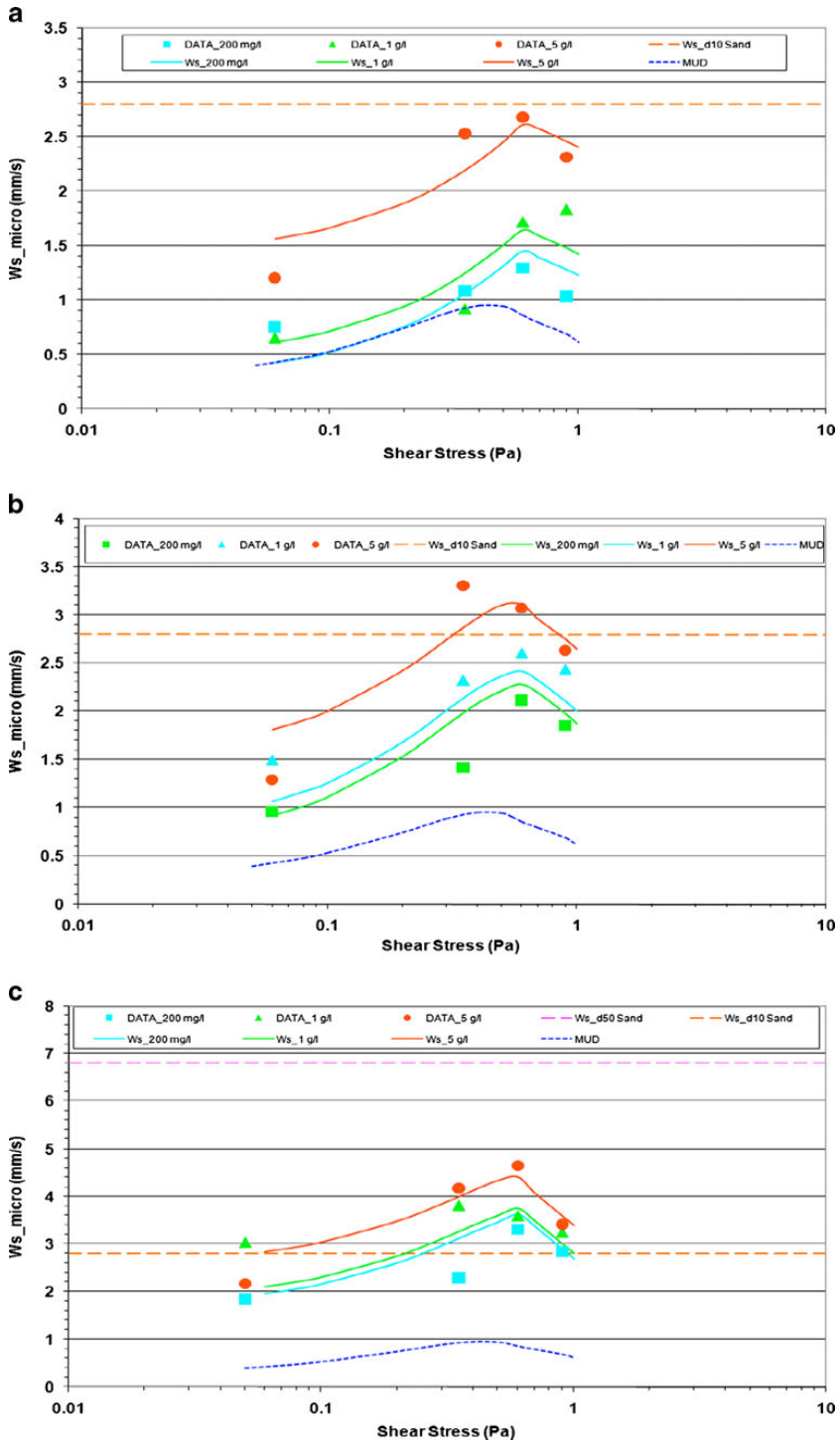

Fig. 8 Ws_{micro_EM} regression curves (*solid lines*) and data points for Tamar Estuary manufactured sediment mixtures at the following ratios: **a** 75% Mud:25% Sand; **b** 50% Mud:50% Sand; and **c** 25% Mud:75% Sand. *Line* representative of constant sand grain and pure Tamar mud settling velocities are also shown

mixed Ws_{micro} tended to produce a maximum at the more turbulent 0.6 Pa. For example, at the lower concentration Ws_{micro_EM} reduced collectively to 0.4 mm s^{-1} within the lower turbulence, increased to 1.5 mm s^{-1} at 0.6 Pa and then reduced again to ~ 1.1 mm s^{-1} at maximum shear stress. The addition of a greater abundance of particulates in suspension (5 g l^{-1}) significantly enhanced the settling dynamics of both fractions at their respective optimum shearing stresses. At 2.6 mm s^{-1}, the Ws_{micro_EM} was 1.8 mm s^{-1} quicker than the MFSV model estimate, where the pure mud microfloc settling rate was over 200% quicker.

If we examine the graphical output from each mixed-sediment microfloc algorithm (see Fig. 8a–c) and compare these to the predicted macrofloc settling (see Fig. 7a–c), we can observe that the Ws_{macro_EM} and Ws_{micro_EM} algorithms all displayed an increase in settling rate with rising total concentration. The macrofloc algorithms predict smaller settling velocities as the percentage of mud decreases, and conversely the microfloc settling velocities increase with decreasing mud content.

4.4 Portsmouth natural mixtures—Ws_{macro_EM} and Ws_{micro_EM}

A comparison of the Tamar mud:sand mixture settling velocity algorithms was made with the Portsmouth Harbour floc/aggregate settling data (Pidduck and Manning 2009). This data was also statistically assessed, so as to produce algorithms which were representative of Ws_{macro_EM} and Ws_{micro_EM}. The settling algorithms equation structure is the same as for the Tamar mixtures and the coefficients are summarised in Table 3. From inspection of the statistical analysis, three quarters of the regression derived equations (Eqs. 4.7–4.9) had highly significant R^2 fit values of over 0.9. The 70M:30S Ws_{micro_EM} algorithms (Eqs. 4.10a and b) had slightly lower statistical fits with the data, but the R^2 values of 0.75 and 0.84 are still respectable for natural sediment data. The output from the Portsmouth Harbour settling algorithms will be compared with those calibrated for the Tamar mixtures in Section 5.

4.5 SPM ratio (SPM_{ratio_EM})

To parameterise the distribution of particulate matter throughout the macrofloc and microfloc sub-populations, the dimensionless SPM ratio (SPM_{ratio_EM}; Manning 2004c) is used. This was calculated by dividing the percentage of SPM_{macro} by the percentage of SPM_{micro} for each floc population. It must be noted that this type of computation is unique to optical floc sampling instruments such as LabSFLOC and INSSEV, which can accurately and reliably estimate the individual effective density of settling flocs and their respective individual floc mass (by simul-

Table 3 Regression coefficients for the Portsmouth Harbour mixed-sediment data

Equation form: $Ws = a + b \times \tau + c \times \tau^2 + d \times SPM$

			Coefficients					
Result	Mud:sand ratio	Shear stress range (Pa)	a (Constant)	b (τ)	c (τ^2)	d (SPM)	R^2	Eqn ref.
Ws_MACRO	38M:62S	0.1–0.6	−0.7175	9.608	−12.564	1.28E−03	0.934	4.7a
Ws_MACRO	38M:62S	0.6–1	1.073	−0.433	−0.417	1.13E−03	0.959	4.7b
Ws_Micro	38M:62S	0.1–0.6	1.4883	11.88	−9.333	4.11E−04	0.987	4.8a
Ws_Micro	38M:62S	0.6–1	8.135	−5.533	1.167	4.34E−04	0.984	4.8b
Ws_MACRO	70M:30S	0.1–0.6	−1.9754	29.469	−37.974	1.39E−03	0.952	4.9a
Ws_MACRO	70M:30S	0.6–1	4.354	−4.075	0.958	1.15E−03	0.992	4.9b
Ws_Micro	70M:30S	0.1–0.6	0.142	11.532	−12.179	6.50E−04	0.843	4.10a
Ws_Micro	70M:30S	0.6–1	4.73	−4.058	1.625	4.32E−04	0.751	4.10b

taneous size and settling velocity observations) for a complete floc/aggregate population. Without this type of measurement, it is not possible to apportion the SPM concentration with any degree of confidence or accuracy between the microfloc and macrofloc groups.

There was a much wider degree of scatter in the SPM ratio data for the various mixed-sediment data, when compared to both the macrofloc and microfloc settling velocity data. Therefore, in order to obtain a set of general algorithms, average SPM ratio values were used in the multiple regression analysis. A mean SPM ratio value was calculated from the four individual experimental SPM ratios that were obtained from all four shear stress levels for each of the three total SPM concentrations (i.e. three SPM ratio values per experimental run). The SPM_{ratio_EM} equations representing each ratio of mud and sand listed below:

75% Mud:25% Sand

$$SPM_{ratio\_EM} = 0.375 + 0.000888 \times SPM - 0.00000007 \times SPM^2 \quad R^2 = 0.999 \tag{4.11}$$

50% Mud:50% Sand

$$SPM_{ratio} = 0.375 + 0.000328 \times SPM - 0.00000002 \times SPM^2 \quad R^2 = 0.999 \tag{4.12}$$

25% Mud:75% Sand

$$SPM_{ratio\_EM} = 0.292 + 0.000091 \times SPM + 0.00000001 \times SPM^2 \quad R^2 = 0.999 \tag{4.13}$$

Each SPM_{ratio} Eq. (4.11–4.13) is valid for the entire experimental total SPM concentration and shear stress ranges (i.e. 200 mg l^{-1}–5 g l^{-1} and 0.06–0.9 Pa, respectively). In contrast to both the Ws_{macro_EM} and Ws_{micro_EM}, the SPM_{ratio_EM} showed a strong dependency solely with the SPM concentration; this was very similar to pure mud algorithms.

The mixed-sediment SPM_{ratio} values estimated by Eqs. 4.11–4.13 are plotted in Fig. 9. The algorithms are represented by the solid lines on Fig. 9 and the corresponding data points upon which the algorithm regressional derivation are based, are also plotted; the dotted line indicates the SPM_{ratio} for pure mud as estimated by the MFSV (Manning 2004b, c). One can observe that the mixed-sediment SPM_{ratio} steadily rises as total concentration increases, which is similar to a pure mud suspension. However, the SPM_{ratio} generally decreases across the suspended particulate matter concentration range, as the mud content diminishes and the sand content rises. This suggests that the microflocs dominate the flocculated suspensions for the sandy–mud suspensions (i.e. 25M:75S) throughout the entire concentration range. In comparison, the MFSV pure mud algorithms produce much higher SPM_{ratio} estimates across the whole range of concentrations. Due to the general nature of the derivation of these SPM_{ratio} algorithms, they were assumed to be sufficiently representative for the Portsmouth Harbour data.

4.6 Mass Settling Flux (MSF_{EM})

The MSSV Eqs. 4.1–4.13 can be combined (using the respective equations pertaining to a mixed-sediment ratio and sediment origin type) to form Eq. 4.14 from which the total mass settling flux, MSF_{EM} (with the units of mg m^{-2} s^{-1}), for a specific mud:sand ratio can be calculated:

$$MSF_{EM} = \left[\left(1 - \frac{1}{1 + SPM_{ratioEM}}\right) \cdot (SPM \cdot Ws_{macroEM})\right] + \left[\frac{1}{1 + SPM_{ratioEM}} \cdot (SPM \cdot Ws_{microEM})\right] \tag{4.14}$$

This is a convenient way of expressing the interrelationship between the three core algorithms and can easily be implemented in mathematical simulation models. Within a sediment transport model framework, each value of MSF_{EM} calculated for a specific point in the water column, can be linked to the depositional flux by either the conventional depositional shear stress threshold (Krone 1962), or the depositional approach advocated by Winterwerp (2006). Some examples of MSSV estimated MSF_{EM} values will be presented in Section 5.

4.7 Distribution of mud:sand across sub-fractions ($M:S_{\_mi:MA\ \_EM}$)

When utilising two or more sediment fractions in a numerical sediment transport model, it is valuable to know where each fraction (i.e. mud and fine sand) is moving within the model grid from a mass-balance perspective. If we consider the hierarchical order of aggregation theory by Krone (1963), the smaller microflocs (D<160 μm) are generally considered to be the building blocks from which the macroflocs are composed. The microfloc class tends to display a much wider range in effective densities and settling velocities than the macrofloc fraction. It is plausible that for mixed sediments, the microfloc fraction will comprise a large proportion of unflocculated sand grains under certain conditions. The macroflocs are composed of microflocs, so this fraction will also contain both cohesive and non-cohesive particulates.

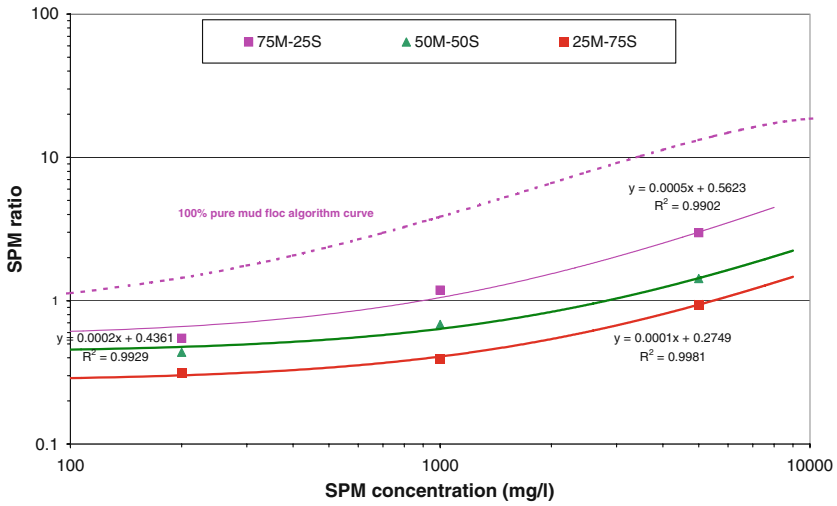

Fig. 9 SPM_{ratio_EM}: regression curves (*solid lines*) and data points for Tamar Estuary manufactured sediment mixtures. Line (*dotted*) representative of pure Tamar mud conditions is also shown

In addition to knowing the SPM_{ratio} for a given suspension, it is important to have an accurate indication of how much sand and mud is contained within both the macrofloc and microfloc sub-fractions of a specific mixed-sediment population. Although this information is not directly required to calculate a single mass settling flux value and solve Eq. 4.14, it allows the modeller to simultaneously track both the flocculation mass settling flux changes, together with the movements of the generic compositional material groups (i.e. mud and sand). This provides the maximum amount of information about the resuspended sediments, creating greater confidence in the calibration, and potentially leading to a more accurate numerical simulation.

Being able to estimate, with a degree of certainty, how much mud and sand is present within a macrofloc or microfloc fraction of a population is not as easy as it first seems. Although traditional mass-balancing theory is relatively straightforward, this is much more complex for observed floc data, due to the added degrees of freedom. As there were no known documented procedures which precisely fitted our analysis requirements, the percentage of sand present in both the macrofloc and microfloc fractions were determined using a combination of both the effective density and porosity data. Benchmark effective density and porosity values were established for both pure sand and pure flocculated mud conditions. These computational stages are detailed by Manning et al. (2011).

By dividing the $\%sand_{micro}$ by the $\%sand_{macro}$ it was possible to calculate the relative distribution of the total sand content, present within a mixed suspension, across the two sub-fractions. For the mixed-sediment empirical model, this component is represented by the following abbreviation: $M{:}S_{\_mi:MA\_EM}$, where:

$$M : S_{\_mi:MA\_EM} = \%sand_{micro}/\%sand_{macro} \tag{4.15}$$

If a value of $M{:}S_{\_mi:MA\_EM}$ is known, it is possible to first calculate the $\%sand_{macro}$ by re-arranging Eq. 4.15, into the form of Eq. 4.16:

$$\%sand_{macro} = 100/(1 + M : S_{\_mi:MA\_EM}) \tag{4.16}$$

Then, by the simple substitution of the $\%sand_{macro}$ value into Eq. 4.17, a corresponding value of $\%sand_{micro}$ can be calculated:

$$\%sand_{micro} = 100 - \%sand_{macro} \tag{4.17}$$

The relationship between values of $M{:}S_{\_mi:MA}$, and the $\%sand_{micro}$ and $\%sand_{macro}$ are quantified in Table 4. For a mixed-sediment floc population which demonstrates a division of $20\%sand_{micro}$ and $80\%sand_{macro}$, this would produce a $M{:}S_{\_mi:MA}$ of 0.25. Once the $M{:}S_{\_mi:MA}$ reaches a value of 100, this indicates that 99% of the total sand content is held in the microfloc size fraction. Therefore, in this latter scenario, very little flocculation would probably be occurring in the microflocs and these would be predominately sand, whilst the macrofloc would still be composed as mud flocs.

In order to provide estimates of the $\%sand_{micro}$ and $\%sand_{macro}$ for numerical sediment transport modelling purposes, it is necessary to parameterise $M{:}S_{\_mi:MA\_EM}$. A multiple linear regression was applied to the mud:sand sub-fractional data, thus using the same statistical analysis

approach used to produce the other components of the mixed-sediment floc settling model. The regression analysis produced a series of M:S$_{_mi:MA_EM}$ equations representing each ratio of mud and sand, for each shear stress and SPM concentration range, as follows:

75% Mud:25% Sand

- For τ ranging between 0.06 and 0.9 Pa; SPM ranging between 200 and 5,000 mg l^{-1}:

$$\mathrm{M:S}_{\_mi:MA\_EM} = 281 - 830 \times \tau + 649 \times \tau^2 - 0.136 \times \mathrm{SPM} + 0.000016 \times \mathrm{SPM}^2 \quad R^2 = 0.894 + 0.174 \times \mathrm{SPM} \times \tau - 0.136 \times \mathrm{SPM} \times \tau^2 \tag{4.18}$$

50% Mud:50% Sand

- For τ ranging between 0.06 and 0.9 Pa; SPM ranging between 200 and 5,000 mg l^{-1}:

$$\mathrm{M:S}_{\_mi:MA\_EM} = 127 - 269 \times \tau + 303 \times \tau^2 - 0.108 \times \mathrm{SPM} + 0.000017 \times \mathrm{SPM}^2 \quad R^2 = 0.764 + 0.044 \times \mathrm{SPM} \times \tau - 0.00001 \times \mathrm{SPM} \times \tau^2 \tag{4.19}$$

25% Mud:75% Sand

- For τ ranging between 0.06 and 0.9 Pa; SPM ranging between 200 and 1,000 mg l^{-1}:

$$\mathrm{M:S}_{\_mi:MA\_EM} = 19.3 + 91.5 \times \tau - 65.6 \times \tau^2 - 0.0021 \times \mathrm{SPM} + \quad R^2 = 0.824 \; 0.00000018 \times \mathrm{SPM}^2 + 0.0205 \times \mathrm{SPM} \times \tau + \; 0.000003 \times \mathrm{SPM} \times \tau^2 \tag{4.20a}$$

- For τ ranging between 0.06 and 0.9 Pa; SPM of 5,000 mg l^{-1}:

$$\mathrm{M:S}_{\_mi:MA\_EM} = 10.7 + 4.7 \times \tau + 5.2 \times \tau^2 \quad R^2 = 0.650 \tag{4.20b}$$

To obtain M:S$_{_mi:MA_EM}$ values for τ ranging between 0.06 and 0.9 Pa and SPM between 1,000 and 5,000 mg l^{-1}, requires a correctly proportioned linear interpolation between the M:S$_{_mi:MA_EM}$ values determined by Eqs. 4.20a and 4.20b at each shear stress increment. These algorithms are illustrated in Fig. 10 and their importance to advancing the insight of mixed-sediment floc structures is discussed in Section 6.2.3.

5 Assessment of MSSV algorithms

When new empirical parameterisations are developed, it must be shown first that they are an accurate representation of the data from which they are originally derived. The statistical "fit" of the regression-derived curves to the data provides an indication of reliability of the algorithms over their operational range, which will give any potential end user confidence during implementation.

Second, it is necessary to demonstrate that new parameterisations of physical processes are an improvement on those which currently exist. There is little point in an end user implementing a new algorithm within a numerical sediment transport model, if only to find that the new parameterisation is either: (a) a less realistic representation of the physical process it is attempting to mimic; (b) significantly more complicated to implement in the main model coding framework; (c) and/or it adds considerable processing time to an iteration due to complex computations, such as where iterative mathematical techniques are required to solve the equations.

Therefore, a series of tests were conducted on the MSSV model. The testing was carried out in two stages. Stage 1 comprised benchmark testing the MSSV algorithms against both the original dataset from which the algorithms were

Table 4 Relationship between ratio values of M:S$_{_mi:MA}$, and the %sand$_{micro}$ and %sand$_{macro}$

Ratio	% Sand_micro	% Sand_MACRO
0.25	20.0	80.0
0.5	33.3	66.7
0.75	42.9	57.1
1	50.0	50.0
2	66.7	33.3
3	75.0	25.0
4	80.0	20.0
5	83.3	16.7
10	90.9	9.1
20	95.2	4.8
30	96.8	3.2
40	97.6	2.4
50	98.0	2.0
75	98.7	1.3
100	99.0	1.0
150	99.3	0.7
200	99.5	0.5
250	99.6	0.4
300	99.7	0.3
350	99.7	0.3

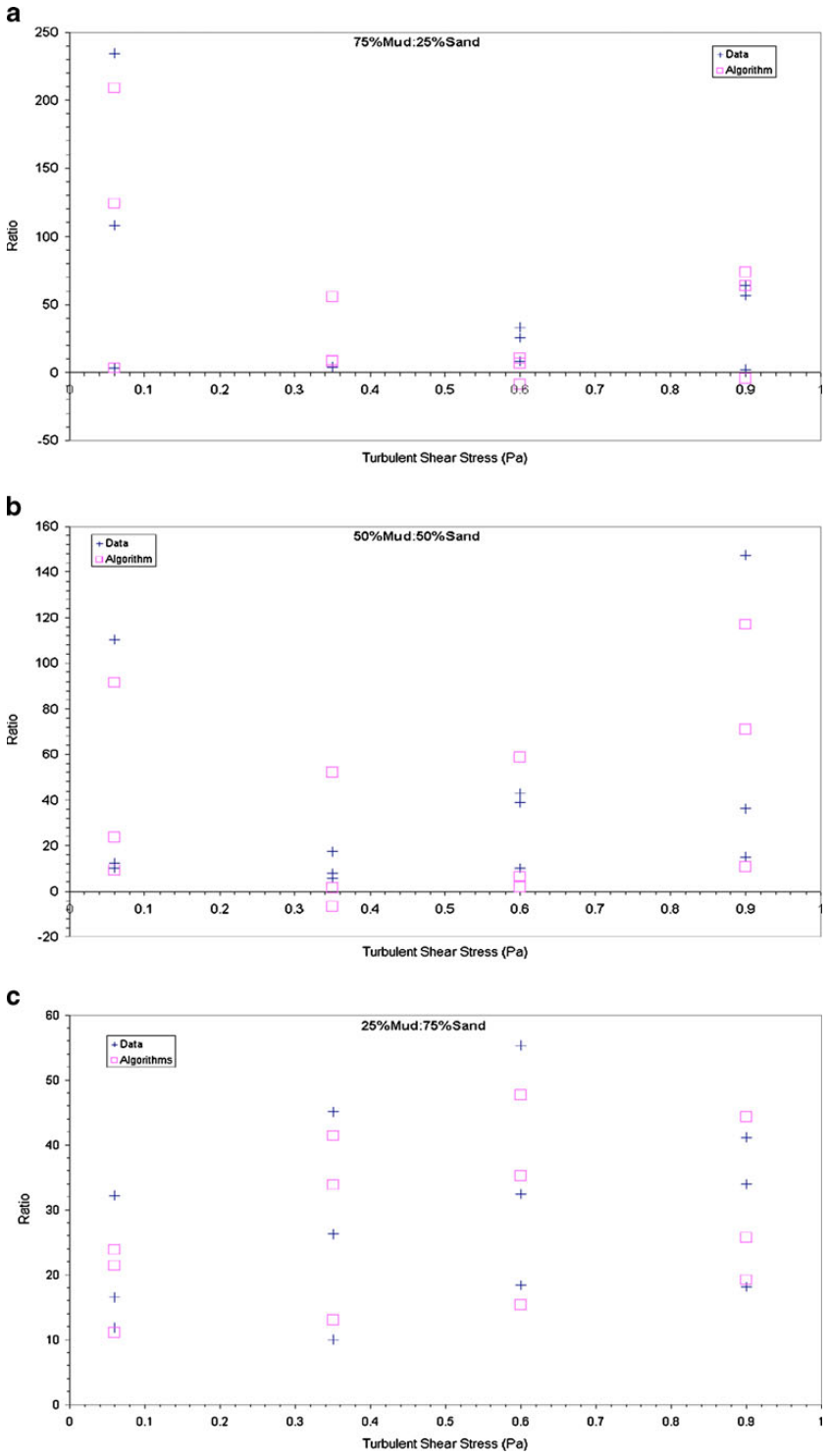

Fig. 10 M:S $_{mi:MA\ \_EM}$ algorithms (Eqs. 4.18–4.20) generated values (*squares*) and data points (*crosses*) for Tamar Estuary manufactured sediment mixtures at the following ratios: **a** 75M:25S; **b** 50M:50S; and **c** 25M:75S

derived, followed by comparisons with a variety of different commonly applied settling velocity parameterisations. Stage 2 of the testing outlines the implementation of the MSSV algorithms within a 1DV numerical sediment transport model (Spearman et al. 2011).

5.1 Comparison of MSSV with Tamar data

5.1.1 Introduction

To initially quantify the accuracy of the empirical MSSV model, it was tested and compared with the original mixed-sediment data set from which the MSSV algorithms are derived. In practice, numerical sediment transport models are used to simulate depositional rates, not settling velocities, so this inter-comparison will be in the form of mass settling fluxes—measured and observed fluxes.

This initial test of the MSSV model compares the model output with the database values from which the model algorithms were derived. Although this is not a very rigorous test, it is an important first step. At this stage, one would expect to have a very high correlation between the data and the algorithm; if not, this could indicate that the structure of the algorithm is incorrect. If the algorithms do not mimic the original data matrix to an acceptable degree of accuracy across the experimental range of conditions, then there is very little chance that the algorithms will produce reliably accurate estimates of MSF if implemented in a predictive sediment transport numerical model.

5.1.2 Individual observed and predicted MSF values

Figure 11 shows the individual MSF values calculated from the measured (i.e. observed) experimental mixed-sediment floc data (x axis), plotted against the corresponding MSF rates as predicted by the MSSV modelling approach for each of the 36 tests. The MSF rates span three orders of magnitude with measured data values ranging from a minimum MSF of 195 mg m^{-2} s^{-1}, and peaking at a maximum observed settling flux of 33 g m^{-2} s^{-1}. The parity line is also plotted (dashed line) on Fig. 11, and initial impressions suggest that there is a good representation of the observations over the full range of the data sets; this suggests that the algorithm structure is correct.

Closer examination indicates that the data have formed three distinct clusters over the MSF range. Of the lower MSF values (195–777 mg m^{-2} s^{-1}) most predictions were within a few percent of the observations. Just two points represented over-predictions of 20–24%.

At the middle region of MSF data, there was under-prediction by six of the 11 data points, for the observed MSFs between 1.6 and 2.9 g m^{-2} s^{-1}. These six points comprised values representing suspension from each mud: sand ratio. The poorest correlation case resulted in an under-prediction in MSF of 34% for a 50M:50S suspension of 1,000 mg l^{-1} at a τ of 0.06 Pa. However, the remaining five data points in this mid-region cluster predominantly exhibited an under-prediction of 25% or less.

The algorithm derived MSFs within the 1.3–21 g m^{-2} s^{-1} cluster, demonstrated an extremely close fit with the data. Even the highest observed MSF of 33 g m^{-2} s^{-1} produced by a 75M:25S mixed suspension, were closely mimicked by the MSSV model (an 18% under-estimate).

5.1.3 Detailed statistical comparison

In order to provide a better idea of how the new MSSV algorithms performed at different suspension concentrations, the data obtained from an individual flume run with a

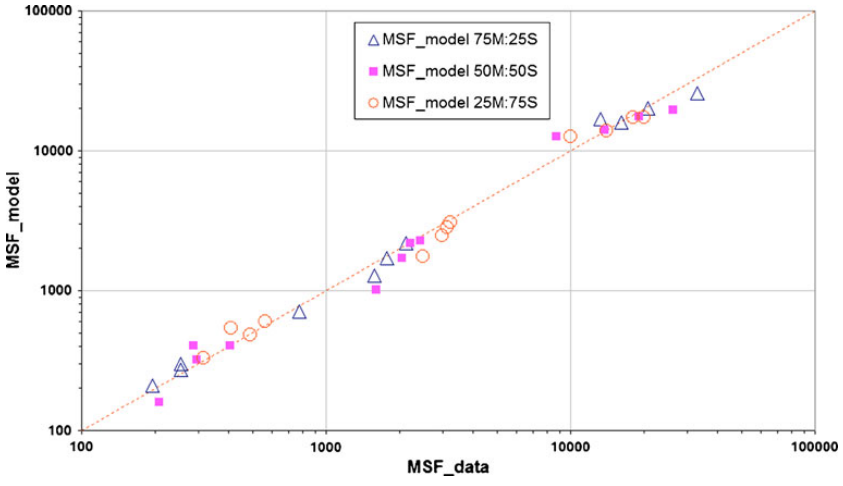

Fig. 11 Comparison of MSSV predicted and observed mass settling fluxes (units = mg m^{-2} s^{-1}) for the different combinations of SPM concentration, shear stress and mud:sand ratio. *Parity line* (*dashed*) also plotted

mixed-sediment suspension, which spanned the experimental shear stress range, was averaged. A statistical assessment was then conducted to quantify the deviation of the 36 observed values (split into their different sub-group scenarios) from their MSSV algorithm derived counterpart, as illustrated by the parity line plotted on Fig. 11.

The statistical assessment was conducted on the MSF values which comprised different sub-grouping scenarios: all SPM, 200, 1,000 and 5,000 mg l^{-1}; each of which were segregated by the mud:sand ratios of: 75M:25S, 50M:50S and 25M:75S.

Five statistical tests were conducted in order to quantify the differences between the observations and predictions: (1) a mean error (ME) expressed as a percentage; (2) standard deviation (SD) and (3) variance; (4) a comparison between the measured total cumulative mass settling flux, i.e. the summation of the flux values for the sub-group scenario under consideration, and the corresponding cumulative flux totals estimated by the MSSV algorithms; (5) and the total cumulative error of the MSF (TCE_{MSF}) computed by first calculating the percentage difference, ± between the predicted and observed MSF for each individual data point, then summing the errors together (for each sub-group scenario) produced a value of TCE_{MSF}. The same combination of five statistical tests was used to assess the MFSV pure mud algorithms (Manning and Dyer 2007).

Table 5 summarises all the statistical results for the MSSV:data comparison and shows that the MSSV predictions represent between 93% and 97% of the total mass settling flux (MSF_{TOTAL}=100%). For the sub-groups of different ratios of mud and sand, and different concentrations, the MSSV predictions represent between 85% and 111% of the total mass settling flux. The MSSV algorithm tends to over-predict the 200 mg l^{-1} values and under-predict for higher values of concentration.

5.2 Comparison methods

To facilitate a rigorous assessment of the empirical MSSV algorithms, a total of nine methods (denoted by *M*) were employed in the comparison with the original data set (a summary is provided in Table 6). The first comparison model (M1) was the MFSV algorithms (e.g. Manning 2008) which are representative of the MSF of pure mud flocculating suspensions. Both the MSSV and MFSV algorithms were derived from empirical data, as opposed to pure theory.

The next four methods (M2–M5) used single constant values of settling velocity. This is a very common approach used in numerical modelling, as it requires the least amount of programming code, and thus reduces a model's processing time. A single settling value says very little about the floc characteristics or how they change throughout a tidal cycle and are generally selected in an arbitrary manner. The settling velocity values employed span commonly quoted values: M2, 0.5; M3, 1; M4, 2.5 and M5, 5 mm s^{-1}. The slowest of these settling velocities is generally representative of mean settling rates determined by gravimetric analysis of field settling tube data, whereas the faster settling rate is a value which has been included in a recent simulation model of the Tamar Estuary by Petersen et al. (2002).

An exponential power regression relationship between the mean settling velocity of mud flocs (Ws_{spm}) and the SPM concentration is the sixth comparative parameterisation (M6)

$$Ws_{spm} = 0.36\,SPM^{0.234} \tag{5.1}$$

and was established from the regression of 157 individually observed pure mud floc populations (Manning and Dyer 2007).

The seventh comparative method (M7) utilised the flocculation formulation advocated by van Leussen (1994). The Ws_{VL} algorithm form is shown in Eq. 5.2, where *G* is a turbulence parameter defined by the root mean square of the gradient in the turbulent velocity fluctuations with the units s^{-1}.

$$Ws_{VL} = Ws_{Ref}\frac{1 + a\,G}{1 + b\,G^2} \tag{5.2}$$

In order to be consistent in the calibration of the coefficients for this expression (Eq. 5.2) and Eq. 5.1, the same data set was used. The best fit (albeit quite poor) to the data matrix was achieved with the constants a=0.3 and b=0.05. The reference settling velocity component (Ws_{Ref}) requires the mean settling rate to be expressed in terms of SPM concentration by a power regression; for this purpose, Eq. 5.1 was used.

M8 was representative of the fall velocity of the median grain size d_{50} of the Redhill 110 sand; a Ws of 7.9 mm s^{-1} (HR Wallingford 1998). These tests were included to indicate what would happen for the extreme case, particularly in terms of predictive MSF error, if the modeller assumed all sediment present at an estuarine location was sand and not a mud:sand mixture. Although it has been noted by Whitehouse (1995) that the grain size for sediment in suspension in tidal waters may often be smaller than d_{50}. The final comparison model, M9, were the MSSV algorithms in the form of Eq. 4.14.

5.3 Segregation and flocculation approaches

5.3.1 Introduction

One of the key issues a sediment transport modeller must address within a coastal and estuarial location is the

Table 5 Summary of statistical tests comparing the observed and MSSV predicted MSFs for each model scenario

	Model scenario		
Statistical test			
	75% Mud_All SPM	50% Mud_All SPM	25% Mud_All SPM
Mean Error (%)	3.9	1.9	0.8
Standard Deviation	20.5	24.6	17.2
Variance	420.7	604.7	296.1
Total Cumulative Error (%)	−46.6	−22.2	−9.5
Total Cumulative MSF (%)	95.0	93.3	96.8
	75% Mud_200 mg/l SPM	50% Mud_200 mg/l SPM	25% Mud_200 mg/l SPM
Mean Error (%)	4.6	−6.4	−11.0
Standard Deviation	31.8	26.3	15.2
Variance	1,010.2	693.1	231.8
Total Cumulative Error (%)	−18.6	25.6	44.0
Total Cumulative MSF (%)	101.2	107.7	110.5
	75% Mud_1,000 mg/l SPM	50% Mud_1,000 mg/l SPM	25% Mud_1,000 mg/l SPM
Mean Error (%)	7.6	15.2	15.2
Standard Deviation	8.9	15.5	10.6
Variance	78.5	241.2	113.3
Total Cumulative Error (%)	−30.5	−60.9	−61.0
Total Cumulative MSF (%)	93.5	86.6	85.6
	75% Mud_5,000 mg/l SPM	50% Mud_5,000 mg/l SPM	25% Mud_5,000 mg/l SPM
Mean Error (%)	−0.6	−3.3	−1.9
Standard Deviation	20.2	30.3	16.3
Variance	407.3	917.8	267.1
Total Cumulative Error (%)	2.5	13.1	7.5
Total Cumulative MSF (%)	95.0	93.9	98.6

Table 6 Summary of paramerisation approaches used during the testing of the MSSV empirical flocculation algorithms

Method Number	Description
M1	MFSV empirical flocculation model for pure mud (Manning 2008)
M2	Constant settling velocity, Ws=0.5 mm s^{-1}
M3	Constant settling velocity, Ws=1 mm s^{-1}
M4	Constant settling velocity, Ws=2.5 mm s^{-1}
M5	Constant settling velocity, Ws=5 mm s^{-1}
M6	Ws_{mean} – SPM concentration power regression relationship (Eq. 5.1).
M7	van Leussen (1994) approach (Eq. 5.2).
M8	Constant settling velocity representative of the average fall velocity of the Redhill 110 sand grains, Ws=7.9 mm s^{-1}
M9	New MSSV empirical flocculation model (Eq. 4.14)

composition of the sediment. If the sediment is mixed, the modeller must then decide how to best represent its features. This is usually a choice between either simplifying the problem by assuming a single sediment type, or using both sediment types simultaneously. If the latter is chosen, the modeller then needs to decide how the two sediment types will be managed: segregated or flocculated.

Mud and sand can be deposited in estuaries either as alternating layers, or mixtures. When the former occurs, the mud content in many parts of an estuary may not be uniform, but can become segregated both vertically and horizontally—a phenomenon known as sand:mud segregation (see van Ledden 2003). This considers the mud and sand to operate as two independent suspensions (van Ledden 2002). When a segregation regime dominates, there is very little bonding and flocculation interaction between the mud and sand fractions is non-existent. Thus, the non-cohesive sand particles and cohesive mud would behave

more or less independently during deposition, resulting in the formation of two well-sorted layers (Ockenden and Delo 1988; Migniot 1968; Williamson and Ockenden 1993; Torfs et al. 1996).

There are also many locations where mud and sand co-exist as a mixture (Mitchener et al. 1996) and this creates the potential for these two fractions to combine within a flocculation matrix when re-entrained into suspension (Manning et al. 2007). When sand is added to a predominantly muddy matrix, Mitchener et al. (1996) found that this increased the binding potential between the clay particles, for example the subtidal mud patches off Sellafield in the Irish Sea (Feates and Mitchener 1998). Thus, the physical effect of adding cohesive mud to a sandy environment can create increased bed stability (Kamphuis and Hall 1983; Alvarez-Herandez 1990; Williamson and Ockenden 1993; Torfs 1994; Mitchener et al. 1996; and Panagiotopoulus et al. 1997), which can potentially lead to mixed-sediment flocs forming when the eroded bed is entrained.

Even where sand and mud are considered to be fairly segregated at the bed, sand and mud can exist as suspended sediment transport. Spearman et al. (2011) describe an example in the outer Thames, renowned for being a sandy area, where the flux of suspended sediment of mud and sand are of the same order.

One can observe that, apart from the empirical MSSV algorithms (M9), all of the modelling approaches listed in Section 5.3 consider the sediment to be either pure mud or pure sand. Also, M9 is the only approach which can represent the flocculation behaviour of mixed suspensions. Therefore, with the exception of M9, the first inter-comparison will assume that the sediments are not mixed. The second inter-comparison treats the sediment as a mixture, but with approaches M1–M8 assuming the sediment operates in a segregated way.

5.3.2 Comparison assuming non-mixed suspensions

The inter-comparisons were made as realistic as practically possible by using only the input values available for each model approach during the MSF computations, namely τ and SPM values. This is similar to how a numerical model would utilise a flocculation algorithm, and thus this provides a realistic and equal test of each method's predictive performance. For these tests, the combinations of τ and SPM concentration, were those values used in the original mud:sand transport laboratory experiments (see Manning et al. 2007); these benchmark values permit a direct comparison between the predicted and observed mixed-sediment MSF values.

The first test assumes that the sediment present in suspension is *not* mixed, even if the mud:sand ratios are known. For example, this would mean that if there is a total concentration of 200 mg l^{-1}, the SPM input would be 200 mg l^{-1}. This assesses how the most simplistic input of SPM would influence the different approaches. The appropriate mud:sand ratio algorithm is still selected for M9 the MSSV, so that the relative improvements/errors can be demonstrated in the inter-comparison between approaches.

As with the initial statistical assessment conducted on the MSSV model in Section 5.1, the inter-comparison tests concentrated on the MSF values which comprised different sub-grouping scenarios. These sub-groups comprised: all SPM, 200, 1,000 and 5,000 mg l^{-1}; each of which were further grouped by the mud:sand ratios of: 75M:25S, 50M:50S, and 25M:75S.

The results of the main MSF inter-comparison tests, assuming the sediment is not mixed, are displayed graphically in Fig. 12. Each scatterplot corresponds to a parameterisation, where the predicted MSF values for each of the 36 experimental conditions (i.e. combinations of τ, SPM and mud:sand ratio) are plotted against the actual observed values of MSF from the experiments (see Manning et al. 2007). In order to place some scale to the mass settling fluxes being used as benchmark values, the total observed MSF from the combination of all 36 benchmark fluxes is 243 g m^{-2} s^{-1}. The division of this combined flux attributes 90 g m^{-2} s^{-1} to the 75% mud suspensions, 76 g m^{-2} s^{-1} to the predominantly sandy mixture (25M:75S) and the remaining 77.4 g m^{-2} s^{-1} encompasses the equal mud:sand suspension.

All of the M2 MSF points were above the parity line Fig. 12, which demonstrates that a constant settling velocity of 0.5 mm s^{-1} under-estimated on every account. The contrary over-estimate resulted from parameterising the suspension solely as sand particles (M8). The original Manning settling floc velocity parameterisation for pure mud (M1), together with the Power Law (M6) and van Leussen (M7) approaches, all resulted in both over- and under-predictions in the MSF, displaying a wide degree of scatter.

Table 7 shows the comparison of MSF values. Focusing on the dilute suspension condition (200 mg l^{-1}) M10 over-predicted the observed MSF (4 g m^{-2} s^{-1}) by just 6%, at a mean error of −4% (SD=24%). In comparison, the pure mud algorithms (M1), together with M2 and M3 (slow constant Ws), produced fairly large under-estimates ranging from 25% to 70%.

The faster constant Ws of 2.5 and 5 mm s^{-1} (M4 and M5) produced highly inflated estimates of MSF at low turbidity: a 73% over-estimate for the former and 246% for the latter; both with high MEs. When comparing M4 and M5 to the slower constant settling parameters (M2 and M3), the former produced significantly greater total cumulative errors in the estimate of the MSF; this was

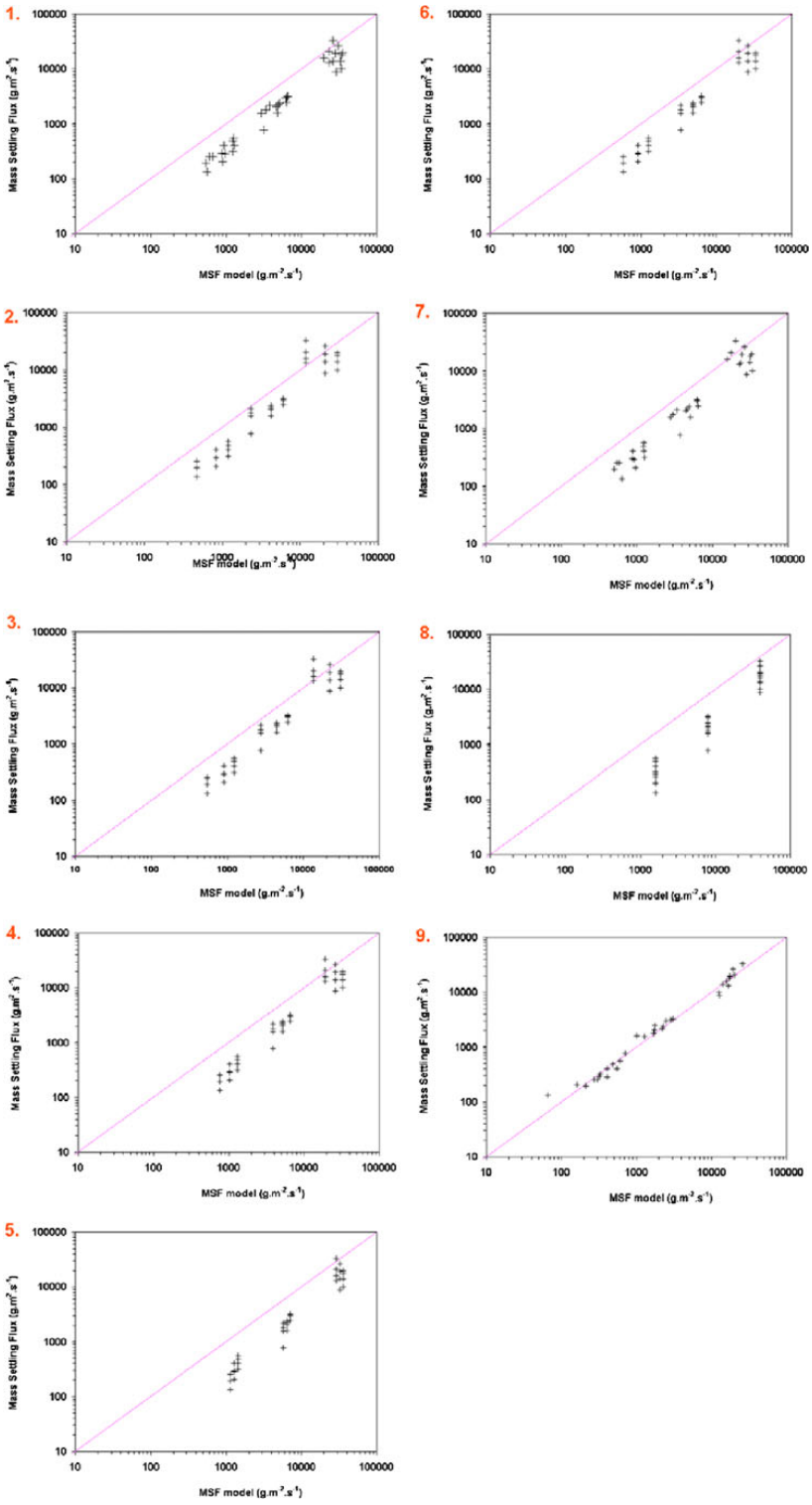

Fig. 12 Comparison of individual MSF values estimated by the nine parametersiation approaches, where a single sediment type is assumed, and the benchmark MSF observation values. *Plot numbers* correspond to parameterisation approaches M1–M9. The *parity line* (*magenta*) indicates a perfect fit between the predicted and observed MSF values

Table 7 Summary of the relative percentage between the MSF determined from the nine parameterisation approaches, where a single sediment type is assumed, and the benchmark MSF observations which equal 100%

	Model scenario		
Parameterisation			
	75% Mud_All SPM	50% Mud_All SPM	25% Mud_All SPM
M1	72	83	85
M2	14	16	16
M3	28	32	33
M4	69	80	82
M5	138	160	164
M6	68	79	81
M7	63	73	75
M8	217	253	259
M9	95	93	97
	75% Mud_200 mg/l SPM	50% Mud_200 mg/l SPM	25% Mud_200 mg/l SPM
M1	103	72	49
M2	48	33	23
M3	95	67	45
M4	238	167	113
M5	477	335	226
M6	119	83	56
M7	110	77	52
M8	753	529	357
M9	101	108	111
	75% Mud_1,000 mg/l SPM	50% Mud_1,000 mg/l SPM	25% Mud_1,000 mg/l SPM
M1	93	71	50
M2	32	24	17
M3	64	48	34
M4	160	121	85
M5	319	241	169
M6	116	87	61
M7	107	81	57
M8	504	381	268
M9	94	87	86
	75% Mud_5,000 mg/l SPM	50% Mud_5,000 mg/l SPM	25% Mud_5,000 mg/l SPM
M1	85	104	93
M2	12	15	16
M3	24	29	32
M4	60	74	81
M5	121	147	161
M6	64	78	85
M7	59	72	79
M8	190	233	255
M9	95	94	99

These sub-groups compared comprised: all SPM, 200 mg l^{-1}, 1,000 mg l^{-1} and 5,000 mg l^{-1}; each of which were segregated by the mud:sand ratios of: 75M:25S, 50M:50S, and 25M:75S

reflected in TCE_{MSF} values exceeding 3,200%, as opposed to just 35–70% for M2 and M3.

M6 and M7 both demonstrated 20% over-estimates for 75M:25S, but sandier mixtures show 50% under-estimates. MEs were double those of M9 predictions. M8 illustrates what happens when the suspensions are represented solely as fine sand. Generally, M8 produced grossly over-estimated fluxes by nearly +450% higher than the observed benchmark. This flux figure was with MEs of −480% (at a SD=170%), and the TCE_{MSF} approaching 4,800%.

Even when the concentrations were raised to either 1 g l^{-1} (mid-range) or 5 g l^{-1} (peak), the MSSV (M9) algorithms estimate of MSF were predominantly within −1% to −6% of the observations. Mean errors were never more than 15%, with many sub-group scenarios producing MEs of less than −3%. TCE_{MSF} values were also characteristically low; −150% for 1 g l^{-1} and down to 23% for the highest SPM.

At 1 g l^{-1}, M2 and M3, continued to under-predict the MSF, but now to an even greater degree. On average M2 estimated only one quarter of the benchmark flux, whilst M3 predicted half the observed MSF. Interestingly, at a SPM of 5 g l^{-1} the MSF values estimated by M1 showed the opposite pattern to that depicted at 1 g l^{-1}, with the closer M1 MSF prediction being made in the more sandy, less cohesive suspension (25M:75S); an under-estimate of less than −7% at a mean error of 2%. Overall, M1 under-estimated the flux at 5 g l^{-1} by −17%, but displayed a mean error five times greater than M9 predictions.

The quicker fixed settling speeds of M4 and M5 did fair better at predicting MSFs at higher concentrations than at dilute suspensions; most estimates showed a 50% reduction in error, with over-predictions now generally ranging between +30 and +220, with some under-estimates of about −20 calculated by M4. Also the M4 and M5 flux estimates were slightly better than their slower settling counterparts at high concentrations. However such findings can lead to potential difficulties if implemented in numerical models; this will be discussed in Section 6.

When averaging the 1 g l^{-1} suspension, methods M6 and M7 (i.e., Power Law, van Leussen) predicted 80–86% of the observed flux; this fell to 63–75% at peak SPM conditions. These MSF differences all brought about MEs and SDs two to three times greater than M9. Thus, all three methods showed inconsistent behaviour throughout the mid- and high concentration tests.

As one would expect, the representation of the benchmark MSF observations by settling parameters representative of sand grains were always going to be in error. M8 produced over-estimates in MSF ranging from +168% for muddy sand (i.e. 25M:75S) to +404% for the more cohesive sandy mud (i.e. 75M:25S) at 1 g l^{-1}. Throughout an SPM of 5 g l^{-1}, the MSF estimates of M8 fell to +155% and +90% for the same respective mixture conditions; the high Ws of the sand grains slightly better suited with the faster settling velocities usually attributed to high concentration fully flocculated suspensions.

5.3.3 Comparison assuming suspensions are mixed

In this section, the same tests used in the previous section are conducted, but now the sediment in suspension is assumed to be mixed and this knowledge should theoretically improve the predictability of MSF, when compared to solely pure mud parameterisations. In application this would mean that if a mixed suspension of 75% mud and 25% sand at a total concentration of 1,000 mg l^{-1} is to be tested, a SPM of 750 mg l^{-1} would be used for the cohesive part of the parameterisation. For the remaining 25% sand content, which is 250 mg l^{-1} in this mixed suspension example, the non-cohesive MSF component would be calculated by multiplying 250 mg l^{-1} by the average fall velocity for a sand particle. The total MSF for each prediction would be obtained by summing both parts.

This dual computation approach would be adopted by M1 to M7; M8 is still only representative of pure sand (as a comparison benchmark). It must be noted that although the sediment in suspension is now being considered as a mixed mud:sand suspension, the two sediment types are still being treated independently. Thus the predictions for M1 to M7 assume no direct mud:sand interaction, i.e. segregation is applied; sand-mud flocculation is only assumed to occur with M9, whose MSSV algorithms are based on flocculating mixed sediments.

The nine predictions of MSF are again plotted as scatterplots in Fig. 13. From inspection of the parity lines, one can immediately see that by allowing the modeller to represent each individual suspension as a two component, segregated mixed sediment (i.e. a mud part and a sandy fraction), all parameterisations were now over-predicting the MSF.

Overall, the implementation of dual fraction settling velocities proved to produce the greatest over-predictions in MSF at a SPM of 200 mg l^{-1}. For instance, the modified M1 over-predicted by nearly 200% across the dilute suspension (see Table 8). The non-cohesively modified constant settling velocities, M2–M5, all over-predicted in MSF. For example, the modified slower settling velocity (M2) now over-estimated the 200 mg l^{-1} SPM mass flux by a concentration average of +160%. This compared to one-third of the observed MSF for the unmodified version of M2; a 325% swing in estimated MSF.

At the quicker end of the constant settling velocity scale, the modified M5 produced over a threefold over-estimate in MSF; an 88% rise from the unaltered format. As with the unmodified constant Ws parameterisations, mean error values were quite high (ME ranging between −171 and −360).

The inclusion of a sand grain fall velocity parameter coupled with the Power Law's (M6) computation of settling flux, resulted MSF values approximately +180% greater than the observations across the ratios of mud:sand mixture. This was a very different flux pattern than that depicted by the sole use of the Power Law, which generally under-estimated by −14% for dilute suspensions; over-estimates of +19% for 75% mud, and it under-estimated by −44% for

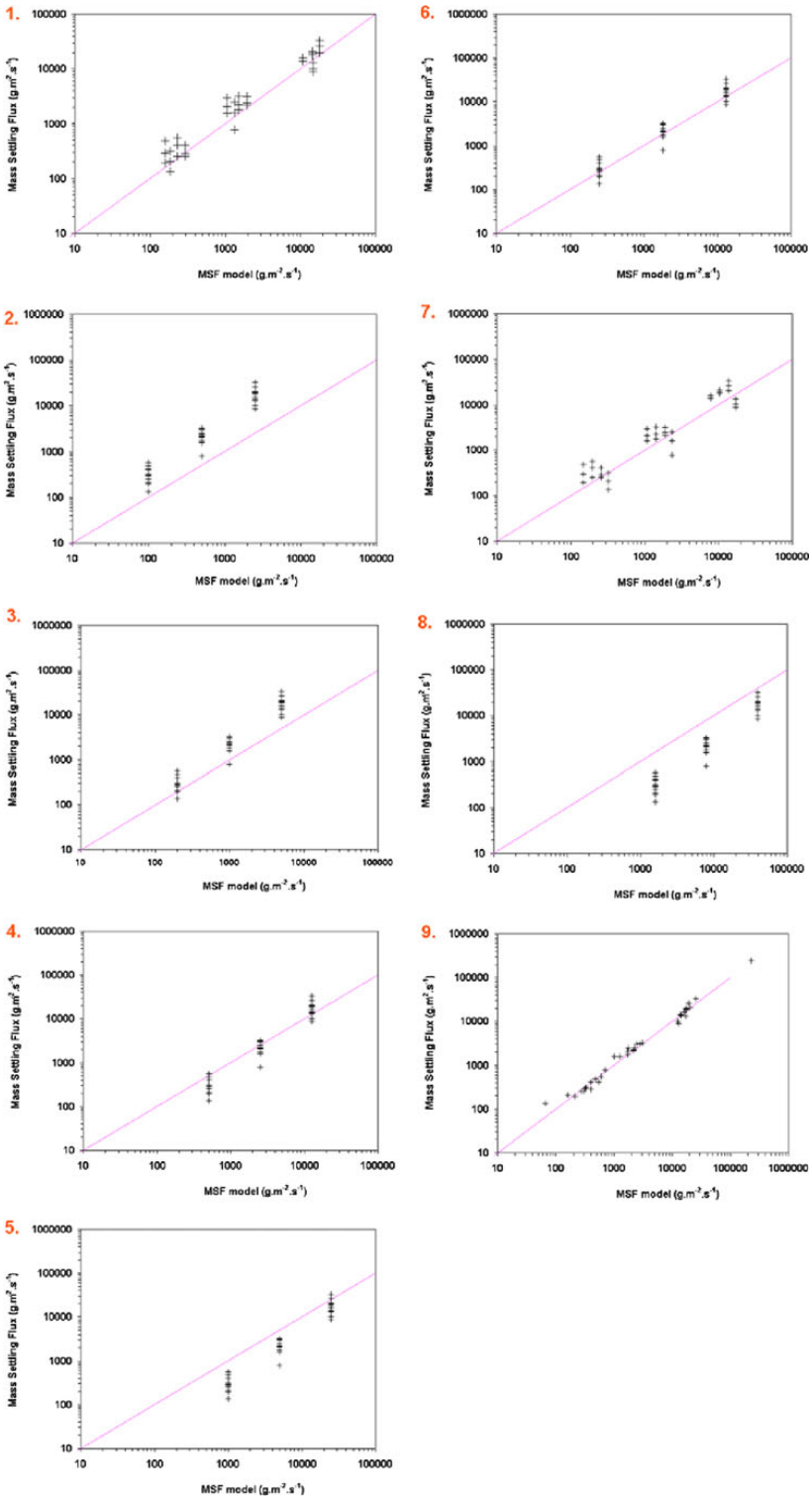

Fig. 13 Comparison of individual MSF values estimated by the nine parametersiation approaches, where a sediment is assumed to be mixed, and the benchmark MSF observation values. Plot numbers correspond to parameterisation approaches M1-M9. The *parity line* (*magenta*) indicates a perfect fit between the predicted and observed MSF values

Table 8 Summary of the relative percentage between the MSF determined from the nine parameterisation approaches, where a sediment is assumed to be mixed, and the benchmark MSF observations which equal 100%

	Model scenario		
Parameterisation			
	75% Mud_All SPM	50% Mud_All SPM	25% Mud_All SPM
M1	111	168	219
M2	57	66	195
M3	66	131	199
M4	93	153	211
M5	138	190	231
M6	95	155	212
M7	92	152	211
M8	190	233	255
M9	95	94	99
	75% Mud_200 mg/l SPM	50% Mud_200 mg/l SPM	25% Mud_200 mg/l SPM
M1	283	308	283
M2	224	149	273
M3	260	298	279
M4	367	348	296
M5	546	432	324
M6	277	306	282
M7	271	303	281
M8	753	529	357
M9	101	108	111
	75% Mud_1,000 mg/l SPM	50% Mud_1,000 mg/l SPM	25% Mud_1,000 mg/l SPM
M1	212	234	216
M2	150	107	205
M3	174	215	209
M4	246	251	222
M5	366	311	243
M6	213	234	216
M7	207	231	215
M8	504	381	268
M9	94	87	86
	75% Mud_5,000 mg/l SPM	50% Mud_5,000 mg/l SPM	25% Mud_5,000 mg/l SPM
M1	111	168	219
M2	57	66	195
M3	66	131	199
M4	93	153	211
M5	138	190	231
M6	95	155	212
M7	92	152	211
M8	190	233	255
M9	95	94	99

These sub-groups compared comprised: all SPM, 200 mg l^{-1}, 1,000 mg l^{-1} and 5,000 mg l^{-1}; each of which were segregated by the mud:sand ratios of: 75M:25S, 50M:50S, and 25M:75S

a 75% sand suspension. The non-cohesive modified M7 parameterisation showed similar levels of over-estimation as the modified M6 approach. These exceptionally poor predictions of MSF are all a long way from the 1–11% over-estimates of the M9 mixed-sediment algorithms across the shear stress and sediment mixture range.

Generally, the over-predictions in MSF by the non-cohesive modified versions of M1–M7, became less as the concentration rose, but were still in the region of over 100%. For example, the sand-modified M1 parameterisation produced greater mean errors at maximum concentration (ME=−84%). This was nearly an order of magnitude more

than the unmodified M1. In contrast to the quasi-random nature of the modified M1–M7 settling flux predictions within high concentration suspensions, M9 never deviated more than 6% from the observational benchmark MSF values.

6 Discussion

In order to produce accurate morphological predictions, sediment transport models require a quantitative description of the various mixed-sediment processes (e.g. Chesher and Ockenden 1997; Le Hir et al. 2007; Waeles et al. 2008). The testing of empirically derived algorithms is a vital procedure, especially for processes such as mixed-sediment flocculation, which have many degrees of freedom. For physical process algorithms which describe natural sediment dynamics and natural processes, it is very important that this testing is conducted against the benchmark of actual observations and carried out in incremental stages. That way the algorithm testing is fully rigorous and would indicate any probable weak areas or limitations prior to numerical model implementation. It is also important to demonstrate whether a new technique is a significant improvement over those which current exist. Also inter-comparisons would demonstrate how new parameterisations compare to existing ones. Findings from the testing operation would provide a potential end user with the required confidence to implement such a set of algorithms in a mathematical model simulation.

6.1 Tamar algorithm assessment

The first part of the testing compared the new MSSV model just with the original data set of 36 mixed-sediment floc population observations, from which the algorithms were derived. The 36 populations produced a combined (measured) MSF benchmark of 243 g m^{-2} s^{-1}. This compares to a total combine mass settling flux of 231 g m^{-2} s^{-1} estimated by the MSSV algorithms; an overall MSF prediction error of just ±5%, which is exceptionally good for such a complex process. It must be remembered that these predictions are valid for: τ ranging from 0.06 to 0.9 Pa, SPM from 200 mg l^{-1}–5 g l^{-1}, and mud:sand ratios from 75M:25S to 25M:75S. Therefore the mixed-sediment flocculation algorithms are mimicking the depositional behaviour of mud:sand flocs to a high level of accuracy and on a reliably, repeatable basis, within a wide range of hydro- and sediment dynamical conditions representative of those typically experienced in many natural north-western European estuaries.

In order to gain a more detailed break-down of how the MSSV model performed, we can assess the algorithm's predictability on a sub-group scenario level in terms of mud: sand ratio. For muddy sand suspensions (i.e. 75M:25S), the model produced MSF predictions of between −6.5% and +1.2% (compared to the benchmark values) across the entire concentration and shear stress range, with mean errors of −0.6 to +7.6%. This resulted in an average under-prediction of −5% for the 75M:25S suspensions. An equal apportioning of mud and sand in suspension, resulted in an over-prediction of +7.7% at the dilute suspension level, followed by under-estimates at 1 g l^{-1} and 5 g l^{-1} of −13.4% and −6.1%, respectively. Generally, the MSFs compare well with the data, even if at times, the raw figures of settling velocity are less accurate.

Sandy mud suspensions (i.e. 25M:75S) also produced a larger under-estimate in MSF at the 1 g l^{-1} concentration of just over −14%. However at 5 g l^{-1} the MSSV algorithms were only −1.4% below the benchmark observed flux. Therefore, with the 200 mg l^{-1} over-estimating by +10.5%, the algorithms were seen to produce a resultant difference in MSF of −3.2%, from the observations. In summary, on a sub-group scenario scale, the gap between the observations and the MSSV predictions is predominantly 3-6% and on no occasion does it exceed 15%. This level of accuracy is fully acceptable for the parameterisation of a natural process, based on real experimental data. Given the variability in composition of a natural estuarine mud and the complexity of the mixed-sediment flocculation process, this level of accuracy displayed by the MSSV algorithms, would potentially provide an end user with the robustness and adaptable qualities which are important for the successful application and implementation of a flocculation algorithm (Baugh and Manning 2007).

It must be stressed that empirical algorithms such as MSSV, which are produced by extended 'curve fitting' to data, will always give a higher level of accuracy than a formula with a sound physical basis with no data. Therefore, one should realize that such curve fitting with a high number of coefficients, is only applicable for that specific situation under the specified circumstances. This emphasizes the pre-requisite requirement of good quality physical process data from a location under consideration.

6.1.1 Potential data and algorithm limitations

The data which was used to derive the mixed-sediment empirical algorithms was generated entirely from a laboratory source. There could be potential implications when using such data to simulate real field situations, which include: spatial scaling, time scaling, sediment mixture composition and the closeness of the flume water column to real estuarine conditions.

The Tamar Estuary sediment mixtures were manufactured slurries, whereby Tamar mud was mixed with a different sand. This is very similar to previous mixed-sediment research conducted by Torfs (1994), Torfs et al. (1996) and Mitchener et al. (1996), who used combinations

of both naturally mixed sediments and prescribed mixtures. This paper also draws on a natural mixed sediment from Portsmouth Harbour. The variability in the algorithms generated by each sediment type illustrates the site specific nature of these algorithms, although some common factors are still evident. For example, high sand contents produce greater microfloc settling velocities and less mass within the macrofloc fractions.

The algorithms presented in this paper are meant to be representative of the floc dynamical changes in terms of: M:S, τ and SPM. The difference between the sediment types is more in terms of the relative magnitudes (e.g. Ws_{macro}) and therefore indicates the importance of data for coefficient calibration. It must be stressed that calibration of these algorithms solely through field observation is potentially very difficult and laboratory simulations of the flocculation processes can provide a clearer picture of floc dynamic variability over a wider range of conditions. A laboratory calibration (based on mixing processes) can then be improved and tuned using in situ data. It must be noted that geotechnical type data alone would not provide enough information about the flocculation of mud:sand mixtures.

In terms of flume scaling, the vertical settling in the flume is much lower than in real circumstances (due to the much smaller water depth. This may influence the mechanism of differential settling. However, Stolzenbach and Elimelich (1994) have suggested that differential settling is not an important interparticle contact mechanism, and may only occur within extremely quiescent waters, less turbulent than those used in this series of flume studies. Furthermore, van Leussen (1988) theoretically assessed the comparative influence of the three main collision mechanisms: Brownian motion, turbulent shear and differential settling and deduced that turbulent shear stresses (particularly those ranging between 0.03 and 0.8 Pa), were the dominant flocculation mechanism within an estuary and these fall within the data range used to generate the algorithms. Turbulent shear stress can impose a maximum floc size restriction on a floc population in tidal waters (McCave 1984). The sediments in the flume were sheared for a duration according to the TF (see Section 2.1). Also the flume water salinity was of a similar scale to in situ conditions. Therefore, it is suggested that the potential limits of these algorithms derived from laboratory data, are most likely to be less than those based solely on in situ data, due to the complex nature of mixed-sediment flocculation; however they are still site-specific and not universally applicable.

6.2 Modelling applications

Generally, the flocculation effects of mixed-sediment suspensions are rarely represented or even considered when parameterising the settling of estuarine sediments. This is primarily because most scientists have not considered mixed-sediment flocculation as an important process, or even acknowledge that mixed-sediment flocculation occurs to any degree. Although this may be true for a segregation-type environment, where the mud and sand do not combine into a single matrix; the previous section demonstrates that when mud and sand form a flocculating matrix, the inclusion of a representative process parameterisation may be very important for accurate estuarine sediment transport modelling, due to flocculation influencing the settling flux. The problem has always been that historically it is a very complex process to describe in a fundamental form, and thus it has always been difficult to represent mud flocculation mathematically. By using the various settling velocity parameterisation approaches listed in Section 5.2, this section will provide an insight into how different assumptions and approaches which could be included in a sediment transport model, compare with the output of the MSSV algorithms, in terms of MSF.

6.2.1 Single sediment type approach (Tamar)

The addition of non-cohesive fine sands to a muddy suspension can make the theoretical description of the flocculation even more difficult. Generally, most modellers will not consider mixed-sediment flocculation effects, as very little quantitative research has been conducted or reported on the effects of mixed-sediment processes as a whole. Under this situation and faced with a mixed-sediment regime, an estuarine sediment transport modeller has two initial basic choices. The first and most simple option, is to assume that the suspended sediments, which in reality are mud:sand mixtures act solely as one sediment type when suspended, thus entirely demonstrating either cohesive or non-cohesive settling characteristics.

Using this single sediment type assumption, the cohesive MFSV algorithms (M1) under-predicted the flux by −28% when there was really a 75M:25S mixture present, but the under-estimate dipped to just −15% as the sand content rose. The slower constant settling velocities (M2–M4) under-predicted by 86–31%, respectively; the fastest fall rate (M5) over-predicted by +38%. The calculated MSFs increased by about 2–26%, with the respective M2–M5 velocities, with decreasing sand content. However, although one may hypothesise that it is potentially possible to pick a single Ws value which would represent the benchmark fluxes, a statistical assessment of the M2-M5 derived MSFs for “all SPM” reveals that the mean error in these calculated fluxes tend to range from 100% to 300%, at SDs of 70–240%. This high degree in ME and its dispersion puts significant doubt into the reliability of a single constant Ws to represent mixed sediments. In contrast, the MSSV

predicted 95% of the MSF for a 75M:25S suspension, and the MEs were extremely small—spanning between −0.8% and −4%, with low degrees of dispersion as indicated by SDs of 17–20%.

Alternatively the modeller may wish to assume the ambient sediment is just sand and therefore use a simple sand grain settling velocity, such as M8. The testing results showed that at an SPM of 200 mg l^{-1}, the fast settling velocity of the pure sand parameterisations over-estimated the mass settling flux by 370–446%. Increasing SPM concentration tends to increase the settling velocity of both naturally flocculating pure mud and mixed sediments, due to an improvement in the particle collisions frequency. Thus over-estimation in MSF reduced to +126% for M8, at 5 g l^{-1}. In terms of real mud:sand ratios, the sand parameterisations produced over-predictions of about +100% for muddy sand suspensions (75M:25S), and this rose to approximately +150% for sandy mud (25M:75S). Therefore we can conclude that if mud:sand mixtures are represented solely by a non-flocculating, non-porous sand mineral suspension, even in the most favourable circumstances (e.g. higher concentrations), one can expect to be producing mass settling fluxes which are double those of the real mixed suspension and beyond.

6.2.2 Mixed sediment type approach (Tamar)

The second option is when a modeller acknowledges the presence of a mud:sand mixed environment; the issue is then how is this information treated. In theory, if the modeller knows how much mud and sand are in suspension, one would imagine the settling flux estimates would be more accurate. However, most research reports on the segregation environment, where the mud and sand do not combine into a single matrix. For example, the mixed-sediment model by van Ledden (2002), employed the segregation criteria for low concentration depositional simulations; flocculation effects are ignored. The problem arises when the modeller assumes the mixed suspensions are acting in a segregated manner, when in fact they are demonstrating a degree of flocculation, a wide range in predicted settling flux errors may arise from the modelling output.

For example, the tests conducted in Section 5.3.3 indicated that for a 75% mud suspension, M1 (The cohesive MFSV algorithms) now over-predicted by +20% and this rose to massive +120% for a 25M:75S mixture. At 75M:25S, the slower constant settling velocities (M2 and M3) under-predicted by 25–35%, the fastest fall rate (M5) over-predicted by +58%, whilst 2.5 mm s^{-1} (M4) was within +6% of the benchmark value. As the mud content decreased and the sand content increased, so the degree of over-estimation by M2–M5 rose. For a 75% sand slurry, all constant Ws parameters displayed over-estimates of 100% or more, when compared to the benchmark observations.

In fact the use of a single, static, constant settling velocity parameterisation to represent mixed-sediment settling behaviour is potentially very risky. This will be demonstrated using some examples from the first part of the inter-comparisons, where the sediment was assumed to be "not mixed" and the cohesive parameters were applied in an unmodified way. For example, a constant Ws of 1 mm s^{-1} (M3) predicted 98% of the MSF for a dilute suspension of 75M:25S; whilst for the same suspension a constant Ws of 5 mm s^{-1} (M5) over-estimated the MSF, at a concentration of 5 g l^{-1}, by just +21% - these are both fairly credible efforts. However if the concentration changed to 1 g l^{-1}, the former settling velocity (M3) would only predict two-thirds of the flux, and M5 would over-estimate by more than 200%. Furthermore, fixed settling values cannot react and adapt to changes in estuarial environmental conditions. Although they were occasionally correct—they were more often than not producing highly erroneous MSF estimates. This effect is analogous to the time output from a clock which has stopped—it will always display the correct time once during every 12-h cycle, although it is not working correctly at any other time.

The van Leussen (1994) approach (M7) is based on theoretical cohesive aggregation concepts, but during the intercomparison M7 showed quite large predictive errors and limited ranges of practical application in calculating MSF values. In pure cohesive form, M7 generally under-predicted by −25% to −37%, with extremely high mean errors (MEs of 163–360%) present in many of the individual flux computations and these errors were widely dispersed at 75–283%. Whilst in a mixed-sediment modified format, M7 was within 2% of the benchmark observations for a 75M:25S slurry, but over-predictions climbed to over 110% for sand dominated suspensions. Although reduced, the MEs and SDs were still comparably high, demonstrating values ranging between 115–150% and 70–140%, respectively. Therefore, in a predictive sense the MSSV empirical model is a significant step in improving mixed-sediment transport numerical simulations. The Power Law (M6) approach followed a similar pattern to M7, with mean errors which were more than ten times greater than the comparable MSSV method (M9), and the standard deviation of these errors two to three times greater than the MSSV.

6.2.3 Sediment apportioning across macrofloc:microfloc fractions

An important aspect for a modeller to consider in mixed-sediment flocs, is estimating how much of the mud and sand present in a suspension volume, is apportioned across

the macrofloc and smaller microfloc sub-fractions. The 75M:25S algorithms (Eq. 4.18) illustrated in Fig. 10a, indicates that for a low SPM concentration (200 mg l^{-1}), the M:S$_{mi:MA\ _EM}$ is 209 in the quiescent low turbulence environment (τ=0.06 Pa); this is suggesting 99.5% of the sand is held within the microflocs. As the turbulence rises, so the sand content slowly increases in the macroflocs, until the M:S$_{mi:MA\ _EM}$ falls to 11 at τ=0.6 Pa, when the microflocs now only contain 91% sand—a decrease of 8.5% from the low shear stress. Thereafter, the shear stress rises and the sand content in the macroflocs starts to decrease again.

For 50M:50S (Eq. 4.19), the algorithm in Fig. 10b show a similar shape to those of the 75% mud suspension. The main difference is that the peak sand content present in the 50M:50S suspension macroflocs, denoted by low M:S$_{mi:MA\ _EM}$ values, tends to occur around the lower shear stress of 0.35 Pa; it was closer to the more turbulent 0.6 Pa for the more cohesive 75% mud sediment. Also, the equal mud:sand ratio suspension M:S$_{mi:MA\ _EM}$ generated values were generally more than half the size of those estimated for a 75% mud suspension.

Due to the nature of the 75% and 50% mud suspension regression curves, it may be possible for them to generate negative M:S$_{mi:MA\ _EM}$ values within the MSSV boundary conditions of SPM concentration and shear stress. Under these conditions, it may be prudent to assume a M:S$_{mi:MA\ _EM}$ value of 0.25, equivalent to the macroflocs containing 80% of the sand content. It may also be advisable to assume a M:S$_{mi:MA\ _EM}$ lower limit of 0.25, as this will potentially minimise any erratic behaviour in the sand distribution across the macrofloc and microfloc populations; i.e. a M:S$_{mi:MA\ _EM}$ of zero suggests the macroflocs are composed entirely of sand, which is not realistic.

When the total sand content rises to 75% and beyond, the form of the M:S$_{mi:MA\ _EM}$ regression curves (see Fig. 10c) are the inverse of those produced by a greater total mud content. This suggests that the M:S$_{mi:MA\ _EM}$ values rise with increasing turbulent shear stress, peaking at a τ of 0.6 Pa. We can also see that M:S$_{mi:MA\ _EM}$ decreases with rising total sand content.

If we use a constant 200 mg l^{-1} concentration as an example, at τ=0.06 Pa the algorithm (Eq. 4.20a) suggests that 96% of the sand was within the smaller microfloc fraction by calculating a M:S$_{mi:MA\ _EM}$ of 24 (185 lower than for a 75% mud suspension). On reaching a τ=0.6 Pa, the algorithm estimates that the M:S$_{mi:MA\ _EM}$ had doubled to 48 (37 higher than for a 75% mud suspension), which is indicative of 98% of the sand in the microflocs. Thereafter, the M:S$_{mi:MA\ _EM}$ dips due to sand content in the macroflocs starting to increase very slightly with rising shear stress.

The importance of accounting for this sediment distribution across the macrofloc:microfloc fractions for a flocculating mixture, can be further demonstrated in a more generic way by a comparison with the MSSV MSF values and those obtained from incorrectly assuming segregation, when flocculation really applies. For example, a flocculating mixed suspension with a total SPM of 200 mg l^{-1} comprising 75M:25S produced a total combined MSF of 849 mg m^{-2} s^{-1} across all four shear stress zones. As the 75M:25S mixture is flocculating and the mud is actively integrating with the sand, one can assume that the mud (i.e. 150 of the 200 mg l^{-1} total SPM) is contributing 75% of the flux which is 637 mg m^{-2} s^{-1}. If, however, the sediments are deemed segregated and acting independently, as in a sand modified M1, the 150 mg l^{-1} represented by the pure mud parameterisation produced a cumulative MSF across the four shear stresses of 790 mg m^{-2} s^{-1}, which infers a 26% over-estimate in settling flux of the cohesive fraction. When both cohesive and non-cohesive components are combined in M1, the total segregated MSF (from all four τ zones) of 2,370 mg m^{-2} s^{-1} is nearly three times the flux estimated in terms of a flocculating suspension.

If we, again, separate the equivalent of the mud fraction (250 mg l^{-1}) from the less cohesive 25M:75S 1 g l^{-1} flocculating mixed suspension, a quarter of the MSSV estimated total flux (10.1 g m^{-2} s^{-1}) is 2.5 g m^{-2} s^{-1}. The pure mud parameterisation (M1) only estimates a MSF of 1.8 g m^{-2} s^{-1} for the 250 mg l^{-1} of cohesive sediment present, which is 72% of the MSSV flux for the cohesive fraction. In order to produce this additional 28% of the cohesive attributed flux, the particles must be settling quicker, as the SPM has not changed. This suggests that the cohesive sediment must be adhering in some shape or form to the more compact sand particles and therefore producing an enhanced fall velocity (see Manning et al. 2009).

6.2.4 Role of aggregate composition and biology in mud: sand mixture flocculation

The significant differences in floc properties, mean that theoretical representation of natural mud:sand flocs is currently not possible to any degree of accuracy. These uncertainties arise from the complexity of the compositional matrix and the resultant floc structures.

The original LabSFLOC data, from which the MSSV algorithms are based, identified that for flocculating mud: sand mixtures, there is a wide range in effective densities across the microfloc fraction, but most were less than pure quartz (1,600 kg m^{-3}). Transmission electron microscopy images have also visually identified the presence of both clay minerals and quartz mineral fragments within natural microfloc structures (Spencer et al. 2010). This all suggests that when mixed sediments flocculate, the sand particles favour the microfloc fractions, probably attributed to the

closer and stronger interparticle bonding potential of the microflocs. The available data suggests that the uptake of individual sand particles is probably much less in the macroflocs. However, the microflocs are recognised as the building blocks of the macroflocs (Eisma 1986; Krone 1986) and will result in the pathway for some sand reaching the larger size fraction.

The combined effects of particle concentration and turbulent shearing have long been attributed to the growth of mud flocs (e.g. Tsai et al. 1987; Burban 1987; Puls et al. 1988; Kranck and Milligan 1992). Under optimum flocculation conditions, Mehta and Lott (1987) suggested that pure mud macroflocs tend to contribute most to the MSF, on account of high instability (van Leussen 1994) due to floc growth potential producing a greater number of larger macroflocs with fast settling velocities. In estuaries, observation reveal these pure mud macroflocs can typically grow to mean a diameter >400 μm, exhibiting effective densities of less than 40–50 kg m^{-3} and becoming more than 95% porous, which mean these macroflocs are highly delicate entities and are easily progressively broken apart as they pass through regions of higher turbulent shear stress (Glasgow and Lucke 1980). However, the MSSV algorithms indicates a trend whereby a rise in sand content, and a subsequent decrease in mud, favours the microflocs as the dominant flux contributor.

For example, if we consider a flocculating mixture comprising 25% mud and 75% sand, at a nominal concentration of 1,000 mg l^{-1} and all sheared at a τ of 0.6 Pa, this results in the microflocs representing three quarters of the SPM. Therefore, the microfloc fraction would be contributing 88% of the total MSF which is 3.08 g m^{-2} s^{-1}. To place this MSF value into perspective: it is approximately double the flux estimated for either a pure mud or a 75% mixed mud suspension; nearly 30% greater than the MSSV flux predicted for a 50:50 mixture; and six times greater than the MSF obtained by using a constant 0.5 mm s^{-1} settling velocity.

In contrast, the MSSV algorithms indicated that by maintaining the ambient SPM at 1 g l^{-1}, but making the suspension 75% cohesive (i.e. 75M:25S), when it is sheared at 0.35 Pa the predicted total MSF (2.2 g m^{-2} s^{-1}) would be weighted 73%:27% in favour of the macroflocs. This settling flux distribution is more characteristic of a fully cohesive suspension (Manning and Bass 2006). This suggests that with just an 8% lower MSF than pure mud, the 75M:25S mixture is behaving, to some degree, predominantly as a cohesive suspension, even with 25% sand present in the mixture.

In terms of the wider picture, the MSSV reveals that for a predominantly sandy suspension (25M:75S), the macroflocs represented only 20% of the total MSF, when averaged across the various SPM and shear stress ranges. In contrast, the macroflocs contributed 58% of the settling flux for the muddier suspensions (75M:25S).

In addition to the physical processes, an important component which makes mixed-sediment flocculation possible is the presence of biological matter. In predominantly muddy/silty environments, benthic microphytobenthos contribute up to half the total autotrophic production in an estuarine system (Underwood and Kromkamp 1999; Cahoon 1999). Biostabilisation can increase particle cohesion, for example: epipelic diatoms (e.g. Paterson and Hagerthey 2001) secrete extra-cellular polymeric substances (EPS; Tolhurst et al. 2002) and are regarded as highly effective stabilisers of muddy sediments. The influence of biology on sand is reported to much lesser extent, however sand grains that are exposed to long-term biological activity, may also develop a cohesive bio-coating which could increase the particle collision efficiency when they are entrained. Hickman and Round (1970) reported that sand particles can be joined by “epipsammic” diatoms which attach to sand grains. Epipsammic macro-algal forms either adnate to the grain surface or attach to sand grains by their mucilage stalks. Epipsammic diatoms which are attached to sand grains, demonstrate strong adhesive properties to the grain surface (Harper and Harper 1967). When the sand and biology are combined into a single matrix, they can form “microbial mats” and the binding strength of these mats can be extremely high. Little (2000) states that because these types of algal threads are sticky with EPS, they can efficiently trap sand grains. These sticky bio-coating can increase collision efficiency (Edzwald and O’Melia 1975) of particle when entrained into suspension, thus allowing fine sand grains to adhere with the clay fraction and form the cage-like structure. Through microscopic photography, Wolanski (2007) reports the formation of large muddy flocs formed by mud creating a sticky membrane around large non-cohesive silt particles.

Also, the process of bioturbation (i.e. the reworking of the bed sediments) can potentially enhance the mixing of bed sediment particles prior to resuspension (e.g. Nowell et al. 1981; Paterson et al. 1990; Widdows et al. 2004). Thus, a bed which is initially deposited as a discretely segregated layering of mud and sand, may be transformed into a quasi-homogeneous mixture through bioturbation.

The parameterisation of biological process for inclusion in numerical sediment transport models is notoriously difficult and the MSSV algorithms do not include a dedicated “biological” term. However, both the Tamar and Portsmouth algorithms are based on data derived from natural sediments, which would include some of the biological effects—most importantly the presence of sticky EPSs. A limitation of many mixed-sediment laboratory studies, is that the mud:sand matrix is over-simplified through the use of a pure clay mineral (e.g. kaolinite)

devoid of any biology. As clay minerals only flocculate through electrostatic (i.e. salt) flocculation, at best a segregated environment may be simulated if the water is brackish, but resultant mixed-sediment flocculation effects will never be observed.

6.2.5 Tamar–Portsmouth settling algorithm comparison

It is generally acknowledged that most empirical data relating to natural cohesive sediments in one form or another tend to be estuary-specific. Therefore, the MSSV algorithms were also calibrated using naturally occurring mud:sand mixtures from Portsmouth Harbour. The Portsmouth algorithm calibrations were presented in Section 4.4 and two examples are presented in Fig. 14. Generally, one can see that the Portsmouth Harbour sediments showed similar general macrofloc and microfloc settling velocity patterns to those of the equivalent Tamar mixed suspensions, however both fractions of the Portsmouth sediment tended to fall quicker than their Tamar mixed-sediment equivalents, except for lower concentrations for microflocs.

If we first consider the scenario of a more cohesive 70M:30S mixture, a dilute 200 mg l^{-1} suspension resulted in a peak Ws_{macro} of 4 mm s^{-1} for the Portsmouth sediment (see Fig. 14a), which quickens to 6.6 mm s^{-1} as the ambient SPM is raised by an order of magnitude (SPM=2 g l^{-1}). This is in stark contrast to the equivalent Tamar Ws_{macro}, which were approximately 40% slower than the respective Portsmouth fall velocities. A similar trend was observed for the 70M:30S microflocs (Fig. 14b), however the microfloc settling rates were slower; a maximum Ws_{micro} of 4.2 mm s^{-1} was predicted for the Portsmouth sediment at an SPM=2 g l^{-1}.

As the sand content doubled to 38M:62S, the Portsmouth microfloc fall rates (see Fig. 15b) increases to speeds of 5.3 and 6.1 mm s^{-1}, (at low and high turbidity), which are more representative of the Ws_{macro} values predicted at a 70M:30S mixture. In comparison, the Tamar mixture predicted a much slower Ws_{micro} of 3 mm s^{-1} ±0.1, across the comparison turbidity range. It is proposed that this could be a result of a different sand grain size distribution combined with stronger bio-film coatings producing added cohesion in the Portsmouth sediment mixtures. This would permit a greater uptake of the sand grains within the macrofloc fraction, whilst also potentially forming the faster settling microflocs observed.

Interestingly, if we examine the 38M:62S equivalent macrofloc predicted settling trends (see Fig. 15b), even though the Portsmouth algorithms predicted that they were the quickest (Ws_{macro}=3.7 mm s^{-1}) by 1.2 mm s^{-1} for the high concentration scenario; at the lower end of the turbidity scale, the Portsmouth macroflocs fell near 0.5 mm s^{-1} slower than their Tamar equivalents. One can see that empirical algorithms generated in the MSSV form will be unique to the sediment tested and therefore not universally applicable, due to the site-specific nature of cohesive mixed sediments. For alternative locations (e.g. estuaries), different algorithm coefficients may be needed, and even these formulas cannot always be applied over the full range of shear stresses. Thus, floc settling, mixture composition, hydrodynamic and suspended solids data will be required in order to correctly tune the algorithms. This demonstrated the necessity to test sediment properties over as wide a range of conditions prior to implementation, as is practically possible. Furthermore, these empirical formulae may need to be modified to account for any seasonal variations. This will give any potential end user greater confidence in using a specific algorithm.

7 Summary and conclusions

The settling characteristics of flocculating mixed-sediment suspensions were investigated through the synthesis of an empirical data set (as opposed to pure physical theory), which was presented as a series of algorithms. Collectively, the algorithms were referred to as the MSSV empirical model and mimicked the mass settling flux of mixed suspensions. The MSSV algorithms were principally derived using manufactured mixtures of Tamar Estuary mud and a fine silica sand, which means that the algorithms presented are site-specific in nature, and not fully universal in application.

As one would expect, the MSSV algorithms are an accurate reflection of the mixed-sediment flocculation data it is based on. However the low standard deviations and scatter demonstrated by the MSSV empirical model, together with fully acceptable levels of mean error, when applied to a wide range of simulated estuarine environmental conditions, in comparison to existing settling flux parameterisations, is a testament to its overall reliability and robustness. For example in terms of MSF: at the lower flux range (195–777 mg m^{-2} s^{-1}) most MSSV predictions were within a few percent of the observations, whilst for the largest observed MSFs (1.3–21 g m^{-2} s^{-1}), the MSSV demonstrated a close fit with the data. Even for the highest observed MSF of 33 g m^{-2} s^{-1} (produced by a 75M:25S mixed suspension), the MSSV only under-estimated the flux by 18%. The MSSV algorithms indicates a trend whereby a rise in sand content, and a subsequent decrease in mud, favours the microflocs as the dominant flux contributor.

In terms of comparing various settling velocity parameterisations, testing revealed that the application of a single sediment assumption to a mixed-sediment environment, the pure mud algorithms (Manning 2008) under-predicted at each concentration by as much as 25% and did not handle sandy mud sediments particularly well. The slower constant settling

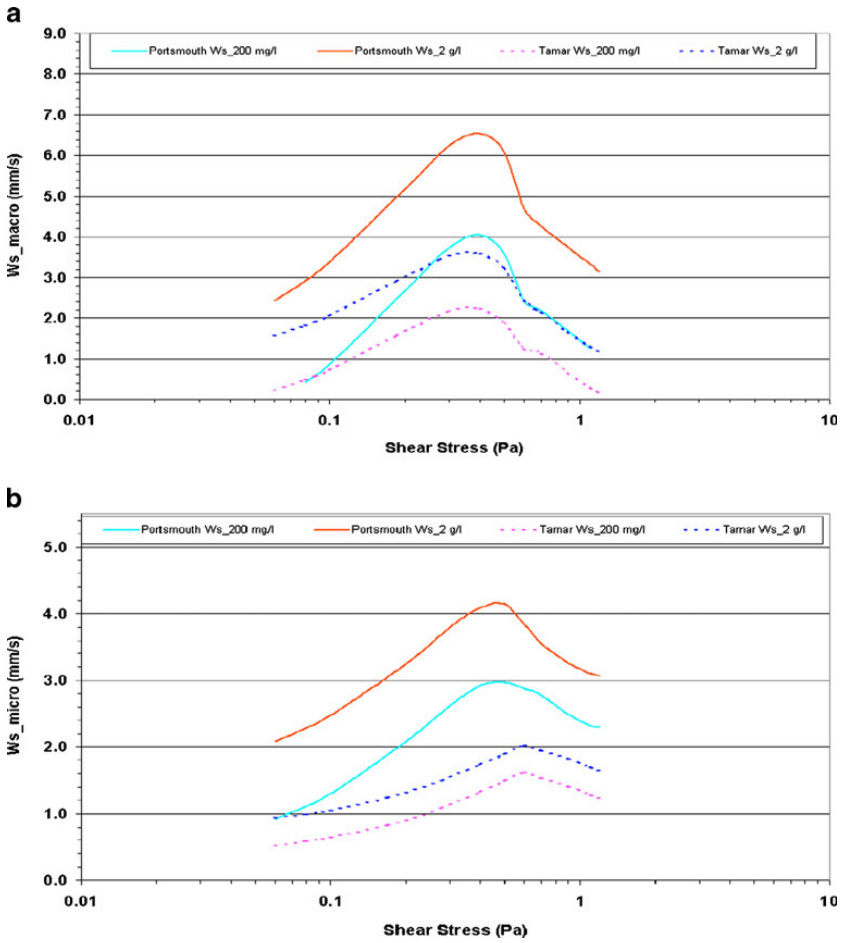

Fig. 14 Comparison of the settling trends in terms of **a** Ws_{MACRO} and **b** Ws_{micro}, for the Tamar and Portsmouth mixed-sediment algorithms for a suspension with a mixture ratio 70% Mud:30% Sand

velocity parameters severely under-predicted MSF (at times down to only 13% of the observed flux), whilst the fastest constant fall rate (5 mm s^{-1}) over-predicted by as much as 246%. Fixed Ws parameters produced quite large mean errors in MSF estimation. The Power Law and van Leussen approaches generally under-predicted by 25–37%, with extremely high mean errors and SDs. By assuming every suspension scenario was pure sand, they over-estimated the mass settling flux by over 400% at dilute suspensions, reducing to about 100% at a concentration of 5 g l^{-1}.

One would assume that if we knew what percentage of mud and sand were in suspension at any one point in time and space, we should be able to predict the MSF with greater accuracy. However, the modification of one of the purely cohesive parameterisations (e.g. M1–M7) with the addition of a pure sand fall velocity to account for the sand fraction, tended to create even greater MSF predictive errors, and in most cases produced excessive over-estimations in MSF. The reason for these predictive errors was that this hybrid approach still treated mud and sand separately. This is potentially reasonable if the sediments are segregated and non-interactive, but appears to be unacceptable when the mud and sand are flocculating via an interactive matrix.

The MSSV empirical model may be regarded as a 'first stage' approximation for scientists and engineers either wishing to investigate mixed-sediment flocculation and its depositional characteristics in a quantifiable framework, or simulate mixed-sediment settling in a numerical sediment transport model where flocculation is occurring. The preliminary assessment concluded that in general when all the SPM and shear stress range data were combined, the net result indicated that the new mixed-sediment settling velocity empirical model was only in error by −3 to −6.7% across the experimental mud:sand

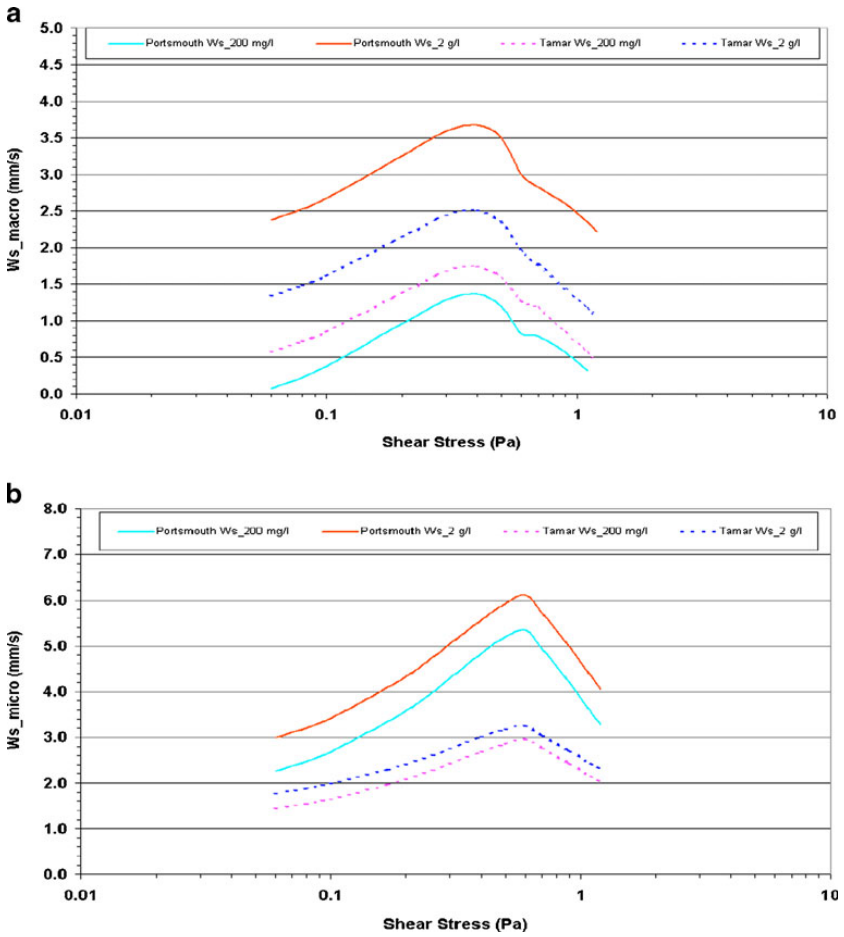

Fig. 15 Comparison of the settling trends in terms of **a** Ws_{MACRO} and **b** Ws_{micro}, for the Tamar and Portsmouth mixed-sediment algorithms for a suspension with a mixture ratio of 38% mud and 62% sand

mixture ratios. The development of a more physics-based model, which captures the essential features of the empirical MSSV model, would be more universally applicable. This transition from empirical to physics-based model has been achieved by Soulsby et al. (2010) for pure cohesive sediment flocculation.

At present, the MSSV algorithms provides a modeller, who is setting up a numerical mud and sand sediment transport simulation model, a starting point from which to work. However, the specific settling velocities and mass distributions predicted by the MSSV algorithms presented in this paper will not be universally applicable to all estuarine locations, as only Tamar Estuary mud was used. Therefore, tuning of the algorithm coefficients is required for the accurate prediction of depositional rates in a specific estuary, as was demonstrated by the calibration to data from Portsmouth Harbour presented in this paper. This type of tuning requires instrumentation which permits unintrusive, simultaneous measurements of floc/aggregate D and Ws across a wide range of suspended concentrations (e.g. video-based devices such as LabSFLOC). Furthermore, these empirical formulae may need to be modified to account for any seasonal variations. Volume 2 of this paper (Spearman et al. 2011) describes the application of the present empirical MSSV model to the outer Thames Estuary.

Acknowledgements The primary data collection and analysis described in this paper was funded by HR Wallingford as part of the Company Research Programme Mud:Sand Transport projects: DDD0301 and DDD0345. The analysis required for the preparation of this paper was part funded by the HR Wallingford Company Research project DDD0360 and completed as part of project DDY0409.

Appendix 1

Table 9 Summary of laboratory flume floc properties for suspensions with a ratio of 75% mud and 25% sand

Mud%	Sand%	SPM (mg l^{-1})	τ (Pa)	microfloc SPM%	microfloc MSF (mg m^{-2} s^{-1})	microfloc SPM ratio	microfloc Effectivity Density (kg m^{-3})	microfloc Ws (mm s^{-1})	microfloc Porosity (%)	MACROFLOC SPM%	MACROFLOC MSF (mg m^{-2} s^{-1})	MACROFLOC SPM ratio	MACROFLOC Effectivity Density (kg m^{-3})	MACROFLOC Ws (mm s^{-1})	MACROFLOC Porosity (%)	Total Mass Setting (mg m^{-2} s^{-1})
75	25	200	0.9	79.10	164.42	0.26	554.60	1.03	55.84	20.90	31.04	0.26	43.46	0.74	96.54	195
75	25	200	0.6	51.23	128.31	0.95	627.13	1.29	50.07	48.77	125.61	0.95	53.19	1.29	95.77	254
75	25	200	0.35	72.34	162.23	0.38	338.46	1.08	73.05	27.66	92.08	0.38	111.87	1.65	91.09	254
75	25	200	0.06	62.78	85.88	0.59	387.01	0.75	69.19	37.22	49.20	0.59	36.91	0.67	97.06	135
75	25	1,000	0.9	68.40	1,253.21	0.46	676.38	1.83	46.15	31.60	322.58	0.46	46.76	1.00	96.28	1,576
75	25	1,000	0.6	48.12	863.27	1.08	880.47	1.72	29.90	51.88	914.14	1.08	69.26	1.64	94.49	1,777
75	25	1,000	0.35	23.37	239.67	2.79	233.56	0.92	81.40	73.59	1,894.75	2.79	79.76	2.47	93.65	2,134
75	25	1,000	0.06	70.61	466.13	0.42	193.09	0.65	84.63	29.39	310.54	0.42	36.60	0.98	97.09	777
75	25	5,000	0.9	31.80	4,025.27	2.15	307.66	2.39	75.50	68.20	12,087.02	2.15	141.93	3.50	88.70	16,112
75	25	5,000	0.6	35.88	4,821.46	1.79	981.06	2.68	21.89	64.12	15,883.29	1.79	151.42	4.57	87.94	20,705
75	25	5,000	0.35	16.15	2,100.35	5.19	628.81	2.53	49.94	83.85	30,821.66	5.19	169.21	7.16	86.53	32,922
75	25	5,000	0.06	26.12	1,586.26	2.83	442.72	1.17	64.75	73.88	11,654.80	2.83	146.39	3.17	88.34	13,241

Table 10 Summary of laboratory flume floc properties for suspensions with a ratio of 50% mud and 50% sand

Mud %	Sand %	SPM (mg l^{-1})	τ (Pa)	microfloc SPM%	microfloc MSF (mg m^{-2} s^{-1})	microfloc SPM ratio	microfloc Effectivity Density (kg m^{-3})	microfloc Ws (mm s^{-1})	microfloc Porosity (%)	MACROFLOC SPM%	MACROFLOC MSF (mg m^{-2} s^{-1})	MACROFLOC SPM ratio	MACROFLOC Effectivity Density (kg m^{-3})	MACROFLOC Ws (mm s^{-1})	MACROFLOC Porosity (%)	Total Mass Setting (mg m^{-2} s^{-1})
50	50	200	0.9	65.63	245.32	0.52	697.88	1.70	4.44	34.37	49.65	0.52	40.00	0.72	96.82	295
50	50	200	0.6	74.85	334.14	0.34	1,510.14	2.14	−20.23	25.15	71.46	0.34	71.25	1.47	94.33	406
50	50	200	0.35	78.42	220.56	0.28	1,283.15	1.42	−2.16	21.58	66.71	0.28	109.07	1.55	91.32	287
50	50	200	0.06	61.99	150.44	0.61	406.68	1.00	67.62	38.01	57.32	0.61	35.39	0.72	97.18	208
50	50	1,000	0.9	61.87	1,534.94	0.62	989.07	2.44	21.25	38.13	511.23	0.62	62.30	1.28	95.04	2,046
50	50	1,000	0.6	55.96	1,479.35	0.79	1,130.90	2.63	9.96	44.04	736.24	0.79	64.38	1.60	94.87	2,216
50	50	1,000	0.35	44.54	1,135.15	1.25	500.84	2.32	60.12	55.46	1,289.50	1.25	111.64	2.33	91.11	2,425
50	50	1,000	0.06	92.22	1,476.50	0.08	833.83	1.54	33.61	7.78	124.51	0.08	101.09	1.60	91.95	1,601
50	50	5,000	0.9	45.35	62.19.09	1.21	1,767.57	2.66	−40.73	54.65	7,634.82	1.21	156.93	2.83	87.51	13,854
50	50	5,000	0.6	47.90	8,362.73	1.09	1,149.98	3.07	8.44	52.10	10,711.97	1.09	148.26	3.89	88.20	19,075
50	50	5,000	0.35	30.19	5,572.68	2.31	883.19	3.32	29.68	69.81	20,691.45	2.31	146.07	5.40	88.37	26,264
50	50	5,000	0.06	47.39	3,143.62	1.11	875.83	1.29	30.27	52.61	5,588.62	1.11	118.31	2.15	90.58	8,732

Table 11 Summary of laboratory flume floc properties for suspensions with a ratio of 25% mud and 75% sand

Mud %	Sand %	SPM ($mg\ l^{-1}$)	τ (Pa)	microfloc SPM%	microfloc MSF ($mg\ m^{-2}\ s^{-1}$)	microfloc SPM ratio	microfloc Effectivity Density ($kg\ m^{-3}$)	microfloc Ws ($mm\ s^{-1}$)	microfloc Porosity (%)	MACROFLOC SPM%	MACROFLOC MSF ($mg\ m^{-2}\ s^{-1}$)	MACROFLOC SPM ratio	MACROFLOC Effectivity Density ($kg\ m^{-3}$)	MACROFLOC Ws ($mm\ s^{-1}$)	MACROFLOC Porosity (%)	Total Mass Setting ($mg\ m^{-2}\ s^{-1}$)
25	75	200	0.9	76.89	449.59	0.30	723.22	2.84	42.42	23.11	37.76	0.30	52.21	0.82	95.84	487
25	75	200	0.6	72.98	501.33	0.37	1,430.47	3.49	−13.89	27.02	60.81	0.37	61.70	1.13	95.09	562
25	75	200	0.35	75.15	358.83	0.33	553.39	2.29	55.94	24.85	47.98	0.33	46.68	0.91	96.28	407
25	75	200	0.06	79.55	280.70	0.26	399.47	1.66	68.19	20.45	33.53	0.26	55.95	0.82	95.55	314
25	75	1,000	0.9	80.20	2,748.83	0.25	953.17	3.28	24.11	19.80	228.59	0.25	63.03	1.15	94.98	2,977
25	75	1,000	0.6	75.92	2,891.37	0.32	1,034.84	3.61	17.61	24.08	329.51	0.32	67.02	1.35	94.66	3,221
25	75	1,000	0.35	64.17	2,556.77	0.56	1,048.80	3.86	16.50	35.83	570.87	0.56	75.00	1.56	94.03	3,128
25	75	1,000	0.06	69.23	2,119.13	0.44	835.43	3.03	33.49	30.77	364.89	0.44	60.60	1.16	95.17	2,484
25	75	5,000	0.9	56.90	9,826.19	0.76	1,025.43	3.42	18.36	43.10	4,226.22	0.76	91.11	1.87	92.75	14,052
25	75	5,000	0.6	45.58	11,246.05	1.19	1,497.18	4.62	−19.20	54.42	6,744.84	1.19	118.37	2.43	90.58	17,991
25	75	5,000	0.35	50.15	10,780.55	0.99	1,205.45	4.18	4.02	49.85	9,218.63	0.99	156.70	3.50	87.52	19,999
25	75	5,000	0.06	58.72	6,460.32	0.70	624.78	2.17	50.26	41.28	3,575.61	0.70	84.28	1.71	93.29	10,036

References

Alvarez-Herandez E (1990) The influence of cohesive sediment on sediment movement in channels of circular cross-section. PhD thesis, University of Newcastle-upon-Tyne

Ayesa E, Margeli MT, Florez J, Garcia-Heras JL (1991) Estimation of break-up and aggregation coefficients in flocculation by a new adjustment algorithm. Chemical Engineering Science 46(1):39–48

Argaman Y, Kaufman WJ (1970) Turbulence and flocculation. J Sanitary Eng, ASCE 96:223–241

Baugh JV, Manning AJ (2007) An assessment of a new settling velocity parameterisation for cohesive sediment transport modelling. Continental Shelf Research. doi:10.1016/j.csr.2007.03.003

Boadway JD (1978) Dynamics of growth and breakage of alum flocs in presence of fluid shear. ASCE, Journal of the Environmental Engineering Division 104(EE5):901–915

Burban PY (1987) The flocculation of fine-grained sediments in estuarine waters. MSc. thesis, Dep. of Mech. Eng. Univ. of Calif., Santa Barbara, USA

Cahoon LB (1999) The role of benthic microalgae in neritic ecosystems. Oceanography and marine biology: an annual review 37:47–86

Casamitjana X, Schladow SG (1991) A dynamic model for particle distribution in a stratified lake. Proceedings of International Association for Hydraulic Research, XXIV Congress, September 1991, Madrid, Spain, Vol C, pp 509–516

Casamitjana X, Schladow SG (1993) Vertical distribution of particles in a lake. ASCE J Env Eng 119(3):443–462

Chen S, Eisma D (1995) Fractal geometry of in situ flocs in the estuarine and coastal environments. Netherlands Journal of Sea Research 32(2):173–182

Chesher TJ, Ockenden MC (1997) Numerical modelling of mud and sand mixtures. In: Burt N, Parker R, Watts J (eds) Cohesive sediments—Proc. of INTERCOH Conf. (Wallingford, England). Wiley, Chichester, pp 395–406

Cuthbertson A, Dong P, Davies P (2008) Hindered settling velocity of cohesive/non-cohesive sediment mixtures. Coastal Engineering. doi:10.1016/j.coastaleng.2008.05.001

Dankers PJT, Sills GC, Winterwerp JC (2007) On the hindered settling of highly concentrated mud-sand mixtures. In: Kudusa T, Yamanishi H, Spearman J, Gailani JZ (eds) Sediment and ecohydraulics—Proc. in Marine Science, INTERCOH 2005. Elsevier, Amsterdam, pp 255–274

Dyer KR (1986) Coastal and estuarine sediment dynamics. Wiley, Chichester, 342 pp

Dyer KR (1989) Sediment processes in estuaries: future research requirements. J Geophys Res 94(C10):14,327–14,339

Dyer KR, Manning AJ (1999) Observation of the size, settling velocity and effective density of flocs, and their fractal dimensions. Journal of Sea Research 41:87–95

Dyer KR, Cornelisse JM, Dearnaley M, Jago C, Kappenburg J, McCave IN, Pejrup M, Puls W, van Leussen W, Wolfstein K (1996) A comparison of in-situ techniques for estuarine floc settling velocity measurements. Journal of Sea Research 36:15–29

Edzwald JK, O'Melia CR (1975) Clay distributions in recent estuarine sediments. Clays and Clay Minerals 23:39–44

Eisma D (1986) Flocculation and de-flocculation of suspended matter in estuaries. Neth J Sea Res 20(2/3):183–199

Eisma D, Dyer KR, van Leussen W (1997) The in-situ determination of the settling velocities of suspended fine-grained sediment – a review. In: Burt N, Parker R, Watts J (eds) Cohesive sediments—Proc. of INTERCOH Conf. (Wallingford, England). Wiley, Chichester, pp 17–44

Feates NG, Mitchener HJ (1998) Properties of dredged material: measurement of sediment properties of dredged material from Harwich Harbour. HR Wallingford Report TR 46

Fennessy MJ, Dyer KR, Huntley DA (1994) Size and settling velocity distributions of flocs in the Tamar Estuary during a tidal cycle. Netherlands Journal of Aquatic Ecology 28:275–282

Fennessy MJ, Dyer KR, Huntley DA, Bale AJ (1997) Estimation of settling flux spectra in estuaries using INSSEV. In: Burt N, Parker R, Watts J (eds) Cohesive sediments—Proc. of INTERCOH Conf. (Wallingford, England). Wiley, Chichester, pp 87–104

Glasgow LA, Lucke RH (1980) Mechanisms of deaggregation for clay-polymer flocs in turbulent systems. Ind Eng Chem Fundam 19:148–156

Gratiot N, Manning AJ (2004) An experimental investigation of floc characteristics in a diffusive turbulent flow. In: Ciavola P, Collins MB (eds) Sediment transport in European Estuaries. J Coast Res SI 41:105–113

Gratiot N, Manning AJ (2008) Flocculation processes in concentrated benthic suspension layer (CBS) using a laboratory diffusive turbulent grid tank. In: Kudusa T, Yamanishi H, Spearman J, Gailani JZ (eds) Sediment and ecohydraulics—Proc. in Marine Science 9. Elsevier, Amsterdam, pp 53–68, ISBN: 978-0-444-53184-1

Harlow D (1980) Sediment processes, Selsey Bill to Portsmouth, PhD thesis, Department of Civil Engineering, University of Southampton

Harper MA, Harper JF (1967) Measurements of diatom adhesion and their relationship with movement. British Phycological Bulletin 3:195–207

Hickman M, Round FE (1970) Primary production and standing crops of epipsammic and epipelic algae. British Phycological Journal 5 (2):247–255

Hill PS (1996) Sectional and discrete representations of floc breakage in agitated suspensions. Deep-Sea Res 43:679–702

Hydraulics Research (1959) Portsmouth harbour investigation, parts I and II. Reports 213b and 214, Technical report, Hydraulics Research

Jacobs W (2006) Eco-morphology of estuaries and tidal lagoons: literature review and experiments on sand-mud mixtures. TU Delft report no. 1–106, March 2006, 101p

Kamphuis W, Hall KR (1983) Cohesive material erosion by unidirectional current. J Hyd Eng, ASCE 109:49–61

Klimpel RC, Hogg R (1986) Effects of flocculation conditions on agglomerate structure. Journal of Colloid Interface Science 113:121–131

Koglin B (1977) Assessment of the degree of aggregation in suspension. Powder Technology 17:219–227

Kranck K, Milligan TG (1992) Characteristics of suspended particles at an 11-hour anchor station in San Francisco Bay, California. Journal of Geophysical Research 97:11373–11382

Kranenburg C (1994) The fractal structure of cohesive sediment aggregates. Estuarine Coastal Shelf Sci 39:451–460

Krishnappan BG (1990) Modelling of settling and flocculation of fine sediments in still water. Canadian Journal of Cibil Engineering 17:763–770

Krishnappan BG (1991) Modelling of cohesive sediment transport. In: International Symposium on the Transport of Suspended Sediments and its Mathematical Modelling, Florence, Italy, pp 433–448

Krone RB (1962) Flume studies of the transport of sediment in estuarial shoaling processes. Final report. Hyd. Eng. Lab. and Sanitary Eng. Lab., University of California, Berkeley

Krone RB (1963) A study of rheological properties of estuarial sediments. Report No. 63–68, Hyd. Eng. Lab. and Sanitary Eng. Lab., University of California, Berkeley

Krone RB (1986) The significance of aggregate properties to transport processes. In: Mehta AJ (ed) Estuarine cohesive sediment dynamics. Springer, Berlin, pp 66–84

Le Hir P, Monbet Y, Ovain F (2007) Sediment erodibility in sediment transport modelling: can we account for biota effects? Cont Shelf Res 27:1116–1142

Lee S-I, Seo I-S, Koopman B (1994) Effect of mean velocity gradient and mixing time on particle removal in sea water induced flocculation. Water, Air and Soil Pollution 78:179–188

Lick W, Huang H, Jepsen R (1993) Flocculation of fine-grained sediments due to differential settling. J Geophs Res 98 (C6):10,279–10,288

Little C (2000) The biology of soft shores and estuaries. Oxford University Press, UK, p 252p, ISBN: 978-0-198-50426-9

Lonsdale BJ (1969) A sedimentary study of the eastern Solent, Master's thesis, Department of Oceanography, University of Southampton

Maggi F (2005) Flocculation dynamics of cohesive sediments. PhD Thesis, TU Delft, 136p

Malcherek A (1995) Mathematische modellierung von stromungen und stofftransportprozessen in Astuaren. Dissertation, Institut fur Stromungsmechanik und Elektronisch Rechen im Bauwessen der Universitat Hannover, Bericht Nr. 44/1995 (in German)

Malcherek A, Markofsky M, Zielke W, Peltier E, Le Normant C, Teisson C, Cornelisse J, Molinaro P, Corti S, Greco G (1996) Three dimensional numerical modelling of cohesive sediment transport in estuarine environments. Final report to the EC contract MAS2-CT92-0013

Manning AJ (2001) A study of the effects of turbulence on the properties of flocculated mud. Ph.D. Thesis. Institute of Marine Studies, University of Plymouth, 282p

Manning AJ (2004a) The observed effects of turbulence on estuarine flocculation. In: Ciavola P, Collins MB (eds) Sediment transport in European estuaries. J Coast Res SI 41:90–104

Manning AJ (2004b) The development of new algorithms to parameterise the mass settling flux of flocculated estuarine sediments. HR Wallingford Ltd (UK) Technical Report No. TR 145, 26p

Manning AJ (2004c) Observations of the properties of flocculated cohesive sediment in three western European estuaries. In: Ciavola P, Collins MB (eds) Sediment transport in European estuaries. J Coast Res SI 41:70–81

Manning AJ (2006) LabSFLOC – A laboratory system to determine the spectral characteristics of flocculating cohesive sediments. HR Wallingford Technical Report, TR 156

Manning AJ (2008) The development of algorithms to parameterise the mass settling flux of flocculated estuarine sediments. In: Kudusa T, Yamanishi H, Spearman J, Gailani JZ (eds) Sediment and Ecohydraulics—Proc. in Marine Science 9. Elsevier, Amsterdam, pp 193–210, ISBN: 978-0-444-53184-1

Manning AJ, Bass SJ (2006) Variability in cohesive sediment settling fluxes: observations under different estuarine tidal conditions. Marine Geology 235:177–192

Manning AJ, Dyer KR (1999) A laboratory examination of floc characteristics with regard to turbulent shearing. Marine Geology 160:147–170

Manning AJ, Dyer KR (2002) A comparison of floc properties observed during neap and spring tidal conditions. In: Winterwerp JC, Kranenburg C (eds) Fine sediment dynamics in the marine environment—Proc. in marine science 5. Elsevier, Amsterdam, pp 233–250, ISBN: 0-444-51136-9

Manning AJ, Dyer KR (2007) Mass settling flux of fine sediments in Northern European estuaries: measurements and predictions. Marine Geology 245:107–122. doi:10.1016/j.margeo.2007.07.005

Manning AJ, Whitehouse RJS (2009) UoP Mini-annular flume—operation and hydrodynamic calibration. HR Wallingford Technical Report, TR169

Manning AJ, Spearman J, Whitehouse RJS (2007) Mud:sand transport—flocculation & settling dynamics within turbulent flows, part 1: analysis of laboratory data. HR Wallingford Internal Report, IT 534:32p

Manning AJ, Baugh JV, Spearman J, Whitehouse RJS (2009) Flocculation settling characteristics of mud: sand mixtures. Ocean Dynamics, PECS2008 SI, doi:10.1007/s10236-009-0251-0

Manning AJ, Baugh JV, Spearman J, Whitehouse RJS (2011) Mud: sand transport – flocculation & settling dynamics within turbulent flows, Part 2: The development of new algorithms to parameterise the mass settling flux of flocculated mixed estuarine sediments. HR Wallingford Internal Report, IT 552 release 2

McAnally WH (1999) Aggregation and deposition of estuarial fine sediment. PhD thesis, University of Florida, Gainesville, Florida, 383p

McCave IN (1984) Size spectra and aggregation of suspended particles in the deep ocean. Deep-Sea Res 31:329–352

Mehta AJ, Lott JW (1987) Sorting of fine sediment during deposition. Proc. Speciality Conf. Advances in Understanding Coastal Sediment Processes. Am Soc Civ Eng, New York, pp 348–362

Mietta F, Maggi F, Winterwerp JC (2008) Sensitivity to break-up functions of a population balance equations for cohesive sediment. In: Kudusa T, Yamanishi H, Spearman J, Gailani JZ (eds) Sediment and ecohydraulics—Proc. in Marine Science 9. Elsevier, Amsterdam, pp 275–286, ISBN: 978-0-444-53184-1

Migniot C (1968) Study of the physical properties of various very fine sediments and their behaviour under hydrodynamic action. La Houille Blanche 23(7). (Translation of French text)

Mitchener HJ, Torfs H, Whitehouse RJS (1996) Erosion of mud/sand mixtures. Coastal Engineering 29:1–25, Errata, 1997, 30, 319

Nowell ARM, Jumars PA, Eckman JE (1981) Effects of biological activities on the entrainment of marine sediments. Mar Geol 42:133–153

Ockenden MC, Delo EA (1988) Consolidation and erosion of estuarine mud and sand mixtures – an experimental study. HR Wallingford Report, SR 149

Panagiotopoulus I, Voulgaris G, Collins MB (1997) The influence of clay on the threshold of movement of fine sandy beds. Coastal Eng 32:19–43

Parker DS, Kaufman WJ, Jenkins D (1972) Floc break-up in turbulent flocculation processes. J Sanitary Eng Div, Proc Am Soc Civil Eng 98(SA1):79–97

Paterson DM, Hagerthey SE (2001) Microphytobenthos in contrasting coastal ecosystems: biology and dynamics. In: Reise K (ed) Ecological comparisons of sedimentary shores. Ecological studies, pp 105–125

Paterson DM, Crawford RM, Little C (1990) Subaerial exposure and changes in the stability of intertidal estuarine sediments. Estuarine Coastal and Shelf Science 30:541–556

Petersen O, Vested HJ, Manning AJ, Christie MC, Dyer KR (2002) Numerical modelling of mud transport processes in the Tamar Estuary. In: Winterwerp JC, Kranenburg C (eds) Fine sediment dynamics in the marine environment—Proc. in Mar. Sci. 5. Elsevier, Amsterdam, pp 643–654

Pidduck EL, Manning AJ (2009) A laboratory examination of flocculation properties exhibited by natural sediment mixtures from Portsmouth Harbour, UK. HR Wallingford Technical Report, TR 182

Puls W, Kuehl H, Heymann K (1988) Settling velocity of mud flocs: results of field measurements in the Elbe and the Weser Estuary. In: Dronkers J, van Leussen W (eds) Physical processes in estuaries. Springer, Berlin, pp 404–424

Raudkivi AJ (1998) Loose boundary hydraulics, 3rd edn. Balkeme, Rotterdam

Sanford LP, Dickhudt PJ, Rubaiano-Gomez L, Yates M, Suttles SE, Friedrichs CT, Fugate DC, Romine H (2005) Variability of suspended particle concentrations, sizes and settling velocities in the Chesapeake Bay turbidity maximum. In: Droppo IG, Leppard GG, Liss P, Milligan T (eds) Flocculation in natural and engineered environmental systems. CRC, Florida, pp 211–236

Soulsby RL, Manning AJ, Whitehouse RJS, Spearman JR (2010). Development of a generic physically-based formula for the settling flux of natural estuarine cohesive sediment. Final Report – summary, HR Wallingford company research project DDY0409, 1p

Spearman JR, Manning AJ, Whitehouse RJS (2011) The settling dynamics of flocculating mud-sand mixtures: Part 2—Numerical modelling. Ocean Dynamics, INTERCOH 2009 special issue

Spencer KL, Manning AJ, Droppo IG, Leppard GG, Benson T (2010) Dynamic interactions between cohesive sediment tracers and natural mud. Journal of Soils and Sediments 10(7), doi:10.1007/s11368-010-0291-6

Stolzenbach KD, Elimelich M (1994) The effect of density on collisions between sinking particles: implications for particle aggregation in the ocean. Journal of Deep Sea Research I 41 (3):469–483

Tambo N, Watanabe Y (1979) Physical characteristics of flocs—I. The floc density function and aluminium floc. Water Research 13:409–419

Tolhurst TJ, Gust G, Paterson DM (2002) The influence on an extracellular polymeric substance (EPS) on cohesive sediment stability. In: Winterwerp JC, Kranenburg C (eds) Fine sediment dynamics in the marine environment—Proc. in Marine Science 5. Elsevier, Amsterdam, pp 409–425, ISBN: 0-444-51136-9

Torfs H (1994) Erosion of layered sand-mud beds in uniform flow. Proc. 24th Int. Conf. Coastal Eng., Kobe, Japan, 23–28 October 1994

Torfs H, Mitchener HJ, Huysentruyt H, Toorman E (1996) Settling and consolidation of mud/sand mixtures. Coastal Engineering 29:27–45

Tsai CH, Iacobellis S, Lick W (1987) Flocculation of fine-grained sediments due to a uniform shear stress. J Great Lakes Res 13:135–146

Uncles RJ, Stephens JA, Harris C (1998) Seasonal variability of subtidal and intertidal sediment distributions in a muddy, macrotidal estuary: the Humber-Ouse, UK. In: Black KS, Paterson DM, Cramp A (eds) Sedimentary processes in the intertidal zone. Geological Society, London, Special Publications, 139, 211–219

Underwood GJC, Kromkamp J (1999) Primary production by phytoplankton and microphytobenthos in estuaries. Advances in ecological research 29:93–153

van Ledden M (2002) A process-based sand-mud model. In: Winterwerp JC, Kranenburg C (eds) Fine sediment dynamics in the marine environment—Proc. in Mar. Science 5. Elsevier, Amsterdam, pp 577–594, ISBN: 0-444-51136-9

van Ledden M (2003) Sand-mud segregation in estuaries and tidal basins. Ph.D. Thesis, Delft University of Technology, The Netherlands, Report No. 03-2, ISSN 0169-6548, 217p

van Leussen W (1988) Aggregation of particles, settling velocity of mud flocs: a review. In: Dronkers J, van Leussen W (eds) Physical processes of estuaries. Springer, Berlin, pp 347–403

van Leussen W (1994) Estuarine macroflocs and their role in fine-grained sediment transport. Ph.D. Thesis, University of Utrecht, The Netherlands, 488p

van Wijngaarden M, Venema LB, De Meijer RJ, Zwolsman JJG, Van Os B, Gieske JMJ (2002a) Radiometric sand-mud characterisation in the Rhine-Meuse estuary, Part A: fingerprinting. Geomorphology 43:87–101

van Wijngaarden M, Venema LB, De Meijer RJ (2002b) Radiometric sand-mud characterisation in the Rhine-Meuse estuary, Part B: in situ mapping. Geomorphology 43:103–116

Waeles B, Le Hir P, Lesueur P (2008) A 3D morphodynamic process-based modelling of a mixed sand/mud coastal environment: the Seine Estuary, France. In: Kudusa T, Yamanishi H, Spearman J, Gailani JZ (eds) Sediment and ecohydraulics—Proc. in marine science 9. Elsevier, Amsterdam, pp 477–498, ISBN: 978-0-444-53184-1

Wallingford HR (1998) SandCalc: Marine sands calculator interface. Version 2.0 for Windows. Software by Tessela & HR Wallingford

Whitehouse RJS (1995) Observations of the boundary layer characteristics and the suspension of sand at a tidal site. Continental Shelf Research 15(13):1549–1567. doi:10.1016/0278-4343(95)00038-3

Whitehouse RJS, Manning AJ (2007) Mixing it: how marine mud and sand interact. Innovation & Research Focus, Institution of Civil Engineering, London, Thomas Telford Services Ltd 71:2

Whitehouse RJS, Soulsby R, Roberts W, Mitchener HJ (2000) Dynamics of estuarine muds. Telford, London, 232p

Widdows J, Blauw A, Heip CHR, Herman PMJ, Lucas CH, Middelburg JJ, Schmidt S, Brinsley MD, Twisk F, Verbeek H (2004) Role of physical and biological processes in sediment dynamics of a tidal flat in Westerschelde Estuary, SW Netherlands. Mar Ecol Prog Series 274:41–56

Williamson HJ (1991) Tidal transport of mud/sand mixtures: Sediment distributions – a literature review. HR Wallingford, Report SR 286

Williamson HJ, Ockenden MC (1993) Laboratory and field investigations of mud and sand mixtures. In: WangSam SY (ed) Advances in hydro-science and engineering, Proceedings of the First International Conference on Hydro-science and Engineering, Washington D.C. (7–11 June 1993), volume 1, pp 622–629

Winterwerp JC (1998) A simple model for turbulence induced flocculation of cohesive sediment. J Hyd Eng 36(3):309–326

Winterwerp JC (2006) On the sedimentation rate of cohesive sediment. In: Maa JP-Y, Sanford LP, Schoellhamer DH (eds) Coastal and estuarine fine sediment processes—Proc. in Marine Science, INTERCOH-2003. Elsevier, Amsterdam, pp 203–220

Winterwerp JC, van Kesteren WGM (2004) Introduction to the physics of cohesive sediment in the marine environment. In: van Loon T (ed) Developments in sedimentology, 56. Elsevier, Amsterdam, p 466p

Winterwerp JC, Manning AJ, Martens C, de Mulder T, Vanlede J (2006) A heuristic formula for turbulence-induced flocculation of cohesive sediment. Estuarine, Coastal and Shelf Science 68:195–207

Wolanski E (2007) Estuarine ecohydrology. Elsevier, Amsterdam, p 157p, ISBN: 978-0-444-53066-0

Appendix D

Paper: On the Consequence of a New Tidal Dock on the Sedimentation Regime in the Antwerpen Area of the Lower Sea Scheldt

Continental Shelf Research 31 (2011) S150–S164

Contents lists available at ScienceDirect

Continental Shelf Research

journal homepage: www.elsevier.com/locate/csr

Research papers

On the consequence of a new tidal dock on the sedimentation regime in the Antwerpen area of the Lower Sea Scheldt

Andrew J. Manning [a,*], Thijs Van Kessel [b], Johan Melotte [c], Marc Sas [c], Han Winterwerp [b,d], Emma L. Pidduck [a]

[a] Marine Physics Research Group, School of Marine Science and Engineering, University of Plymouth, Portland Square Building (A410), Plymouth, Devon PL4 8AA, UK
[b] Deltares, P.O. Box 177, 2600 MH Delft, The Netherlands
[c] International Marine and Dredging Consultants IMDC, Wilrijkstraat 37-45, B-2140, Antwerpen, Belgium
[d] Delft University of Technology, Department of Civil Engineering and Geosciences, Delft, The Netherlands

ARTICLE INFO

Article history:
Received 11 January 2009
Received in revised form
9 October 2010
Accepted 17 October 2010
Available online 21 November 2010

Keywords:
Cohesive sediment
Mass settling flux
Flocculation
Deurganckdok

ABSTRACT

Following the recent completion of the Deurganckdok (DGD) tidal dock in the Port of Antwerpen, Belgium, the Flemish government commissioned a programme of field surveys with the aim to identify potential changes in sediment properties. A significant feature of the Lower Sea Scheldt (LSS) is the presence of a turbidity maximum zone (TMZ) with depth-averaged suspended particulate matter (SPM) concentrations between 50 and 500 mg l^{-1}. This paper highlights aspects of the findings of the suspended sediment properties measured during HCBS1 (conducted in February 2005 prior to DGD construction) and HCBS2 (September 2006 when the dock was open and in operation) surveys, including data comparison.

Floc size (D) and settling velocity (W_s) spectra were measured nominally 0.6 m above the estuary bed every 10–20 min (turbidity dependent), using derivatives of the INSSEV instrument. This instrument permitted the accurate calculation of the following floc properties: effective density, dry mass, porosity and mass settling flux (MSF). To characterise the corresponding near-bed hydrodynamics, the turbulence was measured by a 3-D Acoustic Doppler Velocimeter and the turbidity monitored by an array of Optical Backscatter Sensors. All measurements were conducted for runs of 8–10 h in duration.

HCBS1 was conducted during neap tides in the winter, predominantly during the ebb phase, whilst HCBS2 experienced spring tides in the autumn with sampling generally on the flood. It is therefore important to note that only limited comparison between surveys and the different HCBS locations is possible. Even so, the survey revealed that, following construction of the DGD, turbidity was an order of magnitude higher in the DGD, than in the upper and lower Scheldt Estuary. It was also noted that that the DGD macrofloc fraction settled at $W_{s\,macro}=5.3$ mm s^{-1} in the TMZ, which was 1.4 and 3.2 mm s^{-1} quicker than the fastest settling macrofloc population observed in the LSS during the winter at neap tides and late summer at spring tides, respectively.

The HCBS surveys have highlighted the important role of low density macroflocs in the mass settling flux within the dock. At peak concentration in the DGD produced a MSF of 13.2 g m^{-2} s^{-1}; over an order of magnitude greater than observed within the HCBS1 TMZ. Within DGD the time series MSF of 30,200 mg m^{-2} s^{-1}, was five times the MSF observed at the dock entrance, and 19 times the MSF observed in the Scheldt estuary outside the dock (HCBS2_SS). Over 70% of the total MSF occurred during the TMZ passage through the dock on the flood.

The weaker currents present in the dock, particularly on the ebb, when combined with a near continual abundance of fast settling macroflocs, will tend to trap sediment in the basin, whilst near-bed turbulence damping will reduce the level of bed erosion in DGD. The sedimentation in the dock is stimulated by a significantly less turbid supply of cohesive sediment present in the Scheldt Estuary. It is proposed that the construction of a passive structure, such as a current deflecting wall, may reduce sediment entering the open tidal dock.

1. Introduction

The Scheldt Estuary is the southern branch of the Rhine – Meuse – Scheldt delta. Over the past 150 years, the delta has been subjected to much anthropogenic activity and commercial port development (Nihoul et al., 1978). With the increasing development, the delta has

* Corresponding author.
E-mail addresses: andymanning@yahoo.com, A.Manning@plymouth.ac.uk (A.J. Manning).

0278-4343/$ - see front matter © 2010 Elsevier Ltd. All rights reserved.
doi:10.1016/j.csr.2010.10.008

seen a rise in the number of container shipments; thus, the construction of the Deurganckdok (DGD) tidal dock in the Port of Antwerpen (Belgium).

The DGD has a length of 3000 m, a width of 400 m and a low water depth of 17 m and is located in the Lower Sea Scheldt (LSS), Belgium. In an attempt to evaluate the potential impact of DGD on the sedimentation regime in the Antwerpen region of the Lower Scheldt Estuary (LSE), the Flemish government commissioned a programme of field surveys. These surveys were referred to as "High-Concentration Benthic Suspensions" (HCBS), as the programme was predominantly concerned with their dynamic behaviour, and the conditions and locations of their occurrence in the LSS.

Within an estuarine environment, such as the Scheldt, there are changes in sediment concentration and shear, as well as regular erosion of material from the bed and subsequent settling back to the bed. The movement patterns of cohesive sediments within a tidal estuary create specific problems for the surrounding industry and commerce, which rely on the navigable waterways for access and transportation.

Environmentally, cohesive sediments are recognised as carriers of marine pollutants, which are of particular relevance to industrial waters, as per the Scheldt Estuary. Billen and Smitz (1978) reported that the Scheldt Estuary is heavily polluted by organic matter within the Antwerp region. Historically, the pollution arises from intense heterotrophic activity whereby oxygen is rapidly depleted and other oxidants are used by anaerobic metabolisms. Wollast (1973a) reported that increasing salinity in the Antwerp region of the estuary, produced flocculation and sedimentation of the organic matter. The effects of the organic pollutants have been examined in terms of the marine chemistry, biology and water quality (e.g. Billen, 1975; Wollast, 1973b; Somville and Pauw, 1982; de Jong and de Jonge, 1995).

As with most industrialised estuaries, numerical modelling is an important aspect of water management in the Scheldt Estuary (Fettweis and Sas, 1996). In 2006, a work plan was conceived for the development of a mud transport model for the estuary (see Van Kessel et al., 2006) in the framework of the "Long Term Vision" (LTV) (Winterwerp and De Kok, 2006). The purpose of this model was to support managers of the estuary with the solution to a number of managerial issues (IMDC, 2005). Information on suspended matter could potentially be archived on a geographical information system (GIS) database and enable the suspended particulate matter (SPM) concentration to be determined at different stages of the tide (Sterckx et al., 2007).

It is hence that a primary goal of the HCBS campaign was to establish fluxes of fine sediment in the river with the purpose to calibrate future numerical 3D cohesive sediment transport models of the LSS. Prediction of the transport of fine suspended sediment depends particularly on an accurate specification of the settling velocity and the mass settling flux (MSF). This can only be achieved by using field measurements of floc settling dynamics and bed sediment bed properties that can be implemented in sediment transport models (Winterwerp et al., 2006). This paper highlights aspects of the findings of the suspended sediment properties measured during HCBS1 (conducted in February 2005 prior to DGD construction) and HCBS2 (September 2006 when the dock was open and in operation) surveys, including data comparison. The floc data sets from each survey are compared with each other and also independent comparisons are made with a newly developed flocculation empirical model.

2. Study area

The Lower Sea Scheldt (Beneden Zeeschelde; LSS) is the stretch of the Scheldt Estuary between the Belgium–Dutch border and Rupelmonde, where the entrance channels to the Antwerp sea locks are located. The River Scheldt is situated in the Northeast of France, the West of Belgium and the Southwest of the Netherlands (Fig. 1), and drains a catchment of approximately 22,000 km^2. The tidal regime in the estuary is semi-diurnal with a mean tidal range of 3.85 m at the mouth, increasing up to 5.24 m at Schelle (91 km from mouth), making the estuary macrotidal. The tidal wave can penetrate 156 km inland from the mouth. DGD is located about 60 km upstream of the Scheldt Estuary mouth at Vlissingen. The average fresh water discharge is approximately 100 m^3 s^{-1}, with extreme values ranging between 20 m^3 s^{-1} during summer and 600 m^3 s^{-1} during winter (Belmans, 1991). The river flow tends to be a lesser influence on mixing in the Scheldt Estuary, when compared with the motion of the tide (Nihoul et al., 1978).

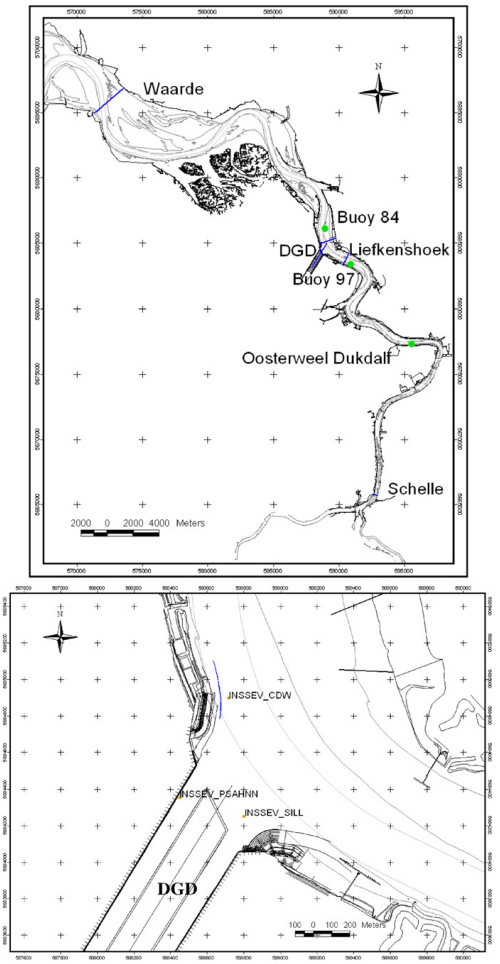

Fig. 1. A map of the Lower Sea Scheldt (top), with a close-up illustrating the DGD (below). The two main sampling locations are shown: in the LSS (INSSEV_CDW) and within DGD (INSSEV_PSAHNN). Supplementary data was collected at the DGD sill (INSSEV_SILL), but this is not presented in this paper.

Verlaan (1998) has reviewed the spatial distribution of bed sediments in the vicinity of LSS. The suspended sediment in the Scheldt Estuary consists of marine and terrestrial mud, the ratio of which tend to increase in downstream direction, with a particular rapid transition from terrestrial to marine mud near the Deurganckdok (Verlaan, 2000). The main navigation channel has a sandy bed, while the shallower areas (intertidal areas, mud flats, salt marshes) consist of sandy clay or even pure mud (Wartel et al., 2007). This part of the Scheldt is characterised by large horizontal salinity gradients, which can generate significant density currents between the river and the entrance channels to the locks, causing large siltation rates. It is to be expected that in the near future the DGD will also suffer from such large siltation rates, and may double the amount of dredging material to be dumped in the LSS (e.g. IMDC, 2004a). Another observation during recent years is that the composition of the sediment dredged at the Sill of Zandvliet became muddier, resulting in a strong increase in dumping volumes at the allocated dumping sites since 2002.

Previous measurements by Fettweis et al. (1998) at Prosperpolder (12 km seaward of DGD in Scheldt Estuary) suggested that the suspended mud concentrations correlated with the tides, spring-neap cycles and with the seasons. The mud concentration in Prosperpolder was, on average, higher during flood than during ebb, which was explained by the flood dominant character of the currents. Also, Fettweis et al. (1998) showed that the tide averaged SPM concentrations at Prosperpolder were 1.3–1.7 times higher during a spring tide than during a neap tide.

A significant feature of the LSS is the presence of a turbidity maximum zone (TMZ). Observations of SPM distributions by Chen et al. (2005a) have confirmed the existence of three TMZs in the Scheldt Estuary; a function of the resultant energy patterns demonstrated by the combined interaction of wave energy, tidal energy and river energy throughout the estuary. The first TMZ is a marine-dominated zone in the lower reaches near the estuary mouth; whilst the second is a more fluvial-dominated TMZ in the upper reaches of the estuary where SPM can reach 200–300 mg l^{-1}.

The third TMZ residing in the middle estuary is tide-dominated and of primary interest to the DGD project. Depth-averaged SPM concentrations typically range from 50 to 500 mg l^{-1} (IMDC, 2004b) and peak at few grams per litre (Chen et al., 2005a). This can compound the siltation problem, as sediment particles which become trapped within the TMZ, will experience a significantly longer residence time in the LSS region of the estuary. The entire estuary demonstrates a net increase in the mud stock. This net increase was completely at the expense of mud deposition in the access channels to the sluice gates giving access to the harbour of Antwerp (Wartel et al., 2007).

In the past, many surveys have been carried out to increase the understanding of the dynamics of fine sediment in the Lower Sea Scheldt. For example, seasonal floc characteristics were examined by Chen et al. (2005b) in the intertidal region. Also, salinity and turbidity have been continuously measured at Prosperpolder and Oosterweel. However, none of these measurements have been carried out in the lower 1 m of the water column.

3. Method and materials

Floc size (D) and settling velocity (W_s) spectra were measured nominally 0.6 m above the estuary bed, where the turbulent shearing tends to be the greatest (Mehta and Partheniades, 1975), at intervals of 10–20 min (turbidity dependent), using various derivatives of the video-based INSSEV – IN-Situ Settling Velocity – instrument (Fennessy et al., 1994; Manning and Dyer, 2002; Manning, 2006). This instrument permitted the accurate calculation of the following floc properties using specially developed algorithms (Fennessy et al., 1997; Manning, 2004a): effective density (ρ_e), floc mass and MSFs.

To characterise the corresponding near-bed hydrodynamics, the turbulent fluctuations were measured by a Nortek 3-D Acoustic Doppler Velocimeter (ADV), and the turbidity monitored by an array of Optical Backscatter Sensors (OBS). The flocculation and hydrodynamic measurements were conducted from the Dredging International workboat *Dommel*, which also housed all surface electronics and the image analysis suite. The vessel remained positioned at the survey site (the entrance to DGD) during the Eulerian sampling using specially deployed moorings.

4. HCBS1 Scheldt estuary observations

4.1. Overview

The High Concentrated Benthic Suspension 1 (HCBS1) survey was conducted on 17th February 2005. At this time the DGD was still under construction; the dock entrance created by excavating a section of the protective dyke that flanks the majority of the hinterland of the LSS. Breaching the dyke would then allow dredging vessels access to remove the sediment within DGD, which was deemed more efficient than other methods. The HCBS1 survey continuously covered the last part of the flood and on through the ebb to low water slack, and then the early part of the following flood during neap tidal conditions. The HCBS1 LSS survey location is indicated as 'INSSEV_CDW' in Fig. 1. For further HCBS1 campaign details, see Manning et al. (2007) and Manning and Sas (2006).

4.2. Time series observations

The variations in turbulent kinetic energy (TKE) time series, derived from turbulent shear stress measurements (Stapleton and Huntley, 1995) from the ADV, and SPM concentration, at the nominal floc sampling height of 0.6 m above the estuary bed, are illustrated in Fig. 2(b). The corresponding water depth and current velocities are shown in Fig. 2(a).

A TMZ was observed, as demonstrated by the peak in Fig. 2(b), at the sampling location between the approximate hours of 0830 and 0930. The TMZ displayed SPM concentrations of 150–300 mg l^{-1} in the vicinity of the estuary bed and remained in the Antwerpen region for just over 1 h. During this time, shear stress rose from 0.04 Pa within the TMZ, to 0.24 Pa. The mean floc size (Fig. 2c) responded by reducing from 313 μm down to less than 100 μm in the same time frame. Similarly, the W_{smean} reduced by nearly an order of magnitude during the early ebb from an initial TMZ settling rate of 2.3 mm s^{-1}. All mean floc properties were calculated as floc 'number' averages.

Once into the ebb, the flow fluctuated between a minimum of 0.4 m s^{-1} and a maximum velocity of 0.7 m s^{-1}. Outside of the TMZ, the SPM concentration remained, predominantly, under 100 mg l^{-1} to mid-ebb, and halved by low water (LW) slack at around 1430 h. As LW approached, and the current velocity slowed, the lower shear stress permitted the D_{mean} to grow to 200 μm and settle at a $W_{s\,mean}$ of about 1.2 mm s^{-1}.

As the tide turned, so the shear stress and SPM conditions returned to those more favourable for flocculation. The mean floc size at the early part of the flood increased from 250 to 375 μm, whilst their $W_{s\,mean}$ fell approximately 20% quicker.

The sample-averaged floc characteristics tend to indicate general trends, whereas the macrofloc and microfloc properties identify more discrete details about the dynamics of the settling floc population. Manning (2001) defines the critical size between these two fractions as 160 μm, and the macrofloc and microfloc properties were determined for each complete INSSEV floc population. Fig. 2(d) illustrates the SPM distribution, representative of all flocs within the macrofloc and microfloc sub-populations.

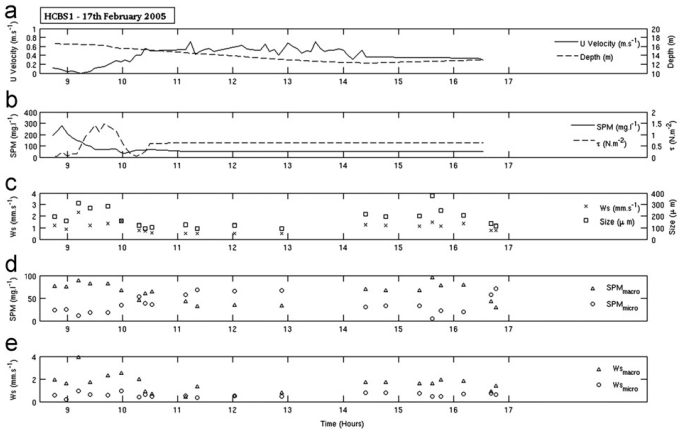

Fig. 2. Time series of floc properties in the Lower Sea Scheldt outside Deurganckdok on 17th February 2005. (a) Shear stress τ and SPM, (b) water depth and alongstream current velocity, (c) Mean floc size and settling velocity, (d) Macrofloc and microfloc SPM distribution, and (e) Macrofloc and microfloc settling velocity.

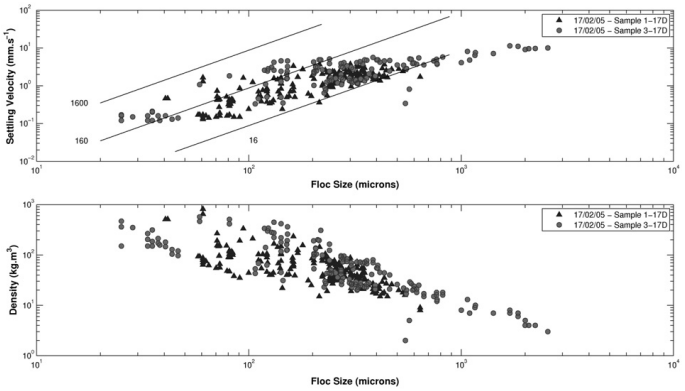

Fig. 3. Settling and density floc characteristics for Sample 1-17D and Sample 3-17D, acquired during HCBS1. Diagonal lines on D vs. W_s scatterplot (a) represent contours of constant Stokes equivalent effective density: top = 1600 kg m^{-3}, middle = 160 kg m^{-3} and bottom = 16 kg m^{-3}.

The denser microflocs are seen to dominate the SPM during the turbulent mid-ebb conditions. They comprised between 40% and 70% of the total SPM and had $W_{s\,micro}$ values of 0.4–0.6 mm s^{-1} (Fig. 2e). Contrastingly, in the TMZ, the faster settling macroflocs ($W_{s\,macro}$ = 3.9 mm s^{-1}) represented over three quarters of the floc mass.

4.3. Detailed floc spectra

To provide more information about the floc populations present at various times in the tidal cycle, a number of spectral floc distributions will be presented.

4.3.1. Floc samples 1-17D and 3-17D

Fig. 3 shows the floc individual floc population for samples 1-17D and 3-17D. The former was collected at 0845 h, just prior to the main body of the turbidity maximum reaching the DGD sampling station, accounting for a concentration of 195 mg l^{-1}. The decreasing flow of high water slack conditions resulted in a turbulent shear stress of only 0.042 Pa. Fig. 3(a) illustrates spherical-equivalent dry mass weighted floc size plotted against settling velocity for the sample. The diagonal lines represent contours of constant floc effective density (units = kg m^{-3}). Fig. 3(b) demonstrates the effective density of flocs plotted against floc size to show a general relationship.

The smallest microflocs were dense (ρ_e up to 818 kg m^{-3}), predominantly mineral aggregates, with voids comprising less than one third of the floc internal structure. As the macroflocs grew, they became progressively less dense and more fragile; with the largest 1-17D macroflocs having effective densities less than 10 kg m^{-3}. When comparing the settling velocities, the macrofloc fraction fell at an average rate of 1.9 mm s^{-1}, whereas the microflocs were settling approximately four times slower.

Sample 3-17D (see Fig. 3) was obtained at 0912 h, from within the turbidity maximum as it was ebbing seaward through the LSS near the site of the proposed DGD. The faster flowing ebb current produced a shear stress of 0.24 Pa. When coupled with an SPM concentration of 277 mg l^{-1}, this appears to have produced ideal conditions to stimulate flocculation.

The main difference between the two distributions is that 80% of the 3-17D floc population were large macrofloc with an average diameter of 507 μm. Individually, the floc size of these 127 aggregates ranged from 202 to 2559 μm in diameter with individual settling velocities of between 1 and 11 mm s^{-1}.

5. HCBS2 observations

The HCBS2 surveys were conducted in September 2006, once the DGD was open and in use by container vessels. The HCBS2 campaign comprised three separate surveys: the first day was at the same general location as the HCBS1 survey in the Scheldt Estuary (HCBS2_SS); the second survey had the survey vessel positioned at the entrance above the sill of the dock (INSSEV_SILL on Fig. 1); and the final survey was located within DGD (HCBS2_DD). Further technical details on HCBS2 are reported by Manning and Melotte (2007).

5.1. HCBS2_SS (Scheldt estuary)—time series

The HCBS2 INSSEV survey was conducted in the same general location as the HCBS1 survey. The HCBS2_SS survey experienced spring tidal conditions. The transition from ebb to flood at the start of the run experienced highly turbulent conditions, with τ increasing from a shear stress of 1.1 Pa to a maximum of 1.4 Pa (Fig. 4b) and the SPM was between 35 and 45 mg l^{-1}. These highly turbulent conditions produced mean floc sizes of ~85 μm and W_{smean} of ~0.6 mm s^{-1}. At this time, the floc mass SPM% was weighted 3:1 in favour of the microflocs.

Thereafter, the shear stress decreased to moderately turbulent flow with τ of 0.6–0.9 Pa. The times when the stress was at the lower values, coincided with the peaks in turbidity. Unlike the HCBS1 survey, the autumn spring tide ambient conditions did not seem to produce a distinctly obvious TMZ in the LSS. The first peak in turbidity (SPM = 134 mg l^{-1}) occurred at approximately 0800 h, just after low water; the mean floc size had now grown by 50% to a D_{mean} of 135 μm, but the $W_{s\,mean}$ remained unchanged at 0.8 mm s^{-1}. The last SPM peak (116 mg l^{-1}) occurred at 1335 (approx. HW), but the fastest settling and largest flocs observed during HCBS2_SS were not formed until 1400 (HW+0:30) when the SPM had decreased to 74 mg l^{-1}. Interestingly, the quickest W_{smacro} was only 2.1 mm s^{-1}; nearly half the macrofloc fall rate observed in the LSS during the winter at neap tides (see Section 4.2).

5.1.1. Floc samples 2-5SS and 14-5SS

Sample 2-5SS (Fig. 5) was collected at 0737 h, just minutes prior to local LW in the LSS near Deurganckdok. The ebb to flood transition meant that the water column at this time was at its most turbulent at the sampling location. A maximum floc diameter of 172 μm, was a reflection of a τ of 1.4 Pa coupled with a concentration of only 35 mg l^{-1}. The 2-5SS settling velocities spanned from 0.1 to 2 mm s^{-1}. When comparing the settling velocities, the macrofloc fraction fell at an average rate of 0.3 mm s^{-1}, whereas the smaller microflocs were settling at a velocity three times quicker. This was reflected in the microflocs effective densities (ρ_{e_micro} ranging from 200 to 850 kg m^{-3}) generally being over an order of magnitude greater than the macroflocs (ρ_{e_macro} from 10 to 30 kg m^{-3}). One can assume that these low-density macroflocs are predominantly organically based.

Also plotted in Fig. 5 is INSSEV sample 14-5SS, acquired towards the end of the HCBS2_SS survey during the afternoon ebb at 1356 h (HW+0:26) when the SPM was 78 mg l^{-1}. This was only two thirds of the turbidity observed during any of the three concentration peaks (see Fig. 4). However, the 14-5SS population exhibits flocs which were more than double the diameter of those present during the turbidity peaks.

The macrofloc sizes ranged from 164 to 451 μm; the largest of the run. This growth was a consequence of the turbulence (τ = 0.38 Pa) becoming more conducive for flocculation. Whereas, the earlier more turbid water column was nearly twice as turbulent and thus created a certain amount of floc break-up. The less turbulent flow allowed the macroflocs, settling at 4 mm s^{-1} (double the speed of the microflocs), to dominate over three quarters of the entrained floc mass. This produced a significantly higher mass settling flux

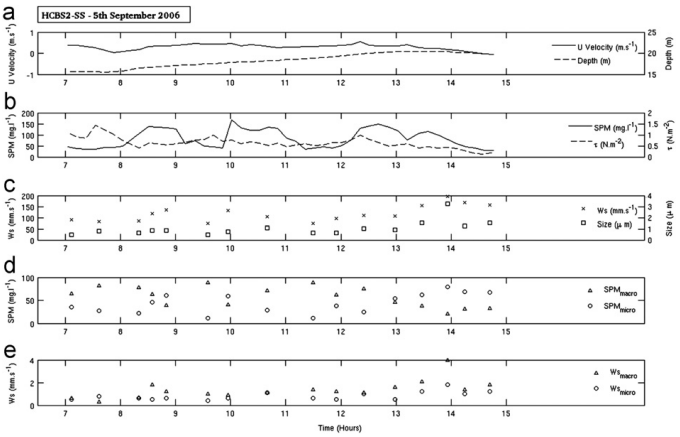

Fig. 4. Time series of floc properties from the Lower Sea Scheldt (HCBS2_SS) on 5th September 2006. (A) Shear stress τ and SPM, (B) water depth and alongstream current velocity, (C) Mean floc size and settling velocity, (D) Macrofloc and microfloc SPM distribution, and (E) Macrofloc and microfloc settling velocity.

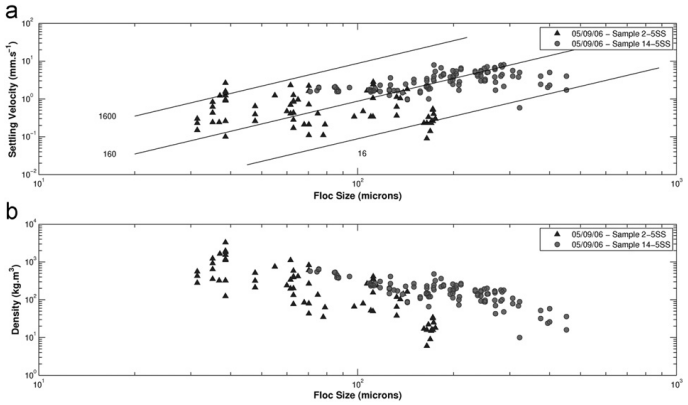

Fig. 5. Settling and density floc characteristics for Sample 2-5SS and Sample 14-5SS, acquired during the HCBS2SS survey. Diagonal lines on D vs. W_s scatterplot (a) represent contours of constant Stokes equivalent effective density: top = 1600 kg m^{-3}, middle = 160 kg m^{-3} and bottom = 16 kg m^{-3}.

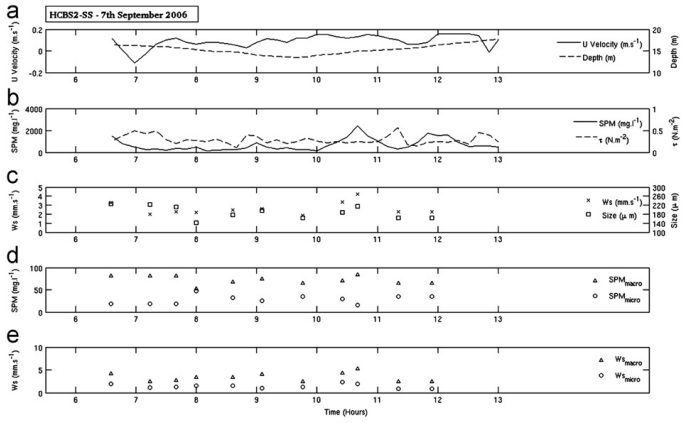

Fig. 6. Time series of floc properties from the Lower Sea Scheldt (HCBS2_DD) on 7th September 2006. (a) Shear stress τ and SPM, (b) water depth and alongstream current velocity, (c) Mean floc size and settling velocity, (d) Macrofloc and microfloc SPM distribution, and (e) Macrofloc & microfloc settling velocity.

(MSF) than from within the earlier higher concentration and more turbulent environments. The MSF issues are assessed later in Section 6.4.

5.2. HCBS2_DD (inside dock)—time series

The HCBS2_DD survey was conducted from within the DGD itself (indicated by 'INSSEV_PSAHNN' on Fig. 1). Data sampling comprised the latter half of the morning ebb, followed by the flood. The shear stress was predominantly under 0.45 Pa for most of the sampling run (Fig. 6).

SPM concentrations in the DGD basin were predominantly an order of magnitude greater than those encountered outside the dock in the Scheldt Estuary channel, or even at the dock entrance. The TMZ concentration peaked at 2400 mg l^{-1}, producing significant floc growth in DGD resulting in a D_{mean} of 215 μm and a $W_{s\,mean}$ of 4.2 mm s^{-1}. In terms of the larger size fraction, the macrofloc fell at $W_{s\,macro}$ of 2.5–5.3 mm s^{-1}, whilst the smaller microflocs settled at comparatively slower 0.9–2.3 mm s^{-1}. The corresponding ρ_{e_macro} ranged between 63 and 164 kg m^{-3}, which suggests these large macroflocs were porous and fragile in construction.

A second lesser peak of 1770 mg l^{-1} appeared an hour after the main TMZ. In between these turbidity peaks, the lowering of the concentration allowed turbulent kinetic energy to produce the highest observed HCBS2_DD shear stress (τ = 0.56 Pa), which resulted in D_{mean} and W_{smean} values reducing by one third and a half, respectively.

5.2.1. Floc samples 6-7DD and 9-7DD

The low turbulent environment during the latter part of the morning ebb in DGD (τ = 0.27 Pa), when the SPM was still only

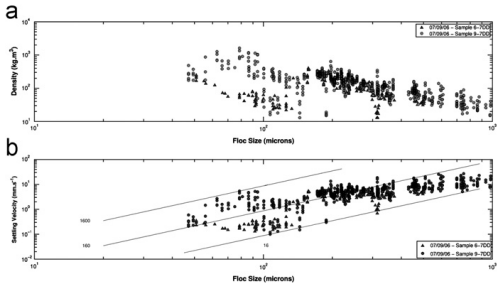

Fig. 7. Settling and density floc characteristics for Sample 6-7DD and Sample 9-7DD, acquired inside DGD during HCBS2_DD. Diagonal lines on D vs. W_s scatterplot (a) represent contours of constant Stokes equivalent effective density: top= 1600 kg m^{-3}, middle=160 kg m^{-3} and bottom=16 kg m^{-3}.

690 mg l^{-1}, produced a distinctly bi-modal floc distribution (Fig. 7). The population was equally apportioned in terms of numbers of microflocs and macroflocs. Most of the former were settling at under 0.5 mm s^{-1}. The second mode comprised macroflocs from 180 to 503 μm in size and settling velocities ranging between 0.7 and 6.6 mm s^{-1}. These 6-7DD macroflocs represented three quarters of the floc mass, settling collectively at a $W_{s\,macro}$ of 4 mm s^{-1}.

Within the main TMZ, the D vs. W_s scatterplot 9-7DD demonstrates a partially distorted dual-modal population; both modes demonstrating very different floc characteristics. The first mode was composed of microflocs up to 150 μm in diameter and these represented a third of the total population. This fraction was a combination of both fast settling (W_s ~4–5 mm s^{-1}), dense (ρ_e up to 1550 kg m^{-3}) microflocs, principally mineral in composition; together with some more loosely constructed (ρ_e ~14 kg m^{-3}), organically based microflocs, settling at 0.1–0.2 mm s^{-1}. The remaining population were macroflocs with an average diameter of 268 μm. Individually, the floc size of these 2402 aggregates ranged from 177 to 986 μm in diameter and had individual settling velocities ranging between 3 and 7 mm s^{-1}.

6. Comparison with an empirical flocculation model

To facilitate the floc data acquired from the Scheldt Estuary/DGD surveys to be assessed in terms of applicability to settling flux predictions, particularly for sediment transport modelling applications, this section compares the parameterised Scheldt Estuary floc data, with generic trends generated by a new model for estuarine flocculation developed by Manning and Dyer (2007): the Manning floc settling velocity empirical (EM) model (also see Baugh and Manning, 2007 for applications of the EM). The EM is calibrated for the Tamar (UK), Gironde (France) and Dollard (The Netherlands) estuaries, and therefore provides a generic inter-comparison with typical floc settling values from these estuarial locations.

The EM algorithms provides estimates of the macrofloc ($D > 160$ μm) and microfloc ($D < 160$ μm) settling velocities (i.e. $W_{s\,macro}$ and $W_{s\,micro}$), whilst a third algorithm predicts the relative distribution of particulate matter throughout each macrofloc and microfloc sub-population. This latter function is termed the SPM_{ratio} (Manning, 2004a) and is a dimensionless parameter calculated by dividing the percentage of SPM_{macro} by the percentage of SPM_{micro} for each floc population.

6.1. Macrofloc settling velocity

Fig. 8 shows $W_{s\,macro}$ values calculated from the INSSEV data for the HCBS1 survey. Qualitatively, the data depicts a similar general pattern to those of the macrofloc settling velocity curves as predicted by the EM algorithm. When comparing the data, the macroflocs in the lower shear stress regions were seen to settle significantly faster than the general algorithm estimates. The fastest HCBS1 macrofloc settled at 3.9 mm s^{-1}, which was 60% quicker than the model algorithm predicted (with the same nominal SM concentration). The HCBS1 $W_{s\,macro}$ were much more in-step with the EM algorithm predictions, once τ exceeded 0.4 Pa. The EM under-estimated the time series averaged $W_{s\,macro}$ value for the HCBS1 by 20%.

Fig. 8 also shows $W_{s\,macro}$ values calculated from the INSSEV data for each HCBS2 survey. As with the HCBS1 flocculation survey data, there is a reasonable general agreement with the data and the general shape of the macrofloc settling velocity curves as predicted by the EM.

There are, however, numerous occasions, particularly during the HCBS2 surveys at the dock location, where the macroflocs are settling between 50% and 80% faster than the MFSV predicted rates. At the extreme, the INSSEV measured $W_{s\,macro}$ was three times faster than the EM estimate.

In terms of the time series (TS) averages, the HCBS2_SS INSSEV measurements found the $W_{s\,macro-TS}$ to be 1.4 mm s^{-1}, which was similar to the EM estimate. The model under-estimation rose to one third once inside the dock, where the predicted $W_{s\,macro-TS}$ was 2.4 mm s^{-1}, compared with the observed $W_{s\,macro-TS}$ of 3.5 mm s^{-1}.

From these points we can draw a number of conclusions about the macrofloc settling dynamics:

- $W_{s\,macro}$ during spring tide conditions were generally higher than the EM estimates. This suggests improved flocculation efficiency within the LSS when compared with the "benchmark" estuaries.
- The $W_{s\,macro}$ progressively rose beyond those predicted by the EM, the further the one ventured from the main Scheldt Estuary (e.g. outside the dock) and into the more turbid, less turbulent environment of the newly constructed Deurganckdok.

6.2. Microflocs settling velocity

The Lower Scheldt Estuary microfloc settling velocities ranged between 0.2 and 1.8 mm s^{-1} (Fig. 9). These $W_{s\,micro}$ values were similar to those estimated by the general EM. For example, the EM gave just a 2% under-estimate in $W_{s\,micro}$ for the HCBS2_SS time series where the INSSEV $W_{s\,micro-TS}$ was 0.8 mm s^{-1}. The microfloc settling rates from the more quiescent environments tended to exceed the predicted values, but as with the macroflocs, showed slightly better agreement with the model in the higher stress region.

Within the DGD basin (HCBS2_DD), the more flocculation conducive, turbulent conditions allowed the microflocs, as well as the macroflocs, to form into aggregates that typically demonstrated $W_{s\,micro}$ which fell one third faster than those observed at the dock entrance, and nearly double the speed in the LSS. The $W_{s\,micro-TS}$ of 1.5 mm s^{-1} in DGD was more than twice the equivalent value estimated by the model. Again, as with the macroflocs, this demonstrates why good quality spectral floc size and settling velocity data is required in order to calibrate numerical models and accurately tune algorithms to local conditions.

6.3. Suspended particulate matter concentration ratio

The majority of the HCBS1 floc populations were dominated by the larger, faster settling macroflocs as SPM_{ratio}s of 2–19 indicate (Fig. 10). These ratios correspond to the macroflocs comprising 67–95% of the suspended matter. From an initial inspection of Fig. 11, it appears that the HCBS1 Scheldt floc mass division shows a wide range of scatter when compared to the SPM_{ratio_EM} values. This is primarily due to the fact that the EM SPM_{ratio} algorithm

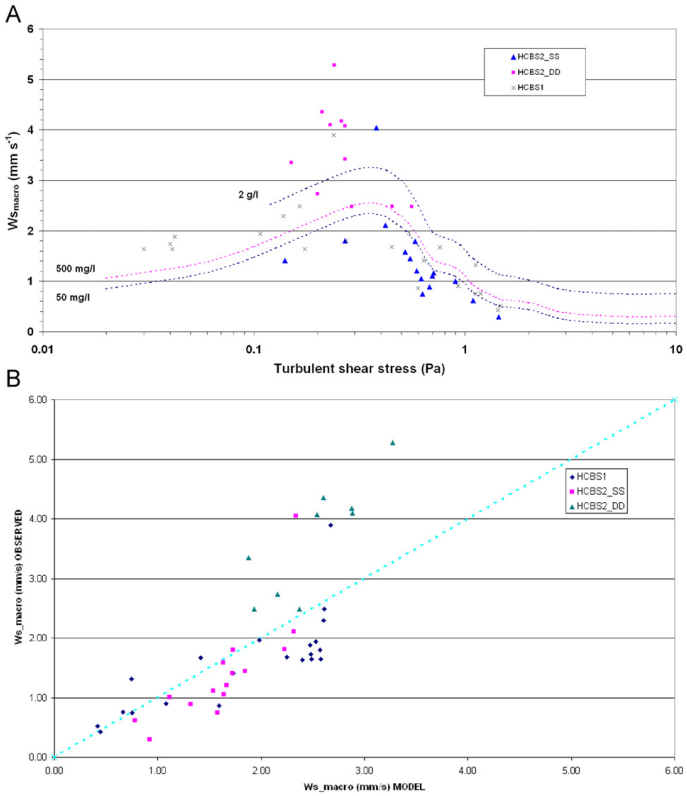

Fig. 8. (A) Plot of $W_{s\,macro}$ from each survey day plotted against the corresponding shear stress. Contours indicate $W_{s\,macro}$ values predicted by the empirical flocculation model (EM) for constant values of SPM concentration. (B) A direct comparison of the Observed and the EM predeicted $W_{s\,micro}$ values.

(the dotted line) is based solely on SPM concentration from a data set, which spanned more than three orders of magnitude, whereas the February 2005 Scheldt Estuary floc survey conditions did not produce concentrations in excess of 300 mg l^{-1}.

The more turbulent spring tide conditions of HCBS2_SS meant the Scheldt Estuary floc populations were dominated by the smaller microflocs, as the SPM_{ratio}s of 0.3–0.74 indicate (up to three quarters of the SPM). In the DGD basin, SPM concentrations rose by an order of magnitude during the TMZ passage and the SPM_{ratio} rose to 5.6; equivalent to three quarters of the floc mass attributed to the macroflocs. This further reinforces the argument that the DGD environment was conducive for macrofloc growth.

Initially, there appears to be a wide amount of scatter when comparing the SPM_{ratio} observations with the EM curve. However, when the time series averages are computed for each day, it shows only +1% difference between the EM estimated values and the $SPM_{ratio-TS}$ for HCBS2_SS. This time series deviation rose to a 9% over-estimate in DGD; all of which are acceptable in terms of predictive modelling.

6.4. Mass settling flux prediction comparisons

The output from three EM component algorithms can be combined to estimate the total mass settling flux, MSF (with the units of mg m^{-2} s^{-1}), can be calculated

$$MSF\__{EM} = \left[\left(1-\frac{1}{1+SPM_{ratio\,EM}}\right)(SPMW_{s\,macro\,EM})\right] + \left[\frac{1}{1+SPM_{ratio\,EM}}(SPMW_{s\,micro\,EM})\right] \quad (1)$$

This is a very practical way of expressing the inter-relationship between the three core EM algorithms and can easily be implemented in mathematical simulation models. This type of expression describes the fundamental aspects of estuarine flocs (i.e. their effect on deposition rates) throughout the changing levels of turbulent mixing and particle entrainment, as opposed to a formulation which just has floc settling velocity or size as the dependent variable.

The other comparative floc parameterisation used is a constant settling velocity 0.5 mm s^{-1} (denoted by $W_{s-0.5}$); typically representative of values obtained from gravimetric analysis from field settling tube instruments. These constant fall rates are often used in numerical modelling as they are simple to implement.

6.4.1. LSS mass settling flux

The cumulative total flux for the 21 HCBS1 INSSEV samples was 4445 mg m^{-2} s^{-1} (Fig. 11a). A peak settling flux of 1326 mg m^{-2}

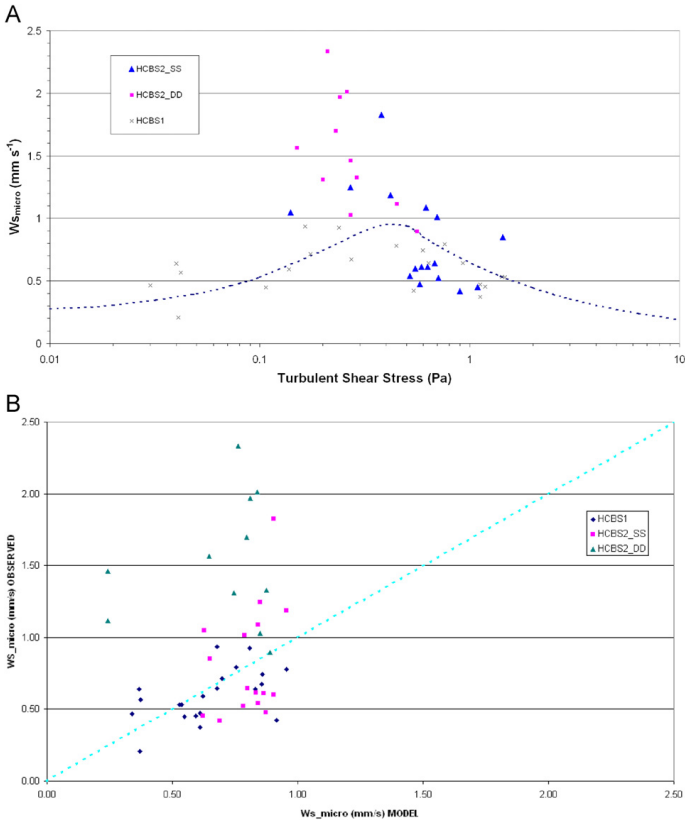

Fig. 9. (A) Plot of $W_{s\ micro}$ from each survey day plotted against the corresponding shear stress. Contours indicate $W_{s\ macro}$ values predicted by the empirical flocculation model (EM) for constant values of SPM concentration. (B) A direct comparison of the Observed and the EM predeicted $W_{s\ micro}$ values.

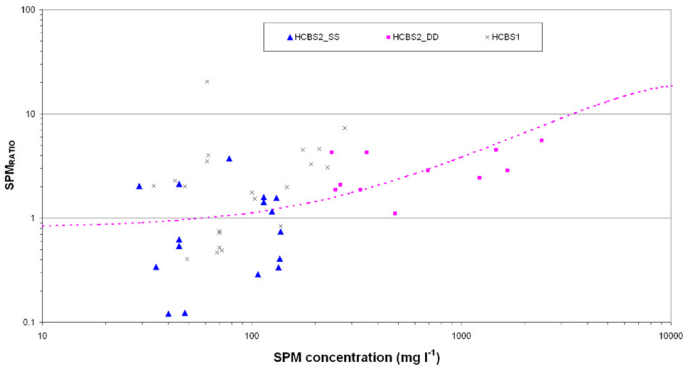

Fig. 10. Plot of SPM_{ratio} from each survey day plotted against the corresponding SPM concentration. Dotted line indicates SPM_{ratio} values predicted by the empirical flocculation model (EM).

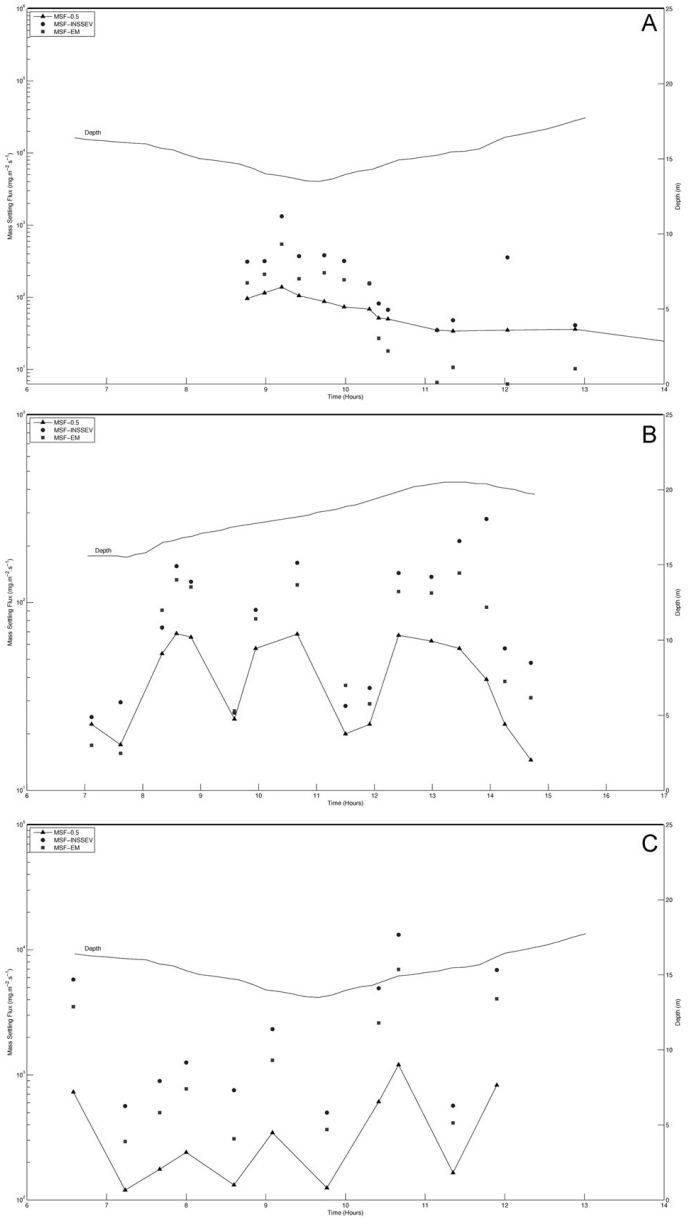

Fig. 11. Time series of INSSEV mass settling flux and corresponding water depth from: (A) HCBS1, (B) HCBS2_SS and (C) HCBS2_DD. Values of MSF predicted by the empirical flocculation model (EM) and applying a constant settling velocity of 0.5 mm s^{-1}.

s^{-1}, sample 3-17D (see Fig. 3), was measured during the TMZ passage. The microflocs encompassed only 12% of the floc mass. This translated into the fast settling macroflocs contributing 97% of the flux; a product of a $W_{s\,macro}$ of 3.9 mm s^{-1}, which was more than four times faster than the $W_{s\,micro}$. To put this all into context, this total MSF was nearly ten times greater than the value computed by the use of an estimated mean settling velocity of 0.5 mm s^{-1}.

The EM shows a reasonable agreement with the pattern of the measured MSF during the early and latter stages of the ebb, although the EM values were lower in each case. The EM only tends to estimate 25–30% of the actual flux during the highly turbulent mid-phase of the ebb, however this was the period when turbidity was at its lowest. This was the only instance when the W_s_0.5 approximation came close to simulating the actual MSF variations. Taking the HCBS1 time series as a whole, the EM approach calculated half of the total cumulative flux, whilst the constant W_s_0.5 only estimated one quarter.

At the same nominal LSS site during the more turbulent spring tides, the total HCBS2_SS sampling run settling flux was only 1600 mg m^{-2} s^{-1} (Fig. 11b). This was nearly a three-fold reduction from the neap tide HCBS1 run. Similarly, the run peak settling flux of 278 mg m^{-2} s^{-1} (sample 14–5SS) was approaching one fifth of the neap tide TMZ peak flux.

Interestingly, the 14–5SS flux figure was significantly higher than within the higher concentration environments present earlier in the tidal cycle, so what could promote this improvement in settling flux? The main difference is that the shear stress for sample 14-5SS (τ=0.38 Pa) was in the range Manning (2004b) terms as the "optimum" range for stimulating constructive inter-particle contacts. For these particular floc samples acquired outside of the Deurganckdok in the Scheldt Estuary, it highlights that the shear stress is a more significant catalyst at furthering floc growth than the simple increase of SPM concentration.

The EM estimated three quarters of the total HCBS2_SS settling flux, whilst the W_s_0.5 parameter calculated less than half the measured flux. The only time when the W_s_0.5 approach showed any kind of reasonably accuracy, was during extremely turbulent episodes which meant the floc settling velocities were consequently severely restricted to the 0.5 mm s^{-1} settling velocity range.

6.4.2. HCBS2_DD mass settling flux

Within DGD (HCBS2_DD) the time series MSF of 30,200 mg m^{-2} s^{-1}, (Fig. 11c) was 19 times the MSF observed in the Scheldt estuary outside the dock (HCBS2_SS). Over 70% of the total MSF occurred during the TMZ passage through the dock on the flood.

The majority of the matter suspended during the entire HCBS2_DD sampling run in Deurganckdok was in the form of macroflocs. For example, the superior dynamics of the 6-7DD macroflocs (see Fig. 7), formed in the latter stages of the ebb (τ=0.27 Pa and SPM=690 mg l^{-1}), contributed 2092 g m^{-2} s^{-1} of the 2322 g m^{-2} s^{-1} sample MSF. In fact the 15 largest macroflocs, represented 7% of the MSF, equivalent to two-thirds of the flux contributed by all the microflocs. The important role of the macrofloc dynamics was further demonstrated during the peak settling flux of 13.2 g m^{-2} s^{-1} (measured an hour after HW; sample 9–7DD), where one fifth of the MSF were accredited to extremely large macroflocs ranging from 700 to 986 μm in diameter (see Fig. 7) and had W_s > 5–27 mm s^{-1}.

The EM algorithms improved its estimate of the HCBS2_DD total MSF by predicting nearly two thirds of the MSF measured by INSSEV. This was a distinct predictive improvement over the Lower Sea Scheldt estuarial environment. The improved EM estimate for HCBS2_DD was partly due to providing improved flux estimations during the TMZ conditions. The performance of the W_s_0.5 approach continued to decrease, by now only estimating 4524 mg m^{-2} s^{-1} of the total MSF present within the HCBS2_DD time series.

7. HCBS1 and HCBS2—inter-comparisons

To enable inter-comparisons between HCBS1 and the various HCBS2 observations, and in particular establish the effects of the DGD construction, there needs to be some degree of commonality between the measurements in the LSS. HCBS1 was in the winter, when the organic matter content may be assumed to be low, while HCBS2 was in the warmer autumn climate and the organic matter content could have been greater. Furthermore, HCBS1 was conducted during neap tides predominantly during the ebb phase, whilst HCBS2 experienced higher spring tides with sampling generally on the flood. There were also, most probably, different river discharges during each campaign. All of these criteria will have a potential impact on the flocculation process.

Within the Antwerpen region, however, the peak HCBS2_SS spring tide SPM concentrations were of a similar range to those observed during the HCBS1 neap tide deployment. The SPM did not exceed 300 mg l^{-1} during any of the deployments within the LSS (i.e. outside of the dock). Also, the ambient current velocities were of a similar range during both HCBS1 and HCBS2_SS surveys in the LSS. A comparison would be fully justified if external forcing conditions were similar (i.e. river flow and tidal range), therefore only a limited inter-comparison between surveys and the various HCBS locations is possible.

7.1. HCBS1 and HCBS2_SS

During the HCBS1 survey in the LSS, there was a clearly defined turbidity maximum present in the estuary around local HW. At the time of the TMZ advection through the sampling location, the τ was about 0.24–0.34 Pa and the peak SPM concentration varied between 220 and 280 mg l^{-1} at the INSSEV floc sampling height (i.e. 0.6 m above the bed). This was in contrast to HCBS2_SS which did not observe a well defined TMZ at the same LSS site outside of the dock, and the maximum concentrations were only half those observed during HCBS1.

Small flocs (D_{mean}=110–135 μm) were observed at the SPM peaks in HCBS2_SS (e.g. samples 4, 8, 11-5SS), which compared with a D_{mean} of 313 μm during the TMZ in HCBS1 (sample 3-17D), which is nearly a factor of three difference in diameter. These mean floc sizes were of a similar order to the maximum floc sizes observed by Chen et al. (2005b) in the vicinity of intertidal mud flats during inundation in the Scheldt Estuary.

The HCBS1 TMZ flocs were settling more than twice as fast as the flocs created during the HCBS2_SS SPM peaks. These smaller, slower settling HCBS2_SS flocs observed during the maximum concentrations can be primarily attributed to the more turbulent water column associated with these events which instigated a certain amount of floc break-up and at that time the macroflocs only represented one quarter of the SPM.

Throughout both time series, however, both the HCBS1 and HCBS2_SS macrofloc settling velocities were very similar ($W_{smacro-TS}$ ~1.5 mm s^{-1}). In terms of time series averaged MSF, HCBS2_SS was 102 mg m^{-2} s^{-1}, which was only half the MSF from the same LSS site from HCBS1. This was a result of more mass present as macroflocs during the quiescent neaps than the more turbulent springs. This demonstrates that a knowledge of floc mass distribution is equally as important as fall velocity data.

7.2. HCBS1 and HCBS2_DD

SPM concentrations within the DGD basin (HCBS2_DD) were significantly higher than those encountered outside the dock in the

Scheldt Estuary channel (during both the winter and autumn surveys) or even at the dock entrance. The TMZ occurred at LW+1 producing a peak concentration of 2400 mg l^{-1}, and floc conducive τ values ranging between 0.2 and 0.43 Pa for approximately 85% of the 6.5 h time series.

During the TMZ advection through DGD, the W_{smean} was 4.2 mm s^{-1}, nearly 50% quicker than from within the HCBS1 TMZ. In the less turbid, but more turbulent HCBS2_SS, D_{mean} were significantly smaller within the TMZ than both the HCBS2_DD and HCBS1.

Although the DGD macrofloc at peak turbidity were half the average diameter of the HCBS1 TMZ, the macrofloc represented the majority of the SPM for both TMZs. However, within DGD TMZ the macrofloc fraction ($W_{s\,macro}$=5.3 mm s^{-1}) settled more than 1 mm s^{-1} faster than the comparative HCBS1 TMZ ($W_{s\,macro}$= 3.9 mm s^{-1}). Thus, the peak SPM in DGD produced a MSF of 13.2 g m^{-2} s^{-1}; over an order of magnitude greater than observed within the HCBS1 TMZ.

In terms of the complete time series average the HCBS2_DD D_{macro} at 259 μm, were just 26 μm smaller than HCBS1. The HCBS2_SS D_{macro} were 90 μm smaller than the HCBS1 winter flocs. Biologically these findings were surprising, as one would expect there to be more biology present during the milder autumn climate and thus a higher level of extracellular polymeric substances (EPS) to adhere to the sediment particles. Therefore the differences in diameters may be explained more by physics, in terms of turbulence and SPM concentration.

The HCBS_DD $W_{s\,macro-TS}$ of 3.5 mm s^{-1}, was twice the average macrofloc fall rate encountered throughout the HCBS1 time series, which in terms of depositional and accretion rates is highly significant. When the macrofloc mass and settling components are combined as the mass settling flux, the much greater SPM concentrations present within the DGD basin produced a time series total MSF of 27 g m^{-2} s^{-1}; most were due to the macroflocs. In fact the HCBS1 flux was only one seventh of cumulative total settling flux observed within the dock. If we average the MSF throughout each sampling run, the dock environment demonstrated a MSF_{mean} of 3.4 g m^{-2} s^{-1}, which was an order of magnitude greater than the mean flux in the LSS (both winter and autumn surveys) and at the DGD entrance.

8. Long-term implications of sedimentation in a tidal dock

8.1. Synopsis of the dock environment

The HCBS surveys have highlighted the importance of the role of the low density macroflocs in the mass settling flux within the dock. This observation concurs with a hypotheses offered by Mehta and Lott (1987) and Van Leussen (1994). Glasgow and Lucke (1980) suggest that macroflocs are also highly delicate entities, and could be easily progressively broken down when passing through regions of higher turbulent shear stress, and returned back to their component microfloc sub-structure. This can lead to continual particle re-cycling and re-entrainment (Mehta and Partheniades, 1975). Therefore the predominantly low turbulent, highly turbid DGD is the ideal environment for long-term macrofloc production.

The sediment transport cycle in DGD predominantly produces large, rapid settling macroflocs. This depositional pattern can produce CBS layers, which eventually lead to the formation of a dense benthic nepheloid layer in the base of the dock. This extremely stratified, turbid, near-bed environment, can potentially lead to the damping of turbulent energy and produce drag reduction effects (Dyer et al., 2004). This can all lead to enhanced flocculation and reductions in erosion.

The resultant weaker currents present in the dock, will tend to trap sediment in the basin, as it is unable to transport out of dock on the less energetic ebb which is not capable of re-entraining sufficient sediment. Turbulence damping will reduce the level of bed erosion. With a net influx of sediment entering the dock, from the less turbid Scheldt Estuary, high accretion rates are, therefore, a potential long-term possibility in DGD. This will arise, primarily, from the mobility of the nepheloid layer forming in the basin, which will tend to produce a poorly consolidated bed. This suggests that the sedimentation within the dock, is not keeping pace with the rate of infilling.

Benthic nepheloid layers characteristically contain fluid mud in which sediment settling rates are governed (hindered) by the rate of dewatering of the slurry. For example, in the highly turbid Severn Estuary (UK) there are numerous lutoclines present (e.g. Kirby, 1986) giving the water column a "step-like" turbidity profile (Whitehouse et al., 2000). The near-bed lutocline is predominantly a result of hindered settling below the lutocline where turbulence damping processes result in low energy conditions and minimal local mixing (Dyer, 1986). In contrast, the less distinct lutoclines in the upper water column are more characteristic of higher-energy hydrodynamics. Minimal vertical mixing occurs there in these surface layer; a function of the non-linear dependence of the diffusive flux on the vertical concentration gradient (Dyer, 1986). As fluid mud density rises it becomes increasingly non-Newtonian, and behaves rheologically, as a pseudo-plastic; i.e. they have high viscosity at low shear rates, but their viscosity reduces at high shear rates. Fluid mud can acquire apparent yield strength at very high concentrations. Fluid mud also moves more as gravity flows, which act independently of the ambient hydrodynamic field.

Thus, a tidal dock with no lock gates has advantage of continual vessel access, but permits a continual supply of sediment (albeit a fairly low concentration) to the dock from the estuary. The surveys showed that the TMZ concentration in the LSS was over an order of magnitude lower than in the dock. This illustrates that a steady supply of a low concentration of cohesive sediment, continually feeding into a tidal basin over several months, is all that is required to quickly instigate the infilling of an anthropogenically manufactured tidal dock. This could demonstrates the estuary trying to achieve a natural sedimentation equilibrium. Estuary sedimentation process seem to respond much more rapidly and extremely (i.e. the process seems to accelerate) when an artificial form of geomorphology/bathymetry is introduced (e.g. a dock or dredged navigation channel).

8.2. Design criteria

The main consideration for dock and harbour entrance design is nautical navigation, and for optimal access, the entrance should be as wide as possible (Barneveld and Hugtenburg, 2008). DGD is 500 m wide. This however maximises the volume of sedimentation within the dock and at the entrance. This becomes partly an economic decision for dock designers and port manager: dock gates limit access, but restrict sedimentation. Open tidal docks promote continual access by both vessels and sediment. The latter decreases the navigable depth basin, thus potentially requiring more costly maintenance dredging, which over time will interfere with dock operations. The intercomparison between the estuary and dock environments, although not fully rigorous, indicated that SPM concentrations and settling fluxes were over an order of magnitude higher in the basin than in the LSS.

To achieve a reduction in sedimentation rate the causes for the sedimentation have to be known. Sediment can be transported into an estuarine dock/harbour by various transport mechanisms (Booij, 1986; Langendoen, 1992). In the long-term, it is better to prevent sediment from entering the basin in the first place. An overview of

methods to reduce harbour siltation are provided by PIANC (2006). At present, there is one solution which is gaining popularity, which can reduce sedimentation in an open tidal dock (such as DGD) without restricting access. These are current deflecting walls (CDW; Winterwerp et al., 1994; Christiansen, 1997). This is a passive structure, usually in the form of a curved (in the horizontal plane), vertical screen. It is generally positioned at the seaward end of a dock or harbour entrance. The aim of a CDW is to alter the flow pattern, typically creating a vortex over the width of the basin entrance which results in a reduction of sediments being transported into the dock (Winterwerp, 2005).

Scale physical model tests have demonstrated that a CDW can produce reductions ranging from 25% to 45% of the inflow of near-bed water during a flood (Kuijper et al., 2005), with the only negative component being a 5% increase of the total water exchange around high slack water (van Leeuwen, 1999). During 1991, a CDW was constructed at the entrance of the tidal Köhlfleet harbour in Hamburg (Germany) and in-situ studies showed that siltation in the Köhlfleet could be reduced by about 40% (Kuijper et al., 2005; Winterwerp, 2005). If such a scheme was applied to DGD, it would slow the rate at which sediment enters the basin from the estuary and could potentially halve the observed mean settling fluxes within the dock from 3400 to 1700 mg m^{-2} s^{-1}. This may eventually slow down the formation of fluid mud, or even decrease the thickness of these layer, thus improving chance for greater bed consolidation; this would eventually reduce the time the sediment remains in suspension and is mobile throughout the dock. A potential location for a CDW at DGD is indicated in Fig. 1.

Further research has indicated that when a CDW is combined with a special sill design, this reduction is potentially increased by a further 10–25%, whereby even more of the flow is guided into the upper water column and thus assisting to reduce siltation (Hofland et al., 2001). This structure would produce even further potential long-term benefits to an open tidal dock like DGD. It could curb the excessive flocculation observed within the dock, through a gradual reduction in SPM. This could limit the formation of fluid mud in DGD, by keeping the average settling fluxes under 800–1000 mg m^{-2} s^{-1} and closing the gap between the MSF in the basin with those observed at the dock entrance and in the LSS. This would bring about an improvement in the longitudinal sedimentary balance between the artificial basin and the natural estuarine environments. A CDW can only function when the sediment concentration in the higher parts of a river is substantially less than in the lower parts; the observations in the Scheldt Estuary indicate that it fits this criteria.

8.3. Modelling considerations

When correctly designed and positioned, a passive structure such as a CDW, encourages the water that flows into a dock/harbour during rising tide predominantly from the less turbid upper water layer. Hereby the influx of sediment-laden near-bed water is substantially decreased (Crowder et al., 1999; Hofland et al., 2001). Therefore the design and locating of a sediment-restriction barrier is crucial to reduce siltation within the basin, whilst not creating adverse geomorphological effects in the surrounding estuary. This objective can only be accurately achieved through numerical and/or physical modelling.

A new fractal-based flocculation model (e.g. Kranenburg, 1994) has been derived by Winterwerp et al. (2006) and calibrated for the LSS. It is also possible to tune the EM (see Section 6) for the various dock and estuarial environments. However, in order to accurately validate and calibrate depositional models, high quality floc data is required. Instruments such as INSSEV, which can simultaneously measure both D and W_s of large, fragile macroflocs is a pre-requisite. Disruptive sampling techniques (e.g. gravimetric analysis of field settling tube water samples) will favour the slower settling microfloc fraction. Whilst optical devices, such as particle sizers, only measure D and therefore can only estimate floc settling velocity, by assuming a floc density. Also optical particle sizers struggle to operate reliably in turbid waters.

The collection of data before and after dock construction is strongly recommended. This provides a "benchmark" for comparison, when assessing potential effects of a dock construction. Although the comparison presented in this paper are not ideal, as many of the conditions were different (tides, season), the data within the estuary before and after dock construction demonstrated similar floc trends, whilst very different floc patterns were observed in DGD. The data reinforced the importance of role of turbulence in flocculation; stimulated macrofloc formation within the dock for more than three quarters of a tidal cycle.

The time series averaged MSF (3400 mg m^{-2} s^{-1}) measured in the dock, when placed in the context of the DGD dimensional scales, would equate to an annual siltation rate of 129 MT per year within the dock. However, modelling predictions estimate the siltation in DGD as only 1–2 MT per year; this is a difference of nearly two orders of magnitude. This discrepancy can be partly explained by a number of factors: primarily INSSEV captures the gross settling flux instead of the net settling flux (i.e. it neglects the upward transport resulting from turbulent mixing). There could have been a high level of continual resuspension present during the early stages of the DGD opening, which would result in a poorly consolidated bed (see the review by Merckelbach, 2000) and result in the high observed MSFs within the dock. Bed sediments from the Scheldt Estuary have been previously assessed via flume studies by Torfs (1994a, b, 1995).

The sedimentation rates predicted by numerical models are heavily influenced by the depositional parameterisation employed. For example, using a Telemac 3D numerical model to test parameterisation sensitivity, Spearman and Manning (2008) found that the use of the classic Krone (1962) depositional formula, produced significantly different siltation results to Winterwerp's (2007) alternative approach. The latter parameterisation assumes that: (i) there is no critical shear stress for deposition; (ii) deposition on the bed occurs at a rate, $W_s \times \mathrm{SPM}$, regardless of the applied shear stress; (iii) deposition occurs simultaneously with erosion; and (iv) changes in the bed are actually caused by net deposition or erosion. Therefore, depending upon the model settings, the MSF may or may not always equal the deposition flux. Van Maren et al. (2009) have applied the Winterwerp et al. (2006) fractal flocculation model to further investigate sediment transport within DGD and predicts that siltation rates are expected to decrease when the dock is fully excavated compared to the initial half-opened dock. Further surveys would provide a greater insight into the long-term siltation within DGD.

9. Summary

The measurements conducted within DGD revealed that the further one moved away from the main Scheldt Estuary channel and ventured into DGD itself, the magnitudes of the TKE and current velocity on both the ebb and flood decreased. In fact during the entire DGD sampling period, the shear stress fell within the zone Manning (2004b) classifies as creating the optimum contacts and impact levels for maximising flocculation potential (τ values generally falling between 0.2 Pa and 0.38–0.43 Pa) for about 85% of the 6.5 h sampling duration.

HCBS1 was conducted during neap tides in the winter predominantly during the ebb phase, whilst HCBS2 experienced spring tides in the autumn with sampling generally on the flood. Therefore only a limited inter-comparison between surveys and the various HCBS

locations is possible. Even so, the survey showed that turbidity was an order of magnitude higher in DGD than those in the Scheldt Estuary. The DGD macrofloc fraction settled at $W_{s\,macro}=5.3$ mm s^{-1} in the TMZ, which was quicker than in the LSS TMZ.

The HCBS surveys have highlighted the importance of the role of the low density macroflocs in the mass settling flux within the dock. At peak concentration in DGD produced a MSF of 13.2 g m^{-2} s^{-1}; over an order of magnitude greater than observed within the HCBS1 TMZ. Within DGD the time series MSF of 30,200 mg m^{-2} s^{-1}, was 19 times the MSF observed in the Scheldt estuary outside the dock (HCBS2_SS). Over 70% of the total MSF occurred during the TMZ passage through the dock on the flood.

The weaker currents present in the dock, particularly on the ebb, when combined with a near-continual abundance of fast settling macroflocs, will tend to trap sediment in the basin. Near-bed turbulence damping will reduce the level of bed erosion in DGD. The sedimentation in the dock is stimulated by a significantly less turbid supply of cohesive sediment present in the Scheldt Estuary. The construction of a passive structure, such as a current deflecting wall, may reduce sediment entering the open tidal dock. Based on previous research, such a device may curb the excessive flocculation observed within the dock, through a gradual reduction in the suspended sediment concentration. This could limit the formation of fluid mud in DGD, by keeping the average settling fluxes under 800–1000 mg m^{-2} s^{-1} and hence closing the gap between the MSF in the basin with those observed at the dock entrance and in the LSS. The accurate design, positioning and estuary-wide impact of a passive structure can only be determine through applied modelling, of which some benchmark sedimentary and hydrodynamic data (i.e. pre-dock construction) is a necessity.

Acknowledgements

The authors would like to thank the Ministry of the Flemish Community for the funding of the project, and their permission to publish the results. Staff from Ms Zeeschelde and Gems Int. are acknowledged for collaboration during the field measurements. Peter Ganderton (Uni. Plymouth), George Graham (Uni. Plymouth), Francesca Mietta (TU Delft) and the crew of the Dredging International workboat *Dommel* are all thanked for their assistance during the INSSEV surveys. The authors would also like to thank Edward Steele (Uni. Plymouth) for data plotting assistance.

References

Barneveld, H.J., Hugtenburg, J., 2008. Feasibility study for implementation of sedimentation reduction measures in river harbours. In: Dohmen, Janssen, Hulscher (Eds.), River, Coastal and Estuarine Morphodynamics: RCEM 2007. Taylor Francis Group, London, pp. 1187–1192, ISBN:978-0-415-45363-9.

Baugh, J.V., Manning, A.J., 2007. An assessment of a new settling velocity parameterisation for cohesive sediment transport modelling. Continental Shelf Research, doi:10.1016/j.csr.2007.03.003.

Belmans, H., 1991. Discharges in the Scheldt basin. Month and year averaged values 1981–1990. Ministry of the Flemish Community. Antwerpse Zeehavendienst (in Dutch).

Billen, G., 1975. Nitrification in the Scheldt Estuary (Belgium and The Netherlands). Estuarine, Coastal, and Marine Science 3, 79–89.

Billen, G., Smitz, J., 1978. Mathematical model of water quality in a highly polluted estuary. In: Nihoul, J.C.J. (Ed.), Hydrodynamics of Estuaries and Fjords. Proceedings of the ninth international liège colloquium on ocean hydrodynamics, vol. 23 of Elsevier Oceanography Series, Issue 23 of Oceanography and Marine Biology Series, pp. 55–62.

Booij, R., 1986. Measurements of exchange between river and harbour. Technical Report, Delft University of Technology, (in Dutch).

Chen, M., Wartel, S., Eck, B., Dirk, M., 2005a. Suspended matter in the Scheldt Estuary. Hydrobiologia 540 (1–3), 79–104.

Chen, M.S., Wartel, S., Temmerman, S., 2005b. Seasonal variation of floc characteristics on tidal flats, the Scheldt estuary. Hydrobiologia 540, 181–195. doi:10.1007/s10750-004-7143-6.

Christiansen, H., 1997. Erfahrungen mit der Strömungsumlenkwand. Hansa 134 (12) (in German).

Crowder, R.A., Kirby, R., Falconer, R.A., 1999. Model Study to reduce siltation in harbours using current deflecting walls. In: Proceedings of the coastal engineering.

Dyer, K.R., 1986. Coastal and estuarine sediment dynamics. Wiley & Sons, Chichester 342 p.

Dyer, K.R., Christie, M.C., Manning, A.J., 2004. The effects of suspended sediment on turbulence within an estuarine turbidity maximum. Estuarine, Coastal and Shelf Science 59, 237–248.

de Jong, D.J., de Jonge, V.N., 1995. Dynamics and distribution of microphytobenthic chlorophyll-*a* in the Western Scheldt estuary (SW Netherlands). Hydrobiologia 311, 21–30.

Fennessy, M.J., Dyer, K.R., Huntley, D.A., 1994. INSSEV: an instrument to measure the size and settling velocity of flocs in-situ. Marine Geology 117, 107–117.

Fennessy, M.J., Dyer, K.R., Huntley, D.A., Bale, A.J., 1997. Estimation of settling flux spectra in estuaries using INSSEV. In: Burt, N., Parker, R., Watts, J. (Eds.), Cohesive Sediments—Proceedings of INTERCOH Conference (Wallingford, England). John Wiley & Son, Chichester, pp. 87–104.

Fettweis, M., Sas, M., 1996. Cohesive sediment transport models and integral water management: applications to the Scheldt estuary. Water 15 (90), 249–256.

Fettweis, M., Sas, M., Monbaliu, J., 1998. Seasonal, neap-spring and tidal variation of cohesive sediment concentration in the Scheldt Estuary, Belgium. Estuarine, Coastal and Shelf Science 47 (1), 21–36.

Glasgow, L.A., Lucke, R.H., 1980. Mechanisms of deaggregation for clay-polymer flocs in turbulent systems. Industrial and Engineering Chemistry Fundamentals 19, 148–156.

Hofland, B., Christiansen, H., Crowder, R.A., Kirby, R., Van Leeuwen, C.W., Winterwerp, J.C., 2001. The current deflecting wall in an estuarine harbour. In: Proceedings of the XXIX IAHR congress, 16–21 September, 2001, Tsinghua University Press, Beijing, China.

IMDC, 2004a. Environmental impact assessment of the deposit of dredged material in the Lower Sea Scheldt. IMDC Report for The Port of Antwerp and AMT.

IMDC, 2004b. Description of the proposed measurements of high concentrated mud suspensions. Report no. 16EB/04/13, 112 p.

IMDC, 2005. Long term vision in the Lower Sea Scheldt: Field Measurements High-Concentration Benthic Suspensions (HCBS) Report 2.1: Deurganckdok 16/02/2005. I/RA/11265/05.009/MSA.

Kirby, R., 1986. Suspended fine cohesive sediment in the Severn estuary and Inner Bristol channel. Reptort ESTU-STP-4042, Department of Atomic Energy, Harwell, UK.

Kranenburg, C., 1994. The fractal structure of cohesive sediment aggregates. Estuaries, and Coastal Shelf Science 39, 451–460.

Krone, R.B., 1962. Flume studies of the transport of sediment in estuarial shoaling processes final report, Hydraulic Engineering and Sanitary Engineering Research Laboratory, University of California, Berkeley, USA.

Kuijper, C., Christiansen, H., Cornelisse, J.M., Winterwerp, J.C., 2005. Reducing harbor siltation. II: case study of Parkhafen in Hamburg. Journal of Waterway, Port, Coastal and Ocean Engineering 131 (6), 267–276.

Langendoen, E.J., 1992. Flow patterns and transport of dissolved matters in tidal harbours. Dissertation, Delft University of Technology.

Manning, A.J., 2001. A study of the effects of turbulence on the properties of flocculated mud. Ph.D. Thesis. Institute of Marine Studies, University of Plymouth, 282 p.

Manning, A.J., 2004a. Observations of the properties of flocculated cohesive sediment in three western European estuaries. Journal of Coastal Research Special Issue, SI 41, 70–81.

Manning, A.J., 2004b. The observed effects of turbulence on estuarine flocculation. Journal of Coastal Research Special Issue, SI 41, 90–104.

Manning, A.J., 2006. LabSFLOC—a laboratory system to determine the spectral characteristics of flocculating cohesive sediments. HR Wallingford Technical Report, TR 156.

Manning, A.J., Dyer, K.R., 2002. The use of optics for the in-situ determination of flocculated mud characteristics. Journal of Optics A: Pure and Applied Optics 4, S71–S81.

Manning, A.J., Dyer, K.R., 2007. Mass settling flux of fine sediments in Northern European estuaries: measurements and predictions. Marine Geology 245, 107–122. doi:10.1016/j.margeo.2007.07.005.

Manning, A.J., Martens, C., de Mulder, T., Vanlede, J., Winterwerp, J.C., Ganderton, P., Graham, G.W., 2007. Mud floc observations in the turbidity maximum zone of the Scheldt Estuary during neap tides. Journal of Coastal Research, SI 50, 832–836.

Manning, A.J., Melotte, J., 2007. Report 9: Settling velocity INSSEV summer 2006. IMDC Technical report of flocculation and hydrodynamic measurements at Deurganckdok location, Lower Scheldt Estuary (Port of Antwerp, Belgium). Project: field measurements—high-concentration benthic suspensions (HCBS2), Doc. Ref.:I/RA/11291/06.102/MSA, 193 p.

Mehta, A.J. and Lott, J.W., 1987. Sorting of fine sediment during deposition. In: Proceedings of the specialty conference. Advances in understanding coastal sediment processes. American Society of Civil Engineers, New York, pp. 348–362.

Mehta, A.J., Partheniades, E., 1975. An investigation of the depositional properties of flocculated fine sediment. J. Hydrol. Res. 92 (C13), 361–381.

Merckelbach, L.M., 2000, Consolidation and strength evolution of soft mud layers, Ph.D. Thesis, Delft University of Technology; also: Delft University of Technology, Faculty of Civil Engineering and Geosciences, Communications on Hydraulic and Geotechnical Engineering, Report 00-2, ISSN 0169-6548.

Manning, A.J., Sas, M., 2006. Report 3: settling velocity of the sediment – INSSEV. IMDC Technical report of flocculation and hydrodynamic measurements at Deurganckdok location, Lower Scheldt Estuary (Port of Antwerp, Belgium). Project: field measurements – high-concentration benthic suspensions (HCBS1), Doc. Ref.:I/RA/11265/05.016/MSA, 212 p.

Nihoul, J.C.J., Rondaya, F.C., Peters, J.J., Sterling, A., 1978. Hydrodynamics of the Scheldt Estuary. In: Nihoul, J.C.J. (Ed.), Hydrodynamics of estuaries and fjords. Proceedings of the ninth international Liège colloquium on ocean hydrodynamics, vol. 23 of Elsevier Oceanography Series, Issue 23 of Oceanography and Marine Biology Series, pp. 55–62.

PIANC, 2006. Minimising harbour siltation. Report of the International Navigation Association, PIANC Working Group 43.

Somville, M., de Pauw, N., 1982. Influence of temperature and river discharge on water quality of the western Scheldt Estuary. Water Research 16 (8), 1349–1356.

Spearman, J., Manning, A.J., 2008. On the significance of mud transport algorithms for the modelling of intertidal flats. In: Kudusa, T., Yamanishi, H., Spearman, J., Gailani, J.Z. (Eds.), Sediment and Ecohydraulics—Proceedings in Marine Science,, vol. 9. Elsevier, Amsterdam, pp. 411–430 ISBN: 978-0-444-53184-1.

Stapleton, K.R., Huntley, D.A., 1995. Sea bed stress determinations using the inertial dissipation method and the turbulent kinetic energy method. Earth Surface Proceedings and Landforms 20, 807–815.

Sterckx, S., Knaeps, E., Bollen, M., Trouw, K., Houthuys, R., 2007. Retrieval of suspended sediment from advanced hyperspectral sensor data in the Scheldt estuary at different stages in the tidal cycle. Marine Geodesy 30 (1–2), 97–108.

Torfs, H., 1994a. Erosion of mixed cohesive/non-cohesive sediments in uniform flow. In: Burt, N., Parker, R., Watts, J. (Eds.), Cohesive Sediments—Proc. of INTERCOH Conference (Wallingford, England). John Wiley & Son, Chichester, pp. 245–252.

Torfs, H., 1994b. Erosion of layered sand – mud beds in uniform flow. In: Proceedings of the 24th international conference on coastal engineering, 23–28 October, Kobe, Japan, pp. 3360–3368.

Torfs, H., 1995. Erosion of mud/sand mixtures. Ph.D. Thesis, Katholieke Universiteit Leuven (Belgium), Department of Civil Engineering.

Van Kessel, T., Vanlede J., Bruens, A., 2006. Development of a mud transport model for the Scheldt estuary in the framework of LTV. WL Delft Hydraulics and WL Borgerhout report Z4210.

Van Leussen, W., 1994. Estuarine macroflocs and their role in fine-grained sediment transport. Ph.D. thesis, University of Utrecht, The Netherlands, 488 p.

Van Maren, D.S., Winterwerp, J.C., Sas, M., Vanlede, J., 2009. The effect of dock length on harbour siltation. Continental Shelf Research 29 (11–12), 1410–1425, doi:10.1016/j.csr.2009.03.003.

van Leeuwen, C.W., 1999. The current deflecting wall in a tidal harbour with density influences. M.Sc. Thesis, Delft University of Technology.

Verlaan, P.A.J., 1998. Mixing of marine and fluvial particles in the Scheldt estuary. Ph.D. Thesis, Delft University of Technology, The Netherlands.

Verlaan, P.A.J., 2000. Marine vs. fluvial bottom mud in the Scheldt Estuary. Estuarine, Coastal and Shelf Science 50, 627–638.

Wartel, S., Chen, M., van Eck, G.T.M., van Maldegem, D., 2007. Influence of harbour construction on mud accumulation in the Scheldt Estuary. Aquatic Ecosystem Health & Management 10 (1), 107–115.

Whitehouse, R.J.S., Soulsby, R., Roberts, W., Mitchener, H.J., 2000. Dynamics of estuarine muds. Thomas Telford Publications, London 232 p.

Winterwerp, J.C., 2005. Reducing harbor siltation. I: methodology. Journal of Waterway, Port, Coastal and Ocean Engineering 131 (6), 258–266.

Winterwerp, J.C., 2007. On the deposition flux of cohesive sediment. In: Maa, J.P.-Y., Sanford, L.P., Schoellhamer, D.H. (Eds.), Estuarine and Coastal Fine Sediment Dynamics—INTERCOH 2003. Elsevier, Amsterdam, pp. 209–226.

Winterwerp, J.C., De Kok, J., 2006. Plan van aanpak LTV-slib: modelinstrumentarium t.b.v.beheersproblematiek slib. Intern document no. Z4210.95—M756/01.

Winterwerp, J.C., Eysink, W.D., Kruiningen, F.E.van, Christiansen, H., Kirby, R., Smith, T.J., 1994. The current deflecting wall: a device to minimise harbour siltation. The Dock and Harbour Authority 74 (849), 243–246 March/April 1994.

Winterwerp, J.C., Manning, A.J., Martens, C., de Mulder, T., Vanlede, J., 2006. A heuristic formula for turbulence-induced flocculation of cohesive sediment. Estuarine, Coastal and Shelf Science 68, 195–207.

Wollast, R., 1973a. Modelling of biological and chemical processes in the Scheldt Estuary. In: Nihoul, J.C.J. (Ed.), Hydrodynamics of estuaries and fjords. Proceedings of the ninth international liège colloquium on ocean hydrodynamics, vol. 23 of Elsevier oceanography series, Issue 23 of Oceanography and Marine Biology Series, pp. 63–78.

Wollast, R., 1973B. Circulation, accumulation et bilan de masse dans l'estuaire de L'Escaut. Rapport de synthese 1972. Commission Interministerielle de la Politique Scientifique (Belgium, in French).

Appendix E

Book Chapter: Flocculation Dynamics of Mud:Sand Mixed Suspensions

Chapter 6

Flocculation Dynamics of Mud: Sand Mixed Suspensions

Andrew J. Manning, Jeremy R. Spearman,
Richard J.S. Whitehouse, Emma L. Pidduck,
John V. Baugh and Kate L. Spencer

Additional information is available at the end of the chapter

http://dx.doi.org/10.5772/55233

1. Introduction

Sediments present in muddy estuaries and tidal inlets are regarded as being predominantly cohesive. These muds are usually composed of both clay and silt minerals combined with organic matter (Winterwerp and van Kesteren, 2004), and with the exception of very low particle concentrations or extremely high energy flow conditions, muddy particles occur as a spectra of floc sizes (D) when entrained into suspension (Kranck and Milligan, 1992).

In reality, natural sediments tend to comprise a mixture of different particle sizes, non-cohesive sediment including fine sands and, because of the interaction between these different fractions, the mixture behaves in a different way than the constituent parts (Whitehouse et al., 2000). Uncles et al. (1998) found that the proportion of mud and sand in subtidal and intertidal sediments can vary both temporally and spatially (e.g. Uncles et al, 1998). Fig. 1 shows an example of mud and sand in close proximity in the Eden Estuary (east coast of Scotland).

Very little is quantitatively known about how mixtures of cohesive and non-cohesive sediments, of different ratios and concentrations, interact whilst in suspension in turbulent flows and the effect this has on the resultant flocs formed and their flocculation properties, in particular the settling velocity. This has important implications for sediment transport modelling. Drawing on key literature and new data, this chapter will provide an overview of mixed sediment flocculation dynamics and how they can influence sediment transport.

The first part of this chapter reviews the theoretical aspects relating to the flocculation of mud:sand mixtures. It commences with a brief review of flocculation processes (2), followed by an overview of segregation environments verses flocculating suspensions (3), and then the biological influences on mixed sediment flocculation are summarised (4). The second part of

Figure 1. Sand and muddy sediments in close proximity, Eden Estuary, Fife (east coast of Scotland).

the chapter (5-7) draws on the findings of recent empirical studies assessing mixed sediment floc behaviour. The laboratory experimental protocols and findings are reported with floc data in spectral and parameterised formats presented and discussed. The potential implications of mud:sand flocculation on sediment transport modelling are also discussed (8-9).

2. Flocculation factors

From a sediment transport perspective, knowledge of the settling rate of sediments in suspension is vital in determining depositional fluxes and sediment transport rates. Sand is a non-cohesive material and therefore does not flocculate in pure sand suspensions. The settling velocity (Ws) is generally proportional to the square of the particle size or diameter (D). Conversely, mud is strongly cohesive and flocculates forming small, compact microflocs as well as larger, more porous macroflocs (Eisma, 1986; Manning, 2001; Manning and Dyer, 2002a,b) – Fig. 2. Flocculation is a dynamically active process which readily reacts to changes in hydrodynamically generated turbulent shear stresses (τ) (e.g. Krone, 1962; Parker et al., 1972; McCave, 1984; van Leussen, 1994; Winterwerp, 1998; Manning, 2004a), suspended particulate matter (SPM) concentration, together with salinity, mineralogy and biological stickiness.

http://dx.doi.org/10.5772/55233

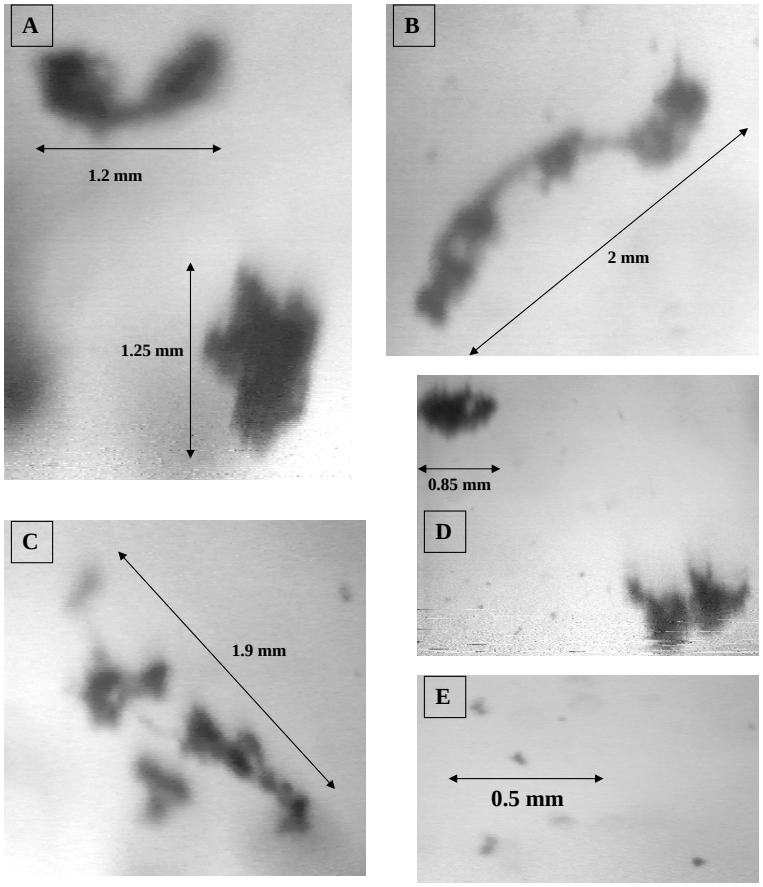

Figure 2. A selection of floc images from a predominantly muddy origin. A) A ragged cluster-type macrofloc (top) and a simple stringer composed of two macroflocs interlinked by organic fibres (bottom); B) a 'string of pearls' type macrofloc; C) a long interlinked stringer comprising two clustered macroflocs; D) ragged macroflocs settling; and E) a selection of small slow settling microflocs, some of which are probably the result of macrofloc fracturing and subsequent break-up during a turbulent event which exceeded the original macrofloc structural integrity threshold.

Flocculation can significantly alter the sediment transport patterns throughout an estuary, and floc properties can vary both in time and space. For example, Manning et al. (2006) showed that during spring tidal conditions in the Tamar Estuary (UK), macroflocs can typically reach 1-2 mm in diameter. These flocs demonstrate settling velocities up to 20 $mm.s^{-1}$, but their effective densities ρ_e (i.e. the floc bulk density less the water density) are generally less than 50 $kg.m^{-3}$, which means they are prone to break-up when settling through a region of high turbulent shear.

There are, however, many estuarial environments where mud and fine sand co-exist as a single mixture (Mitchener et al., 1996) and this creates the potential for these two fractions to combine and exhibit some degree of interactive flocculation (Manning et al., 2007, 2009). The erosion and consolidation of mixtures of mud and sand has been thoroughly reviewed (Williamson, 1991; and Whitehouse et al, 2000), and there have been some studies that have examined mixed sediment settling (e.g. Dankers et al., 2007). However, very little investigation has been devoted to the potential flocculation that may occur when mud and sand mixtures are entrained into suspension, as it was not considered to be an important factor. This could be a valid assumption for a segregational environment, where the mud and sand do not combine into a single matrix.

When we refer to 'mixed sediment flocculation' in this chapter, we are primarily referring to suspension mixtures of mud (typically composed of clay minerals and fine silts up to 63 μm in diameter together with organic matter) and predominantly non-cohesive sediments (typically up to the size of fine sands, i.e. about 100-200 μm, as larger grains are unlikely to directly interact with mud).

Previous research has shown that a clay content of between 5 – 10% can cause natural sediment mixtures to behave in a cohesive manner (Dyer, 1986; Raudviki, 1998). Thus, different ratios of mud and sand can vary the level of cohesion, which will influence the resultant level of flocculation. Biological activity, more commonly associated with cohesive sediments, has been highlighted to play an important role in the cohesion of sediments (e.g. Paterson and Hagerthey, 2001). However, it is extremely difficult to quantify such a complex sedimentary matrix in a fundamental manner, primarily as a result of a lack of verification data.

Of the various processes that occur during a tidal cycle, flocculation of the sediment is regarded as one of the primary mechanisms that can affect the deposition, erosion and consolidation rates. An individual floc may comprise up to 10^6 individual particulates. As flocs grow in size their effective densities generally decrease (Koglin, 1977; Tambo and Watanabe, 1979; Klimpel and Hogg, 1986) and their settling speeds rise due to a Stokes' Law relationship (Dyer and Manning, 1998) between D and Ws. Furthermore, low density flocs also demonstrate settling velocities that are significantly quicker than the individual cohesive particles (~ 1-5 μm in diameter). The cohesive nature of these particulates is a combination of both the electrostatic charging of the clay minerals as they pass through brackish to highly saline water, and various sticky biogenic coatings, such as mucopolysaccharides (e.g. Paterson 1989).

Van Leussen (1988) theoretically assessed the comparative influence of the three main collision mechanisms: Brownian motion, turbulent shear and differential settling, and deduced that turbulent shear stresses, principally those generated by velocity gradients present in an estuarine water column, were the dominant flocculation mechanism. This mechanism was deemed most effective for turbulent shear stresses ranging between 0.03-0.8 Pa. These stresses are representative of those typically experienced in the near bed region of many European macrotidal and mesotidal estuaries and hence estuaries are ideal environments for flocculation.

The energy for turbulent mixing is derived from the kinetic energy dissipated by the water flowing across the sediment bed. The frictional force exerted by the flow per unit area of the

http://dx.doi.org/10.5772/55233

bed is the shear stress (turbulent shear stress during turbulent flow conditions). The efficiency with which the particles flocculate is a reflection of the stability of the suspension (van Leussen, 1994). A suspension is classified as unstable when it becomes fully flocculated, and is stable when all particles remain as individual entities.

As low to medium levels of turbulent shear stress can promote floc growth, high levels of turbulence that occur during a tidal cycle, can cause disruption to the flocculation process by instigating floc break-up, and eventually pull the constituent components of a floc apart. As turbulent activity increases, both turbulent pressure differences and turbulent shear stresses in the flow rise. If the floc structural integrity is less than the imposing turbulent induced forces, the floc will fracture. Also, aggregate break-up can occur as a result of high impact particle collisions during very turbulent events. Floc break-up by three-particle collisions tends to be the most effective (Burban et al., 1989). Hence, turbulent shear stress can impose a maximum floc size restriction on a floc population in tidal waters (McCave, 1984). Eisma (1986) observed a general agreement between the maximum floc size and the smallest turbulent eddies as categorised by Kolmogorov (1941a, b).

3. Segregation and flocculation

This section looks at how mud and sand can co-exist within an aquatic environment. Mud:sand sediment mixtures may behave either in a segregated way, or interact through flocculation. The phenomenon of mud:sand segregation considers the mud and sand to operate as two independent suspensions (van Ledden, 2002) and, as such, very little bonding occurs, and flocculation interactions between the cohesive and non-cohesive sediment fractions are non-existent. Mixed sediment experiments have shown that mud particles and sand grains which behave in a segregated manner, settle simultaneously but as independent fractions to form two well sorted layers at the bed/water interface (Ockenden and Delo, 1991; Migniot, 1968; Williamson and Ockenden, 1993).

Williamson (1991) reviewed a number of the characteristics of mud:sand mixtures in the natural environment (some of the key findings are summarised in this paragraph). The review investigated the distributions and characteristics of mud and sand mixtures based on a literature search and a review of relevant fieldwork data. Some of the features common to both mud and sand, such as: spatial distributions, vertical layering, bioturbation, depositional characteristics and flocculation, were described. The review suggested that muddier sediments were generally found in regions of lower dynamic activity and sandier sediments in higher energy regions. However, the local distributions could only be explained by local hydrodynamic analysis and these data were often lacking, which did not allow a complete picture to be obtained. Flocculation and the effects of salinity distributions were found to be important in governing the mud distributions, with a muddy reach often being found in the flocculation zone. The vertical profile of settled mud and sand was also investigated, with laminations of mud and sand often being found. The thickness of the layers in the laminated sediment profiles were typically sub-millimetre to a few millimetres. The process of bioturbation (i.e. the

reworking of the bed sediments by living organisms) can potentially produce a mixing of bed sediment particles prior to resuspension (e.g. Nowell et al., 1981; Paterson et al., 1990; Widdows et al., 2004). Thus a bed which is initially deposited as a discretely segregated layering of mud and sand may be transformed into a quasi-homogeneous mixture.

Van Ledden (2003) states that mud and sand can be deposited as mixtures or in alternating layers in estuaries. An example of this is visible in the upper part of Fig 1. Additionally, biological activity such as bioturbation (i.e. the reworking of the bed sediments), can mix the sediment particles. As a result the mud content in many parts of an estuary may not be uniform, but can become segregated both vertically and horizontally – a phenomenon known as mud:sand segregation (van Ledden, 2003).

Mud:sand segregation can have a direct influence on the settling velocity of the sediments once entrained. For instance, the settling velocity of individual sand grains could be reduced as they pass through a layer of flocculating muddy sediments in close proximity to the sea bed. Van Ledden (2003) provides three examples which illustrate the importance of why a physical understanding of the distribution of mud and sand in estuarine systems is important:

- Large mud content variations at the bed surface indicate that both mud and sand contribute to bed level changes in estuaries and tidal inlets. These will affect the navigable depth and high water levels.
- Cohesive muddy sediments have the propensity to adsorb contaminants (Förstner and Wittmann,1983). This, in turn, has a direct effect on water quality and related environmental issues (e.g. Uncles et al., 1998). The amount of segregation present on both temporal and spatial scales will provide an indication to the potential degree of pollution in bed sediments.
- The mud content in sediment beds is a crucial habitat parameter, which controls the distribution of flora and fauna in estuarine systems (e.g. Reid and Wood, 1976; Kennish, 1986; Widdows et al., 2004). Dyer et al. (2000), for example, showed that the sediment type and grain size are the best physical descriptors of floral and faunal assemblages in the upper zone of intertidal mudflats.

Van Wijngaarden (2002a, 2002b) examined the mud:sand content distributions in the upper 300 mm of the bed in the Haringvliet – Holland Diep (The Netherlands). Mud content varied from less than 15% at the mouths of most of the river branches feeding into the system, to nearly two thirds mud in the channels of the Holland Diep. Fast settling sand grains accumulated at the end of river branches whereas the slower-settling muddy suspensions were transported further downstream due to settling lag into the central part of the Holland Diep. The segregation is, to a large extent related to varying bed levels throughout the system and variations in the turbulent shear stresses (van Ledden, 2003), which influence erosion, deposition and transport.

There are also many locations where mud and sand co-exist as a mixture (Mitchener et al., 1996) and this creates the potential for these two fractions to combine within a flocculation matrix when re-entrained into suspension (Manning et al., 2007). When sand is added to a predominantly muddy matrix, Mitchener et al. (1996) found that this increased the binding

http://dx.doi.org/10.5772/55233

potential between the clay particles, for example as found in the subtidal mud patches off Sellafield in the Irish Sea (Feates and Mitchener, 1998). Thus the physical effect of adding cohesive mud to a sandy environment can create increased bed stability, which can potentially lead to mixed sediment flocs forming when the eroded bed is entrained (Kamphuis and Hall, 1983; Alvarez-Hernandez, 1990; Williamson and Ockenden, 1993; Torfs, 1994; Mitchener et al., 1996; and Panagiotopoulus et al., 1997). Even where sand and mud are considered to be fairly well segregated at the bed, sand and mud can co-exist in suspended sediment transport. Spearman et al. (2011) describe an example in the outer Thames Estuary (UK), renowned for being a sandy area, where the flux of suspended sediment of mud and sand are of the same magnitude.

Therefore, in a segregated environment, both mud and sand are present acting in a completely independent manner. In a flocculating environment, the mud and sand particles are interacting to form flocs which demonstrate very different characteristics (e.g. D, Ws, ϱ_e) from their compositional base. The nature of the sedimentary regime is best determined by observational measurements rather than being able to be determined *a priori*. This can pose additional problems for the prediction and modelling of suspended sediment transport in mixed sediment estuarine environments and this will be considered in Section 9.

4. Role of biology in mud: Sand mixtures

Although not directly examined in the laboratory experiments which will be discussed later in this chapter, it is important to consider other effects of which a key one is due to biological factors influencing the grains in suspension. These factors work in addition to the primary chemico-physical ones to make mixed sediment flocculation possible. In predominantly muddy/silty environments, benthic microphytobenthos contribute up to half the total autotrophic production in an estuarine system (Underwood and Kromkamp, 1999; Cahoon, 1999). Biostabilisation can increase particle cohesion, for example: epipelic diatoms (e.g. Paterson and Hagerthey, 2001) secrete extra-cellular polymeric substances (EPS; Tolhurst et al., 2002) as they move within the sediments. EPSs are regarded as highly effective stabilisers of muddy sediments (e.g. de Brouwer et al. 2005; Gerbersdorf et al. 2009; Grabowski et al., 2012).

The influence of biology on sand is reported to a much lesser extent in the literature, however sand grains that are exposed to long-term biological activity, may also develop a cohesive bio-coating which could increase the particle collision efficiency when they are entrained. Hickman and Round (1970) reported that sand particles can be joined by 'epipsammic' diatoms which attach to sand grains. Epipsammic macro-algal forms either adnate to the grain surface or attach to sand grains by their mucilage stalks. Epipsammic diatoms which are attached to sand grains, demonstrate strong adhesive properties to the grain surface (Harper and Harper, 1967). When fine sand and biology are combined into a single matrix, they can form “microbial mats” and the binding strength of these mats can be extremely high. Little (2000) states that because these types of algal threads are sticky with EPS, they can efficiently trap fine sand grains. These sticky bio-coatings can increase the collision efficiency (Edzwald and O’Melia,

1975) of particles when entrained into suspension, thus allowing fine sand grains to adhere with the clay fraction and form the cage-like structure around fine sand particles. Through microscopic photography, Wolanski (2007) observed the formation of large muddy flocs formed by mud creating a sticky membrane around large non-cohesive silt particles.

5. Experimental approaches

When investigating the role sand may play in the flocculation process, several important research questions need to be considered, including:

i. How does the settling velocity of mixed sediment flocs vary in response to different mud:sand mixtures?

ii. What effect does turbulence have on mixed sediment flocculation?

iii. Do resuspended sand particles favour interacting with microflocs or macroflocs more, and enhance their settling dynamics?

iv. If mixed sediment flocculation occurs, are sand grains directly incorporated into both microfloc and macrofloc fractions?

v. Does flocculation have an effect on the distribution of the particle mass and the mass settling flux (MSF) of different suspended mud:sand mixtures?

In order to address aspects of the above questions, a series of new controlled laboratory environment research were initiated to quantitatively examine the flocculation and interaction between suspended sand and mud sediment mixtures. Other aspects of mud:sand behaviour have been assessed in laboratory environment measurements (e.g. Ockenden and Delo, 1988; Williamson and Ockenden, 1993; Torfs, 1994; Torfs et al., 1996; Dankers et al., 2007). During the new experiments, suspensions of mud and sand, of different total concentrations, were sheared at different rates in a mini-annular flume and the resultant floc properties observed. The new experimental runs primarily comprised pre-determined mud:sand mixtures complemented with some additional data from naturally occurring mud:sand sediment mixtures.

5.1. Annular flume simulations

This study utilised a mini-annular flume to create a consistent and repeatable turbulent environment (see Fig. 3A) (Manning and Whitehouse, 2009). The annular flume has an outer diameter of 1.2 m, a channel width of 0.1 m and a maximum depth of 0.15 m, along with a detachable motor driven rotating roof (10 mm thick) to create the flow for cohesive sediment experiments (e.g. Manning and Dyer, 1999). Maximum flow speeds of approximately 0.7 $m.s^{-1}$ can be produced in the lower half of the water column, created by 10 mm deep paddles attached to the underside of the roof. A Nortek mini-ADV (Acoustic Doppler Velocimeter) probe was used to calibrate the flow in terms of velocity and turbulent kinetic energy (TKE) at a distance of 22 mm (the floc extraction height) above the flume channel base.

http://dx.doi.org/10.5772/55233

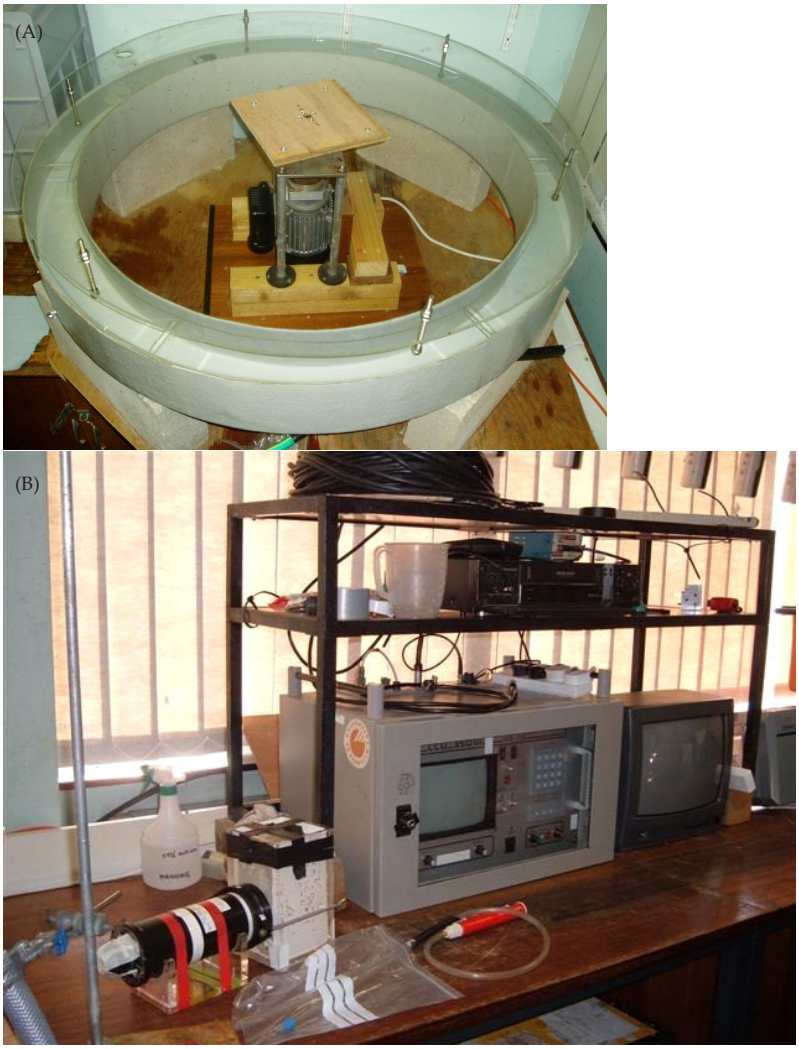

Figure 3. The mini-annular flume (A) and the LabSFLOC instrument set-up (B).

5.2. Floc property measurements

Representative floc populations were measured using the LabSFLOC version 1.0 – Laboratory Spectral Flocculation Characteristics – instrument (Manning, 2006). This utilises

a high magnification Puffin (model UTC 341) monochrome all-magnetic Pasecon tube video camera (Manning and Dyer, 2002a), to observe particles settling in a Perspex settling column (see Fig. 3B), allowing for minimal disruption of the particles. The video camera, positioned 75 mm above the base of the column, views all particles in the centre of the column that pass within a 1 mm depth of field, 45 mm from the lens. The video camera has an annulus of six high intensity red 130 mW LED's (light emitting diodes) positioned around the camera lens, which results in the flocs being viewed as silhouettes and produces a clear image of their size and structure. Whilst other studies may refer to muddy and/or mud-sand mixture particles as aggregates, for simplicity this study will refer to all aggregated combinations of particles as flocs.

5.3. Flume experimental protocols

The flume was filled with 45 litres of saline water (salinity = 20 ±0.2), to a depth of 0.13 m. The mixed sediments (both pre-determined and natural) were introduced into the flume as slurries of known SPM (suspended particulate matter) concentrations. Gravimetric analysis of extracted water samples was used to monitor the ambient concentration during the flume runs and check they were within the required experimental tolerances. For each run, different rotation speeds were used to shear the sediment slurries at shear stresses (τ) ranging from 0.06-0.9 Pa ±5% (equivalent Kolmogorov microscale values are: 381 - 138 μm ; equivalent G-values, the root mean square of the gradient in the turbulent velocity fluctuations, are: 7.1 – 54.2 s^{-1}) at the floc sampling point. Manning and Whitehouse (2009) report the calibration of the mini-flume hydrodynamics. Each run was initiated at the fastest rotational velocity and decreased towards the slowest speed as the run progressed. Further details of the experimental protocols are outlined by Manning et al. (2007).

The mixed sediment slurries were sheared in the flume for 30 minutes at each stress level. This duration of shearing, which was pre-determined in accordance with theoretical flocculation time (T_F), allowed each sediment suspension to attain floc equilibrium. Van Leussen (1994) defines T_F as the time required to decrease the number of individual unflocculated particles in a suspension, to just 10% of the initial number as a result of flocculation.

Floc population sampling comprised careful extraction of a suspension sample from the same height in the water column as the ADV calibration using a bespoke glass pipette. To obtain a floc sample, the rotation was stopped for approximately 6-8 seconds, although flow in the flume still continued through inertia, maintaining particles in suspension throughout this period. Manning and Whitehouse (2009) showed that the flow does not significantly slow until at least 15-20 seconds after stopping the drive motor. The floc sample was then transferred to the LabSFLOC Perspex settling column, whereby each individual floc was observed by the video camera as it was settling. Parameters of individual floc size (D) and settling velocity (Ws) were recorded during settling and the values obtained by video image post-processing. The experimental flow speeds generated in the flume were sufficient to keep the fine sand in suspension. The aperture of the pipette was brought into contact with the settling column water surface and held in place (vertically) allowing the captured flocs to undergo gravitational settling through the still

http://dx.doi.org/10.5772/55233

water column. Extensive testing of this sampling protocol during the EC COSINUS project (e.g. Gratiot and Manning, 2004) revealed that this technique created minimal floc disruption during acquisition. Once floc samples were extracted, the flume lid rotation continued at the next selected velocity.

5.4. LabSFLOC data processing

Parameters D and Ws, for all settling flocs viewed by the LabSFLOC video camera (for each sample), were measured simultaneously from the video recordings. Digitisation of the calibrated images resulted in a pixel resolution of 6.3 μm to determine floc size and position, from which settling velocity is determined by analysis of sequential images at a sampling rate of 25 Hz. The effective density (ϱ_e) of each floc was calculated by applying Stokes' Law relationship; ϱ_e is the difference between the floc bulk density (ϱ_f) and the water density (ϱ_w). To apply Stokes' Law, it is assumed that each sampled floc that fell through the still water enclosed within the settling column was within the viscous Reynolds region; i.e. when the individual floc Reynolds number (R_e) was less than 0.5. For instances where R_e exceeded 0.5, the Oseen modification, as advocated by ten Brinke (1994), was applied in order to correct for the increased inertia during settling. It is assumed that the measured particle is spherical; that is, it is as 'deep' as the measured D size.

The observed flocs were measured within a reference volume of water. By implementing a sequence of algorithms, originally derived by Fennessy et al. (1997) and modified by Manning (2004b), the dry mass of a floc population could be compared with the measured SPM concentration. This provides an estimate of the efficiency of the sampling procedure, and yielded corresponding rates of MSF. By definition, the data obtained from LabSFLOC are both of qualitative and quantitative value.

The floc data is presented as individual scatterplots and also as spectral size-banded (SB) distributions of floc mass and MSF; SB1 represents microflocs less than 40 μm in size and SB12 are macroflocs greater than 640 μm in diameter. Sample mean values are quoted. To provide a quantitative framework for population comparisons, the macrofloc and microfloc range of properties were assessed (Eisma, 1986; Manning, 2001), as these parameters are often used in flocculation modelling. The demarcation point for the macrofloc:microfloc fractions was a floc size of 160 μm (Manning, 2001) and was chosen for two main reasons: i) this was found to be the most statistically significant separation point for the majority of the mixed sediment floc populations in terms of mass settling properties; ii) it also provides computational continuity with previously derived flocculation algorithms for pure mud suspensions, such as the Manning Floc Settling Velocity (MFSV) algorithms which describe floc settling at different concentrations within turbulent flow (Manning and Dyer, 2007). Strictly it should be noted that microflocs are cohesive sediment flocs resistant to break-up by shear, however, in this study, many pure sand particles fall within the microfloc size range. Therefore, in this chapter microflocs refer to the 'fine particle population' < 160 μm in diameter. The sand used in the tests also contains a fraction with grains greater than 160 μm (around 10% by mass). Therefore, the macrofloc fraction may also contain a number of pure sand grains.

5.5. Floc microstructure

In order to examine the floc internal microstructure (matrix) at a sub-micron level (1-2 nm; Buffle and Leppard, 1995), use of transmission electron microscopy (TEM) was employed in a separate series of experiments (see Spencer et al., 2010). In addition, energy dispersive spectroscopy (EDS) was used to provide the elemental composition of the floc components. Samples were prepared for TEM analysis by first stabilising the samples in glutaraldehyde and embedding the samples in Spurr resin. The samples were polymerised at 60 ºC overnight. Ultrathin sections of the polymerised resins (50 nm) were obtained by sectioning with a diamond knife mounted in an ultramicrotome (RMC Ultramicrotome MT-7) and were then mounted on formvar copper grids for analysis. The ultra-thin sections were then observed in transmission mode at an accelerating voltage of 80 kV using a JEOL 1200EXIITEMSCAN scanning transmission electron microscope (STEM). The scanning mode of the STEM was used to generate a microprobe beam for EDS of individual floc components in sections allowing observation of minerals across the aggregates. A Princeton Gamma Tech (PGT) Si[Li] X-ray detector and Imix multichannel analyser provided spectra of all elements, with an atomic number greater than 10, on a "per colloid" basis.

6. Experimental results

Sections 6.1-6.5 report findings from the laboratory studies with pre-determined (PD) mud:sand mixtures conducted by Manning et al. (2007). Sections 6.5-6.6 report a selection of tests on naturally occurring mud and sand mixtures (NM), and analysis of a mixed sediment microfloc internal structure, respectively.

6.1. Sediments (PD)

The sand used in the pre-determined mixtures was named Redhill 110, which is a well-rounded and closely graded silica sand used by HR Wallingford for model testing with mobile sediment beds. Redhill 110 has a d_{50} of about 110 μm, with a d_{10} of 70 μm and a d_{90} of approximately 170 μm (Redhill 110 size values quoted are from independent analysis conducted at HR Wallingford). The experimental mud sample was obtained from the surface down to a depth of about 50 mm from the Calstock region of the upper Tamar Estuary (UK) and had an average organic content of approximately 10%. Fitzpatrick (1991) found Tamar Estuary mud to be generally high in kaolinite clay minerals and Fennessy et al. (1994) also report microscopic fragments of Tourmaline and Hornblende minerals present in Calstock mud. This particular mud was used as its floc properties are widely reported from earlier studies (e.g. Manning and Dyer, 2002b ; Mory et al., 2002 ; Bass et al., 2006). The mud was collected only a few days before the flume experiments were conducted, and cold stored (frozen) in a wet form to maximise organic matter preservation.

http://dx.doi.org/10.5772/55233

6.2. Overview of experimental runs (PD)

These experiments comprised a series of three main flume runs, A to C, based on pre-determined mud:sand (M:S) ratios (i.e. Run A = 75M:25S, Run B = 50M:50S and Run C = 25M:75S; units expressed as percentages). These main runs were each divided into 12 minor runs (based on concentration). This produced a total of 36 mixed sediment floc spectral samples. Three nominal total SPM concentrations were used: 200 $mg.l^{-1}$, 1000 $mg.l^{-1}$ and 5000 $mg.l^{-1}$. Four shear stresses were used per run and these were determined by the ADV records as nominal clearwater τ values of: 0.06, 0.35, 0.6 and 0.9 Pa. The experimental conditions are summarised in Table 1.

Run	Sample	Mud (%)	Sand (%)	τ (Pa)	SPM (mg/l)
A	1	75	25	0.9	200
A	2	75	25	0.6	200
A	3	75	25	0.35	200
A	4	75	25	0.06	200
A	5	75	25	0.9	1000
A	6	75	25	0.6	1000
A	7	75	25	0.35	1000
A	8	75	25	0.06	1000
A	9	75	25	0.9	5000
A	10	75	25	0.6	5000
A	11	75	25	0.35	5000
A	12	75	25	0.06	5000
B	1	50	50	0.9	200
B	2	50	50	0.6	200
B	3	50	50	0.35	200
B	4	50	50	0.06	200
B	5	50	50	0.9	1000
B	6	50	50	0.6	1000
B	7	50	50	0.35	1000
B	8	50	50	0.06	1000
B	9	50	50	0.9	5000
B	10	50	50	0.6	5000
B	11	50	50	0.35	5000
B	12	50	50	0.06	5000
C	1	25	75	0.9	200
C	2	25	75	0.6	200
C	3	25	75	0.35	200
C	4	25	75	0.06	200
C	5	25	75	0.9	1000
C	6	25	75	0.6	1000
C	7	25	75	0.35	1000
C	8	25	75	0.06	1000
C	9	25	75	0.9	5000
C	10	25	75	0.6	5000
C	11	25	75	0.35	5000
C	12	25	75	0.06	5000

Table 1. Overview of experimental runs & samples.

During a pilot study to design and refine experimental protocols on the floc population evolution of a few pre-selected slurries, observations indicated that at a τ of 0.06 Pa the sand in the upper part of the water column settled to the channel base. However, this preliminary inspection indicated that there was still sufficient fine sand in suspension in the lower half of the flume to maintain the nominal mud to sand ratio in the floc sampling region. Furthermore, during the pilot study, checks were made on mixture homogeneity during suspension and revealed a nominal 8% mixture deviation (in terms of the sand) for a 75% sand slurry, reducing to less than 5% for a 75M:25S mixture. These nominal deviations are deemed acceptable for these mixed sediment flocculation experiments, but are taken into consideration when interpreting the study results.

During the main flume run, the total suspended concentrations were monitored by gravimetric analysis of samples withdrawn at the floc sampling point. This analysis indicated that the 200 $mg.l^{-1}$ total SPM varied the least at ±3%; the higher 5000 $mg.l^{-1}$ varied by ±4.7%; and the 1000 $mg.l^{-1}$ slurry nominally varying by ±4.3% by the time of floc sampling. Therefore, these relatively small deviations demonstrate that the majority of the mixed sediment mass was remaining in suspension for the shearing duration. Therefore the floc population characteristics were related closely to the initial total concentrations and mud:sand ratios. Further details on the homogeneity of mud:sand mixing within the mini-annular flume is reported by Manning et al. (2009).

6.3. Floc size and settling velocity spectra with mixtures of mud and sand (PD)

To demonstrate the floc properties for suspensions comprising 75M:25S, 50M:50S and 25M:75S, a number of examples of the individual detailed spherical-equivalent dry mass weighted floc sizes vs. settling velocity spectra are presented (Figs 4Ai-4Av). The plots represent the mass-balance corrected floc distributions, thus an individual point on each graph may represent several flocs with very similar floc characteristics. The diagonal lines on each scatterplot represent contours of constant floc effective density, ρ_e, (units = $kg.m^{-3}$), i.e. the bulk density minus the water density.

For completeness the full set of D vs. Ws floc distributions for all experiments can be found in Figs. 5, 6 and 7. By following the plots in each column, starting at the lower plot, one can track the evolution of the floc populations formed in a constant SPM concentration as the shear stress rises through the various increments. Similarly, by following the plots from left to right, the effect of rising concentration on the floc dynamics can be observed. Sections 6.3 and 6.4 summarise some of the key observations from a selection of the populations.

6.3.1. Run A (75M:25S) (Fig. 5)

The flocs from the lower SPM concentration (200 $mg.l^{-1}$), A1-A4, appear to produce three separate clusters: a sub-70 μm group, a fraction greater than 160 μm; with a third group sandwiched in between. For example, the 204 individual flocs that comprised sample A3 (Fig. 5 box A3) ranged from 42 μm to 182 μm in diameter (also Fig. 4Ai). Corresponding settling velocities spanned 0.3 $mm.s^{-1}$ to 3.4 $mm.s^{-1}$ for sample A3.

http://dx.doi.org/10.5772/55233

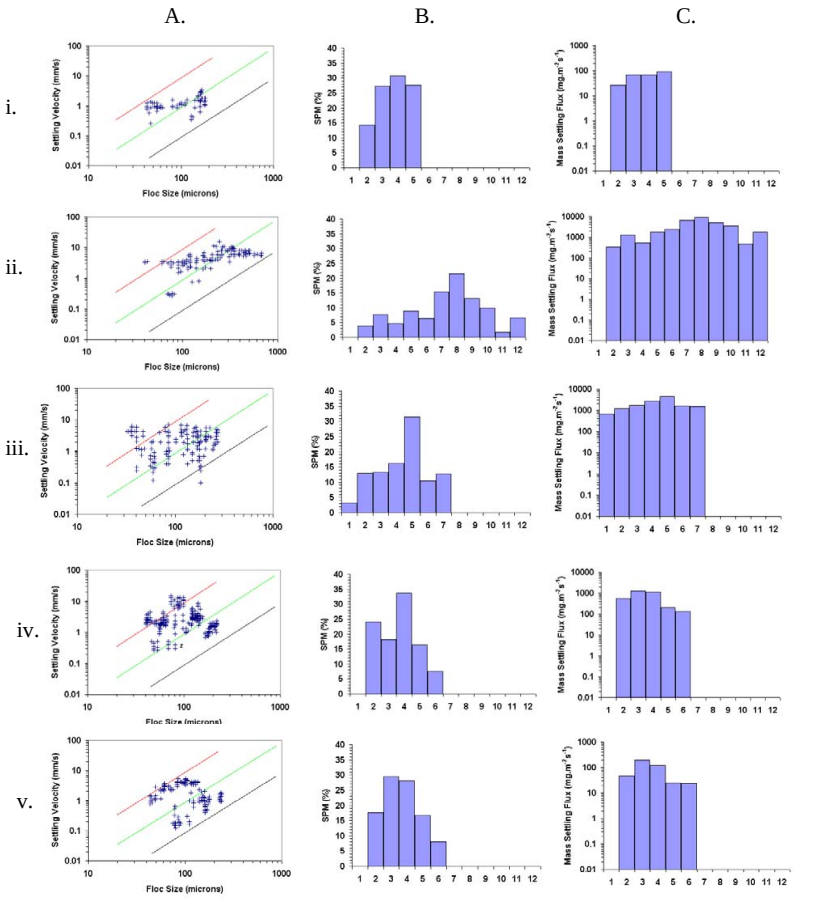

Size Band	1	2	3	4	5	6	7	8	9	10	11	12
Floc size (μm)	< 40	40 -80	80 -120	120 -160	160 -200	200 -240	240 -320	320 -400	400 -480	480 -560	560 -640	> 640

Figure 4. The floc size vs. settling velocity scatter plots (A, left-hand column) for five selected samples: i) A3, ii) A11, iii) B9, iv) C6 and v) C3. Diagonal lines on figures in column A represent contours of constant Stokes equivalent effective density: red = 1600 kgm^{-3}, green = 160 kgm^{-3}, and black = 16 kgm^{-3}. The centre (B) and right-hand (C) columns represent the corresponding size-banded SPM% and mass settling flux distributions (units = mg.m^{-2}s^{-1}). The size bands are illustrated in the table below the plots.

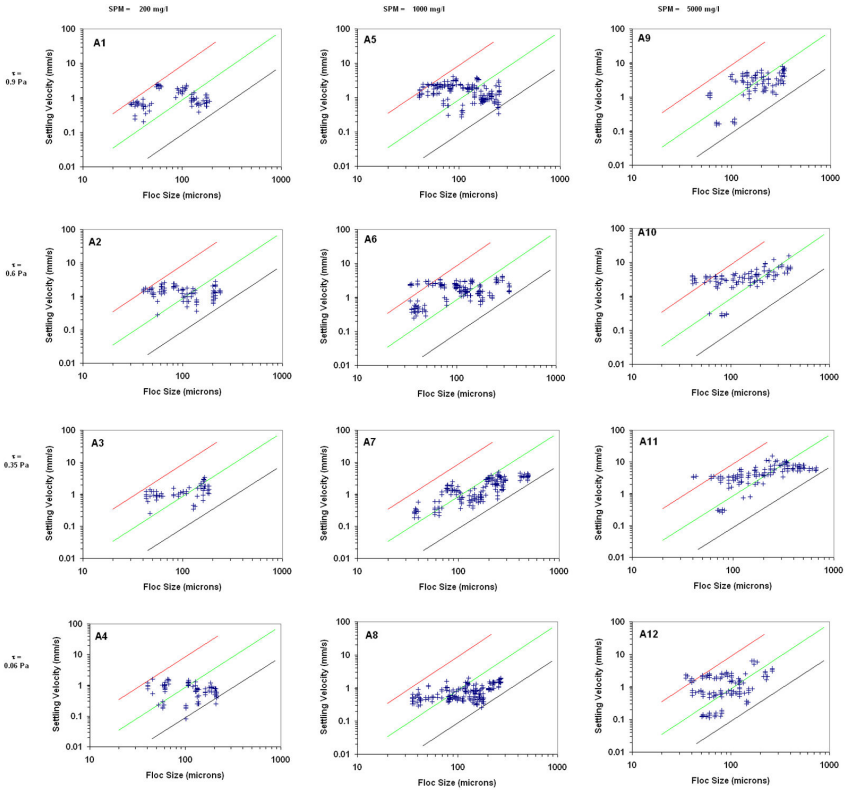

Figure 5. Distribution floc/aggregate size and settling velocity characteristics for the Run A (75M:25S) samples. Diagonal lines represent contours of constant Stokes equivalent effective density: red = 1600 kgm^{-3}, green = 160 kgm^{-3}, and black = 16 kgm^{-3}.

http://dx.doi.org/10.5772/55233

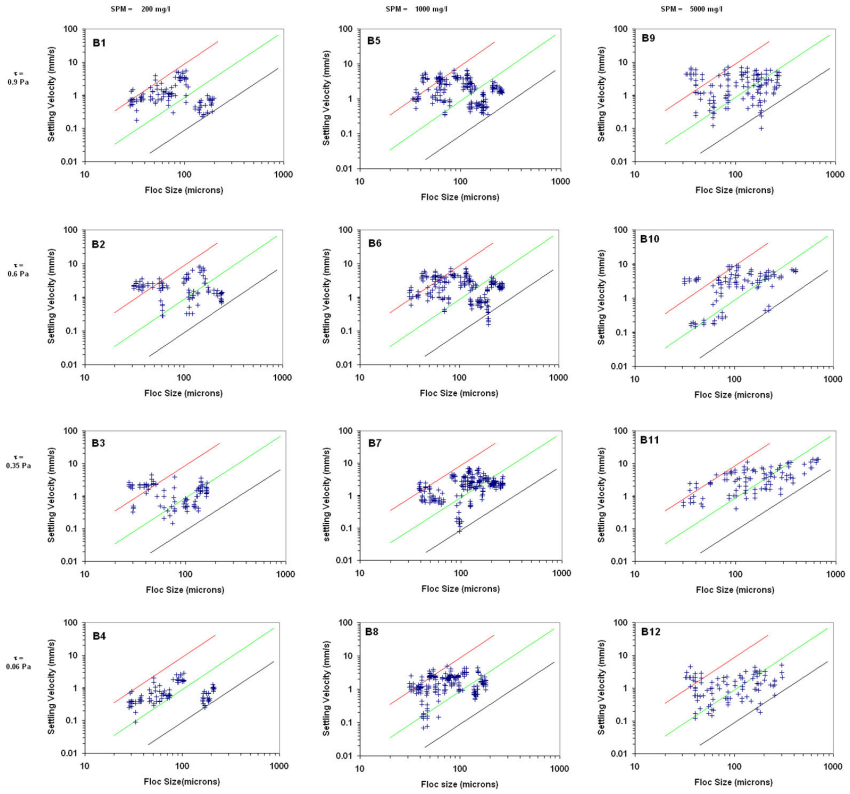

Figure 6. Distribution floc/aggregate size and settling velocity characteristics for the Run B (50M:50S) samples. Diagonal lines represent contours of constant Stokes equivalent effective density: red = 1600 kgm^{-3}, green = 160 kgm^{-3}, and black = 16 kgm^{-3}.

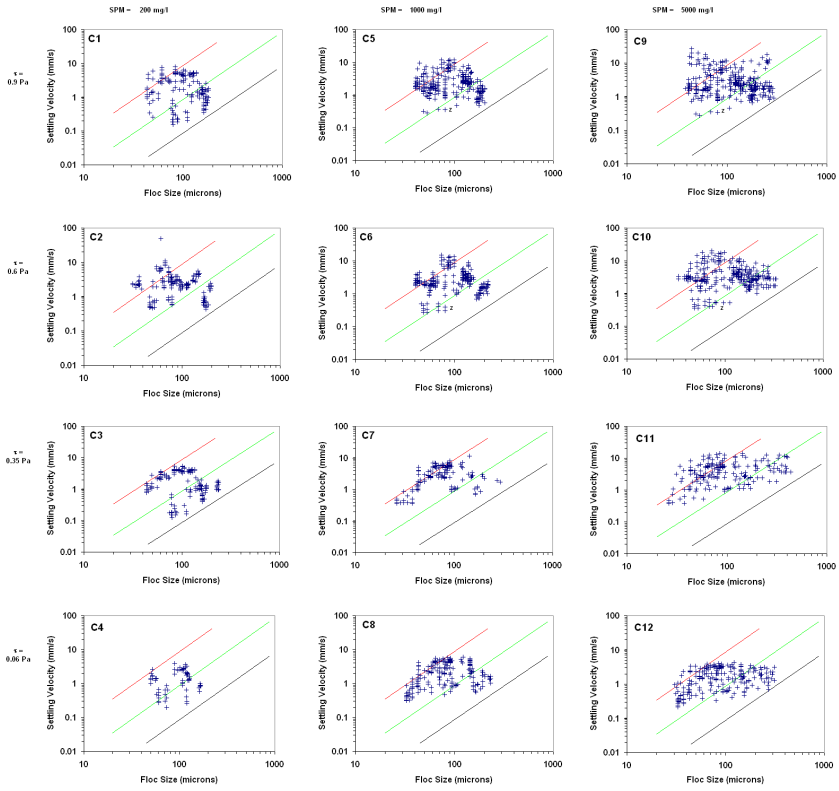

Figure 7. Distribution floc/aggregate size and settling velocity characteristics for the Run C (25M:75S) samples. Diagonal lines represent contours of constant Stokes equivalent effective density: red = 1600 kgm^{-3}, green = 160 kgm^{-3}, and black = 16 kgm^{-3}.

The Run A floc growth was potentially stimulated by a greater abundance of sediment, with D_{Max} (maximum floc diameter) nearly reaching 700 μm at peak turbidity (5000 mg.l^{-1}). The floc growth signified a corresponding quickening in Ws with rising SPM, producing Ws_{Max} (maximum settling velocities) of 7-8 mm.s^{-1} at 5000 mg.l^{-1}; approximately double the speed exhibited by the dilute sandy mud suspensions. This is demonstrated by A11 (Fig. 5 box A11 and Fig. 4Aii) where the shear stress was the same as A3 (0.35 Pa), but the particle mass in suspension were raised by a factor of twenty five. Flocs greater than 160 μm comprised 61% of the total population. In terms of the effects of shear stress, 0.35 Pa seems to produce the largest, fastest settling macroflocs at 75M:25S. These inter-relationships will be further examined in the Discussion (Section 7).

http://dx.doi.org/10.5772/55233

6.3.2. Run B (50M:50S) (Fig. 6)

Increasing the sand content to equal the mud fraction (50M:50S), brought about a general decrease in the macrofloc settling velocity across the entire shear stress range at each base concentration increment.

In contrast to the macroflocs, the smaller 50M:50S microfloc fractions all displayed quicker fall rates when compared to the 75% mud in settling rate for each mixed suspension run, with the 5000 $mg.l^{-1}$ 50M:50S mixed suspension (sample B9, Fig. 6) microfloc fraction settling velocity peaking at a highly turbulent τ of 0.9 Pa.

The B9 size vs. settling velocity floc scatter plot (Fig.6 box B9 and Fig. 4Aiii) shows a "W" or "double-V" pattern to the aggregates distribution. By this we mean there are small, fast settling microflocs (nominal 20-40 μm), whose settling velocity range expands at the mid-size microfloc fraction (nominal 40-80 μm). Then, for the microflocs nominally greater than 80 μm in size, the spread in the microfloc Ws again reduces, thus producing a "V" shaped distribution. This "V" pattern is repeated for the macroflocs, with their largest Ws scatter occurring between 185-230 μm for Sample B9.

The microflocs forming the first "V" spanned from 32 μm and up to 114 μm where they form the apex with the adjacent "V" to form the "W". At each end of the size range there are aggregates settling at 5-7 $mm.s^{-1}$, whilst the middle part of the "V" sections shows flocs falling as slowly as 0.1 $mm.s^{-1}$. In the upper left part of the D vs. Ws scatterplot, there are a number of aggregates which appear to be between 35-50 μm in diameter, settling at 3-6 $mm.s^{-1}$ and exhibiting effective densities of 2000-5000 $kg.m^{-3}$, which is up to three times the effective density of a sand grain. It is most probable that these are individual fragments of either Tourmaline or Hornblende; minerals native to the Tamar Estuary and its catchment. The majority of the aggregate population between 45-90 μm appears to be dominated by sand grains, with a minimum amount of cohesive matter (i.e. mud content) attached to the sand grains. These would form very basic, dense, lower order floc structures, which would trap very little interstitial water. This is indicated by high effective densities (ρ_e ~1200-1400 $kg.m^{-3}$), large fractal dimensions (nf of 2.8-2.9) and low porosities (~10-20%), but they are still not characteristic of pure (i.e. unflocculated) sand grains.

6.3.3. Run C (25M:75S) (Fig. 7)

Reducing the mud content to 25%, meant the microfloc size fraction tended to dominate the size and settling dynamics as the total concentration rose throughout Run C. At dilute conditions, the microflocs represented less than one quarter of the individual flocs for the A1-4 samples; for example C3 (Fig 7. Box C3 and Fig. 4Av). However, with many of the sub-160 μm C1-4 flocs settling at 4-7 $mm.s^{-1}$, they were falling significantly quicker than their muddier Runs A and B counterparts.

A five-fold rise in the total SPM concentration increased the production of smaller flocs, with the macrofloc size fractions only accounting for 10-20% of the individual aggregates. For example, nearly 90% of the C6 flocs (τ = 0.6 Pa, SPM = 1000 $mg.l^{-1}$) were within the microfloc range (Fig. 7 box C6 and Fig. 4Aiv). This was approximately 15-20% more microflocs when

compared to the more cohesive B6 and A6 samples (see relevant boxes in Fig. 6 and Fig 5. respectively).

The accuracy of effective density values is crucial to the determination of when mixed sediment particles are flocculating, or if the fine sand particles remain as individual inert entities. The reliability of the LabSFLOC effective density estimates are demonstrated by their observation of pure sand grains (Fig. 8). The D and Ws fine sand observations produce a distribution which closely follows the 1600 kg.m^{-3} density contour, generally not deviating by no more than ±100 kg.m^{-3} for over three hundred sand grain observations.

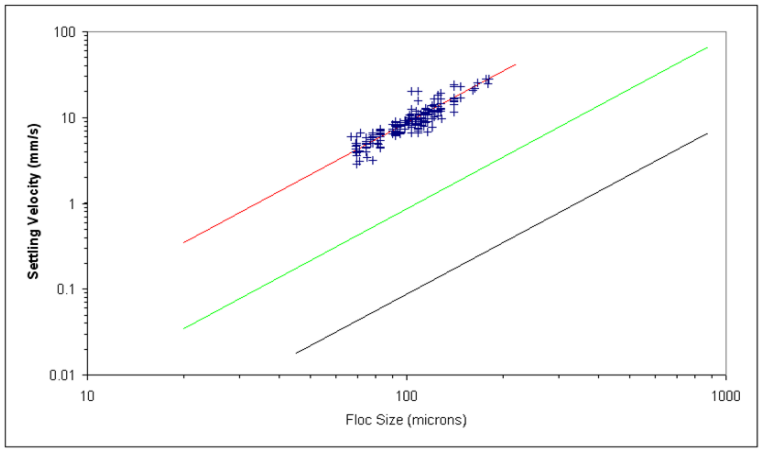

Figure 8. Settling settling vs. floc size for a 100% sand sample. Diagonal lines represent contours of constant Stokes equivalent effective density: red = 1600 kgm^{-3}, green = 160 kgm^{-3}, and black = 16 kgm^{-3}.

6.4. Floc composition with mixtures of mud and sand (PD)

To illustrate how the floc structure varies at different mud:sand ratios, a few examples will be presented with the compositional properties (effective density and SPM) as size band distributions. We start with sample A3 which represents a muddier dilute concentration and the D vs. Ws scatterplot (see Fig. 4Ai) shows that the macrofloc and microfloc fractions formed three distinctively separate groups. From Fig. 4Ai we can determine that the microfloc effective densities (ϱ_{e_micro} ranging from 200-1580 kg.m^{-3}) were generally an order of magnitude greater than the macrofloc (ϱ_{e_macro} from 30-100 kg.m^{-3}). This suggests that together with some individual sand grains, some of the sand grains may have also been included into the microfloc structure during the flocculation process.

In terms of the mass distribution across the dilute concentration floc population, the small microflocs for A3 represented three quarters of the mass (Fig. 4Bi). This is similar to fully cohesive suspensions within a moderately-high shear zone (τ of 0.6-1 Pa) which suggests the

http://dx.doi.org/10.5772/55233

mixture is still behaving as a cohesive suspension, even with 25% sand present in the initial mixture. For this sample, the denser, more compact microflocs represented two thirds of the total 254 $mg.m^{-2}s^{-1}$ mass settling flux (Fig. 4Ci).

At a concentration of 5000 $mg.l^{-1}$, the 75M:25S macroflocs of sample A11 (Fig. 4Aii) the macroflocs were observed to be delicate, low in density (ρ_e ranging from 20-200 $kg.m^{-3}$) entities. The A11 macroflocs now represented 84% of the mass (Fig. 4Bii), which was more than double the A3 macrofloc mass. Higher turbidity stimulated floc growth in A11, resulting in the largest flocs (D_{max}) growing to 670 μm.

The A11 microfloc fraction consisted of higher density flocs, with the smallest flocs (40-80 μm) demonstrating effective densities of over 1100 $kg.m^{-3}$, which are indicative of sand-laden microflocs or sand grains (where the effective density is greater than 1600 $kg.m^{-3}$). With sand accounting for one quarter of the total suspension and the microflocs representing 16% of the A11 mass, continuity of mass dictates that a reasonable portion of the sand must have been incorporated in many of the macrofloc structures during the flocculation process. This is very different from some segregational theories (e.g. van Ledden, 2003) which regard suspensions of sand and mud as completely independent entities.

Collectively, the fast settling A11 macroflocs contributed 94% of the total mass settling flux (33 $g.m^{-2}s^{-1}$; Fig. 4Cii); a result of a macrofloc settling velocity of 7.2 $mm.s^{-1}$, which was nearly three times quicker than the corresponding Ws_{micro}. To put this all into context, the A11 total MSF was 13 times greater than the value computed by the use of an estimated mean settling velocity of 0.5 $mm.s^{-1}$; a typical parameterised cohesive sediment Ws value derived from the gravimetric analysis of Owen tube (Owen, 1976) samples. Dearnaley, (1996) summarised the primary drawback associated with the Owen tube and other field settling tube devices, including the disruptive nature on flocs of the instrument sampling. Even the A11 microflocs were settling five times quicker than a 0.5 $mm.s^{-1}$ parameter value (A11 Ws_{micro} = 2.5 $mm.s^{-1}$).

Examination of the 50M:50S sample B9 D vs. Ws scatterplot (Fig. 4Aiii), reveals the presence of a high density sub-group of flocs (upper left-hand section). These flocs, which are only 35-50 μm in diameter, are settling at 3-6 mms^{-1} and exhibiting effective densities of up to 2000-3500 $kg.m^{-3}$. This is up to three times the typical effective density of a sand grain. It is proposed that these are individual fragments of either Tourmaline or Hornblende; minerals native to the Tamar Estuary and its catchment (Fennessy et al., 1994). However, given the Tamar's history for shipping copper out of Calstock, and the rich mining history for everything from tin to silver, these heavier particles could be from a number of sources. The majority of the floc population between 45-90 μm appears to be dominated by sand grains as their effective densities are typically greater than 1600 $kg.m^{-3}$, with a minimum amount of cohesive matter (i.e. mud content) attached to the sand grains. These would form very basic, dense, lower order floc structures, which would trap very little interstitial water. We could ask the question; if these high density particles were included in the mud used for all mixtures, why are they observed only in this case? It is possibly due to uncertainty made when estimating size and settling velocity of flocs rises as the particles become smaller (i.e. they are harder to detect as their images are formed from less pixels). Furthermore, these very dense mineral fragments only constitute a few percent of the total mass.

To reiterate, the microflocs tended to dominate the less cohesive Run C samples (25M:75S). The C6 (τ = 0.6 Pa and SPM = 1000 mg.l^{-1}) macroflocs did not grow larger than 215 μm (Fig. 4Aiv). This was a 40% reduction in size when compared to the corresponding 75M:25S sample (A6). The low density (effective densities of less than 70 kg.m^{-3}) C6 small macroflocs fell at a combined average Ws_{macro} of 1.35 mm.s^{-1}, whilst the Ws_{micro} was 3.6 mm.s^{-1}. The C6 microflocs also represented three quarters of the SPM and 90% of the C6 MSF of 3.2 g.m^{-2}s^{-1} (see Fig. 4Biv and Fig. 4Civ, respectively). To place this MSF observation into perspective: it was approximately double the flux produced either by pure mud or a 75% mixed mud suspension; 31% greater than a 50:50 mixture could produce, and six times greater than the flux obtained by using a constant 0.5 mm.s^{-1} Ws (a typical settling parameter used in cohesive sediment transport modelling).

The 'clustered' appearance depicted by the lower concentration (SPM = 200 mg.l^{-1}) 25M:75S C3 sample (Fig. 4Av) is similar to Sample C6 (Fig. 4Av). The shear stress was less turbulent (τ = 0.35 Pa) than C6, so one would assume the floc settling dynamics would improve. However, the removal of three quarters of the cohesive matter meant that the Ws_{macro} was only 0.9 mms^{-1}; half the Ws_{macro} for the 75M:25S run A3. As with the 1000 mg.l^{-1} C6 suspension, the C3 macroflocs only represented a quarter of the SPM (Fig. 4Bv). The main difference between the lower and the higher Run C suspension was fewer individual unflocculated sand grains in the suspension at the lower turbidity.

6.5. Analysis of macrofloc: Microfloc trends (PD)

This section will look at the macrofloc and microfloc (Eisma, 1986) settling velocity trends (i.e. Ws_{macro} and Ws_{micro} respectively) calculated from the pre-determined mud:sand mixture data presented earlier in Section 6.3. A dual-modal approach is advised when assessing parameterised floc settling and floc mass population data, as it tends to be more realistically representative than a single sample average (Dyer et al., 1996; Mietta, 2010), especially when considering the effects of mass settling fluxes to the bed (Baugh and Manning, 2007). This approach also permits quantitative inter-comparisons with previous pure mud flocculation studies.

The density contours superimposed on the Ws vs. D scatterplots presented in Section 6.3 indicate that only a minimum number of sand grains remained in an unflocculated state. This was confirmed from an assessment of both the effective density and SPM distributions. Therefore these few grains were included in the microfloc analysis presented in this section, as they form part of the total suspension and this provides the continuity of mass when comparing the different samples. However, to make these assessments fully rigorous, the mud fraction of the samples will be isolated and examined independently in the 'modelling implications' section (see Section 9).

6.5.1. Run a using 75% mud: 25% sand

Fig. 9 shows the macrofloc and microfloc averaged settling velocity plots which cover both the pre-determined mixtures experimental concentration and shear stress ranges. The solid lines

http://dx.doi.org/10.5772/55233

on Figs 9.A and 9.B correspond to the 25% sand mixed suspensions; the dotted curve lines are the contrasting 100% mud suspension outputs from the MFSV (this prediction was calibrated principally for Tamar mud extracted from the same study location). The straight dotted lines represent the d_{50} and d_{10} settling rates of pure sand grains determined by the *SandCalc* sediment transport computational software package (HR Wallingford, 1998).

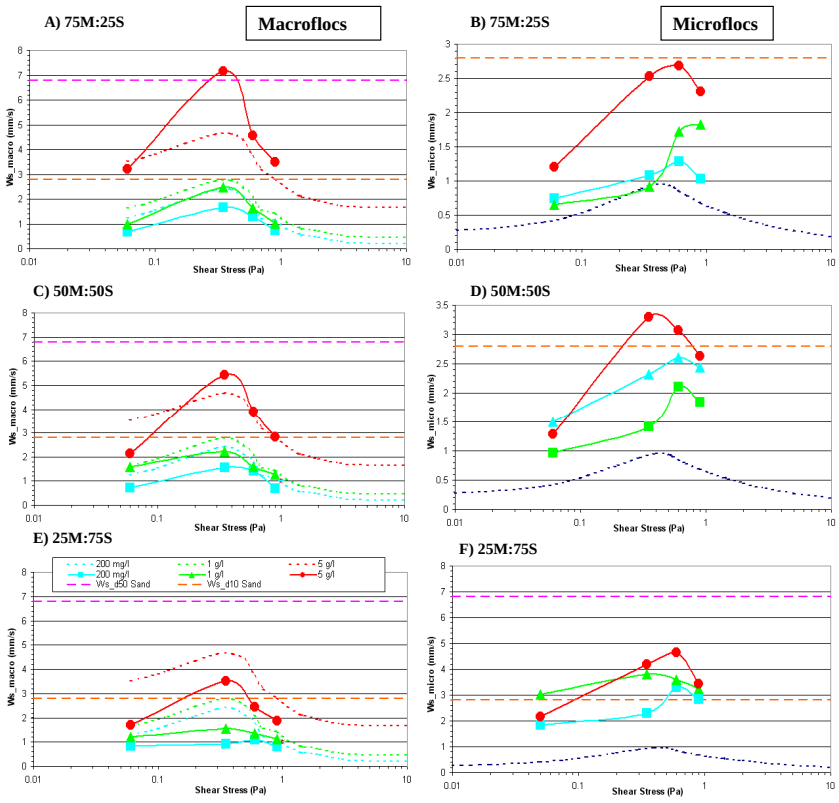

Figure 9. Ws_{macro} (left column, y-axis, units = $mm.s^{-1}$) & Ws_{micro} (right column, y-axis, units = $mm.s^{-1}$) values for runs A (75M:25S), B (50M:50S) and C (25M:75S), plotted against shear stress (x-axis, units = Pa). Solid lines + symbols indicate mixed sediment floc data points. Dashed lines indicate predicted behaviour of 100% mud macroflocs at three concentrations, and 100% mud microflocs at a single concentration. Lines indicating SandCalc estimated settling velocities of unhindered d_{10} and d_{50} pure sand grains are also plotted.

Substituting 25% of the pure mud suspension for sand produced a distinct change to the macrofloc settling velocity (Fig. 9.A). Starting at the lowest concentration (200 $mg.l^{-1}$), the quiescent conditions of 0.06 Pa only produced a Ws_{macro} of 0.65 $mm.s^{-1}$: nearly half the settling

rate of pure mud. As the shear stress increased, the floc dynamics respond and the settling velocity increased to a maximum of 1.7 $mm.s^{-1}$ at 0.35 Pa, which was 0.8 $mm.s^{-1}$ slower than pure mud at the same concentration. The intermediate concentration (1000 $mg.l^{-1}$) Ws_{macro} closely mimicked the settling profile of pure mud macroflocs at the less turbid 200 $mg.l^{-1}$. This is primarily a result of the 75M:25S suspension lacking sufficient cohesion because it only comprises 75% mud and the potential level of flocculation is more restricted than pure mud. The mixed sediment macroflocs also demonstrated lower effective densities (~30-50 $kg.m^{-3}$) than their pure mud counterparts.

The smaller mixed sediment microfloc fractions all settled faster than the pure mud equivalents, at each stress increment (Fig. 9.B). Where the macrofloc mixed fraction showed settling peaks at 0.35 Pa, similar to natural muds (Manning, 2004b), the mixed Ws_{micro} tended to produce a maximum at the higher turbulent shear stress of 0.6 Pa.

At high turbidity (5000 $mg.l^{-1}$), the macroflocs were nearly three time more dense than at lower turbidity. This saw the Ws_{macro} peaking at 7.2 $mm.s^{-1}$, which was 2.5 $mm.s^{-1}$ faster than the 100% mud equivalent, and 0.4 $mm.s^{-1}$ quicker than a d_{50} pure sand. The corresponding Ws_{micro} was 2.7 $mm.s^{-1}$, which was similar to a d_{10} sand grain and 1.7 $mm.s^{-1}$ quicker than pure mud microflocs.

6.5.2. Run B using 50% mud: 50% sand

Increasing the sand content to equal the mud fraction (50M:50S), brought about a general decrease in the macrofloc settling velocity across the entire shear stress range at each base concentration increment (Fig. 9.C). For the 200 $mg.l^{-1}$ slurries sheared at 0.35 Pa, the equally mixed sediment produced a Ws_{macro} of 1.6 $mm.s^{-1}$, a reduction of 0.1 $mm.s^{-1}$ from the 75% mud, and was 0.8 $mm.s^{-1}$ slower at settling than the pure mud benchmark.

At the highest suspended concentration (5000 $mg.l^{-1}$), and again at a turbulent stress of 0.35 Pa, the 50M:50S slurry produced a Ws_{macro} of 5.4 $mm.s^{-1}$. This was 0.8 $mm.s^{-1}$ faster than pure mud, but 1.8 $mm.s^{-1}$ slower than the 75M:25S macroflocs. This large Ws_{macro} difference exhibited between the 75M:25S and 50M:50S mixtures, decreased as the TKE dissipated to a lesser level. However, both mixed suspension macroflocs at the low shear stress were still slower than pure mud, which settled considerably faster.

In contrast to the macroflocs, the smaller 50M:50S microfloc fractions (Fig. 9.D) all displayed quicker settling velocities when compared to 75M:25S. The one main exception was the 5000 $mg.l^{-1}$ concentration, where Ws_{micro} achieved a maximum speed of 3.3 $mm.s^{-1}$; which was 2.3 $mm.s^{-1}$ faster than pure mud and 0.75 $mm.s^{-1}$ quicker than the corresponding 75M:25S microflocs.

6.5.3. Run C using 25%mud: 75% sand

The addition of a greater amount of sand particles in suspension significantly enhanced the settling dynamics at their respective shearing stresses which stimulate maximum flocculation. All 25M:75S values of Ws_{micro} exceeded the purely cohesive suspensions by more than a factor

http://dx.doi.org/10.5772/55233

of two (Fig. 9.F), and the majority of the microfloc samples also exceeded the settling rate of a d_{10} sand grain. At an SPM concentration of 200 mgl^{-1}, the Ws_{micro} at 0.06 Pa was 1.8 $mm.s^{-1}$ and increased to a peak of 3.3 $mm.s^{-1}$ at 0.6 Pa. By increasing the SPM concentration to 5000 $mg.l^{-1}$, the Ws_{micro} maximum peaked at 4.7 $mm.s^{-1}$. This was approximately five times faster than the value for 100% mud, and nearly double the equivalent 75M:25S Ws_{micro} (Fig. 9.F).

Conversely, all macrofloc fractions settled significantly slower within the less cohesive suspensions. At peak turbidity, the macrofloc fraction fell at 3.5 $mm.s^{-1}$; this was the sole macrofloc fraction to exceed the settling velocity of d_{10} sand. In fact, this 25M:75S macrofloc fraction was 1.2 $mm.s^{-1}$ slower than the corresponding Ws_{micro} from the same run.

In terms of the particle mass distribution: as the percentage content of non-cohesive sediment rose (i.e. mud content decreased), the relative contribution of the microfloc fraction to the total SPM concentration in each population increased.

6.6. Comparative data for sediment from Portsmouth Harbour – Natural Mixture (NM)

To support the data derived from the pre-determined mud:sand slurries, a selection of naturally occurring mixed sediment samples collected from within Portsmouth Harbour (a tidal inlet on the southern coast of the UK) were also assessed using the same type of laboratory flume runs (Pidduck and Manning, in prep.). The same protocols used for the pre-determined mixture experiments, were adopted for these runs. Sediment transport in Portsmouth Harbour has been studied by Hydraulics Research (1959), Lonsdale (1969) and Harlow (1980). Regular dredging activities for military vessel access to the Royal Naval Base, combined with an ebb-dominant macrotidal regime, mean that the fine mud and coarser sands that reside in the Harbour can become mixed.

Two Portsmouth Harbour samples at a constant SPM concentration of 2000 $mg.l^{-1}$ and sheared at 0.35 Pa are described. The first suspension, 4_A (Fig. 10a), was a low cohesive sediment composed of 38M:62S (including coarse silts). Loss-on-ignition tests indicated that sediment 4_A was approximately 6% organic. The 4_A flocs ranged in size from 29-313 μm, although there is an absence of particles in the 33 to 69 μm range. The smallest microflocs (2% of the population) all demonstrate effective densities of quartz and beyond, which suggests the presence of some very dense minerals; possibly some metallic particles. The larger microflocs were less dense (~ 700 $kg.m^{-3}$).

The 4_A microflocs comprised just over half of the SPM, with their settling velocities spanning three orders of magnitude from 0.36-34 $mm.s^{-1}$. This resulted in a Ws_{micro} of 5.4 $mm.s^{-1}$, which was 1.3 $mm.s^{-1}$ quicker than the larger macroflocs. This was due to the macroflocs demonstrating effective densities predominantly below 200 $kg.m^{-3}$, which are more indicative of cohesive flocs.

The second sample, 6_B (Fig. 10b), was more cohesive as it contained only 30% sand (70M:30S) and the sediment mixture had 8.4% organic matter present within its matrix. Where the sample 4_A D vs. Ws distribution favoured the smaller size fractions, 6_B depicts a population more characteristic of a pure mud. The microflocs were distinctly slower in settling, ranging from

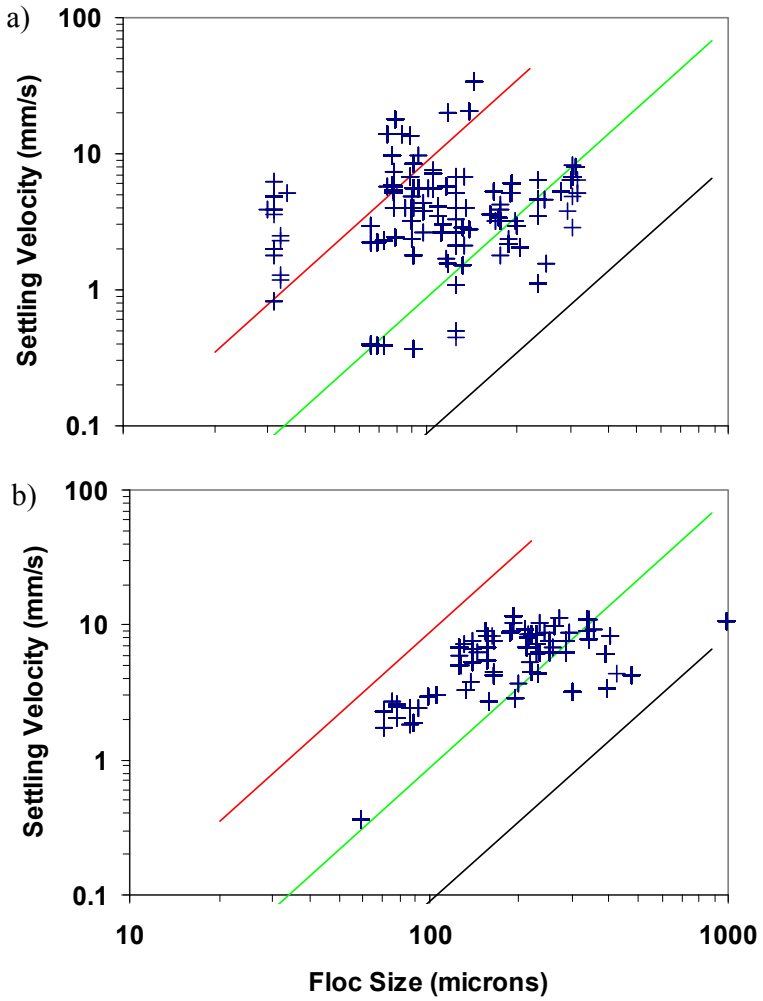

Figure 10. Settling settling vs. floc size for Portsmouth Harbour samples: a) 4_A (38M:62S); b) 6_B (38M:62S). Both samples had nominal 2 $g.l^{-1}$ total SPM concentrations and were sheared at a stress of 0.35 Pa. Diagonal lines represent contours of constant Stokes equivalent effective density: red = 1600 kgm^{-3}, green = 160 kgm^{-3}, and black = 16 kgm^{-3}.

2-8 $mm.s^{-1}$. All flocs were also less dense than 4_A; effective densities under 740 $kg.m^{-3}$, with the largest flocs having a ϱ_e of just 20 $kg.m^{-3}$.

The macroflocs comprised nearly two thirds of 6_B population and over three quarters of the mass. The macrofloc and microfloc settling dynamics of the Portsmouth Harbour samples, at

http://dx.doi.org/10.5772/55233

the three induced shear stresses (0.06, 0.35 and 0.6 Pa; 0.9 Pa was not available for the Portsmouth Harbour tests), are illustrated in Fig. 11. The data reveals some interesting settling velocity trends and these will be discussed in Section 7.

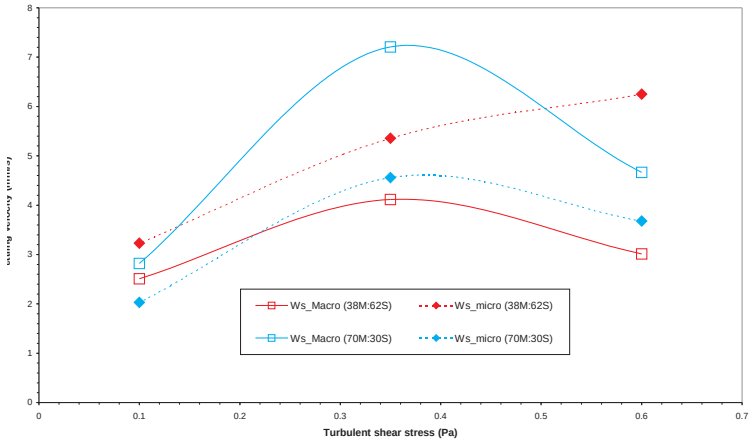

Figure 11. Ws_{macro} and Ws_{micro} values plotted against shear stress for Portsmouth Harbour samples 4_A (38M:62S) and 6_B (70M:30S). Both samples had nominal 2 $g.l^{-1}$ total SPM concentrations and were sheared at a stress of 0.35 Pa.

6.7. Floc microstructure

To illustrate how both non-cohesive and cohesive sediments components can combine in natural microflocs, electron micrographs of cross-sections through natural microflocs from the Tamar Estuary (UK) are shown in Fig. 12. The low resolution TEM image which encompasses the entire microfloc (Fig. 12a) shows the complex matrix of structurally interdependent components of a typical floc section. Both organic and inorganic particles are present creating a highly porous, high water content, three-dimensional sedimentary matrix.

7. Discussion of experimental findings

7.1. Settling velocity

This section addresses issues relating to research questions i-iii listed in Section 5. A number of generalised trends, in terms of the settling velocity, can be deduced from the macrofloc and microfloc data. The macrofloc settling velocities generally slowed as the sand content rose. These macroflocs fell slightly quicker than the microflocs at low turbidity, but almost three-times as quick at the higher suspended concentration. However, as the mud content decreased,

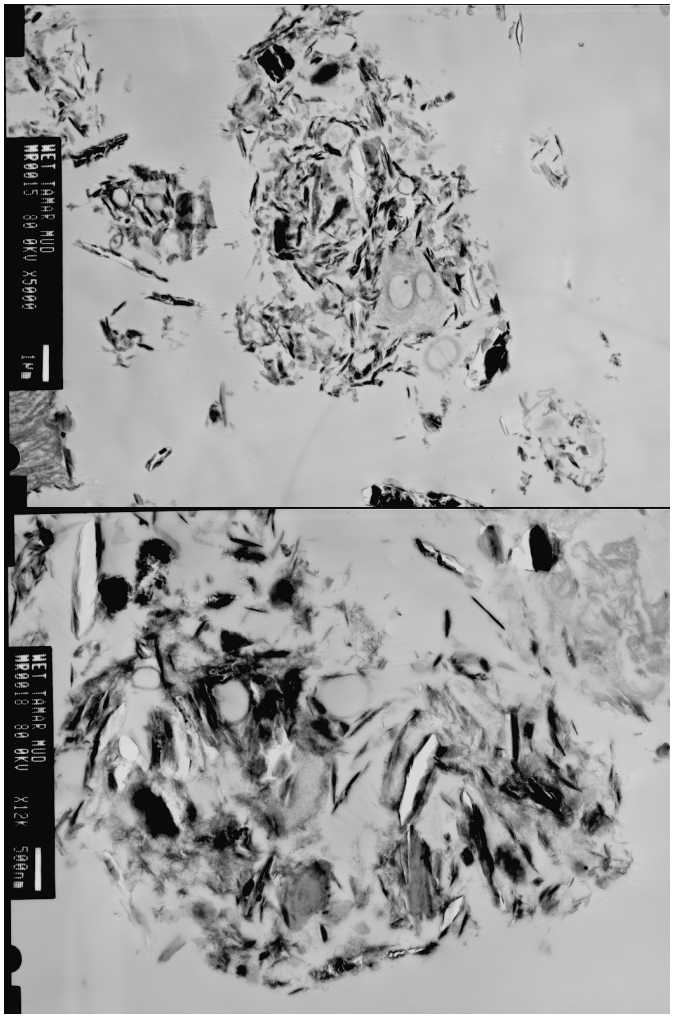

Figure 12. Low resolution (a) and high resolution (b) TEM images of a natural microfloc composed of a mud:sand mixture.

the particle cohesion efficiency would also reduce and could potentially limit the floc growth potential, curbing the equilibrium floc size of the macrofloc fraction.

The microfloc settling responded to a greater abundance of sand, whereby the greater the sand content in a mixed fraction - the faster the Ws_{micro}. For example, for a 25M:75S suspension, the microfloc settling velocities demonstrated a three-fold increase at low turbidity and nearly

http://dx.doi.org/10.5772/55233

doubled in settling speed at high turbidity to produce Ws_{micro} of 3.5 mm.s^{-1} and 4.7 mm.s^{-1}, respectively. The effective density data of many of the microfloc fractions from the pre-determined mixtures tests ranged from 800-1200 kg.m^{-3}. This would suggest that the finer sand grains tended to interact and bond better with the smaller floc structures, accounting for the quicker microfloc settling velocities observed.

The flocs produced from the natural Portsmouth Harbour sediments showed similar general settling velocity patterns to those of the pre-determined Tamar mixed suspensions. For the less cohesive 38M:62S slurry (sample 4_A), the microfloc fraction settled quicker than the macroflocs. By taking into account differences in SPM and M:S ratio, one can deduce that the 4_A microflocs were settling approximately 1.5 mm.s^{-1} quicker than their manufactured slurry equivalents, whilst the Portsmouth macroflocs fell nearly twice as quick as their pre-determined slurry equivalent. This could be a result of slightly larger sand grains present in the Portsmouth 4_A sediment and also stronger bio-film coatings present in the 4_A mixture providing extra adhesion for the sand grains permitting greater uptake within the macrofloc fraction.

It is interesting to observe that the microflocs in 4_A produced their fastest settling velocities at a τ of 0.6 Pa, whilst the Ws_{macro} peaked at a less turbulent 0.35 Pa. This can be explained by the denser microflocs being stronger than the weaker macroflocs, hence they can survive larger stresses. The ratio of a floc's diameter to the corresponding dissipating eddy size, such as the Kolmogorov microscale (1941a, b), in turbulent flow is a fundamental governing condition for estuarine flocculation dynamics (Tomi and Bagster, 1978; Tambo and Hozumi, 1979; McCave, 1984). Furthermore, if settling velocities are large, more turbulent energy is required to keep those flocs in suspension.

7.2. Composition and SPM distribution

Aspects relating to research question iv are now discussed. The LabSFLOC data has provided evidence of how sand grains can be potentially included within a floc matrix. The Ws vs. D spectra show that only a minimal amount of potentially unflocculated pure sand particles are present in a few of the samples; this is in terms of both individual numbers and the percentage of the total SPM (typically less than 1-2% of the total mud:sand concentration). An accurate mass balance between the predetermined mixed suspension introduced into the flume at the commencement of each run and the filtered SPM obtained from each sample promotes confidence in the mixed sediment LabSFLOC floc observations.

The LabSFLOC sampling protocol of measuring D and Ws simultaneously means that data on individual floc effective density is available. The latter provides important information about the composition of each floc (Dyer, 1989). The data identifies that there is a wide range in effective densities exhibited across each spectrum, particularly in the microfloc range, but most are less than pure quartz (~1600 kg.m^{-3}). Transmission electron microscopy (TEM) images have also visually identified the presence of both clay minerals and quartz mineral fragments within natural microfloc structures (Spencer et al., 2010). This leads to the suggestion that when mixed sediments flocculate, the sand particles favour the microfloc fraction, which is logical reasoning: microflocs tend to have the stronger bonding potential due to the closeness of the bonds.

Uptake of individual sand particles will probably be much less in the macroflocs. This is consistent with the order of aggregation theory (Krone, 1962; Eisma, 1986) which states that microflocs will flocculate into macroflocs when the ambient conditions are favourable. This provides a more efficient mechanism / pathway for the fine sand grains to move into the macrofloc fractions.

The EDS floc structural analysis of the TEM floc images presented in Section 6.7, identified that the microfloc inorganic constituents primarily comprised planar clay minerals (identified by the thin dark grey objects in Fig. 12) and fine quartz fragments (all much smaller than the mean sand grain size), evident from concoidal fracturing (the black marks in Fig. 12a and 12b). Other minerals present included Fe and Mn oxides and opaque sub-cubic minerals (probably pyrite), which are all typical of estuarine sediments. The organic constituents are predominantly observed to be bacteria and their EPS (extracellular polymeric substance; see Underwood and Paterson, 2003; Tolhurst et al., 2002) fibrils, which are produced by the bacteria for attachment, assimilation of food (dissolved organic carbon) and for protection from predation and contaminants. In the high resolution TEM image of the microfloc (Fig 12b.), the EPS can be seen linking the biological and inorganic particles and represents a micro-structural framework of the floc matrix (Fig. 12b). The EPS matrix is considered to be the component of the floc that enhances floc building and provides it with its strength.

For the Tamar mixtures, with a sand d_{50} of 0.11 mm, it is geometrically possible that only one sand grain may form a microfloc. The data shows that many of the microflocs exhibited effective densities significantly less than pure quartz, but higher than most pure mud microfloc. This suggests that the mixed sediment microflocs could be either combined mixtures of very fine quartz fragments and mud, as illustrated by the TEM images, or they could be individual larger quartz particles which are coated in organic mud. For example, Whitehouse et al. (2000) offer a scenario where mud can create a 'cage-work' structure which can fully encompass the sand grains, thus trapping the sand within a clay floc envelope. Mehta et al. (2009) observed flocs of various sizes in Lake Apopka (Florida, USA) where the inorganic particles are held together by embayment within a spacious exopolymeric biofilm (e.g. organic mucus) (Fig. 13). Such flocs do not conform to the mathematical fractal description typically attributed to predominantly inorganic flocs (e.g. Winterwerp and van Kesteren, 2004, Winterwerp et al, 2006), because there is no floc formation that can be described as the primary structure. All these cases would produce microflocs which are both less dense than their constituent minerals, but would have the potential to bond with a macrofloc due to their part-biological matrix.

7.3. MSF distributions

By combining the settling velocity and mass distribution findings, it is possible to assess the mass settling flux (i.e. the product of the concentration and the Ws); this enables aspects of research question v to be discussed.

The combined effects of particle concentration and turbulent shearing have long been attributed to the growth of mud flocs (e.g. Tsai et al., 1987; Burban, 1987; Puls et al., 1988; Kranck and Milligan, 1992). Under optimum flocculation conditions, Mehta and Lott (1987) suggested

http://dx.doi.org/10.5772/55233

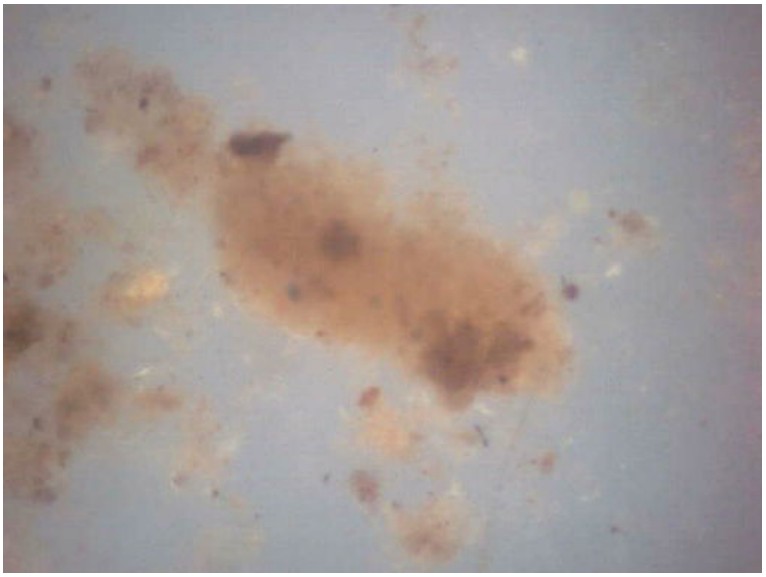

Figure 13. A very porous (low density) floc, composed from a translucent organic coating eveloping a solid (opaque) core (from Mehta et al., 2009).

that pure mud macroflocs tend to contribute most to the MSF, on account of high instability (van Leussen, 1994) due to floc growth potential producing a greater number of larger macroflocs with fast settling velocities. Observations in estuaries reveal these pure mud macroflocs can typically grow to mean a diameter > 400 μm, exhibiting effective densities of less than 40-50 $kg.m^{-3}$ and becoming more than 95% porous. These macroflocs are highly delicate entities and are easily progressively broken apart as they pass through regions of higher turbulent shear stress (Glasgow and Lucke, 1980). However, the data presented in this chapter indicates a trend whereby an increase in sand content, and a subsequent decrease in mud, favours the microflocs as the dominant flux contributor.

For example, if we consider a flocculating mixture comprising 25% mud and 75% sand, at a nominal concentration of 1000 $mg.l^{-1}$ and sheared at a τ of 0.6 Pa (i.e. Sample C6 ; see Fig. 4Civ), this results in the microflocs representing three quarters of the SPM. Therefore, the microfloc fraction would be contributing 88% of the total MSF (3.08 $g.m^{-2}s^{-1}$). To place this MSF value into perspective: it is approximately double the flux estimated for either a pure mud or a 75% mixed mud suspension; nearly 30% greater than the flux for a 50M:50S mixture; and six times greater than the MSF obtained by using a constant 0.5 $mm.s^{-1}$ settling velocity.

In contrast, by maintaining the ambient SPM concentration at 1000 $mg.l^{-1}$, but making the suspension 75% cohesive (i.e. 75M:25S), when it is sheared at 0.35 Pa (Sample A7) the total MSF (2.2 $g.m^{-2}s^{-1}$) would be weighted 73%:27% in favour of the macroflocs. This settling flux

distribution is more characteristic of a fully cohesive suspension (Manning and Bass, 2006). This suggests that with just an 8% lower MSF than pure mud, the 75M:25S mixture is behaving, to some degree, predominantly as a cohesive suspension, even with 25% fine sand present in the mixture.

The data shows that the greater the sand content of a mixed suspension, the higher the total MSF. Although it is not possible to state how much, or even when, cohesive material attaches to individual sand grains, the effective density distributions (see Figs 4Ai-v) indicate that many of the microflocs are less dense than quartz (for a nominally mass-balanced mud:sand mixture). The Ws_{micro} generally rose with rising sand content. One can see that this smaller size fraction is extremely important in terms of the total MSF for less cohesive suspensions. By averaging the MSF over the entire concentration and shear stress ranges for a nominally constant ratio of mud and sand, the data reveals that for a predominantly sandy suspension (Run C - 25M: 75S), the microflocs represented the majority (~80%) of the total MSF. In contrast, the microflocs contributed less than half (~42%) of the settling flux for the muddier 75M:25S slurry (Run A).

With the sandier 4_A Portsmouth microflocs (see Fig. 10a) representing over half of the total 2000 $mg.l^{-1}$ suspension and the macroflocs comprising three quarters of the more cohesive sample 6_B flocs (see Fig. 10b), the Portsmouth samples displayed a similar mass distribution to those of the Tamar pre-determined slurries. In terms of the MSF, Sample 4_A produced a resultant 9.9 $g.m^{-2}s^{-1}$, which was approximately 50% greater than the Tamar manufactured suspension. Whilst the Sample 6_B depositional flux, 13.6 $g.m^{-2}s^{-1}$, was more than three times the settling flux of the Tamar equivalent mixtures. The higher mass settling fluxes were a function of the quicker settling velocities demonstrated by the Portsmouth Harbour suspensions.

A direct comparison of the mass settling fluxes and their associated dynamics, can also provide a practical way to illustrate the enhanced / increased flocculation with respect to turbulent intensity. If we consider the 5000 $mg.l^{-1}$ B9 floc sample from the 50M:50S suspension, the very turbulent (τ = 0.9 Pa) environment produced a net MSF of 13.8 $g.m^{-2}s^{-1}$ (see Fig. 4Ciii), with just half the flux attributed to the macroflocs. In comparison the more advanced flocculation of the less turbulent (τ = 0.35 Pa) Sample B11, resulted in a MSF of 26.2 $g.m^{-2}s^{-1}$. This was nearly double the Sample B9 flux and was primarily due to the B11 macroflocs contributing 80% of the total flux. The fast settling (Ws of 6-14 $mm.s^{-1}$) macroflocs ranging from 482 to 650 μm produced nearly one quarter of the B11 MSF.

8. Parameterisation of mixed sediment flocculation

Since the mid-1990s, much research has been conducted in Europe on the parameterisation of the natural flocculation process, through projects such as COSINUS - *Prediction of COhesive Sediment transport and bed dynamics in estuaries and coastal zones with Integrated NUmerical Simulation models* (see Berlamont, 2002). A significant degree of progress has been achieved on the practical modelling of flocculation (e.g. Winterwerp et al., 2006; Baugh and Manning, 2007, Soulsby and Manning, 2012). In terms of general modelling applicability, these floccu-

http://dx.doi.org/10.5772/55233

lation advancements are still limited to the modelling of solely pure cohesive sediment estuaries. Due to the complexity of the mixed sediment flocculation process (as demonstrated in this chapter), statistical relationships between floc properties acquired from direct empirical observations can be used to quantify the response of flocculation to different environmental conditions (Manning and Dyer, 2007). Fig. 14 shows a conceptual representation of the 25M: 75S data compared to pure mud suspensions, at a SPM concentration of 5000 mg.l^{-1}. The mixed sediment macrofloc settling curve, within a turbulent shear stress (τ) region of 0.06-0.6 Pa, can be quantified by the following algorithm:

$$Ws_{macro} = 0.259 + 5.76*\tau - 7.61*\tau^2 + 0.000317*SPM \quad (1)$$

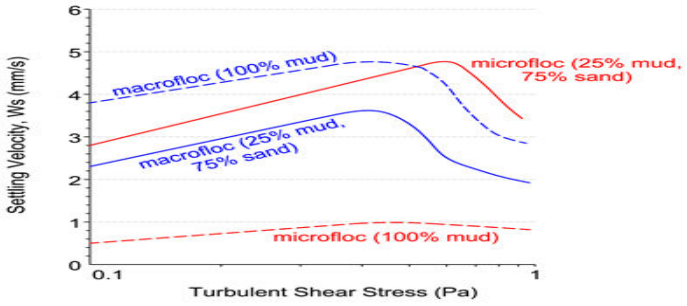

Figure 14. Conceptual illustration of Ws_{macro} (blue lines) & Ws_{micro} (red lines) trends for a mixed sediment suspension of ratio 25M:75S (solid lines) and a pure mud (dotted lines) suspension, all for a total concentration of 5 gl^{-1}, plotted against shear stress.

A parametric multiple regression was used to generate Eqn 1. For this particular type of multi-regression derivation we are using non-homogeneous dimensions, therefore the units used are as follows: Ws_{macro} = mm.s^{-1}, τ = Pa, and SPM = mg.l^{-1}. Demonstrating an R^2 = 0.84, the algorithm is a close approximation of the parameterised observations covering the 200-5000 mg.l^{-1} laboratory experimental SPM concentration range. Eqn 1 is just one form of algorithm and others can be generated from the data depending upon the modelling input variables.

The general structure of Eqn. 1 is similar to the pure mud macrofloc settling velocity relationship derived by Manning (2004a) as part of the Estuary Processes Research Project – EstProc (Estuary Process Consortium, 2005). The general shape of the Eqn. 1 curve is similar to the flocculation schematic proposed by Dyer (1989), with an increase in settling velocity at low stress due to flocculation enhanced by shear, and floc disruption at higher stresses for the same concentration. Also, the combined influence of concentration and turbulent shear on the control of the macrofloc properties, as listed in Eqn. 1, agrees with the hypotheses offered by both Puls et al. (1988) and Kranck and Milligan (1992).

However, the relative magnitudes and peaks in the mixed sediment conceptual curves (illustrated in Fig. 14) differ from the pure mud representations in a number of ways. The microflocs in the 25M:75S mixed suspension microflocs settle at a maximum velocity of 4.7 $mm.s^{-1}$; this is 380% quicker than the equivalent pure mud and nearly double the Ws_{micro} for a 75% mud suspension. Interestingly, the mixed suspension Ws_{micro} is virtually the same as the macrofloc settling velocity for pure mud. The peak 25M:75S Ws_{micro} occurred at a shear stress of 0.6 Pa, which falls within the "moderately-high" shear stress zone (Manning, 2004a); 0.2-0.3 Pa above the shear stress region typically recognised as producing optimum stimulation for pure mud flocculation (Manning, 2004a).

Manning and Dyer (2007) demonstrated that, for varying levels of suspended concentration, mud microfloc settling in turbulent flows could be represented by a single algorithm curve. In contrast, mixed sediment microfloc settling velocities appear to be dependent upon both concentration and shear stress variations, as well as the proportion of mud and sand. This is indicated by different curves representing Ws_{micro} throughout a shear stress range at varying concentration levels, even when the mud:sand ratio is constant. From this we can deduce that the mixed sediment Ws_{micro} parameter is far more sensitive to changes in SPM concentration, compared to pure mud microflocs whose dynamics only seem to vary with turbulent shear stress.

If we now examine the macrofloc settling for the conceptual curve for a 5000 $mg.l^{-1}$ 25M:75S mixed suspension (Fig. 14), one can observe that the maximum Ws_{macro} of 3.5 $mm.s^{-1}$ occurs at a shear stress of about 0.35-0.4 Pa; the same stress range as pure mud macroflocs. However, the 25M:75S macroflocs are settling 1.2 $mm.s^{-1}$ (or 25%) slower than both the Ws_{micro} peak for the mixed sediments and the Ws_{macro} for pure mud.

If we consider the mixed sediment settling velocity variations in terms of Krone's (1963) classic hierarchical order of aggregation theory, the smaller microflocs ($D < 160$ μm) are generally considered to be the building blocks from which the macroflocs are composed. The microflocs tend to display a much wider range in effective densities and settling velocities than the macrofloc fraction. It is highly plausible that for mixed sediments, the microfloc fraction samples may comprise both flocculated mud and some unflocculated sand grains depending on mud:sand ratio, concentration and shear stress. This could account for the faster microfloc settling velocities with rising sand content and concentration.

The macroflocs are deemed to be composed of microflocs, so this fraction will also contain both cohesive and non-cohesive particulates. The intra-bonding of microfloc to microfloc is usually far weaker than the closer internal particle bonds of individual microflocs. This means that macrofloc bonding relies heavily on the sediment cohesional properties (primarily those from extra-cellular polymeric substances), and these will exponentially decrease with muddy sediments being replaced by non-cohesive sands.

The parameterisation of biological process for inclusion in numerical sediment transport models is notoriously difficult, and algorithms such as Eqn. 1 do not include a specific "biological" term. However, where the algorithms are based on data derived from natural sediments which would include some of the biological effect. A limitation of many mixed

http://dx.doi.org/10.5772/55233

sediment laboratory studies, is that the mud:sand matrix is over-simplified through the use of a pure clay mineral (e.g. kaolinite) devoid of any biology. As clay minerals only flocculate through electrostatic (i.e. salt) flocculation, at best a segregated environment may be simulated if the water is brackish, but resultant mixed sediment flocculation effects will never be observed.

9. Modelling implications of mixed sediment flocculation

The prediction and modelling of mud:sand segregation effects on processes such as deposition are very useful from an estuarine management perspective. Numerical models are typically the chosen tools with which estuarine management groups attempt to predict sediment transport rates. In order for these models to provide sufficiently accurate results, a good scientific understanding of the flocculation process and interactions between mud and sand is required (e.g. Chesher and Ockenden, 1997; van Ledden, 2002; Waeles et al., 2008), and these processes need to be adequately described mathematically.

The complexity of mud:sand suspensions and a general lack of suitable experimental data which can describe the resultant dynamics of different mixtures of mud and sand, means that most numerical sediment transport models treat mud and sand as entirely separate entities. These conditions may exist for a segregational environment. However, if the mud:sand particles interact as a combined matrix, it has the potential to flocculate (as demonstrated in this chapter). This research has indicated that when mud and sand are mixed in different ratios and interact, the level of inter-particle cohesion can also vary and this is reflected in the macrofloc:microfloc mass settling flux distributions. Therefore it may be important for modellers to consider potential flocculation effects when parameterising mixed sediment deposition in turbulent flows that are conducive to flocculation.

When faced with a potential mixed sediment regime, an estuarine sediment transport modeller has two initial basic choices. The first and most simple option, is to assume that the mud:sand mixtures act solely as one sediment type when suspended, thus entirely demonstrating either cohesive or non-cohesive settling characteristics. If all sediment is assumed to be non-cohesive, e.g. pure sand grains devoid of any cohesive matter, the SPM would behave as inert particles as their dynamic settling spectrum would not alter greatly with increasing concentration as they do not flocculate. Similarly pure sand grain dynamics are not affected by shear stresses in the same way muddy sediments are. Thus, the settling properties of pure sand suspensions are similar over the SPM concentration range (200-5000 $mg.l^{-1}$) encompassed by the flume experimental data reported in this chapter; this is also because the influence of hindered settling is not important in this range of concentration. In contrast, if all SPM present is deemed to be pure mud, flocculation will completely dominate the settling process.

The second option acknowledges the presence of a mud:sand mixed environment; the issue is then how this is handled. For example, Van Ledden's (2002) mixed sediment model employed the segregational criteria for low concentration depositional simulations in which flocculation effects are ignored. However, if it is assumed that the mixed suspensions are acting in a

segregated manner, when in fact they are demonstrating a degree of flocculation, a wide range in predicted settling flux errors may arise from the modelling output.

To illustrate the potential pitfalls of solely using either a sand or mud settling parameterisation, when there is actually a flocculating mud:sand mixture present, we compare fraction-maximum settling velocities for: pure mud, pure sand and a 50M:50S ratio suspension, all at an SPM concentration of 200 $mg.l^{-1}$. For the 100% mud condition, the respective macrofloc and microfloc settling velocities are 2.4 $mm.s^{-1}$ and 0.9 $mm.s^{-1}$. The contrasting pure sand settling velocity values are Ws_{macro_sand} = 20.1 $mm.s^{-1}$ and Ws_{micro_sand} = 7.4 $mm.s^{-1}$; this was a comparative 7 to 8 -fold settling velocity rise for the two respective pure sand fractions, over the pure mud. An equal division of mud and sand resulted in an observed mixed sediment macrofloc settling velocity of 1.6 $mm.s^{-1}$, which was more than twelve times slower than the pure sand macrofloc-equivalent sized fraction and two thirds the velocity of the pure mud macroflocs. However, the observed 50M:50S microflocs fell at 2.2 $mm.s^{-1}$, which was three-times slower than pure sand, and twice as fast as pure mud suspensions. This example demonstrates the importance of obtaining high quality temporal and spatial settling velocity data of mixed sediments in suspension. It is anticipated that the effects of mixed sediment flocculation on numerical sediment transport modelling, will be the topic of future research and publication.

10. Conclusion

The aim of this chapter was to provide an overview of mixed sediment flocculation dynamics and how they can influence sediment transport. It has drawn on key literature and new data to address this aim. The theoretical aspects relating to the flocculation of mud:sand mixtures include flocculation processes, segregation versus flocculating suspensions, and biological influences on mixed sediment flocculation.

In order to demonstrate the flocculation potential and characteristics of mud:sand mixtures, the second part of the chapter has drawn on the findings from recently completed laboratory studies that examined the flocculation dynamics for mud:sand (M:S) mixtures primarily using Tamar estuary mud and silica sand at different concentrations and shear rates in a mini-annular flume. Turbulent shear stresses during the experimental runs ranged from 0.06-0.9 Pa (±5%), with maximum flow speeds in the annular flume of about 0.7 $m.s^{-1}$, for three total suspended sediment concentrations representative of estuarine concentrations, namely 200, 1000 and 5000 $mg.l^{-1}$. The video-based LabSFLOC instrument was used to determine floc properties including size, settling velocity, density, and mass.

The experiments showed that as mud content decreased, the particle cohesion efficiency reduces which can limit the growth potential of the macrofloc fraction (sizes > 160 μm). For a 75M:25S suspension, the settling velocity Ws_{macro} was slightly quicker than the microflocs at 200 $mg.l^{-1}$, but almost three-times as fast at the higher suspended concentration (5000 $mg.l^{-1}$). Parameterised data indicated that by adding more sand to a mud:sand mixture, the settling velocity of the macrofloc fraction slows and the settling velocity of microflocs (sizes < 160 μm) increases.

http://dx.doi.org/10.5772/55233

In terms of floc composition, effective density data of many of the microfloc fractions ranged between 800-1200 $kg.m^{-3}$. This would suggest that the finer sand grains tended to interact and bond better with the smaller floc structures, accounting for the quicker microfloc settling velocities observed.

The general trends revealed by the pre-determined (Tamar mud and silica) mixtures were also observed with independent tests on naturally mixed Portsmouth Harbour sediments. However, compositionally, the Portsmouth sediment matrix produced differences in the absolute settling velocities of the macrofloc and microfloc fractions from those of the Tamar mixtures. Both fractions of the Portsmouth sediment tended to fall quicker than their Tamar mixed sediment equivalents. It is proposed that this could be a result of a different sand grain size distribution combined with stronger bio-film coatings producing added cohesion in the Portsmouth sediment mixtures. This would permit a greater uptake of the sand grains within the macrofloc fraction, whilst also potentially forming the faster settling microflocs observed.

The data showed that the greater the sand content of a mixed suspension, the higher the total mass settling flux (MSF). As the microflocs have been seen to be more conducive at flocculating with the finer sand grains, and the Ws_{micro} rose with rising sand content, one can see that this smaller size fraction is extremely important in terms of the total MSF for less muddy suspensions. By averaging the MSF over the entire concentration and shear stress ranges for a constant ratio of mud (M) and sand (S), the data revealed that for a predominantly sandy suspension (25M:75S), the microflocs represented the majority of the total MSF. In contrast, the microflocs contributed less than half of the settling flux for a much muddier mixture (75M:25S).

Biology is considered to be extremely important in the mixed sediment flocculation process. For example, the presence of sticky extracellular polymeric substances (EPSs) produced by epipelic and epipsammic diatoms could significantly enhance particle bonding. Energy dispersive spectroscopy analysis confirmed the presence of both clay minerals and quartz mineral fragments within a natural microfloc. A high resolution transmission electron microscopy (TEM) image revealed EPS fibrils linking the biological and inorganic particles within a micro-structural framework of a microfloc matrix.

Since estuaries may have mixed or segregational mud:sand environments and numerical models are used to inform management decisions, some issues relating to the parameterisation of mud:sand flocculation and their implementation in sediment transport models have been discussed. It is anticipated that these two topics will be the subject of future research and publication on mixed sediment flocculation.

Acknowledgements

The mini-annular flume experiments were primarily funded by the HR Wallingford Company Research Programme as part of the 'Mud:Sand Transport' projects (DDD0301 and DDD0345), and completed during the 'Sediment in Transitional Environments' – SiTE project (DDY0427).

Author details

Andrew J. Manning[1,2], Jeremy R. Spearman[1], Richard J.S. Whitehouse[1], Emma L. Pidduck[2], John V. Baugh[1] and Kate L. Spencer[3]

1 HR Wallingford, Howbery Park, Wallingford, Oxfordshire, UK

2 School of Marine Science & Engineering, University of Plymouth, Plymouth, Devon, UK

3 Department of Geography, Queen Mary – University of London, Mile End Road, London, UK

References

[1] Alvarez-Hernandez, E. (1990). The influence of cohesive sediment on sediment movement in channels of circular cross-section. PhD thesis, University of Newcastle-upon-Tyne.

[2] Bass, S.J., Manning, A.J. and Dyer, K.R. (2006). Preliminary findings from a study of the upper reaches of the Tamar Estuary, UK, throughout a complete tidal cycle: Part I. Linking sediment and hydrodynamic cycles. In: J.P.-Y. Maa, L.P. Sanford and D.H. Schoellhamer (eds), Coastal and Estuarine Fine Sediment Processes - Proc. in Marine Science 8, Amsterdam: Elsevier, pp. 1-14, ISBN: 0-444-52238-7.

[3] Baugh, J.V. and Manning, A.J. (2007). An assessment of a new settling velocity parameterisation for cohesive sediment transport modelling. Continental Shelf Research, doi:10.1016/j.csr.2007.03.003.

[4] Berlamont, J.E. (2002). Prediction of cohesive sediment transport and bed dynamics in estuaries and coastal zones with integrated numerical simulation models. In: Winterwerp, J.C., Kranenburg, C. (eds), Fine Sediment Dynamics in the Marine Environment - Proc. in Mar. Sci. 5., Elsevier, Amsterdam, pp. 1-4.

[5] de Brouwer, J.F.C., Wolfstein, K., Ruddy, G.K. (2005). Biogenic stabilization of intertidal sediments: The importance of extracellular polymeric substances produced by benthic diatoms. Microbial Ecology, 49, 501-512.

[6] Buffle, J. and Leppard, G.G. (1995). Characterisation of aquatic colloids and macromolecules. 2. Key role of physical structures on analytical results. Environmental Science and Technology, 29, 2176-2184.

[7] Burban, P.Y. (1987). The flocculation of fine-grained sediments in estuarine waters. MSc. thesis, Dep. of Mech. Eng. Univ. of Calif., Santa Barbara, USA.

http://dx.doi.org/10.5772/55233

[8] Cahoon, L.B. (1999). The role of benthic microalgae in neritic ecosystems. Oceanography and marine biology: an annual review, 37, 47-86.

[9] Chesher, T.J. and Ockenden, M.C. (1997). Numerical modelling of mud and sand mixtures. In: N. Burt, R. Parker and J. Watts (Eds), Cohesive Sediments – Proc. of INTERCOH Conf. (Wallingford, England), Chichester: John Wiley & Son, pp. 395-406.

[10] Dankers, P.J.T., Sills, G.C. and Winterwerp, J.C. (2007). On the hindered settling of highly concentrated mud-sand mixtures. In: T. Kudusa, H. Yamanishi, J. Spearman and J.Z. Gailani (Eds), Sediment and Ecohydraulics - Proc. in Marine Science, INTERCOH 2005, Amsterdam: Elsevier, pp. 255-274.

[11] Dearnaley, M.P. (1996). Direct measurements of settling velocities in the Owen Tube: a comparison with gravimetric analysis. Journal of Sea Research, Vol. 36, Nos. 1-2, 36, 41-47.

[12] Dyer, K.R. (1986). Coastal and Estuarine Sediment Dynamics. Wiley & Sons, Chichester, 342p.

[13] Dyer, K.R. 1989. Sediment processes in estuaries: future research requirements. J. Geophys. Res., 94 (C10): 14,327-14,339.

[14] Dyer, K.R., Cornelisse, J.M., Dearnaley, M., Jago, C., Kappenburg, J., McCave, I.N., Pejrup, M., Puls, W., van Leussen, W. and Wolfstein, K. (1996). A comparison of in-situ techniques for estuarine floc settling velocity measurements. Journal of Sea Research 36, 15-29.

[15] Dyer, K.R. and Manning, A.J. (1998). Observation of the size, settling velocity and effective density of flocs, and their fractal dimensions. Journal of Sea Research 41, 87-95.

[16] Edzwald, J.K. and O'Melia, C.R. (1975). Clay distributions in recent estuarine sediments. Clays and Clay Minerals, 23:39-44.

[17] Eisma, D. (1986). Flocculation and de-flocculation of suspended matter in estuaries. Neth. J. Sea Res., 20 (2/3), 183-199.

[18] Estuary Process Consortium (2005). Final Report of the Estuary Process Research Project (EstProc) – Algorithms and Scientific Information. Integrated Research Results on Hydrobiosedimentary Processes in Estuaries, R & D Technical Report prepared by the Estuary Process Consortium for the Fluvial, Estuarine and Coastal Processes Theme, co-funded by Defra & Environment Agency, Report FD1905/TR3, 140p.

[19] Feates, N.G. and Mitchener, H.J. (1998). Properties of dredged material: measurement of sediment properties of dredged material from Harwich Harbour. HR Wallingford Report TR 46.

[20] Fennessy, M.J., Dyer, K.R. and Huntley, D.A. (1994). Size and settling velocity distributions of flocs in the Tamar Estuary during a tidal cycle. Netherlands Journal of Aquatic Ecology, 28: 275-282.

[21] Fennessy, M.J., Dyer, K.R., Huntley, D.A. and Bale, A.J. (1997). Estimation of settling flux spectra in estuaries using INSSEV. In: N. Burt, R. Parker and J. Watts (Eds), Cohesive Sediments – Proc. of INTERCOH Conf. (Wallingford, England), Chichester: John Wiley & Son, pp. 87-104.

[22] Fitzpatrick, F. (1991). Studies of sediments in a tidal environment. Ph.D. Thesis, Department of Geological Sciences, University of Plymouth, 221p.

[23] Förstner, U. and Wittmann G. T. W. (1983). Metal Pollution in the Aquatic Environment. Springer Verlag, Berlin, Heidelberg et New York, 2nd revised edition, 486p.

[24] Gerbersdorf, S.U., Bittner, R., Lubarsky, H., Manz, W. and Paterson, D.M. (2009). Microbial assemblages as ecosystem engineers of sediment stability. J Soils Sediments, 9, 640–652.

[25] Grabowski, R.C., Droppo, I.G. and Wharton, G. (2011). Erodibility of cohesive sediment: The importance of sediment properties. Earth-Science Reviews, 105, 101-120.

[26] Glasgow, L.A. and Lucke, R.H. (1980). Mechanisms of deaggregation for clay-polymer flocs in turbulent systems. Ind. Eng. Chem. Fundam., 19: 148-156.

[27] Gratiot, N. and Manning, A.J. (2004). An experimental investigation of floc characteristics in a diffusive turbulent flow. In: P. Ciavola and M. B. Collins (Eds), Sediment Transport in European Estuaries, Journal of Coastal Research, SI 41, 105-113.

[28] Harlow, D. (1980). Sediment Processes, Selsey Bill to Portsmouth, PhD thesis, Department of Civil Engineering, University of Southampton.

[29] Harper, M.A. and Harper, J.F. (1967). Measurements of diatom adhesion and their relationship with movement. British Phycological Bulletin, 3, 195-207.

[30] Hickman, M. and Round, F.E. (1970). Primary production and standing crops of epipsammic and epipelic algae. British Phycological Journal, Vol 5 (2), pp. 247-255.

[31] HR Wallingford (1998). SandCalc: Marine Sands Calculator Interface. Version 2.0 for Windows. Software by Tessela & HR Wallingford.

[32] Hydraulics Research (1959). Portsmouth harbour investigation, parts i and ii. Reports 213b and 214, Technical report, Hydraulics Research.

[33] Kamphuis, W and Hall, K.R. (1983). Cohesive material erosion by unidirectional current. J. Hyd. Eng., ASCE, 109, 49-61.

[34] Kennish, M.J. (1986). "Ecology of estuaries Volume 1: Physical and chemical aspects." Boca Raton Florida, CRC Press, 1.

http://dx.doi.org/10.5772/55233

[35] Koglin B. (1977). Assessment of the degree of aggregation in suspension. Powder Technology 17, 219-227.

[36] Klimpel R.C. and Hogg R. (1986). Effects of flocculation conditions on agglomerate structure. Journal of Colloid Interface Science 113, 121-131.

[37] Kolmogorov, A.N. (1941a). The local structure of turbulence in incompressible viscous fluid for very large Reynolds numbers. C. R. Acad. Sci. URSS, 30: 301.

[38] Kolmogorov, A.N. (1941b). Dissipation of energy in locally isotropic turbulence. C. R. Acad. Sci. URSS, 32: 16.

[39] Kranck, K. and Milligan, T.G. (1992). Characteristics of suspended particles at an 11-hour anchor station in San Francisco Bay, California. Journal of Geophysical Research, 97, 11373-11382.

[40] Krone, R.B. (1962). Flume studies of the transport of sediment in estuarial shoaling processes. Final report. Hyd. Eng. Lab. and Sanitary Eng. Lab., University of California, Berkeley.

[41] Krone, R. B. (1963). A study of rheological properties of estuarial sediments. Report No. 63-68, Hyd. Eng. Lab. and Sanitary Eng. Lab., University of California, Berkeley, 63-68.

[42] Little, C. (2000). The biology of soft shores and estuaries. Oxford University Press (UK), 252p., ISBN: 978-0-19850-426-9.

[43] Lonsdale, B. J. (1969). A sedimentary study of the eastern Solent, Master's thesis, Department of Oceanography, University of Southampton.

[44] Manning, A.J. (2001). A study of the effects of turbulence on the properties of flocculated mud. Ph.D. Thesis. Institute of Marine Studies, University of Plymouth, 282p.

[45] Manning, A.J. (2004a). The observed effects of turbulence on estuarine flocculation. In: P. Ciavola and M. B. Collins (eds), Sediment Transport in European Estuaries, Journal of Coastal Research, SI 41, 90-104.

[46] Manning, A.J. (2004b). Observations of the properties of flocculated cohesive sediment in three western European estuaries. In: P. Ciavola and M. B. Collins (Eds), Sediment Transport in European Estuaries, Journal of Coastal Research, SI 41, 70-81.

[47] Manning, A.J. (2006). LabSFLOC – A laboratory system to determine the spectral characteristics of flocculating cohesive sediments. HR Wallingford Technical Report, TR 156.

[48] Manning, A.J., Bass, S.J. and Dyer, K.R. (2006). Floc Properties in the Turbidity Maximum of a Mesotidal Estuary During Neap and Spring Tidal Conditions. Marine Geology, 235, 193-211.

[49] Manning, A.J., Baugh, J.V., Spearman, J. and Whitehouse, R.J.S. (2009). Flocculation Settling Characteristics of Mud:Sand Mixtures. Ocean Dynamics, PECS2008 SI, DOI: 10.1007/s10236-009-0251-0.

[50] Manning, A.J. and Dyer, K.R. (1999). A laboratory examination of floc characteristics with regard to turbulent shearing. Marine Geology 160, 147-170.

[51] Manning, A.J. and Dyer, K.R. (2002a). The use of optics for the in-situ determination of flocculated mud characteristics. J. Optics A: Pure and Applied Optics, Institute of Physics Publishing, 4, S71-S81.

[52] Manning, A.J. and Dyer, K.R. (2002b). A comparison of floc properties observed during neap and spring tidal conditions. In: J.C. Winterwerp and C. Kranenburg (Eds), Fine Sediment Dynamics in the Marine Environment - Proc. in Marine Science 5, Amsterdam: Elsevier, pp. 233-250, ISBN: 0-444-51136-9.

[53] Manning, A.J. and Dyer, K.R. (2007). Mass settling flux of fine sediments in Northern European estuaries: measurements and predictions. Marine Geology, 245, 107-122, doi:10.1016/j.margeo.2007.07.005.

[54] Manning, A.J., Spearman, J. and Whitehouse, R.J.S. (2007). Mud:Sand Transport – Flocculation & Settling Dynamics within Turbulent Flows, Part 1: Analysis of laboratory data. HR Wallingford Internal Report, IT 534, 32p.

[55] Manning, A.J. and Whitehouse, R.J.S. (2009). UoP Mini-annular flume – operation and hydrodynamic calibration. HR Wallingford Technical Report, TR 169.

[56] McCave, I.N. (1984). Size spectra and aggregation of suspended particles in the deep ocean. Deep-Sea Res., 31: 329-352.

[57] Mehta, A.J., Jaeger, J.M., Valle-Levinson, A., Hayter, E.J., Wolanski, E. and Manning, A.J. (2009). Resuspension Dynamics in Lake Apopka, Florida. Final Synopsis Report, submitted to St. Johns River Water Management District, Palatka, Florida, June 2009, Report No. UFL/COEL-2009/00, 158p.

[58] Mehta, A.J. and Lott, J.W. (1987). Sorting of fine sediment during deposition. Proc. Speciality Conf. Advances in Understanding Coastal Sediment Processes. Am. Soc. Civ. Eng., New York, pp. 348-362.

[59] Mietta, F. (2010). Evolution of floc size distribution of cohesive sediments. Ph.D. Thesis, Delft University of Technology, Faculty of Civil Engineering and Geosciences, The Netherlands, 169p.

[60] Migniot, C. (1968). Study of the physical properties of various very fine sediments and their behaviour under hydrodynamic action. La Houille Blanche, 23 (7). (Translation of French text).

[61] Mitchener, H.J., Torfs, H. and Whitehouse, R.J.S. (1996). Erosion of mud/sand mixtures. Coastal Engineering, 29, 1-25 [Errata, 1997, 30, 319].

[62] Mory, M., Gratiot, N., Manning, A.J. and Michallet, H. (2002). CBS layers in a diffusive turbulence grid oscillation experiment. In: J.C. Winterwerp and C. Kranenburg (Eds.), Fine Sediment Dynamics in the Marine Environment - Proc. in Mar. Science 5, Amsterdam: Elsevier, pp.139-154, ISBN: 0-444-51136-9.

[63] Nowell, A.R.M., Jumars, P.A. and Eckman, J.E. (1981). Effects of biological activities on the entrainment of marine sediments. Mar. Geol., 42, 133-153.

[64] Ockenden, M.C. and Delo, E.A. (1988). Consolidation and erosion of estuarine mud and sand mixtures – an experimental study. HR Wallingford Report, SR 149.

[65] Owen, M.W. (1976). Determination of the settling velocities of cohesive muds. Hydraulics Research, Wallingford, Report No. IT 161, 8p.

[66] Panagiotopoulus, I., Voulgaris, G. and Collins, M.B. (1997). The influence of clay on the threshold of movement of fine sandy beds. Coastal Eng., 32, 19-43.

[67] Parker, D.S., Kaufman, W.J. and Jenkins, D. (1972). Floc break-up in turbulent flocculation processes. J. Sanitary Eng. Div., Proc. Am. Soc. Civil Eng., 98 (SA1): 79-97.

[68] Paterson, D.M. (1989). Short-term changes in the erodibility of intertidal cohesive sediments related to the migratory behaviour of epipelic diatoms. Limnol. Oceanogr. 34: 223-234.

[69] Paterson, D.M., Crawford, R.M. and Little, C. (1990). Subaerial exposure and changes in the stability of intertidal estuarine sediments. Estuarine Coastal and Shelf Science, 30, 541-556.

[70] Paterson, D.M. and Hagerthey, S.E. (2001). Microphytobenthos in contrasting coastal ecosystems: Biology and dynamics. In: Ecological comparisons of sedimentary shores (K. Reise, Ed.), Ecological studies, pp. 105-125.

[71] Pidduck, E.L. and Manning, A.J., in prep. A Laboratory Examination of Flocculation Properties Exhibited by Natural Sediment Mixtures from Portsmouth Harbour, UK. HR Wallingford Technical Report, TR 182.

[72] Puls, W., Kuehl, H. and Heymann, K. (1988). Settling velocity of mud flocs: results of field measurements in the Elbe and the Weser Estuary. In: J. Dronkers, and W. van Leussen, (eds), Physical Processes in Estuaries. Berlin: Springer-Verlag, pp. 404-424.

[73] Raudkivi, A.J. (1998). Loose boundary hydraulics. 3rd Edition. Balkema, Rotterdam.

[74] Reid, G.K. and Wood, R.D. (1976). "Ecology of inland water and estuaries." New York: D. Van Nostrand Company.

[75] Soulsby, R.L. and Manning, A.J. (2012). Cohesive sediment settling flux: settling velocity of flocculated mud. Technical Note DDY0409-01, HR Wallingford, Wallingford, UK.

[76] Spearman, J.R., Manning, A.J. and Whitehouse, R.J.S. (2011). The settling dynamics of flocculating mud:sand mixtures: Part 2 – Numerical modelling. Ocean Dynamics, INTERCOH 2009 special issue, DOI: 10.1007/s10236-011-0385-8.

[77] Spencer, K.L., Manning, A.J., Droppo, I.G., Leppard, G.G. and Benson, T. (2010). Dynamic interactions between cohesive sediment tracers and natural mud. Journal of Soils and Sediments, Volume 10 (7), doi:10.1007/s11368-010-0291-6.

[78] Tambo, N. and Hozumi, H. (1979). Physical characteristics of flocs – II. Strength of flocs. Water Research, 13, 409-419.

[79] Tambo, N. and Watanabe, Y., (1979). Physical characteristics of flocs-I. The floc density function and aluminium floc. Water Research 13, 409-419.

[80] ten Brinke, W.B.M. (1993). The impact of biological factors on the deposition of fine grained sediment in the Oosterschelde (The Netherlands). Ph.D. Thesis, University of Utrecht, The Netherlands, 252p.

[81] Tolhurst, T.J., Gust. G. and Paterson, D.M. (2002). The influence on an extra-cellular polymeric substance (EPS) on cohesive sediment stability. In: J.C. Winterwerp and C. Kranenburg (Eds), Fine Sediment Dynamics in the Marine Environment - Proc. in Marine Science 5, Amsterdam: Elsevier, pp. 409-425, ISBN: 0-444-51136-9.

[82] Tomi, D.T., Bagster, D.F. (1978). The behaviour of aggregates in stirred vessels: Part I - Theoretical considerations on the effects of agitation. Trans. Inst. Chem. Eng., 56, 1-8.

[83] Torfs, H. (1994). Erosion of layered sand-mud beds in uniform flow. Proc. 24th Int. Conf. Coastal Eng., Kobe, Japan, 23-28 October 1994.

[84] Torfs, H., Mitchener, H.J., Huysentruyt, H. and Toorman, E. (1996). Settling and consolidation of mud/sand mixtures. Coastal Engineering, 29, 27-45.

[85] Tsai, C.H., Iacobellis, S. and Lick, W. (1987). Flocculation of fine-grained sediments due to a uniform shear stress. J. Great Lakes Res., 13: 135-146.

[86] Uncles, R.J., Stephens, J.A. and Harris, C. (1998). Seasonal variability of subtidal and intertidal sediment distributions in a muddy, macrotidal estuary: the Humber-Ouse, UK. In: Sedimentary Processes in the Intertidal Zone, Black, K.S., Paterson, D.M. and Cramp, A. (Eds), Geological Society, London, Special Publications, 139, 211-219.

[87] Underwood, G.J.C. and Kromkamp, J. (1999). Primary production by phytoplankton and microphytobenthos in estuaries. Advances in ecological research, 29, 93-153.

[88] Underwood, G.J.C. and Paterson, D.M. (2003). The importance of extracellular carbohydrate production by marine epipelic diatoms. Advances in Botanical Research (incorporating Advances in Plant Pathology), Vol. 40, Elsevier, Amsterdam, pp.183-240, ISBN: 0-12-005940-1.

http://dx.doi.org/10.5772/55233

[89] Van de Ven, T.G. and Hunter, R.J. (1977). The energy dissipation in sheared coaggulated soils. Rheologica Acta, 16, 534-543.

[90] van Ledden, M. (2002). A process-based sand-mud model. In: J.C. Winterwerp and C. Kranenburg (Eds.), Fine Sediment Dynamics in the Marine Environment - Proc. in Mar. Science 5, Amsterdam: Elsevier, pp.577-594, ISBN: 0-444-51136-9.

[91] van Ledden, M. (2003). Sand-mud segregation in estuaries and tidal basins. Ph.D. Thesis, Delft University of Technology, The Netherlands, Report No. 03-2, ISSN 0169-6548, 217p.

[92] van Leussen, W. (1988). Aggregation of particles, settling velocity of mud flocs: a review. In: Dronkers, J., van Leussen, W. (Eds), Physical Processes of Estuaries, Berlin: Springer, pp. 347-403.

[93] van Leussen, W. (1994). Estuarine macroflocs and their role in fine-grained sediment transport. Ph.D. Thesis, University of Utrecht, The Netherlands, 488p.

[94] van Wijngaarden, M., Venema, L.B., De Meijer, R.J., Zwolsman, J.J.G., Van Os, B. and Gieske, J.M.J. (2002a). Radiometric sand-mud characterisation in the Rhine-Meuse estuary, Part A: Fingerprinting. Geomorphology, 43, 87-101.

[95] van Wijngaarden, M., Venema, L.B., and De Meijer, R.J. (2002b). Radiometric sand-mud characterisation in the Rhine-Meuse estuary, Part B: In situ mapping. Geomorphology, 43, 103-116.

[96] Waeles, B., Le Hir, P. and Lesueur, P. (2008). A 3D morphodynamic process-based modelling of a mixed sand/mud coastal environment : the Seine Estuary, France. In: T. Kudusa, H. Yamanishi, J. Spearman and J.Z. Galiani, (eds.), Sediment and Ecohydraulics - Proc. in Marine Science 9, Amsterdam: Elsevier, pp. 477-498, ISBN: 978-0-444-53184-1.

[97] Whitehouse, R.J.S., Soulsby, R., Roberts, W. and Mitchener, H.J. (2000). Dynamics of Estuarine Muds. Thomas Telford Publications, London, 232p.

[98] Widdows, J., Blauw, A., Heip, C.H.R., Herman., P.M.J., Lucas, C.H., Middelburg, J.J., Schmidt, S., Brinsley, M.D., Twisk, F. and Verbeek, H. (2004). Role of physical and biological processes in sediment dynamics of a tidal flat in Westerschelde Estuary, SW Netherlands. Mar. Ecol. Prog. Series, 274, 41-56.

[99] Williamson, H.J. (1991). Tidal transport of mud / sand mixtures: Sediment distributions – a literature review. HR Wallingford, Report SR 286.

[100] Williamson, H.J. and Ockenden, M.C. (1993). Laboratory and field investigations of mud and sand mixtures. In: Sam S.Y Wang (Ed.), Advances in Hydro-science and Engineering, Proceedings of the First International Conference on Hydro-science and Engineering, Washington D.C. (7-11 June 1993), volume 1, pp. 622-629.

[101] Winterwerp, J. C. (1998). A simple model for turbulence induced flocculation of cohesive sediment, J. Hyd. Eng., 36 (3), 309-326.

[102] Winterwerp, J.C. and van Kesteren, W.G.M. (2004). Introduction to the physics of cohesive sediment in the marine environment. Developments in Sedimentology, 56, van Loon, T. (Ed.), Amsterdam: Elsevier, 466p.

[103] Winterwerp, J.C., Manning, A.J., Martens, C., de Mulder, T., and Vanlede, J. (2006). A heuristic formula for turbulence-induced flocculation of cohesive sediment. Estuarine, Coastal and Shelf Science, 68, 195-207.

[104] Wolanski, E. (2007). Estuarine Ecohydrology. Elsevier (Amsterdam, The Netherlands), 157p, ISBN: 978-0-444-53066-0.